University of Essex

Thermal responses of marine phytoplankton: Implications to their biogeography in the present and future oceans

Brisneve Edullantes

A thesis submitted for the degree of Doctor of Philosophy

School of Life Sciences

University of Essex

September 2020

This page is intentionally left blank.

I dedicate this work to my family and friends, especially to SCE, PCE, and GCB, who are my inspirations in life.

This page is intentionally left blank.

ABSTRACT

Phytoplankton are ecologically significant as primary producers and as regulators of the biogeochemical cycle. However, some may form harmful algal blooms that are a global problem due to the production of toxins that pose a risk to public health, the environment, and our economy. Climate change poses a serious threat to phytoplankton communities. It is, therefore, crucial to advance our knowledge on how they respond to the changes in temperature that is projected to increase in the next decades. The main aim of this thesis is to investigate how temperature limits biogeography, growth, toxin production, and competition in marine phytoplankton. To achieve this aim, the thesis presents a series of chapters with independent objectives. In Chapter 2, I analysed a global dataset of species occurrence data to examine the global patterns in the realised thermal niche and geographic range of marine phytoplankton. In Chapter 3, I investigated the global patterns of thermal traits, thermal sensitivity, and exposure and vulnerability to warming in marine phytoplankton. In Chapter 4 and 5, I conducted laboratory experiments to examine the temperature dependence of growth and toxin production in marine dinoflagellates. In Chapter 6, I also conducted laboratory experiments to test the effect of increased temperature on growth and competition in marine phytoplankton using dinoflagellates as test organisms. The key results of this thesis are as follows: (1) the current distribution of marine phytoplankton is limited by temperature, (2) their thermal traits are contingent on their biogeography and phylogeny, (3) their growth and toxin production is affected by temperature, and (4) interspecific competition in dinoflagellates is altered by increasing temperature. The findings of this thesis advance our current predictive understanding of the ecological responses of marine phytoplankton to climate change.

ACKNOWLEDGEMENTS

TABLE OF CONTENTS

This page is intentionally left blank.

LIST OF TABLES

This page is intentionally left blank.

LIST OF FIGURES

scenario ($WR_{8.5}$* and $V_{8.5}$*, respectively). S_{min}*, S_{max}*, $WR_{8.5}$*, and $V_{8.5}$* were fitted against latitude using generalised additive models (*GAM*; see Supplementary Table 3.3 *GAM* 17, 18, 22, and 26, respectively, for the summary statistics). The regression lines are indicated in blue solid lines with 95% confidence interval in grey shading. Except for $V_{8.5}$*, estimates for S_{min}*, S_{max}*, $WR_{8.5}$* did vary non-monotonously with latitude (A – D). Furthermore, S_{min}*, S_{max}*, $WR_{8.5}$*, and $V_{8.5}$* were fitted against *TA* and *TS* using generalised linear models (*GLM*; see Supplementary Table 3.5 *GLM* 33, 34, 38, and 42, respectively, for the summary statistics). The *GLMs* were used to construct the contour plots (E – H). The colour bars indicate the estimates of S_{min}*, S_{max}*, $WR_{8.5}$*, and $V_{8.5}$*.

marine phytoplankton. *CTMI*-derived TT_p* (A – D) and seasonal extreme *SST*-derived TT_o* (E – H) were used to compute for the difference between physiology- and occurrence-based thermal traits (I – L). $S_{min}*$, $S_{max}*$, $WR_{8.5}*$ and $V_{8.5}*$ were obtained from *CTMI*-derived datasets (M – P) and the warming rate and vulnerability were computed based on *RCP* 8.5 climate scenario. The solid black lines indicate the Moran's *I* index autocorrelation, and the dashed black lines indicate the 95% confidence interval. The horizontal black lines represent the estimated value of Moran's *I* under the null hypothesis of no phylogenetic autocorrelation. The red and blue colored bars indicate significant positive and negative autocorrelation, respectively; whilst, the black colored bars indicate a non-significant autocorrelation.

between the thermal traits, i.e. thermal optimum (T_{opt}), critical thermal minimum (CT_{min}), critical thermal maximum (CT_{max}), and fundamental thermal niche (FTN) (A – D, respectively) in marine phytoplankton and the ambient temperatures (mean, minimum, maximum, and range of sea surface temperature (SST), respectively) they experienced in their local habitat. Circles indicate the mean estimates of the traits in non-toxic (blue) and potentially toxic (red) strains with error bars representing the standard error of the mean. Generalised linear mixed models ($GLMM$) were used to model the trait-environment relationships with toxicity, strain identity, and source of experimental data as random factors. The solid lines represent the linear fit with 95% confidence interval in grey shading. The broken lines represent the equality between the thermal traits and the environment.

examined under a Leica DMI6000B inverted light microscope at 100x magnification (A). Each sample in a well was scanned (the red lines indicate the scanning path) on a 3x5 rectangular pattern producing 15 image tiles per sample (B). Each microscope image (C1) was processed (C2 – C7) by executing an ImageJ macro in FIJI to produce a spreadsheet of parameters (C8) and an image overlaid with outlines (C9). Input and output files for each samples for every sampling date were organised in a directory with a structure shown in D.

species in the competition. The solid lines represent the fits with the linear model displayed at the bottom. The points above the horizontal broken lines or at the right side of the vertical broken lines indicate that focal species outcompetes competitor, whilst points below or at the left side of the broken lines indicates that competing species outcompetes focal species.

percentage of new and loss habitats in the future may vary across phytoplankton species and between non-toxic and toxic species. The results are based on the preliminary analysis, which will not be discussed in details since it is not within the scope of this chapter. This figure is for demonstration purpose only to show how correlative and mechanistic *ENM* projections are used to examine ecological response of marine phytoplankton to climate change.

composition of toxic species decreased in lower latitude. However, this projection is different from the correlative *ENM* that show a complex latitudinal pattern in $\Delta PT - NT$. The results are based on the preliminary analysis, which will not be discussed in details since it is not within the scope of this chapter. This figure is for demonstration purpose only to show how correlative and mechanistic *ENM* projections are used to examine ecological response of marine phytoplankton to climate change.

This page is intentionally left blank.

DECLARATION OF THE CONTRIBUTION TO THE THESIS

In all chapters, I was responsible for the conception of the study design, development of methods, data collection, data processing, data analysis, data interpretation, and writing the initial and final drafts. Tom Cameron, Michael Steinke, and Etienne Low-Decarie assisted me in the data analysis and interpretation in Chapter 2 to Chapter 6. They also provided feedback and assisted me in the revision of all drafts. Andrew Turner and Ben Maskrey from Center for Environment, Fisheries and Aquaculture Science (CEFAS) analysed the samples for the detection and quantification of toxins presented in Chapter 5. All contribution to this thesis is acknowledged as co-authorship in the following papers, which are currently *in preparation* for possible publication:

Chapter 1

- Edullantes, B., Cameron, T., Steinke, M., and Low-Decarie, E. Review of the evolution and ecology of toxin production by phytoplankton. (*In preparation*)

Chapter 2

- Edullantes, B., Cameron, T., Steinke, M., and Low-Decarie, E. Thermal biogeography of marine phytoplankton in the contemporary ocean. (*In preparation*)

Chapter 3

- Edullantes, B., Low-Decarie, E., Steinke, M., and Cameron, T. Congruence and inequality between fundamental and realised thermal niche in marine phytoplankton. (*In preparation*)

- Edullantes, B., Low-Decarie, E., Steinke, M., and Cameron, T. Warming vulnerability differs across biogeographic and thermal affinities in marine phytoplankton. (*In preparation*)
- Edullantes, B., Low-Decarie, E., Steinke, M., and Cameron, T. Phylogenetic pattern in thermal traits explain warming vulnerability in marine phytoplankton. (*In preparation*)

Chapter 4

- Edullantes, B., Low-Decarie, E., Steinke, M., and Cameron, T. Difference in the thermal growth response between non-toxic and toxic marine phytoplankton. (*In preparation*)

Chapter 5

- Edullantes, B., Turner, A., Maskrey, B., Low-Decarie, E., Steinke, M, and Cameron, T. Effect of temperature on growth and toxin production in a toxigenic dinoflagellate species. (*In preparation*)

Chapter 6

- Edullantes, B., Low-Decarie, E., Steinke, M., and Cameron, T. Application of high throughput microscopy, reproducible image analysis, and deep learning to quantify growth and competition in a phytoplankton community**.** (*In preparation*)
- Edullantes, B., Low-Decarie, E., Steinke, M., and Cameron, T. The effect of warming on growth and competition in marine dinoflagellates**.** (*In preparation*)

Chapter 7

- Edullantes, B., Low-Decarie, E., Steinke, M., and Cameron, T. Predicting the biogeography of marine phytoplankton in present and future climate scenarios. (*In preparation*)

CHAPTER 1

This page is intentionally left blank.

This page is intentionally left blank.

GENERAL INTRODUCTION

1.1 PHYTOPLANKTON AND THEIR IMPACTS

Phytoplankton are unicellular photosynthetic microorganisms that are drifting with the current in the euphotic layer of the oceans (Falkowski and Raven, 2007). They are widespread and diverse group of organisms, which are distributed across the major taxonomic groups including the prokaryotes (i.e. cyanobacteria) and the eukaryotes (e.g. diatoms, dinoflagellates, and chlorophytes) that acquired photosynthesis via endosymbiosis (Simon et al., 2009). These autotrophic organisms are ecologically important as primary producers, biological carbon pump regulators, and biogeochemical cycle mediators (Barsanti and Gualtieri, 2005; Behrenfeld et al., 2006; Falkowski, 2012; Falkowski and Oliver, 2007).

As the base of aquatic food web, they make their own food by harnessing sunlight to combine carbon dioxide and water, and produce excess carbohydrates and oxygen that are made available to organisms at higher trophic levels, fueling the entire (Falkowski and Raven, 2007). They account for 1% of the photosynthetic biomass at a global scale and contribute almost half of our planet's annual net primary production (Falkowski, 2012). As regulator in the biological carbon pump, they transfer tons of carbon dioxide from the atmosphere to the water bodies each year. They fix inorganic carbon (Falkowski and Oliver, 2007) into more usable organic material, transfer it to other organisms when they are consumed, and deposit it into the sea floor when they die or decompose (Behrenfeld *et al.*, 2006). As mediator of the biogeochemical cycles, they also provide a link between metabolic processes and the flux of nutrients other than carbon (C), such as nitrogen (N), phosphorus (P), silicon (Si), sulfur (S), iron

(*Fe*), and other trace elements (Barsanti and Gualtieri, 2005). Key functional phytoplankton groups have their role in various marine biogeochemical cycles. Silicifiers (e.g. diatoms and silicoflagellates) play a major role of the biogeochemical cycle of *C*, *Si*, *N*, and *Fe* in open ocean, and some are chain forming species that contribute to the downward export of *Si* especially after bloom events (Tréguer and De La Rocha, 2013). Calcifiers (e.g. coccolithopores) control the air-sea carbon dioxide equilibrium, alkalinity, and surface carbonate chemistry and contribute for more than the marine carbonate export (Schiebel, 2002). Nitrogen fixers (e,g. *Trichodesmium* spp. and diazotrophs) regulate the balance of total oceanic nitrogen and drive new and export production by providing a new bioavailable nitrogen source to the ocean (Montoya et al., 2004). Dimethyl sulfate (*DMS*) producers (e.g. diatoms, dinoflagellates, and *Phaeocystis* spp.) influence the atmospheric sulfur cycle by converting dimethyl-sulfoniopropionate (*DMSP*) to *DMS* (Simó, 2001). Picoautotrophs (e.g. *Synechococcus* spp. and *Prochlorococcus* spp.) play a significant role in microbial food web, ocean nitrogen cycles, and global carbon biogeochemistry (Boyd et al., 2010).

Regardless of their ecological importance, some phytoplankton species, under certain circumstances, may form harmful algal bloom (*HAB*) that pose human health risks, environmental degradation, and economic losses (Berdalet et al., 2016). *HAB* species (*HABs*) may harm marine organisms by production of excessive biomass. The bacterial degradation of high biomass during the decline phase of the bloom can diminish the concentration of dissolved oxygen in coastal waters. This results to hypoxic condition that may cause massive mortalities of fish and invertebrates (Hallegraeff et al., 2004). Furthermore, high algal biomass in coastal waters may also reduce light penetration and produce excessive ammonia. This condition degrades the coastal water

with scums and bad odours, making the area unsuitable for recreation (Berdalet et al., 2016).

Other *HABs* produce compounds (e.g. reactive oxygen species (*ROS*), polyunsaturated fatty acids (*PUFAs*, mucilage) that are noxious to fish and invertebrates (Hallegraeff et al., 2004). Fish kills by these harmful species has been suggested to be caused by impairment in fish respiratory system by: (1) mechanical damage to the gills due to serrated algal spines, (2) clogging of gills by the excess mucus produced at the site of penetration by the spines, and (3) hemorrhage of gill capillaries due to hemolytic substance produce by the algae (Kent et al., 1995; Yang and Albright, 1992). Some fish kill is associated with algal blooms that produce extracellular toxins (Bourdelais et al., 2002).

Some *HABs* present risk to human health by production of potent biotoxins, which have been linked to food-borne poisonings. They can be filtered from the water by bivalve mollusks, which bio-concentrate the algal toxins. These toxic *HABs*, especially dinoflagellate species, can cause harm at low abundances by contaminating shellfish with toxins that are harmful or even lethal to humans (Hallegraeff et al., 2004). Economic impacts of toxic *HABs* include commercial fishery losses due to closure of aquaculture, fish mortalities, and shellfish poisoning scare, and the associated high cost of monitoring and management of toxic harmful blooms (Anderson et al., 2000).

The well-documented impacts of phytoplankton to the marine environment, to humans and to other organisms have generated ongoing interests in the physiology and ecology of phytoplankton, but more especially their response to changes in temperature (e.g. Litchman et al., 2012; Righetti et al., 2019; Thomas et al., 2012), and particularly in the context of contemporary climate change (IPCC, 2013).

1.2 PHYTOPLANKTON IN THE WARMING OCEAN

Excessive emissions of CO_2 in the atmosphere from anthropogenic activities lead to ocean warming (IPCC, 2013). The ocean absorbs more than 93% of the enhanced heat since 1970s which warms the ocean at a rate of ~0.13 °C per decade (Rhein et al., 2013). Ocean warming is not just an increase in the sea surface temperature (SST); in fact, two thirds of the excess heat has been absorbed by the upper ocean whilst one third is taken up into deep ocean (Laffoley and Baxter, 2016). Ocean heat uptake is not uniform spatially with warming greater in mid-latitude regions and greatest in the southern hemisphere (Laffoley and Baxter, 2016; Rhein et al., 2013). These changes in temperature in ocean is likely to have a profound effect on phytoplankton physiology and ecology, and consequently altering marine ecosystem structure and function (Regaudie-De-Gioux and Duarte, 2012; Thomas et al., 2012; Toseland et al., 2013).

Phenology is regarded as the simplest process to track changes in response to climate change (Rosenzweig et al., 2007). It refers to a naturally recurring phenomenon in organisms governed by seasonal and interannual variations in climate. The shifts in phenology are widely recorded impacts of global warming (Root et al., 2003). It is expected that the increasing temperature allows organisms to initiate activity earlier in spring and maintain the activity later in fall (Angilletta, 2009). A recent study that conducted a meta-analysis of recorded impacts of climate change on marine organisms suggests that phytoplankton phenology have shifted earlier in the year (Poloczanska et al., 2016). Several phytoplankton species have advanced their timing of the spring bloom, which may be crucial to the subsequent productivity of the marine ecosystems (Edwards and Richardson, 2004). The annual phytoplankton spring bloom governs the seasonal cycle of primary production in many regions (Gran and Braarud, 1935).

Furthermore, the timing of oceanic CO_2 uptake is considered to be under the influence of phytoplankon phenology (Bennington et al., 2009; Palevsky and Quay, 2017), and the carbon export and storage efficiency is controlled by the seasonal variability in primary production (Lutz et al., 2007). Hence, the climate-induced changes in the timing of the phytoplankton bloom are likely to impact the primary production and carbon cycling in the future ocean.

Aside from the changes in the timing of biological events, activities of organisms are also expected to shift in space due to the warming climate. In recent decades, many plant and animal species have shifted their geographical ranges in response to climate change (Parmesan et al., 2003). Biogeographical distribution and community structure of phytoplankton are also expected to shift in the warming ocean due to alteration in their thermal tolerance. Recent studies have demonstrated the effect of elevated temperature on metabolic and growth rates in phytoplankton (Boyd et al., 2013; de Boer et al., 2004; Krol et al., 1997; Levasseur et al., 1990; Maxwell et al., 1994; Mortain-Bertrand et al., 1988; Regaudie-De-Gioux and Duarte, 2012; Thomas et al., 2017; Toseland et al., 2013) and on phytoplankton biogeographical repartition (Chen, 2015; Righetti et al., 2019; Thomas et al., 2016). Increasing SST enhances stratification that variably affects nutrient and light availability for phytoplankton growth in the global ocean (Behrenfeld et al., 2006). Growth of the phytoplankton in the tropics and mid-latitudes will be limited by nutrients because the increased stratification reduces upwelling of nutrient-rich water to the surface. On the other hand, phytoplankton growth will be light-limited at higher latitudes, and the increased stratification retains phytoplankton within the euphotic zone. Certain phytoplankton species will likely be favoured if the increased thermal stratification will deplete resources for growth within the euphotic zone. For instance, flagellated phytoplankton,

such as most harmful dinoflagellates, are capable to vertically migrate to nutrient replete regions, and therefore are expected to dominate over non-motile species (Falkowski et al., 2004; Tozzi et al., 2004). Increasing SST will likely trigger the poleward shifts in thermal niches of phytoplankton species (Barton et al., 2016). It may also trigger to the decline of phytoplankton diversity in the tropics (Thomas et al., 2012). Warming may also result to the occupancy of non-indigenous and invasive species in new thermally defined habitats (Sorte et al., 2010). Furthermore, it may cause the shift towards a smaller size community structure (Acevedo-Trejos et al., 2015).

In the context of harmful bloom-forming phytoplankton, some specie produce toxin in response to stressful thermal conditions when growth is strongly inhibited (Aquino-Cruz, 2012). Long-term starvation also allows toxic phytoplankton to accumulate toxins (Lee et al., 2016), which can be induced when increased temperature limits their capacity to uptake nutrients (Sterner and Grover, 1998). Increased toxicity to elevated temperature could be attributed to the reduction of toxin-consuming bacterial symbionts (Ashton et al., 2003). Furthermore, warming may also shift the abundance, distribution, and timing of toxic bloom forming phytoplankton. Abundance of *Gambierdiscus toxicus*, a tropical HAB, increases with elevated SST during El Niño events (Hales et al., 1999), and its range may expand to higher latitudes as the ocean gets warmer (Tester, 1994). Moreover, toxic bloom of *Alexandrium catenella* occurs usually at SST greater than 13°C in late summer and early fall in Puget Sound (Washington) (Gessner and Middaugh, 1995), and the annual occurrence of this bloom in this region may expand as a result of warming (Moore et al., 2008). Ocean warming may also indirectly influence phytoplankton blooms. It can cause coral-macroalgal phase shifts (Hughes et al., 2007), that may increase habitat for toxic HAB epiphytes like *G. toxicus* (Moore et al., 2008). Climate change may provide favourable

conditions for toxic algae to occur (Hallegraeff, 2010). It is likely that toxic blooms and their impacts may be exacerbated in the future where their duration, intensity, and frequency may increase in response to changes in the climate (Moore et al., 2008; Tatters et al., 2013).

With these known effects of ocean warming due to climate change to phytoplankton, it is crucial to advance our understanding on the physiological and ecological adaptations of marine phytoplankton to temperature.

1.3 DIRECT EFFECTS OF TEMPERATURE

Growth of phytoplankton depends on the abiotic factors such as light, nutrients, temperature, as well as biotic factors such as competition and predation. Among these variables, temperature is one of the most fundamental factors that determines the niche of phytoplankton (Boyd et al., 2013; de Boer et al., 2004). The direct effect of temperature on metabolic and growth rates in phytoplankton are well recognised in literature (Baker et al., 2016; Boyd et al., 2013; de Boer et al., 2004; Geider et al., 1997; Krol et al., 1997; Levasseur et al., 1990; Maxwell et al., 1994; Mortain-Bertrand et al., 1988; Regaudie-De-Gioux and Duarte, 2012; Thomas et al., 2017; Toseland et al., 2013).

Growth of phytoplankton is contingent on the two temperature-dependent metabolic fluxes: photosynthesis and respiration (Raven and Geider, 1988). Typically, photosynthesis rises with elevated temperature until it reaches its optimum, and decreases with further increase in temperature; whilst respiration, on the other hand, increases with increasing temperature. The influence of temperature on metabolic

9

processes in phytoplankton is mainly driven by the kinetics of enzymes. One important

temperature-sensitive enzyme is ribulose-1,5-bisphosphate (Rubisco) with carboxylase

and oxygenase activity that catalyzes two competing biochemical reactions -

photosynthesis and photorespiration, respectively (Hikosaka et al., 2005).

Modification of Rubisco activity is one of the acclimation strategies of

phytoplankton in response to changes in temperature. Some phytoplankton species that

are acclimated to low temperature reduce Rubisco carboxylase activity to decrease the

energy transfer efficiency between the antennae and photosystem II (PS II) reaction

centers and consequently prevent photoinhibition (Krol et al., 1997; Levasseur et al.,

1990; Maxwell et al., 1994), whilst others enhance this enzymatic activity to ensure the

utilization of excess energy and increase photosynthetic rates (Mortain-Bertrand et al.,

1988). Phytoplankton that grow beyond the optimal growth temperature inactivates or

denatures their photosynthetic enzymes that unbalances ATP consumption and

production, and eventually affects photosynthesis, respiration and growth (Raven and

Geider, 1988). Furthermore, adaptation to varying temperature for growth in

phytoplankton involve changes in the quantity of enzymes, light-harvesting pigments

and thylakoid membrane integrity (Raven and Geider, 1988).

Increasing temperature enhances growth until it reaches the optimal

temperature, whilst elevated temperature beyond the optimal is lethal and declines

growth. These thermal responses characterise the typical asymmetry of growth-

temperature curve (Figure 1.1), with asymptotic increase in one side, and an abrupt

decline in another side (Ras et al., 2013). The curves can be used to estimate

maximum growth rate (r_{max}) and the thermal traits such as the (i) the cardinal

temperatures that corresponds to the boundaries of thermal tolerance (i.e. thermal

optima (T_{opt}), critical thermal minima (CT_{min}), and critical thermal maximum (CT_{max}), and

(ii) the fundamental thermal niche breadth (*FTN*) that correspond to the thermal range on which the species can physiologically tolerate. The shape of the curves reflects the effect of temperature on enzymatic rate process and on enzyme activation and stability at high temperatures (Knies and Kingsolver, 2010). Growth rates increase gradually with increasing temperature below the thermal optimum (T_{opt}), which is attributed to the exponential increase of the reaction rates with increasing temperature following the Arrhenius kinetics (Arrhenius, 1915). On the other hand, growth rate decreases with further increase in temperature above T_{opt}, which is attributed to the denaturation of essential proteins (Hochachka and Somero, 2002).

The physiological range of temperature at which phytoplankton can survive defines the thermal "window" or thermal tolerance limit of species (Boyd et al., 2013; Chen, 2015). This temperature range is species-specific that reflects the physiological plasticity of species in response to changes in temperature (de Boer et al., 2004). Species that are heat stress sensitive have narrow thermal tolerance limit, whilst those that can survive through acclimation or adaptation have wider range (Chen, 2015).
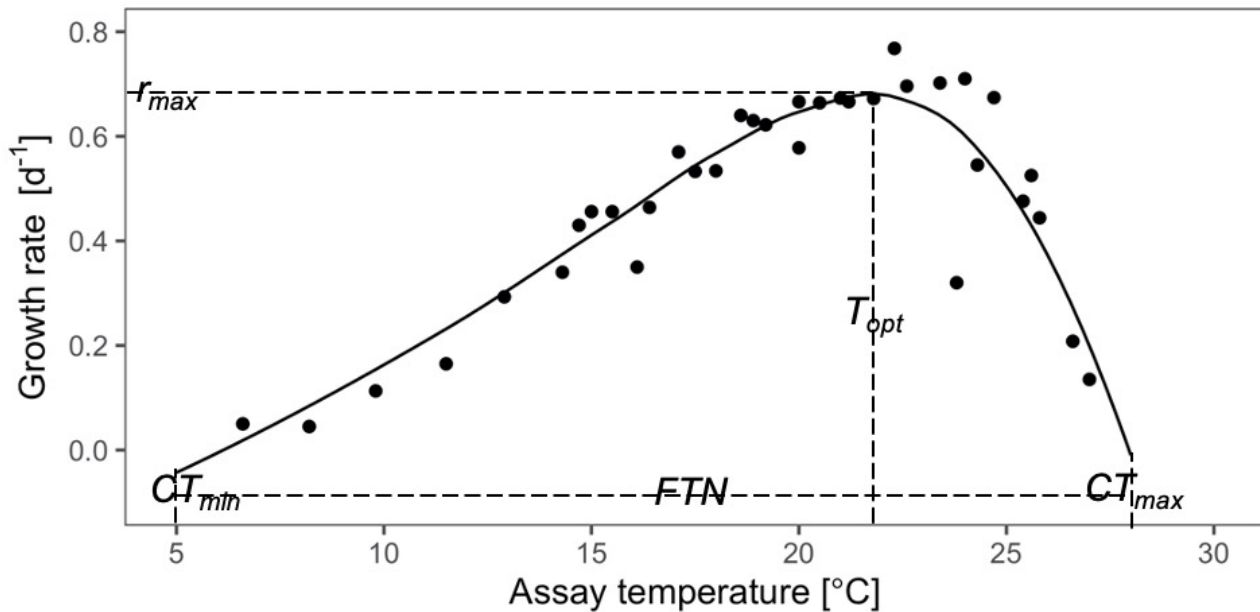
Figure 1.1. A typical thermal growth curve which can be used to estimate the maximum growth rate (r_{max}), the cardinal temperatures i.e. thermal optima (T_{opt}), critical thermal minima (CT_{min}), and critical thermal maximum (CT_{max}), and the fundamental thermal niche breadth (FTN). This figure was drawn using the temperature growth data of *Emiliana huxleyi* available in the R package *temperatureresponse* (Low-Décarie *et al.* 2017).

The fundamental thermal niche of a species is defined by species' physiological tolerance range to temperature in the absence of biotic interactions (Hutchinson, 1957). However, the presence of biotic interactions (Jankowski et al., 2013), species dispersal limitation (Sánchez-Fernández et al., 2016), and limited climate availability (Soberón and Nakamura, 2009) reduce the fundamental niche to realised niche. Most phytoplankton studies are focused on the single-species population responses that reflect the direct physiological response of organism to changing temperature (e.g. Boyd et al., 2013; Coello-Camba and Agustí, 2017; Huertas et al., 2011), but often disregarded the contribution of biotic interaction that may either improve or aggravate a species' response to increased temperature. The effect of temperature on interspecific interactions such as competition is recognised in prior works (e.g. Dunson and Travis, 1991; Park, 1954; Tilman, 1981) and in recent studies (e.g Amarasekare, 2008, 2007; Gilman et al., 2010; Kordas et al., 2011; Tylianakis et al., 2008; Woodward et al., 2010). Temperature influences species interaction, and changes in species interaction may

influence the impacts of climate change on populations (Bellard et al., 2012; Cahill et al., 2013; Tylianakis et al., 2008). Hence, understanding how temperature influences species interaction is critical for predicting how climate change will alter the structure and function of phytoplankton communities in the future oceans.

Metabolic theory of ecology (*MTE*), also known as the metabolic scaling theory (*MST*), attempts to provide mechanistic links between the different levels of organisation in biology and ecology, e.g. from organelles to ecosystems (Brown et al., 2004). Generally, MTE utilises the fundamental roles of size, temperature, and metabolism of organisms in determining various patterns within and across individuals, species, population, community (Brown et al., 2004). Based on this theory, the effect of temperature on competitive interaction is mainly through its influence on the metabolic traits of the organisms (Brown et al., 2004; Van Der Meer, 2006). As a fundamental dimension of the *MTE*, temperature plays a key role in shaping the ecosystem structure and function (Brown et al., 2004; Gillooly, 2001).

However, the complexity of the effect of temperature makes it challenging to develop a mechanistic model to predict responses to climate change. This is because the processes at different biological and ecological levels (i.e. from organism to ecosystem) do not just depend on the direct effects of temperature on physiology, but also on how these direct effects occur in the context of other processes. For example, the species distribution along the environmental temperature reflects interactions of species, not just the direct effects of temperature (e.g. Gross and Price, 2000; Price and Kirkpatrick, 2009). The effect of temperature on interspecific interactions such as competition is recognised in prior works (e.g. Dunson and Travis, 1991; Park, 1954; Tilman, 1981) and in recent studies (e.g Amarasekare, 2008, 2007; Gilman et al., 2010; Kordas et al., 2011; Tylianakis et al., 2008; Woodward et al., 2010). Despite these

efforts, more studies are needed to elucidate the physiological mechanism of interspecific competition in response to temperature.

The thermal performance curves (*TPC*) between two species can be compared to predict the outcome of competition. In a given temperature, patterns of species replacement with the dominance of species with the higher growth rate can be observed along a thermal gradient, which can occur in several ways. One way is when both species are generalists with similar *TPC* but have different thermal optimum (T_{opt}). Another way is when one species is a specialist and the other is a generalist, but both have the same T_{opt}. In both ways, dominance of a species is dependent on local temperature. Species replacement patterns can also occur when the competing species have unequal strengths of density dependence that differ with temperature. In this scenario, a species can be outcompeted by competitor due to its sensitivity to the per capita effects of the competing species in a given temperature, and not because it has low carrying capacity (Reuman et al., 2014).

In the context of toxic species, temperature is one of the most fundamental abiotic factors that may have a direct effect, or an indirect effect if growth and toxin production is uncoupled (Cembella, 1998). Temperature-dependent effect of toxin production is associated with species-specific growth rate, and hence production of toxins is dependent on the thermal tolerance of the species. Hence, the effect of temperature on toxin production has implication on how toxic species may influence the structure and function of marine ecosystems in the future climate scenarios. Supplementary Information 1.1 presents a review that summarises our current knowledge on the evolution and ecology of toxin production by phytoplankton, and provided ecophysiological insights into the expected change in toxic bloom formation with climate change, which brings issues to the debate whether toxin production may

provide a competitive advantage among phytoplankton in the future climate change scenarios.

Concisely, the critical roles of temperature on the physiology, growth, and species interaction of phytoplankton are recognised in numerous studies (e.g. Bestion et al., 2018; Brun et al., 2015; Coello-Camba et al., 2015; Grimaud et al., 2017; Raven and Geider, 1988). Despite these efforts, our knowledge is still limited, particularly on how toxic phytoplankton respond to changes in temperature. Elucidating the thermal response of non-toxic and toxic marine phytoplankton will advance our ability to predict the biogeographic distribution of harmful blooms in the future climate scenarios.

1.4 PREDICTING BIOGEOGRAPHY IN THE FUTURE CLIMATE

In recent years, there have been an impressive growth in use of modeling approaches to predict the biological impacts of climate change (for reviews see Araújo and Guisan, 2006; Austin, 2006, 2002; Guisan and Thuiller, 2005; Guisan and Zimmermann, 2000; Jiménez-Valverde et al., 2008; Morin and Lechowicz, 2008; Peterson, 2006; Rushton et al., 2004). These modeling approaches are empirical or mathematical approximations to ecological niche of a species (Márcia Barbosa et al., 2012), and are often termed as ecological niche models (*ENM*), species distribution models (*SDM*), habitat distribution models (*HDM*), or climate envelope models (*CEM*). These models use the concept of ecological niche to predict the distribution of species in geographic space.

There are several definitions of ecological niche that have been proposed over the years. The earliest definition is by Grinnell (1917) who proposed that a niche is a portion of the habitat that contains the environmental conditions necessary for the

survival and reproduction of individuals of a species. Conversely, Elton (1927) defined a niche with the emphasis of the functional role of species in community, particularly its position in food webs. Grinell's niche concept is based on the broad-scale variables such as the climate that are not affected by the density of species, whereas Elton's niche concept is based on fine-scale variables such as the nutrients that a species can consume or modify (Soberón, 2007). Hence, these two niche concepts associated the term niche with the environmental space for species to occupy. Contrary to this, Hutchinson (1957) defined the niche as an innate property of a species not of the environment. The Huchinson's concept of fundamental and realised niches is widely used in the modeling to predict the geographic distributions in the changing climate. The fundamental niche represents the abiotic factors (i.e. one dimension for each variable) that regulate the success of a species (Wiens and Graham, 2005).

In practice, a limited number of factors is used to define the niches, and among the abiotic factors, temperature have played a critical role in characterising the fundamental niches of species (Lima et al., 2007; Thomas et al., 2012; Walther et al., 2002). The fundamental niche of a species is reduced into realised niche when a species does not occupy the entirety of the fundamental niche due to niche exclusion by competition (Hutchinson, 1957). The concept of realised niche is replaced by Jackson and Overpeck (2000) who introduced potential niche, which is the intersection between available environmental space and the fundamental niche space. Some part of the fundamental niche space may lie outside the environmental space at a given time. Hence, the realised niche is a subset of the potential niche. Three different niches, i.e. fundamental niche, potential niche, and realised niche, have been adapted in several studies (e.g. Colwell and Rangel, 2009; Soberón and Nakamura, 2009).

Another theory is the occupied niche concept that postulates that the species distribution are constrained by geographical and historical factors, as wells as biotic interactions, such as competition, predation, symbiosis and parasitism (Pearson, 2007). Unlike the realised niche as defined by Hutchinson (1957) was only limited by species competition, not by other factors such as dispersal limitations. Therefore, it is expected that the occupied niche is smaller than the realised niche. Another important concepts to consider are the source-sink theory and the dispersal limitation. In a source-sink theory, some populations may occupy unsuitable habitats (sinks) because of the immigration from healthier nearby populations (sources), and individuals in the sinks may die by unfavorable environmental conditions and are replaced by new immigrants (Pulliam, 2000). Here, the realised niche is larger than the fundamental niche when species occupies habitats that are inadequate and not contained in the fundamental niche (Pulliam, 2000). On the other hand, a species may not occupy suitable habitats due to historical reason and dispersal limitations (Holt, 2003).

The effect of climate change on species can be examined by modeling the ecological niche and then projecting the model into the future to determine any changes on the location of the niche. Mechanistic and correlative *ENM* have been used to model the ecological niche (Pearson and Dawson, 2003).

Mechanistic *ENM* is based on mathematical description that relate the environmental tolerance of a species to its population dynamics. These models are calculated with physiological data, and are used to establish a causal relationship among the species distribution and the variables, independently of the species records (Kearney, 2006; Kearney and Porter, 2009, 2004). Hence, the fundamental niche can be derived from mechanistic models. Mechanistic models provide an explicit approach to predict geographic distribution of species with assumptions that can be modified to

integrate further biological detail, such as biotic interactions, dispersal limitations, and evolutionary adaptation. However, extensive knowledge of the biology of the species (e.g. the behavior, physiology, and life history) is required to implement these models (Angilletta, 2009). On the other hand, correlative *ENM* links present geographic distribution of a species to its local environmental conditions to determine its niche and can be used to predict a biogeographic shift during climate change (Elith et al., 2006; Hijmans and Graham, 2006).

Correlative *ENM* provide convenient approach to predict global biogeography since these models only need environmental data that are related to the occurrence locations of species (Graham et al., 2004; Guisan and Thuiller, 2005), and to a certain extent, these models can also deal with geographic variation (Murphy and Lovett-Doust, 2007) and species interactions such as competition and predation (Araújo and Luoto, 2007; Sutherst et al., 2007) (Araujo and Luoto, 2007; Sutherst et al. 2007). However, dispersal and evolutionary responses are not accounted in the correlative models (Pearson and Dawson, 2003). Correlative *ENM* are calculated with species distribution records, and depending on the type of species' records, each model is a different representation of the realised niche. Correlative models using pseudo-absences or absences and presence records forecast the probability of finding the species in a particular place, whereas correlative models using only presence records forecast the suitability of a particular habitat for the species .

Ecological niche modeling has been used in recent phytoplankton studies. Thomas et al. (2012) used a mechanistic *ENM* to investigate how warming leads to poleward shifts in species' thermal niches and cause the decline of phytoplankton diversity in the absence of an evolutionary response. Also, Irwin et al. (2012) compiled occurrence data for 119 phytoplankton species obtained from plankton recorder with

climatological environmental variables in the North Atlantic to obtain ecological response functions of each species using correlative *ENM*. Brun et al. (2015) characterised the realised niche of 133 open ocean phytoplankton taxa species using correlative *ENM* with observations from the MAREDAT initiative. Furthermore, Ajani et al. (2018) obtained long-term phytoplankton community composition and environmental data from a Pacific Ocean coastal station offshore from Sydney, Australia, and used correlative *ENM* to examine whether the realised niches of phytoplankton are fixed or shift in response to changing environmental conditions. More recently, Righetti et al. (2019) investigated the monthly phytoplankton species richness by using correlative *ENM* and global phytoplankton observations to predict global biogeographic patterns of 536 species of phytoplankton. All these studies have demonstrated the usefulness of ecological niche modeling as valuable tool to improve our understanding on how phytoplankton will respond to the expected changes in the climate.

1.5 THESIS STRUCTURE

Given the introductions above, the main aim of this thesis is to investigate how temperature limits biogeography, growth, toxin production, and competition in marine phytoplankton. To achieve this aim, the thesis presents a series of chapters with independent objectives, which is structured as follows:

- Chapter 2 presents the analysis of species occurrence records to investigate the thermal limits to the current biogeographic distribution of marine phytoplankton. Here, I examined whether the patterns in the biogeography of marine phytoplankton follow classical macroecological theories (e.g. Janzen's Rule, Rapoport's rule, and niche breadth–range size hypothesis). Also, I tested if the observed patterns can be explained by environmental temperature, habitat availability, phytoplankton diversity, and the seasonal variability of these factors.

- Chapter 3 presents the global pattern of thermal biology in marine phytoplankton using the thermal traits derived from the published laboratory results and from sea surface temperature of the species' occurrence. In this chapter, I determined the congruence and inequality between physiology- and occurrence-based thermal traits. I also evaluated the variation in the inequality between physiology- and occurrence-based thermal traits, thermal sensitivity, exposure and vulnerability to warming across the gradient of latitude, thermal affinity, and thermal specialisation. Furthermore, I assessed the phylogenetic effect on these thermal attributes in marine phytoplankton.

- Chapter 4 reports the findings of the laboratory experiments that test the temperature dependence of the growth in marine phytoplankton. Here, I determined whether non-toxic and potentially toxic marine phytoplankton exhibit variation in (i) temperature dependence of growth, (ii) maximum growth rates and thermal traits,

(iii) relationship between maximum growth rates and thermal traits, (iv) trait-environment relationship, and (v) thermal safety and vulnerability.

- Chapter 5 reports the results of the laboratory experiments that examine the temperature dependence of toxin production in marine phytoplankton. Here, I examined the temperature dependence of the concentration, cellular content, relative composition, and cellular production rate of toxins and their relationship with growth in a toxic model organism.

- Chapter 6 reports the results of laboratory experiment that examine the effect of warming on growth and competition in phytoplankton using marine dinoflagellates as model organisms. In this chapter, I evaluated the growth responses of species to warming in the absence and presence of competitors. I also tested whether the growth and competitive responses to different temperature treatments are dependent or not on the taxonomic identity and toxicity of focal and competitor species. Moreover, I assessed the relationship between growth rates and competition coefficients across the different temperature treatments.

- Chapter 7 provides a general discussion of this thesis. In this final chapter, I synthesised the key findings of the research and discussed their implications to the global change ecology of marine phytoplankton. I also discussed the future work that come to light from the thesis.

This page is intentionally left blank.

22

This page is intentionally left blank.

CHAPTER 2

This page is intentionally left blank.

24

This page is intentionally left blank.

24

THERMAL LIMITS TO THE BIOGEOGRAPHY OF MARINE PHYTOPLANKTON IN THE CONTEMPORARY OCEAN

ABSTRACT

Temperature plays a critical role in shaping the geographic distribution of marine phytoplankton. Current theories suggest that species that experience greater climate variability will be adapted to a wider thermal range than those species thriving in a stable thermal condition. It remains unclear whether the biogeographical patterns of marine phytoplankton conform to these theories. Here, we analysed the global dataset of species occurrence data to investigate the latitudinal patterns in the realised thermal niche and geographic range of marine phytoplankton. Our findings show complex patterns in the biogeography of marine phytoplankton that do not strictly conform to the classical macroecological theories. We found (1) non-monotonous latitudinal trend in niche breadth, (2) narrower niche in the tropics, (3) unclear latitudinal variation in geographic range, and (4) weak positive relationship between thermal niche and geographic range. These complex patterns are driven by temperature, climate variability, habitat availability, and diversity. Our findings support our current expectation that highly diverse phytoplankton communities in the tropics may be the most at threat from ocean warming.

2.1 INTRODUCTION

The biogeographic distribution of organisms is regulated in part by climatic conditions. Among the climate variables, temperature plays one of the most fundamental roles in limiting the biogeography of organisms from polar to tropical oceans (Stuart-Smith et al., 2017, 2015; Tittensor et al., 2010). The range of temperatures at which organisms can survive defines the thermal 'window' or thermal niche (Boyd et al., 2013; Chen, 2015), the width of which reflects the physiological plasticity to temperature of a given organism (de Boer et al., 2004). Species that are temperature sensitive have narrow thermal tolerance ranges, whilst those that can survive through acclimation or adaptation have wider ranges (Chen, 2015). Understanding the mechanisms by which thermal niche influence the distribution of species will improve our ability to predict their ecological and evolutionary responses to changes in temperatures under ongoing global climate change.

Theories linking niche breadth with latitude are well established. One remarkably prominent idea is that niches become narrower toward the tropics. Janzen's Rule suggests that reduced seasonal thermal variation selects for narrower thermal tolerance (Janzen, 1967). It is expected that tropical species living in a stable thermal condition will be adapted to a narrower thermal range than the temperate species that experience greater seasonal temperature extremes (Sunday et al., 2011). This pattern has been demonstrated in several studies on terrestrial and marine species (Deutsch et al., 2008; Stuart-Smith et al., 2017; Sunday et al., 2011). Following the premise of lower variability in the tropics, the geographic extent of species ranges is expected to decrease at lower latitude as postulated in Rapoport's rule (Stevens, 1989). Furthermore, species in the temperate regions are expected to become more

widespread as they can utilise resources (e.g. light and nutrients) within a wider thermal condition as posited in the niche breadth–range size hypothesis (Slatyer et al., 2013). The patterns predicted by the Rapoport's rule and the niche breadth–range size hypothesis are confounded by the effect of latitudinal gradients in habitat (temperature) availability and the effect of seasonality (Tomašových et al., 2016). The concept that narrower niches in the tropics serve as a premise to several hypotheses that explain the latitudinal trends in species richness (Willig et al., 2003; Willig and Presley, 2018). Alternatively, species richness has been proposed to indirectly affect the latitudinal changes in niche breadth (Vázquez and Stevens, 2004).

Here, we tested whether marine phytoplankton conforms with classical macroecological pattern and whether these patterns can be explained by temperature, habitat availability, diversity, and their seasonal variability. The effect of temperature on phytoplankton has been well studied (Barton et al., 2018; Boyd et al., 2013; Righetti et al., 2019; Thomas et al., 2012; Wang et al., 2018), however, the relationship of niche breadth and geographic range to latitude and temperature is still unclear in marine phytoplankton. Our current understanding of the global patterns in thermal tolerance of phytoplankton has been predominantly inferred from compiling the results of laboratory experiments that quantify the effect of temperature on growth (Chen, 2015; Thomas et al., 2012). In these studies, the relationship between the fitness of phytoplankton and temperature are expressed using thermal performance curves (*TPC*). However, inference from *TPC* is influenced by model choice and data quality (Low-Décarie et al., 2017). Most phytoplankton studies have largely focused on thermal optima that have been shown to decrease with increasing latitude (Chen, 2015; Thomas et al., 2012). However, no clear latitudinal pattern has been observed for the thermal niche breadth in phytoplankton based on the experimental results (Chen, 2015; Thomas et al., 2012). It

remains unknown whether phytoplankton will have the same pattern using a global dataset of species occurrences as demonstrated in several studies on other ectotherms such as macro-invertebrates and fishes (Deutsch et al., 2008; Stuart-Smith et al., 2017).

In this study, we analyse species occurrence records to investigate the thermal limits to biogeographic distribution of marine phytoplankton. We examine whether the patterns in the biogeography of marine phytoplankton would follow the classical macroecological theories. Also, we test if the observed patterns can be explained by temperature, habitat availability, diversity, and their seasonal variability. We hypothesise that species thriving in thermally stable and warmer oceans would have narrower thermal and geographical ranges than the temperate species that experience higher seasonal temperature extremes. We discuss our results in light of their congruency with the existing theories and highlight possible mechanisms that could explain the observed biogeographical patterns in marine phytoplankton.

2.2 MATERIALS AND METHOD

2.2.1 Occurrence data collection and processing

Occurrence records of phytoplankton species from major taxonomic groups were downloaded from Ocean Biogeographic Information System (*OBIS*) (GBIF.org, 2018) and Global Biodiversity Information Facility (*GBIF*) (OBIS, 2018). Additional occurrence records of coccolithophores (O'Brien et al., 2013), diatoms (Leblanc et al., 2012), and *Phaeocystis* spp. (Vogt et al., 2012) were collected from the Marine Ecosystem Data (*MAREDAT*) initiative (Buitenhuis et al., 2013). Also, supplementary records of phytoplankton in the tropical and subtropical regions were obtained from Estrada *et al*. (Estrada et al., 2016).

The data were compiled and curated to only include records with complete spatial and temporal information (i.e. Global Positioning System (*GPS*) coordinates and year of the collection), records reported from 2000 to 2014, and records of phytoplankton identified at the species level. Species names in the original data were validated against the reference list in *GBIF* Backbone Taxonomy (GBIF Secretariat, 2019). The species names were subsequently curated to merge spelling variants and synonymous names and to exclude records that could not be traced on the checklist dataset. This resulted in occurrence dataset with 771,286 observations representing 1,681 species recorded from 89°N to 78°S between 2000 and 2014 (Figure 2.1; Supplementary Figure 2.1). These observations were spatially biased, with the majority of the observations originating from temperate coastal regions in the northern hemisphere (Supplementary Table 2.1).
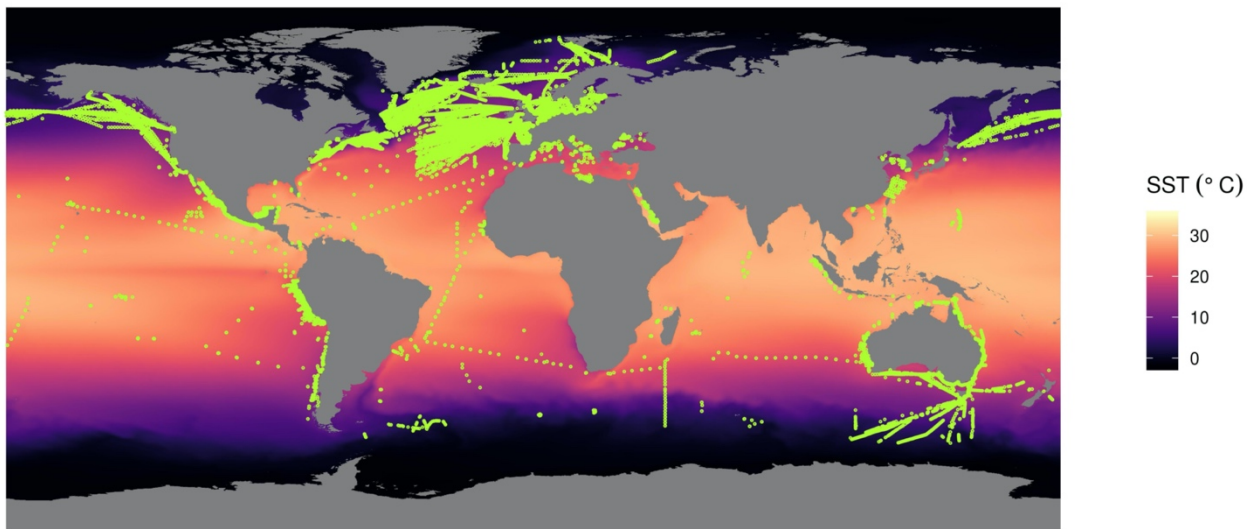
Figure 2.1. Geographic locations of the occurrence records of phytoplankton species retrieved from the four data sources used in this study. The curated dataset is comprised of 62,597 observations from 1,062 geographic variants of phytoplankton representing 331 species from 13 taxonomic classes across 43 regions recorded between 2000 and 2014, which were retrieved from OBIS, GBIF, MAREDAT, and Estrada et. al. (2016). The colour gradient indicates the long-term annual average SST data at 5 arcmin between 2000 and 2014 retrieved from BioORACLE.

To minimise the effects of spatial bias, the occurrence dataset was further curated to exclude duplicates and records verified being on land. Furthermore, the data

were spatially filtered to ensure that no two records were within 10 km of one another.

Spatial filtering can reduce the effect of sampling bias and commonly used to improve

the performance of ecological niche model (Boria et al., 2014). Subsequently, the

records were clustered into regions based on the Longhurst's division of the world's

oceans (Flanders Marine Institute, 2009; Longhurst, 2007). The dataset was screened

to exclude species that has less than 10 records in a region, and the total number of

regional records for species ranged from 10 to 2,456. The final dataset contained

62,597 observations from 1,062 geographic variants of phytoplankton representing 331

species from 13 taxonomic classes across 43 regions (Supplementary Figure 2.2).

2.2.2 Sea surface temperature data collection and processing

Global sea surface temperature (*SST*, °C) data at 5 arcmin (*c.* 0.08° or 9.2 km

at the equator) between 2000 and 2014 were downloaded from *Bio-ORACLE* (Ocean

Rasters for Analysis of Climate and Environment) (Assis et al., 2018). Specifically,

long-term average annual *SST* and seasonal *SST* extremes, i.e. the average

temperature of the warmest and coolest months (Supplementary Figure 2.3) were

downloaded to examine spatial variability of surface water temperature and to examine

the contemporary thermal conditions experienced by marine phytoplankton. These data

were matched with the georeferenced species occurrence data and were used in the

subsequent thermal biogeographic analysis.

2.2.3 Estimation of thermal niche and geographic range

Thermal traits were calculated in two ways following by Stuart-Smith *et al*.

(Stuart-Smith et al., 2017): (i) the 5th and 95th percentiles of long-term average annual

SST (across all locations for which species occurrence was recorded) were determined

to represent the lower and upper thermal limits, respectively (*LTL* and *UTL*, respectively) and to provide a measure of realised thermal breadth (*RTN*; i.e. the average temperature range experienced by a species across its geographic range); (ii) the 5th percentile of the long-term minimum *SST* and the 95th percentile of the long-term maximum *SST* (across all locations for which species occurrence was recorded) were used to represent the extreme thermal limits (*LTL** and *UTL**, respectively) and to estimate realised extreme thermal breadth (*RTN**; i.e. niche that covered the thermal extremes experienced by species throughout its geographic range). The thermal midpoints (*TM* and *TM**) between the 5th and 95th percentiles of the thermal distribution occupied by a species was used to estimate the central tendency of the realised thermal distribution of the species and was considered a proxy for optimal temperature for the ecological success of the species (Stuart-Smith et al., 2015). This approach has the advantage of avoiding the previously mentioned challenges of model choice and the influence of data quality arising from models of *TPC* (Low-Décarie et al., 2017). Geographic range size (*GR*, km^2) was calculated as the area of a polygon in angular coordinates on an ellipsoid (Karney, 2013).

To account for uncertainty arising from the error in the estimate of thermal traits, bootstrapping technique was used to determine the standard error of thermal limits, thermal midpoint, thermal niche breadth, geographic range size and the latitudinal midpoint of each geographic variants of phytoplankton species. In this, re-sampling with replacement was conducted on the sample for 10,000 times and the estimates were made from every bootstrap re-sample. The bootstrap estimate of bias (i.e. difference between the estimate calculated using the original sample and the mean of the bootstrap estimate), the standard error of estimate (i.e. standard deviation of the bootstrapped estimates), and the confidence interval (i.e. the lower and upper limits of

95% confidence interval) were determined (Supplementary Figure 2.4). The bias-corrected estimates (i.e. the difference between the original sample estimate and the bootstrap estimate of bias) were used in the succeeding regression analysis, the estimates in geographic range size of which the bias correction was too strong producing estimates below zero (30% of the dataset).

2.2.4 Analysis of trends in thermal limits, niche breadth, and range size

Relationships between variables were initially examined using generalised linear mixed-effects model (*GLMM*) (Bolker et al., 2009). Latitude and temperature were used as fixed predictors for thermal limits, thermal niche breadth and geographic range size in marine phytoplankton. Thermal limits and niche breadth were also considered as a predictor for geographic range size to examine their postulated relationship in marine phytoplankton. The random effects of ocean regions and taxonomic class were included in the mixed models to account for the possible and biogeographic structure and phylogenetically-conserved effects. All models were conducted separately for the average annual and seasonal extreme *SST* to account for the effect of average and extreme thermal conditions experienced by species across their geographic range, weighted by the number of unique locations.

To assess the non-linearity of the relationship between variables, both the linear and quadratic terms were included in the *GLMM*. Likelihood ratio (*LR*) test was used to determine the significance of a single factor by comparing the fit for models with and without the factor. Akaike information criterion (*AIC*) was used to determine whether a full model with linear and quadratic terms would describe the relationship better than a reduced model. Coefficient of determination for each model was estimated to describe the proportion of variance explained by the fixed factor alone (i.e. mariginal R^2) and by

both the fixed and random factors (i.e. conditional R^2) following Nakagawa and

Schielzeth (Nakagawa and Schielzeth, 2013). In addition to *GLMM*, generalised additive

mixed model (*GAMM*) (Pedersen et al., 2019) with cubic regression splines was used to

gain more insight into any non-linear responses that may exist. In this function, the

smooth is treated as a fixed effect, whilst the wiggly components of the smooth are

treated as random effects. *GAMM* and *GLMM* were used to ensure higher confidence in

the interpretation of the relationships. Regression diagnostics were used to evaluate the

residuals of the models and to examine whether or not there are observations with a

large, undue influence on the analysis (Supplementary Figure 2.5). Using this graphical

method, we found that the residuals of the models predicting geographic ranges

deviated from normality, and hence we log$_{10}$-transformed the estimates to improve the

linearity of the residuals.

In summary, 21 models were fitted in *GLMM* with the linear term only, in *GLMM*

with linear and quadratic terms, and in *GAMM*. The model fits are visualised in

Supplementary Figure 2.6 – 2.9 and are summarised in Supplementary Table 2.2 – 2.3

(*GLMM*) and in Supplementary Table 2.4 – 2.5 (*GAMM*). Generally, the *GAMM* models

had a better fit than *GLMM* models, and hence results of the *GAMM* were preferably

reported in the text.

2.2.5 Estimation of climate variability, habitat availability, and diversity

Additionally, the three environmental factors were estimated to be used as

explanatory variables in the subsequent analysis. Climate variability (*CV*) is defined

here as the long-term mean environmental temperature range (2000-2014). This was

estimated from the difference between the average *SST* of the warmest and coolest

months (maximum and minimum *SST*, hereinafter). The *SST* data were obtained from

Bio-ORACLE as mentioned above and extracted from the raster at 1° resolution. For

every 1° latitudinal band, the minimum *SST* was subtracted from the maximum value to

estimate the temperature range and was summarised to obtain the mean range, which

is referred hereinafter as climate variability (°C). Habitat availability (*HA)* is the total

number of thermally suitable habitats (i.e. cells or pixels at 0.08° resolution) available for

species to occupy. For every 1° latitudinal band, all cells within the band that had *SST*

values (based on long-term average annual *SST*) within the species' extreme thermal

range (i.e. *RTN**) was counted, and the resulting habitat availability statistic is

expressed in # cells per latitudinal degree. Diversity (*D*) is referred to here as the

species richness. For every 1° latitudinal band, the total number of unique species

within the latitudinal coverage of its thermal range was counted, and the resulting

diversity statistic is expressed in # species per latitudinal degree. Estimates of the

variability in habitat availability and diversity were computed as the square root of the

squared difference between the values derived from the maximum and minimum *SST*.

These variability estimates represent the seasonality of these variables.

2.2.6 Analysis of latitudinal trends in environmental variables

Sea surface temperature, habitat availability, diversity, and their seasonal

variability were fitted against latitude using generalised additive models (*GAM*).

Gaussian distribution was used for *GAM* fitting *SST* and climate variability with latitude.

Whereas, a Poisson distribution was used for *GAM* fitting habitat availability, diversity,

and their seasonal variability with latitude. The residuals of the *GAM* models were

evaluated as described above, and all models passed the regression diagnostics. All

GAM models are summarised in Supplementary Table 2.6.

2.2.7 Assessment of the effect of environmental variables on niche breadth and range size

The effects of *SST*, habitat availability, diversity, and their seasonal variability on the thermal niche breadth and geographic range size were determined. Extreme thermal niche breadth (i.e. *RTN**) and geographic range size were binned at 1° latitudinal resolution to obtain the mean estimates for every latitude, which were then merged with the environmental data. Before model fitting, collinearity and relative importance of the variables were assessed as the basis for variable selection. Pearson correlation was implemented to assess the collinearity between environmental variables. The result of this analysis is summarised in Supplementary Figure 2.10. To assess the relative importance of the environmental variables, niche breadth and range size were fitted against the environmental variables in random forest regression models with 500 number of tress and with two variables tried at each split. The variable importance measures produced by the random forest model were extracted. Partial response plots for each environmental variable are available in Supplementary Figure 2.11 for niche breadth and in Supplementary Figure 2.12 for geographic range size.

Generalised linear models (*GLM*) was used to fit niche breadth and range size against SST, habitat availability, diversity, and their seasonal variability. The variables were added sequentially in the nested models based on their relative importance as determined previously. Significance of a factor added in a nested model was assessed using likelihood ratio test (*LRT*) by comparing the fit for models with and without the factor. Interaction between significant terms was also tested for their significance in the model. *AIC* was used for model selection. Results of this analysis are accessible in Supplementary Table 2.7. Summary statistics of the *GLM* models are available in Supplementary Table 2.8.

2.2.8 Data processing and analysis software

Data processing and analyses were implemented in *R* version 3.5.1 (R Core Team, 2019) using packages listed in the supplementary information 2.1.

2.3 RESULTS

2.3.1 Trends in thermal limits, niche breadth, and rang size

Marine phytoplankton displayed a complex latitudinal patterns in thermal limits and niche breadth (Figure 2.2 A and B, respectively; Supplementary Figure 2.6; Supplementary Table 2.2 and 2.3 *GLMM* 01 – 06; Supplementary Table 2.4 and 2.5 *GAMM* 01 – 06). Thermal limits decreased with latitude, and the relationship was nonlinear (Figure 2.2 A). Lower thermal limit (*LTL*; *GAMM* 01) gradually declined from the equator to ~40° and it decreased steeply towards the pole. Whilst the upper thermal limit (*UTL*; *GAMM* 02) remained constant from the equator to ~23°. *UTL* declined steeply to ~50°C and then slowed down towards the pole. This asymmetry between the latitudinal change of *LTL* and *UTL* was matched with non-monotonous relationship between the latitude and realised thermal niche (*RTN*; *GAMM* 03). This asymmetry coincided to the narrowing of *RTN* in the tropics. *RTN* peaked at ~23° and declined towards the equator and towards ~40°. It remained constant between ~40° – 50° and begun to widen towards the pole. This asymmetry was more pronounced when seasonality in the *LTL** (*GAMM* 04) and *UTL** (*GAMM* 05) was taken into account, making *RTN** (*GAMM* 06) higher than the average annual estimates in niche breadth. *RTN** had declined from the pole to ~38°, and peaked at ~25°. Generally, *RTN** in the tropics are narrower than the estimates in temperate regions. Latitude explained $\geq 60\%$

(adjusted R^2 : 0.60 – 0.78) of the variation in the thermal limits but it insignificantly explained the variation in niche breadth.

Our results showed opposite monotonous patterns of thermal limits across the temperature gradient, leading to non-monotonous behavior of niche breadth (Figure 2.2 C and D, respectively; Supplementary Figure 2.7; Supplementary Table 2.2 and 2.3 *GLMM* 07 – 12; Supplementary Table 2.4 and 2.5 *GAMM* 07 – 12). Temperature explained > 80% (adjusted R^2 : 0.83 – 0.91) of the variation the thermal limits higher (>1.25 times) than the explained variance by latitude. On the other hand, temperature alone failed to explain the variation in niche breadth similar to the effect of latitude.

There was no clear evidence that geographic range (*GR*) in marine phytoplankton changes with latitude nor with temperature (Supplementary Figure 2.8; Supplementary Table 2.2 and 2.3 *GLMM* 13 – 15; Supplementary Table 2.4 and 2.5 *GAMM* 13 – 15). Furthermore, *GR* had no clear relationship with thermal limits, but had a positive relationship with thermal niche breadth (Supplementary Figure 2.9; Supplementary Table 2.2 and 2.3 *GAMM* 16 – 21; Supplementary Table 2.4 and 2.5 *GAMM* 16 – 21). However, the niche breadth–range size relationship was weak (adjusted R^2 : 0.05 – 0.14).
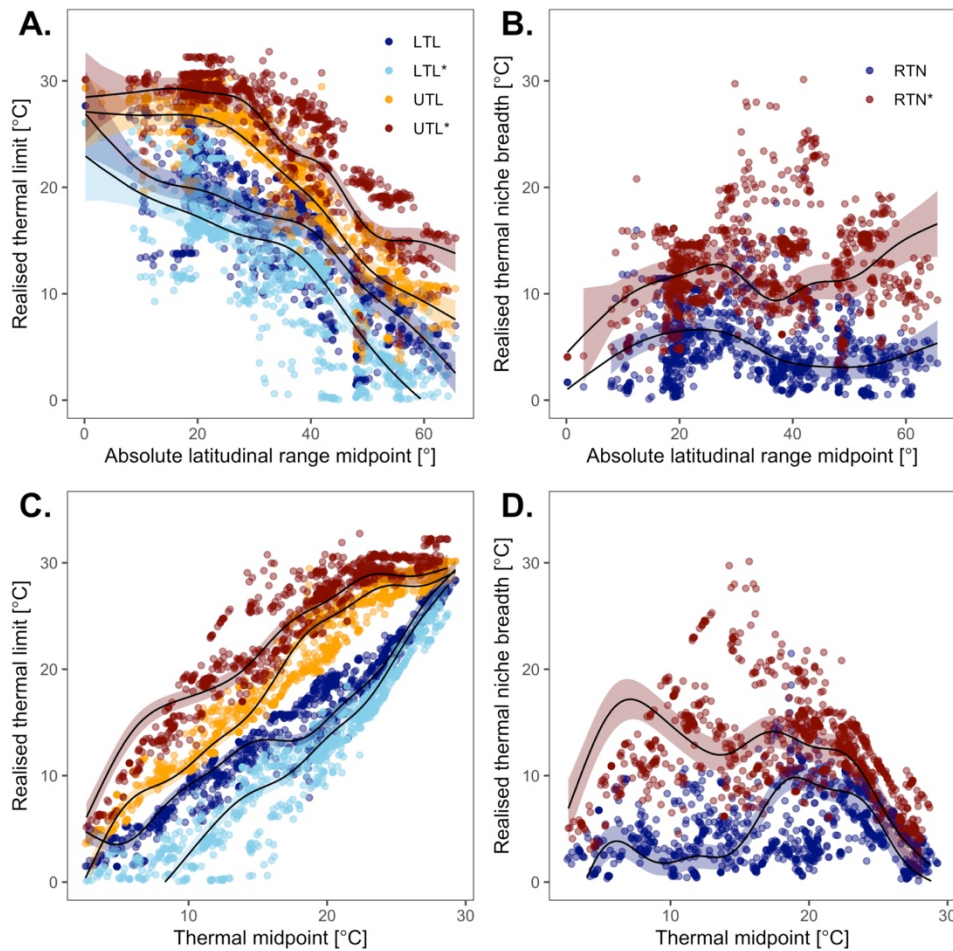
Figure 2.2. Trends in the realised thermal limits and niche breadth of marine phytoplankton across the gradient of latitude and temperature. The thermal limits decrease with increasing latitude (A) and increase with increasing temperature (C). The monotonous asymmetrical behaviour of the lower and upper thermal limits (*LTL* and *UTL*, respectively) leads to the non-monotonous pattern in the niche breadth (*RTN*) across the latitudinal and temperature gradient (B and D, respectively). These findings reveal a narrower niche in tropics, consistent to Janzen's rule. Thermal limits and niche breadths are derived from the average annual sea surface temperature (*SST*) and seasonal extremes *SST* (i.e. *LTL**, *UTL**, and *RTN**). The asymmetry between the limits is more pronounced when seasonality in *SST* is taken into account, suggesting the influence of climate variability on the niche breadth in marine phytoplankton. The solid lines are fit from the generalised additive mixed model with cubic regression splines (*GAMM*) with 95% confidence intervals as error of the regression.

2.3.2 Trends in climate variability, habitat availability, and diversity

Our results showed evident latitudinal trends in sea surface temperature (*SST*), habitat availability, diversity, and their seasonal variability (Figure 2.3; Supplementary Table 2.6). All variables, except for *SST*, showed a clear non monotonously behaviour along the latitudinal gradient.

38

SST reached its peak near the equator and gradually decreased poleward (Figure 2.3 A). However, climate variability (*CV*) dipped near the equator, peaked at mid latitudes, and then declined towards the pole (Figure 2.3 B). Clearly, *SST* was more variable in mid latitudes than in tropical and polar regions. Also, climate of the temperate regions in the northern hemisphere had more variability than in the southern hemisphere. Nearly all of the variation in the mean *SST* and *CV* was explained by latitude (Supplementary Table 2.6 *GAM* 1 – 2; adjusted R^2: 0.99 and 0.96, respectively).

Furthermore, mean habitat availability (*HA*) was low near the equator and reached its peak at ~35° in southern hemisphere and at ~20° in northern hemisphere (Figure 2.3 C). There are more thermally suitable habitats available in the southern hemisphere than in the northern hemisphere. More than 75% of the variation in *HA* was explained by latitude (Supplementary Table 2.6 *GAM* 3; adjusted R^2: 0.76). On the other hand, seasonal change in habitat availability (*HAV*) showed a complex pattern (Figure 2.3 D), and only about a third of its variation was explained by latitude (Supplementary Table 2.6 *GAM* 4; adjusted R^2: 0.31).

Bimodality with a dip in the diversity near the equator was observed (Figure 2.3 E). Diversity reached its highest peak at ~23°, showing greater tropical diversity in northern hemisphere than in the southern hemisphere. Diversity eventually declined from the peak towards the polar regions. Latitude explained 88% of the variation in the diversity (Supplementary Table 2.6 *GAM* 5; adjusted R^2: 0.88). Moreover, variability in the diversity (*DV*) was high across the tropics (Figure 2.3 E). It dipped in the mid latitudes and peaked at ~45°, higher than the observed peak in southern hemisphere. However, only 29% of the variation in *DV* was accounted by the latitude (Supplementary Table 2.6 *GAM* 6; adjusted R^2: 0.29).
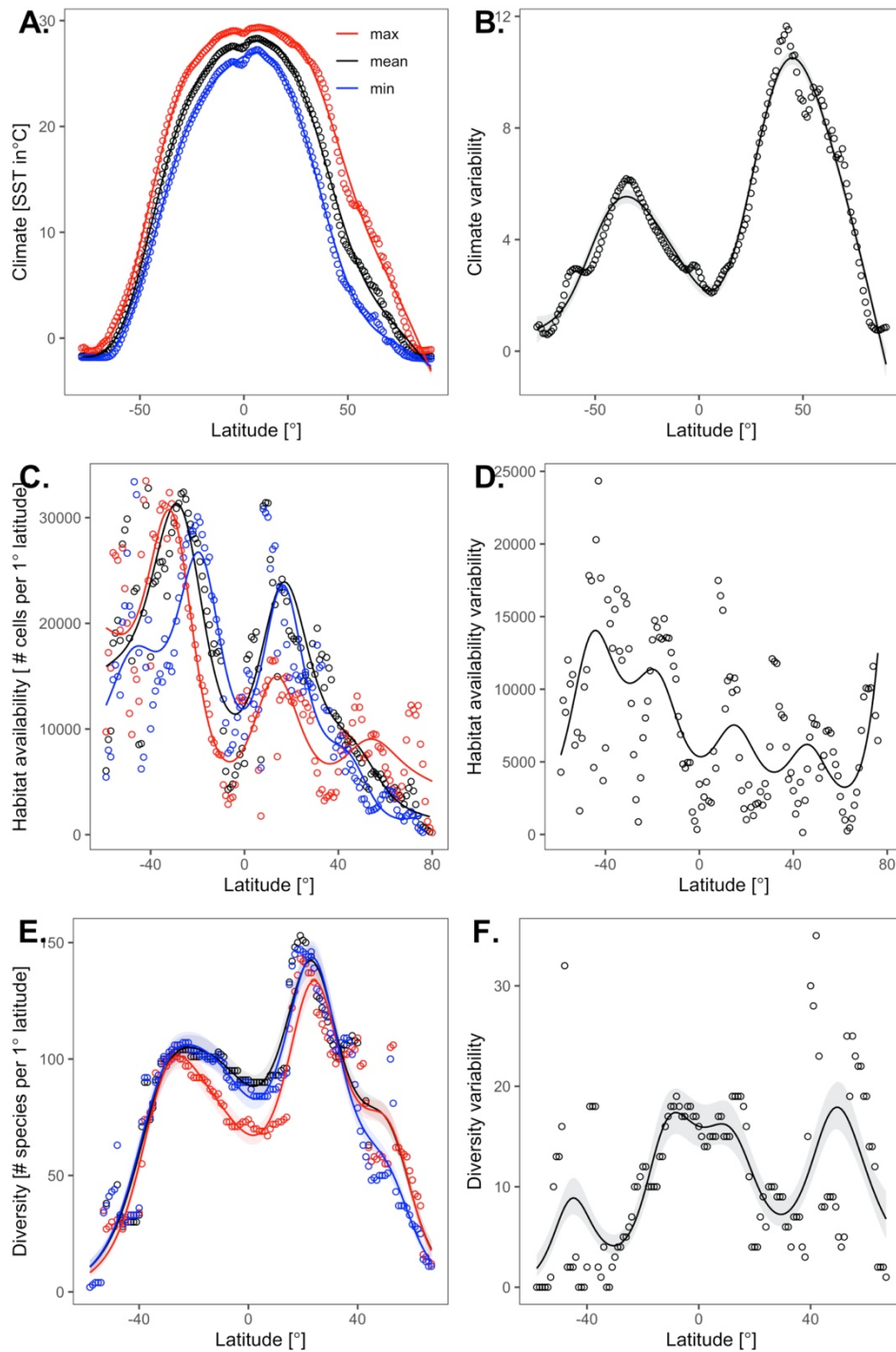
Figure 2.3. Latitudinal trend in mean, minimum, and maximum sea surface temperature (*SST*), habitat availability and diversity (left panel) and their seasonal variability (right panel). Except for *SST*, all variables have non-monotonous relationship with latitude. The solid lines are fit from the generalised additive model with cubic regression splines (*GAM*) with 95% confidence intervals as error of the regression.

2.3.3 Correlation and relative importance of environmental variables

Generally, results of the Pearson correlation indicated that there was a

significant association between the environmental variables (Supplementary Figure

2.10). *SST* had a negative association with *CV*, whilst it had positive associations with *HA* and *DV*. On the other hand, *CV* was negatively associated with *HA* and *HAV*. Moreover, *HA* was positively associated with *HAV* and *D*, but negatively associated with *DV*.

Random forest regression analyses revealed the relative importance of environmental variables as explanatory factors for thermal niche breadth (*RTN**) and geographic range size (*GR*) in marine phytoplankton (Supplementary Figure 2.13). Results showed that *CV* and *SST* are the most important explanatory variables for *RTN**. Whereas, *D* and *HA* are relatively more important than *CV* and *SST* in predicting the *GR*.

2.3.4 Significant effect of environmental variables on niche breadth and range size

The generalised linear regression models revealed the degree of significance of the effect of environmental variables on thermal niche breadth (*RTN**) and geographic range size (*GR*) in marine phytoplankton (Supplementary Table 2.7). The additive model with *CV* and *SST* as explanatory variables for *RTN** (*GLM* 2) described the relationship better than the other models (*GLM* 1 and *GLM* 3 – 7). The main effects of *CV* and *SST* on the *RTN** were significant (*GLM* 2), but the interaction between these terms was not significant (*GLM* 7). *RTN** was observed to be directly proportional to *CV* and *SST* (Supplementary Table 2.8 *GLM* 2). On the other hand, *GR* was best explained by the additive model with *D* and *HA* as predictors (*GLM* 9) in comparison to other models (*GLM* 8 and *GLM* 10 – 14). There was significant effects of *D* and *HA* on *GR* (*GLM* 9) but their interaction was not significant (*GLM* 14). *GR* decreased with increasing *D*, and it increased with increasing *HA* (Supplementary Table 2.8 *GLM* 9).

2.4 DISCUSSION

Our analysis of the species occurrence data provides new insights of the biogeographical patterns of marine phytoplankton in the contemporary ocean. We discuss our findings in light of the conformity or non-conformity with the existing hypotheses and deliberate the possible mechanisms that explain the observed trends.

2.4.1 Narrower niches in the tropics

Our results reveal non-linearity of the latitudinal trend in thermal niche breadth of marine phytoplankton. This trend can be attributed to the latitudinal variation in the difference between the minimum and maximum average annual *SST* or in the difference between the seasonal temperature extremes (i.e. average *SST* of the warmest and coolest months) experienced by phytoplankton in the contemporary ocean (Figure 2.2 A and C). Alternatively, this pattern in the thermal niche breadth reflects the asymmetrical variation in the thermal limits, in which the irregular monotonous behaviour of the lower and upper thermal limits leads to the non-monotonous latitudinal pattern in the niche breadth. The asymmetry is evident in the tropics where the latitudinal decrease in lower thermal limit is steeper than the upper thermal limit. This results in the narrowing of the thermal niche in the tropics that inevitably converges the limits in the warmest latitude (i.e. near the equator), which is evident when seasonality is taken into account (Figure 2.2 B and D). Our results conform to the prediction of Janzen's rule (Janzen, 1967) that expect niches to become narrower in the tropics. Furthermore, our results support previous works showing the relationship between latitude and thermal niche (Addo-Bediako et al., 2000; Stuart-Smith et al., 2017; Sunday et al., 2011) as biogeographical pattern (Gaston et al., 2009). The validity of these relationships in marine phytoplankton

is unclear to date (Chen, 2015; Thomas et al., 2012) but has emerged in our analysis of the species occurrence data.

2.4.2 Limits are sensitive to temperature

The significant influence of latitude on the thermal limits is inevitable since there is a clear monotonous relationship between latitude and temperature (Figure 2.3 A). As expected, thermal limits increase with increasing temperature, opposite to their latitudinal trends (Figure 2.2 A and C). This demonstrates the sensitivity of the thermal limits to annual and seasonal temperatures, suggesting that the contemporary sea surface temperature influences the distribution limits of marine phytoplankton, a trend that was also observed in numerous marine organisms shifting poleward in response to ocean warming (Poloczanska et al., 2013). This temperature dependence can be explained by the metabolic scaling hypothesis (Padfield et al., 2018), which posits that the metabolic rate of organisms regulates the biological processes and patterns in ecology. It is well established that temperature is a key regulator for photosynthesis and respiration in phytoplankton (Barton et al., 2018). The relationship between temperature and physiological performance can are linked to evolutionary history traits of species. Cardinal temperatures are strongly linked to the environmental temperature as an indication of local adaptation and show clear latitudinal trends (Chen, 2015; Thomas et al., 2012) consistent with our results.

2.4.3 Climate variability influences niche breadth

Non-significance of the effect of latitude and temperature on the thermal niche breadth indicates that other factors other than the temperature influence its pattern. The distinctive asymmetry between thermal limits when seasonality is taken into account

(Figure 2.2 B and D) suggests that seasonality in temperature (i.e. climate variability) is a key determinant in linking environmental temperature to the niche in marine phytoplankton. This is further substantiated when climate variability has emerged as the most relatively important variable for niche breadth (Supplementary Figure 2.13). Climate variability is higher in mid-latitudes, whilst the tropics (and polar regions) have more stable water temperature (Figure 2.3 B). The significant effect of climate variability is directly proportional to niche, suggesting that the narrowing of the niche in the tropics is due to reduced climate variability, consistent to the premise of Janzen's rule (Janzen, 1967). Compared to trends observed in terrestrial plants and animals (Araújo et al., 2013), the patterns of the thermal niche in marine phytoplankton are less pronounced but are quite similar to that of marine invertebrates (Stuart-Smith et al., 2017). This could be attributed to the 'buffering' of temperature in water that results in the lesser variability in the annual temperature ranges in seawater as compared to land (Parmesan et al., 2005; Steele, 1985).

Furthermore, the main effect of temperature is significant only when the seasonality in climate is considered. The additive effect of climate variability and temperature is directly positive to niche breadth, suggesting that niches are wider in thermally variable and warmer oceans. This explains why the niches in marine phytoplankton have peaked at ~23° (Figure 2.2 B). At mid-latitudes, it may be possible to deal with much lower and higher temperatures (i.e. generalism is possible but not necessary), whereas in the tropics or polar regions a more extreme temperature (whether colder or hotter) ecological specialisation may be needed. Our results suggest that, other than climate variability, temperature-dependent mechanisms acting at physiological, ecological, and evolutionary levels may also drive the latitudinal patterns of the niche in marine phytoplankton. In light with the metabolic scaling hypothesis

(Padfield et al., 2018), tropical species can perform over a narrower thermal range because of the scaling of physiological rates with the temperature that influences their ecological success in warmer conditions (Payne and Smith, 2017). Recent work on ectotherms have attributed the biogeographic patterns in niche breadth to (i) lower plasticity and evolutionary lability of the upper thermal limits relative to lower thermal limits (Gunderson and Stillman, 2015; Pörtner, 2002), (ii) lowering of the upper thermal limit due to intensification of predation and competition in warmer waters (Stuart-Smith et al., 2017), (iii) tenacity of species at the cool edge of their range by decreasing their metabolism (Masuda, 2008), and (iv) vagrancy of individuals at the cool range edge creating bias in the observation (Bates et al., 2014). Also, the pattern could also be attributed to the negative skewness of the thermal growth response curves in phytoplankton, a condition which makes these organisms more sensitive to warming than cooling (Thomas et al., 2012). Temperature response and biogeography in phytoplankton could also be driven in part by temperature and biogeography of competitors and predators (Wang et al., 2018).

2.4.4 Diversity indirectly affects niche breadth

The strong correlation between diversity and *SST* (r = 0.88, p < 0.05) suggests the important role of temperature in regulating the diversity of phytoplankton (Righetti et al., 2019; Thomas et al., 2012). It is inevitable that the diversity varies across latitude and is highest in the tropics. The latitudinal trend in the diversity of marine phytoplankton shows bimodality with a dip near the equator (Figure 2.3 E) similar to the observed pattern in several marine species (Chaudhary et al., 2016). However, this deviates from the unimodal pattern with a tropical peak that is inferred from the species distribution models in the recent phytoplankton study (Righetti et al., 2019). The

bimodality would suggest that the phytoplankton in the tropics are evolving to temperature variation and are moving away from the equator, and these are likely to happen due to ocean warming.

The positive correlation between diversity and habitat availability (r = 0.28, p < 0.05) indicates that the high tropical diversity is associated to the high availability of habitats (i.e. suitable temperatures) in tropics since it is inevitable that larger area acccommodates more species (Rosenzweig, 1995). The larger habitat areas and little climate variability in tropics may produce high speciation and low extinction rates (Willig and Presley, 2018). It is therefore plausible that the more available habitats in the tropics may influence the latitudinal diversity gradient in marine phytoplankton.

The variation in diversity across latitude may also be a consequence of the decline in geographic range sizes from high to low latitudes as postulated Rapoport's rule (Stevens, 1989). Marine phytoplankton shows a complex relationship between latitude and geographic range size (Supplementary Figure 2.8 A) that does not follow Rapoport's rule despite the presence of clear latitudinal diversity gradient (Figure 2.3 E). In theory, tropical species are predicted to have a small range size due to their adaptation to little seasonal variation in climate. Whereas, temperate species are expected to have a large range size due to their tolerance to greater climate variability. This pattern has been documented for trees, fish, amphibians, reptiles, and mammals (Willig and Presley, 2018), but is not universal, e.g. marine invertebrates (Stuart-Smith et al., 2017), green turtles (Angielczyk et al., 2015), bats and marsupials (Willig and Lyons, 1998), and molluscs (Roy et al., 1994). The inconsistency of the observed pattern to the theory would suggest that several factors other than climate variability may influence the geographic range size in marine phytoplankton. For instance, transport may contribute to the variability in range size of phytoplankton across latitudes

(Gaylord and Gaines, 2000; Hernández-Carrasco et al., 2018), or the niche breadth may influence species range size.

We found a weak trend of increasing geographical range size with increasing thermal niche breadth in marine phytoplankton (Supplementary Figure 2.9 C), suggesting that niche breadth to some extent limit the geographic distribution. This observation supports the validity of the niche breadth–range size hypothesis, which suggests that marine phytoplankton become more widespread when they can utilise resources (e.g. light and nutrients) within a wider thermal condition (Slatyer et al., 2013). Similar to Rapoport's rule, this hypothesis also operates under the premise of climate variability and is also compounded with other factors.

Our findings show that diversity and habitat availability are relatively more important as variables for range size than the seasonal changes in the climate. Geographic range size decreases with increasing diversity and increases with increasing habitat availability. Hence, species may have large range size without adapting to high climate variability if exposed to the environment with low diversity and more thermally suitable habitats. Climate variability may indirectly related to geographic range size via the climate effect on the niche breadth, and on the other hand, diversity may be indirectly linked to niche breadth via diversity effect on range size. Hence, the latitudinal trend of diversity may also explain the observed pattern in niche breadth.

Vázquez and Stevens (Vázquez and Stevens, 2004) proposed a mechanism that relates species diversity with the latitudinal pattern in niche breadth. They suggested that the greater specialisation may be a by-product of the latitudinal gradient in species diversity. The increased nestedness and asymmetric specialisation would suggest that the number of specialists increases faster thus higher species which can result in high specialisation (Vázquez and Stevens, 2004). In this proposed mechanism,

there is an indirect effect of latitude on niche breadth via the effect of diversity which would occur only when species interactions are structured in an asymmetrically specialised and nested way. Hence, the pattern of niche breadth in marine phytoplankton, despite the clear latitudinal diversity trend, can only be explained by this mechanism if a clear nestedness and assymmetric specialisation exist in the structure of species interaction in the phytoplankton. A knowledge gap that limits our current understanding of the biogeography of marine phytoplankton.

2.4.5 Caveats

Our analysis should be interpreted with caution in consideration of the caveats with our approach. First, occurrence records remain geographically incomplete and biased (Isaac and Pocock, 2015). Occurrence data is likely to be driven by survey extent (Supplementary Figure 2.1). There are more and longer transects in the North Atlantic ocean, North Eastern Pacific ocean, American west coasts, and Australian coasts and adjacent waters, whereas such long survey routes are inadequate from the tropics. Second, all locations with recorded occurrences are treated equally independent of phytoplankton abundance, which produce a bias in the estimation of thermal and geographical range. Therefore, it is possible that the species included in the analysis may not have been observed across their full potential thermal and geographical range. Third, data processing, such as excluding data points based on criteria (i.e. dates) and clustering the points into groups (i.e. oceanic regions) may produce possible artefacts by underestimation of the ranges of species. Lastly, the relationship between thermal niches and geographic ranges among species is confounded by the interacting effects of drivers other than the temperature (Sexton et al., 2009; Wiens, 2011) such as light, nutrients, and predation.

2.5 CONCLUSION

Based on our findings from the global analysis of species occurrence data, we conclude that marine phytoplankton exhibit complex biogeographical patterns that do not strictly conform to the classical macroecological rules, and this complexity is partly explained by climate variability, habitat availability, and/or diversity. In summary, the following patterns have emerged from our analysis: (i) the non-monotonous latitudinal pattern in the niche breadth is consequent of the asymmetry between the thermal limits, (ii) the narrowing niches in the tropics is due to reduced seasonal variation in the climate, consistent to Janzen's rule , (iii) the latitudinal pattern in geographic range size of marine phytoplankton invalidates Rapoport's rule but is explained by diversity and habitat availability, and (iv) the direct relationship between niche breadth and range size links diversity effect to the latitudinal trend in thermal niches. From these observed patterns, we conclude that species in tropical oceans have a narrower range making them more vulnerable to ocean warming than those in temperate oceans.

This page is intentionally left blank.

This page is intentionally left blank.

CHAPTER 3

This page is intentionally left blank.

This page is intentionally left blank.

BIOGEOGRAPHIC AND PHYLOGENETIC PATTERNS OF TEMPERATURE RESPONSES IN MARINE PHYTOPLANKTON

ABSTRACT

Understanding the physiological and ecological adaptations of species to temperature is important in predicting their responses to climate change. This study aims to examine the biogeographic and phylogenetic patterns of physiology- and occurrence-based thermal traits (TT_p and TT_o), their inequalities, thermal sensitivity, exposure and vulnerability to warming in marine phytoplankton. Here, TT_p were obtained from the published laboratory results on growth rates across a temperature gradient, whereas TT_o were derived from the sea surface temperature of the species' occurrence locations. The congruence and inequality between TT_p and TT_o were assessed. Also, the variations in the inequality, thermal sensitivity, exposure and vulnerability to warming across the gradient of latitude, thermal affinity, thermal specialisation were determined. Finally, the phylogenetic effect on the thermal attributes was assessed. The findings of this study reveal that TT_p and TT_o are congruent but not equal. Results also show the inequality between TT_p and TT_o and the thermal sensitivity in marine phytoplankton vary across latitude, thermal affinity, thermal specialisation; whereas, the exposure and vulnerability to warming vary non-monotonously with latitude. Interspecific variation in thermal attributes is evident in marine phytoplankton, but no clear evidence of the presence of phylogenetic conservatism in the traits. This empirical investigation of the macroecological patterns of these thermal attributes will provide new insights into distribution of marine phytoplankton in the current and future climate scenarios.

3.1 INTRODUCTION

The critical role played by temperature on phytoplankton physiology, growth, and biogeographical distribution are well recognised (Brun et al., 2015; Coello-Camba et al., 2015; Grimaud et al., 2017; Raven and Geider, 1988). Contemporary rates of warming are shifting the global distributions of marine species (Poloczanska et al., 2013). Recent studies have provided important information on the effect of changes in the temperature on the physiological processes and growth in phytoplankton, consequently altering marine ecosystem structure and function (Behrenfeld et al., 2015; Chust et al., 2014; Huertas et al., 2011; Regaudie-De-Gioux and Duarte, 2012; Thomas et al., 2012). Since the changing climate have serious consequences, it is imperative to have a robust framework to predict the responses of marine phytoplankton on changing climate.It is therefore crucial to understand the physiological and ecological adaptations of marine phytoplankton to temperature to improve our ability to predict their distribution in future climate scenarios.

The direct effect of temperature on phytoplankton growth is typically represented by asymmetric curve, with asymptotic increase in one side, and an abrupt decline in another side (Ras et al., 2013). Several thermal traits can be extracted from this curve including (1) the cardinal temperatures that corresponds to the boundaries of thermal tolerance (i.e. thermal optima, critical thermal minima, and critical thermal maximum), and (2) the thermal niche breadths that correspond to the thermal range on which the species can physiologically tolerate. These physiology-based thermal traits are linked to the biogeographical distribution in ectotherms (Sunday et al., 2012, 2011). However, this physiology-based estimation present a major issue relating to the biases introduced from experimental design, model choice, and data quality (Boyd et al., 2013;

Low-Décarie et al., 2017; Salvador et al., 2019). These biases could be avoided by estimating thermal traits from distribution or species occurrence data (Chapter 2), however occurrence-based estimation is still challenged with spatial, temporal, and taxonomic biases (Isaac and Pocock, 2015). Physiology- and occurrence-based thermal traits may express different aspects of thermal niche of species. Physiology-based thermal traits may represent the fundamental niche, whereas the occurrence-based thermal traits represent the realised niche. Biotic interaction, species dispersal limitation, and limited climate availability reduce fundamental niche to realised niche (Jankowski et al., 2013; Sánchez-Fernández et al., 2016; Soberón and Nakamura, 2009), and hence the realised niche is expected to be smaller than and within fundamental niche (Hutchinson, 1957). Whilst there have been some investigations into the link between physiology- and occurrence-based estimates (Sánchez-Fernández et al., 2012), there are no detailed studies about this relationship in marine phytoplankton. Understanding this link will provide ecophysiological and evolutionary insight on the vulnerability of marine phytoplankton to the warming climate.

In recent years, there has been an increase in the utility of the concept of thermal safety margin (*TSM*) to understand the global patterns of the warming vulnerability in ectotherms (Bennett et al., 2019; Clusella-Trullas et al., 2011; Deutsch et al., 2008; Diamond et al., 2012; Huey et al., 2009; Sunday et al., 2014). *TSM* can be extrapolated from species' thermal sensitivity wherein a physiological thermal safety is inferred if a species' upper (lower) tolerance limit exceeds the warmest temperature (falls short the coldest temperature) it experiences, otherwise species is at risk of thermal danger (Sunday et al., 2014). Furthermore, vulnerability to warming can be explicitly estimated as a function of inherent thermal sensitivity to warmest temperature and the warming exposure (i.e. warming rate) of a species in a given location (Bennett

et al., 2019). The recent developments in the field (i.e. new information and tools) have heightened the need to reassess the vulnerability to warming in marine phytoplankton.

Macroecological patterns of traits has long been a question of great interest. Latitudinal trends in the thermal traits have been demonstrated in previous studies using the physiology data (Chen, 2015; Thomas et al., 2016, 2012) and occurrence data (Chapter 2). Therefore, latitudinal variation in the inequality between physiology- and occurrence-based thermal traits in marine phytoplankton is expected. Also, previous studies have shown the increase of thermal safety margin with increasing latitude, suggesting that tropical species are more vulnerable to warming than temperature species (Clusella-Trullas et al., 2011; Diamond et al., 2012; Sunday et al., 2014).

Other than the latitude, the variation in physiology- and occurrence-based thermal traits, their inequalities, thermal sensitivity, exposure and vulnerability to warming (collectively referred hereinafter as thermal attributes) could also be related to species' thermal affinity, thermal specialisation, and phylogenetic relationship, which previous phytoplankton studies have not dealt with (Chen, 2015; Thomas et al., 2016, 2012). Thermal affinity (*TA*) can be expressed as an index of the degree of preference of species to warm or cold temperatures relative to the average preference in the species pool. Positive *TA* indicates affinity of species to warm temperatures, whilst a negative *TA* indicates affinity to cold temperatures. Thermal specialisation (*TS*) can be expressed as an index of the degree of species thermal tolerance relative to the average tolerance in the species pool. Positive *TS* suggests that a species is relatively more a thermal generalist, whilst a negative *TS* suggests that a species is relatively more a thermal specialist.

Although the phylogenetic effects on thermal traits have been previously demonstrated in phytoplankton (Chen, 2015; Thomas et al., 2016, 2012), there is still very little scientific understanding of whether the thermal attributes are shared with closely related species (i.e. phylogenetic signal) and whether these thermal attributes are evolutionary labile or conserved (i.e. phylogenetic conservatism). Historically, the terms "phylogenetic signal" and "phylogenetic conservatism" has been used synonymously, but in this present study these terms are differentiated. Here, phylogenetic signal is defined as the tendency of closely related species to be similar to each other more than expected from a null model from the same phylogeny (Blomberg et al., 2003). On the other hand, phylogenetic conservatism is the tendency of species to retain their ancestral traits more than expected from a Brownian null model of evolution (Felsenstein, 1985), which can be considered as an extreme case of phylogenetic signal (Loza et al., 2017).

To advance our current knowledge on the microalgal thermal biology, this study sets out to investigate global patterns of physiology- and occurrence-based thermal traits, their inequalities, thermal sensitivity, exposure and vulnerability to warming in marine phytoplankton. Specifically, this study aims to determine the: (1) congruence and inequality between physiology- and occurrence-based thermal traits, (2) variation in the inequality between physiology- and occurrence-based thermal traits, thermal sensitivity, exposure and vulnerability to warming across the gradient of latitude, thermal affinity, and thermal specialisation, and (3) phylogenetic effect on these thermal attributes in marine phytoplankton.

3.2 MATERIALS AND METHOD

3.2.1 Data collection and processing of thermal traits

Physiology-based thermal traits (TT_p; Supplementary Information 3.1) such as the cardinal temperatures (i.e. thermal optimum (T_{opt}), critical thermal minimum (CT_{min}), and critical thermal maximum (CT_{max})), the fundamental thermal niche breadth (FTN) and the maximum growth rate (r_{max}) in marine phytoplankton were compiled from previous studies. Data were obtained from Chen (2015) that compiled 275 records of T_{opt} and r_{max}, 125 records of CT_{min} and 158 records of CT_{max}, and 93 records of FTN in 243 marine phytoplankton strains from 141 unique isolation locations in tropical and temperature regions. Additional data from recently published literature (Coello-Camba and Agustí, 2017) were collected to include 43 records of T_{opt} and r_{max} in 31 marine phytoplankton strains from 21 unique locations in the polar regions. The data were merged into one dataset (referred hereinafter as published dataset) with 318 records of r_{max} and T_{opt}, 125 records of CT_{min}, 158 records of CT_{max} and 93 records of FTN, ranging in latitude from ~75°S to ~81°N (Figure 3.1). The studies included in this published dataset employ different approaches in estimating the cardinal temperature and niche (e.g. different models used for curve fitting), which may introduce some bias. To minimise the effect of this bias, a second dataset of all thermal physiology traits in marine phytoplankton was assembled by fitting growth rates against temperature using the same model. Here, the database of laboratory results on growth rates across a temperature gradient (Litchman and Klausmeier, 2014; Thomas et al., 2016, 2012) was used. The datasets with positive rates for at least four different temperatures were selected. Growth rates were fitted against temperature in a unimodal response curve using the different non-linear functions (i.e. equ04 – equ15 in the *temperatureresponse*

R package (Low-Décarie *et al.* 2017)). Also, the data were fitted using Cardinal Temperature Model with Inflexion (*CTMI*; equ16, hereinafter) (Rosso et al., 1993) (see Supplementary Information 3.2 for the model formulas). The data were fitted to equations using a modified Levenberg-Marquardt algorithm. The fitted equations were compared in terms of Akaike Information Criteria (*AIC*), Bayesian Information Criterion (*BIC*), coefficient of determination (*pseudo R^2*), and the number of successful fits (Supplementary Figure 3.1). Both equ10 and equ16 were initially selected as the best models since they had relatively lower *AIC* and *BIC* values and had relatively higher *pseudo R^2*. *CTMI* model (i.e. equ16) had yielded more realistic estimates of *CT$_{min}$* and *CT$_{max}$* (Supplementary Figure 3.2) and hence was preferably used in the succeeding analysis. *CTMI* allows identifying the cardinal temperatures from experimental data (Grimaud, 2016), which proves useful for the objective of this study. The *CTMI* model successfully fits growth rates with temperature (Supplementary Figure 3.3), generating 197 curve fits. These curves were used to extract the thermal physiological traits in 85 marine phytoplankton strains from 60 unique isolation locations from ~65°S to ~75°N (Figure 3.1) (referred hereinafter as *CTMI*-derived dataset). The *CTMI*-derived dataset was screened with the following inclusion criteria: (1) *CT$_{min}$* > –7 °C, and (2) *CT$_{max}$* < 40 °C and *CT$_{max}$* $\geq$ *T$_{opt}$* + 1°C. The resulting dataset comprised of 168 records of *r$_{max}$* and *T$_{opt}$*, 165 records of *CT$_{min}$*, and 120 records of *CT$_{max}$* and *FTN*. Published and *CTMI*-derived *TT$_p$* are summarised in Supplementary Figure 3.4.
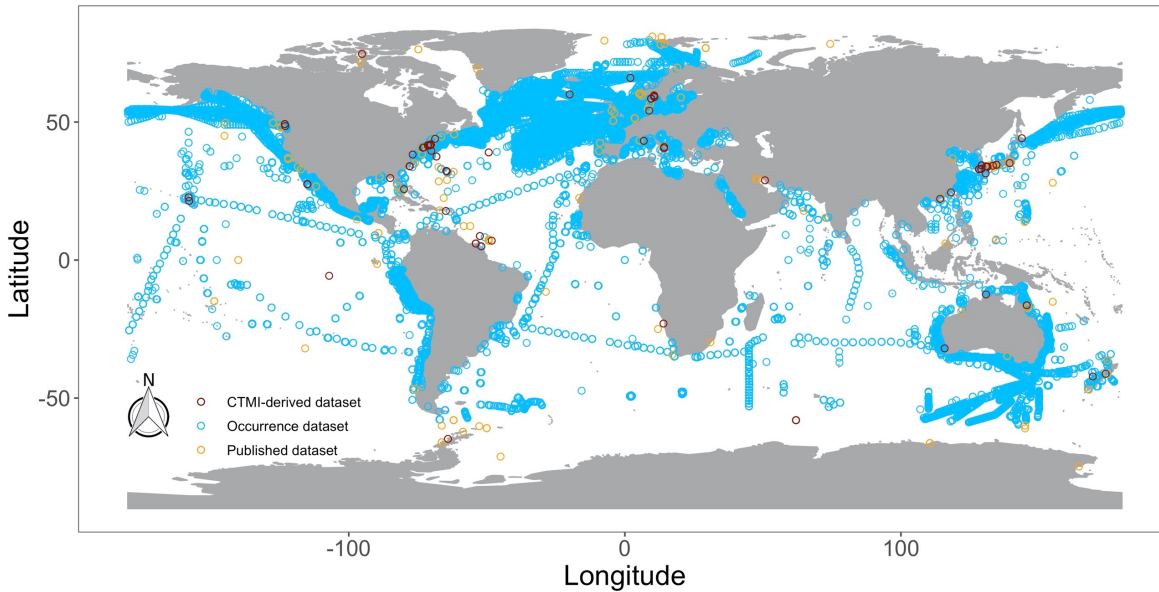
Figure 3.1. Isolation locations of marine phytoplankton listed in the physiology datasets (i.e. published and *CTMI*-derived datasets) and occurrence locations of species listed in occurrence dataset.

Thermal traits derived from species occurrence data (TT_o) was also assembled following Edullantes et al. (unpublished) with modifications. Briefly, occurrence data for each species were downloaded from the databases and recent literature (GBIF.org, 2018; OBIS, 2018; Buitenhuis et al., 2013; Estrada et al., 2016). The collected datasets were curated to only include unique occurrences recorded in marine waters from 2000 to 2014 with complete spatial, temporal, and taxonomic information (i.e. GPS coordinates, year of collection, and identified at species level). To reduce the effect of sampling bias, the species-specific occurrences were spatially filtered to ensure that no two records were within 10 km of one another, which generated a dataset with 98,286 observations representing 1,419 species recorded between 2000 and 2014 (Figure 3.1). The occurrence records were matched with the Sea Surface Temperature (*SST*) values (annual mean *SST*, long-term minimum and maximum *SST*) from 2000 to 2014 that were downloaded from *Bio-ORACLE* (Assis et al., 2018). Lower thermal limit (*LTL*), upper thermal limit (*UTL*), thermal midpoint (*TM*), and realised thermal niche breadth (*RTN*) (Supplementary Information 3.1 for description) were estimated in every species

with $\geq$ 10 unique occurrence records. These traits were derived from both the annual average SST and seasonal extreme SST, i.e. average temperature of the warmest and coldest months. A bootstrapping technique was implemented to account for uncertainty arising from the error in the estimate of thermal traits. The resulting dataset contains the annual average (AA) and seasonal extreme (SE) SST-derived TT_o in 562 marine phytoplankton species, which are summarised in Supplementary Figure 3.4.

TT_p (obtained from published literature and $CTMI$-derived*) and TT_o (derived from annual average and seasonal extreme* SST) were merged and matched up by taxonomic identity at least at species level. This resulted to four combined datasets: (1) TT_p* and TT_o, (2) TT_p* and TT_o*, (3) TT_p and TT_o, and (4) TT_p and TT_o*. These datasets were used in the subsequent analyses and were compared. For simplicity purposes, results of the analyses using the second dataset (i.e. TT_p* and TT_o*) were preferably highlighted in the main text. TT_p* avoids the curve fitting bias introduced in the published dataset as described above, whilst TT_o* is previously shown to account better for biogeographical pattern of niche in phytoplankton than the parameters derived from the annual mean SST (Edullantes et al., n.d.).

3.2.2 Comparing physiology and occurrence-based thermal traits

The congruence in the thermal traits derived from physiological and species occurrence data (TT_p and TT_o, respectively) was assessed following Sánchez-Fernández et al. (2012). TT_p were fitted against TT_o via generalised linear models (GLM) using a Gaussian distribution with link identity (see Supplementary Table 3.1 for the summary statistics). A statistically significant relationship suggests that two approaches of thermal trait estimation are congruent. The slopes of the relationships were tested of their difference from 1 using Chi-squared tests. Deviation of the slope

from 1 suggests that the thermal trait derived from two methods are different. The regression slopes between TT_p and TT_o were also compared across four different datasets using Student t-tests (Andrade and Estévez-Pérez 2014).

Furthermore, the differences between TT_p and TT_o (i.e. difference in optimal temperature (*DOT*), cold tolerance limit (*DCL*), heat tolerance limit (*DHL*), and thermal range (*DTR*); Supplementary Information 3.1 for description; Supplementary Figure 3.5 for summary) were calculated as an additional measure of congruence in the thermal traits estimations. Deviation from 0 was tested using one-sample t-test to indicate mismatch between the two approaches. Positive (or negative) values indicate that the physiology-based estimates are higher (or lower) than the occurrence-based estimates.

3.2.3 Estimation of thermal sensitivity, exposure and vulnerability to warming

Thermal sensitivity, exposure and vulnerability to warming were calculated as described in Supplementary Information 3.1. Sensitivity to cold and warm temperature (S_{min} and S_{max}, respectively) were estimated by obtaining the difference between the species' critical thermal limits (CT_{min} and CT_{max}, respectively) and the ambient sea surface temperature extremes (H_{min} and H_{max}, respectively) it experiences in its local habitat (Bennett et al., 2019). Warming vulnerability (*V*) is a function of inherent thermal sensitivity (S_{max}) and warming exposure (*WR*) of a species in a given location. *V* describes the number of years prior the local temperatures are expected to exceed CT_{max} in a given location (Bennett et al., 2019). SST of the warmest month predicted in the year 2050 and 2010 based on the climate scenarios (i.e. *RCP 2.6*, *RCP 4.5*, *RCP 6.0*, and *RCP 8.5*) were downloaded from *Bio-ORACLE* (Assis et al., 2018) and were used to compute for the warming rate. The estimates of thermal sensitivity, warming rate, and vulnerability to warming are summarised in Supplementary Figure 3.6.

3.2.4 Analysis of latitudinal trends

The differences between physiology- and occurrence-based thermal traits, thermal sensitivity, exposure, and vulnerability to warming were fitted against the absolute latitude of the isolation location using generalised additive models (*GAM*). Gaussian distribution with link identity was used for the *GAM* fitting. Latitudinal trends in the differences between physiology- and occurrence-based thermal traits are summarised in Supplementary Table 3.2. Latitudinal trends in thermal sensitivity, exposure, and vulnerability to warming are summarised in Supplementary Table 3.3.

3.2.5 Analysis of the effect of thermal affinity and specialisation

Thermal affinity *(TA)* and thermal specialisation *(TS)* were computed as described in Supplementary Information 3.1. The main and interactive effects of thermal affinity and thermal specialisation on the differences between thermal traits, thermal sensitivity, exposure and vulnerability to warming were determined by *GLM* models using a Gaussian distribution with link identity. *GLM* models for these relationships of differences between physiology- and occurrence-based thermal traits with thermal affinity and specialisation are summarised in Supplementary Table 3.4. *GLM* models for the relationship of thermal sensitivity, exposure, and vulnerability with thermal affinity and specialisation are summarised in Supplementary Table 3.5.

3.2.6 Analysis of the phylogenetic effect

All species were pooled to construct a backbone phylogeny based on the *NCBI* taxonomy database (Benson et al., 2009; Sayers et al., 2009), which resulted to a topology with all species in the pool. A phylogenetic tree for each of the dataset was constructed using the software program Phylomatic (Webb and Donoghue, 2005), that

matches a pool of species against the backbone phylogeny and returns a trimmed tree. Unresolved relationships between genera and all species within genera were treated as polytomies. Estimated divergence time on the several nodes in the backbone phylogeny (Supplementary Information 3.3) were obtained from TimeTree (www.timetree.org), a public knowledge-base for information of on the evolutionary timescale of life derived using molecular sequence data (Kumar et al., 2017). This information was used to adjust the evolutionary branch lengths in the phylogeny using the *BLADJ* algorithm in the program Phylocom (Webb et al., 2008). The reconstruction of phylogeny was implemented in *R* using the *phylocomr* package (Ooms and Chamberlain, 2019). These reconstructed phylogenies were used to determine the phylogenetic effect.

The presence and strength of phylogenetic signal and phylogenetic conservatism for each trait were quantified. Three approaches were employed to examine the phylogenetic effect on the traits: (1) variance partitioning analysis, (2) autocorrelation using Moran's I and Abouheif's C_{mean} indices, and (3) Brownian motion model of evolution using Blomberg's K and K^* and Pagel's λ indices. The first two approaches tested only for phylogenetic signal, whereas the third approach tested for both phylogenetic signal and phylogenetic conservatism. In the first approach, the phylogenetic signal was tested by comparing the observed variation within hierarchical taxonomic levels with expected values according to a tip randomisation null model following Loza et al. (2017) (citing (Prinzing et al., 2001)). The observed values were examined whether these values were found within the 95% confidence intervals for expected variation within the hierarchical taxonomic level. The confidence intervals were calculated as the interval between the 2.5 and 97.5 percentiles of 10,000 iterations of the null model. Indices in the second and third approaches were calculated using the *phylosignal* package in R (Keck et al., 2016). Local Moran's I index (I_i), a Local

Indicator of Phylogenetic Association (*LIPA*; synonymous to Local Indicator of Spatial Association (*LISA*) (Anselin, 2010)) was also computed to detect hotspots of positive and negative autocorrelation and a phylogenetic correlogram was constructed to visualise the phylogenetic signal in the taxonomy using the *phylosignal* package in R (Keck et al., 2016).

3.2.7 Data processing and analysis software

Data processing and analyses were implemented in *R* version 3.5.1 (R Core Team, 2019) using packages listed in the Supplementary Information 3.4.

3.3 RESULTS

3.3.1 Relationship between physiology- and occurrence based thermal traits

Generalised linear models (*GLM*) were used to assess the relationships between physiology- and occurrence-based thermal traits (TT_p and TT_o, respectively) in marine phytoplankton. Supplementary Table 3.1 provides summary statistics of the linear relationships. Figure 3.2 presents the direct linear relationship of the TT_p* and TT_o* (see Supplementary Figure 3.7 for the linear relationship in all four datasets). Chi-squared tests were used to determine whether the regression slopes are different from the slope = 1.

The direct relationship of optimal temperature estimated from physiological experiments (T_{opt}*) and occurrence data (*TM**) were significant (*GLM* 05: $F_{(1,122)}$ = 94.25, $p < 0.05$; Figure 3.2 A). The slope of the relationship was 1.29 $\pm$ 0.13, which was significantly higher than the slope = 1 ($\chi^2_{(1,123)}$ = 4.71, $p < 0.05$). Approximately 44% of the variance in physiology-based optimal temperature was explained by the variance in

occurrence-based estimates. The regression slopes between physiology- and occurrence-based optimal temperature were the same across the four datasets (Supplementary Figure 3.7 A; Supplementary Table 3.1 *GLM* 01, 05, 09, and 13).

There was also a significant positive relationship between the physiology- and occurrence-based cold tolerance limits (CT_{min}* and *LTL*, respectively) (*GLM* 06: $F_{(1,121)}$ = 99.42, $p < 0.05$; Figure 3.2 B). The slope of the relationship between the cold tolerance limits was 0.67 ± 0.07, which was significantly lower to slope= 1 ($\chi^2_{(1,122)}$ = 24.86, $p < 0.05$). Occurrence-based cold tolerance limits did account for 45% variance in the physiology-based estimates. Similar to the slopes in temperature optimum, the regression slopes between the physiology- and occurrence-based cold tolerance limits were the same across the four datasets (Supplementary Figure 3.7 B; Supplementary Table 3.1 *GLM* 02, 06, 10, and 14).

Furthermore, the heat tolerance limits estimated from physiology and occurrence data (CT_{max}* and *UTL*, respectively) had a significant positive relationship (*GLM* 07: $F_{(1,89)}$ = 46.81, $p < 0.05$; Figure 3.2 C). The regression slope was 1.00 ± 0.15, and was not significantly different to the slope = 1. About 34% of the variation in the physiology-based estimates was accounted for the occurrence-based upper thermal limits. The slopes of the relationship between physiology- and occurrence-based heat tolerance limits did not vary across the four datasets (Supplementary Figure 3.7 C; Supplementary Table 3.1 *GLM* 03, 07, 11, and 15).
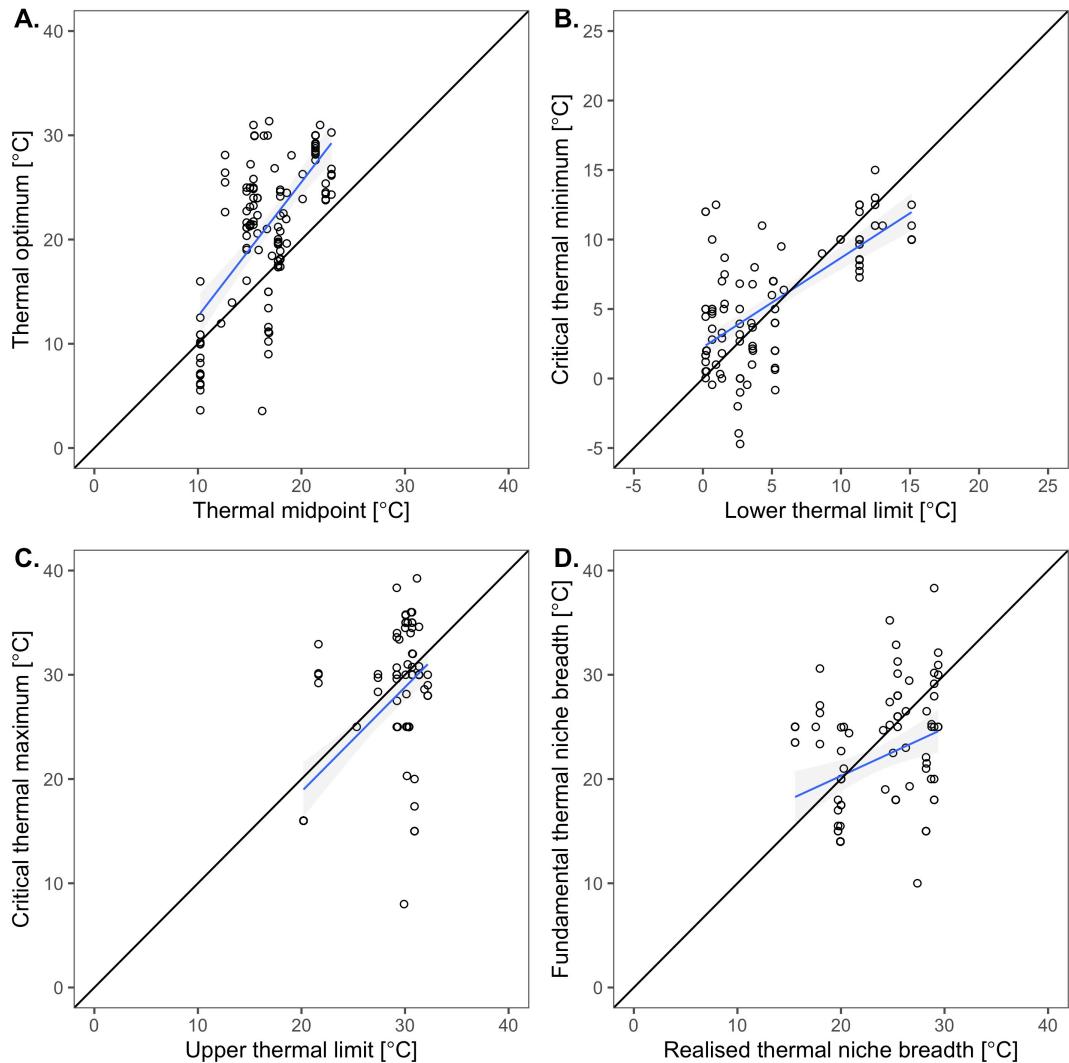
Figure 3.2. Relationship between physiology- and occurrence-based estimates of thermal traits (TT_p and TT_o, respectively) in marine phytoplankton. TT_p* (*CTMI*-derived) were fitted against TT_o* (derived from a seasonal extreme (*SE*) sea surface temperature (*SST*)) using generalised linear models (*GLM*; see Supplementary Table 3.1 *GLM* 05 – 08 for the summary statistics). The regression lines are indicated in blue solid lines with 95% confidence interval in grey shading. The black solid lines represent equality between TT_p* and TT_o*. Generally, there was significant positive relationship between TT_p* and TT_o*, suggesting congruence in estimation approaches. Except for the slope between heat tolerance limits, the slopes of the relationship between TT_p* and TT_o* were different to the slope = 1, indicating thermal traits derived from physiology and occurrence data are not the same. Also, the regression slopes were the same across the datasets, except for the regression slope between the thermal ranges (see Supplementary Figure 3.7).

The positive relationship between the physiology- and occurrence-based thermal ranges (*FTN** and *RTN*,* respectively) was also significant (*GLM* 07: $F_{(1,89)}$ = 10.39, $p < 0.05$; Figure 3.2 D). The slope of the relationship between *FTN** and *RTN** (0.46 ± 0.14) was different to the slope = 1 ($\chi^2_{(1,90)}$ = 14.76, $p < 0.05$). Occurrence-based thermal range only accounted 10% of the variation in the physiology-based

thermal range. The slopes of the relationship between physiology- and occurrence-based thermal range did vary across datasets (Supplementary Figure 3.7 D; Supplementary Table 3.1 *GLM* 04, 08, 12, and 16), e.g. *GLM* 12 slope was different from the slope in *GLM* 4 ($t_{(135)}$ = -2.19; $p < 0.05$) and *GLM* 8 ($t_{(135)}$ = -2.68; $p < 0.05$).

3.3.2 Inequality across latitude, thermal affinity and specialisation

Except for the difference in cold and heat tolerance limits (i.e. DCL_2 and DHL_2, respectively), the mean estimated differences between TT_p* and TT_o* were significantly different from zero, i.e. the difference in optimal temperature ($DOT_2 = T_{opt}$* − *TM**) was 4.56 $\pm$ 0.49 °C ($t_{(123)}$ = 9.25, $p < 0.05$), and the difference in thermal range ($DTR_2 =$ *FTN** − *RTN**) was −1.56 $\pm$ 0.64 °C ($t_{(90)}$ = -2.42, $p < 0.05$). Similar patterns was generally observed in all the datasets. Except for *DOT*, *DCL* ($F_{(3,382)}$ = 45.01, $p < 0.05$), *DHL* ($F_{(3,348)}$ = 7.61, $p < 0.05$), and *DTR* ($F_{(3,274)}$ = 35.00, $p < 0.05$) varied across the four datasets.

Latitudinal trends in the difference between TT_p and TT_o were examined using generalised additive models (*GAM*; Supplementary Table 3.2 for the summary statistics). The difference TT_p* and TT_o* did vary non-monotonously with latitude (Figure 3 A – D). These non-monotonous relationships were generally observed in other datasets (Supplementary Figure 3.8), where latitude accounted for <50% of the variation in the difference between TT_p and TT_o.

Latitude accounted for 29% of the variation in DOT_2 (Supplementary Table 3.2 *GAM* 05). Generally, the DOT_2 was higher than zero across all latitude except for several species close to ~40° and beyond ~60° latitude (Figure 3.3 A). This latitudinal pattern was generally consistent across all datasets (Supplementary Figure 3.8 A).
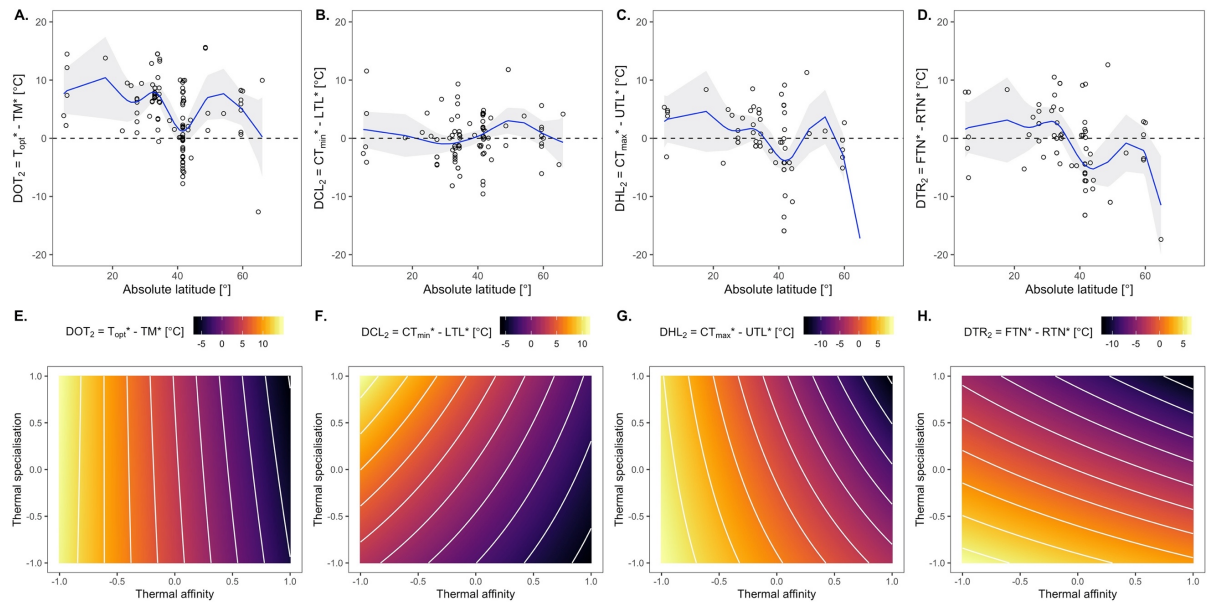
Figure 3.3. Difference between physiology- and occurrence-based thermal traits (TT_p and TT_o, respectively) in marine phytoplankton across latitude (A – D) and across thermal affinity and thermal specialisation (E – H). The estimates of the difference between TT_p^* (*CTMI*-derived) and TT_o^* (derived from a seasonal extreme (*SE*) sea surface temperature (*SST*)) ($TT_p^* - TT_o^*$) were fitted against latitude using generalised additive models (*GAM*; see Supplementary Table 3.2 *GAM* 05 – 08 for the summary statistics). The regression lines are indicated in blue solid lines with 95% confidence interval in grey shading. The horizontal broken line indicates the difference is zero. As presented, $TT_p - TT_o$ did vary non-monotonously with latitude (A – D). Moreover, $TT_p^* - TT_o^*$ were fitted against thermal affinity and thermal specialisation using generalised linear models (*GLM*; see Supplementary Table 3.4 *GLM* 05 – 08 for the summary statistics). The *GLMs* were used to construct the contour plots (E – H). The colour bars indicate the estimates of $TT_p^* - TT_o^*$.

On the other hand, latitude only explained 6% of the variance in DCL_2 (Supplementary Table 3.2 *GAM* 06). DCL_2 did not deviate from zero across all latitude (Figure 3.3 B). However, this pattern was different in DCL_1 and DCL_3 that were generally below zero across latitude (Supplementary Figure 3.8 B). Also, DCL_1 had no clear latitudinal pattern.

About 34% of variance in DHL_2 was explained by latitude (Supplementary Table 3.2 *GAM* 07), which generally did not differ from zero across latitude, except for the estimates near ~40° latitude and beyond ~60° (Figure 3.3 C). This trends varied from DHL_1 and DHL_3 that were generally higher than zero at lower latitude (< 40° latitude) (Supplementary Figure 3.8 C).

69

Approximately 31% of the variance in DTR_2 was explained by latitude (Supplementary Table 3.2 *GAM* 08). DTR_2 did not vary from zero at lower latitude, but it was lower than zero at higher latitude (Figure 3.3 D). Different pattern was observed in DTR_1 and DTR_3, where estimates were generally higher than zero across the latitude (Supplementary Figure 3.8 D).

The effects of thermal affinity (*TA*) and thermal specialisation (*TS*) on the difference between TT_p and TT_o were tested using the generalised linear model (*GLM*; Supplementary Table 3.4 for the summary statistics). Generally, the difference TT_p* and TT_o* did vary with thermal affinity and thermal specialisation (Figure 3 E – H). These patterns were also observed in other datasets (Supplementary Figure 3.9).

The main effect of *TA* on DOT_2 was significant (*GLM* 21). Neither *TS* nor its interaction with *TA* had an effect on DOT_2. DOT_2 had decreased with increasing *TA* (Figure 3 E). Similar pattern was observed in all datasets, but both DOT_3 and DOT_4 were influenced by the main and interaction of the effects of *TA* and *TS* (Supplementary Figure 3.9).

The main effects of *TA* and *TS* on DCL_2 were significant (*GLM* 22). DCL_2 had decreased with increasing *TA* and had increased with increasing *TS* (Figure 3 F), and these were consistent in all datasets (Supplementary Figure 3.9).

The main and interactive effects of *TA* and *TS* on DHL_2 were significant (*GLM* 23). DHL_2 had decreased with increasing *TA* and *TS* (Figure 3 G). Similar patterns were observed in all datasets, except for DHL_3 that was not affected by the interaction between *TA* and *TS* (Supplementary Figure 3.9).

The main effects of *TA* and *TS* on DTR_2 were significant (*GLM* 24). DTR_2 had decreased with increasing *TA* and *TS* (Figure 3 H). This pattern were the same across datasets, except for DTR_4 that did not vary across *TA* (Supplementary Figure 3.9).

3.3.3 Thermal sensitivity, warming exposure and vulnerability across latitude, thermal affinity and specialisation

Latitudinal trends in sensitivity to cold and warm temperature (S_{min} and S_{max}, respectively), warming exposure (WR), and vulnerability to warming (V) in marine phytoplankton were determined using generalised additive model (GAM; Supplementary Table 3.3 for the summary statistics). S_{min} *, S_{max}*, WR*, and V* (estimated from the $CTMI$-derived dataset) were found to vary non-linearly across latitude (Figure 3.3), which generally similar to the patterns observed from the data in the published dataset (Supplementary Figure 3.10).

Exactly half of the variation in S_{min} * was explained by latitude. As observed, S_{min} * rose evidently to high point and peaked at ~50° (Figure 3.4 A). Estimates of S_{min} * were generally lower than zero, except for the observations beyond the peak that were not different from zero. This patterns in S_{min} * had a notable difference from the trends in S_{min} estimated from the published dataset that had dipped at ~50° (Supplementary Figure 3.10 A),

About 31% of the variance in S_{max}* was explained by latitude. S_{max}* had no clear latitudinal variation in lower latitude but the estimates were generally above zero. S_{max}* had dropped at ~40°, then increased to a peak (15°C) at ~55°, and declined to ~65° (Figure 3.4 B). These patterns were generally retained in the latitudinal trends in S_{max} estimated from the published dataset, but had remarkable differences: (1) the decline of S_{max} from 0° to ~23°, (2) the peak at ~35°, and the increasing pattern of S_{max} beyond ~65° (Supplementary Figure 3.10 B).

On the other hand, latitude accounted for the 43% of the variance in warming exposure based on RCP 8.5 climate scenario ($WR_{8.5}$*). $WR_{8.5}$* evidently increased with latitude until it reached a peak at ~45, and declined at ~65° (Figure 3.4 C).

Successively, $WR_{8.5}*$ rose to high point and peaked in the highest latitude. Warming

exposure did vary significantly across climate scenarios ($F_{(3,612)}$ = 925.36, p < 0.05). As

expected, $WR_{8.5}*$ were higher than the WR projected in RCP 2.6, RCP 4.5, and RCP

6.0 climate scenarios. These trends did not differ from the trends in WR estimated from

the published dataset (Supplementary Figure 3.10 C – F).
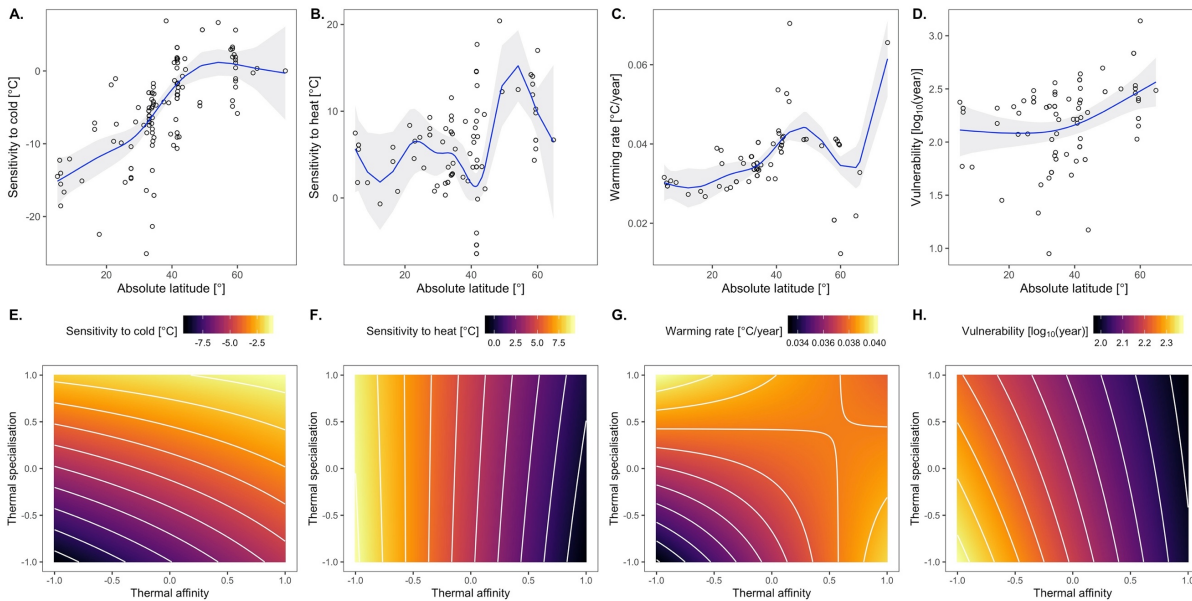
Figure 3.4. Sensitivity to cold and warm temperature (S_{min} and S_{max}, respectively), warming exposure (WR), and vulnerability to warming (V) in marine phytoplankton across latitude (A – D) and across thermal affinity (TA) and thermal specialisation (TS) (E – H). All estimates were obtained from $CTMI$-derived datasets (indicated by an asterisk), and the warming rate and vulnerability were computed based on RCP 8.5 climate scenario ($WR_{8.5}*$ and $V_{8.5}*$, respectively). $S_{min}*$, $S_{max}*$, $WR_{8.5}*$, and $V_{8.5}*$ were fitted against latitude using generalised additive models (GAM; see Supplementary Table 3.3 GAM 17, 18, 22, and 26, respectively, for the summary statistics). The regression lines are indicated in blue solid lines with 95% confidence interval in grey shading. Except for $V_{8.5}*$, estimates for $S_{min}*$, $S_{max}*$, $WR_{8.5}*$ did vary non-monotonously with latitude (A – D). Furthermore, $S_{min}*$, $S_{max}*$, $WR_{8.5}*$, and $V_{8.5}*$ were fitted against TA and TS using generalised linear models (GLM; see Supplementary Table 3.5 GLM 33, 34, 38, and 42, respectively, for the summary statistics). The $GLMs$ were used to construct the contour plots (E – H). The colour bars indicate the estimates of $S_{min}*$, $S_{max}*$, $WR_{8.5}*$, and $V_{8.5}*$.

Warming vulnerability based on RCP 8.5 climate scenario ($V_{8.5}*$) appeared to

behave monotonously (Figure 3.4 D). About 14% of the variance in $V_{8.5}*$ was explained

by latitude. $V_{8.5}*$ remained constant in lower latitude and gradually increased in higher

latitude. There was a significant difference in $V_{8.5}*$ across the climate scenarios ($F_{(3,361)}$

= 35.27, p < 0.05). $V_{8.5}*$ were lower than the warming vulnerability projected in other

climate scenarios. Contrastingly, trends in warming vulnerability estimated from published dataset were non-monotonous (Supplementary Figure 3.10 G – J).

Furthermore, significant effects of thermal affinity (TA) and thermal specialisation (TS) on sensitivity to cold and warm temperature (S_{min} and $S_{max,}$ respectively), warming exposure (WR), and vulnerability to warming (V) in marine phytoplankton were tested using generalised linear model (GLM; Supplementary Table 3.5 for the summary statistics).

Only the main effect of TS on S_{min}* was significant (GLM 33), increasing S_{min}* with increasing TS (Figure 3.4 E). On the other hand, only the main effect of TA on S_{max}* was significant (GLM 34), decreasing S_{max}* with increasing TA (Figure 3.4 F). These trends were similar to the patterns observed in S_{min} and S_{max} estimated from the published dataset (Supplementary Figure 3.11 C and D, respectively).

There was no significant effect of TA and TS on warming exposure and on warming vulnerability based on RCP 8.5 climate scenario ($WR_{8.5}$* and $V_{8.5}$*, GLM 38 and 42, Figure 3.4 G and H, respectively). However, the significance of these effects were dependent on climate scenarios and on the composition of the datasets. Supplementary Figure 3.11 presents contour plots showing the variation of warming exposure (Supplementary Figure 3.11 F – L) and warming vulnerability (Supplementary Figure 3.11 M – T) across thermal affinity and thermal specialisation.

3.3.4 Phylogenetic effect on the thermal traits, thermal sensitivity, exposure and vulnerability to warming

The phylogenetic distribution of the physiology- and occurrence-based thermal traits (TT_p and TT_o, respectively), their difference ($TT_p – TT_o$), thermal sensitivity (S_{min} and S_{max}), warming exposure (WR), and warming vulnerability (V) in marine

phytoplankton (Figure 3.5; Supplementary Figure 3.12 – 3.14) were examined to determine the phylogenetic effect. Three approaches were employed: (1) variance partitioning (*VP*) (Figure 3.6; Supplementary Figure 3.15 – 3.17), (2) autocorrelation (*AC*) using Moran's *I* (Figure 3.7; Supplementary Figure 3.18 – 3.20) and Abouheif's C_{mean} indices, and (3) Brownian motion model of evolution (*BM*) using Blomberg's *K* and *K** and Pagel's λ indices. Supplementary Table 3.6 presents the summary statistics for these three approaches.

Variation in TT_p across taxonomic groups was evident (Figure 3.5 A – D; Supplementary Figure 3.12 A – H). For instance, cyanobacteria had higher $T_{opt}^{(*)}$, $CT_{min}^{(*)}$, and $CT_{max}^{(*)}$, and lower $FTN^{(*)}$ compared to other taxonomic groups. Based on *VP*, about 24 – 63% of the variation in TT_p was explained by species, and a significant smaller proportions of the variance was explained by supra-specific taxonomic levels (Figure 3.6 A – D; Supplementary Figure 3.15 A – H). *AC*-based phylogenetic signal was present in $T_{opt}^{(*)}$ (*I* and $C_{mean} > 0$, $p < 0.05$; Figure 3.7 A and Supplementary Figure 3.18 A and E), but *BM*-based signal was absent. Both *AC* and *BM*-based phylogenetic signals were detected in $CT_{min}^{(*)}$ (*I*, C_{mean}, *K*, *K**, and $\lambda > 0$, $p < 0.05$; Figure 3.7 B and Supplementary Figure 3.18 B and F), but the *BM*-based signal was weak to detect phylogenetic conservatism in $CT_{min}^{(*)}$ (*K, K**, and $\lambda < 1$). However, no *AC*-based phylogenetic signal was detected in CT_{max}^{*} (Figure 3.7 C), but CT_{max} estimated from the published dataset had produced a significant *AC*-based phylogenetic signal (*I* and C_{mean} > 0, $p < 0.05$; Supplementary Figure 3.18 G). Furthermore, phylogenetic signal was absent in FTN^{*} (Figure 3.7 D), but, both *AC* and *BM*-based signals were detected in *FTN* estimated from the published dataset (*I*, C_{mean}, *K*, *K**, and $\lambda > 0$, $p < 0.05$; Supplementary Figure 3.18 H). The *BM*-based signal was weak to infer presence of phylogenetic conservatism in *FTN* (*K, K**, and $\lambda < 1$).

Figure 3.5. Phylogenetic distribution of the thermal traits estimated from physiology data (TT_p) and occurrence data (TT_o), their difference ($TT_p - TT_o$), thermal sensitivity (S_{min} and S_{max}), warming exposure (WR), and warming vulnerability (V) in marine phytoplankton. $CTMI$-derived TT_p* (A – D) and seasonal extreme SST-derived TT_o* (E – H) were used to compute for the difference between physiology- and occurrence-based thermal traits (I – L). S_{min}*, S_{max}*, $WR_{8.5}$* and $V_{8.5}$* were obtained from $CTMI$-derived datasets (M – P) and the warming rate and vulnerability were computed based on RCP 8.5 climate scenario. Colours indicate trait value, as shown by the colour bar below each tree.
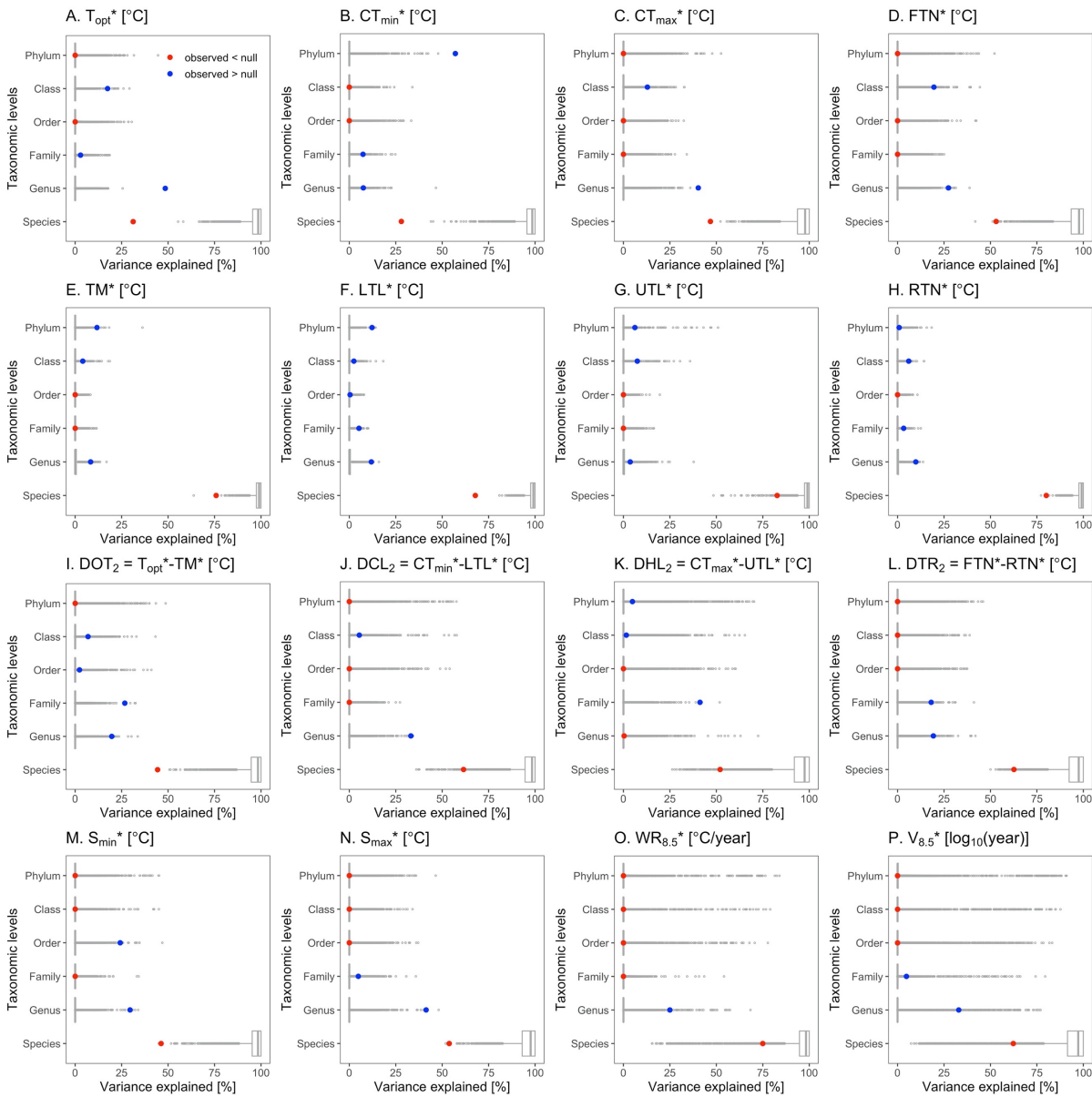
Figure 3.6. Percentage of variation in thermal traits estimated from physiology data (TT_p) and occurrence data (TT_o), their difference ($TT_p – TT_o$), thermal sensitivity (S_{min} and S_{max}), warming exposure (WR), and warming vulnerability (V) in marine phytoplankton explained by different taxonomic levels according to a variance partitioning analysis. *CTMI*-derived TT_p* (A – D) and seasonal extreme *SST*-derived TT_o* (E – H) were used to compute for the difference between physiology- and occurrence-based thermal traits (I – L). $S_{min}*$, $S_{max}*$, $WR_{8.5}*$ and $V_{8.5}*$ were obtained from *CTMI*-derived datasets (M – P) and the warming rate and vulnerability were computed based on *RCP* 8.5 climate scenario. Solid points represent the observed values, whilst the boxplots represent the distribution of values generated by the tip randomisation null model. All observed values are significant different from the null model at 95% confidence interval. The red and blue points indicate that observed values are lower and higher than the null model, respectively.
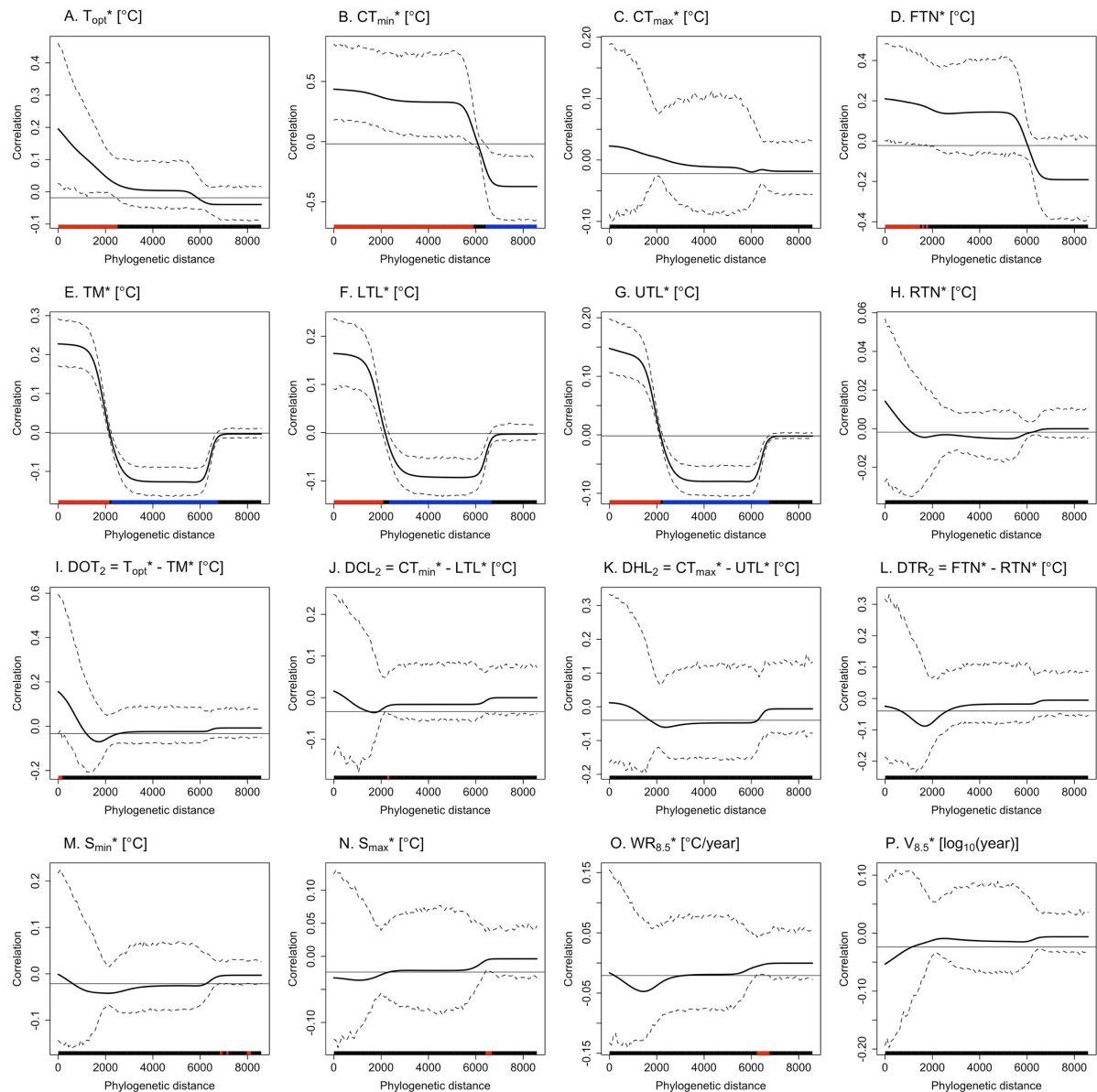
Figure 3.7. Phylogenetic correlograms for the thermal traits estimated from physiology data (TT_p) and occurrence data (TT_o), their difference ($TT_p - TT_o$), thermal sensitivity (S_{min} and S_{max}), warming exposure (WR), and warming vulnerability (V) in marine phytoplankton. $CTMI$-derived TT_p* (A – D) and seasonal extreme SST-derived TT_o* (E – H) were used to compute for the difference between physiology- and occurrence-based thermal traits (I – L). $S_{min}*$, $S_{max}*$, $WR_{8.5}*$ and $V_{8.5}*$ were obtained from $CTMI$-derived datasets (M – P) and the warming rate and vulnerability were computed based on RCP 8.5 climate scenario. The solid black lines indicate the Moran's I index autocorrelation, and the dashed black lines indicate the 95% confidence interval. The horizontal black lines represent the estimated value of Moran's I under the null hypothesis of no phylogenetic autocorrelation. The red and blue colored bars indicate significant positive and negative autocorrelation, respectively; whilst, the black colored bars indicate a non-significant autocorrelation.

TT_o also appeared to vary across taxonomic groups (Figure 3.5 E – H; Supplementary Figure 3.12 I – P). Approximately, 68 – 88% of the variation in TT_o was largely explained by species (Figure 3.6 E – H; Supplementary Figure 3.15 I – P). *AC-*

77

based phylogenetic signal was present in $TM^{(*)}$ (I and $C_{mean} > 0$, $p < 0.05$; Figure 3.7 E

and Supplementary Figure 3.18 I and M). Also, BM-based signal was detected in TM^*

(based only on $\lambda > 0$, $p < 0.05$) and in TM (based on K and $\lambda > 0$; $p < 0.05$), however

this signal was weak to detect phylogenetic conservatism in $TM^{(*)}$ (K and $\lambda < 1$). $LTL^{(*)}$

had produced significant AC- and BM-based phylogenetic signals (I, C_{mean}, K, K^*, and λ

> 0, $p < 0.05$; Figure 3.7 F and Supplementary Figure 3.18 J and N). However,

phylogenetic conservatism was absent in $LTL^{(*)}$ (K, K^*, and $\lambda < 1$). Also, AC- and BM-

based phylogenetic signals were also detected in $UTL^{(*)}$ (I, C_{mean}, and $\lambda > 0$, $p < 0.05$;

Figure 3.7 G; Supplementary Figure 3.18 K and O) but failed to detect phylogenetic

conservatism in $UTL^{(*)}$ ($\lambda < 1$). AC-based phylogenetic signal was present in RTN^*

(based only on $C_{mean} > 0$, $p < 0.05$) and in RTN (I and $C_{mean} > 0$, $p < 0.05$; Figure 3.7 H

and Supplementary Figure 3.18 L and P). Neither the phylogenetic signal nor the

phylogenetic conservatism based on BM analysis were detected in $RTN^{(*)}$.

The difference between $TT_p^{(*)}$ and $TT_o^{(*)}$ was also found to vary across

taxonomic groups (Figure 3.5 I – L; Supplementary Figure 3.13), and significant

proportion of the variation in $TT_p^{(*)} - TT_o^{(*)}$ was explained by the species (25 – 70%)

and supra-specific taxonomic levels (Figure 3.6 I – L; Supplementary Figure 3.16).

However, both AC- and BM-based analyses did not reveal statistically significant

phylogenetic signal and conservatism in $TT_p^* - TT_o^*$ (Figure 3.7 I –L and

Supplementary Figure 3.19). In contrast, $TT_p - TT_o$ estimated from published dataset

produced a significant AC-based phylogenetic signal (I and/or $C_{mean} > 0$, $p < 0.05$),

except for the difference in heat tolerance limits ($DHL^{(*)}$) .

Thermal sensitivity (S_{min} and S_{max}), warming exposure (WR), and warming

vulnerability (V) in marine phytoplankton also seemed to vary across taxonomic groups

(Figure 3.5 M – P; Supplementary Figure 3.14), and significant percentage of the

variation was explained by species and supra-specific taxonomic levels (Figure 3.6 M – P; Supplementary Figure 3.17). However, phylogenetic signal and conservatism were absent in S_{min}* (Figure 3.7 M and Supplementary Figure 3.20 A). In contrast, S_{min} estimated from published dataset had detected a statistically significant phylogenetic signal based on *AC* (*I* and C_{mean} > 0, p < 0.05; Supplementary Figure 3.20 C) and *BM* (*K** and λ > 0, p < 0.05). However, *BM*-based signal was too weak to detect phylogenetic conservatism in S_{min}. Also, There was no significant phylogenetic signal in $S_{max}^{(*)}$ (Figure 3.7 N and Supplementary Figure 3.20 B and D), with the exception of the analysis based on C_{mean} that had detected a statistically significant phylogenetic signal in S_{max} estimated from published dataset (C_{mean} > 0, p < 0.05). Generally, phylogenetic signal was absent in $WR^{(*)}$ across all climate scenarios (Figure 3.7 O and Supplementary Figure 3.20 E and L), except for the analysis based on *K* and *K** that had detected significant phylogenetic signal in $WR_{2.6}$* but was weak to detect phylogenetic conservatism in the trait (*K* and *K** < 1). Furthermore, significance of the phylogenetic signal in $V^{(*)}$ across all climate scenarios was not detected (Figure 3.7 P and Supplementary Figure 3.20 M and T), except for the λ that had detected statistically significant signal in $V_{2.6}$, $V_{6.0}$, and $V_{8.5}$ (λ > 0, p < 0.05). The λ-based signals were close to 1 (i.e. 0.96 – 1.00), which may indicate the presence of phylogenetic conservatism in warming vulnerability in marine phytoplankton.

3.4 DISCUSSION

3.4.1 Congruence and inequality between physiology- and occurrence-based thermal

The significance of the direct relationship between the thermal traits derived from physiology and occurrence data (TT_p and TT_o, respectively) in marine phytoplankton (Figure 3.2) suggests congruence between the estimation approaches. However, the degree of congruence is not high as inferred from the lower proportion of the variance in TT_p explained by TT_o (< 50 %). Furthermore, the TT_p and TT_o are not equal as indicated by the non-conformity of the slopes to 1 (Figure 3.2) and the non-equality of $TT_p – TT_o$ to zero (Figure 3 A – D), with the exception of the heat tolerance limits. Taken together, these results support the hypothesis of the link between TT_p and TT_o that may express different aspects of the thermal niche of species. TT_p is expected to estimate the fundamental niche of a species, which is defined by species' physiological tolerance range to environmental factors such as temperature in the absence of biotic interactions (Hutchinson, 1957). However, the presence of biotic interaction such as predation, competition, mutualisms, parasites and pathogens (Jankowski et al., 2013), species dispersal limitation (Sánchez-Fernández et al., 2016), and limited climate availability (Soberón and Nakamura, 2009) reduce the fundamental niche to realised niche that may be estimated by the TT_o. Hence, it is expected that the TT_p is higher than TT_o.

Contrary to expectations, the extreme cold and heat tolerance limits as estimated from occurrence data in several species are close, or even exceed their physiological thermal limits (Figure 3 B and C), resulting to the extreme realised range equal to or wider than the fundamental range (Figure 3 D). However, this is not case for

the thermal ranges estimated from the annual average *SST* that are generally smaller than the physiological thermal range (Supplementary Figure 3.7 D). Therefore, the thermal range derived from annual average- and seasonal extreme-*SST* may estimate a different aspect species niche, the former being limited by thermal availability and is generally smaller than and is within the fundamental niche (Supplementary Figure 3.21 A and C), conforming to the prediction by Hutchinson (1957).

The biases associated with physiology data (Boyd et al., 2013; Low-Décarie et al., 2017; Salvador et al., 2019) and occurrence data (Isaac and Pocock, 2015); cannot be ignored that may introduce uncertainties in the estimation of the thermal traits, and thus possibly violate the prediction by Hutchinson (1957). For instance, strains/isolates of species may possess different thermal niche and species may not be represented across their geographic range, which may underestimate the fundamental thermal niche. Also, the spatial, temporal, and taxonomic bias in the occurrence dataset may underestimate or overestimate the species' realised niche.

Setting these biases aside, the predictions by Hutchinson (1957) can be violated in several ways: (1) niche evolution can change the physiological limits in a population relative to their baseline; (2) natural or anthropogenic mechanisms can facilitate the occurrence of species outside their physiological limits; and (3) failure to account for the variation in physiological requirements across species life history may introduce inaccuracies of the estimation of fundamental thermal niche (Soberon and Arroyo-Peña 2017).

3.4.2 Variation of the inequality between physiology- and occurrence-based thermal traits

Generally, thermal traits in marine phytoplankton vary across latitude as demonstrated in previous studies using the physiology data (Chen, 2015; Thomas et al., 2016, 2012) and occurrence data (Edullantes et al., n.d.). Hence, the difference between physiology- and occurrence-based thermal traits ($TT_p - TT_o$) is also likely to vary across latitude. As observed, $TT_p - TT_o$ generally vary non-monotonously with latitude (Figure 3 A – D), suggesting that $TT_p - TT_o$ may increase or decrease depending on the geographic locations where the species are collected/isolated. Moreover, the significance of the main effects of thermal affinity (*TA*) and thermal specialisation (*TS*) on $TT_p - TT_o$ reveals remarkable contrasts between the cooler- and warmer-affinity species, and between the specialists and generalists (Figure 3 E – H; Supplementary Figure 3.9).

The estimates of the difference in optimal temperature (*DOT*) across latitude are mostly above the equality line (Figure 3 A; Supplementary Figure 3.8 A), indicating that the optimal temperature for growth of a species is higher than that the optimal temperature for their ecological success. Hence, it is possible to hypothesise that presence of the biotic interactions is likely to reduce the optimal thermal preference of species. Also, the results also show the decline of *DOT* near the equality line at ~40° where variability in *DOT* is high. These findings may be explained by the fact that climate variability is highest at mid latitude (Chapter 2). A high climate variability inevitably widens the realised niche breadth to an extent where the midpoint will be closer or exceed the physiological thermal optimum. Furthermore, *DOT* decreases with *TA* (Figure 3 E; Supplementary Figure 3.9), suggesting that the greater the affinity of

species to warm temperature, the closer their thermal optimum for growth to their

optimal temperature for ecological success.

On the other hand, the latitudinal trend in *DCL* (i.e. difference in cold tolerance

limit) is generally close to or below the equality line (Figure 3 B; Supplementary Figure

3.8 B), entailing that the species' lower thermal limits in the presence of biotic

interaction are equal or greater than their physiological thermal minima. Contrastingly,

the latitudinal trend in *DHL* (i.e. difference in heat tolerance limit) is commonly near or

above the equality line (Figure 3 C; Supplementary Figure 3.8 C), suggesting that the

realised upper thermal limits of species are equal or lower than their critical thermal

maxima. These findings support the hypothesis that the species' realised thermal limits

are within their fundamental thermal niche. However, there are several notable

observations that contradict this hypothesis. For instance, estimates of *DCL* and *DHL*

are highly variable at ~40°, where some estimates are above and below the equality

line, respectively. Therefore, in this case, the realised thermal limits are not contained

by the fundamental thermal range, and the realised thermal niche may be wider than

the fundamental niche (Figure 3 D), which is inconsistent to the prediction by

Hutchinson (1957). As described earlier, these discrepancies are obvious with

occurrence-based thermal traits derived from seasonal extreme *SST*. In addition, both

DCL and *DHL* also decline with increasing *TA* (Figure 3 F and G, respectively;

Supplementary Figure 3.9), indicating that warmer-affinity species have lesser

inequality between physiological and realised thermal limits as compared to the cooler

water species. The direct relationship between *DCL* and *TS* suggests that the more

specialist a species, the lesser is the difference in cold tolerance limits. On the other

hand, the inverse relationship between *DHL* and *TS* implies that the difference in heat

tolerance limits is greater in the thermal specialist than in the thermal generalist.

The latitudinal trends in *DTR* (difference in thermal range) with realised thermal limits derived from annual average *SST* are generally above the equality line (Supplementary Figure 3.8 D), conforming to the hypothesis. As observed, *DTR* in lower latitude are greater than the estimates in higher latitude, suggesting that the realised thermal niche in temperate species are much closer to the their fundamental thermal niche as compared to the niches in tropical and sub-tropical species. Furthermore, *DTR* declines with increasing *TA* and *TS* (Figure 3 H; Supplementary Figure 3.9), implying that the difference between fundamental and realised thermal range is greatest among species with greater affinity to cold temperature and with higher degree of thermal specialisation. This trend could be explained by the reduced climate variability in lower latitude, constraining the species' realised thermal niche (Stuart-Smith et al., 2017) and physiological thermal niche (Addo-Bediako et al., 2000; Janzen, 1967; Sunday et al., 2011) in the tropics. In addition, the high biodiversity of marine phytoplankton in the tropics (Righetti et al., 2019) entails intensification of the biotic interaction in the tropical phytoplankton community, and hence may narrow the realised thermal niche in the tropics. Accordingly, the rates of biotic interactions and processes, or the rate of evolutionary diversification are higher in a warmer climate than the rates in a colder climate (Allen et al., 2002; Mittelbach et al., 2007). Several literature provide persuasive empirical evidence to support that thermal niche breadth increases with increasing latitude (Addo-Bediako et al., 2000; Stuart-Smith et al., 2017; Sunday et al., 2011). In spite of this, the generalisation of the relationship is still unclear mainly due to several analytical issues associated with macroecological studies (Blackburn and Gaston, 1998; Gaston et al., 2009).

3.4.3 Variation of thermal sensitivity, exposure and vulnerability to warming

Thermal sensitivity (S_{min} and S_{max}) is the proximity between species' physiological thermal limits (CT_{min} and CT_{max}, respectively) and the ambient temperature extremes it experiences in its local habitat (H_{min} and H_{max}). This can be used to infer species' thermal safety margin (*TSM*), a useful concept to understand global patterns of the vulnerability of ectotherms to warming (Bennett et al., 2019; Clusella-Trullas et al., 2011; Deutsch et al., 2008; Diamond et al., 2012; Huey et al., 2009; Sunday et al., 2014). A positive *TSM* ($CT_{min} < H_{min}$, hence $S_{min} < 0$; $CT_{max} > H_{max}$, hence $S_{max} > 0$) suggests that a species has a physiological thermal safety since the lower and upper tolerance limits are below the coldest temperature and above the warmest temperature it experiences, respectively. In contrast, a negative *TSM* ($CT_{min} > H_{min}$, hence $S_{min} > 0$; $CT_{max} < H_{max}$, hence $S_{max} < 0$) indicates that a species has to avoid the extreme temperatures or else it is at risk of thermal danger (Sunday et al., 2014). The results of the study show that S_{min} and S_{max} are generally below and above zero, respectively (Figure 3.4 A and B; Supplementary Figure 3.10 A and B), indicating positive *TSM*. Hence, the marine phytoplankton are generally living in the present climate scenario within the thermal safety zone.

Thermal sensitivity in marine phytoplankton varies across latitude (Figure 3.4 A and B; Supplementary Figure 3.10 A and B), which can be explained by the fact that species in the tropics are more exposed to warmer temperature as compared to temperate species that are more exposed to cold temperature. This suggests that temperate species have low cold safety margins and therefore they are at risk to live beyond the limit of their cold tolerance as compared to species in the tropics. On the other hand, the tropical species have low heat safety margins and hence they are more vulnerable to warming than the species thriving at higher latitudes (Clusella-Trullas et

al., 2011; Deutsch et al., 2008; Diamond et al., 2012; Huey et al., 2009). This is further supported by the latitudinal trend in warming vulnerability (Figure 3.4 D; Supplementary Figure 3.10 G – J), indicating that the local temperatures will surpass the physiological upper thermal limits in tropical species faster than the temperate species despite the warming rate is slower in the lower latitudes (Figure 3.4 C; Supplementary Figure 3.10 C – F).

Moreover, S_{min} is independent on species' thermal affinity (TA) but depends on the degree of their thermal specialisation (TS) (Figure 3.4 E). This suggests that the more specialist the species, the lower their physiological lower thermal limits relative to the coldest temperature they experience, regardless of their degree of affinity to warm and cold temperature. It can therefore be inferred that the specialists have higher cold safety margin than the generalist.

On the other hand, S_{max} is dependent on TA but not on TS (Figure 3.4 F), suggesting that the sensitivity to warm temperature is different between the cooler- and warmer-affinity species regardless of their degree of specialisation. This further implies that cooler-affinity species tend to have high physiological upper thermal limits relative to the highest temperature they experience in their local habitat as compared to that of the warmer-affinity species. Hence, species that have higher affinity to warm temperature have low heat safety margin, which makes them more vulnerable to warming. Contrary to expectations, this study is unable to find a clear effect of TA and TS on exposure and vulnerability to warming (Figure 3.4 G – H; Supplementary Figure 3.11 M – T). This result however is contingent on the climate scenarios and the composition of datasets.

3.4.4 Presence of phylogenetic signal in thermal attributes

This study also set out to assess the phylogenetic effect on the thermal attributes in marine phytoplankton such as the physiology- and occurrence-based thermal traits, their inequalities, thermal sensitivity, warming exposure, and warming vulnerability. This aim is attained by assessing the presence and strength of phylogenetic signal and/or phylogenetic conservatism using three approaches: (1) variance partitioning, (2) autocorrelation, and (3) Brownian motion model of evolution. Generally, the results provide support for the hypothesis that thermal attributes are more similar among closely related species than expected from a null model from the same phylogeny. However, the findings provide no clear evidence of the presence of phylogenetic conservatism in the thermal attributes. The implications of these findings and a number of caveats with respect to our analyses are discussed below.

The first approach is based on variance partitioning (*VP*) in which the phylogenetic pattern of thermal attributes is inferred from the significant difference between the observed variation within hierarchical taxonomic levels and the variation expected by the tip randomisation null models. There are several null models used to deduce phylogenetic patterns of traits (Krasnov et al., 2011; Machac et al., 2011; Silvertown et al., 2006; Waldron, 2007), however the explicit null models used for this hypothesis testing (i.e. tip randomization) remove any attribution to shared ancestry by randomly assigning species traits values across a given phylogeny (Loza et al., 2017). The findings reveal that the significant proportion of the variation in all thermal attributes is mainly explained by species, which generally exceeds the proportion of variance explained by supra-specific taxonomic levels. This suggests that the thermal attributes are most variable among species within genera with few notable exceptions (Figure 3.6; Supplementary Figure 3.15 – 3.17). Although the variation is largely explained by

species, the supra-specific taxonomic levels frequently explained more variation than expected by the tip randomisation null models. This indicates presence of phylogenetic signal in the physiology- and occurrence-based thermal traits, their inequalities, thermal sensitivity in marine phytoplankton. This study demonstrates the utility of variance partitioning across taxonomic levels in assessing the phylogenetic patterns of thermal attributes. However, this approach does not require a dated phylogeny nor assume any evolutionary model premises, hence this can only be used to test the phylogenetic signal and not phylogenetic conservatism.

The second approach is based on autocorrelation (AC) using Moran's I and Abouheif's C_{mean} indices. Moran's I index measures spatial autocorrelation (Moran, 1950, 1948), which later used to tests phylogenetic autocorrelation that relates cross-taxonomic trait variation to phylogeny (Gittleman and Kot, 1990). Whereas, Abouheif's C_{mean} index measures for serial independence (Abouheif, 1999), which is the mean value of a random subset of possible ways to represent the order of branches in a phylogenetic tree. Both indices are not under an assumption of evolutionary model and are not suited as an effect size measure. Since both are restricted to comparisons among different traits in the same phylogeny, the resulting values do not offer interpretation when comparing values between phylogenetic trees. However, the deviation from zero (i.e. null model) indicates the relationship between trait values in the same phylogeny (Münkemüller et al., 2012). The results of this study generally show the significant difference in the AC-based indices for physiology- and occurrence-based thermal traits from the null model, suggesting the presence of phylogenetic signal in the thermal traits. On the other hand, the findings generally suggest absence of phylogenetic signal in the inequality between physiology- and occurrence-based thermal traits, thermal sensitivity, and exposure and vulnerability to warming.

The third approach is based on the Brownian motion model of evolution (*BM*) using Blomberg's *K* and *K** and Pagel's λ indices. Blomberg's *K* and *K** expresses the strength of phylogenetic signal as a scaled ratio of observed distribution of tip data to expectations derived from a Brownian motion model of evolution (Blomberg et al., 2003). *K* uses the phylogenetically correct mean, whereas *K** uses the observed data on a star phylogeny with contemporaneous tips, but both indices are highly correlated (Blomberg et al., 2003). A *K* or *K** value close to 1 implies that relatives resemble each other more than expected under a Brownian motion model of evolution, whereas a value close to 0 indicates absence of phylogenetic conservatism (Blomberg et al., 2003). Similar to Blomberg's indices, Pagel's *λ* index operates under the assumption of Brownian evolution model in which it measures a scaling parameter for the correlations between species relative to the expected correlation (Pagel, 1999). A *λ* value close to 1 indicates that traits evolve under a Brownian model of evolution, whereas a value of 0 indicates no phylogenetic signal in the trait. Depending on the shape of phylogeny, *λ* value may exceed to 1 (Freckleton et al., 2002). Generally, the results of this study reveal no significant difference in the *BM*-based indices for the thermal attributes from the null model, suggesting the absence of phylogenetic signal in the thermal attributes. A notable exception is the patterns in physiology- and occurrence-based estimate of the lower thermal limits, which appear to have significant phylogenetic signal based on the *BM*-based indices. However, the detected phylogenetic signals are weak, suggesting the absence of phylogenetic conservatism in both the physiology- and occurrence-based estimate of the lower thermal limits.

These results however must be interpreted with caution because of the possible biases from the composition of the datasets. For instance, several *AC*-based indices show significant difference from the null model for traits in *CTMI*-derived dataset but not

in the published dataset. Another source of uncertainty is the estimate of the trait values

due to potential biases associated with physiology and occurrence data (Boyd et al.,

2013; Isaac and Pocock, 2015; Low-Décarie et al., 2017; Salvador et al., 2019) as

described earlier. Furthermore, there is also a potential bias form the estimates of the

phylogeny since indices and tests for phylogenetic signals are dependent on tree

topologies (Blomberg et al., 2003; Freckleton et al., 2002, 2011; Ives et al., 2007; Rohlf,

2001). The findings may be somewhat limited by the genetic information used to

reconstruct phylogeny and to estimate the divergence time of major taxon in

phytoplankton.

3.5 CONCLUSIONS

The present study examines the global pattern of the congruence between

physiology- and occurrence-based thermal traits, thermal sensitivity, and exposure and

vulnerability to warming in marine phytoplankton. To our knowledge, this has been one

of the first attempts to thoroughly investigate the biogeographic and phylogenetic

patterns of these thermal attributes in marine phytoplankton. Key findings in this study

are summarised as follows: (1) physiology- and occurrence-based thermal traits are

congruent but not equal, (2) the inequality between these traits and thermal sensitivity

vary across latitude, thermal affinity, thermal specialisation, (3) exposure and

vulnerability to warming vary non-monotonously with latitude, (4) interspecific variation

in thermal attributes is evident, and (5) phylogenetic signals are present, but no clear

evidence of the presence of phylogenetic conservatism in the thermal attributes. The

study has identified emerging patterns of thermal attributes in marine phytoplankton,

contributing to our understanding of how these species respond to climate change.

CHAPTER 4

This page is intentionally left blank.

92

TEMPERATURE DEPENDENCE OF GROWTH IN NON-TOXIC AND TOXIC MARINE PHYTOPLANKTON

ABSTRACT

Toxic algal blooms appear to expand globally and their duration, frequency, and intensity may increase in response to climate change. Hence, it is important to assess the effect of temperature on growth in marine phytoplankton. This present study examined the temperature dependence of the growth in non-toxic and toxic marine phytoplankton. Using strains of dinoflagellates, growth rates were measured along a wide temperature gradient to estimate the maximum growth rates and thermal traits. The data obtained from this study were supplemented with datasets compiled from published laboratory culture experiments to allow comparison with an adequate number of observations. The results revealed no difference in the (i) temperature dependence of growth, (ii) thermal traits, (iii) relationship between maximum growth rates and thermal traits, (iv) trait-environment relationship, and (v) thermal safety and vulnerability between non-toxic and potentially toxic phytoplankton. These findings improve our current knowledge on the growth in marine phytoplankton in response to temperature, advancing our ability to predict toxic blooms in response to ongoing climate change.

4.1 INTRODUCTION

Phytoplankton are ecologically important as primary producers and biological carbon pump regulators (e.g. Behrenfeld et al., 2006; Falkowski, 2012; Falkowski and Oliver, 2007). However, some phytoplankton species may form harmful algal blooms (HAB) that are a global problem due to the production of toxins that pose a risk to public health, the environment, and our economy (Berdalet et al., 2015). Toxic blooms are already a global problem and their current distribution is alarming. Climate change may provide favourable conditions for toxic algae to occur (Hallegraeff, 2010). It is likely that toxic blooms and their impacts may be exacerbated in the future where their duration, intensity, and frequency may increase in response to changes in the climate (Moore et al., 2008; Tatters et al., 2013). The well-documented effects of toxins to humans and to other organisms (Berdalet et al., 2016) and the potential effect of climate change on toxic blooms in the future (Fu et al., 2012) have stimulated studies on the ecophysiology of toxic phytoplankton (e.g. Kellmann et al., 2010a; Perini et al., 2014; Ramsey et al., 1998; Stüken et al., 2011). Hence, it is crucial to be able to assess the sensitivity of HAB species to changes in the temperature, which is projected to increase under climate change (IPCC, 2013).

Temperature is one of the most fundamental abiotic factors that influence the niche of phytoplankton (Boyd et al., 2013; de Boer et al., 2004). Increasing temperature enhances growth until it reaches the optimal temperature, whilst elevated temperature beyond the optimal decreases growth and can be lethal. These thermal responses characterise the typical asymmetry of the growth-temperature curve, with an asymptotic increase on the colder side, and an abrupt decline on the warmer side (Ras et al., 2013). The influence of temperature on physiological processes in phytoplankton is

mainly driven by the kinetics of enzymes. One important temperature-sensitive enzyme is ribulose-1,5-bisphosphate (Rubisco) with carboxylase and oxygenase activity that catalyzes two competing biochemical reactions - photosynthesis and photorespiration, respectively (Hikosaka et al., 2005). Modification of Rubisco activity is one of the acclimation strategies of phytoplankton in response to changes in temperature. Some phytoplankton species that are acclimated to low temperature reduce Rubisco carboxylase activity to decrease the energy transfer efficiency between the antennae and photosystem II (PS II) reaction centers and consequently prevent photoinhibition (Krol et al., 1997; Levasseur et al., 1990; Maxwell et al., 1994), whilst others enhance this enzymatic activity to ensure the utilization of excess energy and increase photosynthetic rates (Mortain-Bertrand et al., 1988). Phytoplankton that grow beyond the optimal growth temperature inactivates or denatures their photosynthetic enzymes that unbalances ATP consumption and production, and eventually affects photosynthesis, respiration and growth (Raven and Geider, 1988). Furthermore, adaptation to varying temperature for growth in phytoplankton involves changes in the quantity of enzymes, light-harvesting pigments and thylakoid membrane integrity (Raven and Geider, 1988).

Several non-linear models have been used to describe the growth response to temperature (Low-Décarie et al., 2017; Rosso et al., 1993). These models are also used to predict the maximum growth rate (r_{max}) and the thermal traits such as the (i) the cardinal temperatures that corresponds to the boundaries of thermal tolerance (i.e. thermal optima (T_{opt}), critical thermal minima (CT_{min}), and critical thermal maximum (CT_{max}), and (ii) the fundamental thermal niche breadth (*FTN*) that correspond to the thermal range on which a species can physiologically tolerate. This temperature range is species-specific that reflects the physiological plasticity of species in response to

changes in temperature (de Boer et al., 2004). The relationship between the maximum growth rate of phytoplankton and temperature is initially described by an exponential envelope function (Eppley, 1972), which the "hotter is better" hypothesis is based on. Under this hypothesis, the maximum growth rate is expected to be greater at higher optimal temperature. However, several works have challenged the validity of this hypothesis (Bissinger et al., 2008; Brush et al., 2002). Several studies have examined the effect of temperature on phytoplankton growth rate (Thomas et al., 2012), but the differences in the temperature-growth relationship between non-toxic and toxic phytoplankton species is understudied. Understanding the effect of temperature on growth in non-toxic and toxic marine phytoplankton is crucial in predicting the biogeography of harmful blooms in future climate scenarios.

To improve our understanding on the effect of temperature on the growth of the phytoplankton, this chapter sets out to determine whether non-toxic and potentially toxic marine phytoplankton exhibit variation in (i) temperature dependence of growth, (ii) maximum growth rates and thermal traits, (iii) relationship between maximum growth rates and thermal traits, (iv) trait-environment relationship, and (v) thermal safety and vulnerability. It is hypothesized that there will be no significant variation in these responses between the toxicity of marine phytoplankton. To test this hypothesis, plate-based and tube-based growth experiments were conducted to determine the growth response of non-toxic and potentially toxic strains of phytoplankton. The data obtained from these experiments were supplemented with the datasets compiled from laboratory culture experiments to allow comparison with an adequate number of observations. The variation in these responses were then examined across strain identity, toxicity, and experiments.

4.2 MATERIALS AND METHOD

4.2.1 Test organisms

Six cultures of dinoflagellate strains were obtained from different culture collections (Table 4.1). They are ecologically relevant organisms belonging to the phytoplankton genera that make up the majority of the toxic bloom-forming species, i.e. *Prorocentrum* and *Alexandrium* (Abdenadher et al., 2012; Ben-Gharbia et al., 2016; Grzebyk et al., 1997; Quilliam et al., 1996; Vlamis et al., 2015). Three of the strains are listed as "toxic" from their respective culture collections but only one strain was detected for the presence of toxins (e.g. okadaic acid (*OA*) and dinophysistoxins (*DTX1 and DTX2*)), henceforth all of these strains were referred as potentially toxic. Another three strains congeneric to the potentially toxic strains were non-toxic. To minimise the effect of the differences in source's culture conditions, all strains were maintained in 35 mL batch cultures in artificial seawater (*ASW*) (Berges et al., 2001) enriched with *K* minimum nutrients (Keller et al., 1987). Cultures were regularly transferred to a fresh *K* medium to maintain the exponential growth. The cultures were not axenic. To minimize contamination, all *ASW* and *K* media were autoclaved, and all transfers were performed in a class II biosafety cabinet. The batch cultures were maintained at a constant temperature of 15°C and under a 12:12 hour light-dark cycle at a mean light intensity (± standard error) of 221 ± 12, measured using a light meter (Li-Cor Li-250A). They were allowed to grow at this condition for at least four transfers prior to experimental procedures.

Table 4.1. Information on the identity, origin, culture condition, and toxicity of experimental organisms obtained from different culture collections.

Experimental Organism	Origin	Source's culture condition	Toxicity
Prorocentrum sp. (NRR 188) *	Maintained at University of Essex culture collection; Information on isolate's origin is not available.	Medium: f/2 in natural sea water (*NSW*) Temperature: 15 °C Light intensity: 100 µmol m^{-2} s^{-1}	non-toxic
Prorocentrum micans (CCAP 1136/15)	Isolated at Lynn of Lorne, Argyll, Scotland, UK; maintained at Culture Collection of Algae and Protozoa (*CCAP*) at the Scottish Association for Marine Science (*SAMS*)	Medium: L1 in *NSW* Temperature: 15 – 20 °C Light intensity: 30 – 40 µmol m^{-2} s^{-1}	non-toxic
Alexandrium tamutum (PARALEX 242)	Isolated at Kerloc'h, Dinan, English Channel, France; maintained at Roscoff Culture Collection (ID: RCC 3034)	Temperature: 19 °C Light intensity: 100 µmol m^{-2} s^{-1}	non-toxic
Prorocentrum minimum (Poulet)	Maintained at *RCC* (ID: RCC 291); Information on isolate's origin is not available.	Medium: K in *NSW* Temperature: 20 °C Light intensity: 100 µmol m^{-2} s^{-1}	potentially toxic
Prorocentrum lima (CCAP 1136/11)	Isolated from Vigo, Spain; maintained at CCAP at SAMS	Medium: L1 in *NSW* Temperature: 15 – 20 °C Light intensity: 30-40 µmol m^{-2} s^{-1}	potentially toxic*
Alexandrium minutum (PARALEX 246)	Isolated from Britanny coast, English Channel, France; maintained at RCC (ID: RCC 2649)	Medium: f/2 in NSW Temperature: 18 °C Light intensity: 100 µmol m^{-2} s^{-1}	potentially toxic

* The he species name needed to be confirmed.
** Lipophilic toxins (e.g. okadaic acid (*OA*) and dinophysistoxins (*DTX1 and DTX2*)) were detected in the samples.

4.2.2 Growth experiments

Plate- and tube-based experiments (Figure 4.1; Table 4.2**)** were designed to examine the growth of non-toxic and toxic marine phytoplankton across a wide range of temperature.

Table 4.2. Description of the experimental design in plate- and tube-based experiments.

Experimental design	Plate-based experiments		Tube-based experiments	
Growth conditions	*Chamber 1*	*Chamber 2*		
Air temperature	10°C	20°C	20°C	
Relative humidity	80%	80%	80%	
Light:dark cycle (hours)	12:12	12:12	12:12	
Light intensity (μmol m^{-2} s^{-1})	268 ± 11	257 ± 13	251 ± 10	
Thermal gradient				
Temperature range	7.1– 18.6 °C	16.8 – 35.1°C	5 – 30 °C	
Stepwise variation	0.7 °C	1.0 °C	5.0 °C	
Samples	3 replicates of 2 mL per culture per well		3 replicates of 40 mL per culture per tube	
Incubation			*1st tube-based experiment*	*2nd tube-based experiment*
Stepwise acclimatisation	No		No	Yes
Incubation period	9 days		16 days	28 days
Growth measurement	Optical density at 660 nm		Fluorescence	

4.2.2.1 Plate-based experiments

In the plate-based experiments, temperature gradient was maintained using thermoblocks that were housed in separate growth chambers (Conviron Adaptis CMP6010) with similar growth conditions, except for the air temperature which needed to be different in order to achieve the desired thermal gradient. Each of the thermoblocks were custom-made metal blocks that were temperature-regulated wih flow-through fluid. The temperature gradient of the thermoblock was regulated by the flow of fluid to an external cooling or heating device connected via insulated flexible PVC hoses. At one end of the block, a water bath chiller was used as a cooling device to circulate antifreeze fluid. Whereas, a water bath was used as a heating device to circulate distilled water at the other end of the block. Temperature set points for external cooling and heating devices are adjusted to attain the desired temperature gradient and stepwise variation in each thermoblock (Table 4.2).

To determine the thermal growth response in each experimental organism, three replicates of 0.2 mL of each of the culture were inoculated into 1.8 mL *K* medium in each well of the first three rows of the 24-well microplates. Wells in the last row were inoculated with *K* medium to serve as blank. Algal cells in the microplates were incubated in the above mentioned plate-based thermoblocks for nine days. The microplates were covered with lids with pores that sheathed with polyvinylidene chloride gas-permeable membranes to ensure gas exchange during the incubation period and were removed aseptically every growth measurement.

Growth rates were quantified from the changes in cell density that were estimated from the optical density (*OD*) measured daily (between 14:00 to 16:00) for nine days using a FLUOstar Omega spectrophotometer (BMG Labtech, Germany) with the following endpoint protocol settings: excitation of 660 nm that corresponds to the long wavelength absorption peak of chlorophyll *a*, horizontal bidirectional reading (start top left), and a shaking with frequency of 400 rpm for 60 seconds before plate reading to homogenize the sample.

OD values were blank corrected and were pre-processed to detect outliers prior to regression analyses. A total of 324 triplicated observations (36 assay temperatures x 9 days) for every experimental organism were obtained and were quality controlled. The data were trimmed to capture growth within the exponential phase. These pre-processed data were used subsequently in the regression analyses to estimate the growth rates.

4.2.2.2 Tube-based experiments

Tube-based experiments were performed inside a growth chamber with conditions described in Table 4.2. The thermal gradient in these experiments ranged

from 5°C to 30°C at 5°C stepwise variation. Each assay temperature was maintained inside a glass water-jacketed bath using circulating distilled water. The temperature of the circulated distilled water was regulated by external recirculating water baths connected via flexible PVC hoses.

Triplicates of 4 mL of each of the culture were inoculated into 36 mL *K* medium contained in 50 mL glass test tubes. The tubes were capped with autoclaved foam stoppers to allow gas exchange during the incubation period. Algal cells in the test tubes were incubated in the above-mentioned temperature regulated water-jacketed bath. Two tube-based experiments were performed. In the first experiment, the cells were incubated for 16 days without a stepwise acclimatisation. Whilst in the second experiment, the strains were allowed to acclimatise to a new thermal condition for 14 days prior the incubations to another 14 days of incubation.

Growth of the cultures were determined using in *in vivo* fluorescence as a proxy for phytoplankton biomass, which was measured daily (between 14:00 to 16:00) using a Turner Designs Trilogy Fluorometer. Prior to the fluorescence measurement, each culture in a test tube was homogenised using a vortex mixer. The test tube was subsequently placed in the fluorometer and a fluorescence reading was obtained. The estimated fluorescence in all samples was corrected with the fluorescence in a blank sample (i.e. 0.04). The corrected estimates of fluorescence were used to compute for the growth rates as described in the section below.

A. Plate-based experimental design

A1. Without stepwise acclimatisation   A2. Thermal gradient and set up
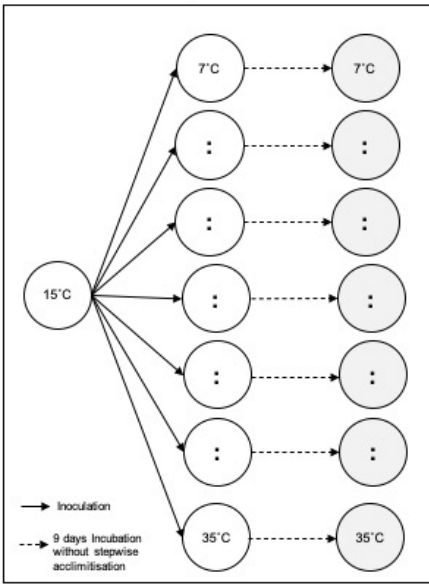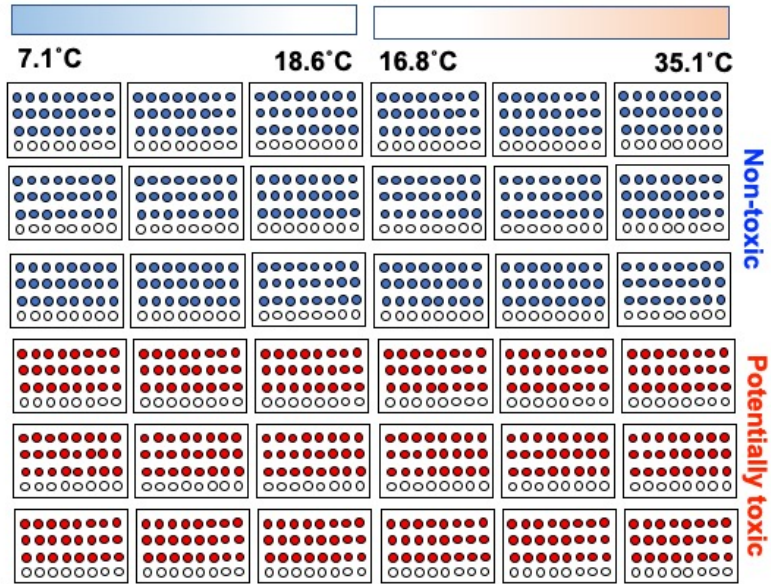
B. Tube-based experimental design

B1. Thermal gradient and set up
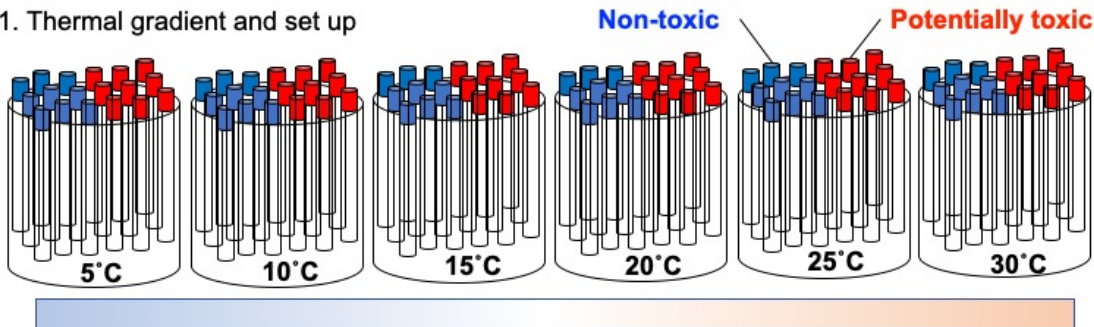
B2. Without stepwise acclimatisation   B3. With stepwise acclimatisation
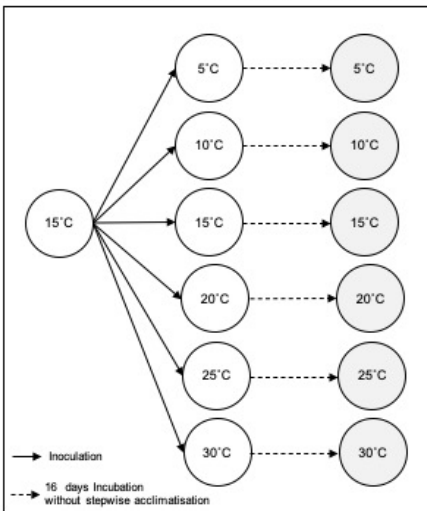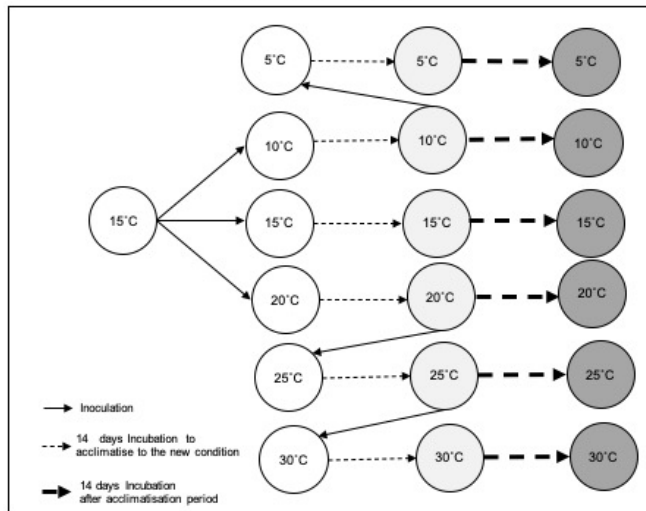
Figure 4.1. Schematic representation of the plate- and tube-based experimental designs to examine effect of temperature on growth and toxin production in marine phytoplankton.

4.2.3 Determination of growth rates and thermal attributes

Natural log of *OD* or the fluorescence estimates were fitted against time in a linear model to estimate the growth rate (Supplementary Figure 4.1 – 4.4). Only the positive growth rates were included in the subsequent analysis. The growth rates were fitted against temperature in a unimodal response curve using the different non-linear functions (i.e. equ04 – equ15 in the R package *temperatureresponse* (Low-Décarie *et al.* 2017) and Cardinal Temperature Model with Inflexion (*CTMI*; equ16) (Rosso et al., 1993)) presented in Table 4.3. The fitting of all equations was implemented in *R* version 3.6.1 (R Core Team, 2019).

A modified Levenberg–Marquardt algorithm was used for robust fitting of non-linear equations to data (Low-Décarie *et al.* 2017). The starting values were estimated from the dataset when the equation parameter values represent features of the dataset, otherwise the starting values for the parameters were derived the fitted parameters from the source publication of equation or were set to ensure a downward parabola-like shape. Equations were ranked on each dataset using Bayesian information criterion (BIC). Similar results of the ranking of equations was observed when other measures of model quality were used such as Akaike information criterion (AIC) and the AIC corrected for finite sample sizes (AICc).

Table 4.3. List of equations used to fit growth rates (*r*) against temperature (*T*) (adapted from Low-Décarie *et al.* 2017 and Rosso et al., 1993).

ID	Formula
equ04	$r = a \cdot exp\left(\frac{-b}{R \cdot T}\right) - c \cdot exp\left(\frac{-d}{R \cdot T}\right)$
equ05	$r = \dfrac{a \cdot T \cdot exp\left(\frac{-b}{R \cdot T}\right)}{1 + exp\left(\frac{-c}{R}\right) \cdot exp\left(\frac{-d}{R \cdot T}\right)}$
equ06	$r = \dfrac{a \cdot \left(\frac{T}{298.15}\right) \cdot exp\left(\frac{b}{R} \cdot \left(\frac{1}{298.15} - \frac{1}{T}\right)\right)}{1 + exp\left[\frac{c}{R} \cdot \left(\frac{1}{d} - \frac{1}{T}\right)\right] + exp\left[\frac{e}{R}\left(\frac{1}{f} - \frac{1}{T}\right)\right]}$
equ07	$r = \dfrac{a \cdot \left(\frac{T}{293.15}\right) \cdot exp\left(\frac{b}{R} \cdot \left(\frac{1}{293.15} - \frac{1}{T}\right)\right)}{1 + exp\left[\frac{c}{R} \cdot \left(\frac{1}{d} - \frac{1}{T}\right)\right]}$
equ08	$r = a \cdot exp\left[-0.5 \cdot \left(\frac{[T - T_{ref}]}{b}\right)^2\right]$
equ09	$r = a \cdot exp\left[-0.5 \cdot \left(\frac{abs[T - T_{ref}]}{b}\right)^c\right]$
equ10	$r = a \cdot exp(c \cdot T)\left[1 - \left(\frac{T - T_{ref}}{b}\right)^2\right]$
equ11	$r = a + b \cdot T + c \cdot T^2$
equ12	$r = \dfrac{1}{1 + (a + b \cdot T + c \cdot T^2)}$
equ13	$r = [a \cdot (T - CT_{min})]^2 \cdot \left[1 - exp\left(b \cdot (T - CT_{max})\right)\right]^2$
equ14	$r = a \cdot \{1 - exp[-b \cdot (T - CT_{min})]\} \cdot \{1 - exp[-c \cdot (CT_{max} - T)]\}$
equ15	$r = r_{max} \cdot \left\{sin\left[\pi \cdot \left(\frac{T - CT_{min}}{CT_{max} - CT_{min}}\right)^a\right]\right\}^b$
equ16	$\begin{cases} r = 0 \;, if\; T < CT_{min} \\ r = r_{max} \cdot \theta, if\; CT_{max} \leq T \leq CT_{max} \\ r = 0 \;, if\; T > CT_{max} \end{cases}$

with:

$$\theta = \frac{(T - CT_{max}) \cdot (T - CT_{min})^2}{(T_{opt} - CT_{min}) \cdot [(T_{opt} - CT_{min}) \cdot (T - T_{opt}) - (T_{opt} - CT_{max}) \cdot (T_{opt} + CT_{min} - 2T)]}$$

under the condition:

$$T_{opt} > \frac{CT_{min} + CT_{max}}{2}$$

Abbreviations: *a – f* are the model coefficients; *R* is the universal gas (Boltzmann) constant; T_{ref} is reference temperature; CT_{min} is the critical thermal minimum; CT_{max} is the critical thermal maximum; T_{opt} is the thermal optimum; r_{max} is the maximum growth rate.

These non-linear models were used to estimate the following thermal traits: (1) the maximum growth rate (r_{max}, d^{-1}; the highest growth rate within the temperature range), (2) the cardinal temperatures such as the thermal optimum (T_{opt},°C) ; temperature that corresponds to r_{max}), critical thermal minimum (CT_{min},°C; the lowest temperature at which no positive growth), and critical thermal maximum (CT_{max},°C; the highest temperature at which no positive growth), and (3) the fundamental thermal niche breadth (*FTN*,°C; the width of the temperature range). The skewness of the curve was also calculated as the difference between activation and deactivation rates, which were derived from the mean of value of the derivative across sub- (CT_{min} to T_{opt}) and supra- (T_{opt} to CT_{max}) optimal temperatures, respectively. The skewness was used as a measure of asymmetry of the thermal growth curve. A positive skew indicates activation is steeper than deactivation, whereas a negative skew indicates that deactivation is steeper than activation.

Thermal sensitivity, exposure and vulnerability to warming were also calculated as described in Chapter 3. Longitude and latitude coordinates were approximated based on the isolation location of the strains. These coordinates were used to

determine the sea surface temperature (*SST*) of the coldest and warmest months from

2000 to 2014, which were downloaded from *Bio-ORACLE* (Assis et al., 2018).

The *SST* were used to represent the ambient temperature extremes that the

strains experience in their local habitats (H_{min} and H_{max} in °C, respectively). The

difference between a strain's critical thermal limits (CT_{min} and CT_{max}) and the

temperature extremes it experiences represent its sensitivity to cold and warm

temperature (S_{min} and S_{max} in °C, respectively) (Bennett et al., 2019). The thermal

sensitivity was used to infer species' thermal safety margin (*TSM*). A positive *TSM*

($CT_{min} < H_{min}$, hence $S_{min} < 0$; $CT_{max} > H_{max}$, hence $S_{max} > 0$) suggests that a species

has a physiological thermal safety, whereas a negative *TSM* ($CT_{min} > H_{min}$, hence $S_{min} >$

0; $CT_{max} < H_{max}$, hence $S_{max} < 0$) indicates that a species has to avoid the extreme

temperatures or else it is at risk of thermal danger (Sunday et al., 2014). Warming

vulnerability (*V*, year) describes the number of years prior the local temperatures are

expected to exceed CT_{max} in a given location (Bennett et al., 2019). This was calculated

by dividing the species' sensitivity to warm temperature (S_{max}) by the warming rate (*WR*,

°C per year) it experiences in a given location. *WR* was derived from the slope of SST

of the warmest month between the contemporary and future climate scenarios (i.e. SST

predicted in 2050 and 2010 based on *RCP 2.6*, *RCP 4.5*, *RCP 6.0*, and *RCP 8.5*, which

were also downloaded from *Bio-ORACLE* (Assis et al., 2018)). Thermal sensitivity,

exposure and vulnerability to warming in *Prorocentrum minimum* strains were not

determined because their isolation locations were unknown.

To obtain an adequate number of observations, this study was supplemented

with the dataset from the published experimental results on marine phytoplankton

growth rates across temperature (Litchman and Klausmeier, 2014; Thomas et al., 2016,

2012). The species in the dataset that were listed in the IOC-UNESCO Taxonomic

Reference List of Harmful Micro Algae (Moestrup et al., 2009) were categorised as potentially toxic, otherwise they are categorised as non-toxic. Out of 545 phytoplankton strains/isolates in the dataset, 74 of which represent 25 potentially toxic species and about 20% belong to the same taxonomic class as the experimental organisms in this study.

However, only few of the temperature-growth relationships in these potentially toxic strains (not more than 14) were successfully fitted by the non-linear models. In Chapter 3, *CTMI* was preferably used in the analysis since this model yielded more realistic estimates of the cardinal temperatures from the published experimental data. Out of the 18 temperature-growth relationships expected in each of the experiments in this study, 80 to 90% of these relationships in the tube-based experiments were successfully fitted by *CTMI*, whilst only 40% in the plate-based experiments.

In this study, the variations in traits across different models were observed (Supplementary Figure 4.5). To simplify the results, model averaging was used to estimate the mean trait values were across models weighted by BIC median rank.

In this study, all temperature growth models were used, and the variation by these models was explored as described in the next section. All estimates derived from this study and published experimental data were pooled into one dataset. This dataset was curated to exclude unrealistic estimates of thermal traits with the following inclusion criteria (1) r_{max} within 0.01 to 3.00 d^{-1}range, and (2) cardinal temperatures within the -7 to 40 °C range.

4.2.4 Data processing and analyses

Generalised linear mixed models (*GLMM*) were used to analyse the variation using the *glmer* function in lme4 package implemented in *R* version 3.6.1 (R Core Team, 2019). All the GLMM were compared to a null model using likelihood ratio (*LR*) test to determine the significance of a single factor by comparing the fit for models with and without the factor. Coefficient of determination for each model was estimated to describe the proportion of variance explained by the fixed factor alone (i.e. mariginal R^2) and by both the fixed and random factors (i.e. conditional R^2) (Nakagawa and Schielzeth, 2013). These statistics were implemented as described below.

To analyse the variation in the maximum growth rates, thermal traits, thermal sensitivity, and warming vulnerability (collectively known as response variables), the fixed and random effects of strain identity, toxicity, and source of experimental data were determined. Specifically, (1) variation in a response variable across phytoplankton strains was analysed whilst taking into account the random effects of toxicity and experiments, i.e. glmer(response ~ strain identity + (1|toxicity) + (1|experiments),data); (2) variation in a response variable between non-toxic and potentially toxic species was analysed whilst taking into account the random effects of strain identity and experiments, i.e. glmer(response ~ toxicity + (1|strain identity) + (1|experiments),data); and (3) variation in a response variable across the experiments (fixed effect) was analysed whilst taking into account the random effects of strain identity and toxicity, i.e. glmer(response ~ experiments + (1|strain identity) + (1| toxicity),data).

To examine the relationships between the maximum growth rates (r_{max}) and thermal traits (i.e. T_{opt}, CT_{min}, CT_{max}, and *FTN*), the fixed effect of a thermal trait on r_{max} was examined whilst taking into account the random effects of strain identity, toxicity

and experiments with following structure: glmer(r_{max} ~ thermal trait + (1|strain identity) +

(1|toxicity) + (1|experiments),data).

To examine the trait-environment relationships, the fixed effect of the

environmental temperature (e.g. mean, minimum, maximum, and range of SST) on the

thermal trait (e.g. T_{opt}, CT_{min}, CT_{max}, and *FTN,* respectively) was examined whilst taking

into account the random effects of strain identity, toxicity and experiments with following

structure: glmer(thermal trait ~ environmental temperature + (1|strain identity) +

(1|toxicity) + (1|experiments),data).

4.3 RESULTS

4.3.1 Growth across temperature

Growth rates of non-toxic and potentially toxic marine phytoplankton exhibited

sensitivity to temperature as observed in plate- and tube-based experiments (Figure

4.2). Generally, the growth rate had increased gradually with temperature until it

reached its peak at the optimal temperature, and it decreased substantially with further

increase in temperature. The shapes of the thermal performance curves varied

considerably from a more asymmetric for potentially toxic *P. minimum* and *A. minutum*

to a nearly symmetric response for *P. lima*. In tube-based experiments, the growth

response across temperatures below the optimal temperature was found to vary among

species from a more linear trend in potentially toxic *P. minimum* to a more non-linear

pattern in non-toxic *Prorocentrum* spp. Also, the asymmetric shape was more evident

from the thermal performance curves obtained from the tube-based experiments.
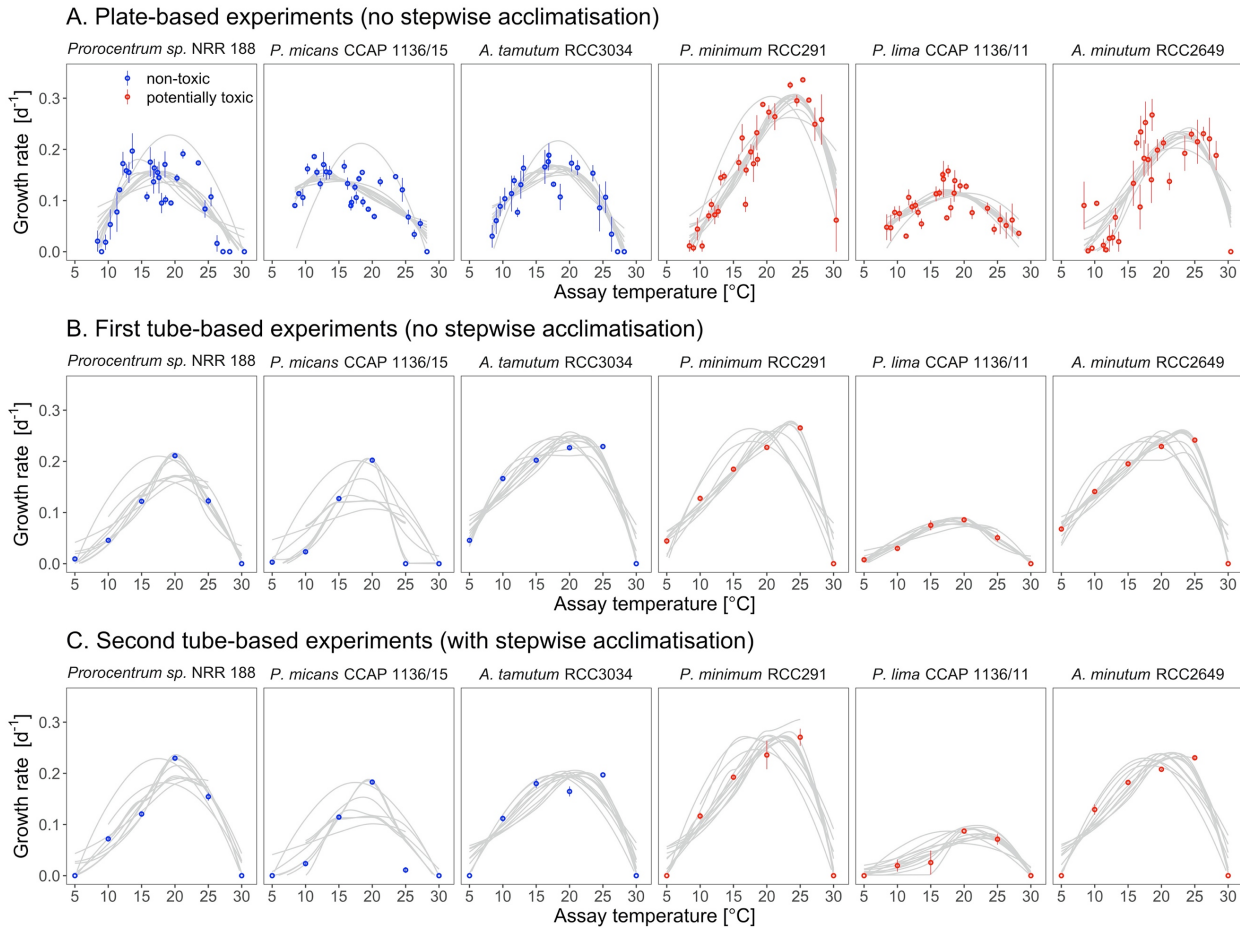
Figure 4.2. Growth rates in non-toxic and potentially toxic strains of marine phytoplankton across temperature obtained from plate-based experiments (*PB*) and tube-based experiments without and with stepwise acclimatisation (*TB1* and *TB2*, respectively). Each data point shows the mean growth rate with standard error as error bars. The grey solid lines denote all the non-linear models fitting growth rate against temperature.

4.3.2 Variation in maximum growth and thermal traits

4.3.2.1 Maximum growth rate

Dinoflagellate strains exhibit significant variation in maximum growth rates (r_{max}) ($\chi^2_{(1, N = 54)}$ = 74.39, p < 0.05) (Figure 4.3). *P. lima* had the lowest r_{max} (0.11 $\pm$ 0.03 d^{-1}), whilst potentially toxic *P. minimum* had the highest r_{max} (0.28 $\pm$ 0.03 d^{-1}). Variation in r_{max} between non-toxic (0.18 $\pm$ 0.04 d^{-1}) and potentially toxic (0.21 $\pm$ 0.09 d^{-1}) dinoflagellate strains was not significant ($\chi^2_{(1, N = 54)}$ = 0.46, p > 0.05). The mean r_{max} in plate-based experiment was 0.19 $\pm$ 0.02 d^{-1}, whereas the mean r_{max} in tube-based experiments

without and with stepwise acclimatisation were both 0.20 ± 0.04 d^{-1}. No significant variation in r_{max} was observed across experiments ($\chi^2_{(1, N = 54)} = 1.22$, p > 0.05).
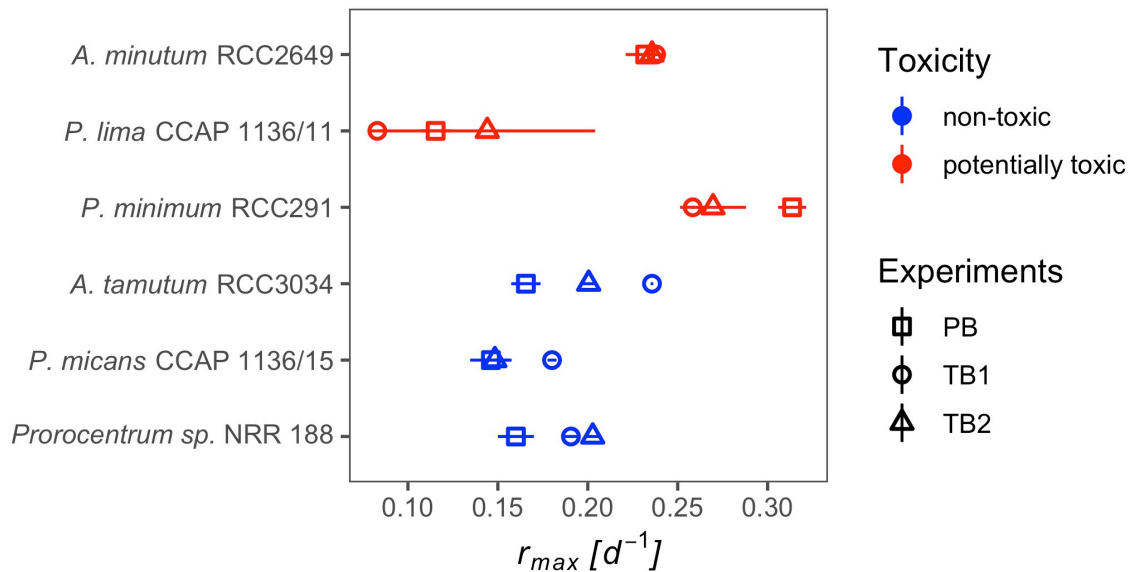
Figure 4.3. Variations in the mean growth rates (r_{max}, d^{-1}) across non-toxic and potentially toxic dinoflagellates strains estimated across different experiments (PB, TB1, and TB2 refers to plate-based experiments and tube-based experiments without and with stepwise acclimatisation, respectively). Each point indicates a mean estimate with error bar showing the standard error of the mean.

4.3.2.2 Thermal optimum

There was a significant variation in the mean thermal optimum (T_{opt}) across dinoflagellates strains ($\chi^2_{(1, N=54)} = 37.86$, p < 0.05) (Figure 4.4). On average, T_{opt} in *P. micans* was lowest (16.45 ± 3.10 °C) among the strains. On the other hand, mean T_{opt} in potentially toxic *P. minimum* was highest among strains (23.16 ± 2.13 °C). Mean T_{opt} in potentially toxic strains was 21.60 ± 2.57 °C, which 3.06 ± 1.46 °C higher than the mean T_{opt} in non-toxic strains (18.54 ± 1.11 °C) ($\chi^2_{(1, N=54)} = 4.3$, p < 0.05). There was a significant variation in mean T_{opt} across experiments ($\chi^2_{(1, N=54)} = 7.81$, p < 0.05). Mean T_{opt} obtained in plate-based experiment was 19.14 ± 1.57 °C, which was 1.28 and 1.51 °C higher than estimates from tube-based experiments. Mean T_{opt} obtained in tube-based experiment without acclimatisation (20.42 ± 2.14 °C) was lower compared to the

average estimate obtained in tube-based experiment with acclimatisation (20.65 ± 2.14 °C).
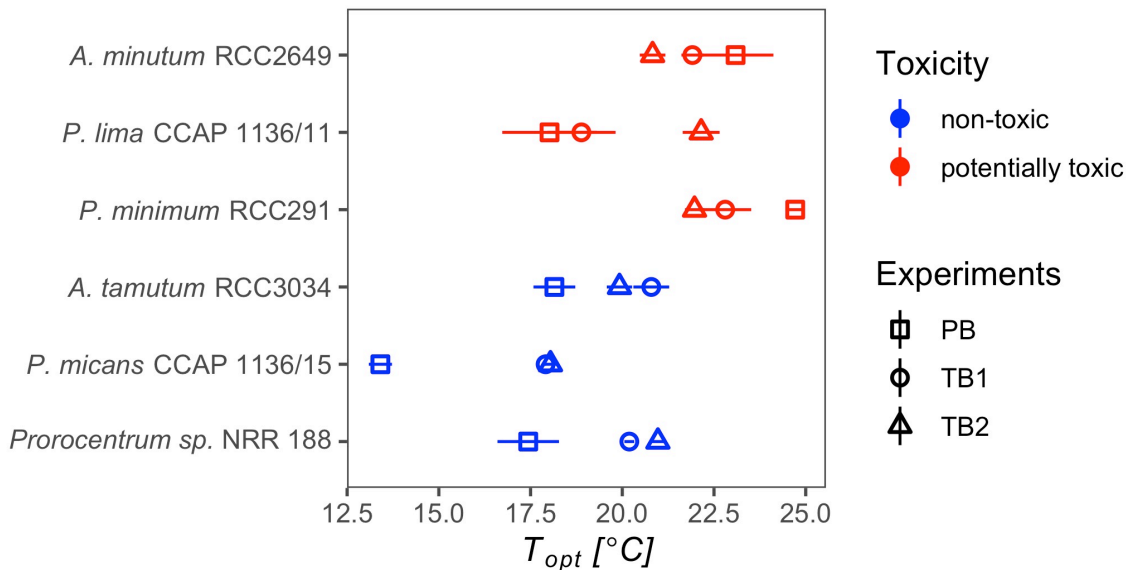
Figure 4.4. Variations in the mean thermal optimum (T_{opt}, °C) across non-toxic and potentially toxic dinoflagellates strains estimated across different experiments (PB, TB1, and TB2 refers to plate-based experiments and tube-based experiments without and with stepwise acclimatisation, respectively). Each point indicates a mean estimate with error bar showing the standard error of the mean.

4.3.2.3 Critical thermal minimum

The mean critical thermal minimum (CT_{min}) did not vary across strains ($X^2_{(1, N=54)}$ = 1.25, p > 0.05) (Figure 4.5). Average CT_{min} in dinoflagellate strains ranged from 4.27 °C to 5.1 °C. Also, the mean CT_{min} did not differ significantly between non-toxic ($4.59 \pm$ 0.60 °C) and potentially toxic dinoflagellates (4.56 ± 1.08 °C) ($X^2_{(1, N=54)}$ = 0.0033, p > 0.05). However, the variation in mean CT_{min} across the experiments was significant ($X^2_{(1, N=54)}$ = 8.78, p < 0.05). Average CT_{min} estimated from plate-based experiments was 5.61 ± 0.43 °C, which was 1.70 °C and 1.40 °C higher than the mean estimates from the tube-based experiments. Mean T_{opt} obtained in tube-based experiment without acclimatisation (3.91 ± 1.03 °C) was lower than the average estimate obtained in tube-based experiment with acclimatisation (4.21 ± 1.03 °C).
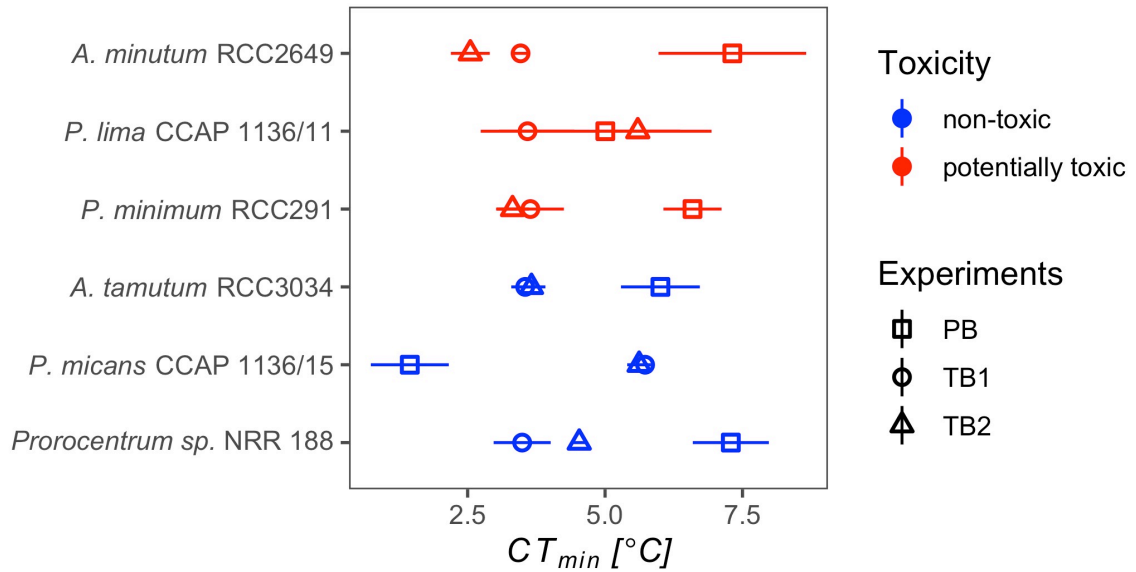
Figure 4.5. Variations in the critical thermal minimum (CT_{min}, ℃) across non-toxic and potentially toxic dinoflagellates strains estimated across different experiments (PB, TB1, and TB2 refers to plate-based experiments and tube-based experiments without and with stepwise acclimatisation, respectively). Each point indicates a mean estimate with error bar showing the standard error of the mean.

4.3.2.4 Critical thermal maximum

Significant variation in the mean critical thermal maximum (CT_{max}) across dinoflagellate strains was found ($X^2_{(1,\ N=54)}$ = 11.19, p < 0.05) (Figure 4.6).   On average, *A. minutum* had higher CT_{max} (30.80 ± 0.50 °C) than the estimates in other strains, with difference ranging between 0.06 °C and 1.17 °C. There was also a significant variation in the mean CT_{max} between non-toxic and potentially toxic dinoflagellates ($X^2_{(1,\ N=54)}$ = 4.02, p < 0.05). Potentially toxic strains had higher CT_{max} (30.66 ± 0.63 °C) than the average estimate in non-toxic strains (29.95 ± 0.26 °C), with a difference of 0.72 °C. However, no significant variation in CT_{max} was observed across experiments ($X^2_{(1,\ N = 54)}$ = 1.06, p > 0.05). The mean CT_{max} in plate-based experiment was 30.32 ± 0.41 °C, whereas the mean CT_{max} in tube-based experiments without and with stepwise acclimatisation were 30.48 ± 0.77 °C and 30.12 ± 0.77 °C.
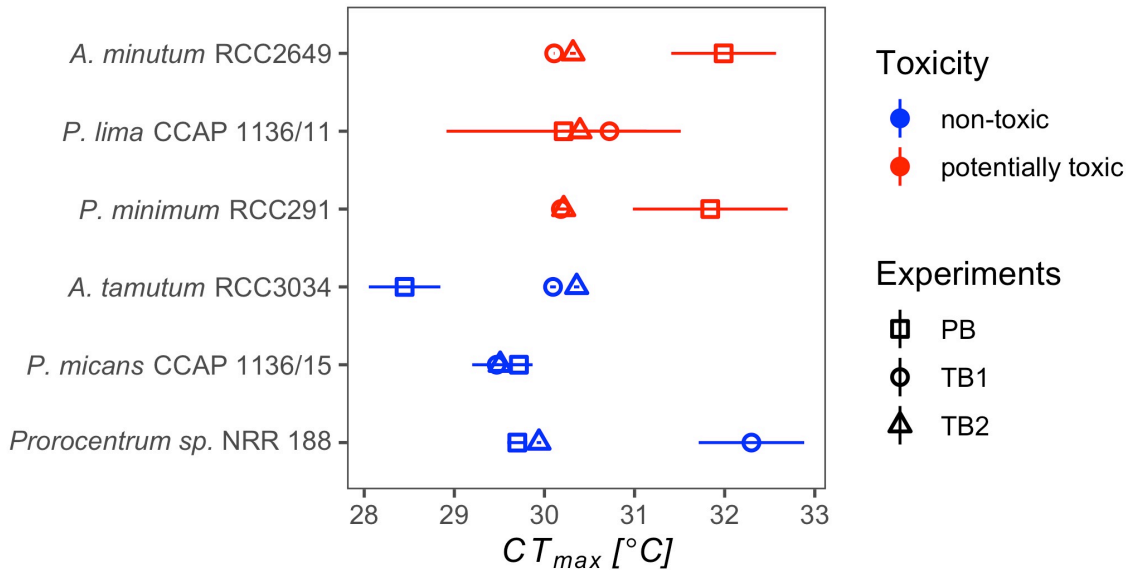
Figure 4.6. Variations in the critical thermal maximum (CT_{max}, °C) across non-toxic and potentially toxic dinoflagellates strains estimated across different experiments (PB, TB1, and TB2 refers to plate-based experiments and tube-based experiments without and with stepwise acclimatisation, respectively). Each point indicates a mean estimate with error bar showing the standard error of the mean.

4.3.2.5 Fundamental thermal niche

The mean fundamental thermal niche breadth (*FTN*) did not differ significantly across dinoflagellate strains ($X^2_{(1, N=54)}$ = 2.56, p > 0.05) (Figure 4.7). Average *FTN* in dinoflagellate strains ranged from 25.23 °C to 26.36 °C. There was no significant difference in mean *FTN* between non-toxic (25.36 ± 0.61 °C) and potentially toxic dinoflagellates (26.10 ± 1.14 °C) ($X^2_{(1, N=54)}$ = 1.95, p > 0.05). Significant variation in mean *FTN* was found across experiments ($X^2_{(1, N=54)}$ = 8.03, p < 0.05). Plate-based experiments yielded a lower mean *FTN* (24.71 ± 0.53 °C) as compared to the mean estimates from tube-based experiments without and with stepwise acclimatisation with difference of 1.86 °C and 1.20 °C, respectively.
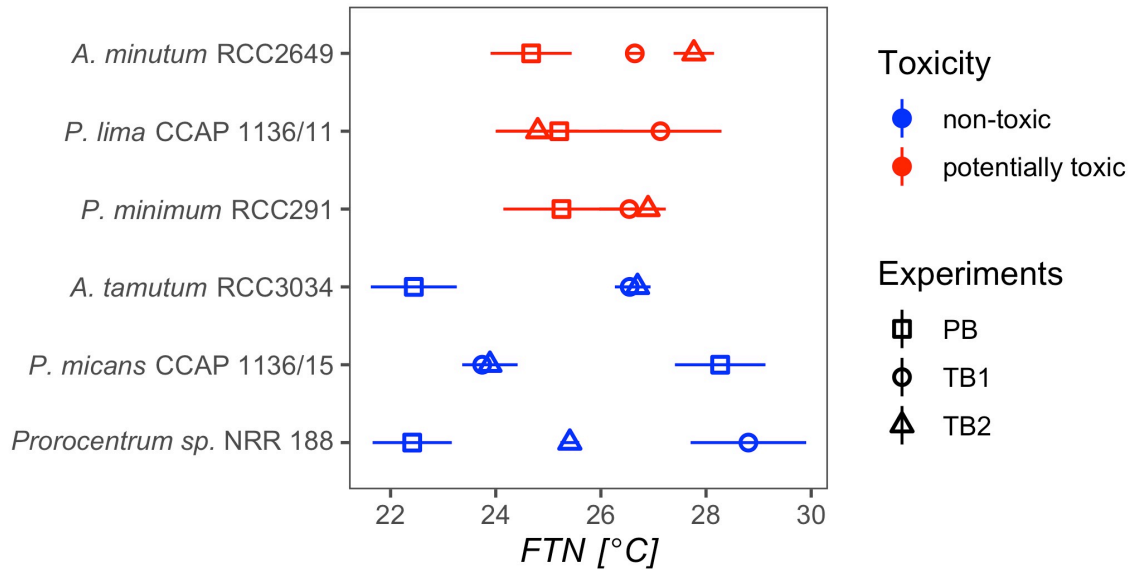
Figure 4.7. Variations in the fundamental thermal niche breadth (*FTN*, ℃) across non-toxic and potentially toxic dinoflagellates strains estimated across different experiments (PB, TB1, and TB2 refers to plate-based experiments and tube-based experiments without and with stepwise acclimatisation, respectively). Each point indicates a mean estimate with error bar showing the standard error of the mean.

4.3.2.6 Skewness

Dinoflagellate strains exhibit significant variation in mean skewness ($\chi^2_{(1, N = 54)}$ = 30.58, p < 0.05) (Figure 4.8). Potentially toxic *P. minimum* had the lowest skewness (-1.03 $\pm$ 0.46), whilst *P. micans* had the highest skewness (0.0016 $\pm$ 0.58). The mean skewness did not differ significantly between non-toxic (-0.18 $\pm$ 0.28) and potentially toxic dinoflagellates (-0.57 $\pm$ 0.58 °C) ($X^2_{(1, N=54)}$ = 1.92, p > 0.05). The variation in mean skewness across the experiments was significant ($X^2_{(1, N=54)}$ = 20.86, p < 0.05). Average skewness estimated from plate-based experiments was -0.05 $\pm$ 0.21, which was 0.65 and 0.32 higher than the mean estimates from the tube-based experiments. Mean skewness obtained in tube-based experiment without acclimatisation (-0.71 $\pm$ 0.34) was lower than the mean skewness obtained in tube-based experiment with acclimatisation (-0.37 $\pm$ 0.34). Most if not all of the thermal performance curves were asymmetric based on skewness. About 78% of the curves were left skewed, and the remaining 12% were right skewed.
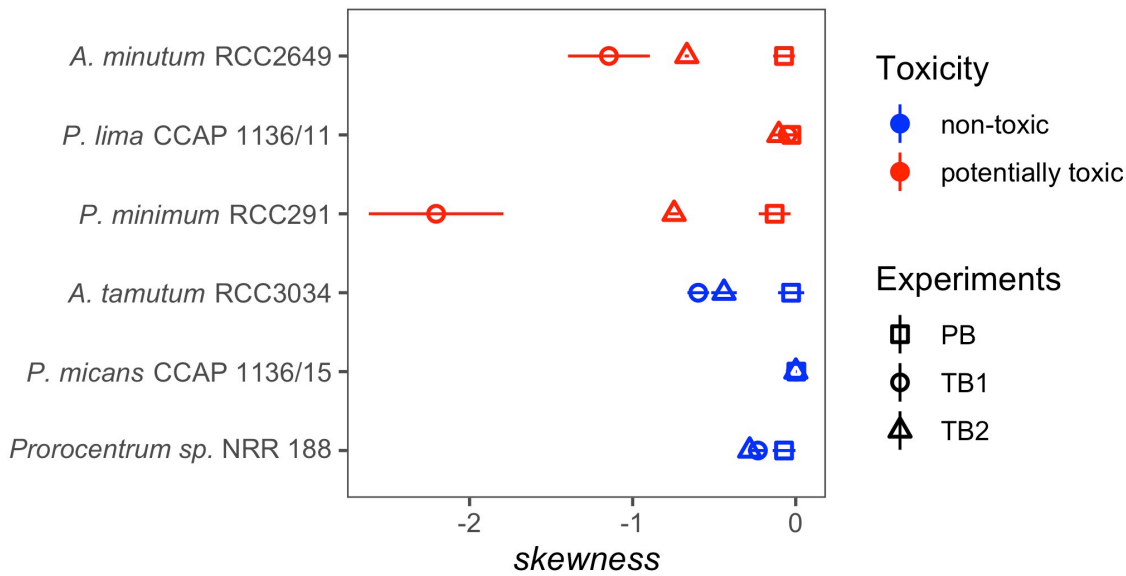
Figure 4.8. Variations in the skewness across non-toxic and potentially toxic dinoflagellates strains estimated across different experiments (PB, TB1, and TB2 refers to plate-based experiments and tube-based experiments without and with stepwise acclimatisation, respectively). Each point indicates a mean estimate with error bar showing the standard error of the mean.

4.3.2.7 Variation in growth rates and thermal traits in combined studies

Analysis of the pooled experimental results from the present and published studies revealed no significant differences in maximum growth rates and thermal traits between non-toxic and potentially toxic phytoplankton (Figure 4.9).

Most potentially toxic strains observed in the present study had r_{max} close to the median, except for *P. lima* of which the estimate was within the first quartile of the distribution (Figure 4.9 A). Estimates of r_{max} in all non-toxic strains in the present study were near the lower limit of the distribution. About 3% of the variation in r_{max} was explained by the fixed effect of toxicity, and 82% of the variation was explained by both the fixed effect and random effects of strain identity and study design.
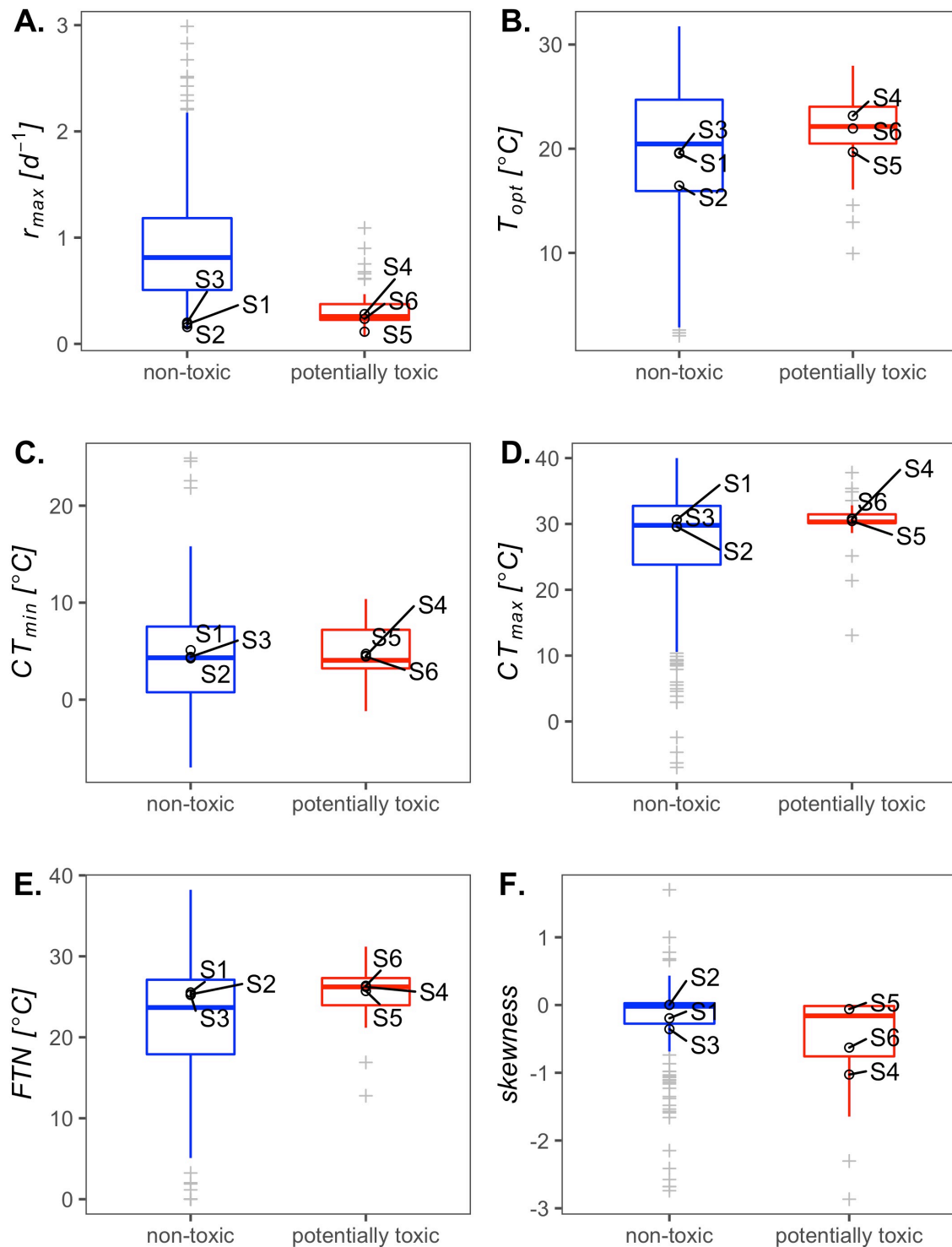
Figure 4.9. Variation in maximum growth rates and thermal traits between toxicity in marine phytoplankton. Box plots show the distribution of maximum growth rates (r_{max}), thermal optimum (T_{opt}), critical thermal minimum (CT_{min}), critical thermal maximum (CT_{max}), fundamental thermal niche (FTN), and skewness in non-toxic (blue) and potentially toxic (red) strains from the combined present and published experimental data. Outliers are indicated as grey crosses. Traits in strains (S1 – S3 refers to non-toxic strains of *Prorocentrum sp.*, *P. micans*, and *A. tamutum*, respectively; whilst S4 – S6 refers to potentially toxic strains of *P. minimum*, *P. lima*, and *A. minutum*, respectively) used in this present study are labelled and indicated as black circles.

Thermal traits of the strains used in this present study were generally within the interquartile range of the distribution of the traits (Figure 4.9 B – F). The range of thermal traits in non-toxic and potentially toxic strains were overlapping. Analysis of variance in these traits revealed no significant difference. The proportion of the variance in these traits explained by toxicity was less than 2%. The fixed effect of toxicity and the random effects of strain identity and study design explained about 40% – 92% of the variance in these traits. Majority of the variation in these traits was explained largely by taxonomic affinity.

4.3.3 Trade-offs between maximum growth rate and thermal traits

There was no clear linear relationship between r_{max} and thermal traits in marine phytoplankton (Figure 4.10). Less than 15% of the variation in r_{max} was explained by the fixed effects of thermal traits. About 83 – 86% of the variation in r_{max} was explained by both the fixed and random effects.

4.3.4 Trait-environment relationship

There was a clear evidence of the direct relationship between the cardinal temperatures and the ambient temperature experienced by marine phytoplankton at their local habitat (Figure 4.11).

Thermal optimum (T_{opt}) had increased at 0.61 ± 0.06 °C per degree increase of mean SST (Figure 4.11 A). The fixed effect of mean SST on T_{opt} explained 40% of the variance, whilst 91% of the variance was explained by both the fixed effect and random effects of toxicity, strain identity, and source of experimental data. Among these random effects, strain identity explained the most variation in T_{opt}. About 85% of the phytoplankton strains (83% of non-toxic and 100% of potentially toxic) had higher

average T_{opt} than the local mean SST, with the difference varying between 0.17 and

19.00 °C and the mean difference of 6.25 ± 0.24 °C. T_{opt} in the remaining 15% of the

phytoplankton strain was 3.64 ± 0.35°C lower than the local mean SST.
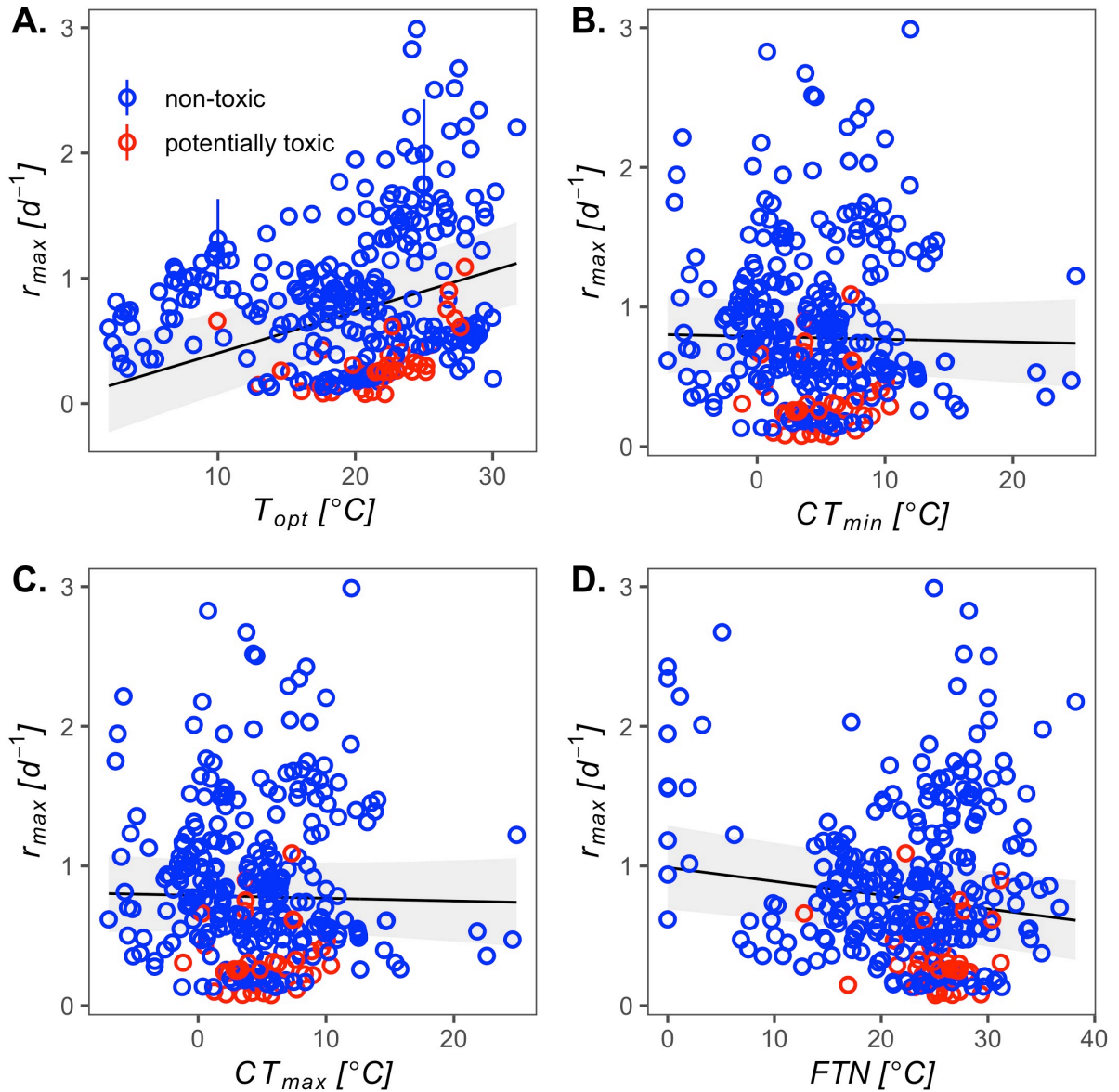
Figure 4.10. Trade-offs between maximum growth rate (r_{max}) and thermal traits in non-toxic and potentially toxic marine phytoplankton. The scatter plots show the relationship between r_{max} and thermal optimum (T_{opt}), critical thermal minimum (CT_{min}), critical thermal maximum (CT_{max}), and fundamental thermal niche (FTN) (A – D, respectively). Circles indicate the mean estimates of the traits in non-toxic (blue) and potentially toxic (red) strains with error bars representing the standard error of the mean. r_{max} was fitted against T_{opt}, CT_{min}, CT_{max}, and FTN using generalised linear mixed models ($GLMM$) with toxicity, strain identity, and source of experimental data as random factors. The solid lines represent the linear fit with 95% confidence interval in grey shading.
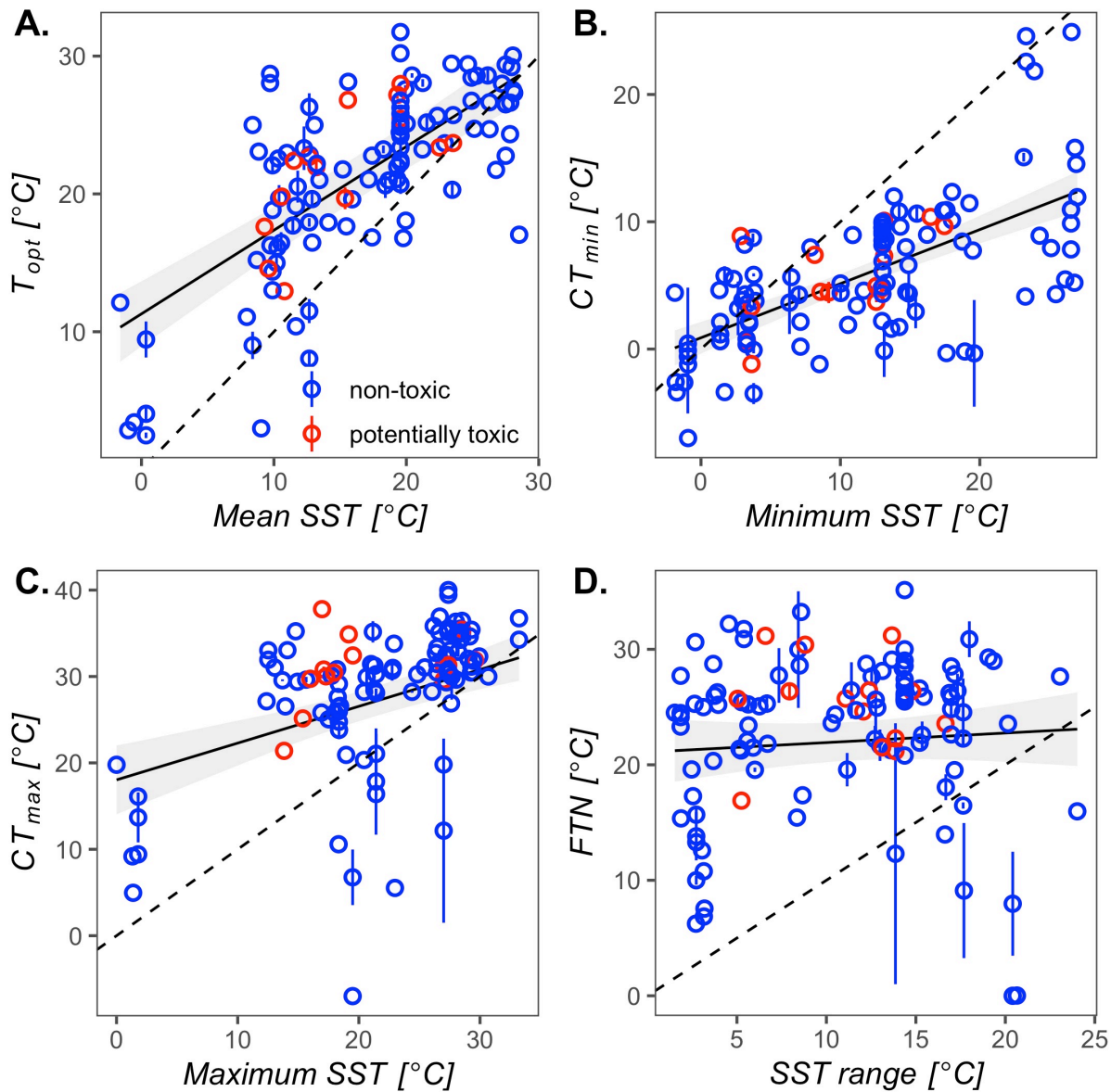
Figure 4.11. Relationship between thermal traits in marine phytoplankton and environment. The scatter plots present the relationship between the thermal traits, i.e. thermal optimum (T_{opt}), critical thermal minimum (CT_{min}), critical thermal maximum (CT_{max}), and fundamental thermal niche (FTN) (A – D, respectively) in marine phytoplankton and the ambient temperatures (mean, minimum, maximum, and range of sea surface temperature (SST), respectively) they experienced in their local habitat. Circles indicate the mean estimates of the traits in non-toxic (blue) and potentially toxic (red) strains with error bars representing the standard error of the mean. Generalised linear mixed models (*GLMM*) were used to model the trait-environment relationships with toxicity, strain identity, and source of experimental data as random factors. The solid lines represent the linear fit with 95% confidence interval in grey shading. The broken lines represent the equality between the thermal traits and the environment.

Also, critical thermal minimum (CT_{min}) had increased with increasing minimum

SST at rate of 0.43 ± 0.05 °C per degree increase in local temperature (Figure 4.11 B).

About 33% of the variance in CT_{min} was explained by the fixed effect of minimum SST and 73% of variance was explained by both the fixed effect and random effects of toxicity, strain identity, and source of experimental data. Strain identity also explained the highest proportion of the variation in CT_{min} among the random effects. Approximately 34% of the strains (35% of non-toxic and 26% of potentially toxic strains) had higher average CT_{min} than the minimum SST they experienced at their local habitat with the difference of 2.59 ± 0.28 °C, ranging from -0.24 to 0.93 °C. The majority of the strains (66%) had CT_{min} lower than the local minimum SST with the mean difference of 6.66 ± 0.34 °C.

There was an increasing trend in critical thermal maximum (CT_{max}) with the local maximum SST experienced by marine phytoplankton (Figure 4.11 C). CT_{max} had increased at 0.43 ± 0.07 °C per degree increased local maximum SST. The fixed effect of maximum SST explained 13% of the variance in CT_{max}, and both the fixed and random effects explained 75% of the variation. Among the random effects, the source of experimental data explained the highest proportion of the variation in CT_{max}, whilst strain identity explained the variation the least. Majority (85%) of the phytoplankton (83% non-toxic and 100% potentially toxic strains) had CT_{max} higher than the local maximum SST with the difference ranging from 0.07 °C to 20.83 °C and the average difference of 8.70 ± 0.31 °C. CT_{max} of the 15% of the phytoplankton strains was 8.10 ± 0.99 °C lower than the maximum SST they experienced at their local habitat.

On the other hand, fundamental thermal niche (FTN) did not change with increasing SST range (Figure 4.11 D). The fixed effect of SST range explained a negligible proportion (less than 1%) of the variation in FTN. Whereas, both the fixed and the random effects explained 62% of the variation. Most of the variation in FTN was also explained by the source of experimental data.

4.3.5 Thermal safety and vulnerability

Majority of the phytoplankton had higher critical thermal maxima (CT_{max}) than the maximum sea surface temperature (SST) projected in 2050 and 2010 at different climate scenarios (RCP 2.6 and RCP 2.8) (Figure 4.12). About 82% of the marine phytoplankton (79% of the non-toxic strains and 100% of the potentially toxic strains) had CT_{max} higher than the environmental temperature projected in 2050 at RCP 2.6, with the mean difference of 7.86 $\pm$ 0.30 °C (Figure 4.12 A). The remaining 18% of the marine phytoplankton (all were non-toxic; 21% of the non-toxic strains) had mean CT_{max} that was 8.56 $\pm$ 0.98 °C lower than the projected local environmental temperature. Similar observations were found in the projections in 2050 at RCP 8.5 (Figure 4.12 B) and in 2100 at RCP 2.6 (Figure 4.12 C). However, a noticeable difference in the statistics was observed for the projections in 2100 at RCP 8.5 (Figure 4.12 D). Approximately, 73% of the marine phytoplankton (70% of the non-toxic strains and 94% of the potentially toxic strains) had CT_{max} higher than the environmental temperature projected in 2100 at RCP 8.5, with the mean difference of 6.26 $\pm$ 0.30 °C. The remaining 27% of the marine phytoplankton (30% of the non-toxic strains and 6% of the potentially toxic strains) had mean CT_{max} that was 7.99 $\pm$ 0.87 °C lower than the projected local environmental temperature in 2100 at RCP 8.5.
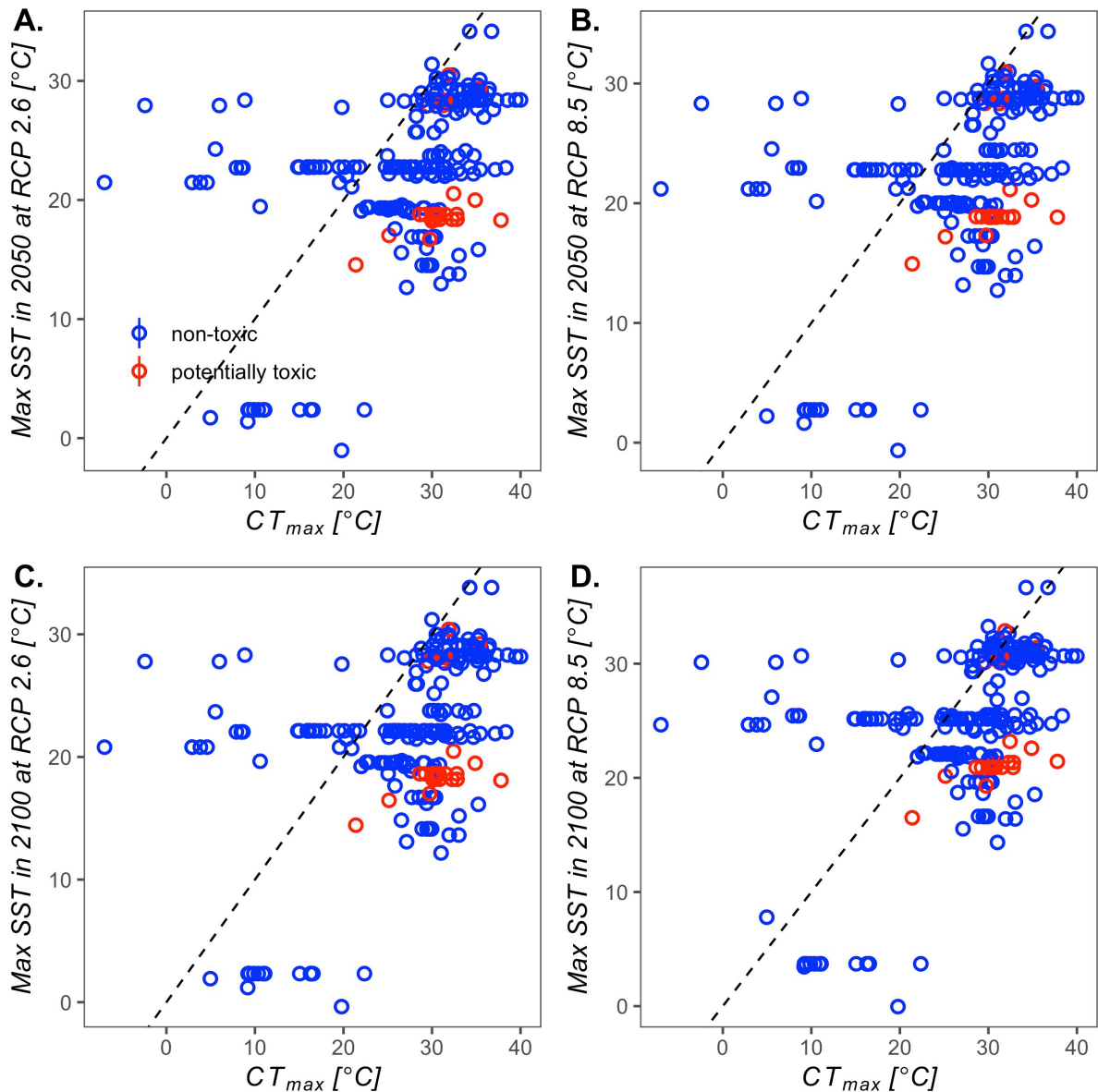
Figure 4.12. Scatter plots showing the critical thermal maximum (CT_{max}) of non-toxic (blue) and potentially toxic (red) marine phytoplankton strains in relation to their habitat"s maximum sea surface temperate (SST) projected in 2050 and 2100 at different climate scenarios (RCP 2.6 and RCP 2.8). The points above the threshold (broken line) indicates that the projected SST exceeds the CT_{max}.

Majority of the phytoplankton strains had lower CT_{min} and higher CT_{max} than the local minimum and maximum *SST*, respectively. As a result, they had sensitivity to cold (S_{min}) and sensitivity to warm (S_{max}) temperatures below and above zero, respectively, occupying the thermal safety zone (Figure 4.13). About 62% of the strains had thermal safety, whereas the remaining 38% were at risk of cooling (21.38%), warming (13.77%), or both (2.29%).
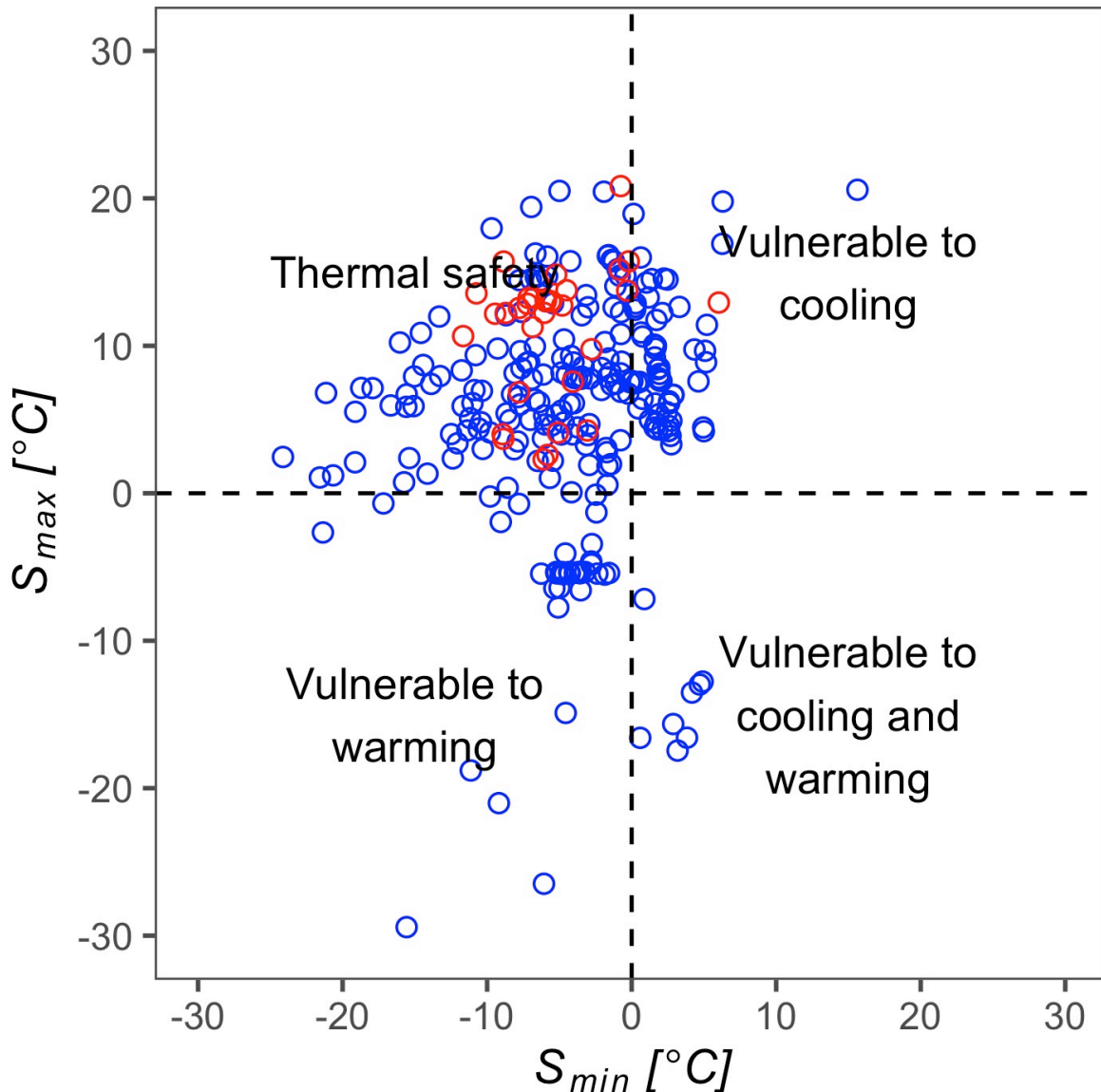
Figure 4.13. Scatter plot of the sensitivity to cold (S_{min}) and sensitivity to warm (S_{max}) temperatures in non-toxic (blue) and potentially toxic (red) marine phytoplankton strains. This plot is divided into four quadrants, categorising the strains that are safe and vulnerable to warming and/or cooling in the present climate scenario.

Average S_{min} in non-toxic strains was -5.06 ± 0.77 °C, which was not statistically different from the average S_{min} in potentially toxic strains (-4.73 ± 2.61 °C) ($X^2_{(1, N=276)}$ = 0.04, p > 0.05) (Figure 4.14 A). Furthermore, non-toxic had a mean S_{max} of 5.75 ± 1.00 °C, which was similar to the mean S_{max} of potentially toxic strain (6.61 ± 2.93 °C) ($X^2_{(1, N=276)}$ = 0.14, p > 0.05) (Figure 4.14 B). Toxicity explained a negligible proportion of

variation in S_{min} and S_{max}. Both the fixed effect of toxicity and random effects of taxonomic affinity and study design explained more than 75% of the variation in S_{min} and S_{max} . The source of experimental data explained more proportion of the variance in S_{min} and S_{max} than the strain identity.

No significant difference in the vulnerability to warming between toxicity in marine phytoplankton at all climate scenarios (Figure 4.14 C – F). The local maximum temperature was projected to exceed the CT_{max} of non-toxic phytoplankton after 859.86 $\pm$ 71.46 years, 541.38 $\pm$ 52.96 years, 529.85 $\pm$ 114.20 years, and 251.02 $\pm$ 26.57 years at RCP 2.6, RCP 4.5, RCP 6.0, and RCP 8.5 climate scenarios, respectively, which were similar to projections in potentially toxic phytoplankton, i.e. 944.83 $\pm$ 241.78 years, 512.11 $\pm$ 171.08 years, 367.21 $\pm$ 253.43 years, and 218.01 $\pm$ 81.76 years, respectively. Toxicity alone had negligible effect on warming vulnerability. However, taking into account the taxonomic affinity and study design, both the fixed and random effects explained more than 78% of the variation. Between the random effects, majority of the variation was also explained by strain identity.
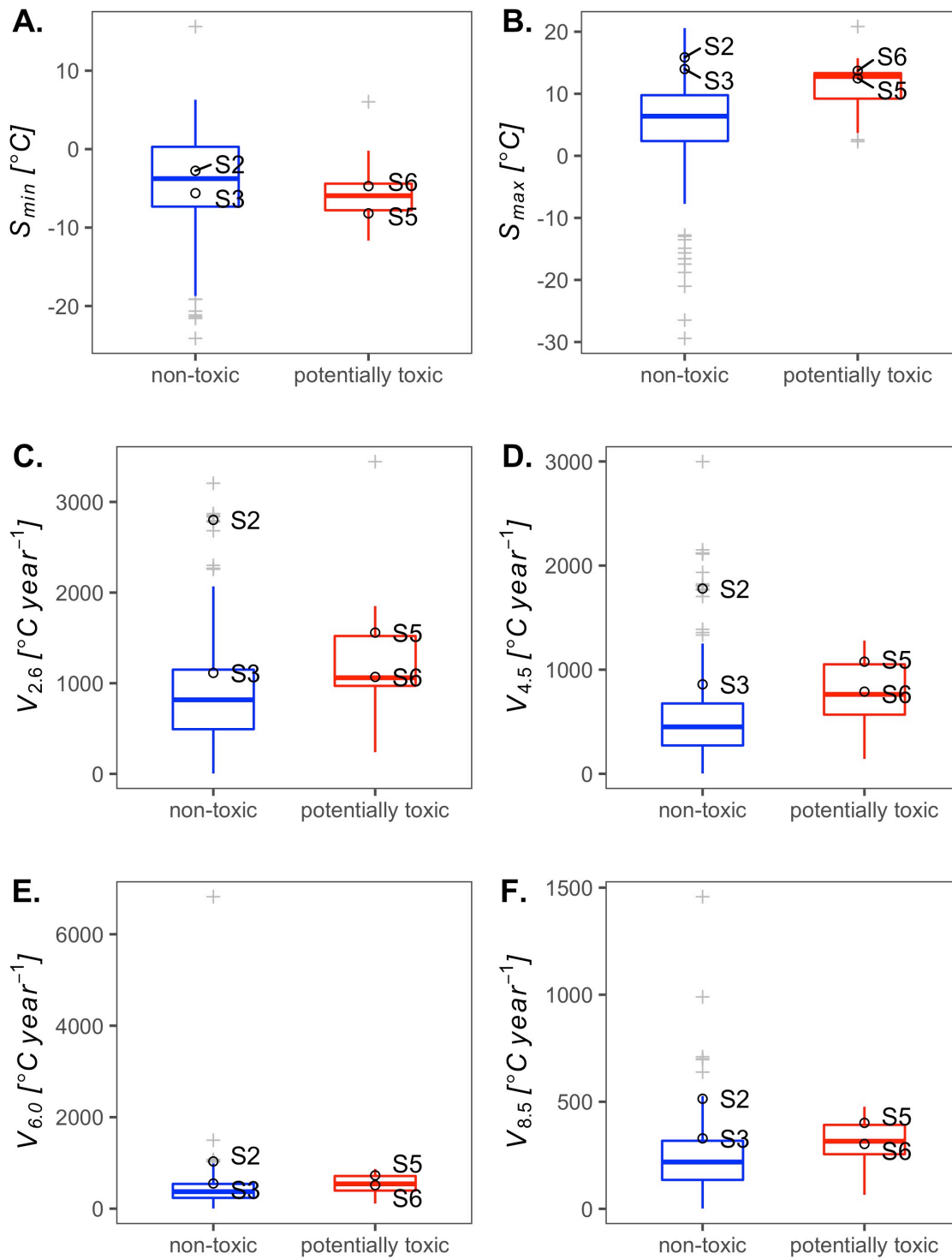
Figure 4.14. Variation in thermal sensitivity and vulnerability between toxicity in marine phytoplankton. Box plots show the distribution of thermal sensitivity to cold and warm temperature (S_{min} and S_{max}, respectively; A and B, respectively) and vulnerability to warming at *RCP* 2.6, *RCP* 2.6, *RCP* 2.6, and *RCP* 2.6 climate scenarios ($V_{2.6}$, $V_{4.5}$, $V_{6.0}$, and $V_{8.5}$, respectively; C – F, respectively) in non-toxic (blue) and potentially toxic (red) strains from the combined present and published experimental data. Outliers are indicated as grey crosses. Traits in strains (S2 – S3 refers to non-toxic strains of *P. micans*, and *A. tamutum*, respectively; whilst S5 – S6 refers to potentially toxic strains of *P. lima*, and *A. minutum*, respectively) used in this present study are labelled and indicated as black circles. Data for *Prorocentrum* sp. (S1) and P. minimum (S4) were not available.

4.4 DISCUSSION

4.4.1 Thermal dependence of growth in test organisms

The results of this study indicate the dependence of growth in non-toxic and potentially toxic dinoflagellates on temperature as evidently depicted by the thermal growth curves. These curves, also known as the thermal performance curves or the thermal reaction norms, are often unimodal and negatively skewed in ectotherms (Eppley, 1972; Kingsolver, 2009; Knies and Kingsolver, 2010). The shape of the curves reflects the effect of temperature on enzymatic rate process and on enzyme activation and stability at high temperatures (Knies and Kingsolver, 2010). Growth rates increase gradually with increasing temperature below the thermal optimum (T_{opt}), which is attributed to the exponential increase of the reaction rates with increasing temperature following the Arrhenius kinetics (Arrhenius, 1915). On the other hand, growth rate decreases with further increase in temperature above T_{opt}, which is attributed to the denaturation of essential proteins (Hochachka and Somero, 2002). The variability in the trends in growth below or above T_{opt} can be explained by the probability of the activation of rate-limiting enzymes that declines at high and low temperature (Knies and Kingsolver, 2010; Ratkowsky et al., 2005).

The asymmetrical pattern of the thermal growth curve is observed in the majority of strains based on the estimates of the skewness of the curves which were generally below zero. This suggests that their growth is more sensitive to warming than cooling, which is an important trait given the projected change in temperature in the next decades. On the contrary, few species exhibit a less skewed curve (i.e. nearly symmetrical), a trait characterised by a constant growth over an optimal temperature range that deceases at extreme temperatures at similar rates. The symmetrical thermal

growth curve suggests that the growth of the species is equally sensitive to decreasing and increasing temperature from the T_{opt}.

The findings reveal differences in the growth rates across strains. Generally, thermal traits were found to be vary across strains, toxicity, and experimental design. Interspecific and intraspecific variations in growth rates and thermal traits of marine phytoplankton have been demonstrated in several studies (Boyd et al., 2013; Chen and Laws, 2016; Kremp et al., 2012; Thomas et al., 2016). These differences in the traits among species and strains implies that the phytoplankton community composition may be altered as a results of climate change. Species that are heat stress sensitive have narrow thermal tolerance limit, whilst those that can survive through acclimation or adaptation have a wider range (Chen, 2015). Thermal acclimation is part of the phenotypic plasticity in phytoplankton to increase growth or survival under sub- and supra-optimal conditions over short term periods (Raven and Geider, 1988; Staehr and Birkeland, 2006), and is believed to be linked to the adaptive changes in their genes. Thermal adaptation of phytoplankton has been developed as a result of the evolutionary process (Hanelt et al., 2003), and has been demonstrated in several studies (Huertas et al., 2011; Iglesias-Prieto et al., 1992). The difference in temperature dependence of growth between the non-toxic and potentially toxic phytoplankton has an ecological implication. Toxic species may dominate over the non-toxic species (or vice versa) in the changing climate. Toxic species could employ thermal acclimation and adaptive strategies to expand their thermal tolerance, and toxin production may provide toxic species a selective advantage under future climate scenario.

However, the outcome of the experiments should be interpreted with caution as there are several caveats as described subsequently. First, the rates derived from the log increase of optical density and fluorescence over time may present two different

measures of growth. Optical density-based growth may be governed by a set of enzymes that are different from the enzymes acting on the fluorescence-based growth. Hence, It is possible for different approaches to the measurement of growth rates to yield different results. Second, one challenge of modeling the thermal growth response is that there is no single equation that fits all data (Low-Décarie et al., 2017). This suggests that different equations may describe different processes that are still unresolved. Finally, extrapolation of the thermal response of dinoflagellates as model organisms to the whole phytoplankton is inherently problematic. Although the majority of toxic species belong to dinoflagellates, characterisation of the thermal response curves in representatives from the other taxa, i.e. diatoms, haptophytes and cyanobacteria, is crucial to advance our knowledge on the taxon-specific differences in the growth thermotolerance between non-toxic and toxic phytoplankton. Pooling the experimental data obtained from this study with the datasets compiled from other laboratory culture experiments allows the comparison of thermal growth response between phytoplankton groups with an adequate number of observations.

4.4.2 Differences in growth and thermal traits

Results of the analysis of the pooled datasets suggest the maximum growth rates and thermal traits between non-toxic and potentially toxic phytoplankton are comparable. However, toxicity explained only a small part of the variation in the all of the traits. Generally, the majority of the variation in the traits is explained by strain identity and source of experimental data. These results from the thermal growth curves describe the growth constraint experienced by species at their maximum and minimum temperature limits, and the range between these limits define their niche, which can vary among strains and experiments, suggesting that growth and thermal traits are

dependent to physiological plasticity and evolutionary history (Kremer et al., 2017; Thomas et al., 2016, 2012). Overall, the results suggest that non-toxic and toxic phytoplankton may co-exist in the same thermal condition, but in terms of growth rates, toxic species are weak competitors against non-toxic species.

These findings may be somewhat biased in several ways. One of the limitations includes the statistical uncertainty of the estimation of the thermal physiological limits and thermal niche breadth, as these parameters are frequently extrapolated beyond the data. This constrain our understanding of the responses of non-toxic and toxic phytoplankton to climate extremes. There are also limitations linked with low temperature resolution, incomplete observation of full thermal range, over representation of non-toxic phytoplankton, and few observations on toxic species that are mostly dinoflagellates. Furthermore, the multifaceted interference from different protocols implemented across individual studies may also limit the usefulness of the compiled datasets. However, the experimental results generated in this present study provide the groundwork to evaluate of the value of the published datasets in comparing traits between toxicity in marine phytoplankton. As observed, there is a discrepancy in the findings between the analyses using the present and published experimental results, which may be related to the data quality used in thermal trait analysis. For instance, the present experiments reveal that that the maximum growth rates in toxic strains are higher than the rates in non-toxic strains of dinoflagellates, which are found to be comparable in the analyses of the pooled datasets. This suggests that the maximum growth rates between non-toxic and toxic phytoplankton are not robust across a range of the experimental protocols, which may be attributed to the sensitivity of the trait to light or nutrient conditions (Boyd et al., 2013).

4.4.3 Uncoupling of growth rates and thermal traits

The results demonstrate that maximum growth rates have no clear linear relationship with thermal traits. The variation of the growth rates explained a negligible variation in the thermal traits. This suggests that there is no clear trade-off between maximum growth rate and thermal traits. The latest work reveals that there is a thermal limit for thermal optimum and the maximum growth rate is highly constrained by this limit, which is highly variable among functional groups in phytoplankton (Grimaud, 2016). The difference in maximum growth rate among the taxonomic groups was attributed to the various physiological limits, photosynthesis yields, and biovolume (Grimaud, 2016; Marãnón et al., 2014; Raven and Geider, 1988). However, our current understanding of the link between maximum growth rates and the thermal limits and niche breadth is still limited.

4.4.4 Linking thermal traits with environment

The findings reveal a clear linear relationship between thermal traits and the temperature experienced by marine phytoplankton at their local environment, except for the temperature range. The ambient temperature explained significantly the variation in cardinal temperatures. Results suggest that there is a strong link between the cardinal temperatures and the ambient temperature experienced by marine phytoplankton at their local habitat, indicative of local adaptation (Thomas et al., 2012). Recent work by Chen (2015) found similar results and demonstrated the importance of the temperature in shaping the physiology of phytoplankton. Chen (2015) emphasized that the these thermal traits can be inherited for a long period of time even if the phytoplankton have been cultured over multiple generations. Thermal traits obtained from physiology

experiments are different from the traits derived from the temperature experienced by

organism in its local environment. As observed, all physiology-based thermal traits are

generally higher than the environmental temperatures, except for the lower temperature

limit. As examined in Chapter 2, this difference can be explained by the reduction of the

fundamental thermal niche in nature due to biotic interaction, species dispersal

limitation, and limited climate availability (Jankowski et al., 2013; Sánchez-Fernández et

al., 2016; Soberón and Nakamura, 2009). Furthermore, the results suggest that this link

is highly variable among taxonomic groups in marine phytoplankton, but is less variable

between non-toxic and potentially toxic phytoplankton.

4.4.5 Vulnerability to climate change

Findings of this current study show that nearly all the non-toxic and potentially

toxic phytoplankton were thriving within the thermal safety zone in the present climate

scenario. Also, results show comparable estimates of thermal sensitivity and warming

vulnerability between non-toxic and potentially toxic phytoplankton. However, toxicity

explained insignificant variation in these estimates. Overall, the results indicates that the

vulnerability to climate change is highly variable among the strains, and less variable

between toxicity in marine phytoplankton.

Vulnerability of phytoplankton to climate change is attributed to the influence of

temperature change on the physiological processes and growth, which consequently

alter marine ecosystem structure and function (Regaudie-De-Gioux and Duarte, 2012;

Thomas et al., 2012; Toseland et al., 2013). Recent studies have demonstrated the

effect of elevated temperature on metabolic and growth rates in phytoplankton (de Boer

et al., 2004; Regaudie-De-Gioux & Duarte, 2012; Boyd *et al.*, 2013; Toseland *et al.*,

2013). Typically, photosynthesis rises with elevated temperature until it reaches its

optimum, and decreases with further warming; whilst respiration, on the other hand, increases with increasing temperature. This elevation in metabolic rates is likely to expand the growth rate of photoautotrophs in warming conditions (Hochachka and Somero, 2002). Several species exposed to high temperature display higher photosynthesis and lower respiration rates, but exhibit reduction in their cell size (Staehr and Birkeland, 2006). Shrinking their size can neutralize the imbalance between these metabolic processes (Peter and Sommer, 2013). Also, nutrient uptake by phytoplankton becomes strongly limiting at elevated temperatures (Sterner and Grover, 1998). Cell size reduction can improve nutrient uptake rates and lessen metabolic costs, which is a good strategy in response to increasing resources demand due to warming (Atkinson et al., 2006). Furthermore, cyst germination in dinoflagellate is controlled by temperature (Anderson et al., 2005), which may be altered in changing climate. It can be increased under warmed condition, and can be inhibited at extreme temperature (Anderson et al., 2005).

4.4.6 Implication to future algal blooms

The effect of temperature change on their physiological processes and growth may alter marine ecosystem structure and function. As observed, majority of the marine phytoplankton are generally living in the present climate scenario within the thermal safety zone. However, the warming temperature may likely exceed the physiological limits of marine phytoplankton species. They must avoid the extreme temperatures or else they are at risk of the thermal danger. They may either adapt or migrate to new favourable habitats to survive, otherwise, their extinction is inevitable.

In the context of harmful algal blooms, warming may provide favourable conditions for toxic algae to occur. It is likely that toxic blooms and their impacts may

be exacerbated in the future where their duration, intensity, and frequency may increase in response to changes in the climate. The possible impacts of climate change on toxic blooms have important implications on how to manage and control harmful algal blooms (HAB) in the future.

The findings of this study improve our predictive understanding on the ecological responses of non-toxic and toxic marine phytoplankton to future climate scenarios. The thermal performance curves (*TPC*) obtained in this study can be used to develop a mechanistic ecological niche model to establish a causal relationship between species distribution and temperature. This mechanistic model is useful in predicting the climate-induced ecological trends such as changes in range, habitat suitability, diversity, and community composition.

4.5 CONCLUSIONS

This chapter investigates the effect of temperature on growth and toxin production in marine phytoplankton. Here, six strains of dinoflagellates were used as model organisms to examine the temperature dependence of growth in non-toxic and potentially toxic phytoplankton. Generally, the results of this study reveal a asymmetrical pattern of the thermal growth curve in these model organisms, suggesting that their growth is more sensitive to warming than cooling. The data obtained from this present study was supplemented with the datasets compiled from laboratory culture experiments to allow comparison with an adequate number of observations. The results of the analysis of the pooled datasets show that the maximum growth rates and the thermal traits are comparable. Furthermore, the findings reveal unclear trade-off between the maximum growth rates and thermal traits in marine phytoplankton but

show evident trait-environment relationships. The results also demonstrate that nearly all the non-toxic and potentially toxic phytoplankton were thriving within the thermal safety zone in the present climate scenario. However, the trait tradeoff, trait-environment relationships, thermal sensitivity, and warming vulnerability are comparable between non-toxic and potentially toxic phytoplankton.

This page is intentionally left blank.

This page is intentionally left blank.

CHAPTER 5

This page is intentionally left blank.

This page is intentionally left blank.

TEMPERATURE DEPENDENCE OF TOXIN PRODUCTION IN MARINE DINOFLAGELLATES

ABSTRACT

Assessing the effect of temperature on toxin production in marine phytoplankton is important to improve our predictive understanding of toxic blooms in the future ocean. This present study examined the temperature dependence of toxin production in a marine phytoplankton. Here, a tube-based growth experiment was conducted using dinoflagellate strains as the test organism under different thermal conditions. Paralytic shellfish poisoning (*PSP*) toxins such as saxitoxin (*STX*) and its derivatives and lipophilic toxins such as okadaic acid (*OA*) and dinophysistoxins (e.g. *DTX1 and DTX2*) were extracted from the algal samples collected at the end of the incubation period. Standardised protocols using ultrahigh-performance liquid chromatography (UHPLC) coupled to the mass spectrometer (MS/MS) were implemented to detect and quantify toxins in the extracted algal samples. Among the test organisms, only the *Prorocentrum lima* strain was detected for the presence of *OA*, *DTX1, and DTX2*. Results showed (1) cell density dependence of toxin concentration, (2) inter-strain variability in cellular toxin content, (3) temperature dependence of the concentration, cellular content, relative composition, and cellular production rate of toxins, and (4) inverse linear relationship between toxin production rates and growth rates. These findings improve our current knowledge on the toxin production in marine phytoplankton in response to temperature, advancing our understanding of toxic blooms in response to ongoing climate change.

5.1 INTRODUCTION

Toxic blooms are already a global problem and their current distribution is alarming. Climate change may provide favourable conditions for toxic algae to occur (Hallegraeff, 2010). It is likely that toxic blooms and their impacts may be exacerbated in the future where their duration, intensity, and frequency may increase in response to changes in the climate (Moore et al., 2008; Tatters et al., 2013). The well-documented effects of toxins to humans and to other organisms (Berdalet et al., 2015) and the potential effect of climate change on toxic blooms in the future (Fu et al., 2012) have stimulated studies on the ecophysiology of toxic phytoplankton (e.g. Kellmann et al., 2010a; Perini et al., 2014; Ramsey et al., 1998; Stüken et al., 2011).

The advantages of toxin production would lead to the expectation of the ubiquity of toxicity in phytoplankton. Surprisingly toxin production is only known for few phytoplankton species (150 species in 50 genera listed in Moestrup et al. (2009)). Despite the rarity of toxicity in phytoplankton lineage, the toxins are diverse with distinct chemical structure, biosynthetic pathways and mode of actions (Rossini and Hess, 2010). The toxin diversity may be attributed to its widespread distribution in phytoplankton lineage and may reveal putative physiological and ecological roles beyond their assumed primary role as a defense mechanism. Physiological roles of toxins may have evolved in response to stressful abiotic conditions to improve efficiency in nutrient acquisition and storage, excretion, osmoregulation, scavenging mechanisms, biosynthesis, structural organisation, and cell signalling (Alexova et al., 2011; Bar-Yosef et al., 2010; Bates, 1998; Cembella, 1998). Ecological roles of toxins may have evolved from the need for infochemicals for biotic interaction to improve efficiency in mating,

alarm signals, defense/offense mechanism, and symbiosis (Bates, 1998; Cembella, 1998; Pohnert et al., 2007).

Toxin production is influenced by a number of abiotic factors such as temperature, pH, light, nutrients and biotic factors such as competition and grazing. Temperature is one of the most fundamental abiotic factors that may have a direct effect, or an indirect effect if growth and toxin production is uncoupled (Cembella, 1998). Temperature dependence of toxin production is associated with species-specific growth rate, and hence production of toxins is dependent on the thermal tolerance of the species. Hence, the effect of temperature on toxin production has implication on how toxic species may influence the structure and function of marine ecosystems in the future climate scenarios. However, our current knowledge on how toxin production is influenced by temperature is still lacking.

To improve our understanding on the microalgal toxin production, this study was set out to examine (1) the temperature dependence of the concentration, cellular content, relative composition, and cellular production rate of toxins, and (2) the relationship between toxin production and growth. This study hypothesized that concentration, cellular content, relative composition, and cellular production rate of toxins are dependent on temperature. This study also hypothesized that there is an inverse relationship between production of toxin and growth. To test these hypotheses, a tube-based experiment using *Prorocentrum* and *Alexandrium* strains (see description in Chapter 4) as the test organisms under different thermal conditions. Dinoflagellates of genus *Prorocentrum* and *Alexandrium* are among the best-studied toxic phytoplankton because of their production of toxins (Abdenadher et al., 2012; Ben-Gharbia et al., 2016; Grzebyk et al., 1997; Quilliam et al., 1996; Vlamis et al., 2015). Toxic *Prorocentrum* species are known producers of lipoliphic toxins such as okadaic

acid (OA) and dinophysistoxins (e.g. DTX1 and DTX2), which are responsible for

diarrhetic shellfish poisoning (DSP. On the other hand, toxic *Alexandrium* species are

known producers of saxitoxins (STX) and its derivate, which are responsible for

paralytic shellfish poisoning (PSP). The findings of this study will improve our current

knowledge of how production of toxins will be affected by temperature that is expected

to change with climate.

5.2 MATERIALS AND METHOD

5.2.1 Test organisms

Cultures of *Prorocentrum* and *Alexandrium* strains were obtained from different

culture collections (see Chapter 4 for description). They are ecologically relevant

organisms belonging to the phytoplankton genera that make up the majority of the toxic

bloom-forming species (Abdenadher et al., 2012; Ben-Gharbia et al., 2016; Grzebyk et

al., 1997; Quilliam et al., 1996; Vlamis et al., 2015). To optimize growth for the conduct

of the experiment, the culture was maintained in 35 mL batch culture in artificial

seawater (ASW) (Berges et al., 2001) enriched with K minimum nutrients (Keller et al.,

1987). The culture was regularly transferred to a fresh K medium to maintain the

exponential growth. The culture was not axenic. To minimize contamination, all ASW

and K media were autoclaved, and all transfers were performed in a class II biosafety

cabinet. The batch culture was maintained at a constant temperature of 15°C and under

a 12:12 hour light-dark cycle at a mean light intensity (± standard error) of 221 ± 12,

measured using a light meter (Li-Cor Li-250A). The culture was allowed to grow at this

condition for at least four transfers prior to experimental procedures.

5.2.2 Growth experiments

Tube-based experiments were performed inside a growth chamber (Conviron Adaptis CMP6010) with the following conditions: 20°C air temperature, 80% relative humidity, 12:12 light to dark cycle in hours, and 251 ± 10 light intensity. The thermal gradient in these experiments ranged from 5°C to 30°C at 5°C stepwise variation. Each assay temperature was maintained inside a glass water-jacketed bath using circulating distilled water. The temperature of the circulated distilled water was regulated by external recirculating water baths connected via flexible PVC hoses.

Triplicates of 4 mL of each of the culture were inoculated into 36 mL K medium contained in 50 mL glass test tubes. The tubes were capped with autoclaved foam stoppers to allow gas exchange during the incubation period. Algal cells in the test tubes were incubated in the above-mentioned temperature regulated water-jacketed bath.

Two tube-based experiments were performed. In the first experiment, the cells were incubated for 16 days without a stepwise acclimatisation. Whilst in the second experiment, the strains were allowed to acclimatise to a new thermal condition for 14 days prior the incubations to another 14 days of incubation.

Growth of the cultures were determined using in in vivo fluorescence as a proxy for phytoplankton biomass, which was measured daily (between 14:00 to 16:00) using a Turner Designs Trilogy Fluorometer. Prior to the fluorescence measurement, each culture in a test tube was homogenised using a vortex mixer. The test tube was subsequently placed in the fluorometer and a fluorescence reading was obtained. The estimated fluorescence in all samples was corrected with the fluorescence in a blank sample (i.e. 0.04).

The corrected estimates of fluorescence were used to compute for the growth rates. Natural log of the fluorescence estimates were fitted against time in a linear model to estimate the growth rate.

5.2.3 Toxin production experiments

5.2.3.1 Collection of toxin samples

Algal toxin samples were collected at the last day of the incubation period. Here, 1 mL samples were collected for cell counting to determine the algal cell density (cells mL^{-1}), and 30 mL samples were collected into 50 mL centrifuge tubes for toxin measurement. The algal toxin samples were centrifuged at 5000 rpm for 10 min. The cell pellets were stored at -20 °C until the sonication extraction method described in the subsequent section.

5.2.3.2 Extraction of toxins from algal samples

The samples were thawed for toxin extraction. Toxins in *Alexandrium* spp. (i.e. Paralytic Shellfish Poisoning (*PSP*) toxins) were extracted in 1.5 mL 0.05 M acetic acid, whilst toxins in *Prorocentrum* spp. (i.e. lipoliphic toxins (*LT*) such as okadaic acid (*OA*) and its derivatives) were extracted in 1.5 mL methanol:water (90:10 v:v). The resulting solutions were transferred into 15 mL centrifuge tubes and were sonicated for 30 seconds using a sonicator. The supernatants were collected and filtered through 0.2 µm pore size filters into 2 mL autosampler vials. The vials were covered with screw cap with hole and septum. The samples were kept frozen at -20 °C prior to toxin analyses.

5.2.3.3 Toxin analyses

The toxin analyses were conducted at the Centre for Environment, Fisheries and Aquaculture Science (*CEFAS*) using their in house protocols for the detection and quantification of *PSP* toxins (Turner et al., 2019) and lipophilic toxins (Dhanji-Rapkova et al., 2019, 2018) using the Waters Corp. (Manchester, UK) Acquity ultrahigh-performance liquid chromatography (*UHPLC*) coupled to the Xevo TQ-S tandem quadrupole mass spectrometer (*MS/MS*). The *UHPLC-MS/MS* system was equipped with (i) a binary solvent system capable of delivering up to four mobile phases with uniform flow of up to 0.8 mL min^{-1}; (ii) an autosampler capable of 2 μL injections; (iii) a temperature-regulated liquid chromatography (*LC*) column compartment, capable of holding the column at 60°C; (iv) a tandem mass spectrometer for operation in *MS/MS* mode, capable of positive/negative mode switching; and (v) a software system for instrument control and capable of processing quantitative data.

5.2.3.4 Analysis of *PSP* toxins in *Alexandrium* spp.

Samples of *Alexandrium* strains extracted in acetic acid were cleaned up through amorphous polymer graphitized-carbon solid-phase extraction (*SPE*) cartridges (i.e. Supelclean ENVI-Carb 250 mg/3 mL *SPE* cartridges; Sigma-Aldrich, St. Louis, MO) following the method of Turner et al. (2019). The cartridges were conditioned with 3 mL 20% acetonitrile + 1% acetic acid at 6 mL min^{-1} and followed by 3 mL 0.025% ammonia. These were eluted to the top of the frit and the eluents were discarded to waste. The cartridges were loaded with 400 μL acetic acid extract and eluted to the top of the frit at a flow rate of 3 mL min^{-1} and the eluents were also discarded to waste. The cartridges were washed with 700 μL deionized water and eluted to dryness, discarding the eluent to waste, with a flow rate of 3 mL min^{-1}. The sample extracts were eluted and collected

by adding 2 mL 20% acetonitrile and 1% acetic acid in a clean polypropylene tube at a

flow rate of 3 mL min^{-1}. The eluents were vortex-mixed, and 100 µL aliquots were

diluted with 300 µL acetonitrile in autosampler vials. The diluted extracts were then

analysed by *UHPLC-MS/MS* utilizing hydrophilic interaction LC (*HILIC*) following Turner

et al. (2019). This *UHPLC-MS/MS* system used a *HILIC* analytical column (i.e. 1.7 µm,

2.1 × 150 mm Waters Corp. (Manchester, UK) Acquity BEH Amide UPLC column

together with a Waters Corp. (Manchester, UK) VanGuard^{TM} BEH Amide guard

cartridge) held at 60°C with all the mobile phases connected and reagent lines

assembled to eliminate air bubbles.

The instrument conditions for the use of the *HILIC* analytical column were as

follows: (i) mobile phases were A1 (i.e. water with 0.015% formic acid and 0.015%

ammonia), B1 (i.e. 70% acetonitrile + 0.01% formic acid), A2 (i.e. water with 0.5%

formic acid), and B2 (i.e. methanol); (ii) seal and needle washes were 10% and 70%

acetonitrile, respectively; (iii) injection volume was 2 µL; (iv) run time for conditioning,

start-up, shutdown, and analysis were 30, 17.5, 15, and 11 min, respectively; and, (v)

temperature for column and autosampler held at 60°C and 4°C, respectively. Mobile

phases were delivered at the gradient throughout the conditioning, start-up, shutdown,

and analysis runs as described in Turner et al. (2019). In conditioning run, new columns

were conditioned before use for the first time with 100% of mobile phase A1 (0% B1) at

a flow rate of 0.10, 0.20, 0.30, 0.35, and 0.35 mL min^{-1} at time 0.0,1.5, 3.0, 4.0, and

30.0 min, respectively. If columns were already conditioned and used, the flow rate was

set to 0.35 ml min^{-1} throughout the conditioning run. The column conditioning was

performed using a blank injection, followed by the shutdown gradient and then the start-

up gradient prior to the analysis of standards and samples. The gradient during the

start-up run was initially 50% A1 (50% B1) at 0.3 mL min^{-1} for the first 4.0 min, and this

rate flow rate was increased to 0.50 mL min^{-1} starting at time 6.0 min for the next 9.0 min. Then, the gradient was decreased from 50% to 2.0% A1 (i.e. increased from 50% to 98% B1) with a flow rate of 0.50 mL min^{-1} for next 1.0 min until 16.0 min, and this rate was slowed down to 0.40 mL min^{-1} for the remaining 1.5 min. Whereas, the gradient during the shutdown run was initially 100% A1 (0% B1) at 0.30 mL min^{-1} for the first 4.0 min, and the concentration of A1 was dropped to 0% (100% B1) for the next 4.0 min. This gradient was kept steady for a minute, and the flow rate was doubled (i.e. 0.60 mL min^{-1}) starting at the time 11.0 min for the remaining 4 min. The LC gradient used for the analysis of standards and samples was initially 2% A1 (98% B1) at 0.4 mL min^{-1} for the first 5 min. Then, the gradient was increased from 2% to 50% A1 (dropped from 98% to 50% B1) for the next 2.5 min, before ramping the flow rate to 0.5 mL min^{-1} over the next 1.5 min until 9.0 min. The gradient then decreased to 2% A1 (increased to 98%) by 9.5 min, increasing to a flow rate of 0.8 mL min^{-1} at 10.0 min, holding until 10.6 min, and dropping back to 0.4 mL min^{-1} for the remaining 0.4 min.

The tandem quadrupole mass spectrometer (*MS/MS*) coupled to the *UHPLC* was used for the quantification of *PST* toxins. The *MS/MS* acquisition methods are set up using the specific multiple reaction monitoring (*MRM*) transitions recommended for *PST/TTX* acquisition as summarized in Turner et al. (2019). Toxins were monitored using positive and negative electrospray ionization modes (*ESI+* and *ESI-*, respectively). Saxitoxin (*STX*), neosaxitoxin (*NEO*), decarbamoyl saxitoxin (*dcSTX)*, decarbamoyl neosaxitoxin (*dcNEO*), deoxydecarbamoyl-STX (*doSTX*), and tetrodotoxin (*TTX*) were monitored using *ESI+* mode. Gonyautoxins 1 (*GTX 1*), gonyautoxins 2 (*GTX 2*), decarbamoyl gonyautoxins 1 (*dcGTX 1*), decarbamoyl gonyautoxins 2 (*dcGTX 2*), and N-sulfocarbamoyl toxins (*C1*) are monitored in *ESI-* mode. The remaining analogues of gonyautoxins (i.e. *GTX3, GTX4, GTX5*, GTX6), decarbamoyl

gonyautoxins (i.e. dcGTX3, dcGTX4), and N-sulfocarbamoyl toxins (i.e. C2, C3, and

C4) are monitored with both *ESI*+ and *ESI*-. Validation protocol was applied to certified

reference toxins as described in Turner et al. (2019). Quantification of the *PSP* toxins

was not performed since their presence in the extracted samples of *Alexandrium* strains

were not detected.

5.2.3.5 Analysis of lipophilic toxins in *Prorocentrum* spp.

Samples of *Prorocentrum* strains extracted in methanol were remained

unhydrolysed. The crude methanolic extracts were analysed for the presence of

lipophilic toxins (*LT*) such as okadaic acid (*OA*), dinophysis toxins (*DTX1* and *DTX2*),

pectenotoxins (*PTX1* and *PTX2*), azaspiracids (*AZA1*, *AZA2* and *AZA3*), and

yessotoxins (*YTX*, *homo YTX*, *45−OH YTX*, and *45−OH homo-YTX*) by *UHPLC-*

MS/MS using the method described in Dhanji-Rapkova et al. (2019, 2018).

The *UHPLC-MS/MS* system for LT analysis used a Waters Corp. (Manchester,

UK) BEH C18 column (50 x 2.1 mm, 1.7 µm) in conjunction with Waters Corp.

(Manchester, UK) VanGuard^{TM} BEH C18 (5 x 2.1 mm, 1.7 µm) held at 50°C. The

chromatography was performed in an alkaline condition (pH 11), which was achieved

by adjusting the alkalinity of mobile phases A (2mM ammonium bicarbonate) and B

(2mM ammonium bicarbonate in 90% acetonitrile) to pH 11$\pm$ 0.2 with ammonium

hydroxide following the method by Gerssen, Mulder, McElhinney, & de Boer (2009) with

modifications described in Dhanji-Rapkova et al. (2019, 2018). The mobile phases were

delivered at 0.6 mL min^{-1} in a gradient mode. The gradient was initially set at 75% A for

the first 0.2 min. This was decreased from 75% A to 50% A for the next 1.4 min and the

gradient was kept steady for 1.0 min. The composition of mobile phase A was

sequentially decreased by half every minute until it reached 0% by 3.0 min, holding it

until 3.5 min. The composition was ramped from 0% A to 75% A for the next 0.5 min,

keeping It steady for the remaining 0.5 min. A total cycle run time of 4.5 min. The

injection volume was set to 3 μL.

The *MS/MS* acquisition methods were set up using the *MRM* transitions

recommended for *LT* acquisition as summarized in Dhanji-Rapkova et al. (2019, 2018).

OA, DTX1, DTX2, *YTX, homo YTX, 45−OH YTX*, and *45−OH homo-YTX* were

monitored using negative electrospray ionization modes (*ESI-*). *PTX1*, *PTX2*, *AZA1*,

AZA2, and *AZA3* were monitored using positive electrospray ionization modes (*ESI+*).

Certified reference materials for *LT* were obtained from the Institute of Biotoxin

Metrology, National Research Council Canada (NRCC, Halifax, Nova Scotia, Canada),

which were diluted in 100% methanol to form concentrated stock standard solutions

prior to further dilution to make the calibration standards. Among the lipoliphic toxins,

the presence of *OA*, *DTX1*, and *DTX2* were detected in the *Prorocentrum* samples, and

hence, only these toxins were quantified.

The peak area response was measured using instrument quantitative data

processing software (i.e. Waters Corp. MassLynxTM v.4.1). The peak area response

data for the calibration standards were fitted against the concentration of the certified

reference toxins in linear regression curves. These linear regression models were used

to interpolate the concentration of the toxins in the sample using the following equation:

Equation 5.1 $\qquad Toxin\ concenration\ ([T];\ \mu g\ L^{-1}) = \frac{y-b}{a}$

where y is the peak response area, b is the intercept of the regression line, and a is the

slope of the calibration curve.

The cellular toxin content and cellular toxin production were computed using the

equations as shown below:

Equation 5.2 $\qquad Cellular\ toxin\ content\ (T_c;\ pg\ cell^{-1})\ = \frac{[T]}{N}$

Equation 5.3 $\quad\quad$ Cellular toxin production $(T_p; \mathrm{pg\ cell^{-1}\ d^{-1}}) = \dfrac{final\ T_c - initial\ T_c}{t}$

where $[T]$ is the toxin concentration (μg L^{-1}), N is the cell density (cells L^{-1}), and t is the

incubation time (in days).

5.2.4 Data processing and analyses

Analysis of variance (ANOVA) and *post hoc* Tukey were used (1) to determine

the cell-density dependence of toxin concentration and whether this dependence varies

across thermal conditions (2) to determine the temperature dependence of the

concentration, cellular content, and relative composition of toxins and whether this

dependence varies between experiments without and with thermal acclimatisation, (3)

to test the main effect temperature on cellular toxin production rates. A simple linear

regression was used to examine the relationship between cellular toxin production rates

and growth rates. Data processing and analyses were implemented in R version 3.6.1

(R Core Team, 2019).

5.3 RESULTS

5.3.1 Variation in toxin production

5.3.1.1 Toxin concentration

This study revealed that *P. lima* CCAP 1136/11 strain is highly toxigenic. This

strain produced a detectable concentration of okadaic acid (*OA*; 713.49 ± 106.12 μg L^{-1}; 116.80 – 2375.50 μg L^{-1}), dinophysistoxins 1 (*DTX1*; 74.45 ± 10.72 μg L^{-1}; 17.30 –

241.50 μg L^{-1}), and dinophysistoxins 2 (*DTX2*; 0.63 ± 0.17 μg L^{-1}; 0.20 – 5.40 μg L^{-1}).

Toxin concentration appeared to vary across cell density (Figure 5.1). Analysis of

variance revealed cell density dependency in the concentration of *OA* ($F_{(1,26)}$ = 6.88, *p* < 0.05) and *DTX1* ($F_{(1,26)}$ = 16.14, *p* < 0.05), but not in *DTX2* ($F_{(1,26)}$ = 1.08, *p* > 0.05). Among the toxins, only the concentration of *OA* showed to vary between experimental designs ($F_{(1,26)}$ = 7.60, *p* < 0.05). There was no significant interaction between the effects of the cell density and the experimental design on the toxin concentration.
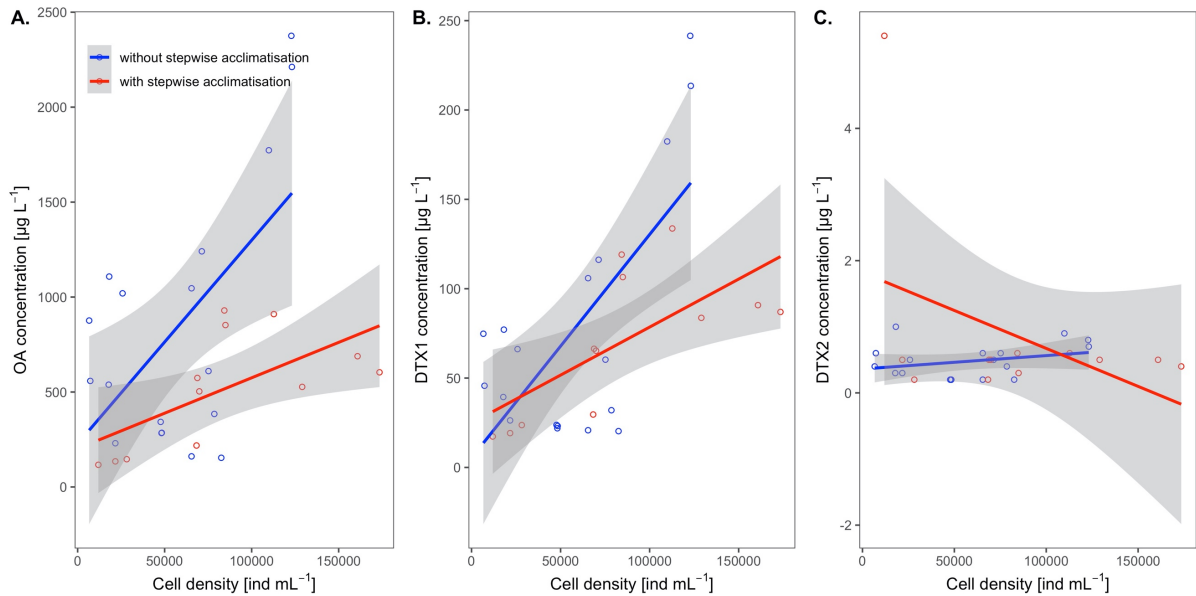
Figure 5.1. Cell density dependence of toxin concentration. The concentration of okadaic acid (*OA*) and dinophysistoxins (*DTX1* and *DTX2*) in *Prorocentrum lima* CCAP 1136/11 strain were fitted against cell density in a linear regression (A – C, respecitvely). Blue and red circles represent the toxin concentration estimated in the tube-based experiments without and with stepwise acclimatisation, respectively. The solid lines represent the linear fit with 95% confidence interval in grey shading.

The analysis of variance on the concentration of okadaic acid (*OA*) yielded significant variation across temperatures ($F_{(4,21)}$ = 10.15, *p* < 0.05), experimental designs ($F_{(1,21)}$ = 10.14, *p* < 0.05) and their interaction ($F_{(3,21)}$ = 11.95, *p* < 0.05) (Figure 5.2 A). The mean concentration of *OA* at 25 °C was 1363.18 $\pm$ 348.50 μg L^{-1}, which was significantly higher than the mean estimate at 10 °C (364.40 $\pm$ 146.97 μg L^{-1}), 15 °C (517.33 $\pm$ 127.01 μg L^{-1}), and 20 °C (640.08 $\pm$ 129.69 μg L^{-1}). On average, *OA* concentration estimated from tube-based experiments without stepwise acclimatisation (*TB1*) was 844 .42 $\pm$ 161.84 μg L^{-1} that was significantly higher than the mean

concentration estimated from the experiments with stepwise acclimatisation (*TB2*) (517.08 $\pm$ 87.50 μg L^{-1}). The highest mean *OA* concentration was 2120 $\pm$ 180 μg L^{-1} at 25 °C from *TB1*, which was 1222.60 – 1987.33 μg L^{-1} greater than the mean estimates from other groups of the two-way interaction.

The concentration of dinophysistoxins 1 (*DTX1*) also vary across temperatures ($F_{(4,21)}$ = 10.39, *p* < 0.05), but did not vary between experiments (Figure 5.2 B). However, the two-way interaction was significant ($F_{(3,21)}$ = 14.62, *p* < 0.05). Mean *DTX1* concentration at 25 °C was 149.81 $\pm$ 29.05 μg L^{-1}, which was 71.17 – 117.80 μg L^{-1} higher than the mean concentration at lower temperatures. The highest mean *DTX1* concentration was 212.47 $\pm$ 17.07 μg L^{-1} at 25 °C from *TB1*, which was 92.7 – 192.40 μg L^{-1} greater than the mean estimates from other groups of the two-way interaction. Also, *DTX1* concentration at 20 °C from *TB1* was higher than the concentration at 20 °C from *TB1* and at 10 °C from *TB2*.

There was no significant variation in the concentration of dinophysistoxins 2 (*DTX2*) across temperatures and experimental designs (Figure 5.2 C).
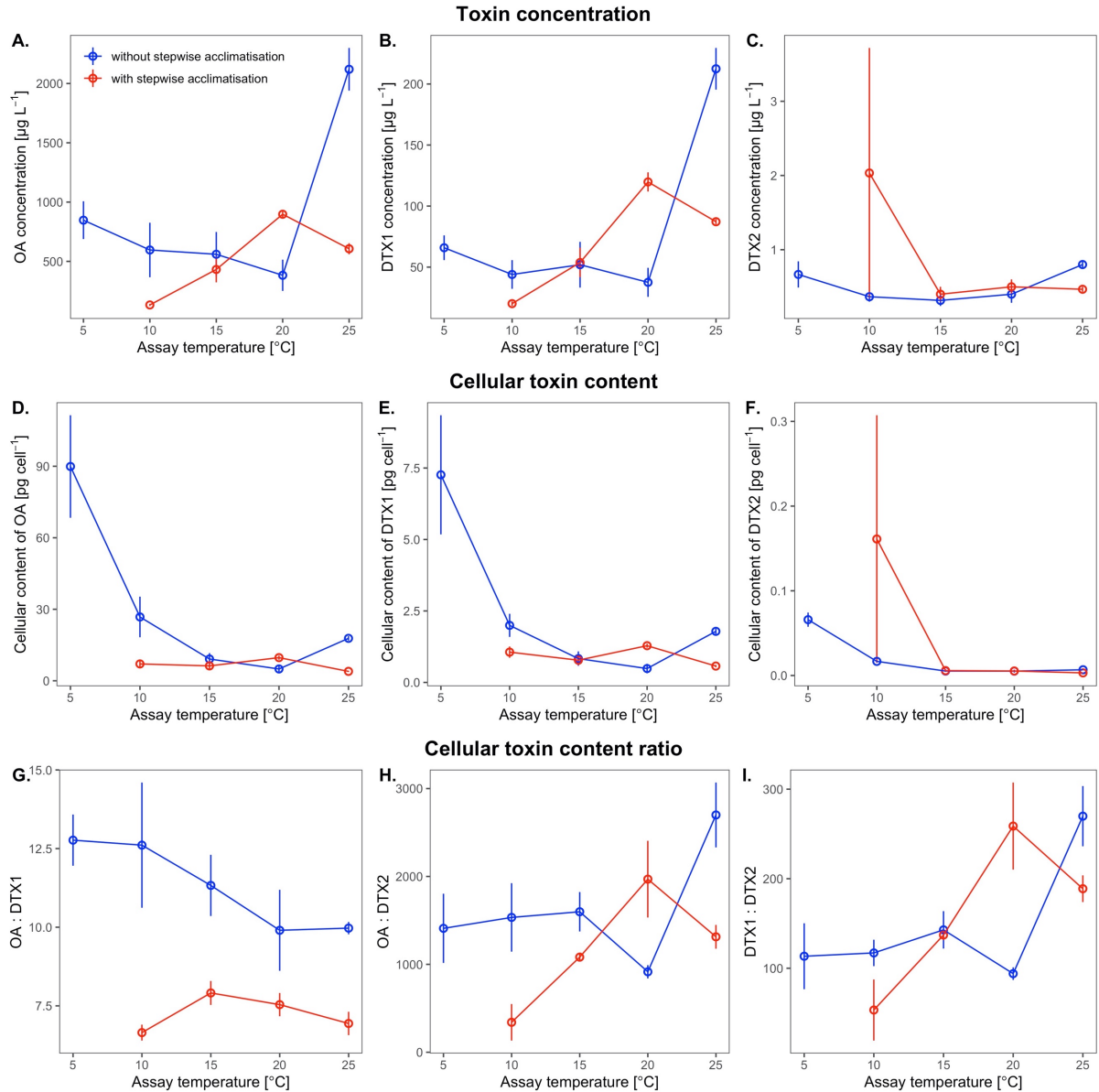
Figure 5.2. Temperature dependence of the concentration and cellular content of toxins. The mean concentration of okadaic acid (*OA*) and dinophysistoxins (*DTX1* and *DTX2*) in *Prorocentrum lima* CCAP 1136/11 strain across the temperature gradient in the tube-based experiments without and with stepwise acclimatisation (colored blue and red, respectively) are presented (A – C) as circles with error bars that represents the standard error of the mean. The mean cellular content of *OA*, *DTX1* and *DTX2* (D – F) and their relative proportion (G – I) across the assay temperatures in the culture experiments are also presented.

5.3.1.2 Cellular content of toxins

There was a significant difference in the cellular content of *OA* across temperatures ($F_{(4,21)}$ = 26.44, *p* < 0.05) (Figure 5.2 D). Neither the experimental design nor its interaction with temperature yielded a significant variation in the cellular content of *OA*. Mean cellular content at 5 °C was 89.90 ± 21.50 pg cell^{-1}, which was 63.12 –

85.95 pg cell^{-1} higher than the temperature in *TB1* and *TB2*. Mean cellular content of *OA* were the same across temperatures below 5 °C.

Similar pattern was observed in the cellular content of *DTX1*. It varied significantly with temperature ($F_{(4,21)}$ = 105.69, $p < 0.05$) and not with experimental design (Figure 5.2 E). Also, the two-way interaction was not significant. The mean cellular content of *DTX1* was 7.26 $\pm$ 2.08 pg cell^{-1}, which was 5.27 – 6.78 pg cell^{-1} higher than the temperatures in *TB1* and *TB2*. There was no evident variation in mean cellular content of *DTX1* across temperatures below 5 °C.

Analysis of variance revealed no significant difference in the cellular content of *DTX2* across temperatures and experimental designs (Figure 5.2 F). However, post hoc Tukey test showed significant variations between groups paired by temperature and its interaction with experimental design.

5.3.1.3 Cellular content of toxins ratio

The relative proportion between cellular content of *OA* and *DTX1* varied significantly across temperatures ($F_{(4,21)}$ = 3.45, $p < 0.05$) and between experiments ($F_{(1,21)}$ = 26.61, $p < 0.05$) (Figure 5.2 G). However, the two-way interaction between variables were not significant. *OA:DTX1* at 5 °C was 12.67 $\pm$ 0.81, which was significantly higher than the relative proportion at 20 °C (8.72 $\pm$ 0.80) and 25 °C (8.46 $\pm$ 0.70). Differences in *OA:DTX1* between several of the paired groups in two-way interaction were significant.

On the other hand, there was a significant variation in the ratio between *OA* and *DTX2* across temperatures ($F_{(4,21)}$ = 3.16, $p < 0.05$), experimental designs ($F_{(1,21)}$ = 6.23, $p < 0.05$), and their interaction ($F_{(3,21)}$ = 6.76, $p < 0.05$) (Figure 5.2 H). *OA:DTX1* at 25 °C (2006 $\pm$ 356.28) was significantly higher than the ratio at 10 °C (937.44 $\pm$ 331.95).

Also, significant differences in *OA:DTX2* between several of the paired groups in two-way interaction were found.

Ratio between *DTX1* and *DTX2* also differed significantly across temperatures ($F_{(4,21)}$ = 7.21, $p < 0.05$) but not between experimental designs (Figure 5.2 I). There was a significant interaction between the variables ($F_{(3,21)}$ = 7.60, $p < 0.05$). However, the post hoc Tukey tests did not reveal significant differences between paired groups.

5.3.1.4 Cellular toxin production rates

There was a significant effect of temperature on the production rate of *OA* ($F_{(4,10)}$ = 72.86, $p < 0.05$). On average, the highest production rate of *OA* was 6.37 $\pm$ 1.54 pg cell^{-1} d^{-1} at 5 °C, which was 4.51 – 6.12 pg cell^{-1} d^{-1} greater than the rates at higher temperatures (Figure 5.3 A). *OA* production drastically dropped to 1.86 $\pm$ 0.61 pg cell^{-1} d^{-1} at 10 °C, and it gradually declined to its lowest rate (0.03 $\pm$ 0.01 pg cell^{-1} d^{-1}) at 20 °C. It then slightly increased to 1.21 $\pm$ 0.07 pg cell^{-1} d^{-1} at 25 °C. However, the difference in *OA* production across temperatures above 5 °C was not significant.

The main effect of temperature on *DTX1* production was also significant ($F_{(4,10)}$ = 7.60, $p < 0.05$). Similar trend was observed in *DTX1* production in which the highest rates (0.52 $\pm$ 0.15 pg cell^{-1} d^{-1}) was observed at 5 °C (Figure 5.3 B). Also, it steeply declined to 0.14 $\pm$ 0.03 pg cell^{-1} d^{-1} at 10 °C and slowly dipped to 0.03 $\pm$ 0.01 pg cell^{-1} d^{-1} at 20 °C. Finally, it increased to 0.12 $\pm$ 0.01 pg cell^{-1} d^{-1} at 25 °C. Still, there was no significant variation in *DTX1* production across temperatures above 5 °C.

Furthermore, the significance of the effect of temperature on *DTX2* production was found ($F_{(4,10)}$ = 7.60, $p < 0.05$). *DTX2* production at 5 °C was 0.005 $\pm$ 0.0006 pg cell^{-1} d^{-1}, which was 4x – 11x greater than the rates at higher temperatures (Figure 5.3 C). Also, a sharp decline of rates was observed from 5 °C to 10 °C, followed by a gradual

155

decline of the rates until it reached the lowest rate at 20 °C. Mean production of *DTX2*

were statistically similar across 10 °C – 25 °C.
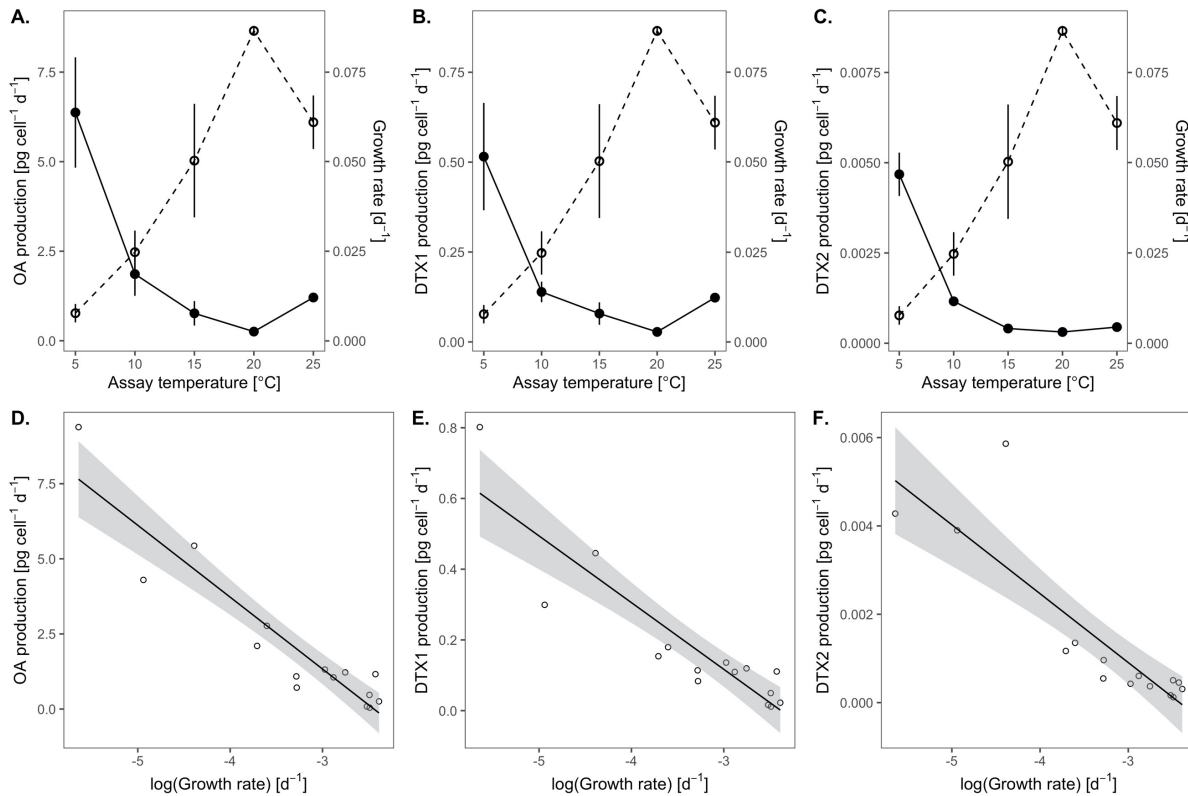
Figure 5.3. Temperature dependence of toxin production and growth rate and their relationship. The mean rates of production (solid circles connected with solid lines) of okadaic acid (*OA*) and dinophysistoxins (*DTX1* and *DTX2*) and the mean growth rate (open circles connected with dashed lines) in *Prorocentrum lima* CCAP 1136/11 strain across the temperature gradient in the first tube-based experiments are presented (A – C) with error bars representing the standard error of the mean. Toxin production rates were fitted against the log of growth rates in a linear regression (D – F). The solid lines represent the linear fit with 95% confidence interval in grey shading.

5.3.2 Relationship between toxin production and growth rates

Trends in the production of toxins across the temperature was opposite to

observed patterns observed in growth rates (Figure 5.3 A – C). As presented in Figure

5.3 D – F, toxin production and growth rates appeared to be inversely related. A simple

linear regression was used to determine significance of the inverse relationship. A

significant linear relationship with the growth rate was found for the production of *OA*

($F_{(1,13)}$ = 86.88, $p < 0.05$; adjusted R^2 of 0.86), *DTX1* ($F_{(1,13)}$ = 57.36, $p < 0.05$; adjusted

R^2 of 0.80), and *DTX2* ($F_{(1,13)}$ = 40.20, $p < 0.05$; adjusted R^2 of 0.74). For every log

increase in growth rate, production of *OA* decreased by 2.39 ± 0.26 (with the intercept

of -5.84 ± 0.89), *DTX1* production decreased by 0.18 ± 0.02 (with the intercept of $-$

0.45 ± 0.09), and *DTX2* production decreased by 0.0016 ± 0.0002 (with the intercept

of -0.0037 ± 0.0008).

5.4 DISCUSSION

5.4.1 Toxin production in dinoflagellates

This study examined the presence of saxitoxin (*STX*) and its derivatives in

Alexandrium spp. These toxins are comprised of a tri-cyclic perhydropurine, a nitrogen-

rich alkaloid (Gupta et al., 1989). Despite its similarity to purines of primary metabolism,

STX and its derivatives appears to be synthesized by a totally different pathway

(Shimizu et al., 1984). It has been suggested that arginine, acetate, and methionine

serve as the building blocks of this compound (Gupta et al., 1989; Shimizu et al., 1984).

STX modifies ion channels specifically by binding to voltage-gated sodium channels. It

blocks the opening and prevents the sodium ion flux across the membrane. This

neurotoxin alters the propagation of action potential generated across the nerve

membrane and thus prevents normal nerve function. *STX* is the causative agent for

paralytic shellfish poisoning (*PSP*) (Cusick and Sayler, 2013). As expected, these toxins

were not detected in *A. tamutum*. Surprisingly, the strain of *A. minutum* was tested

negative for the presence of *PSP* toxins. *A. minutum* is a dinoflagellate species known

to produce toxins (Flores-Moya et al., 2012; Wang et al., 2005), but non-toxic strains

are reported in several studies (Touzet et al., 2007; Yang et al., 2010). It is also likely

that their ability to produce toxins have lost because they possibly have been cultivated in the laboratory for a long period.

Among the model organisms in this present study, only *Prorocentrum lima* CCAP 1136/11 strain was found to produce okadaic acid (*OA*) and dinophysistoxins (*DTX1 and DTX2*). These toxins are linear polyethers that are linked to diarrhetic shellfish poisoning (*DSP*) (Hackett et al., 2009; Quilliam et al., 1996). These lipoliphic toxins are known to bind to the phosphatase proteins, specifically serine/threonine phosphatases, and inhibit the activity of the protein by hyperphosphorylation that modifies secretion of sodium ions and cell permeability of solutes (Garibo et al., 2013).

5.4.2 Cell density dependence of toxin concentration

The *P. lima* CCAP 1136/11 strain is highly toxigenic, with variable toxin concentration across all experimental conditions. This variability can be attributed to the cell density in the cultures. The results in this study show direct linear relationship between toxin concentration and cell density (Figure 5.1). Only *OA* and *DTX1* exhibit this relationship, suggesting that the concentration of these toxins is dependent on the cell density of the culture. The cell density dependence of *OA* and *DTX1* concentration substantiates the importance of population growth in promoting production of these toxins in *P. lima*. As secondary metabolites, the synthesis of *OA* and its analogues is completely uncoupled from cell growth (López-Rosales et al., 2013). These toxins are mainly accumulated during the stationary phase of growth at which cells are under long-term starvation (López-Rosales et al., 2013). However, it is assumed in this present study that toxins are produced during the exponential growth phase. Hence, the estimates of toxin concentration are lower compared to the values expected during the stationary growth phase that takes time to achieve in sub- and supra- optimal

conditions. It is therefore reasonable to take into account the effect of cell density when comparing toxin production across treatments by normalising the toxin concentration by cell density to produce the cellular toxin content that is expressed in pg cell^{-1}. Figure 5.4 presents the variation of cellular content of *OA*, *DTX1*, and *DTX2* in *P. lima* observed in this study and in literature.

5.4.3 *Inter-strain variability in cellular toxin content*

The results from the present study show that the cultured *P. lima* CCAP 1136/11 strain is actively producing *OA*. Varkitzi et al. (2010) reported that the *OA* cellular content for this CCAP 1136/11 strain ranges from 0.10 – 1.25 pg cell^{-1} within 1 – 15 days of incubation at 20°C, and it reaches the maximum value of 11.27 ± 3.30 pg cell^{-1} after 34 days of incubation. However, our findings show higher *OA* cellular content, varying between 1.86 and 11.02 pg cell^{-1} after 14 – 16 days of incubation at 20°C. This *P. lima* CCAP 1136/11 strain was isolated from Ria de Vigo in Spain, similar to the isolation location of the toxic *P. lima* strains reported in previous studies (Barbier et al., 1999; Bravo et al., 2001; Lee et al., 1989; Martine Morlaix and Patrick Lassus, 1992). Bravo et al. (2001) reported a range of *OA* cellular content (0.19 – 12.87 pg cell^{-1}) in 19 strains of *P. lima* isolated in the Pontevedra and Ria de Vigo, which is comparable to the present study. On the other hand, several studies have reported higher *OA* cellular content (5 – 24.5 pg cell^{-1}) in the isolates from Ria de Vigo than the reported estimates in CCAP 1136/11 strain (Barbier et al., 1999; Lee et al., 1989; Martine Morlaix and Patrick Lassus, 1992). This discrepancy suggests the inter-strain variability in *OA* cellular content within the same or adjacent isolation location, which may be linked to the differences in the environment, including temperature, light, and nutrient conditions employed in the cultivation.
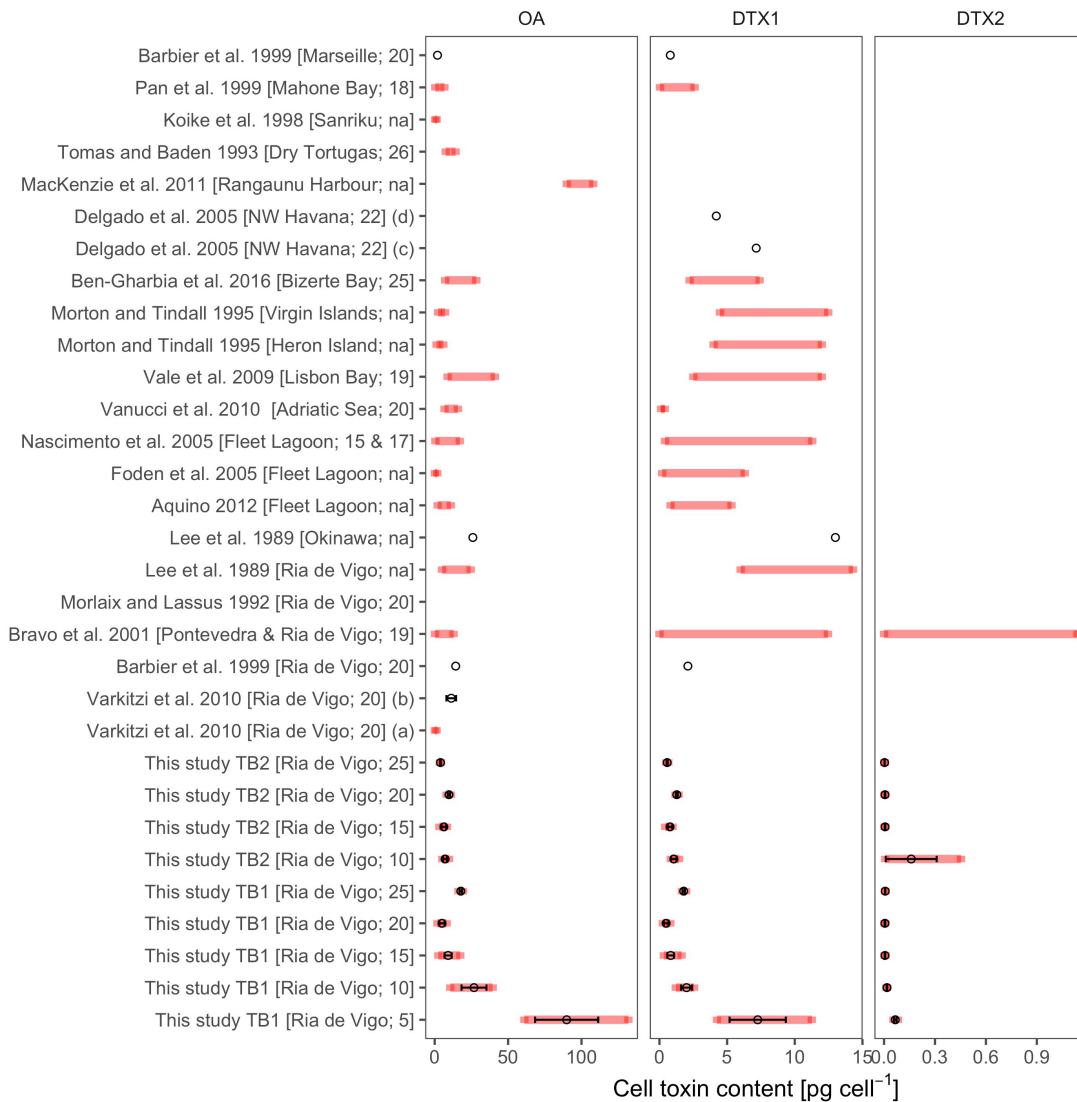
Figure 5.4. Inter-strain variability of cellular toxin content in *Prorocentrum lima* observed in this present study and in literature. The circles indicate the reported estimates or the observed mean estimates of cell toxin content with error bars representing the standard error. The red solid line indicates the reported/observed range. Enclosed in the bracket is the isolation location followed the assayed temperature in °C. This data is also summarised in Supplementary Table 5.1. [Abbreviations: (na) not available/acquired; (a) within 1 – 15 days incubation; (b) after 34 days of incubation; (c) cultured cells; (d) natural cells]

Comparing the results to other strains from other isolation locations, the mean estimates of *OA* cellular content at 10 – 25 °C in this present study are higher than the values reported for isolates from Fleet Lagoon, Dorset in UK (0.1 – 1.8 pg cell^{-1}) (Foden et al., 2005) but are generally within the reported range in several studies in the same location (0.42 – 17.13 pg cell^{-1}) (Aquino-Cruz, 2012; Nascimento et al., 2005). Furthermore, the mean estimates at 20 °C are also within the lower half of the range

reported for isolates from Adriatic Sea in Italy (6.69 – 15.8 pg cell^{-1}) (Vanucci et al., 2010) and Lisbon Bay in Portugal (8.8 – 41 pg cell^{-1}) (Vale et al., 2009), but are generally lower than the reported value for isolates from Marseille in France (1.9 pg cell^{-1}) (Barbier et al., 1999) and from Heron Island in Australia (1.31 – 5.88 pg cell^{-1}) (Morton and Tindall, 1995). The mean estimate 20 °C in the first test tube experiments (*TB1*) is within the range of the *OA* cellular content for isolates from Virgin Islands in USA (2.33 – 7.06 pg cell^{-1}) (Morton and Tindall, 1995) and from Mahone Bay in Nova Scotia, Canada (0.37 – 6.6 pg cell^{-1}) (Pan et al., 1999), but the mean estimate in the second test tube experiment (*TB2*) is higher than the reported range in the same isolation locations. At higher temperature (25 °C), the mean *OA* cellular content values observed in *TB2* is generally lower than the reported estimates for isolates from Bizerte Bay in Tunisia (7.13 – 28.33 pg cell^{-1}) (Ben-Gharbia et al., 2016) and from Dry Tortugas in Florida, USA (7.5 – 14.2 pg cell^{-1}) (Tomas and Baden, 1993), but the mean value observed in *TB1* is generally within and higher than the estimates reported in these isolation locations, respectively. Lee et al. (1989) recorded a cellular toxin content of 26 pg cell^{-1} in isolates from Okinawa, Japan, which was comparable to the mean estimate at 10°C in *TB1*. Moreover, Mackenzie et al. (2011) reported *OA* cellular content for isolates from Rangaunu Harbour in New Zealand, varying between 90 – 108 26 pg cell^{-1}. These values are the highest reported in literature, and are comparable to the range of *OA* cellular content in *P. lima* strains incubated at 5 °C observed in this present study. Overall, these results suggest the *OA* cellular content in *P. lima strains* is contingent to the geographic locations where the strains are isolated, which may be linked to variable environmental conditions that were experienced by *P. lima* strains at that time.

Furthermore, results of this present study revealed that the cultured *P. lima* CCAP 1136/11 strain is also actively producing *OA* analogues such as lipophilic dinophysistoxins (*DTX1* and *DTX2*). To our knowledge, this is the first study that demonstrated the presence of *DTX1* and *DTX2* in *P. lima* CCAP 1136/11 strain. *DTX1* cellular content in *P. lima* CCAP 1136/11 strain is 1.69 ± 0.40 pg cell^{-1} on average, varying between 0.25 and 11.26 pg cell^{-1} across temperature range of 5 – 25 °C. Except at 5°C, the mean estimates of *DTX1* cellular content found in this present study are lower compared to that of *P. lima* strain isolated from the same locations (i.e. Ria de Vigo, Spain) with the value of 2.10 pg cell^{-1} (Barbier et al., 1999). Furthermore, these mean estimates are within the lower half of the range reported for the isolates from Ria de Vigo, varying between 0 and 14.3 pg cell^{-1} (Bravo et al., 2001; Lee et al., 1989). Comparing to isolates from other location, the results at 20°C are within the reported range for the isolates from Mahone Bay (0.04 – 2.60 pg cell^{-1}) (Pan et al., 1999), lower than the values for isolates from Adriatic Sea (0.12 – 0.39 pg cell^{-1}) (Vanucci et al., 2010), and higher than the estimates for isolates from Lisbon Bay (2.5 – 12 pg cell^{-1}) (Vale et al., 2009). Moreover, the mean estimates observed in this present study are generally within the lower half of the range of *DTX1* cellular content observed for isolates from Fleet Lagoon (0.2 – 11.29 pg cell^{-1}) (Aquino-Cruz, 2012; Foden et al., 2005; Nascimento et al., 2005). Barbier et al. (1999) reported a *DTX1* cellular content value of 0.8 pg cell^{-1} at 20 °C, which was higher and lower than the estimates observed at 20 °C in *TB1* and *TB2*, respectively. At 25 °C, the present study yields a lower estimate of *DTX1* cellular content compared to the values for isolates from Bizerte Bay, which vary from 2.23 to 7.4 pg cell^{-1} (Ben-Gharbia et al., 2016). Delgado et al. (2005) reported *DTX1* cellular content for cultured (7.15 pg cell^{-1}) and natural population (4.20 pg cell^{-1}) of *P. lima* cells isolated from Havana City in Cuba (Delgado et al., 2005),

which was generally higher than the observed values in this present study. Morton and Tindall (1995) reported higher estimates of *DTX1* cellular content for Heron Island isolates, varying between 4 and 8 pg cell^{-1}, which are also higher than observations at 10 – 25 °C in this present study. *P. lima* isolates from Okinawa is reported to contain 13 pg cell^{-1} of *DTX1* (Lee et al., 1989), which is the highest value found in literature. On the other hand, *DTX2* cellular content in *P. lima* CCAP 1136/11 strain is 0.028 ± 0.015 pg cell^{-1} on average, varying between 0.0023 and 0.45 pg cell^{-1} across temperature range of 5 – 25 °C. Bravo et al. (2001) reported the *DTX2* cellular content for isolates from Ria de Vigo, ranging from 0 to 1.14 pg cell^{-1}. The mean estimates of *DTX2* cellular content observed in this present study is generally within the lowest extreme of the range reported in Bravo et al. (2001). These findings also suggest inter-strain variability of *DTX1* and *DTX2* in *P. lima* and this large variability may also be explained by the varying environmental conditions experienced by strains in the different isolation locations.

As observed, both the content and composition in *P. lima* CCAP 1136/11 strain are variable across the experimental conditions. Cellular content of *OA* is 9.70 ± 0.50 times (6.17 – 15.40 times) higher than *DTX1*, and it is 1446.16 ± 137.29 times (21.63 – 3159.30 times) higher than the *DTX2*. On the other hand, cellular content of *DTX1* is 151.83 ± 14.41 times (3.20 – 355 times) higher than *DTX2*. Studies on the relative composition of cellular toxin in *P. lima* is limited. *OA:DTX1* of *P. lima* CCAP 1136/11 strain observed in this present study is higher than the reported estimates in *P. lima* isolates from Mahone Bay in Nova Scotia, Canada (*OA:DTX1* is nearly 1:1) (Jackson et al., 1993; Marr et al., 1992) and from El Pardito in Gulf of California, Mexico (*OA:DTX1* is 1:2) (Heredia-Tapia et al., 2002). This suggests variability in the relative composition of toxins within the *P. lima* species.

Cellular toxin content indicates the amount of toxin initially accumulated in a cell and the gross toxin production that reflects the balance between the net production and loss of toxins (Kamiyama et al., 2010). Catabolism, leakage, and/or cell division contribute to the net toxin loss (Anderson et al., 1990), and among these processes, cell division is thought to be crucial in laboratory experiments (Kamiyama et al., 2010). In this present study, cellular toxin production rates were determined to examine further the dynamics of toxin production in *P. lima* CCAP 1136/11 strain for each of the thermal condition in *TB1*. The initial cellular toxin content was not obtained in *TB2*, and hence, the cellular toxin production rate for this experimental condition cannot be computed. However, it is assumed that the rates will be the same with the estimates in *TB1*, since the variation in cellular toxin content between the experimental designs was not significant. Results showed the cellular toxin production for *OA* is 2.09 ± 0.66 pg cell^{-1} d^{-1} ($0.045 - 9.38$ pg cell^{-1} d^{-1}), for *DTX1* is 0.18 ± 0.05 pg cell^{-1} d^{-1} ($0.01 - 0.80$ pg cell^{-1} d^{-1}), and for *DTX2* is 0.0014 ± 0.0004 pg cell^{-1} d^{-1} ($0.0001 - 0.0059$ pg cell^{-1} d^{-1}). Cellular toxin production rate in *P. lima* is not well studied, but it expected to vary among strain since the cell toxin content is highly variable. Comparing the results of this study to the rates of other species found in literature, the mean cellular production rate of *OA* in *P. lima* is within the reported range of rates in *Dinophysis acuminata* ($1.18 - 2.31$ pg cell^{-1} d^{-1}) (Kamiyama et al., 2010). However, *DTX1* cellular production rates in *P. lima* estimated in this present study is higher than the reported values in *D. acuminate* ($0.06 - 0.08$ pg cell^{-1} d^{-1}) (Kamiyama et al., 2010). This suggests inter-species variability of the cellular toxin production rates in toxic dinoflagellates.

P. lima is not only known to accumulate intracellular toxins, but it also releases considerable amount of toxins to the surrounding (Nascimento et al., 2005; Vale et al., 2009). Furthermore, the filtration employed in the extraction of algal toxins may have

produced enough pressure on cells, forcing to leak extracellularly. In this study, toxins were not obtained, hence our findings may be biased by this, which underestimates the toxin production in *P. lima* CCAP 1136/11 strain.

5.4.4 Thermal dependence of toxin production

Another objective of this study was to examine the effect of varying temperature on the total concentration, cellular content, composition, and production rates of toxins in marine phytoplankton, using *Prorocentrum lima* as a model organism. The results revealed that the concentration of *OA* and *DTX1* in *P. lima* CCAP 1136/11 strain are temperature dependent (Figure 5.2 A). The temperature dependence in the *OA* and *DTX1* concentration was contingent on whether the test organism was drastically or gradually (without or with stepwise acclimatisation, respectively) exposed to new thermal condition. Drastic exposure of *P. lima* strain to 25 °C yielded higher *OA* and *DTX1* concentration than the estimates at 15°C, but the gradual exposure produced no difference from the estimates at 15°C. However, this is unlikely an indication of response to heat stress since the total toxin concentration is also dependent on cell density (Figure 5.1). Furthermore, the findings show temperature dependence of the cellular content of *OA* and *DTX1* in *P. lima* CCAP 1136/11 strain (Figure 5.2 B). This dependence on temperature is attributed to cellular toxin content at 5 °C, which was greater than the estimates at higher temperature. However, no difference in the cellular content across 10 – 25 °C, regardless of whether the strain is exposed drastically or gradually to new temperature. This suggest that the cellular accumulation of *OA* and *DTX1* in *P. lima* strain is not a response of heat stress. However, production of these toxins in response to cold stress warrants further investigation. The relative proportion between *OA* and its analogues (*DTX1* and *DTX2*) in *P. lima* CCAP 1136/11 strain varies

across thermal conditions (Figure 5.2 C). Across all temperatures, drastic exposure to new temperature yielded higher estimates of *OA*:*DTX1* as compared to the ratios produced by strains that undergo a stepwise acclimatisation. These findings suggest that the relative toxin composition is also dependent on the thermal exposure conditions. Cellular production rate of *OA*, *DTX1*, *DTX2* in *P. lima* CCAP 1136/11 strain exhibit temperature dependence (Figure 5.3 A). Low cellular toxin production rates are observed at thermal optimum for growth (20°C), whilst higher production rates are observed at sub- and supra-optimal temperatures. This suggests that temperature may indirectly affect toxin production and that the temperature-dependence of population growth influences toxin production in *P. lima* strain.

5.4.5 Inverse relationship between growth and toxin production

The results of this study indicate there is an inverse linear relationship between toxin production rates and growth rates in *P. lima* CCAP 1136/11 strain (Figure 5.3 B), suggesting that the toxin production rate increases with decreasing growth rates. Toxin production is postulated to dispense with excess photosynthetic energy when toxic species growth is no longer optimal (Bates, 1998; Pan et al., 1996). Growth at the sub-optimal thermal range was observed to favour a high cell *PSP* toxin quota in *Alexandrium* spp. (Usup et al., 1994), which may suggest that cellular nitrogen is more allocated to toxin synthesis than protein biosynthesis at this condition (Anderson et al., 1990). The same observation was found in *Pseudo-nitzchia seriata* where growth at lower temperature produce higher levels of cellular DA, but it is still unclear whether this is due to physiological stress at this condition (Bates, 1998). It is also observed that cellular OA/DTX content is increased in *P. lima* at lower temperature which may be also attributed to a division rate rather an increase in production (Wright and Cembella,

1998). Furthermore, cell growth in *Pseudo-nitzchia multiseries* at higher temperature and light did increase the cellular DA content, which may suggest increase supply of photosynthetic energy to enhance DA production (Bates, 1998). Some species produce toxin in response to stressful thermal conditions when growth is strongly inhibited (Aquino-Cruz, 2012). Long-term starvation allows toxic species to accumulate toxins (Lee et al., 2016), which can be induced when increased temperature limits their capacity to uptake nutrients (Sterner and Grover, 1998).

5.5 CONCLUSIONS

This present study demonstrated the toxigenicity of *Prorocentrum lima* CCAP 1136/11 strain. The strain has variable concentrations of okadaic acid (*OA*) and dinophysistoxins (DTX1 and DTX2) across all experimental conditions, which can be attributed to the cell density in the cultures. The strain also has cellular contents of OA, DTX1, and DTX2 that were comparable to the reported values in the literature. Furthermore, the concentration, cellular content, relative composition, and cellular production rate of toxins in this strain was temperature dependent. The findings also present an inverse linear relationship between toxin production rates and growth rates in this strain. Overall, the results in this present study improve our current understanding on the toxin production in marine phytoplankton, which have a potential implication on the toxic blooms in the future climate scenarios.

This page is intentionally left blank.

This page is intentionally left blank.

CHAPTER 6

This page is intentionally left blank.

This page is intentionally left blank.

THE EFFECT OF WARMING ON GROWTH AND COMPETITION IN MARINE DINOFLAGELLATES

ABSTRACT

Ocean warming is having a profound impact on the physiology and ecology of phytoplankton. This present study examines how warming affects the growth and competition of marine dinoflagellate, some of which are responsible for toxic algal blooms. Specifically, this study sets out to determine (1) the growth responses of species to warming, (2) the species specificity of the temperature dependence of growth and competition, and (3) the relationship between growth response and competition response to warming. Six phytoplankton species representing two co-occurring genera of dinoflagellates (i.e. *Prorocentrum* and *Alexandrium*) were incubated at three temperatures(15, 20, and 25 °C) in monocultures and pairwise mixed cultures. Results showed that (1) temperature is a limiting factor for growth and competition in marine dinoflagellates, (2) temperature dependence of growth and competition is specific to the species identity of the focal and competitor strain, and not to their toxicity, (3) interspecific competition influence the growth responses to temperature, (4) warming affects interspecific competition, (5) strong direct relationship between growth and competition, and (6) ecological response is predictable from growth responses. In light of these findings, it is expected that interspecific competition of marine phytoplankton is likely to change the community structure under a future climate scenario.

6.1 INTRODUCTION

Climate change is recognised as a major threat to global biodiversity and predicted to be the main cause of the extinction of thousands of species over the next century (Bellard et al., 2012; Thomas et al., 2004). There has been recent advancement of our understanding of the ecological consequence of climate change (Hoegh-Guldberg and Bruno, 2010; McCarty, 2001; Pecl et al., 2017). In fact, a rapid increase in the number of experiments has been conducted in the last decades with the aim to establish mechanistic understanding of how climate change might transform the biological world (Wernberg et al., 2012). Despite the considerable efforts, our current knowledge of the role of species interactions in responses to climate change is still limited, especially the ecological responses of the aquatic primary producers to ocean warming.

Due to climate change, the oceans are warming at a rate of ~0.13 °C per decade (Rhein et al., 2013), and is having a profound effect on phytoplankton from its physiology to ecology (Regaudie-De-Gioux and Duarte, 2012; Thomas et al., 2012; Toseland et al., 2013). Most phytoplankton studies are focused on the response of single-species population that reflect the direct physiological response of organism to changing temperature (e.g. Boyd et al., 2013; Coello-Camba and Agustí, 2017; Huertas et al., 2011), but often disregarded the contribution of species interaction that may either improve or aggravate a species' response to increased temperature. Warming affects species interaction, and changes in species interaction may influence the impacts of climate change on populations (Bellard et al., 2012; Cahill et al., 2013; Tylianakis et al., 2008). Hence, understanding how warming affects species interaction

is critical for predicting how climate change will alter the structure and function of phytoplankton communities in the future oceans.

Competition exists in nature between organisms with similar needs and habits living in the same environment (Keddy, 2001). This interaction occurs when more than one organisms demand for the same resources of the environment that are limited in availability, causing a negative effect to one or more organisms (Crombie, 1947). At the species level, two species that are competing for the same limited resources in the same environment cannot survive together unless they have equal competitive ability (Crombie, 1947). Hence, competition can cause the exclusion of a species that has lower competitive ability than other species (Chesson, 2000). Several studies have demonstrated the significance of competition and the environment in predicting the community composition and diversity (Durant et al., 2012; Grover, 2000; Hodge and Fitter, 2013; Kennedy, 2010; Stenseth et al., 2015), but there have been very few empirical studies that assess how temperature influences community structure through its effects on interspecific competition.

Temperature has effects on species interaction, mainly through its influence on the metabolism of organism (Brown et al., 2004; Van Der Meer, 2006). Several life history traits that determine fitness (e.g. population growth and biotic interactions) are governed by the most fundamental biological rate – the metabolic rate (Brown et al., 2004). Temperature dependence of metabolic rates vary across species, and this interspecific differences in the thermal performance curves can greatly influence species interactions (Dell et al., 2014). The key role of metabolic traits, i.e. the temperature dependence of growth and resource acquisition can be used to predict the outcome of interspecific competition in phytoplankton (Bestion et al., 2018). The temperature dependence of growth rate is directly relevant to species interactions, and

the effect of temperature on growth rate is expected to change the competitive interactions among species in a community (Lord and Whitlatch, 2015). Changes in growth with temperature can be used to predict the outcome of competition (Clusella-Trullas et al., 2011; Milazzo et al., 2013). The growth responses to temperature are typically characterised as asymmetrical curves, known as the thermal performance curves or the thermal reaction norms, which are often unimodal and negatively skewed in ectotherms (Eppley, 1972; Kingsolver, 2009; Knies and Kingsolver, 2010). The range of temperature at which organism can survive defines the thermal niche of species (Boyd et al., 2013; Chen, 2015). Vulnerability to warming is dependent on the thermal niche of species, and it is expected that those with narrower thermal tolerance range are more susceptible to warming (Magozzi and Calosi, 2015; Pacifici et al., 2015).

Different growth responses to temperature drive the changes in the interspecific competition in several groups of organism including bacteria, phytoplankton, plants, and invertebrates (Bestion et al., 2018; Chu et al., 1978; Johannes et al., 1983; Nedwell and Rutter, 1994). Thermal tolerance differs between toxic and non-toxic phytoplankton within genus (Rhodes et al., 1994), but not within species (Huisman et al., 2005). Hence, it is expected that the warming will have an effect the competitive interaction between non-toxic and toxic species.

Hence, in this chapter, the main objective is to examine the effect of warming on the growth and competition in phytoplankton using marine dinoflagellates as test organisms. Specifically, this chapter aims to (1) evaluate the growth responses of species to warming in the absence and presence of competitors, (2) test whether the growth and competitive responses to different temperature treatments are dependent or not on the taxonomic identity and toxicity of focal and competitor species, and (3)

assess the relationship between growth rates and competition coefficients across the different temperature treatments.

6.2 MATERIALS AND METHOD

6.2.1 Experimental design

Six phytoplankton species representing two co-occurring genus of dinoflagellates (i.e. *Prorocentrum* and *Alexandrium*) were used as model organisms, i.e. (1) *Prorocentrum* sp. NRR 188, (2) *Prorocentrum micans* CCAP 1136/15, (3) *Alexandrium tamutum* PARALEX 242, (4) *Prorocentrum minimum* Poulet, (5) *Prorocentrum lima* CCAP 1136/11,and (6) *Alexandrium minutum* PARALEX 246, which were obtained from different culture collections. The first three species are categorised as non-toxic, whereas the remaining three species are categorised as potentially toxic. Further information about their origin, culture condition, and toxicity is available in Chapter 4. These species belonging to a taxonomic group that consist the majority of the toxic bloom-forming species. The ecological and economic relevance of dinoflagellates are very important and understudied. Dinoflagellates can be mixotrophic and endosymbiotic, but can cause economically damaging tides.

Cultures were maintained in 30 mL stock cultures in artificial seawater (ASW) enriched with K minimum nutrients (K medium), which were stored in T25 cell culture flask with filter caps. They were kept inside a growth chamber at 15 °C, under a continuous light cycle at irradiance levels of 221 ± 12 µmol m^{-2} s^{-1}. All stock cultures were maintained in exponential growth with a 1:10 dilution every 14 days.

Prior to the experiment (see Figure 6.1 for schematic representation of the experimental design), each strain was acclimated for two weeks at three different

temperature treatments (i.e. 15, 20, and 25 °C) under 12:12 hr light:dark cycle at irradiance levels of 251 ± 10 µmol m^{-2} s^{-1}. In each temperature treatment, six stocks of monocultures (single-species cultures) and 15 stocks of pairwise co-cultures (mixed-species cultures) were prepared (Figure 6.1 A). These stock cultures were prepared by inoculating the same biomass (using fluorescence as proxy) of the pre-acclimated cultures into 250 mL Erlenmeyer flask. All experiments were conducted in triplicates in T25 cell culture flask (with filter caps), containing 20 mL of the stock cultures. The single- and mixed-species cultures were incubated for 20 days at three different temperature treatments (i.e. 15, 20, and 25 °C) inside custom-built water baths (Figure 6.1 B) with circulating water. The temperature of the circulated water was regulated by external recirculating water baths. The water baths were placed on platform rockers set to 70 rotations per minute (rpm) and kept inside a growth chamber (Adaptis CMP6010, Conviron, Canada).

To monitor changes in the cultures throughout the experiment, 200 µL samples were collected from all cultures every 48 hours for 20 days (the cultures were shaken to homogenise the cells prior to collection). The samples were placed into 96-well microtiter plates and were immediately fixed with Lugol's solution (1% final concentration). For every sampling, each sample was consistently inoculated into a well following the well plate format in Figure 6.2. The samples were then stored at 4°C until they were analysed through microscopy.

A. Phytoplankton cultures
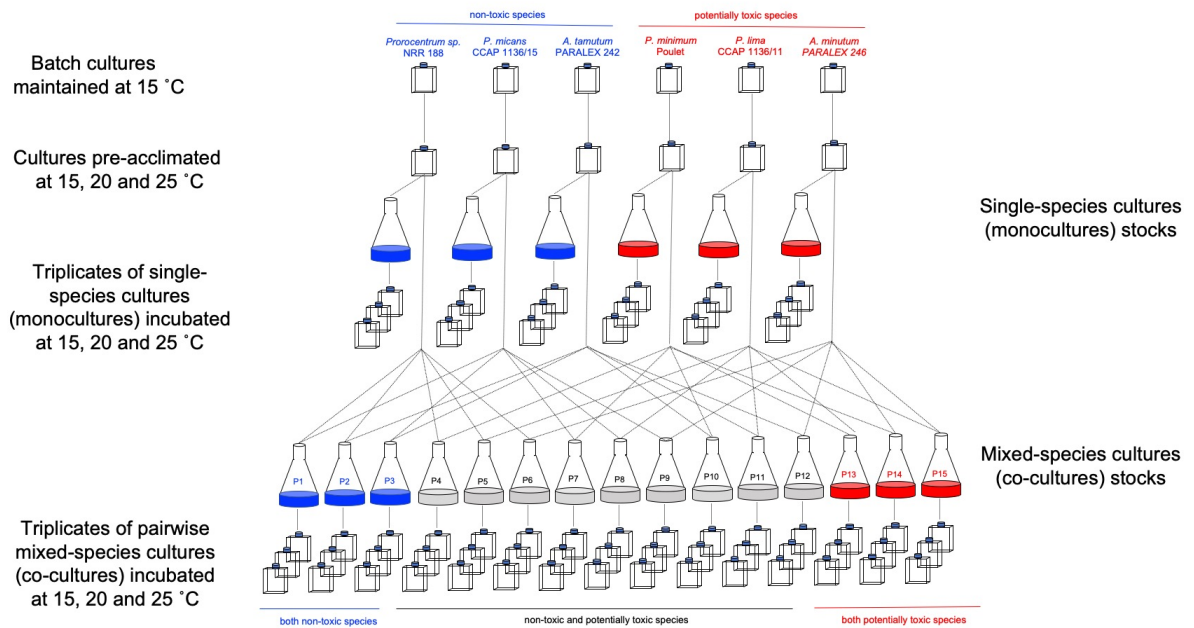
B. Temperature treatments
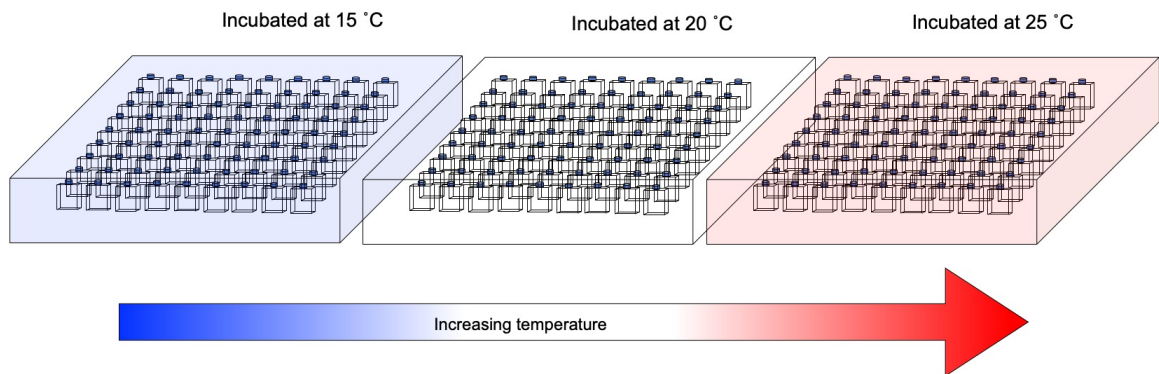
Figure 6.1. Schematic representation of the experimental designs to examine effect of temperature on the competition in marine phytoplankton.

6.2.2 High throughput microscopy

Microscopy was performed with a Leica DMI6000B inverted light microscope equipped with Leica DFC310FX camera (Figure 6.2 A), and the acquisition and device control were performed by Leica AF6000 Modular Systems (LAS AF) v4.6 (Leica Microsystems CMS GmbH, Ernst-Leitz-Strasse, Wetzlar, Germany).
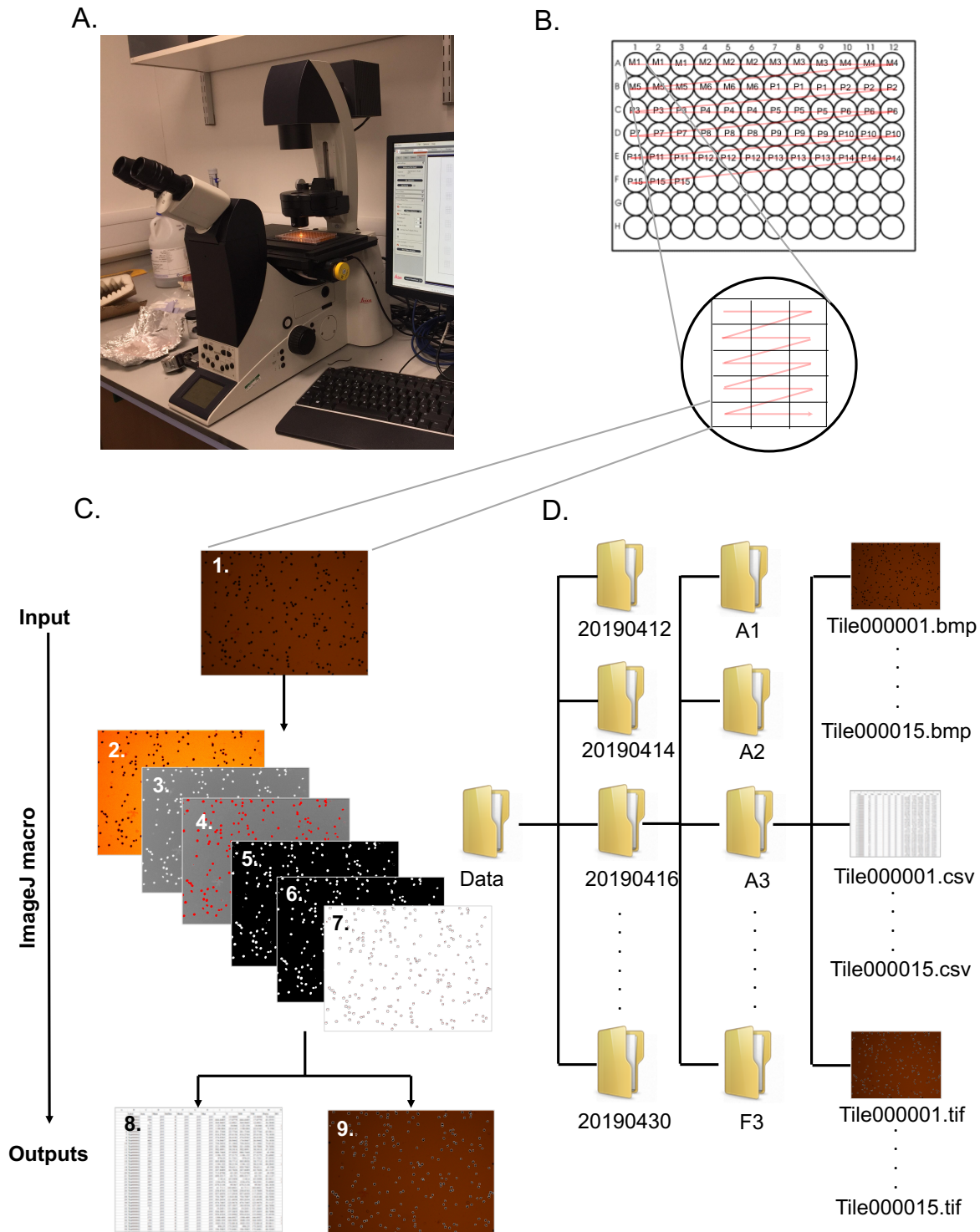
Figure 6.2. Workflow of high throughput microscopy and image processing and analysis. The samples in the 96-well microplate were examined under a Leica DMI6000B inverted light microscope at 100x magnification (A). Each sample in a well was scanned (the red lines indicate the scanning path) on a 3x5 rectangular pattern producing 15 image tiles per sample (B). Each microscope image (C1) was processed (C2 – C7) by executing an ImageJ macro in FIJI to produce a spreadsheet of parameters (C8) and an image overlaid with outlines (C9). Input and output files for each samples for every sampling date were organised in a directory with a structure shown in D.

The 96-well plate without the lid was placed securely on a multi-well plate stage insert. The samples were initially examined through the eyepiece under 50x magnification with a bright field illumination and to have a clear view of the stained specimen. We then switched to a colour camera under 100x magnification to have a live view of the specimen on the LAS AF screen and the focus was adjusted to obtain optimal image quality. A 3x5 rectangular pattern was constructed repeatedly for each of 96 wells to acquire 15 image tiles for each well (Figure 6.2 B). Images were acquired with an automated scanning of the pattern with autofocus. All images were saved as bitmap files in best resolution of 1392 × 1040 pixels and kept in a directory with a structure shown in Figure 6.2. In this directory, the images were organised by folders that correspond to the sampling date (e.g. ./Data/20190412). Within these folders are subfolders that correspond to the well position of the sample in the microplate (./Data/20190412/A1), which in every subfolder contains all the 15 image tiles from each replicate in every sample.

6.2.3 Image processing for cell characterisation

FIJI (FIJI is Just ImageJ) software was used to process and analyse the microscope image data (Schindelin et al., 2012). The processing was automated using a script written in ImageJ Macro programming language (Supplementary Information 6.1). The script was executed one sampling date at a time in the macro interface in FIJI as soon as the image data were acquired. The script requires the path of the working directory. The function in the macro script has 9 major steps to process and analyse an image (Figure 6.2 C Step 1 – 9): (1) opening and duplication of an image file; (2) enhancement of contrast of the image; (3) converting to 8-bit image and inverting the look-up table; (4) setting the threshold using MaxEntropy; (5) converting to Mask; (6)

opening, filling the holes, and watershading; (7) setting the measurements, analysing

particles with parameters set to size = 50 – Infinity and circularity=0.50-1.00, and

displaying the outputs; and saving the outputs that includes (8) a spreadsheet (in .csv

format) enumerating all the detected cells and their corresponding size and shape

parameters and (9) an image overlaid with outlines of the detected cells (in .tif format)

that were labelled with identification number matching to the identification number in the

spreadsheet. The script performs a for loop of this function for every image in every

subfolder in the specified directory (Figure 6.2 D).

The spreadsheet data produced in FIJI were processed and analysed in *R*

version 3.6.1 (R Core Team, 2019) . We collated all spreadsheet data into one data

frame and curated it to retain records within the expected range of species-specific

dimensions. This resulted to a data frame with observations for 45 variables. Five

identification parameters (treatment, date, trial, culture, code) and 13 morphometric

features (Area, Perimeter, Width, Height, Circularity, Feret, FeretX, FeretY, Feret Angle,

Mini, AR, Roundness, and Solidity; see

https://imagej.nih.gov/ij/docs/menus/analyze.html for description) were selected and

used for the succeeding analysis.

6.2.4 Deep learning for species identification

A deep neural network model for each pairwise combination was developed

using the 13 morphometric features to predict the species identity in mixed-species

cultures. In each combination, a dataset of 30,000 observations for each species

sampled randomly from the single-species dataset was assembled. The dataset was

split into training (80%) and test (20%) datasets using the R package *rsample* (Kuhn et

al., 2019). The predictor variables were normalised (scaled and centered), whilst the

categorical response variables were one-hot encoded. Both the training and test datasets were pre-processed using the *recipes* package in R (Kuhn and Wickham, 2019).

The training dataset was used to train and validate a four-layer neural network model using the *keras* package in R (Allaire and Chollet, 2019). A sequential model was initialised, and an input layer with 13 variables, three hidden layers with 16, 8, and 4 nodes, and an output layer with 2 nodes were applied (Figure 6.3). All hidden layers were set with a uniform kernel initialiser and a rectified linear unit activation function. The input shape in the first hidden layer was set to the number of variables in the input layer (i.e. 13). A dropout layer after each hidden layer was added at a rate of 0.10, which eliminate weights below the cut-off threshold (i.e. 10%) to prevent overfitting. Also, the output layer was set with a uniform kernel initialiser and a sigmoid activation function. The model was compiled with a common optimisation algorithm (i.e. adam), categorical cross entropy loss, and accuracy metrics. The model was trained with a training cycle set to 100 epochs (i.e. iterations), a batch size set to 100 samples per gradient update within each epoch, and a validation split set to 0.10 to include 10% of the data for model validation. All the settings for the neural network model described above are results of tuning.

The model was assessed based on the cross entropy loss and accuracy of the training and validation (Figure 6.4 A). Also, the true performance of the model was assessed by generating the class predictions from the model on the test datasets using the *yardstick* package in R (Kuhn and Vaughan, 2020), which was then inspected using a confusion matrix (Figure 6.4 B). From the confusion matrix, the accuracy of the model was calculated by determining the proportion of correctly classified individuals against the total population (i.e. total number of individuals that have been classified). The

accuracy of the models used to classify species in pairwise mixed-species cultures is summarised in Supplementary Table 6.1. The model accuracy was used as inclusion criteria for the succeeding data analysis. Pairs with average model accuracy of <0.80 (highlighted in grey) were included in the dataset (referred as *filtered dataset* hereinafter), which was used in the succeeding data analysis. The identity of species in a mixed-species culture was predicted using the morphometrics data (centered and scaled similar to the normalisation rule of the training dataset) observed in the co-culture dataset, which were fed into the trained model.
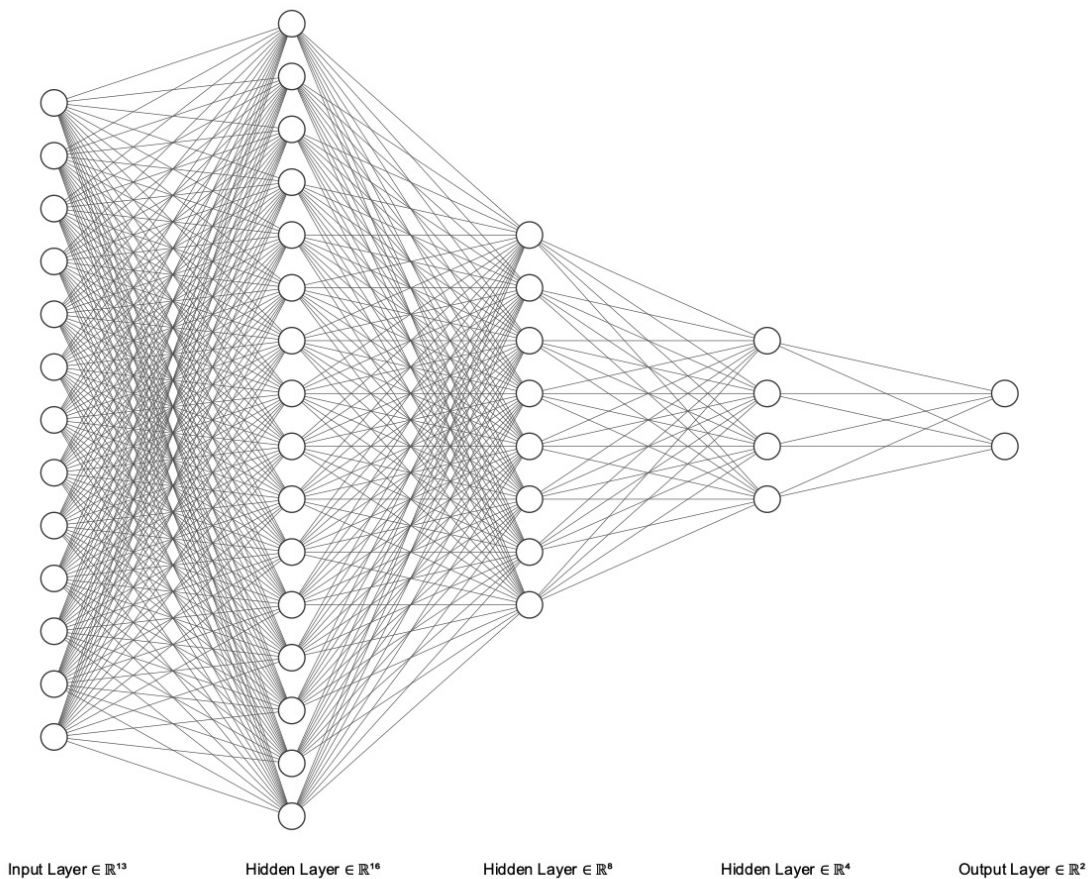
Figure 6.3. A deep neural network architecture showing an input layer with 13 variables, three hidden layers with 16, 8, and 4 nodes, and an output layer with 2 nodes used to classify species in pairwise mixed cultures.

A.

B.
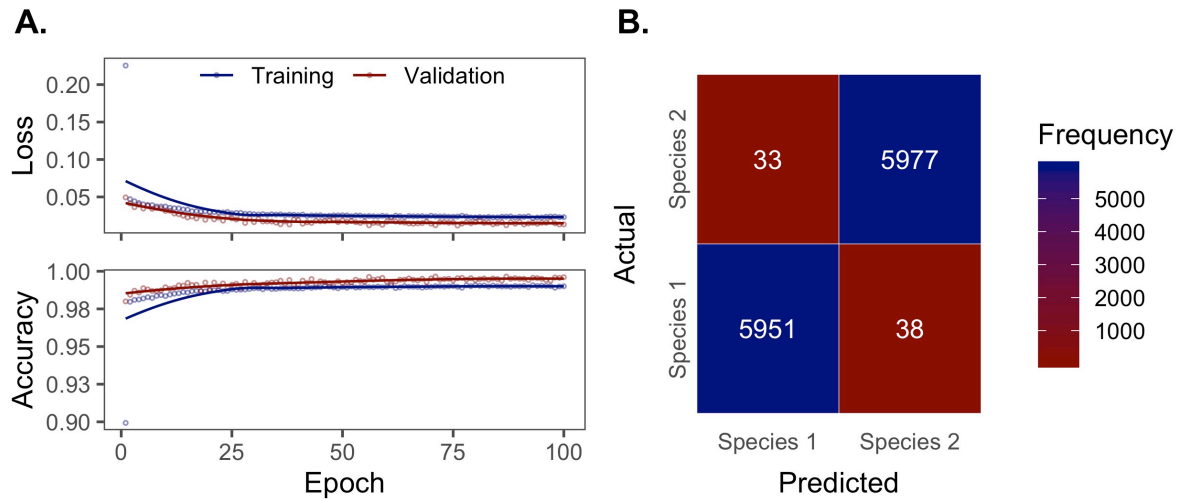
Figure 6.4. Diagnostic plots used to assess the performance of the deep neural network models used in this study. The line plots (A) show the cross-entropy loss and classification accuracy over epochs for the training (blue) and validation (red) datasets. The confusion matrix heat map (B) shows the counts of correct and incorrect classification of species in a pairwise mixed-species culture. The loss and accuracy of models used to classify species in pairwise mixed-species cultures at three different temperature treatments are shown in Supplementary Figure 6.1 – 6.3. The confusion matrices of these models are shown in Supplementary Figure 6.4 – 6.6.

6.2.5 Quantitation of growth and competition

Growth for each species in monocultures and co-cultures was quantified in terms of change in total biomass accumulated per day as described subsequently. First, the biovolume (BV) for each cell was computed using the linear dimensions (i.e. length and width) following the equation of Sun and Liu (2003) (BV = 1/6 x 3.1416 x length x width x height) and was converted to biomass (BM) using the equation of Eppley et al. (1970) (BM = 0.251 x $BV^{0.94}$). It was assumed that the height of the cell is equivalent to its width in *Alexandrium* spp. whilst it is equal to one-third of the width in *Prorocentrum* spp. The total biomass (pg C) was estimated by multiplying the sum of the biomass or cellular carbon content (pg C cell^{-1}) and total cell count. Finally, the log of total biomass within the exponential phase was fitted against time in a linear model to estimate the growth rate in monocultures and co-cultures (*r* and *r**, respectively; expressed in d^{-1}) (Supplementary Figure 6.7). Relative growth index (*RG*) was determined by the proportion between growth rate in monocultures and co-cultures (*RG = r*/r*). *RG* was

used to examine whether the presence of the competitors has decreased ($RG < 1$) or increased ($RG > 1$) the growth of species. The nature of the species interaction between pairs in the mixed-species growth experiments was also examined RG. $RG < 1$ indicates a fitness cost incurred by interspecific competition since growth rate in co-culture is lower than the rate that the species achieved in monoculture. On the other hand, $RG > 1$ indicates facilitation since growth rate is increased in the presence of other species.

Competition coefficients (c) of two competing species, i.e. (1) focal species and (2) its competitor were computed following Low-Decarie et al. (2011) using the equation below:

Equation 6.1 $$c_1 = \frac{r_1 - r_2}{r_c} = \frac{1}{g_c} \ln\left(\frac{\frac{b_{1_{final}}}{b_{2_{final}}}}{\frac{b_{1_{initial}}}{b_{2_{initial}}}}\right) = -c_2$$

The predicted competition coefficients or PCC (c_1 and c_2) were calculated as the difference between the growth rates of species in monocultures (r_1 and r_2) standardised by the growth rate of the community (r_c). The realised competition coefficients or RCC (c_1* and c_2*) were calculated as a function of observed change in relative total biomass (b) of each species in a co-culture through time accounting for the growth of the community overall (g_c, number of generations across the community). Competition coefficients were used to examine whether focal species outcompete competitors (PCC or $RCC > 0$).

6.2.6 Data analyses

Response of growth rates and relative growth index were assessed using an analysis of variance (ANOVA). The main effects and interactions of temperature and competition on the response variables among six different species, between two

different genera, and between non-toxic and potentially toxic dinoflagellates were tested. Also, the main effects and interactions of the focal species and competitors taxonomic identity and toxicity on the response variables among the three different temperature treatments (i.e. 15, 20, and 25 °C) were tested. Post hoc Tukey tests were also conducted to determine the significant difference in the mean estimates between paired groups. A total of 18 analyses were conducted using ANOVA and post hoc Tukey tests (see Supplementary Table 6.2 for description). Results of ANOVA are summarised in Supplementary Table 6.3 – 6.7, whereas the results of post hoc Tukey tests are visualised in Supplementary Figure 6.8 – 6.12. Generally, the statistical results for filtered and full datasets were comparable. Hence, the results for the filtered dataset are preferably reported in the main text. Finally, to examine the relationship between growth rates and competition coefficients, a simple linear regression was used. Data processing and analyses were implemented in *R* version 3.6.1 (R Core Team, 2019) using packages implemented in the previous chapters.

6.3 RESULTS

6.3.1 Growth response in monocultures

The main effect of temperature on growth in monocultures was significant in all six species (Figure 6.5; *ANOVA* 1 in Supplementary Table 6.3). All six species showed a significant increase in growth at higher temperature (Supplementary Figure 6.8 A), except for the growth in *Prorocentrum* sp. and *Prorocentrum micans* that declined at 25 °C. On average, growth of *Prorocentrum* increased at 20 °C and then declined at 25 °C whereas growth of *Alexandrium* increased with increasing temperature (*ANOVA* 2 in Supplementary Table 6.3; Supplementary Figure 6.8 B). Similarly, non-toxic

dinoflagellates showed increase in growth at 20 °C, which subsequently declined at 25

°C; however, potentially toxic dinoflagellates had higher growth at higher temperature

(*ANOVA* 3 in Supplementary Table 6.3; Supplementary Figure 6.8 C).
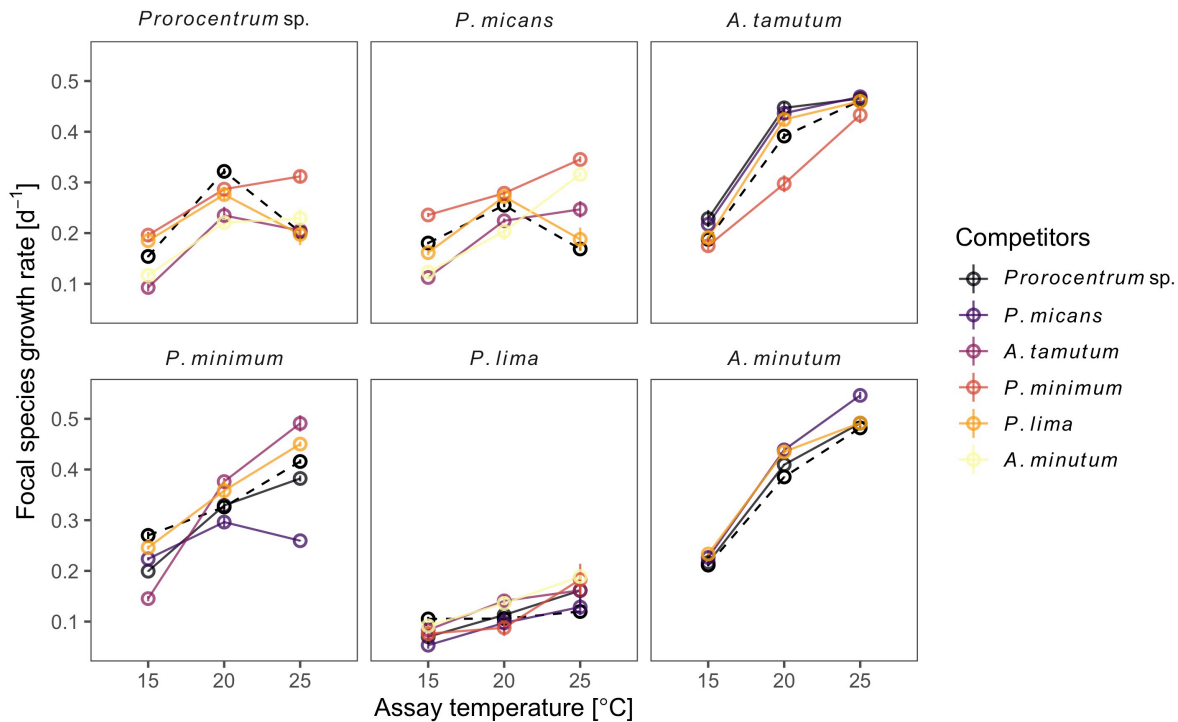
Figure 6.5. Growth rates of marine dinoflagellates in monocultures and co-cultures across temperature treatments. The points represent the growth rates of focal species in monocultures (black) and co-cultures (coloured), whereas the lines represent the trend of growth in monocultures (broken) and co-cultures (solid) over temperature.

Significance of the main effects of taxonomic identity and toxicity of

dinoflagellate species on growth in monoculture were found in all temperature

treatments, except for the effect of genus identity and toxicity at 15 °C (*ANOVA* 4 – 6 in

Supplementary Table 6.3). Growth in pure culture in all temperature treatments were

different across dinoflagellate species, ranging from 0.11 – 0.48 d^{-1}. Among

dinoflagellate species, *P. lima* had the lowest growth across all temperature, whilst *P.*

minimum, *A. tamutum* and *A. minutum* had the highest growth at 15, 20, and 25°C,

respectively (Supplementary Figure 6.8 D). There was no difference in growth between

the two genus of dinoflagellate at 15 °C, but growth of *Alexandrium* was significantly

higher than the growth of *Prorocentrum* at higher temperature (Supplementary Figure 6.8 E). Similarly, growth between non-toxic and toxic dinoflagellates were similar at 15 °C but different at higher temperature. Non-toxic dinoflagellates had a higher growth at 25°C, whilst potentially toxic dinoflagellates had a higher growth at 25°C (Supplementary Figure 6.8 F).

6.3.2 Growth response in co-cultures

Generally, the main effects of temperature and competitor species identity and their interaction effect on growth in co-cultures were significant in all species (Figure 6.5; *ANOVA* 7 in Supplementary Table 6.4) with few notable exceptions (e.g. interaction effect on growth in *Alexandrium tamutum* and *Prorocentrum lima*). Growth in co-cultures significantly increased at higher temperature in most dinoflagellate species. Trends in the growth in co-cultures were generally comparable to the patterns observed in monoculture. Notably, a different trend was observed in the growth of *Prorocentrum* sp. at 25 °C where growth had increased when paired with *P. minimum*. Similar increasing pattern was observed in the growth of *P. micans* when paired with *A. tamutum*, *P. minimum,* and *P. lima*. On the other hand, growth of *P. minimum* at 25 °C had decreased when paired with *P. micans*, which is different from pattern observed in monoculture. All species differed in growth response to temperature that is generally dependent on the identity of competitor species (Supplementary Figure 6.9 A).

Temperature and competitors had significant effect on growth in both the dinoflagellate genera but their interaction effect on growth was significant only in *Alexandrium* (*ANOVA* 8 in Supplementary Table 6.4). The average growth in *Prorocentrum* species in co-cultures increased at 20°C that subsequently decreased at 25°C whilst average growth in *Alexandrium* in increased with increasing temperature,

which is a similar pattern observed in monocultures (Supplementary Figure 6.9 B). Average growth of *Prorocentrum* species in co-cultures was higher when paired with *P. lima* compared to the growth when paired with *P. micans* and *A. minutum*. On the other hand, average growth of *Alexandrium* species in co-cultures was lower when paired with *P. minimum* compared to the growth when paired with the other Prorocentrum species. Furthermore, the average growth in *Prorocentrum* species in co-cultures increased at 20°C that subsequently decreased at 25°C whilst average growth in *Alexandrium* in increased with increasing temperature, which is a similar pattern observed in monocultures. The effect of temperature on the average growth in *Alexandrium* was dependent on the competing species.

Also, the significance of the effects of temperature and competitors on growth was found in non-toxic and potentially toxic dinoflagellates, but the interaction effect on growth was significant only in non-toxic species (*ANOVA* 9 in Supplementary Table 6.4). Average growth of non-toxic and potentially toxic dinoflagellates in co-cultures at 15°C was higher than the average growth at higher temperatures, but average growth in co-cultures at 20°C and at 25°C were comparable, deviating from the patterns observed in monocultures (Supplementary Figure 6.9 C). Average growth of non-toxic species in co-cultures was lower when paired with *A. minutum* compared to the growth when paired with other species except for *P. lima*. On the other hand, average growth of potentially toxic dinoflagellates in co-cultures was higher when paired with *P. lima* compared to the growth when paired with the other species. Unlike non-toxic species, average growth of potentially toxic dinoflagellates differed across temperature independent of the competitors.

The growth was dependent on the taxonomic identity of focal and competitor species in all temperature treatments (*ANOVA* 10 – 11 in Supplementary Table 6.4).

The range of the difference in growth across focal species identity was from -0.28 d^{-1} to 0.33 d^{-1} across temperature (Supplementary Figure 6.9 D). On the other hand, the difference in growth across competitor species identity ranged from –0.063 d^{-1} to 0.073 d^{-1} across temperature. The difference in growth across the interaction between focal and competitive species identity ranged from –0.39 d^{-1} to 0.42 d^{-1} across temperature. The average growth in *Prorocentrum* and *Alexandrium* were different across all temperature and the scale of difference was independent on the genus of competitor species at higher temperature (Supplementary Figure 6.9 E). *Alexandrium* had a higher growth compared to the estimate in *Prorocentrum*, and this difference increased with increasing temperature. Average growth in co-cultures had decreased when a dinoflagellate was competing against *Alexandrium* at 15 °C. Furthermore, the average growth was independent of toxicity of focal and competitor species in all temperature treatments (*ANOVA* 12 in Supplementary Table 6.4; Supplementary Figure 6.9 F).

6.3.3 Relative growth index

Sensitivity of relative growth index (*RG*) to temperature and competitor species identity was generally significant (Figure 6.6; *ANOVA* 13 in Supplementary Table 6.5). Generally, *RG* significantly increased at higher temperature in all species, except for *Alexandrium* species (Supplementary Figure 6.10 A). The difference in relative growth across the competitive species identity ranged from -0.46 to 0.50. *Prorocentrum* sp. had lower *RG* when paired with *A. tamutum* than with *P. minimum* and *P. lima*, but it had higher *RG* when paired with *P. minimum* than with other potentially toxic dinoflagellates. On the other hand, *RG* in *P. micans* was higher when paired with *P. minimum* compared to *RG* when paired to *P. minimum* and *Alexandrium* species. *A. tamutum* had lower *RG* when paired with *P. minimum* than with other *Prorocentrum* species. *P.*

minimum had higher *RG* when paired with *P. lima* than with non-toxic *Prorocentrum* species. It also had higher *RG* when paired with *A. tamutum* than with *P. micans*. Furthermore, *RG* in *P. lima* was higher when paired with *A. minutum* compared to the index when paired with *P. micans*. *A. minutum* had higher *RG* when paired with *P. micans* than with *Prorocentrum* sp. *Prorocentrum* species differed in growth response to temperature that is generally dependent on the identity of competitor species.

The main effects of temperature and competitors and their interaction on *RG* were generally significant in *Prorocentrum* species (*ANOVA* 14 in Supplementary Table 6.5). However, only the significance of the effect of competitor was found in *Alexandrium* species. *RG* in *Prorocentrum* species was significantly higher at higher temperature whilst *RG* in Alexandrium species was similar across temperature treatments (Supplementary Figure 6.10 B). Furthermore, *Prorocentrum* species had higher *RG* when paired with *P. minimum* than with other species, except with *A. minutum*. However, they had lower *RG* when paired with *P. micans* than with *P. lima* and *A. minutum*. On the other hand, *Alexandrium* species had lower *RG* when paired with *P. minimum* than with other *Prorocentrum* species. The effect of temperature on *RG* in *Prorocentrum* species was dependent on the identity of competing species.

Significance of the effect of temperature and competitors and their interaction on the *RG* was found in both non-toxic and potentially toxic dinoflagellates (*ANOVA* 15 in Supplementary Table 6.5). *RG* in non-toxic species was highest at 25 °C (Supplementary Figure 6.10 C). Whereas, *RG* in potentially toxic species was lowest at 15 °C. Relative growth varied across temperature in both non-toxic and toxic dinoflagellate dependent of the toxicity of competitor species.

The main effects of the species identity of focal and competitor species and their interaction effect on *RG* were significant in all temperature treatments (*ANOVA* 16

in Supplementary Table 6.5). The difference in relative growth ranged from -1.23 to 1.43 across focal species identity whilst it ranged from -0.29 to 0.36 across competitor species identity across temperature (Supplementary Figure 6.10 D). Significance of the effect of the genus identity of focal and competitor species was found (*ANOVA* 17 in Supplementary Table 6.5). *Alexandrium* had higher *RG* compared to the *RG* in *Prorocentrum* at 15°C, opposite to the trend at 25 °C (Supplementary Figure 6.10 E). *RG* was decreased when a dinoflagellate was competing against *Alexandrium* at lower temperature. Toxicity of focal species had significant effect on *RG* in all temperature treatments, except at 25 °C (*ANOVA* 18 in Supplementary Table 6.5). At 25 °C, toxicity of competitor species had significant effect on *RG*. Non-toxic dinoflagellates had higher *RG* compared to potentially toxic counterparts at 15 °C, opposite to the trend at 20 °C (Supplementary Figure 6.10 F). Surprisingly, *RG* was higher when competing against potentially toxic species at 25 °C. Interaction effect between toxicity of focal and competitor species on *RG* was not significant.

Based on the *RG* estimates, three species interaction scenarios were observed. Overall, 14 % of pairs demonstrated a mutual competition scenario, 63 % of pairs fell into intermediate scenario where one species was facilitated while the other experienced interspecific competition, and the remaining 23 % of pairs exhibited a full facilitation scenario. Hence, the interactions in the experiment are mostly competitive *sensu stricto*.
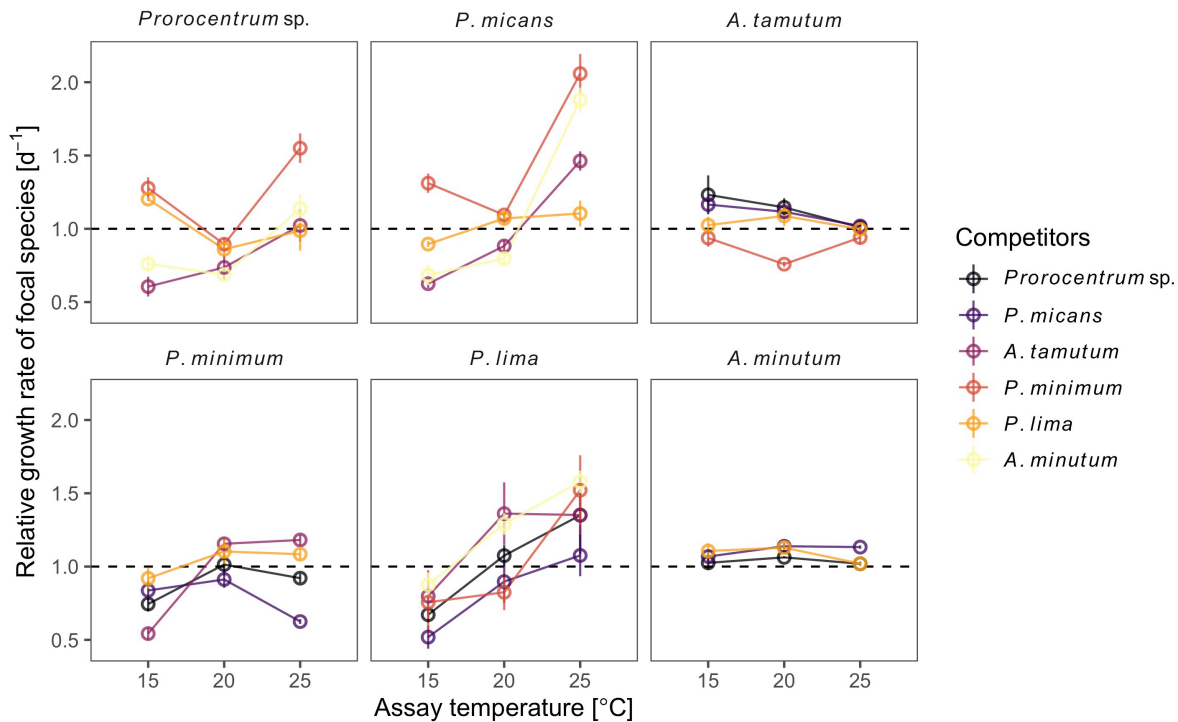
Figure 6.6. Relative growth rates of marine dinoflagellates across temperature. The points represent the growth rates of focal species in monocultures (black) and co-cultures (coloured), whereas the lines represent the trend of growth in monocultures (broken) and co-cultures (solid) over temperature. Points above the horizontal line indicate higher growth in co-culture than in monoculture.

6.3.4 Relationship between growth and competition

There were direct proportional relationship between growth and competition in all temperature treatments (Figure 6.7). The slope between the growth in monocultures and predicted competition coefficient (*PCC*) had decreased with increasing temperature (Figure 6.7 A). On the other hand, the slope between the growth in co-cultures and realised competition coefficient (*RCC*) was lower at 25 °C compared to the slope at lower temperatures (Figure 6.7 B). Among the dinoflagellate species, *P. lima* had the lowest growth rates in monocultures and co-cultures across all temperature treatments. Hence, it had the lowest *PCC* and *RCC* across all temperature treatments (except for *RCC* at 25 °C), which were below zero regardless of its competitors. On the other hand, growth of non-toxic *Prorocentrum* species (i.e. *Prorocentrum* sp., and *P. micans*) in monocultures and co-cultures were higher than the estimates in *P. lima*. Similar trend to

their *PCC* and *RCC* in all temperatures, which were either below or above zero depending on their competitors. Among *Prorocentrum* species, the potentially toxic *P. minimum* had the highest growth rates in monocultures and co-cultures across all temperature treatments. Their *PCC* and *RCC* were generally above zero across all temperatures. Furthermore, growth of *Alexandrium* species in monocultures and co-cultures were the higher than the estimates in *Prorocentrum* species across all temperatures. They had the highest *PCC* ad *RCC* across all temperatures, which above zero regardless of their competitors.

6.3.5 Relationship between predicted and realised competition

Also, there were direct proportional relationships between predicted and realised competition coefficient in all temperature treatments (Figure 6.7 C). The slope of the linear relationship between *PCC* and *RCC* peaked at 20 °C (i.e. ~0.17), whilst the slopes at extreme temperatures were comparable (i.e. ~0.10). Generally, *P. minimum* and *Alexandrium* species outcompeted other dinoflagellates species, whereas *P. lima* and non-toxic *Prorocentrum* species fell behind the competition. These outcomes of the competition inferred from *PCC* and *RCC* were comparable at 20 °C. However, a few discrepancy of the outcomes was observed at extreme temperatures. For instance, *PCC* and *RCC* differed from their outcomes of competition in several co-cultures that paired with *Prorocentrum* sp. at 15 °C. Also, *PCC* and *RCC* had a mismatch of the outcomes of the competition in several co-cultures that paired with *P. micans* and *P. minimum* at 25 °C.
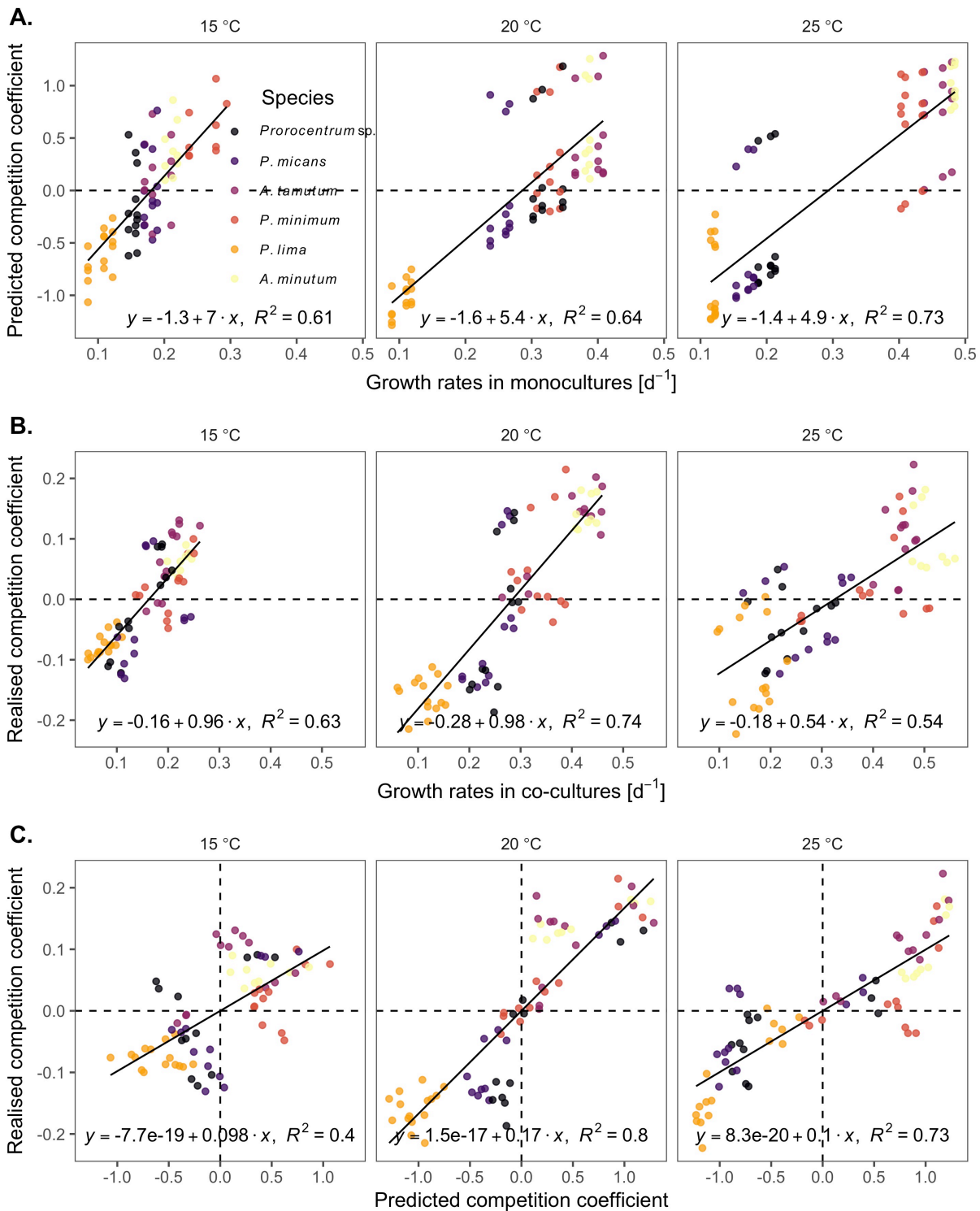
Figure 6.7. Linear relationship between growth and competition in marine dinoflagellate in three temperature treatments. Relationship between growth in monocultures and predicted competition coefficient (*PCC*) and the relationship between growth in co-cultures and realised competition coefficient (*RCC*) are presented (A and B, respectively). Also, the relationship between *PCC* and *RCC* is also presented (C). The colour-coded points represent the estimates obtained from focal species in the competition. The solid lines represent the fits with the linear model displayed at the bottom. The points above the horizontal broken lines or at the right side of the vertical broken lines indicate that focal species outcompetes competitor, whilst points below or at the left side of the broken lines indicates that competing species outcompetes focal species.

6.4 DISCUSSION

6.4.1 Temperature as a limiting factor

Competitive performance of a species can be measured in terms of growth rate, which is dependent on temperature (Amarasekare and Savage, 2011; Savage et al., 2004). The findings in this study reveal the temperature dependence of growth and competition in marine dinoflagellates, suggesting that temperature is a limiting factor. These results are not surprising since existing studies recognised the critical role of temperature on the physiology, growth, species interaction, biogeographical distribution in phytoplankton (Bestion et al., 2018; Brun et al., 2015; Coello-Camba et al., 2015; Grimaud et al., 2017; Raven and Geider, 1988). This present study provides new empirical evidence of the effect of temperature on interspecific competition in non-toxic and potentially toxic dinoflagellates, which is limited in literature.

6.4.2 Focal and competitor species-specificity of responses to temperature

Generally, the main effects of temperature and competitor species identity and the interaction effect on growth and competition were significant, suggesting that the temperature dependence of the responses in the pairwise mixed-species cultures is contingent on the identity of the competitor species.

In single-species growth experiments, there were significant differences in growth rates across the focal species identity and toxicity, suggesting the dependence of the growth on the focal species identity and toxicity. These patterns were observed in warmer temperature, but not evident in 15 °C where no significant variation in the average growth was found between the genera *Alexandrium* and *Prorocentrum* and between non-toxic and potentially toxic dinoflagellates.

On the other hand, in the mixed-species growth experiments, there were significant variations in growth rates and competition across the taxonomic identity of the focal and competitor species, but no significant difference in the responses between non-toxic and potentially toxic species. The results suggest the dependence of growth on both the focal and competitor species identity and not on their toxicity. These patterns were observed across all temperature treatments.

Overall, these findings suggest the importance of focal and competitor species-specificity of the competitive response to warming. This species-specificity of competition is expected since the temperature dependence of metabolic rates varies across species, and this interspecific differences in the thermal performance can greatly influence species interactions (Dell et al., 2014). Furthermore, the results suggest that the toxicity of focal species influence growth in the absence of competition at elevated temperature. These results are anticipated since the average thermal optimum (T_{opt}) in potentially toxic species was higher than the average T_{opt} in non-toxic species (see previous chapter). The toxicity of the focal and competitor species does not influence the growth and competition across all temperature. This findings does not provide evidence to support the hypothesis that warming will affect the competitive interaction between non-toxic and toxic dinoflagellates.

6.4.3 Competition effect on growth responses to temperature

Interspecific competition is defined here as the interaction between species, which leads to a decline in the growth rate of a species by the presence of another. In this study, the relative growth (RG) index was used to identify the nature of the species interaction between pairs in the mixed-species growth experiments. RG is referred here as the ratio between the growth rates in mixed- and single-species cultures, which

similar at some extent to the relative density or yield reported in recent studies (Bestion et al., 2018; Fritschie et al., 2014). Based on the relative growth (*RG*) index, majority of the interactions in the experiment are competitive.

Moreover, this present study used the relative growth index to investigate the competition effect on temperature response. The results show the significance of the main effects of temperature and competitor species identity and their interaction effect on *RG* in all species, generally. These indicate the dependency of the effect of competition on the growth to temperature, which is contingent on the competitors identity. Also, the findings generally reveal the significance of the main effects of the taxonomic identity of focal and competitor species on *RG* in all temperature treatments. These results suggest that the competition effect on growth depends on the interacting species. However, *RG* is independent on the toxicity of focal and competitor species.

Overall, the findings of this study support the hypothesis that interspecific competition modifies temperature dependence of growth in marine dinoflagellates. Previous studies have demonstrated the dependence of growth rates on interspecific interactions (e.g. Anholt and Werner, 1995; Baker, 1982). A recent study found that temperature responses are modified by competitive interactions, and the strength of their effect is species-specific (Nilsson-Örtman et al., 2014). Therefore, temperature dependence of growth rates in laboratory may be different at some extent from the temperature responses in natural conditions (Gilman et al., 2010; Moenickes et al., 2012). Moreover, species-specific variation in physiological response leads to a surprising shift in species interactions with increasing temperatures (Davis et al., 1998; Lang et al., 2012).

6.4.4 Effect of warming on interspecific competition

In this study, the competitive interaction is also expressed as predicted and realised competition coefficients (*PCC* and *RCC*, respectively). Results of the study reveal that warming alters the competitive interaction in marine dinoflagellates, which further suggest that the competitive response is dependent on temperature. The temperature dependence of competition can be explained by the metabolic theory of ecology (*MTE*). *MTE* attempts to provide mechanistic links between the different levels of organisation in biology and ecology, e.g. from organelles to ecosystems (Brown et al., 2004). As a fundamental dimension of the *MTE*, temperature plays a key role in shaping the ecosystem structure and function (Brown et al., 2004; Gillooly, 2001). The effect of temperature on interspecific interactions such as competition is recognised in prior works (e.g. Dunson and Travis, 1991; Park, 1954; Tilman, 1981) and in recent studies (e.g Amarasekare, 2008, 2007; Gilman et al., 2010; Kordas et al., 2011; Tylianakis et al., 2008; Woodward et al., 2010).

This temperature dependence of competition coefficients is also contingent on the competitors species identity. This can be explained by the species specificity of the growth responses to temperature. The thermal performance curves (*TPC*) between two species can be compared to predict the outcome of competition. In a given temperature, patterns of species replacement with the dominance of species with the higher growth rate can be observed along a thermal gradient, which can occur in several ways. One way is when both species are generalists with similar *TPC* but have different thermal optimum (T_{opt}). Another way is when one species is a specialist and the other is a generalist, but both have the same T_{opt}. In both ways, dominance of a species is dependent on local temperature. Species replacement patterns can also occur when the competing species have unequal strengths of density dependence that differ with

temperature. In this scenario, a species can be outcompeted by competitor due to its sensitivity to the per capita effects of the competing species in a given temperature, and not because it has low carrying capacity (Reuman et al., 2014).

A most recent study has developed a simple theoretical model that demonstrated the key role of metabolic traits, i.e. the temperature dependence of growth and resource acquisition, in determining the effect of temperature on interspecific competition in phytoplankton (Bestion et al., 2018). The model assumes that the population are initially rare and the cells are exponentially growing at a constant rate (Bestion et al., 2018). This model differs in several aspects from the assumption of resource competition (Tilman, 1981) and adaptive dynamic (Dieckmann and Law, 1996) theories that assume that a rare species must have lower equilibrium resource requirements (R^*) than that of the resident (at population dynamics equilibrium) in order to successfully invade. Moreover, the model is able to predict the outcomes of the competition experiment with good accuracy, suggesting that metabolic rates are useful in predicting the effects of warming on the ecological dynamics of phytoplankton communities (Bestion et al., 2018).

6.4.5 Direct relationship between growth and competition

The findings reveal the strong direct proportional relationships between growth rates and competition coefficients, suggesting that growth clearly influence competition in marine dinoflagellates. This direct effect of growth on competition is also demonstrated in bacteria (Nedwell and Rutter, 1994), plants (Goldberg and Landa, 1991), marine invertebrates (Johannes et al., 1983; Lord and Whitlatch, 2015). Furthermore, the slope of the linear relationship between growth and competition were found to vary across temperature, suggesting the temperature dependence of the effect

of the growth on competition. This further imply that warming could lead to shift in community composition in marine dinoflagellates where growth rates strongly influence competition. The results also show that the variation in growth explain the majority of the variation in competition, however more than 25% of variation remained unexplained. These results suggest that other than the growth, other factors may also influence competition.

However, the complexity of the effect of temperature makes it challenging to develop a mechanistic model to predict responses to climate change. This is because the processes at different biological and ecological levels (i.e. from organism to ecosystem) do not just depend on the direct effects of temperature on physiology, but also on how these direct effects occur in the context of other processes. For example, the species distribution along the environmental temperature reflects interactions of species, not just the direct effects of temperature (e.g. Gross and Price, 2000; Price and Kirkpatrick, 2009).

6.4.6 Predictable ecological response

The findings also reveal the direct proportional relationships between predicted and realised competition coefficients (*PCC* and *RCC*, respectively) in all temperature treatments (with average $R^2 = 0.64$), suggesting the predictability of the realised competition. Hence, the growth rates of species in monocultures can be used to predict the outcomes of competition in co-cultures. The outcomes of the competition inferred from *PCC* and *RCC* were comparable with 92% of the outcomes are matched. Generally, the results show that *P. minimum* and *Alexandrium* species outcompete other dinoflagellates species, whereas *P. lima* and non-toxic *Prorocentrum* species fall behind the competition.

The study attempts to use competition coefficients to infer the possible community composition at three different temperature treatments. In each treatment, the number of instances that a focal species outcompete competitors is determined based on *PCC* and *RCC* and is expressed as relative frequency. Figure 6.8 shows the *PCC*- and *RCC*-based relative frequency of species in all temperature treatments.
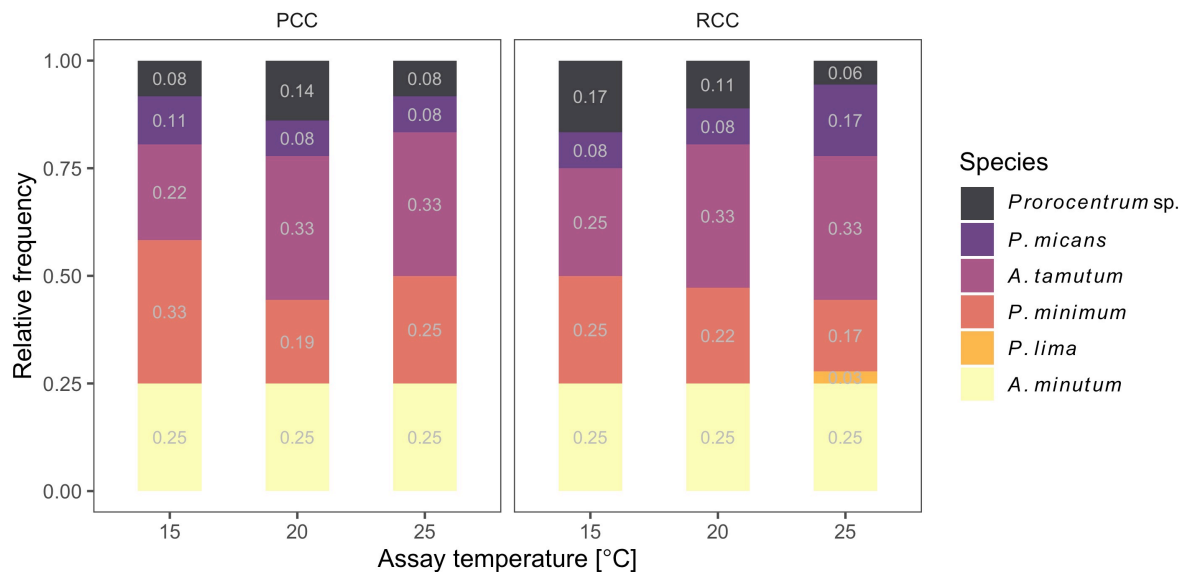
Figure 6.8. Predicted community structure of marine dinoflagellates in three temperature treatments. Filled bars represent the relative frequency of non-toxic and potentially toxic dinoflagellate species across, which were based from the predicted and realised competition coefficients (*PCC* and *RCC*, respectively).

Based on *PCC*, *A. tamutum* is expected to dominate across all temperatures (i.e. 33%), except at 15 °C. This is followed by *A. minutum* with relative frequency of 25% that remains constant in all temperatures. It is expected that *P. minimum* will dominate at 15 °C (33%), but it is predicted to decreased at higher temperatures (19% – 25%). Relative frequency of *Prorocentrum* sp. peaks at 20 °C (14%) whilst the estimates at extreme temperatures are comparable (8%). *P. micans* yields a relative frequency of 11% at 15 °C, and is expected to decrease at higher temperatures (8%). *P. lima* is expected to be extinct across all temperatures. Potentially toxic species is expected to dominate over non-toxic species at 15 °C, whilst non-toxic species is

predicted to dominate at 20 °C. Both non-toxic and potentially toxic species are expected to co-exist at 20 °C. These *PCC*-based patterns are comparable to *RCC*-based relative frequency with few exceptions. For instance, *RCC*-based relative frequency of *Prorocentrum* sp. is expected to decrease with increasing temperature. Also, *RCC*-based relative frequency of *P. micans* is expected to be higher at 15 °C than the estimates at lower temperatures.

On the other hand, *P. lima* is expected to contribute the least to the community composition 25 °C but predicted to be extinct at lower temperature. Both non-toxic and potentially toxic species are expected to co-exist at 15 °C. *RCC*-based relative frequency of non-toxic species is expected to increase with temperature, opposite to the pattern observed in potentially toxic species. Therefore, competition coefficients can be used to predict the structure of the community. However, the accuracy of the prediction cannot be determined since the study is limited to pairwise competition. A full community competition experiment (e.g. Low-Décarie et al., 2011; Pardew et al., 2018) is required to test accuracy of the prediction.

6.4.7 Caveats

The findings presented in this study should be interpreted with caution in consideration of the following caveats with the design: (1) Marine dinoflagellates species were used because they are ecologically relevant organisms comprising the majority of the toxic bloom-forming species. Expanding the results to other taxonomic phytoplankton groups (e.g. diatoms, cyanobacteria, haptophytes) certainly needs additional experimental validation. (2) These test organisms are also easy to keep in good condition over many transfers; however, they are not maintained in axenic cultures. The results may be suffered from the interference from the possible effect of

the presence of bacteria in the culture. (3) Among the test organisms, only *P. lima* is confirmed to produce toxins (see the previous chapter) and it is grouped with *P. minimum* and *A. minutum* as potentially toxic species. Extending the results to toxic phytoplankton species also requires further experimental validation. (4) Prior the experiment, the cultures were pre-acclimated at three different temperature treatments and two weeks may not be enough to fully acclimatised to the new thermal conditions. (5) In few samples, low quality of image data acquired through high throughput microscopy affects the image processing to detect the cells. It is for this reason why the image acquisition is done semi-automatedly per well and not completely automated per plate in order to improve the quality of the image data. (6) Few of the deep learning models yielded a low accuracy in discriminating one species from another species in pairwise mixed cultures (Supplementary Table 6.1), and pairs with low model accuracy were excluded in the analysis. The results of the analysis using the filtered dataset were comparable to that of the full dataset, and hence the findings presented in this study were robust. (7) Growth rate was used as proxy for fitness, which are dependent on specific experimental conditions that vary for different organisms and from lab to lab. (8) The design allows the treatment effect to be partitioned among species, genera, and toxicity and the replication is small. Additional experiments are needed to establish the generality of the conclusions.

With these caveats, the experiment can be used to evaluate the effect of warming on the growth rate in monocultures and the competitive response of two species in mixed cultures.

6.5 CONCLUSIONS

This chapter concludes the following: (1) temperature limits growth and competition, (2) growth response to temperature depends on the interacting focal and competitor species, (3) interspecific competition modifies temperature dependence of growth, (4) warming alters interspecific competition, (5) growth rates strongly influence competition, (6) ecological response to warming is predictable. The results provide new empirical evidence of the effect of warming on growth and competition in marine dinoflagellates. Concisely, this study helps the advancement of our current knowledge on how species respond to climate change, and challenges the use of single-species laboratory experiments for predicting community responses to climate change.

CHAPTER 7

This page is intentionally left blank.

This page is intentionally left blank.

GENERAL DISCUSSION

Climate change poses a serious threat to phytoplankton communities. Recognising the beneficial and harmful impacts of phytoplankton to the environment, to humans, and to other organisms, it is crucial to understand how physiology and ecology of phytoplankton are affected by temperature, which is expected to change with climate. In this thesis, I have addressed some of the existing gaps in our knowledge of the thermal responses in marine phytoplankton. Specifically, I analysed species occurrence data (Chapters 2 and 3), published temperature-growth data (Chapter 3), and data from laboratory experiments (Chapters 4 to Chapter 6) to provide new information on the thermal limitation to the distribution, growth, toxin production, and competition in marine phytoplankton. In the following sections, key findings of the research and their implications are discussed, and future research directions that have come to light from the work are presented.

7.1 KEY RESEARCH FINDINGS

7.1.1 Temperature limits the current biogeography

In Chapter 2, an analysis of the global dataset of species occurrence data was conducted to examine the global patterns in the realised thermal niche and geographic range of marine phytoplankton. Overall, the findings shed light on the complexity of biogeographical patterns of marine phytoplankton species, which do not necessarily conform to classical macroecological rules. Below are the key results of this chapter:

Thermal niches vary non-monotonously with latitude. This trend is due to the latitudinal variation in the difference between the minimum and maximum average

annual *SST* or in the difference between the seasonal temperature extremes experienced by phytoplankton in the contemporary ocean. This pattern in the thermal niche breadth reflects the asymmetrical variation in the thermal limits, in which the irregular monotonous behaviour of the lower and upper thermal limits leads to the non-monotonous latitudinal pattern in the niche breadth.

Thermal niches in the tropics are narrower. The thermal niches of phytoplankton species in the tropics are narrower than those in higher latitudes following Janzen's rule. Thermal limits are influenced by climate variability and in turn affect the distribution of marine phytoplankton. In general, temperature is linked to the role of phytoplankton in regulating biological processes and patterns in ecology as per the metabolic scaling hypothesis, therefore impacting the extent and rate of their metabolic performance rate. Tropical phytoplankton species achieve ecological success in warmer conditions (Payne and Smith, 2017), due to their ability to perform over a narrower thermal range based on the scaling of physiological rates in higher temperatures.

Latitudinal variation in geographic range is not evident. The results showcase a complex relationship between latitude and geographic size range that contradicts Rapoport's rule which dictates that tropical species have small range sizes due to their adaptation to little seasonal variation in climate whereas temperate species are expected to occupy a larger range size due to their tolerance to greater climate variability. This contradiction of the results to the theory suggests that several factors (such as transport or thermal niche breadth) may influence the geographic range size in marine phytoplankton other than climate variability.

Thermal niches and geographic range are related. A weak trend of geographical range size increasing with increasing thermal niche breadth in marine phytoplankton was detected in the data, suggesting that niche breadth to some extent

limits the geographic distribution of these communities. This observation supports the validity of the niche breadth–range size hypothesis, which suggests that marine phytoplankton become more widespread when they can utilise resources (e.g. light and nutrients) within a wider thermal condition (Slatyer et al., 2013).

Patterns are explained by temperature and other environmental factors. Temperature and climate variability are important explanatory variables for the trends in thermal niche breadth. The diversity and habitat availability are relatively more influential as variables for range size than the climate variability since geographic range size decreases with increasing diversity which in turn increases with higher habitat availability. Thus, species may have large range size without adapting to high climate variability if exposed to the environment with low diversity and more thermally suitable habitats.

7.1.2 Biogeography and phylogeny explain variability in thermal attributes

In Chapter 3, the global patterns of physiology- and occurrence-based thermal traits (TT_p and TT_o), thermal sensitivity, and warming exposure and vulnerability in marine phytoplankton were examined. Generally, the findings indicate that the variation of these thermal attributes can be attributed to biogeography and phylogeny of marine phytoplankton. The key findings in this chapters are as follows:

Physiology- and occurrence-based thermal traits are congruent but not equal. These support the hypothesis that TT_p and TT_o express different aspects of species thermal niche. TT_p is expected to estimate the fundamental niche of a species, defined by their physiological tolerance range to environmental factors (e.g. temperature) in the absence of biotic interactions (Hutchinson, 1957). However, the fundamental niche may

be reduced in the presence of biotic interaction such as predation, competition, mutualisms, species dispersal limitation (Sánchez-Fernández et al., 2016), and limited climate availability (Soberón and Nakamura, 2009), resulting in TT_p becoming higher than TT_o.

Thermal attributes vary across latitude. Generally, thermal traits in marine phytoplankton vary across latitude as demonstrated in previous studies using data on algal physiology (Chen, 2015; Thomas et al., 2016, 2012) and occurrence (Chapter 2). As observed, the difference between TT_p and TT_o generally vary non-monotonously with latitude, suggesting that the inequality between these traits may increase or decrease depending on the geographic locations where the species are collected/isolated. Thermal sensitivity in marine phytoplankton also varies across latitude, indicating that temperate species experience low cold safety margins and therefore they are at risk to live beyond the limit of their cold tolerance as compared to species in the tropics. On the other hand, tropical species have low heat safety margins and hence they are more vulnerable to warming than the species thriving at higher latitudes (Clusella-Trullas et al., 2011; Deutsch et al., 2008; Diamond et al., 2012; Huey et al., 2009). This is further supported by the latitudinal trend in warming vulnerability, indicating that the local temperatures will surpass the physiological upper thermal limits in tropical species faster than the temperate species, despite the warming rate being slower in the lower latitudes.

Interspecific variations in thermal attributes is evident. The results reveal that a significant proportion of the variation in all thermal attributes is mainly explained by taxonomic identity, suggesting that the thermal attributes are most variable among species within genera. Although the variation is largely explained by species, the supra-specific taxonomic levels frequently explained more variation than expected by the tip-

randomisation null-models. This indicates presence of phylogenetic signal in the physiology- and occurrence-based thermal traits, their inequalities, and thermal sensitivity in marine phytoplankton.

Phylogenetic conservatism in the thermal attributes is absent. The results suggest that phylogenetic signals are present, but too weak to detect the presence of phylogenetic conservatism. These results further suggest that the thermal attributes are more similar among closely related species than expected from a null model from the same phylogeny, but there is no evidence of the tendency of species to retain their ancestral thermal traits more than expected from a Brownian null model of evolution.

7.1.3   Temperature influences the algal growth

In Chapter 4, laboratory experiments were conducted to examine the temperature dependence of growth in marine dinoflagellates. In general, the findings reveal the comparison between non-toxic and potentially toxic phytoplankton in terms of how temperature change affects their growth. Below are the key results in this chapter:

Growth is temperature-dependent. Generally, the results revealed an asymmetrical pattern of the thermal growth curve indicating that their growth is more sensitive to warmer conditions. This can be attributed towards the physiological processes in phytoplankton that is mainly driven by the kinetics of enzymes which is influenced by temperature. When temperature increases, it affects the enzyme activation and its process rate finding stability at high temperatures (Knies and Kingsolver, 2010). This in turn impacts growth rates which increase exponentially with increasing temperature below the thermal optimum (T_{opt}), following the Arrhenius

kinetics (Arrhenius, 1915). Once the T_{opt} is reached, growth rate decreases due to the denaturation of essential proteins (Hochachka and Somero, 2002).

Thermal traits in non-toxic and toxic species are comparable, but not their growth rates. This variation in temperature dependence of growth between the non-toxic and potentially toxic phytoplankton has an ecological implication especially in the changing climate, as toxic species may dominate over the non-toxic species (or vice versa). Under future climate scenarios, toxic species could employ adaptive strategies to expand their thermal tolerance, while toxin production may provide toxic species a selective advantage.

Maximum growth rates and thermal traits are unrelated. Results suggests that there is no clear trade-off between maximum growth rate and thermal traits. The relationship between the maximum growth rate of phytoplankton and temperature is initially described by an exponential envelope function (Eppley, 1972), which the "hotter is better" hypothesis is based on. Under this hypothesis, the maximum growth rate is expected to be greater at higher optimal temperature.

Thermal traits are linked to environmental temperatures. Results suggest that there is a strong link between the cardinal temperatures and the ambient temperature experienced by marine phytoplankton at their local habitat, indicative of local adaptation (Thomas et al., 2012). This shows the importance of the environment in shaping the physiology of phytoplankton.

Warming vulnerability in non-toxic and toxic species is comparable. Nearly all the non-toxic and potentially toxic phytoplankton species were thriving within the thermal safety zone in the present climate scenario. Thermal sensitivity also remain comparable between non-toxic and potentially toxic phytoplankton. Overall, vulnerability

to climate change is highly variable among the strains, and less variable between

toxicity in marine phytoplankton.

7.1.4 Temperature affects toxin production

In Chapter 5, laboratory experiments were also conducted to examine the

temperature dependence toxin production in marine dinoflagellates. The findings

elucidate how change in temperature influences the production of toxins in a toxic

phytoplankton. Below are the key results in this chapter:

Toxin production is temperature-dependent. The concentration, cellular content,

relative composition, and cellular production rate of toxins are dependent on

temperature. The temperature dependence of toxin production is contingent on whether

the test organism is drastically or gradually exposed to new thermal conditions. Drastic

exposure to higher temperature yielded higher toxin concentration than the estimates at

lower temperature, but the gradual exposure produced no difference from the estimates

at lower temperature. The results of this study indicate there is an inverse linear

relationship between toxin production rates and growth rates, suggesting that the toxin

production rate increases with decreasing growth rates. Toxin production is believed to

dispense with excess photosynthetic energy when toxic species growth is no longer

optimal (Bates, 1998; Pan et al., 1996).

7.1.5 Warming alters growth and competition

In Chapter 6, laboratory experiments were conducted to examine the effect of

increased temperature on growth and competition in marine phytoplankton using

dinoflagellates as test organisms. Overall, the findings provide a new insight on how

warming influences interspecific competition in marine phytoplankton, which is crucial

for predicting the change in the phytoplankton communities in response to climate change. The key results of this chapter are as follows:

*Temperature is a limiting factor for growth and competiti*on. The findings reveal the temperature dependence of growth and competition in marine dinoflagellates, suggesting that temperature is a limiting factor. These results are not surprising since existing studies recognised the critical role of temperature on the physiology, growth, species interaction, biogeographical distribution in phytoplankton (Bestion et al., 2018; Brun et al., 2015; Coello-Camba et al., 2015; Grimaud et al., 2017; Raven and Geider, 1988).

Temperature dependence of growth and competition is specific to the species identity of the focal and competitor species, and not to their toxicity. The results suggest the importance of focal and competitor species-specificity to the competitive response to warming. This species-specificity of competition is expected since interspecific differences in the thermal performance can greatly influence species interactions (Dell et al., 2014). However, the toxicity of the focal and competitor species does not influence the growth and competition across all temperatures. The results are insufficient to support the hypothesis that warming will affect the competitive interaction between non-toxic and toxic dinoflagellates.

Interspecific competition influences the growth responses to temperature. Results support the hypothesis that the interspecific competition modifies temperature dependence of growth in marine dinoflagellates. Previous studies demonstrate the dependence of growth rates on interspecific interactions (e.g. Anholt and Werner, 1995; Baker, 1982) while recent studies report that temperature responses are modified by competitive interactions, and the strength of their effect is species-specific (Nilsson-Örtman et al., 2014). Therefore, there may be slight variations between the temperature

dependence of growth rates in laboratories compared to those in natural conditions (Gilman et al., 2010; Moenickes et al., 2012).

Warming affects interspecific competition. Warming alters the competitive interaction in marine dinoflagellates, which further suggests that the competitive response is temperature dependent. This could be explained by metabolic theory of ecology (*MTE*) that attempts to provide mechanistic links between the different levels of organisation in biology and ecology (Brown et al., 2004). Temperature plays a key role in shaping the ecosystem structure and function as a fundamental dimension of the *MTE* (Brown et al., 2004; Gillooly, 2001) and its effect on interspecific interactions such as competition is recognised in previous studies (e.g. Dunson and Travis, 1991; Park, 1954; Tilman, 1981; Amarasekare, 2008, 2007; Gilman et al., 2010; Kordas et al., 2011; Tylianakis et al., 2008; Woodward et al., 2010).

Growth and competition is are related. There were strong direct proportional relationships between growth rates and competition coefficients, suggesting that growth clearly influences competition in marine dinoflagellates. The slope of the linear relationship between growth and competition were found to vary across temperature, suggesting the temperature dependence of the effect of the growth on competition. This further implies that warming could lead to shifts in community composition in marine dinoflagellates where growth rates strongly influence competitive ability.

Ecological response is predictable from growth responses. There were also direct proportional relationships between predicted and realised competition coefficients (*PCC* and *RCC*, respectively) in all temperature treatments, suggesting the predictability of the realised competition. Hence, the growth rates of species in monocultures can be used to predict the outcomes of competition in co-cultures. The competition coefficients can be used to predict the structure of the community.

7.2 IMPLICATIONS TO CLIMATE CHANGE ECOLOGY

The vulnerability of phytoplankton to climate change is attributed to the impact of temperature change on their physiological processes and growth, which may alter marine ecosystem structure and function. Marine phytoplankton are generally living in the present climate scenario within the thermal safety zone. However, with the ongoing climate change, the warming temperature may likely exceed the physiological limits of marine phytoplankton species. They must avoid the extreme temperatures or else they are at risk of the thermal danger. They may either adapt or migrate to new favourable habitats to survive, otherwise, their extinction is inevitable.

The findings of this thesis reinforce the current thought that ocean warming will likely trigger the poleward shifts in thermal niches of marine phytoplankton species (Barton et al., 2016), the decline of phytoplankton diversity in the tropics (Thomas et al., 2012), the occupancy of non-indigenous and invasive species in new thermally defined habitats (Sorte et al., 2010), and the shift in phytoplankton community structure (Acevedo-Trejos et al., 2015). Hence, highly diverse communities of phytoplankton in the tropics may be the most at threat from global warming. The high biodiversity of marine phytoplankton in the tropics (Righetti et al., 2019) entails intensification of the biotic interaction in the tropical phytoplankton community and hence may narrow the realised thermal niche in the tropics. Narrowing of the niche in tropics may also be attributed to the rates of biotic interactions and processes, or the rate of evolutionary diversification, which are higher in a warmer climate than in a colder climate (Allen et al., 2002; Mittelbach et al., 2007). The findings further imply that species in the tropics are thermal specialists and have a higher affinity to warm temperature than the temperate species. Despite the advantage of having these traits, tropical species have a low heat safety margin, which makes them more vulnerable to warming.

The warming of the climate is likely affecting the distribution of marine phytoplankton in time and space. Consequently, the climate-induced changes in the phenology and biogeography of the phytoplankton bloom are likely to impact the primary production and carbon cycling in the future ocean. It is expected that phytoplankton species will advance their timing of the spring bloom and will persist during fall because of the ocean warming. This advanced timing will be relevant to the subsequent productivity of the marine ecosystems. Along with the shift in phenology, biogeographical distribution and community structure of phytoplankton are also expected to shift in the warming ocean due to alteration in their thermal tolerance. It is expected that species range will shift towards the poles and may contract or expand in response to climate change.

The changes in phenology and biogeography due to warming are also likely to change the ecological interactions. Since different phytoplankton species have different ecological responses to temperature, it is expected that they differ in vulnerability to warming and dispersal capability, and hence changes in the community composition are inevitable in the future. It is predicted that climate change will decrease diversity in the lower latitudes and increase diversity in higher latitudes. Also, it is expected that more changes in phytoplankton community composition will occur in tropics as compared to the temperate regions in response to climate change.

The shifts in the structure and function of the ecosystem are inevitable under the climate change. It is expected that the primary production will be enhanced in many regions in the future since phytoplankton growth is enhanced at an increased temperature below their thermal optimum. This change in the primary productivity will support more aquatic life in the future, and therefore the present biodiversity can be sustained. However, the enhancement of primary production has possible feedback on

global warming. A sink for carbon dioxide may be formed due to higher primary production of phytoplankton. Increased emission of carbon dioxide and increased temperature can enhance primary production by phytoplankton.

In the context of harmful bloom-forming phytoplankton, climate change may provide favourable conditions for toxic algae to occur (Hallegraeff, 2010). It is likely that toxic blooms and their impacts may be exacerbated in the future where their duration, intensity, and frequency may increase in response to changes in the climate. The possible impacts of climate change on toxic blooms have important implications on how to manage and control harmful algal blooms (HAB) in the future. At present, our projections of the HAB response to the future climate scenarios are highly speculative. Our predictive understanding can be improved if evidence for the effect of change in environmental and ecological factors, not just temperature change, on the biogeography and phenology of toxic phytoplankton species is obtained.

7.3 FUTURE RESEARCH DIRECTIONS

7.3.1 Predicting ecological response to climate change

This thesis provides new information on how marine phytoplankton respond to temperature. However, our current understanding on the ecological responses of non-toxic and toxic marine phytoplankton to future climate scenarios is still limited. Other than simple inductive reasoning, further studies are required to advance our knowledge of the climate change ecology of marine phytoplankton. Correlative and mechanistic ecological niche modeling (introduced in Chapter 1) can be applied to examine the effect of climate change on non-toxic and toxic phytoplankton species. In correlative *ENM*, the species occurrence data collected in Chapters 2 and 3 can be linked to

environmental data (e.g. temperature, salinity, nutrients, photosynthetically active radiation, salinity, current velocity, and others) to forecast the suitability of a particular habitat for the species. In mechanistic *ENM*, the thermal performance curves (*TPC*) obtained in Chapters 3 and 4 can be used to establish a causal relationship between species distribution and temperature. Mechanistic *ENM* can be further improved by integrating the findings in Chapter 6 to take into account the effect of biotic interaction on the temperature dependence of growth. Both the correlative and mechanistic *ENM* can be projected into the present and future climate scenarios and can be compared to provide a better insight on the ecological responses of non-toxic and toxic phytoplankton to climate change. Hence, the correlative and mechanistic *ENM* projections can be used to examine the following climate-induced trends in marine phytoplankton:

Latitudinal range shifts. Latitudinal limits and range of species can be projected in the present and future climate scenarios (Figure 7.1). The projected limits can be compared to investigate the magnitude and direction of the climate-induced shift in the equatorial and polar boundaries of species range. Furthermore, the projected latitudinal range can be compared to examine the extent of expansion or contraction of species range in response to climate change.
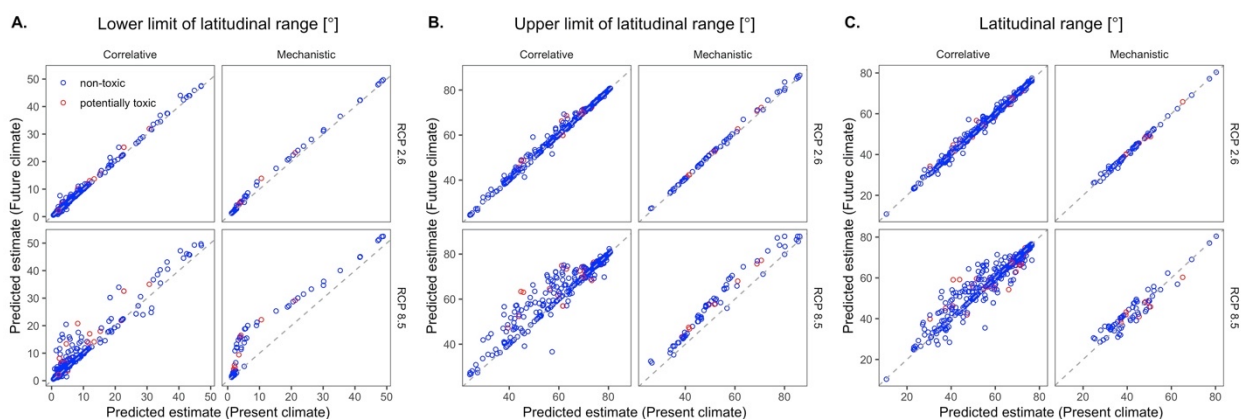
Figure 7.1. Predicted shifts in the latitudinal limits and range of marine phytoplankton. These are projected using correlative and mechanistic ecological niche models (*ENM*) based on the present and

future climate scenarios (*RCP* 2.6 and *RCP* 8.5). The points indicate the projected estimates in non-toxic and potentially toxic species (coloured blue and red, respectively). The points above the 1:1 dashed line indicate a poleward shift in the lower and upper limits of latitudinal range (A and B, respectively) and expansion of latitudinal range (C). On the other hand, the points below the 1:1 dashed line indicate a shift towards the equator in the limits of species range (A and B) and a range contraction (C). As shown, most of the species are expected to experience no change or poleward shift in the lowest and highest latitude at which they can exist. It is also expected that the species range may expand, contract, or remain unchanged in the future climate scenarios. The shifts in the latitudinal limits and range may be dependent on the taxonomic identity and toxicity of phytoplankton species. The results are based on the preliminary analysis, which will not be discussed in detail since it is not within the scope of this chapter. This figure is for demonstration purpose only to show how correlative and mechanistic *ENM* projections are used to examine ecological response of marine phytoplankton to climate change.

Changes in habitat suitability. The number of suitable and unsuitable habitats can also be estimated from the *ENM* projections (Figure 7.2 A and B). The relative change in the predicted number of suitable habitats can be determined to examine how habitat suitability of marine phytoplankton is shifted in response to changes in the climate. This can be expressed by finding the difference between the number of suitable habitats projected in the future and present climate scenarios over the present projections. Based on the implemented *ENM*, that relative change in habitat suitability differ across latitude and the latitudinal variation may also vary across species' taxonomic identity and toxicity. Furthermore, the percentage of habitat loss and gain can also be investigated to examine how much of the suitable habitats can be disappeared or emerged in the future climate scenario (Figure 7.2 C).
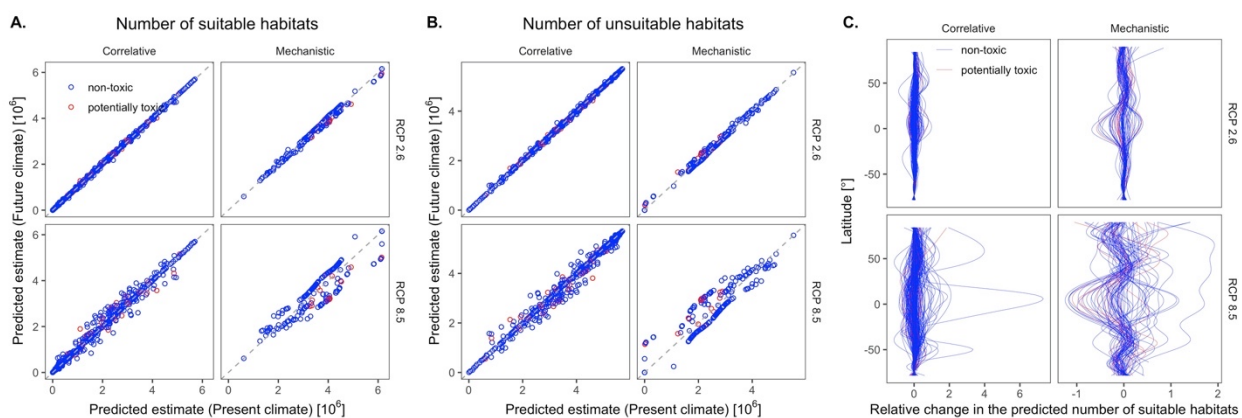
Figure 7.2. Predicted changes in the habitat suitability for marine phytoplankton. The number of suitable and unsuitable habitats are projected using correlative and mechanistic ecological niche models (*ENM*) based on the present and future climate scenarios (*RCP* 2.6 and *RCP* 8.5). The points indicate the projected estimates in non-toxic and potentially toxic species (coloured blue and red, respectively). The points above the 1:1 dashed line indicate an increase in number of suitable and unsuitable habitats, and

points below this line indicate the decline in the estimates (A and B). The latitudinal variation of the relative change in the predicted number of suitable habitats is also presented (C). It is predicted that the percentage of new and loss habitats in the future may vary across phytoplankton species and between non-toxic and toxic species. The results are based on the preliminary analysis, which will not be discussed in details since it is not within the scope of this chapter. This figure is for demonstration purpose only to show how correlative and mechanistic *ENM* projections are used to examine ecological response of marine phytoplankton to climate change.

Changes in the community structure. Phytoplankton diversity in terms of species richness can be obtained by summing the ENM projections of all species. In this, the total number of unique species that are projected to exist in a particular location (0.08° spatial resolution) is determined. To examine the climate-induced change in diversity, the difference in species richness between the present and future projections can be estimated, which can be expressed as change in species richness per decade (Figure 7.3). Furthermore, Sorensen's index in each location can be estimated to examine how similar the phytoplankton community in the present and future climate (Figure 7.4).

Changes in relative composition of toxic species. The difference between the relative proportion of the number of non-toxic and potentially toxic species can also be estimated (Figure 7.5). This projected estimates in the present and future climate scenarios can be compared to examine how climate change affect the dominance of toxic species.
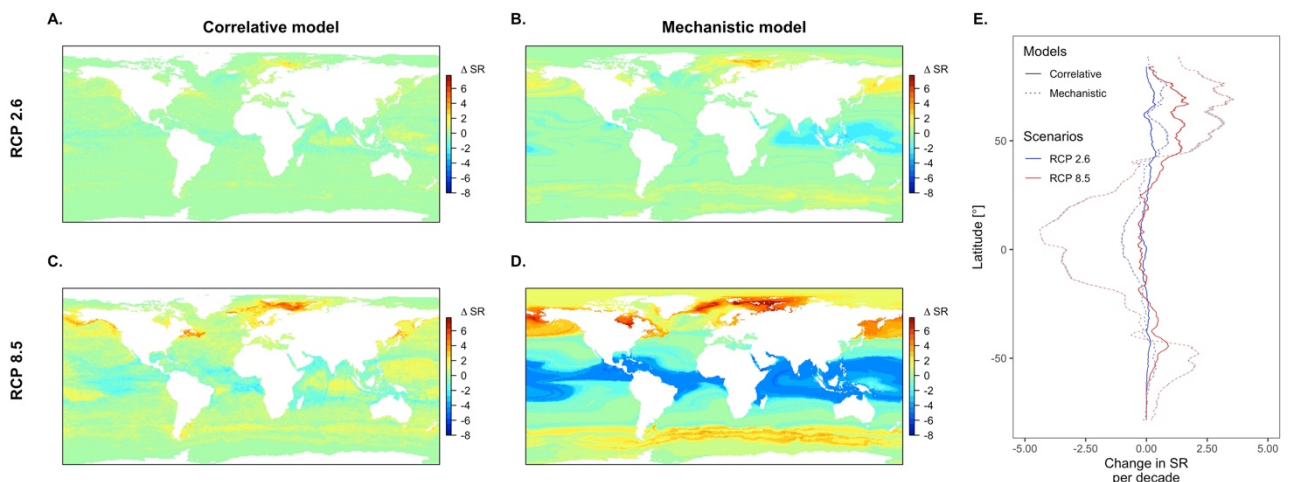
Figure 7.3. Predicted changes in the diversity of marine phytoplankton. The species richness (*SR*) is

projected using correlative and mechanistic ecological niche models (*ENM*) based on the present and future climate scenarios (*RCP* 2.6 and *RCP* 8.5). The colour gradient represents the change in species richness per decade (ΔSR) (A to D). The latitudinal variation of ΔSR is also presented (E). It is predicted that climate change will decrease of diversity in the lower latitudes and increase diversity in higher latitudes. The results are based on the preliminary analysis, which will not be discussed in details since it is not within the scope of this chapter. This figure is for demonstration purpose only to show how correlative and mechanistic *ENM* projections are used to examine ecological response of marine phytoplankton to climate change.
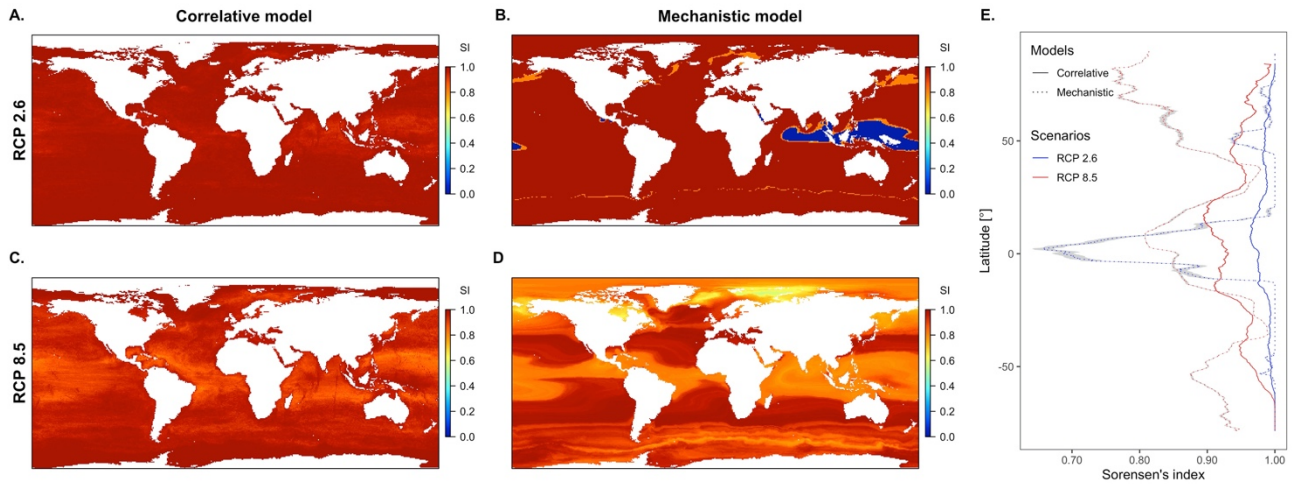
Figure 7.4. Predicted changes in the community composition of marine phytoplankton. The Sorensen's index (*SI*) is projected using correlative and mechanistic ecological niche models (*ENM*) based on the present and future climate scenarios (*RCP* 2.6 and *RCP* 8.5). The colour gradient represents the projected estimates of *SI* (A to D). The latitudinal variation of *SI* is also presented (E). It is predicted that more changes in phytoplankton community composition is expected in tropics as compared to the temperate regions in response to climate change. The results are based on the preliminary analysis, which will not be discussed in details since it is not within the scope of this chapter. This figure is for demonstration purpose only to show how correlative and mechanistic *ENM* projections are used to examine ecological response of marine phytoplankton to climate change.
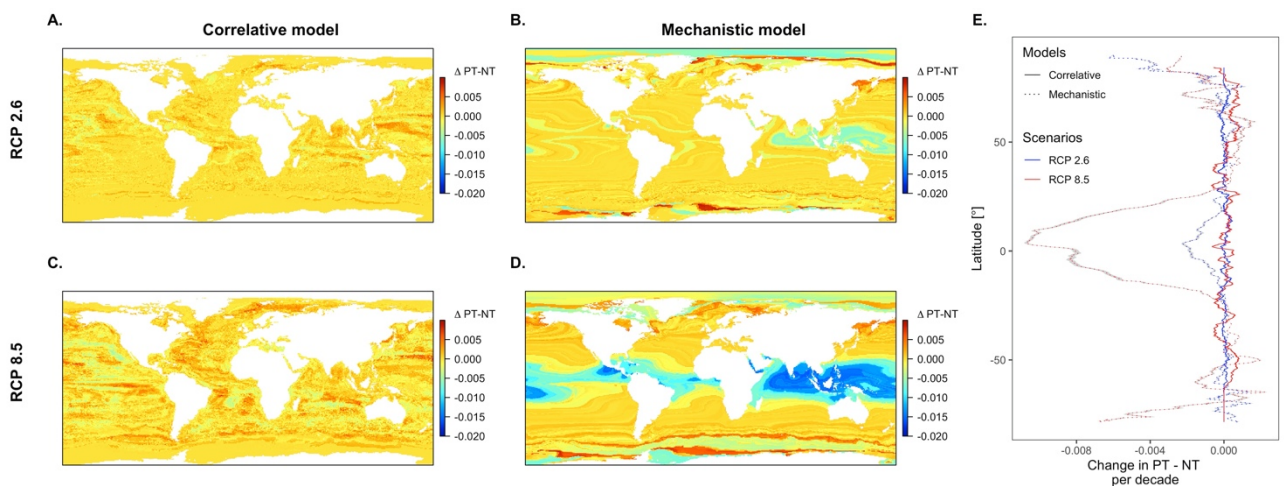
Figure 7.5. Predicted changes in the relative proportion of potentially toxic and non-toxic phytoplankton (Δ *PT - NT*). The relative proportion of the number of non-toxic and potentially toxic species are projected using correlative and mechanistic ecological niche models (*ENM*) based on the present and future climate scenarios (*RCP* 2.6 and *RCP* 8.5). The colour gradient represents the projected estimates of Δ *PT - NT* (A to D). The latitudinal variation of Δ *PT - NT* is also presented (E). As per mechanistic *ENM*, it is expected that the relative composition of toxic species decreased in lower latitude. However, this

projection is different from the correlative *ENM* that show a complex latitudinal pattern in $\Delta\ PT – NT$. The results are based on the preliminary analysis, which will not be discussed in details since it is not within the scope of this chapter. This figure is for demonstration purpose only to show how correlative and mechanistic *ENM* projections are used to examine ecological response of marine phytoplankton to climate change.

However, the ecological niche models are only as good as the data that were used for calibration. As discussed in the previous chapters, there are a number of caveats associated with the use of species occurrence data (Chapter 2 and 3) and temperature-growth data (Chapter 3 and 4), which are needed to be considered when interpreting the findings of *ENM*.

7.3.2 Assessing the thermal growth curve in toxic species from other major taxa

Even though the majority of harmful bloom-forming species and toxigenic strains belong to dinoflagellates (Anderson et al., 2012), characterisation of the thermal response curves in representatives from other phytoplankton taxa, i.e. diatoms, haptophytes and cyanobacteria, is crucial to advance our knowledge on the taxon-specific differences in the growth thermotolerance between non-toxic and toxic phytoplankton. Pooling the experimental data obtained from this study with the datasets compiled from published laboratory culture experiments allows the comparison of thermal growth response between phytoplankton groups with an adequate number of observations (Chapter 4). However, there are still limitations linked with this dataset even if this was compiled from several studies. The limitations include studies with low temperature resolution, incomplete observation of full thermal range, over representation of non-toxic phytoplankton, few observations on toxic species that are mostly dinoflagellates, and insufficient number of freshwater species. Hence, future

work will include examination of growth thermotolerance in toxigenic algal strains from other major taxa.

7.3.3 Determining the physiological responses across thermal gradients

Physiological responses across thermal gradient have to be determined in order to examine the trade-offs between toxicity-related traits (i.e. toxin production and reactive oxygen species (ROS)) and biomass-related traits (i.e. photophysiology, photosynthesis and respiration), which may provide ecological advantages for toxigenic strains to survive thermal stress. These additional physiological measurements will improve our understanding of the bloom-forming capacity of toxic phytoplankton to adjust to changing ocean conditions and will provide insights of the phenotypic responses in current and future climate scenarios.

7.3.4 Determining the combined effects of warming and acidification

This study only accounts the effect of increasing temperature. Single factor experiments (e.g. de Boer *et al.*, 2004; Hikosaka *et al.*, 2005; Low-Décarie *et al.*, 2011) may not lead to an accurate predictions of the physiological and ecological responses of phytoplankton in natural habitats, where phytoplankton are under the influence of the interacting multiple environmental stressors like warming and acidification (Häder & Gao, 2015). The possible additive or multiplicative effects of warming and acidification suggest that single-factor experiments may provide misleading implications about ecophysiological responses of phytoplankton in a multivariate natural environment. However, information about the combined effects of warming and acidification on the ecophysiology of phytoplankton, especially relative success of non-toxic and toxic

species, is scarce but of critical importance for linking ecological shift of toxic blooms with climate change.

7.3 CONCLUDING REMARKS

In this thesis, I have provided new information about the thermal responses of marine phytoplankton. The main findings of this thesis are as follows: (1) the current distribution of marine phytoplankton is limited by temperature, (2) their thermal traits are contingent on their biogeography and phylogeny, (3) their growth and toxin production is affected by temperature, and (4) interspecific competition in dinoflagellates is altered by increasing temperature. The findings of this thesis advance our current predictive understanding on the ecological responses of marine phytoplankton to climate change. In particular, the information collected in this thesis can be used to develop models to predict climate-induced ecological trends such as changes in range, habitat suitability, diversity, and community composition. Accurate predictions are challenging to produce, but the existing models are useful to improve our insights of the climate change biology of marine phytoplankton.

This page is intentionally left blank.

This page is intentionally left blank.

SUPPLEMENTARY TABLES

This page is intentionally left blank.

This page is intentionally left blank.

Supplementary Table 2.1. Total number of observations and unique phytoplankton taxa in the raw and processed data (i.e. data before and after spatial filtering, respectively) across hemispheres, climate zones, and habitats.

Datasets	Factors	Levels	No. of observations (% contribution)		No. of unique taxa					
					Species	*Genus*	*Family*	*Order*	*Class*	*Phylum*
Raw	Hemispheres	North	665058	(86.23)	1514	468	191	84	16	8
		South	106228	(13.77)	975	351	151	69	16	8
	Climate zones	Polar	7533	(0.98)	204	124	85	51	12	6
		Temperate	704462	(91.34)	1561	466	190	83	16	8
		Tropics	59291	(7.69)	917	338	144	69	16	8
	Habitats	Coastal	711113	(92.20)	1644	488	195	84	16	8
		Ocean	60173	(7.80)	469	209	107	56	14	7
Processed	Hemisphere	North	53799	(85.95)	247	125	74	41	13	7
		South	8798	(14.05)	178	96	58	34	8	5
	Climate zones	Polar	787	(1.26)	12	7	4	4	3	3
		Temperate	52877	(84.47)	318	151	86	47	13	7
		Tropics	8933	(14.27)	171	82	53	31	10	6
	Habitats	Coastal	45705	(73.01)	306	149	85	47	13	7
		Ocean	16892	(26.99)	147	75	49	32	6	5

Supplementary Table 2.2. Summary statistics of the likelihood ratio (*LR*) test used to determine the significance of the linear and quadratic terms in the generalized linear mixed model (*GLMM*) (i.e. intercept only (*M1*: y ~ 1), linear term of the predictor (*M2*: y ~ x), and linear and quadratic terms of the predictor (*M3*: y ~ x + x^2). Akaike information criterion (*AIC*) was used to determine whether a full model with linear and quadratic terms would describe the relationship better than a reduced model. Coefficient of determination for each model was estimated to describe the proportion of variance explained by the fixed factor alone (i.e. mariginal *R^2*) and by both the fixed and random factors (i.e. conditional *R^2*). Summary of *GLMM*s can be found in Supplementary Table 2.3.

GLMM ID	Variables			AIC	Likelihood ratio test statistics				Coefficient of Determination	
	Dependent	Independent	Model Structure ID		Test	X^2	df	p-value	R$^2_{GLMM}$^{m}	R$^2_{GLMM}$^{c}
GLMM 01	LTL	LM	M1	4350.01						
			M2	4059.87	M1 vs M2	292.14	1	<0.01	0.13	0.39
			M3	4002.03	M2 vs M3	59.83	1	<0.01	0.19	0.42
GLMM 02	UTL	LM	M1	4831.28						
			M2	4448.57	M1 vs M2	384.71	1	<0.01	0.19	0.31
			M3	4411.02	M2 vs M3	39.55	1	<0.01	0.25	0.34
GLMM 03	RTN	LM	M1	5063.91						
			M2	5054.62	M1 vs M2	11.29	1	<0.01	<0.01	0.05
			M3	5056.54	M2 vs M3	0.08	1	0.78	<0.01	0.05
GLMM 04	LTL*	LM	M1	4971.27						
			M2	4702.36	M1 vs M2	270.91	1	<0.01	0.14	0.27
			M3	4645.52	M2 vs M3	58.84	1	<0.01	0.19	0.33
GLMM 05	UTL*	LM	M1	4517.39						
			M2	4153.92	M1 vs M2	365.47	1	<0.01	0.17	0.34
			M3	4136.46	M2 vs M3	19.45	1	<0.01	0.21	0.35
GLMM 06	RTN*	LM	M1	5360.44						
			M2	5360.14	M1 vs M2	2.30	1	0.13	<0.01	0.10
			M3	5356.41	M2 vs M3	5.73	1	0.02	<0.01	0.12
GLMM 07	LTL	TM	M1	4350.01						
			M2	3562.92	M1 vs M2	789.08	1	<0.01	0.51	0.54
			M3	3506.42	M2 vs M3	58.51	1	<0.01	0.55	0.57
GLMM 08	UTL	TM	M1	4831.28						
			M2	3562.53	M1 vs M2	1270.75	1	<0.01	0.63	0.65
			M3	3506.20	M2 vs M3	58.33	1	<0.01	0.64	0.66
GLMM 09	RTN	TM	M1	5063.91						
			M2	5034.49	M1 vs M2	31.42	1	<0.01	0.02	0.08
			M3	4978.14	M2 vs M3	58.35	1	<0.01	0.03	0.09

GLMM 10	LTL*	TM*	M1	4971.27						
			M2	3844.69	M1 vs M2	1128.57	1	<0.01	0.55	0.60
			M3	3738.40	M2 vs M3	108.30	1	<0.01	0.58	0.61
GLMM 11	UTL*	TM*	M1	4517.39						
			M2	3844.03	M1 vs M2	675.35	1	<0.01	0.38	0.45
			M3	3737.62	M2 vs M3	108.41	1	<0.01	0.43	0.47
GLMM 12	RTN*	TM*	M1	5360.44						
			M2	5316.47	M1 vs M2	45.97	1	<0.01	0.03	0.13
			M3	5210.16	M2 vs M3	108.30	1	<0.01	0.05	0.12
GLMM 13	GR	LM	M1	3438.61						
			M2	3439.39	M1 vs M2	1.22	1	0.27	<0.01	0.01
			M3	3428.36	M2 vs M3	13.02	1	<0.01	<0.01	0.01
GLMM 14	GR	TM	M1	3438.61						
			M2	3439.68	M1 vs M2	0.92	1	0.34	<0.01	0.01
			M3	3441.60	M2 vs M3	0.08	1	0.77	<0.01	0.01
GLMM 15	GR	TM*	M1	3438.61						
			M2	3436.80	M1 vs M2	3.81	1	0.05	<0.01	0.01
			M3	3438.74	M2 vs M3	0.06	1	0.81	<0.01	0.01
GLMM 16	GR	LTL	M1	3438.61						
			M2	3418.38	M1 vs M2	22.22	1	<0.01	<0.01	0.01
			M3	3412.32	M2 vs M3	8.06	1	<0.01	0.01	0.02
GLMM 17	GR	UTL	M1	3438.61						
			M2	3431.01	M1 vs M2	9.60	1	<0.01	<0.01	0.01
			M3	3429.97	M2 vs M3	3.04	1	0.08	<0.01	0.02
GLMM 18	GR	RTN	M1	3438.61						
			M2	3328.30	M1 vs M2	112.30	1	<0.01	0.01	0.02
			M3	3280.41	M2 vs M3	49.89	1	<0.01	0.01	0.02
GLMM 19	GR	LTL*	M1	3438.61						
			M2	3429.16	M1 vs M2	11.45	1	<0.01	<0.01	0.01
			M3	3431.10	M2 vs M3	0.06	1	0.81	<0.01	0.01
GLMM 20	GR	UTL*	M1	3438.61						
			M2	3440.58	M1 vs M2	0.02	1	0.88	<0.01	0.01
			M3	3438.51	M2 vs M3	4.08	1	0.04	<0.01	0.01
GLMM 21	GR	RTN*	M1	3438.61						
			M2	3421.71	M1 vs M2	18.90	1	<0.01	<0.01	0.01
			M3	3360.28	M2 vs M3	63.43	1	<0.01	0.01	0.02

Supplementary Table 2.3. Summary of the generalised linear mixed models (*GLMM*) models used to determine the effect of latitude (expressed as absolute latitudinal midpoint, *LM*, °) and the effect of temperature (expressed as thermal midpoint, *TM*, °C) on the thermal niche parameters (i.e. lower thermal limit (*LTL*, °C), upper thermal limits (*UTL*, °C), and realised thermal niche breadth (*RTN*, °C) derived from long-term annual average and seasonal extreme (indicated by an asterisk) sea surface temperature (*SST*)) (*GLMM* 01 – 12) and geographic range size (*GR*, km^2 in log_{10} scale) (*GLMM* 13 – 15) of marine phytoplankton. *GLMM*s were also used to test the relationship between thermal niche parameters and geographic range size (*GLMM* 16 – 21). Random effects taxonomic class nested in ocean realms was incorporated in all *GLMM*s that were weighted by the number of unique occurrence locations. (Notes: *SE* = standard error; *t* = t value; *SD* = standard deviation).

GLMM ID	Dependent Variables	Models with linear term only (M2)						Models with linear and quadratic terms (M3)					
		Fixed				Random		Fixed				Random	
		Coefficients	Estimates	SE	t	Variables	SD	Coefficients	Estimates	SE	t	Variables	SD
GLMM 01	LTL	Intercept	23.61	0.82	28.75	class:region	0.61	Intercept	20.62	0.86	23.93	class:region	0.73
		LM	-0.23	0.01	-19.03	region	4.58	LM	0.06	0.04	1.49	region	4.28
						residual	7.15	LM^2	<-0.01	<0.01	-7.96	residual	6.91
GLMM 02	UTL	Intercept	31.04	0.74	41.85	class:region	0.90	Intercept	28.28	0.81	34.89	class:region	0.87
		LM	-0.32	0.01	-22.87	region	3.53	LM	-0.05	0.04	-1.17	region	2.93
						residual	8.67	LM^2	<-0.01	<0.01	-6.48	residual	8.58
GLMM 03	RTN	Intercept	6.52	0.71	9.19	class:region	1.02	Intercept	6.35	0.96	6.64	class:region	1.01
		LM	-0.06	0.02	-3.38	region	2.39	LM	-0.04	0.06	-0.72	region	2.39
						residual	11.92	LM^2	<-0.01	<0.01	-0.26	residual	11.93
GLMM 04	LTL*	Intercept	22.36	0.85	26.33	class:region	0.73	Intercept	18.26	0.99	18.44	class:region	0.82
		LM	-0.30	0.02	-18.83	region	4.11	LM	0.08	0.05	1.61	region	4.18
						residual	9.89	LM^2	-0.01	<0.01	-7.83	residual	9.56
GLMM 05	UTL*	Intercept	32.57	0.73	44.69	class:region	0.79	Intercept	30.86	0.78	39.45	class:region	0.78
		LM	-0.27	0.01	-21.50	region	3.76	LM	-0.10	0.04	-2.48	region	3.31
						residual	7.48	LM^2	<-0.01	<0.01	-4.53	residual	7.46
GLMM 06	RTN*	Intercept	10.32	1.01	10.23	class:region	1.02	Intercept	12.17	1.27	9.56	class:region	1.05
		LM	0.03	0.02	1.51	region	4.35	LM	-0.14	0.07	-1.99	region	4.71
						residual	13.61	LM^2	<0.01	<0.01	2.53	residual	13.52
GLMM 07	LTL	Intercept	-0.17	0.43	-0.40	class:region	0.49	Intercept	3.20	0.60	5.32	class:region	0.49
		TM	0.88	0.02	43.75	region	1.44	TM	0.34	0.07	4.57	region	1.35
						residual	5.87	TM^2	0.02	<0.01	7.74	residual	5.72
GLMM 08	UTL	Intercept	0.18	0.43	0.42	class:region	0.49	Intercept	-3.18	0.60	-5.30	class:region	0.49
		TM	1.12	0.02	55.61	region	1.44	TM	1.66	0.07	22.67	region	1.35
						residual	5.87	TM^2	-0.02	<0.01	-7.73	residual	5.72
GLMM 09	RTN	Intercept	0.35	0.85	0.41	class:region	0.97	Intercept	-6.38	1.20	-5.31	class:region	0.97
		TM	0.24	0.04	5.92	region	2.88	TM	1.33	0.15	9.04	region	2.70
						residual	11.74	TM^2	-0.03	<0.01	-7.73	residual	11.43
GLMM 10	LTL*	Intercept	-8.71	0.57	-15.27	class:region	0.52	Intercept	-2.24	0.75	-2.98	class:region	0.47
		TM*	1.17	0.02	47.06	region	2.26	TM*	0.23	0.09	2.62	region	1.69
						residual	6.64	TM^{*2}	0.03	<0.01	10.88	residual	6.39
GLMM 11	UTL*	Intercept	8.71	0.57	15.28	class:region	0.52	Intercept	2.24	0.75	2.98	class:region	0.47
		TM*	0.83	0.02	33.33	region	2.26	TM*	1.77	0.09	20.07	region	1.69
						residual	6.64	TM^{*2}	-0.03	<0.01	-10.89	residual	6.38
GLMM 12	RTN*	Intercept	17.41	1.14	15.27	class:region	1.04	Intercept	4.48	1.50	2.98	class:region	0.94

		TM*	-0.34	0.05	-6.87	region	4.52	TM*	1.54	0.18	8.72	region	3.38
						residual	13.28	TM*^{2}	-0.06	0.01	-10.88	residual	12.77
GLMM 13	GR	Intercept	5.21	0.20	26.05	class:region	0.28	Intercept	6.23	0.35	18.01	class:region	0.29
		LM	0.01	<0.01	1.09	region	0.39	LM	-0.07	0.02	-3.27	region	0.39
						residual	5.84	LM^2	<0.01	<0.01	3.62	residual	5.80
GLMM 14	GR	Intercept	5.57	0.19	29.31	class:region	0.29	Intercept	5.50	0.35	15.84	class:region	0.29
		TM	-0.01	0.01	-0.93	region	0.39	TM	<0.01	0.05	0.03	region	0.39
						residual	5.84	TM2	<-0.01	<0.01	-0.24	residual	5.84
GLMM 15	GR	Intercept	5.75	0.20	29.24	class:region	0.29	Intercept	5.69	0.38	15.04	class:region	0.29
		TM*	-0.02	0.01	-1.94	region	0.38	TM*	-0.01	0.05	-0.23	region	0.39
						residual	5.83	TM*^{2}	<-0.01	<0.01	-0.19	residual	5.83
GLMM 16	GR	Intercept	6.13	0.18	34.66	class:region	0.28	Intercept	6.99	0.30	23.29	class:region	0.29
		LTL	-0.05	0.01	-4.78	region	0.44	LTL	-0.19	0.04	-4.65	region	0.61
						residual	5.77	LTL^2	<0.01	<0.01	3.29	residual	5.69
GLMM 17	GR	Intercept	4.61	0.24	19.59	class:region	0.28	Intercept	3.88	0.45	8.66	class:region	0.27
		UTL	0.04	0.01	3.71	region	0.57	UTL	0.14	0.05	2.59	region	0.61
						residual	5.76	UTL^2	<-0.01	<0.01	-1.81	residual	5.75
GLMM 18	GR	Intercept	4.72	0.11	42.95	class:region	0.25	Intercept	4.20	0.13	32.03	class:region	0.22
		RTN	0.14	0.01	10.94	region	0.46	RTN	0.37	0.03	10.90	region	0.47
						residual	5.53	RTN^2	-0.02	<0.01	-7.16	residual	5.40
GLMM 19	GR	Intercept	5.74	0.13	43.36	class:region	0.28	Intercept	5.77	0.15	38.10	class:region	0.28
		LTL*	-0.03	0.01	-3.41	region	0.42	LTL*	-0.04	0.03	-1.54	region	0.43
						residual	5.80	LTL*^{2}	<0.01	<0.01	0.32	residual	5.80
GLMM 20	GR	Intercept	5.34	0.26	20.72	class:region	0.29	Intercept	4.37	0.55	7.98	class:region	0.28
		UTL*	<0.01	0.01	0.26	region	0.41	UTL*	0.11	0.05	2.02	region	0.41
						residual	5.83	UTL*^{2}	<-0.01	<0.01	-2.01	residual	5.83
GLMM 21	GR	Intercept	4.78	0.17	28.52	class:region	0.28	Intercept	2.85	0.29	9.88	class:region	0.26
		RTN*	0.05	0.01	4.56	region	0.50	RTN*	0.37	0.04	8.98	region	0.43
						residual	5.76	RTN*^{2}	-0.01	<0.01	-8.09	residual	5.61

Supplementary Table 2.4. Summary statistics of the intercept and smooth terms in generalized additive mixed models (*GAMM*) models used to determine the effect of latitude (expressed as absolute latitudinal midpoint, *LM*, °) and the effect of temperature (expressed as thermal midpoint, *TM*, °C) on the thermal niche parameters (i.e. lower thermal limit (*LTL*, °C), upper thermal limits (*UTL*, °C), and realised thermal niche breadth (*RTN*, °C) derived from long-term annual average and seasonal extreme (indicated by an asterisk) sea surface temperature (*SST*)) (*GAMM* 01 – 12) and geographic range size (*GR*, km^2 in log$_{10}$ scale) (*GAMM* 13 – 15) of marine phytoplankton. *GAMMs* were also used to test the relationship between thermal niche parameters and geographic range size (*GAMM* 16 – 21). Random effects taxonomic class nested in ocean realms was incorporated in all *GLMM*s that were weighted by the number of unique occurrence locations. (Notes: *SD* = standard deviation; *t* = t value*; edf* = estimated degrees of freedom; *Ref df* = Reference degree of freedom; *Adj. R^2*= adjusted coefficient of determination).

GAMM ID	Variables Dependent	Variables Independent	Intercept Term Estimate	SD	t	p-value	Smooth Terms Coefficients	edf	Red df	F	p-value	Adj. R^2
GAMM 01	LTL	LM	15.76	0.58	27.00	<0.01	s(LM)	7.45	7.45	69.80	<0.01	0.65
GAMM 02	UTL	LM	20.37	0.38	53.20	<0.01	s(LM)	6.94	6.94	123.00	<0.01	0.78
GAMM 03	RTN	LM	4.77	0.40	11.90	<0.01	s(LM)	5.68	5.68	9.46	<0.01	-0.39
GAMM 04	LTL*	LM	12.31	0.62	20.00	<0.01	s(LM)	6.56	6.56	74.80	<0.01	0.60
GAMM 05	UTL*	LM	23.64	0.44	53.50	<0.01	s(LM)	8.39	8.39	90.50	<0.01	0.66
GAMM 06	RTN*	LM	11.42	0.74	15.40	<0.01	s(LM)	7.45	7.45	8.63	<0.01	-0.38
GAMM 07	LTL	TM	15.85	0.24	65.90	<0.01	s(TM)	8.77	8.77	312.00	<0.01	0.91
GAMM 08	UTL	TM	20.73	0.24	86.20	<0.01	s(TM)	8.77	8.77	504.00	<0.01	0.91
GAMM 09	RTN	TM	4.88	0.48	10.20	<0.01	s(TM)	8.77	8.77	54.80	<0.01	-0.90
GAMM 10	LTL*	TM*	12.28	0.34	36.10	<0.01	s(TM*)	8.53	8.53	370.00	<0.01	0.85
GAMM 11	UTL*	TM*	23.83	0.34	70.00	<0.01	s(TM*)	8.53	8.53	203.00	<0.01	0.83
GAMM 12	RTN*	TM*	11.54	0.68	17.00	<0.01	s(TM*)	8.53	8.53	43.90	<0.01	-0.21
GAMM 13	GR	LM	5.36	0.09	59.80	<0.01	s(LM)	5.25	5.25	5.21	<0.01	-0.08
GAMM 14	GR	TM	5.38	0.08	66.00	<0.01	s(TM)	4.31	4.31	2.44	0.06	-0.20
GAMM 15	GR	TM*	5.38	0.08	63.50	<0.01	s(TM*)	7.42	7.42	6.48	<0.01	-0.21
GAMM 16	GR	LTL	5.30	0.11	48.30	<0.01	s(LTL)	7.91	7.91	9.12	<0.01	-0.08
GAMM 17	GR	UTL	5.48	0.14	40.20	<0.01	s(UTL)	8.03	8.03	8.29	<0.01	-0.60
GAMM 18	GR	RTN	5.32	0.10	55.80	<0.01	s(RTN)	6.82	6.82	38.50	<0.01	0.05
GAMM 19	GR	LTL*	5.36	0.09	62.50	<0.01	s(LTL*)	1.00	1.00	11.50	<0.01	-0.10
GAMM 20	GR	UTL*	5.38	0.09	56.70	<0.01	s(UTL*)	5.77	5.77	8.92	<0.01	-0.17
GAMM 21	GR	RTN*	5.41	0.09	62.80	<0.01	s(RTN*)	8.69	8.69	20.60	<0.01	0.14

Supplementary Table 2.5. Summary statistics of the fixed and random effects in generalized additive mixed models (*GAMM*) used to determine the effect of latitude (expressed as absolute latitudinal midpoint, *LM*, °) and the effect of temperature (expressed as thermal midpoint, *TM*, °C) on the thermal niche parameters (i.e. lower thermal limit (*LTL*, °C), upper thermal limits (*UTL*, °C), and realised thermal niche breadth (*RTN*, °C) derived from long-term annual average and seasonal extreme (indicated by an asterisk) sea surface temperature (*SST*)) (*GAMM* 01 – 12) and geographic range size (*GR*, km^2 in log$_{10}$ scale) (*GAMM* 13 – 15) of marine phytoplankton. *GAMMs* were also used to test the relationship between thermal niche parameters and geographic range size (*GAMM* 16 – 21). Random effects taxonomic class nested in ocean realms was incorporated in all *GLMM*s that were weighted by the number of unique occurrence locations. (Notes: *AIC* = Akaike information criteria; *SD* = standard deviation; *SE* = standard error).

GAMM ID	Variables		AIC	Fixed Effects			Random Effects	
	Dependent	Independent		Coefficients	Estimates	SE	Coefficients	SD
GAMM 01	LTL	LM	3993.8	Intercept	0.34	0.13	class:region	0.72
				s(LM)	0.13	3.35	region	3.67
							residual	6.83
GAMM 02	UTL	LM	4367.7	Intercept	0.15	0.06	class:region	0.81
				s(LM)	0.06	2.63	region	2.28
							residual	8.40
GAMM 03	RTN	LM	5028.4	Intercept	0.16	0.04	class:region	0.92
				s(LM)	0.04	2.67	region	2.29
							residual	11.72
GAMM 04	LTL*	LM	4628.0	Intercept	0.38	0.12	class:region	0.81
				s(LM)	0.12	3.53	region	3.82
							residual	9.41
GAMM 05	UTL*	LM	4035.6	Intercept	0.19	0.12	class:region	0.72
				s(LM)	0.12	4.12	region	2.70
							residual	7.04
GAMM 06	RTN*	LM	5319.7	Intercept	0.55	0.25	class:region	0.96
				s(LM)	0.25	8.94	region	4.56
							residual	13.15
GAMM 07	LTL	TM	3233.0	Intercept	0.06	0.00	class:region	0.53
				s(TM)	0.00	0.90	region	1.45
							residual	4.83
GAMM 08	UTL	TM	3233.1	Intercept	0.06	0.00	class:region	0.53
				s(TM)	0.00	0.90	region	1.45
							residual	4.83
GAMM 09	RTN	TM	4704.7	Intercept	0.23	-0.02	class:region	1.07
				s(TM)	-0.02	3.61	region	2.90
							residual	9.66

GAMM 10	LTL*	TM*	3595.9	Intercept	0.12	-0.02	class:region	0.42
				s(TM*)	-0.02	1.26	region	2.12
							residual	5.81
GAMM 11	UTL*	TM*	3594.8	Intercept	0.12	-0.02	class:region	0.42
				s(TM*)	-0.02	1.26	region	2.12
							residual	5.80
GAMM 12	RTN*	TM*	5067.8	Intercept	0.46	-0.06	class:region	0.84
				s(TM*)	-0.06	5.03	region	4.24
							residual	11.61
GAMM 13	GR	LM	3425.6	Intercept	0.01	0.00	class:region	0.29
				s(LM)	0.00	0.36	region	0.42
							residual	5.74
GAMM 14	GR	TM	3442.5	Intercept	0.01	0.00	class:region	0.30
				s(TM)	0.00	0.17	region	0.35
							residual	5.81
GAMM 15	GR	TM*	3415.5	Intercept	0.01	0.00	class:region	0.29
				s(TM*)	0.00	0.54	region	0.38
							residual	5.69
GAMM 16	GR	LTL	3398.3	Intercept	0.01	0.00	class:region	0.33
				s(LTL)	0.00	0.52	region	0.56
							residual	5.56
GAMM 17	GR	UTL	3419.4	Intercept	0.02	0.00	class:region	0.28
				s(UTL)	0.00	1.18	region	0.75
							residual	5.59
GAMM 18	GR	RTN	3231.4	Intercept	0.01	0.00	class:region	0.21
				s(RTN)	0.00	0.22	region	0.50
							residual	5.21
GAMM 19	GR	LTL*	3431.2	Intercept	0.01	0.00	class:region	0.28
				s(LTL*)	0.00	0.00	region	0.40
							residual	5.80
GAMM 20	GR	UTL*	3411.1	Intercept	0.01	0.00	class:region	0.27
				s(UTL*)	0.00	0.43	region	0.46
							residual	5.69
GAMM 21	GR	RTN*	3294.6	Intercept	0.01	0.00	class:region	0.29
				s(RTN*)	0.00	0.37	region	0.42
							residual	5.31

Supplementary Table 2.6. Summary of the generalised additive models (*GAM*) for the relationship of latitude with sea surface temperature (*SST*), climate variability (*CV*), habitat availability (*HA*) habitat availability variability (*HAV*), diversity (*D*), and diversity variability (*DV*). (Notes: *SD* = standard deviation; *t* = t value*; edf* = estimated degrees of freedom; *Ref df* = Reference degree of freedom; *Adj. R²*= adjusted coefficient of determination).

GAM ID	Variables		Intercept Term				Smooth Terms					Adj. R²
	Dependent	Independent	Estimate	SD	t	p-value	Coefficients	edf	Red df	F	p-value	
GAM 01	SST	Latitude	13.43	0.04	358.50	<0.01	s(Latitude)	8.9	9.0	9968.0	<0.01	0.998
GAM 02	CV	Latitude	4.76	0.04	111.10	<0.01	s(Latitude)	8.8	9.0	496.1	<0.01	0.964
GAM 03	HA	Latitude	9.42	<0.01	10270.00	<0.01	s(Latitude)	9.0	9.0	500000.0	<0.01	0.761
GAM 04	HAV	Latitude	8.85	<0.01	8312.00	<0.01	s(Latitude)	9.0	9.0	156225.0	<0.01	0.309
GAM 05	D	Latitude	4.28	0.01	363.90	<0.01	s(Latitude)	8.8	9.0	1518.0	<0.01	0.880
GAM 06	DV	Latitude	2.28	0.03	74.86	<0.01	s(Latitude)	8.9	9.0	228.1	<0.01	0.285

Supplementary Table 2.7. Summary statistics of the likelihood ratio (*LR*) test used to determine the significance of the variables added sequentially in the nested generalised linear models (GLM) for the relationship of different environmental variables (i.e. sea surface temperature (*SST*), climate variability (*CV*), habitat availability (*HA*) habitat availability variability (*HAV*), diversity (*D*), and diversity variability (*DV*)) with the extreme thermal niche breadth (*RTN**) (GLM 01 – 07) and with geographic range size (*GR*) (GLM 08 – GLM 14). Akaike information criterion (*AIC*) was used to determine which model would describe the relationship best. Selected models are highlighted in grey

Model ID	Model Structure	AIC	Null df	Null Deviance	Residual df	Residual Deviance	Test	p -value
GLM x	RTN* ~ 1	531.36			96	1304.42		
GLM 01	RTN* ~ CV	475.56	1	585.6	95	718.82	GLM x vs GLM 1	<0.01
GLM 02	RTN* ~ CV + SST	463.69	1	95.72	94	623.1	GLM 1 vs GLM 2	<0.01
GLM 03	RTN* ~ CV + SST + D	465.07	1	4.02	93	619.08	GLM 2 vs GLM 3	0.43
GLM 04	RTN* ~ CV + SST + D + HA	465.66	1	8.94	92	610.14	GLM 3 vs GLM 4	0.24
GLM 05	RTN* ~ CV + SST + D + HA + HAV	467.61	1	0.27	91	609.88	GLM 4 vs GLM 5	0.84
GLM 06	RTN* ~ CV + SST + D + HA + HAV + DV	464.74	1	29.9	90	579.98	GLM 5 vs GLM 6	0.03
GLM 07	RTN* ~ CV + SST + CV:SST	462.23	1	21.86	93	601.24	GLM 2 vs GLM 7	0.07
GLM y	GR ~ 1	145.63			96	24.46		
GLM 08	GR ~ D	141.75	1	1.44	95	23.02	GLM y vs GLM 8	0.01
GLM 09	GR ~ D + HA	137.38	1	1.46	94	21.56	GLM 8 vs GLM 9	0.01
GLM 10	GR ~ D + HA + CV	136.35	1	0.66	93	20.89	GLM 9 vs GLM 10	0.09
GLM 11	GR ~ D + HA + CV + SST	138.3	1	0.01	92	20.88	GLM 10 vs GLM 11	0.82
GLM 12	GR ~ D + HA + CV + SST + HAV	140.09	1	0.04	91	20.84	GLM 11 vs GLM 12	0.66
GLM 13	GR ~ D + HA + CV + SST + HAV + DV	141.99	1	0.02	90	20.82	GLM 12 vs GLM 13	0.76
GLM 14	GR ~ D + HA + D:HA	136.21	1	0.69	93	20.86	GLM 13 vs GLM 14	0.08

Supplementary Table 2.8. Summary of the generalised linear models (GLM) for the relationship of different environmental variables (i.e. sea surface temperature (*SST*), climate variability (*CV*), habitat availability (*HA*) habitat availability variability (*HAV*), diversity (*D*), and diversity variability (*DV*)) with the extreme thermal niche breadth (*RTN**) (GLM 01 – 07) and with geographic range size (*GR*) (GLM 08 – GLM 14). Selected models are highlighted in grey. (Notes: *SE* = standard error; *t* = t value*; df =* degrees of freedom).

GLM ID	Dependent Variables	Terms	Coefficients				Null		Residual	
			Estimate	SE	t	p-value	df	Deviance	df	Deviance
GLM 01	RTN*	Intercept	5.92	0.72	8.23	0.00			96	1304.42
		CV	0.93	0.11	8.80	0.00	1	585.60	95	718.82
GLM 02	RTN*	Intercept	2.10	1.21	1.73	0.09			96	1304.42
		CV	1.13	0.11	10.06	0.00	1	585.60	95	718.82
		SST	0.14	0.04	3.80	0.00	1	95.72	94	623.10
GLM 03	RTN*	Intercept	2.28	1.24	1.84	0.07			96	1304.42
		CV	1.08	0.13	8.34	0.00	1	585.60	95	718.82
		SST	0.09	0.08	1.22	0.23	1	95.72	94	623.10
		D	0.01	0.02	0.78	0.44	1	4.02	93	619.08
GLM 04	RTN*	Intercept	1.37	1.46	0.94	0.35			96	1304.42
		CV	1.14	0.14	8.19	0.00	1	585.60	95	718.82
		SST	0.07	0.08	0.92	0.36	1	95.72	94	623.10
		D	0.01	0.02	0.87	0.39	1	4.02	93	619.08
		HA	4.51E-05	3.88E-05	1.16	0.25	1	8.94	92	610.14
GLM 05	RTN*	Intercept	1.46	1.54	0.95	0.34			96	1304.42
		CV	1.14	0.14	8.14	0.00	1	585.60	95	718.82
		SST	0.07	0.08	0.93	0.35	1	95.72	94	623.10
		D	0.01	0.02	0.73	0.47	1	4.02	93	619.08
		HA	4.76E-05	4.11E-05	1.16	0.25	1	8.94	92	610.14
		HAV	-1.22E-05	6.09E-05	-0.20	0.84	1	0.27	91	609.88
GLM 06	RTN*	Intercept	2.66	1.61	1.66	0.10			96	1304.42
		CV	1.12	0.14	8.08	0.00	1	585.60	95	718.82
		SST	0.06	0.08	0.72	0.47	1	95.72	94	623.10
		D	0.02	0.02	1.12	0.27	1	4.02	93	619.08
		HA	1.75E-05	4.26E-05	0.41	0.68	1	8.94	92	610.14
		HAV	-2.10E-06	5.99E-05	-0.04	0.97	1	0.27	91	609.88
		DV	-0.08	0.04	-2.15	0.03	1	29.90	90	579.98
GLM 07	RTN*	Intercept	4.58	1.81	2.54	0.01			96	1304.42
		CV	0.72	0.25	2.85	0.01	1	585.60	95	718.82
		SST	-1.61E-03	0.09	-0.02	0.99	1	95.72	94	623.10

		CV:SST	0.03	0.01	1.84	0.07	1	21.86	93	601.24
GLM 08	GR	Intercept	5.96	0.13	44.26	0.00			96	24.46
		D	-3.51E-03	1.44E-03	-2.44	0.02	1	1.44	95	23.02
GLM 09	GR	Intercept	5.80	0.15	39.80	0.00			96	24.46
		D	-4.57E-03	1.46E-03	-3.12	0.00	1	1.44	95	23.02
		HA	1.46E-05	5.76E-06	2.53	0.01	1	1.46	94	21.56
GLM 10	GR	Intercept	6.15	0.25	24.37	0.00			96	24.46
		D	-4.52E-03	1.45E-03	-3.12	0.00	1	1.44	95	23.02
		HA	7.76E-06	6.94E-06	1.12	0.27	1	1.46	94	21.56
		CV	-0.04	0.02	-1.72	0.09	1	0.66	93	20.89
GLM 11	GR	Intercept	6.13	0.27	22.68	0.00			96	24.46
		D	-0.01	2.84E-03	-1.79	0.08	1	1.44	95	23.02
		HA	7.37E-06	7.18E-06	1.03	0.31	1	1.46	94	21.56
		CV	-0.04	0.03	-1.37	0.17	1	0.66	93	20.89
		SST	3.29E-03	0.01	0.23	0.82	1	0.01	92	20.88
GLM 12	GR	Intercept	6.09	0.28	21.47	0.00			96	24.46
		D	-4.57E-03	3.08E-03	-1.49	0.14	1	1.44	95	23.02
		HA	6.32E-06	7.59E-06	0.83	0.41	1	1.46	94	21.56
		CV	-0.04	0.03	-1.35	0.18	1	0.66	93	20.89
		SST	1.58E-03	0.01	0.11	0.92	1	0.01	92	20.88
		HAV	4.96E-06	1.13E-05	0.44	0.66	1	0.04	91	20.84
GLM 13	GR	Intercept	6.06	0.30	19.93	0.00			96	24.46
		D	-4.75E-03	3.14E-03	-1.51	0.13	1	1.44	95	23.02
		HA	7.14E-06	8.08E-06	0.88	0.38	1	1.46	94	21.56
		CV	-0.03	0.03	-1.32	0.19	1	0.66	93	20.89
		SST	2.07E-03	0.02	0.14	0.89	1	0.01	92	20.88
		HAV	4.68E-06	1.14E-05	0.41	0.68	1	0.04	91	20.84
		DV	2.14E-03	0.01	0.31	0.76	1	0.02	90	20.82
GLM 14	GR	Intercept	6.19	0.27	23.10	0.00			96	24.46
		D	-0.01	3.55E-03	-2.89	0.00	1	1.44	95	23.02
		HA	-1.05E-05	1.54E-05	-0.68	0.50	1	1.46	94	21.56
		D:HA	3.34E-07	1.90E-07	1.76	0.08	1	0.69	93	20.86

Supplementary Table 3.1. Summary of the generalised linear models (*GLM*) for testing the relationship between physiology- and occurrence-based thermal traits (TT_p and TT_o, respectively). Highlighted in grey are reported in the main text. (Notes: *SE* = standard error; *t* = t value*; df* = degrees of freedom; *AIC* = Akaike information criteria; *Adj. R^2* = coefficient of determination).

Model ID	Dependent Variables	Terms	Coefficients				Null		Residual		AIC	Adj. R^2
			Estimate	SE	t	p	df	Deviance	df	Deviance		
GLM 01	T_{opt} *	Intercept	-1.48	2.22	-0.67	0.51			123	6334.32	766.16	0.47
		TM	1.27	0.12	10.47	<0.01	1	2997.73	122	3336.59		
GLM 02	CT_{min}*	Intercept	-1.82	0.86	-2.13	0.04			122	2559.04	668.64	0.38
		LTL	0.68	0.08	8.70	<0.01	1	984.63	121	1574.41		
GLM 03	CT_{max}*	Intercept	3.75	3.04	1.24	0.22			90	4538.52	572.32	0.41
		UTL	0.92	0.12	7.83	<0.01	1	1851.18	89	2687.34		
GLM 04	FTN*	Intercept	16.49	2.29	7.21	<0.01			90	3258.40	583.98	0.06
		RTN	0.36	0.15	2.44	0.02	1	203.67	89	3054.73		
GLM 05	T_{opt}*	Intercept	-0.25	2.27	-0.11	0.91			123	6334.32	774.66	0.44
		TM*	1.29	0.13	9.71	<0.01	1	2760.78	122	3573.53		
GLM 06	CT_{min}*	Intercept	1.90	0.44	4.28	<0.01			122	2559.04	654.62	0.45
		LTL*	0.67	0.07	9.97	<0.01	1	1154.24	121	1404.80		
GLM 07	CT_{max}*	Intercept	-1.24	4.18	-0.30	0.77			90	4538.52	581.55	0.34
		UTL*	1.00	0.15	6.84	<0.01	1	1564.35	89	2974.17		
GLM 08	FTN*	Intercept	11.17	3.37	3.32	<0.01			90	3258.40	579.81	0.10
		RTN*	0.46	0.14	3.22	<0.01	1	340.55	89	2917.85		
GLM 09	T_{opt}	Intercept	1.77	2.26	0.78	0.43			156	8107.20	1005.20	0.34
		TM	1.07	0.12	8.97	<0.01	1	2768.60	155	5338.60		
GLM 10	CT_{min}	Intercept	1.55	1.68	0.93	0.36			69	2361.46	432.04	0.24
		LTL	0.56	0.12	4.59	<0.01	1	559.08	68	1802.38		
GLM 11	CT_{max}	Intercept	0.34	5.21	0.07	0.95			84	4387.27	553.93	0.28
		UTL	1.09	0.19	5.75	<0.01	1	1250.15	83	3137.11		
GLM 12	FTN	Intercept	23.13	2.51	9.23	<0.01			47	1145.94	293.94	0.01
		RTN	-0.12	0.16	-0.74	0.46	1	13.64	46	1132.30		
GLM 13	T_{opt}	Intercept	3.07	2.47	1.24	0.22			156	8107.20	1020.68	0.27
		TM*	1.06	0.14	7.63	<0.01	1	2215.37	155	5891.82		
GLM 14	CT_{min}	Intercept	3.18	1.10	2.88	0.01			69	2361.46	422.33	0.34
		LTL*	0.69	0.12	5.86	<0.01	1	792.49	68	1568.97		
GLM 15	CT_{max}	Intercept	-6.04	6.30	-0.96	0.34			84	4387.27	553.83	0.29
		UTL*	1.22	0.21	5.76	<0.01	1	1253.83	83	3133.44		
GLM 16	FTN	Intercept	17.75	3.68	4.82	<0.01			47	1145.94	293.49	0.02

RTN*	0.17	0.17	0.99	0.33	1	24.05	46	1121.89			

Supplementary Table 3.2. Summary statistics of the intercept and smooth terms in generalized additive models (*GAM*) models used to determine the effect of latitude (expressed as absolute latitude, *lat,°*) on the difference between physiology- and occurrence-based thermal traits (TT_p and TT_o, respectively), i.e. difference in optimal temperature (*DOT*), cold tolerance limit (*DCL*), heat tolerance limit (*DHL*), and thermal range (*DTR*)(see Supplementary Information SI1 for description). Highlighted in grey are reported in the main text. (Notes: *SD* = standard deviation; *t* = t value*; edf* = estimated degrees of freedom; *Ref df* = Reference degree of freedom; *Adj. R²* = coefficient of determination).

GAM ID	Variables		Intercept Term				Smooth Terms					Adj. R²	AIC	N
	Dependent	Independent	Estimate	SD	t	p-value	Coefficients	edf	Red df	F	p-value			
GAM 01	DOT_1	*abs(lat)*	3.27	0.42	7.82	<0.01	*s(abs(lat))*	6.67	7.65	7.13	<0.01	0.31	687.59	116.00
GAM 02	DCL_1	*abs(lat)*	-5.04	0.37	-13.77	<0.01	*s(abs(lat))*	1.00	1.00	0.07	0.79	-0.01	644.78	115.00
GAM 03	DHL_1	*abs(lat)*	1.62	0.48	3.36	<0.01	*s(abs(lat))*	6.61	7.66	5.62	<0.01	0.32	524.08	88.00
GAM 04	DTR_1	*abs(lat)*	6.69	0.60	11.18	<0.01	*s(abs(lat))*	7.01	8.00	3.92	<0.01	0.24	562.82	88.00
GAM 05	DOT_2	*abs(lat)*	4.50	0.44	10.27	<0.01	*s(abs(lat))*	6.64	7.62	6.68	<0.01	0.29	698.38	116.00
GAM 06	DCL_2	*abs(lat)*	0.30	0.34	0.86	0.39	*s(abs(lat))*	4.61	5.56	1.58	0.15	0.06	633.95	115.00
GAM 07	DHL_2	*abs(lat)*	-1.34	0.50	-2.68	0.01	*s(abs(lat))*	6.36	7.42	6.14	<0.01	0.34	530.83	88.00
GAM 08	DTR_2	*abs(lat)*	-1.64	0.55	-3.01	<0.01	*s(abs(lat))*	6.10	7.17	5.86	<0.01	0.31	545.76	88.00
GAM 09	DOT_3	*abs(lat)*	3.01	0.40	7.51	<0.01	*s(abs(lat))*	7.66	8.52	7.01	<0.01	0.27	955.41	156.00
GAM 10	DCL_3	*abs(lat)*	-3.99	0.58	-6.86	<0.01	*s(abs(lat))*	3.80	4.68	4.66	<0.01	0.23	426.99	70.00
GAM 11	DHL_3	*abs(lat)*	2.83	0.49	5.79	<0.01	*s(abs(lat))*	6.53	7.72	9.51	<0.01	0.46	506.26	85.00
GAM 12	DTR_3	*abs(lat)*	6.47	0.87	7.47	<0.01	*s(abs(lat))*	5.47	6.59	3.15	0.01	0.27	316.12	48.00
GAM 13	DOT_4	*abs(lat)*	4.13	0.41	10.07	<0.01	*s(abs(lat))*	7.65	8.52	8.18	<0.01	0.30	963.10	156.00
GAM 14	DCL_4	*abs(lat)*	0.67	0.53	1.28	0.21	*s(abs(lat))*	3.06	3.79	5.73	<0.01	0.23	412.36	70.00
GAM 15	DHL_4	*abs(lat)*	0.53	0.48	1.11	0.27	*s(abs(lat))*	6.77	7.92	10.26	<0.01	0.49	502.99	85.00
GAM 16	DTR_4	*abs(lat)*	-0.25	0.76	-0.34	0.74	*s(abs(lat))*	5.70	6.82	2.73	0.02	0.25	303.70	48.00

Supplementary Table 3.3. Summary statistics of the intercept and smooth terms in generalized additive models (*GAM*) models used to determine the effect of latitude (expressed as absolute latitudinal midpoint, *lat*, °) on the sensitivity to cold temperature (S_{min}) sensitivity to warm temperature (S_{max}), warming exposure (*WR*) and vulnerability (*V*) based on different climate scenarios (i.e. *RCP* 2.6, *RCP* 4.5, *RCP* 6.0, and *RCP* 8.5) (Supplementary Information SI1 for description). *GAM* 17 – 26 shows the fits of the data in *CTMI*-derived datasets, whilst *GAM* 27 – 36 shows the fits of data in published datasets. Highlighted in grey are reported in the main text. (Notes: *SD* = standard deviation; *t* = t value; *edf* = estimated degrees of freedom; *Ref df* = Reference degree of freedom; *Adj. R^2*= adjusted coefficient of determination).

GAM ID	Variables		Intercept Term				Smooth Terms					Adj. R^2	AIC	N
	Dependent	Independent	Estimate	SD	t	p-value	Coefficients	edf	Red df	F	p-value			
GAM 17	S_{min} *	abs(lat)	-4.40	0.35	-12.73	<0.01	s(abs(lat))	4.27	5.21	29.16	<0.01	0.50	878.96	152
GAM 18	S_{max}*	abs(lat)	4.67	0.48	9.81	<0.01	s(abs(lat))	7.41	8.33	6.34	<0.01	0.31	697.44	113
GAM 19	$WR_{2.6}$*	abs(lat)	0.01	<0.01	42.73	<0.01	s(abs(lat))	8.05	8.75	5.77	<0.01	0.22	-1355.13	154
GAM 20	$WR_{4.5}$*	abs(lat)	0.02	<0.01	78.66	<0.01	s(abs(lat))	7.28	8.24	19.67	<0.01	0.51	-1368.10	154
GAM 21	$WR_{6.0}$*	abs(lat)	0.02	<0.01	90.71	<0.01	s(abs(lat))	8.05	8.75	11.18	<0.01	0.38	-1352.33	154
GAM 22	$WR_{8.5}$*	abs(lat)	0.04	<0.01	89.58	<0.01	s(abs(lat))	7.55	8.44	14.10	<0.01	0.43	-1178.83	154
GAM 23	$V_{2.6}$*	abs(lat)	2.74	0.04	78.03	<0.01	s(abs(lat))	2.15	2.63	2.72	0.04	0.08	62.41	90
GAM 24	$V_{4.5}$*	abs(lat)	2.51	0.03	72.17	<0.01	s(abs(lat))	2.20	2.70	6.72	<0.01	0.16	62.33	91
GAM 25	$V_{6.0}$*	abs(lat)	2.42	0.04	68.16	<0.01	s(abs(lat))	2.17	2.66	9.44	<0.01	0.21	68.11	92
GAM 26	$V_{8.5}$*	abs(lat)	2.19	0.04	61.35	<0.01	s(abs(lat))	2.08	2.55	6.00	<0.01	0.14	68.53	92
GAM 27	S_{min}	abs(lat)	-5.22	0.30	-17.40	<0.01	s(abs(lat))	8.12	8.80	8.32	<0.01	0.36	655.57	123
GAM 28	S_{max}	abs(lat)	7.10	0.32	22.17	<0.01	s(abs(lat))	8.24	8.83	8.40	<0.01	0.31	866.40	153
GAM 29	$WR_{2.6}$	abs(lat)	0.01	<0.01	33.25	<0.01	s(abs(lat))	7.69	8.56	11.83	<0.01	0.24	-2430.31	311
GAM 30	$WR_{4.5}$	abs(lat)	0.02	<0.01	50.53	<0.01	s(abs(lat))	6.59	7.73	15.56	<0.01	0.29	-2365.08	311
GAM 31	$WR_{6.0}$	abs(lat)	0.02	<0.01	60.06	<0.01	s(abs(lat))	7.69	8.56	14.74	<0.01	0.29	-2307.54	311
GAM 32	$WR_{8.5}$	abs(lat)	0.03	<0.01	66.65	<0.01	s(abs(lat))	7.08	8.14	23.34	<0.01	0.38	-2020.13	311
GAM 33	$V_{2.6}$	abs(lat)	2.89	0.02	127.00	<0.01	s(abs(lat))	7.22	8.19	4.87	<0.01	0.20	43.28	143
GAM 34	$V_{4.5}$	abs(lat)	2.64	0.02	121.60	<0.01	s(abs(lat))	6.30	7.41	7.51	<0.01	0.27	30.17	144
GAM 35	$V_{6.0}$	abs(lat)	2.51	0.02	116.80	<0.01	s(abs(lat))	6.46	7.56	5.97	<0.01	0.23	27.83	144
GAM 36	$V_{8.5}$	abs(lat)	2.28	0.02	105.90	<0.01	s(abs(lat))	6.64	7.73	5.35	<0.01	0.21	28.94	144

Supplementary Table 3.4. Summary of the generalised linear models (GLM) for testing the main and interactive effects of thermal affinity (*TA*) and thermal specialisation (*TS*) on the difference between physiology- and occurrence-based thermal traits (TT_p – TT_o) (i.e. difference in optimal temperature (*DOT*), cold tolerance limit (*DCL*), heat tolerance limit (*DHL*), and thermal range (*DTR*); see Supplementary Information SI1 for description). Highlighted in grey are reported in the main text. (Notes: *SE* = standard error; *t* = t value*; df* = degrees of freedom; *AIC* = Akaike information criteria; *Adj. R^2* = coefficient of determination).

Model ID	Dependent Variables	Coefficients					Null		Residual		AIC	Adj. R^2
		Terms	Estimate	SE	t	p	df	Deviance	df	Deviance		
GLM 17	DOT_1	Intercept	3.10	0.42	7.31	<0.01			90	2305.04	502.35	0.48
		TA	-8.75	1.04	-8.38	<0.01	1	1097.86	89	1207.18		
		TS	-0.46	0.65	-0.72	0.48	1	11.04	88	1196.13		
		TA:TS	-0.49	0.91	-0.54	0.59	1	4.04	87	1192.09		
GLM 18	DCL_1	Intercept	-4.19	0.36	-11.69	<0.01			90	1315.66	471.80	0.35
		TA	-3.73	0.88	-4.22	<0.01	1	71.01	89	1244.65		
		TS	3.45	0.55	6.31	<0.01	1	377.85	88	866.79		
		TA:TS	-0.94	0.77	-1.22	0.22	1	14.68	87	852.12		
GLM 19	DHL_1	Intercept	2.35	0.36	6.50	<0.01			90	2701.35	473.14	0.68
		TA	-7.82	0.89	-8.79	<0.01	1	1239.46	89	1461.89		
		TS	-3.43	0.55	-6.23	<0.01	1	522.31	88	939.58		
		TA:TS	-2.13	0.77	-2.74	0.01	1	74.82	87	864.76		
GLM 20	DTR_1	Intercept	6.54	0.42	15.45	<0.01			90	3719.62	501.99	0.68
		TA	-4.10	1.04	-3.93	<0.01	1	718.47	89	3001.15		
		TS	-6.89	0.65	-10.68	<0.01	1	1791.39	88	1209.76		
		TA:TS	-1.16	0.91	-1.28	0.20	1	22.39	87	1187.37		
GLM 21	DOT_2	Intercept	4.49	0.42	10.67	<0.01			90	2555.14	500.89	0.54
		TA	-9.76	1.04	-9.42	<0.01	1	1361.57	89	1193.56		
		TS	-0.45	0.64	-0.70	0.48	1	12.22	88	1181.35		
		TA:TS	-0.71	0.90	-0.79	0.43	1	8.33	87	1173.02		
GLM 22	DCL_2	Intercept	1.41	0.32	4.38	<0.01			90	1227.46	452.83	0.44
		TA	-5.32	0.80	-6.69	<0.01	1	225.92	89	1001.54		
		TS	3.07	0.49	6.24	<0.01	1	282.76	88	718.78		
		TA:TS	-1.28	0.69	-1.84	0.07	1	27.00	87	691.78		
GLM 23	DHL_2	Intercept	-0.47	0.42	-1.12	0.26			90	2974.18	499.91	0.61
		TA	-8.25	1.03	-8.01	<0.01	1	1307.85	89	1666.33		
		TS	-3.03	0.64	-4.76	<0.01	1	424.34	88	1241.99		
		TA:TS	-2.22	0.90	-2.47	0.02	1	81.44	87	1160.55		
GLM 24	DTR_2	Intercept	-1.88	0.48	-3.91	<0.01			90	3401.70	525.50	0.55
		TA	-2.94	1.19	-2.48	0.01	1	449.31	89	2952.39		

		TS	-6.12	0.73	-8.33	<0.01	1	1401.20	88	1551.18		
		TA:TS	-0.92	1.03	-0.89	0.38	1	13.91	87	1537.27		
GLM 25	*DOT$_3$*	*Intercept*	4.54	0.32	14.30	<0.01			47	1064.80	207.85	0.84
		TA	-14.34	1.14	-12.60	<0.01	1	842.59	46	222.21		
		TS	-2.09	0.59	-3.52	<0.01	1	17.63	45	204.58		
		TA:TS	3.57	1.27	2.82	0.01	1	31.25	44	173.34		
GLM 26	*DCL$_3$*	*Intercept*	-1.70	0.55	-3.09	<0.01			47	1295.05	260.49	0.60
		TA	-3.27	1.97	-1.66	0.10	1	176.99	46	1118.06		
		TS	5.73	1.03	5.58	<0.01	1	568.46	45	549.60		
		TA:TS	-3.54	2.19	-1.61	0.11	1	30.64	44	518.96		
GLM 27	*DHL$_3$*	*Intercept*	3.57	0.41	8.75	<0.01			47	1261.23	231.93	0.77
		TA	-8.27	1.46	-5.66	<0.01	1	572.42	46	688.81		
		TS	-2.54	0.76	-3.33	<0.01	1	381.17	45	307.64		
		TA:TS	-2.96	1.63	-1.81	0.08	1	21.41	44	286.23		
GLM 28	*DTR$_3$*	*Intercept*	5.27	0.43	12.13	<0.01			47	2317.28	237.91	0.86
		TA	-4.99	1.56	-3.21	<0.01	1	112.87	46	2204.41		
		TS	-8.26	0.81	-10.17	<0.01	1	1879.38	45	325.03		
		TA:TS	0.57	1.73	0.33	0.75	1	0.79	44	324.24		
GLM 29	*DOT$_4$*	*Intercept*	5.67	0.26	21.68	<0.01			47	1144.59	189.12	0.90
		TA	-15.26	0.94	-16.31	<0.01	1	918.99	46	225.60		
		TS	-3.03	0.49	-6.21	<0.01	1	65.66	45	159.94		
		TA:TS	4.17	1.04	4.00	<0.01	1	42.60	44	117.34		
GLM 30	*DCL$_4$*	*Intercept*	2.85	0.50	5.64	<0.01			47	1045.78	252.27	0.58
		TA	-5.97	1.81	-3.31	<0.01	1	317.83	46	727.95		
		TS	3.93	0.94	4.17	<0.01	1	278.05	45	449.90		
		TA:TS	-2.27	2.01	-1.13	0.27	1	12.62	44	437.28		
GLM 31	*DHL$_4$*	*Intercept*	1.29	0.39	3.34	<0.01			47	1168.16	226.35	0.78
		TA	-7.42	1.38	-5.38	<0.01	1	483.68	46	684.48		
		TS	-2.64	0.72	-3.66	<0.01	1	407.14	45	277.34		
		TA:TS	-3.03	1.54	-1.97	0.05	1	22.54	44	254.81		
GLM 32	*DTR$_4$*	*Intercept*	-1.56	0.45	-3.44	<0.01			47	1727.09	241.83	0.80
		TA	-1.46	1.62	-0.90	0.37	1	17.51	46	1709.57		
		TS	-6.56	0.85	-7.76	<0.01	1	1356.33	45	353.24		
		TA:TS	-0.75	1.81	-0.42	0.68	1	1.39	44	351.85		

Supplementary Table 3.5. Summary of the generalised linear models (GLM) for testing the main and interactive effects of thermal affinity (*TA*) and thermal specialisation (*TS*) on the sensitivity to cold temperature (S_{min}), sensitivity to warm temperature (S_{max}), warming exposure (*WR*) and vulnerability (V) based on different climate scenarios (i.e. *RCP* 2.6, *RCP* 4.5, *RCP* 6.0, and *RCP* 8.5) (Supplementary Information SI1 for description). GLM 33 – 42 shows the fits of the data in *CTMI*-derived datasets. GLM 43 – 52 shows the fits of the data in published dataset. Highlighted in grey are reported in the main text. (Notes: *SE* = standard error; *t* = t value; *df* = degrees of freedom; *AIC* = Akaike information criteria; *Adj. R²* = coefficient of determination).

Model ID	Dependent Variables	Terms	Coefficients Estimate	SE	t	p	Null df	Null Deviance	Residual df	Residual Deviance	AIC	Adj. R²
GLM 33	S_{min} *	Intercept	-4.41	0.71	-6.14	<0.01			85	3315.74	560.14	0.09
		TA	1.21	1.77	0.69	0.49	1	61.64	84	3254.10		
		TS	2.74	1.10	2.49	0.01	1	224.18	83	3029.92		
		TA:TS	-0.75	1.57	-0.48	0.63	1	8.48	82	3021.44		
GLM 34	S_{max}*	Intercept	4.33	0.73	5.94	<0.01			85	3373.47	562.82	0.08
		TA	-4.61	1.79	-2.57	0.01	1	252.17	84	3121.30		
		TS	0.18	1.12	0.16	0.87	1	2.38	83	3118.91		
		TA:TS	0.36	1.59	0.23	0.82	1	1.96	82	3116.95		
GLM 35	$WR_{2.6}$*	Intercept	0.01	<0.01	23.54	<0.01			85	<0.01	-714.61	0.06
		TA	1.17 x 10^{-04}	<0.01	0.11	0.91	1	<0.01	84	<0.01		
		TS	7.11 x 10^{-04}	<0.01	1.07	0.29	1	<0.01	83	<0.01		
		TA:TS	-2.21 x 10^{-03}	<0.01	-2.33	0.02	1	<0.01	82	<0.01		
GLM 36	$WR_{4.5}$*	Intercept	0.02	<0.01	36.06	<0.01			85	<0.01	-685.48	0.04
		TA	-1.83 x 10^{-04}	<0.01	-0.14	0.89	1	<0.01	84	<0.01		
		TS	1.16 x 10^{-03}	<0.01	1.48	0.14	1	<0.01	83	<0.01		
		TA:TS	-1.89 x 10^{-03}	<0.01	-1.68	0.10	1	<0.01	82	<0.01		
GLM 37	$WR_{6.0}$*	Intercept	0.02	<0.01	44.32	<0.01			85	<0.01	-692.17	0.06
		TA	5.27 x 10^{-04}	<0.01	0.43	0.67	1	<0.01	84	<0.01		
		TS	6.05 x 10^{-04}	<0.01	0.80	0.43	1	<0.01	83	<0.01		
		TA:TS	-2.38 x 10^{-03}	<0.01	-2.20	0.03	1	<0.01	82	<0.01		
GLM 38	$WR_{8.5}$*	Intercept	0.04	<0.01	44.94	<0.01			85	<0.01	-601.26	0.02
		TA	9.08 x 10^{-04}	<0.01	0.44	0.66	1	<0.01	84	<0.01		
		TS	1.23 x 10^{-03}	<0.01	0.96	0.34	1	<0.01	83	<0.01		
		TA:TS	-2.12 x 10^{-03}	<0.01	-1.16	0.25	1	<0.01	82	<0.01		
GLM 39	$V_{2.6}$*	Intercept	2.70	0.04	64.97	<0.01			63	7.59	38.74	0.23
		TA	-0.55	0.15	-3.67	<0.01	1	0.67	62	6.92		
		TS	-0.08	0.06	-1.36	0.18	1	0.32	61	6.61		
		TA:TS	-0.39	0.14	-2.74	<0.01	1	0.74	60	5.87		
GLM 40	$V_{4.5}$*	Intercept	2.44	0.05	51.39	<0.01			64	8.08	57.27	0.03

		TA	-0.06	0.12	-0.49	0.63	1	0.04	63	8.04		
		TS	-0.06	0.07	-0.98	0.33	1	0.07	62	7.97		
		TA:TS	0.08	0.09	0.84	0.40	1	0.09	61	7.87		
GLM 41	$V_{6.0}$*	Intercept	2.38	0.05	44.55	<0.01			65	10.70	75.38	0.03
		TA	-0.15	0.14	-1.11	0.27	1	0.22	64	10.49		
		TS	-0.03	0.08	-0.44	0.66	1	0.01	63	10.48		
		TA:TS	0.07	0.11	0.65	0.52	1	0.07	62	10.41		
GLM 42	$V_{8.5}$*	Intercept	2.15	0.05	42.74	<0.01			65	9.47	67.11	0.03
		TA	-0.16	0.13	-1.20	0.24	1	0.25	64	9.23		
		TS	-0.04	0.07	-0.56	0.58	1	0.04	63	9.19		
		TA:TS	0.03	0.10	0.25	0.80	1	0.01	62	9.18		
GLM 43	S_{min}	Intercept	-5.57	0.82	-6.78	<0.01			46	1263.17	292.37	0.11
		TA	6.38	2.94	2.17	0.04	1	94.51	45	1168.65		
		TS	2.11	1.53	1.38	0.17	1	15.95	44	1152.70		
		TA:TS	-3.71	3.27	-1.14	0.26	1	33.57	43	1119.13		
GLM 44	S_{max}	Intercept	7.52	0.65	11.55	<0.01			46	818.36	270.48	0.14
		TA	-6.10	2.33	-2.62	0.01	1	74.75	45	743.61		
		TS	-1.75	1.21	-1.44	0.16	1	2.18	44	741.43		
		TA:TS	4.01	2.59	1.55	0.13	1	39.11	43	702.31		
GLM 45	$WR_{2.6}$	Intercept	0.01	<0.01	19.16	<0.01			46	<0.01	-416.15	0.25
		TA	2.09×10^{-03}	<0.01	1.34	0.19	1	<0.01	45	<0.01		
		TS	1.81×10^{-03}	<0.01	2.22	0.03	1	<0.01	44	<0.01		
		TA:TS	-0.01	<0.01	-3.45	<0.01	1	<0.01	43	<0.01		
GLM 46	$WR_{4.5}$	Intercept	0.02	<0.01	32.78	<0.01			46	<0.01	-410.38	0.20
		TA	7.03×10^{-04}	<0.01	0.42	0.67	1	<0.01	45	<0.01		
		TS	9.68×10^{-04}	<0.01	1.12	0.27	1	<0.01	44	<0.01		
		TA:TS	-4.54×10^{-03}	<0.01	-2.45	0.02	1	<0.01	43	<0.01		
GLM 47	$WR_{6.0}$	Intercept	0.02	<0.01	40.46	<0.01			46	<0.01	-404.58	0.29
		TA	1.08×10^{-03}	<0.01	0.61	0.54	1	<0.01	45	<0.01		
		TS	1.50×10^{-03}	<0.01	1.63	0.11	1	<0.01	44	<0.01		
		TA:TS	-0.01	<0.01	-3.24	<0.01	1	<0.01	43	<0.01		
GLM 48	$WR_{8.5}$	Intercept	0.03	<0.01	44.33	<0.01			46	<0.01	-364.70	0.16
		TA	2.27×10^{-03}	<0.01	0.84	0.41	1	<0.01	45	<0.01		
		TS	1.68×10^{-03}	<0.01	1.19	0.24	1	<0.01	44	<0.01		
		TA:TS	-0.01	<0.01	-2.38	0.02	1	<0.01	43	<0.01		
GLM 49	$V_{2.6}$	Intercept	2.90	0.04	69.30	<0.01			43	2.67	6.33	0.11

		TA	-0.29	0.15	-1.93	0.06	1	0.09	42	2.58	
		TS	-0.17	0.09	-1.82	0.08	1	0.13	41	2.46	
		TA:TS	0.41	0.34	1.22	0.23	1	0.09	40	2.37	
GLM 50	$V_{4.5}$	*Intercept*	2.63	0.04	65.62	<0.01			44	2.85	7.59	0.12
		TA	-0.20	0.15	-1.30	0.20	1	0.02	43	2.83	
		TS	-0.14	0.08	-1.85	0.07	1	<0.01	42	2.83	
		TA:TS	0.38	0.16	2.35	0.02	1	0.34	41	2.50	
GLM 51	$V_{6.0}$	*Intercept*	2.51	0.04	61.75	<0.01			44	2.96	8.77	0.13
		TA	-0.23	0.16	-1.48	0.15	1	0.01	43	2.95	
		TS	-0.16	0.08	-2.03	0.05	1	<0.01	42	2.95	
		TA:TS	0.41	0.17	2.48	0.02	1	0.38	41	2.56	
GLM 52	$V_{8.5}$	*Intercept*	2.28	0.04	55.09	<0.01			44	2.90	10.54	0.08
		TA	-0.23	0.16	-1.45	0.15	1	<0.01	43	2.90	
		TS	-0.14	0.08	-1.71	0.09	1	0.01	42	2.89	
		TA:TS	0.31	0.17	1.85	0.07	1	0.22	41	2.67	

Supplementary Table 3.6. Phylogenetic signal of the thermal traits estimated from physiology data (TT_p) and occurrence data (TT_o), their difference ($TT_p - TT_o$), thermal sensitivity (S_{min} and S_{max}), warming exposure (WR), and warming vulnerability (V) in marine phytoplankton measured using three approaches: (1) variance component analysis, (2), autocorrelation (i.e. Moran's I index and Abouheif's C_{mean} index), and (3) Brownian motion model of evolution (i.e. Blomberg's K and K^* and Pagel's λ). Highlighted in grey are reported in the main text. Indices in bold face indicates significance at 95% confidence interval.

Thermal traits and their descriptions	Symbols	Variance component analysis (% variation explained)						Autocorrelation		Brownian motion model of evolution		
		Species	Genus	Family	Order	Class	Phylum	Moran's I	Abouheif's C_{mean}	Blomberg's K	Blomberg's K^*	Pagel's λ
Physiology-based thermal traits (TT_p) obtained from $CTMI$* model and published literature	T_{opt}*	**31.21**	**48.48**	**2.89**	**<0.01**	**17.42**	**<0.01**	**0.05**	**0.21**	0.05	0.08	0.14
	CT_{min}*	**28.01**	**7.54**	**7.38**	**<0.01**	**<0.01**	**57.08**	**0.06**	**0.36**	**0.12**	**0.12**	**0.59**
	CT_{max}*	**46.81**	**40.28**	**<0.01**	**<0.01**	**12.90**	**<0.01**	0.00	0.06	0.05	0.07	<0.01
	FTN*	**53.05**	**27.38**	**<0.01**	**<0.01**	**19.57**	**<0.01**	0.01	0.12	0.06	0.07	0.25
	T_{opt}	**63.19**	**24.17**	**<0.01**	**<0.01**	**12.64**	**<0.01**	0.04	0.12	0.02	0.03	<0.01
	CT_{min}	**24.12**	**22.54**	**12.71**	**<0.01**	**2.51**	**38.12**	**0.19**	**0.34**	**0.11**	**0.15**	**0.45**
	CT_{max}	**30.29**	**37.34**	**19.95**	**<0.01**	**12.42**	**<0.01**	**0.11**	**0.25**	0.06	0.10	<0.01
	FTN	**34.58**	**<0.01**	**10.47**	**9.15**	**33.56**	**12.23**	**0.27**	**0.46**	**0.16**	**0.21**	**0.81**
Occurrence-based thermal traits (TT_o) derived from annual average and seasonal extreme* SST	TM	**76.07**	**6.91**	**<0.01**	**<0.01**	**10.29**	**6.72**	**0.14**	**0.27**	0.03	0.05	**0.27**
	LTL	**75.88**	**9.58**	**1.87**	**1.43**	**1.38**	**9.86**	**0.11**	**0.26**	**0.03**	**0.06**	**0.34**
	UTL	**78.11**	**3.53**	**<0.01**	**<0.01**	**17.25**	**1.12**	**0.10**	**0.19**	0.02	0.04	**0.20**
	RTN	**88.48**	**6.41**	**0.42**	**4.69**	**<0.01**	**<0.01**	0.00	**0.07**	0.02	0.04	<0.01
	TM*	**75.87**	**8.31**	**<0.01**	**<0.01**	**4.08**	**11.73**	**0.14**	**0.28**	**0.03**	0.05	**0.27**
	LTL*	**67.82**	**11.86**	**5.21**	**0.42**	**2.46**	**12.24**	**0.11**	**0.27**	**0.04**	**0.08**	**0.69**
	UTL*	**82.74**	**3.65**	**<0.01**	**<0.01**	**7.46**	**6.16**	**0.09**	**0.18**	0.02	0.04	**0.15**
	RTN*	**80.04**	**9.81**	**3.28**	**<0.01**	**6.00**	**0.87**	**0.01**	**0.11**	0.03	0.05	0.24
Difference in physiology and occurrence-based thermal traits ($TT_p - TT_o$) estimated from four sets of datasets: (1) TT_p* and TT_o, (2) TT_p* and TT_o*, (3) TT_p and TT_o, and (4) TT_p and TT_o*, specifically to compute for the difference in	DOT_1	37.10	29.01	8.32	25.57	<0.01	<0.01	0.00	0.10	0.06	0.10	<0.01
	DCL_1	56.54	40.37	<0.01	<0.01	3.09	<0.01	-0.05	-0.04	0.04	0.07	<0.01
	DHL_1	31.40	<0.01	30.10	15.36	23.14	<0.01	-0.03	0.04	0.07	0.13	<0.01
	DTR_1	39.86	15.55	8.04	21.14	15.40	<0.01	-0.03	0.05	0.06	0.10	<0.01
	DOT_2	44.35	19.69	26.71	2.33	6.92	<0.01	0.01	0.11	0.06	0.10	<0.01
	DCL_2	61.49	33.13	<0.01	<0.01	5.38	<0.01	-0.04	-0.03	0.04	0.07	<0.01
	DHL_2	52.03	0.38	41.21	<0.01	1.54	4.84	-0.03	0.04	0.06	0.09	<0.01
	DTR_2	62.64	19.27	18.09	<0.01	<0.01	<0.01	-0.05	-0.01	0.04	0.07	<0.01
	DOT_3	70.13	3.26	<0.01	26.61	<0.01	<0.01	**0.04**	**0.15**	0.03	0.06	<0.01
	DCL_3	46.09	5.81	<0.01	2.92	45.18	<0.01	**0.07**	**0.28**	0.07	0.13	<0.01
	DHL_3	28.30	<0.01	16.09	55.62	<0.01	<0.01	0.04	0.08	0.05	0.10	<0.01
	DTR_3	25.15	<0.01	6.95	31.62	36.28	<0.01	**0.14**	**0.26**	0.10	0.16	0.57

optimal temperature (*DOT*), cold tolerance limit (*DCL*), heat tolerance limit (*DHL*), and thermal range (*DTR*)	DOT_4	**65.61**	**4.83**	**<0.01**	**29.56**	**<0.01**	**<0.01**	**0.04**	**0.15**	0.04	0.07	<0.01
	DCL_4	**49.11**	**<0.01**	**<0.01**	**6.78**	**44.11**	**<0.01**	0.01	**0.17**	0.07	0.12	<0.01
	DHL_4	**32.60**	**<0.01**	**25.43**	**41.97**	**<0.01**	**<0.01**	0.02	0.05	0.05	0.09	<0.01
												<0.01
	DTR_4	**31.62**	**6.91**	**2.86**	**38.29**	**20.31**	**<0.01**	**0.06**	0.16	0.08	0.12	
Sensitivity to cold and warm temperature estimated from *CTMI*-derived* and published datasets	$S_{min}*$	**46.25**	**29.52**	**<0.01**	**24.23**	**<0.01**	**<0.01**	-0.03	-0.01	0.05	0.08	<0.01
	S_{min}	**53.80**	**41.35**	**4.85**	**<0.01**	**<0.01**	**<0.01**	**0.12**	**0.28**	0.08	**0.13**	0.55
	$S_{max}*$	**56.07**	**0.49**	**<0.01**	**2.56**	**0.80**	**40.08**	-0.05	-0.05	0.03	0.04	<0.01
												<0.01
	S_{max}	**53.10**	**29.64**	**2.84**	**<0.01**	**<0.01**	**14.43**	0.00	**0.10**	0.04	0.08	
Warming exposure based on different climate scenarios (i.e. *RCP* 2.6, *RCP* 4.5, *RCP* 6.0, and *RCP* 8.5) estimated from *CTMI*-derived* and published datasets	$WR_{2.6}*$	**54.27**	**7.30**	**<0.01**	**38.43**	**<0.01**	**<0.01**	-0.02	-0.04	**0.12**	**0.17**	<0.01
	$WR_{4.5}*$	**53.52**	**<0.01**	**13.70**	**32.78**	**<0.01**	**<0.01**	-0.04	0.00	0.05	0.08	<0.01
	$WR_{6.0}*$	**74.07**	**19.23**	**6.70**	**<0.01**	**<0.01**	**<0.01**	-0.05	-0.10	0.04	0.07	<0.01
	$WR_{8.5}*$	**75.00**	**25.00**	**<0.01**	**<0.01**	**<0.01**	**<0.01**	-0.08	-0.13	0.02	0.04	<0.01
	$WR_{2.6}$	**94.84**	**<0.01**	**<0.01**	**0.16**	**4.99**	**<0.01**	0.01	0.05	0.02	0.04	<0.01
	$WR_{4.5}$	**93.48**	**5.39**	**<0.01**	**1.13**	**<0.01**	**<0.01**	0.00	-0.07	0.02	0.03	<0.01
	$WR_{6.0}$	**89.55**	**10.45**	**<0.01**	**<0.01**	**<0.01**	**<0.01**	0.00	0.00	0.01	0.03	<0.01
	$WR_{8.5}$	**94.79**	**5.21**	**<0.01**	**<0.01**	**<0.01**	**<0.01**	0.00	-0.01	0.01	0.02	<0.01
Warming vulnerability based on different climate scenarios (i.e. *RCP* 2.6, *RCP* 4.5, *RCP* 6.0, and *RCP* 8.5) estimated from *CTMI*-derived* and published datasets	$V_{2.6}*$	**7.91**	**15.67**	**<0.01**	**69.37**	**<0.01**	**7.05**	-0.02	-0.01	0.12	0.19	0.94
	$V_{4.5}*$	**67.56**	**32.44**	**<0.01**	**<0.01**	**<0.01**	**<0.01**	-0.03	-0.05	0.08	0.14	<0.01
	$V_{6.0}*$	**76.15**	**14.40**	**2.22**	**<0.01**	**<0.01**	**7.23**	-0.01	0.00	0.07	0.11	<0.01
	$V_{8.5}*$	**62.29**	**32.93**	**4.78**	**<0.01**	**<0.01**	**<0.01**	-0.04	-0.05	0.03	0.05	<0.01
	$V_{2.6}$	**34.46**	**<0.01**	**0.39**	**12.45**	**52.71**	**<0.01**	0.00	-0.06	0.13	**0.23**	0.97
	$V_{4.5}$	**11.35**	**8.28**	**1.54**	**0.17**	**76.35**	**2.30**	-0.01	-0.03	0.06	0.12	0.79
	$V_{6.0}$	**4.78**	**2.64**	**0.77**	**<0.01**	**91.82**	**<0.01**	-0.01	-0.06	0.11	0.20	**0.96**
	$V_{8.5}$	**0.06**	**0.04**	**0.01**	**<0.01**	**99.90**	NA	-0.01	-0.02	0.51	0.90	**1.00**

Supplementary Table 5.1. Cellular content of okadaic acid (*OA*), dinophysistoxins (*DTX1* and *DTX2*) in *Prorocentrum lima* found in various studies. Highlighted in grey are the cellular toxin content for *Prorocentrum lima* CCAP 1136/11 strain observed in this present study. Asterisk (*) indicate that the information is not available/acquired.

Isolation location	Strain (Notes)	Temperature	Cellular toxin content (pg cell^{-1})			Reference
			OA	DTX1	DTX2	
Adriatic Sea Goro, Italy	*	*	6.69 - 15.8	0.12 - 0.39	*	(Vanucci et al., 2010)
Bizerte Bay Tunisia	PLBZT14	25	7.13 - 28.33	2.23 - 7.4	*	(Ben-Gharbia et al., 2016)
Dry Tortugas Florida, USA	*	26	7.5 - 14.2	*	*	(Tomas and Baden, 1993)
Fleet Lagoon Dorset, UK	*	*	2.05 - 10.99	0.82 - 5.32	*	(Aquino-Cruz, 2012)
Fleet Lagoon Dorset, UK	*	*	0.1 - 1.8	0.2 - 6.3	*	(Foden et al., 2005)
Fleet Lagoon Dorset, UK	(20 strains)	15,17	0.42 - 17.13	0.41 - 11.29	*	(Nascimento et al., 2005)
Marseille France	MARS1	20	1.9	0.8	*	(Barbier et al., 1999)
Heron Island Australia	*	*	1.31 - 5.88	4 - 12	*	(Morton and Tindall, 1995)
Lagoon of Goro Adriatic Sea, Italy	*	20	6.69 - 15.8	0.12 - 0.39	*	(Vanucci et al., 2010)
Lisbon Bay Portugal	IO66-01	19	8.8 - 41	2.5 - 12	*	(Vale et al., 2009)
Mahone Bay Nova Scotia, Canada	*	18	0.37 - 6.6	0.04 - 2.6	*	(Pan et al., 1999)
NW Havana City Cuba	(cultured cells)	22	*	7.15	*	(Delgado et al., 2005)
NW Havana City Cuba	(natural cells)	22	*	4.2	*	(Delgado et al., 2005)
Okinawa Japan	*	*	26	13	*	(Lee et al., 1989)
Pontevedra and Ria de Vigo, Spain	(19 strains)	19	0.19 - 12.87	0 - 12.45	0 - 1.14	(Bravo et al., 2001)
Rangaunu Harbour	*	*	90 - 108	*	*	(MacKenzie et al., 2011)

New Zealand

Ria de Vigo Spain	CCAP1136/11 (Day 1 - 15)	20	0.1 - 1.25	*	*	(Varkitzi et al., 2010)
Ria de Vigo Spain	CCAP1136/11 (Day 34)	20	11.27	*	*	(Varkitzi et al., 2010)
Ria de Vigo Spain	PL2V	20	14.3	2.1	*	(Barbier et al., 1999)
Ria de Vigo Spain	(5 strains)	*	5 - 24.5	6 - 14.3	*	(Lee et al., 1989)
Ria de Vigo Spain	CCAP1136/11 (TB1)	5	89.9 ± 21.5 (61.05 - 131.93)	7.26 ± 2.08 (4.25 - 11.26)	0.066 ± 0.0084 (0.055 - 0.082)	This study
Ria de Vigo Spain	CCAP1136/11 (TB1)	10	26.78 ± 8.51 (10.63 - 39.49)	2 ± 0.4 (1.21 - 2.56)	0.017 ± 0.0016 (0.014 - 0.019)	This study
Ria de Vigo Spain	CCAP1136/11 (TB1)	15	9.14 ± 2.48 (2.46 - 17.39)	0.83 ± 0.25 (0.32 - 1.63)	0.0053 ± 0.0009 (0.0031 -0.0092)	This study
Ria de Vigo Spain	CCAP1136/11 (TB1)	20	4.96 ± 1.81 (1.86 - 8.11)	0.49 ± 0.17 (0.25 - 0.8)	0.0052 ± 0.0016 (0.0024 - 0.008)	This study
Ria de Vigo Spain	CCAP1136/11 (TB1)	25	17.81 ± 0.93 (16.14 - 19.34)	1.79 ± 0.09 (1.66 - 1.97)	0.0068 ± 0.0007 (0.0057 -0.0082)	This study
Ria de Vigo Spain	CCAP1136/11 (TB2)	10	7.07 ± 1.4 (5.18 - 9.8)	1.06 ± 0.2 (0.84 - 1.45)	0.16 ± 0.15 (0.0071 -0.4532)	This study
Ria de Vigo Spain	CCAP1136/11 (TB2)	15	6.25 ± 1.56 (3.2 - 8.34)	0.78 ± 0.17 (0.43 - 0.97)	0.0058 ± 0.0014 (0.0029 -0.0073)	This study
Ria de Vigo Spain	CCAP1136/11 (TB2)	20	9.71 ± 0.87 (8.07 - 11.02)	1.28 ± 0.07 (1.19 - 1.41)	0.0053 ± 0.001 (0.0035 -0.0071)	This study
Ria de Vigo Spain	CCAP1136/11 (TB2)	25	3.95 ± 0.24 (3.48 - 4.28)	0.57 ± 0.04 (0.5 - 0.65)	0.0031 ± 0.0005 (0.0023 -0.0039)	This study
Sanriku Japan	*	*	0.3 - 1.3	*	*	(Koike et al., 1998)
Virgin Islands US	*	*	2.33 - 7.06	4.47 - 12.47	*	(Morton and Tindall, 1995)

Supplementary Table 6.1. Accuracy of the deep learning models used to classify species in pairwise mixed-species cultures. This metrics was used as inclusion criteria for the succeeding data analysis. Pairs with average model accuracy of <0.80 (highlighted in grey) were included in the dataset used to determine the effect of warming on growth and competition in non-toxic and potentially toxic dinoflagellates.

Pairs	Pairwise combinations		Model Accuracy				
	Species 1	Species 2	15 °C	20 °C	25 °C	Mean	SE
P1	*Prorocentrum* sp.	*Prorocentrum micans*	0.5095	0.5246	0.5625	0.5322	0.0158
P2	*Prorocentrum* sp.	*Alexandrium tamutum*	0.9498	0.9437	0.8082	0.9005	0.0462
P3	*Prorocentrum micans*	*Alexandrium tamutum*	0.9485	0.9382	0.7821	0.8896	0.0538
P4	*Prorocentrum* sp.	*Prorocentrum minimum*	0.8647	0.8562	0.7775	0.8328	0.0278
P5	*Prorocentrum* sp.	*Prorocentrum lima*	1.0000	1.0000	1.0000	1.0000	0.0000
P6	*Prorocentrum* sp.	*Alexandrium minutum*	0.9872	0.9811	0.9759	0.9814	0.0033
P7	*Prorocentrum micans*	*Prorocentrum minimum*	0.8701	0.8445	0.7401	0.8182	0.0398
P8	*Prorocentrum micans*	*Prorocentrum lima*	0.9969	0.9987	0.9977	0.9978	0.0005
P9	*Prorocentrum micans*	*Alexandrium minutum*	0.9847	0.9787	0.9576	0.9737	0.0082
P10	*Alexandrium tamutum*	*Prorocentrum minimum*	0.6929	0.6680	0.6164	0.6591	0.0225
P11	*Alexandrium tamutum*	*Prorocentrum lima*	0.9897	0.9944	0.9947	0.9929	0.0016
P12	*Alexandrium tamutum*	*Alexandrium minutum*	0.5255	0.5784	0.7362	0.6134	0.0633
P13	*Prorocentrum minimum*	*Prorocentrum lima*	0.9941	0.9947	0.9953	0.9947	0.0004
P14	*Prorocentrum minimum*	*Alexandrium minutum*	0.7598	0.7295	0.8090	0.7661	0.0232
P15	*Prorocentrum lima*	*Alexandrium minutum*	0.9908	0.9951	0.9915	0.9925	0.0013

Supplementary Table 6.2. Description of analysis of variance (ANOVA) implemented in this present study. Results of the ANOVA and post hoc Tukey tests are tabulated and plotted, respectively. Asterisk (*) indicates the results of analysis using the filtered datasets.

ANOVA	Description	Model	Data separation	ANOVA summary	Post hoc Tukey test
1	Effect of temperature on growth rate of six different species of dinoflagellates	Growth rate in monocultures ~ Temperature	Focal species	Supplementary Table 5.3	Supplementary Figure 5.8
2	Effect of temperature on growth rate of two different genera of dinoflagellates	Growth rate in monocultures ~ Temperature	Focal genus	Supplementary Table 5.3	Supplementary Figure 5.8
3	Effect of temperature on growth rate of non-toxic and potentially toxic dinoflagellates	Growth rate in monocultures ~ Temperature	Focal toxicity	Supplementary Table 5.3	Supplementary Figure 5.8
4	Species specificity of growth in different temperature treatments	Growth rate in monocultures ~ Focal species	Temperature	Supplementary Table 5.3	Supplementary Figure 5.8
5	Variation in growth between two different genera of dinoflagellates in different temperature treatments	Growth rate in monocultures ~ Focal genus	Temperature	Supplementary Table 5.3	Supplementary Figure 5.8
6	Variation in growth between non-toxic and potentially toxic dinoflagellates in different temperature treatments	Growth rate in monocultures ~ Focal toxicity	Temperature	Supplementary Table 5.3	Supplementary Figure 5.8
7	Effect of temperature and competitors on growth rate of six different species of dinoflagellates	Growth rate in co-cultures ~ Temperature x Competitor species	Focal species	Supplementary Table 5.4* Supplementary Table 5.6	Supplementary Figure 5.9* Supplementary Figure 5.11
8	Effect of temperature and competitors on growth rate of two different genera of dinoflagellates	Growth rate in co-cultures ~ Temperature x Competitor species	Focal genus	Supplementary Table 5.4* Supplementary Table 5.6	Supplementary Figure 5.9* Supplementary Figure 5.11
9	Effect of temperature and competitors on growth rate of non-toxic and potentially toxic dinoflagellates	Growth rate in co-cultures ~ Temperature x Competitor species	Focal toxicity	Supplementary Table 5.4* Supplementary Table 5.6	Supplementary Figure 5.9* Supplementary Figure 5.11
10	Focal and competitor species specificity of growth in different temperature treatments	Growth rate in co-cultures ~ Focal species x Competitor species	Temperature	Supplementary Table 5.4*	Supplementary Figure 5.9*

				Supplementary Tables	
				Supplementary Table 5.6	Supplementary Figure 5.11
11	Dependence of growth on focal and competitor genera in different temperature treatments	Growth rate in co-cultures ~ Focal genus x Competitor genus	Temperature	Supplementary Table 5.4* Supplementary Table 5.6	Supplementary Figure 5.9* Supplementary Figure 5.11
12	Dependence of growth on toxicity of focal and competitor species in different temperature treatments	Growth rate in co-cultures ~ Focal toxicity x Competitor toxicity	Temperature	Supplementary Table 5.4* Supplementary Table 5.6	Supplementary Figure 5.9* Supplementary Figure 5.11
13	Effect of temperature and competitors on relative growth of six different species of dinoflagellates	Relative growth ~ Temperature x Competitor species	Focal species	Supplementary Table 5.5* Supplementary Table 5.7	Supplementary Figure 5.10* Supplementary Figure 5.12
14	Effect of temperature and competitors on relative growth of two different genera of dinoflagellates	Relative growth ~ Temperature x Competitor species	Focal genus	Supplementary Table 5.5* Supplementary Table 5.7	Supplementary Figure 5.10* Supplementary Figure 5.12
15	Effect of temperature and competitors on relative growth of non-toxic and potentially toxic dinoflagellates	Relative growth ~ Temperature x Competitor species	Focal toxicity	Supplementary Table 5.5* Supplementary Table 5.7	Supplementary Figure 5.10* Supplementary Figure 5.12
16	Focal and competitor species specificity of relative growth in different temperature treatments	Relative growth ~ Focal species x Competitor species	Temperature	Supplementary Table 5.5* Supplementary Table 5.7	Supplementary Figure 5.10* Supplementary Figure 5.12
17	Dependence of relative growth on focal and competitor genera in different temperature treatments	Relative growth ~ Focal genus x Competitor genus	Temperature	Supplementary Table 5.5* Supplementary Table 5.7	Supplementary Figure 5.10* Supplementary Figure 5.12
18	Dependence of relative growth on toxicity of focal and competitor species in different temperature treatments	Relative growth ~ Focal toxiciy x Competitor toxicity	Temperature	Supplementary Table 5.5* Supplementary Table 5.7	Supplementary Figure 5.10* Supplementary Figure 5.12

Supplementary Table 6.3. Summary statistics of the analysis of variance (ANOVA) conducted to determine the effect of temperature, taxonomic identity, and toxicity on growth of dinoflagellates in monocultures. Asterisk indicates significance at 95% confidence interval.

ANOVA	Model	Data separation		Terms	df	Sum Sq.	Mean Sq.	F value	p-value	
			Prorocentrum sp.	Temperature	2	0.22	0.11	627.66	<0.05	*
				Residuals	42	0.01	0			
			Prorocentrum micans	Temperature	2	0.07	0.03	266.04	<0.05	*
				Residuals	42	0.01	0			
1	Growth rate ~ Temperature	Focal species	*Alexandrium tamutum*	Temperature	2	0.61	0.3	918.7	<0.05	*
				Residuals	42	0.01	0			
			Prorocentrum minimum	Temperature	2	0.16	0.08	235.11	<0.05	*
				Residuals	42	0.01	0			
			Prorocentrum lima	Temperature	2	0	0	6.98	<0.05	*
				Residuals	42	0.01	0			
			Alexandrium minutum	Temperature	2	0.56	0.28	10401.75	<0.05	*
				Residuals	42	0	0			
2	Growth rate ~ Temperature	Focal genus	*Prorocentrum*	Temperature	2	0.17	0.09	10.28	<0.05	*
				Residuals	177	1.49	0.01			
			Alexandrium	Temperature	2	1.17	0.58	2230.16	<0.05	*
				Residuals	87	0.02	0			
3	Growth rate ~ Temperature	Focal toxicity	non-toxic	Temperature	2	0.52	0.26	36.51	<0.05	*
				Residuals	132	0.94	0.01			
			potentially toxic	Temperature	2	0.47	0.23	15.37	<0.05	*
				Residuals	132	2	0.02			
4	Growth rate ~ Focal species	Temperature	15 °C	Focal species	5	0.23	0.05	205.52	<0.05	*
				Residuals	84	0.02	0			
			20 °C	Focal species	5	0.85	0.17	782.01	<0.05	*
				Residuals	84	0.02	0			
			25 °C	Focal species	5	1.97	0.39	2933.6	<0.05	*
				Residuals	84	0.01	0			
5	Growth rate ~ Focal genus	Temperature	15 °C	Focal genus	1	0.01	0.01	3.61	0.06	
				Residuals	88	0.24	0			
			20 °C	Focal genus	1	0.37	0.37	66.07	<0.05	*
				Residuals	88	0.49	0.01			
			25 °C	Focal genus	1	1.2	1.2	135.19	<0.05	*
				Residuals	88	0.78	0.01			
6	Growth rate ~ Focal toxicity	Temperature	15 °C	Focal toxicity	1	0.01	0.01	3.87	0.05	
				Residuals	88	0.24	0			
			20 °C	Focal toxicity	1	0.06	0.06	6.19	<0.05	*
				Residuals	88	0.81	0.01			
			25 °C	Focal toxicity	1	0.09	0.09	4	<0.05	*
				Residuals	88	1.9	0.02			

Supplementary Table 6.4. Summary statistics of the analysis of variance (ANOVA) conducted to determine the effect of temperature, taxonomic identity, and toxicity on growth of dinoflagellates in co-cultures using the filtered datasets. Notes: asterisk * indicates significance at 95% confidence interval; superscript [a] indicates different statistical result from the analysis using the full datasets; and, superscript [b] indicates statistical computation is not possible.

ANOVA	Model	Data separation		Terms	df	Sum Sq.	Mean Sq.	F value	p-value	
7	Growth rate ~ Temperature x Competitor species	Focal species	*Prorocentrum sp.*	Temperature	2	0.08	0.04	89.28	<0.05	*
				Competitor species	3	0.04	0.01	31.30	<0.05	*
				Temperature: Competitor	6	0.02	0.00	6.01	<0.05	*
				Residuals	24	0.01	0.00			
			Prorocentrum micans	Temperature	2	0.09	0.04	124.43	<0.05	*
				Competitor	3	0.05	0.02	44.30	<0.05	*
				Temperature: Competitor	6	0.04	0.01	18.50	<0.05	*
				Residuals	24	0.01	0.00			
			Alexandrium tamutum	Temperature	2	0.43	0.21	459.96	<0.05	*
				Competitor	3	0.03	0.01	24.94	<0.05	*
				Temperature: Competitor	6	0.02	0.00	6.12	<0.05	*
				Residuals	24	0.01	0.00			
			Prorocentrum minimum	Temperature	2	0.23	0.12	412.91	<0.05	*
				Competitor	3	0.04	0.01	52.79	<0.05	*
				Temperature: Competitor	6	0.08	0.01	44.15	<0.05	*
				Residuals	24	0.01	0.00			
			Prorocentrum lima	Temperature	2	0.06	0.03	37.27	<0.05	*
				Competitor	4	0.01	0.00	3.26	<0.05	*
				Temperature: Competitor	8	0.01	0.00	0.78	0.62	
				Residuals	30	0.02	0.00			
			Alexandrium minutum	Temperature	2	0.39	0.19	1092.45	<0.05	*
				Competitor	2	0.00	0.00	12.55	<0.05	*
				Temperature: Competitor	4	0.00	0.00	4.94	<0.05	*
				Residuals	18	0.00	0.00			
8	Growth rate ~ Temperature x	Focal genus	*Prorocentrum*	Temperature	2	0.39	0.20	26.78	<0.05	*
				Competitor	5	0.11	0.02	3.08	<0.05	*a

No	Model	Factor	Sublevel	Term	df	SS	MS	F	p	
		Competitor species		Temperature:Competitor	10	0.06	0.01	0.78	0.65	
				Residuals	135	0.99	0.01			
			Alexandrium	Temperature	2	0.81	0.41	664.01	<0.05	*
				Competitor	3	0.05	0.02	26.83	<0.05	*
				Temperature:Competitor	6	0.01	0.00	3.93	<0.05	*
				Residuals	51	0.03	0.00			
9	Growth rate ~ Temperature x Competitor species	Focal toxicity	non-toxic	Temperature	2	0.49	0.24	83.33	<0.05	*
				Competitor	5	0.42	0.08	28.76	<0.05	*
				Temperature:Competitor	10	0.08	0.01	2.63	<0.05	*a
				Residuals	90	0.26	0.00			
			potentially toxic	Temperature	2	0.55	0.28	21.52	<0.05	*
				Competitor	5	0.54	0.11	8.40	<0.05	*
				Temperature:Competitor	10	0.05	0.00	0.37	0.96	
				Residuals	90	1.16	0.01			
10	Growth rate ~ Focal species x Competitor species	Temperature	15 °C	Focal	5	0.19	0.04	193.66	<0.05	*
				Competitor	5	0.03	0.01	34.36	<0.05	*
				Focal:Competitor	13	0.04	0.00	16.23	<0.05	*
				Residuals	48	0.01	0.00			
			20 °C	Focal	5	0.85	0.17	381.75	<0.05	*
				Competitor	5	0.01	0.00	6.51	<0.05	*
				Focal:Competitor	13	0.07	0.01	12.11	<0.05	*
				Residuals	48	0.02	0.00			
			25 °C	Focal	5	1.09	0.22	311.17	<0.05	*
				Competitor	5	0.05	0.01	13.91	<0.05	*
				Focal:Competitor	13	0.13	0.01	14.14	<0.05	*
				Residuals	48	0.03	0.00			
		Temperature	15 °C	Focal genus	1	0.07	0.07	30.67	<0.05	*
				Competitor genus	1	0.04	0.04	15.65	<0.05	*
				Focal genus:Competitor genus						b

258

11				Residuals	69	0.17	0.00			
	Growth rate ~ Focal genus x Competitor genus		20 °C	Focal genus	1	0.49	0.49	73.79	<0.05	*
				Competitor genus	1	0.00	0.00	0.75	0.39	
				Focal genus: Competitor genus						b
				Residuals	69	0.46	0.01			
			25 °C	Focal genus	1	0.71	0.71	82.44	<0.05	*
				Competitor genus	1	0.00	0.00	0.01	0.94	
				Focal genus: Competitor genus						b
				Residuals	69	0.59	0.01			
12	Growth rate ~ Focal toxicity x Competitor toxicity	Temperature	15 °C	Focal toxicity	1	0.00	0.00	0.90	0.35	
				Competitor toxicity	1	0.00	0.00	0.39	0.54	
				Focal toxicity: Competitor toxicity	1	0.00	0.00	0.00	0.98	
				Residuals	68	0.27	0.00			
			20 °C	Focal toxicity	1	0.02	0.02	1.38	0.24	
				Competitor toxicity	1	0.02	0.02	1.65	0.20	
				Focal toxicity: Competitor toxicity	1	0.00	0.00	0.32	0.58	
				Residuals	68	0.91	0.01			
			25 °C	Focal toxicity	1	0.00	0.00	0.03	0.86	
				Competitor toxicity	1	0.01	0.01	0.27	0.60	
				Focal toxicity: Competitor toxicity	1	0.01	0.01	0.29	0.59	
				Residuals	68	1.29	0.02			

Supplementary Table 6.5. Summary statistics of the analysis of variance (ANOVA) conducted to determine the effect of temperature, taxonomic identity, and toxicity on relative growth of dinoflagellates using the filtered datasets. Notes: asterisk * indicates significance at 95% confidence interval; superscript [a] indicates different statistical result from the analysis using the full datasets; and, superscript [b] indicates statistical computation is not possible.

ANOVA	Model	Data separation		Terms	df	Sum Sq.	Mean Sq.	F value	p-value	
			Prorocentrum sp.	Temperature	2	0.87	0.43	23.31	<0.05	*
				Competitor species	3	1.08	0.36	19.32	<0.05	*
				Temperature: Competitor	6	0.59	0.10	5.25	<0.05	*
				Residuals	24	0.45	0.02			
			Prorocentrum micans	Temperature	2	4.03	2.01	148.32	<0.05	*
				Competitor	3	1.41	0.47	34.60	<0.05	*
				Temperature: Competitor	6	1.30	0.22	15.90	<0.05	*
				Residuals	24	0.33	0.01			
			Alexandrium tamutum	Temperature	2	0.06	0.03	2.87	0.08	a
				Competitor	3	0.34	0.11	10.93	<0.05	*
	Relative growth ~ Temperature x Competitor species	Focal species		Temperature: Competitor	6	0.13	0.02	2.05	0.10	
13				Residuals	24	0.25	0.01			
			Prorocentrum minimum	Temperature	2	0.51	0.25	28.67	<0.05	*
				Competitor	3	0.29	0.10	10.94	<0.05	*
				Temperature: Competitor	6	0.58	0.10	10.98	<0.05	*
				Residuals	24	0.21	0.01			
			Prorocentrum lima	Temperature	2	3.20	1.60	24.07	<0.05	*
				Competitor	4	0.92	0.23	3.45	<0.05	*
				Temperature: Competitor	8	0.43	0.05	0.82	0.60	
				Residuals	30	1.99	0.07			
			Alexandrium minutum	Temperature	2	0.01	0.01	2.65	0.10	a
				Competitor	2	0.03	0.01	5.17	<0.05	*
				Temperature: Competitor	4	0.02	0.00	1.67	0.20	a
				Residuals	18	0.05	0.00			
14	Relative growth ~ Temperature x	Focal genus	*Prorocentrum*	Temperature	2	5.66	2.83	48.17	<0.05	*
				Competitor	5	2.46	0.49	8.39	<0.05	*

	Model	Factor	Level	Effect	df	Sum Sq	Mean Sq	F	p	
			Competitor species	Temperature:Competitor	10	3.28	0.33	5.59	<0.05	*
				Residuals	135	7.93	0.06			
			Alexandrium	Temperature	2	0.04	0.02	2.45	0.10	a
				Competitor	3	0.34	0.11	13.92	<0.05	*
				Temperature:Competitor	6	0.11	0.02	2.18	0.06	a
				Residuals	51	0.42	0.01			
15	Relative growth ~ Temperature x Competitor species	Focal toxicity	non-toxic	Temperature	2	2.38	1.19	22.43	<0.05	*
				Competitor	5	1.25	0.25	4.71	<0.05	*
				Temperature:Competitor	10	3.02	0.30	5.70	<0.05	*
				Residuals	90	4.77	0.05			
			potentially toxic	Temperature	2	2.20	1.10	24.32	<0.05	*
				Competitor	5	0.88	0.18	3.91	<0.05	*
				Temperature:Competitor	10	1.62	0.16	3.59	<0.05	*
				Residuals	90	4.07	0.05			
16	Relative growth ~ Focal species x Competitor species	Temperature	15 °C	Focal	5	1.43	0.29	16.33	<0.05	*
				Competitor	5	0.95	0.19	10.87	<0.05	*
				Focal:Competitor	13	1.52	0.12	6.69	<0.05	*
				Residuals	48	0.84	0.02			
			20 °C	Focal	5	0.79	0.16	9.13	<0.05	*
				Competitor	5	0.22	0.04	2.58	<0.05	*a
				Focal:Competitor	13	1.12	0.09	5.02	<0.05	*
				Residuals	48	0.83	0.02			
			25 °C	Focal	5	4.08	0.82	24.39	<0.05	*
				Competitor	5	1.57	0.31	9.39	<0.05	*
				Focal:Competitor	13	1.71	0.13	3.94	<0.05	*
				Residuals	48	1.61	0.03			
		Temperature	15 °C	Focal genus	1	0.97	0.97	20.77	<0.05	*
				Competitor genus	1	0.57	0.57	12.23	<0.05	*
				Focal genus:Competitor genus						b

17				Residuals	69	3.21	0.05			
	Relative growth ~ Focal genus x Competitor genus		20 °C	Focal genus	1	0.10	0.10	2.47	0.12	
				Competitor genus	1	0.00	0.00	0.05	0.83	
				Focal genus: Competitor genus						[b]
				Residuals	69	2.86	0.04			
			25 °C	Focal genus	1	1.07	1.07	9.64	<0.05	*
				Competitor genus	1	0.26	0.26	2.37	0.13	
				Focal genus: Competitor genus						[b]
				Residuals	69	7.64	0.11			
18	Relative growth ~ Focal toxicity x Competitor toxicity	Temperature	15 °C	Focal toxicity	1	0.43	0.43	7.20	<0.05	*
				Competitor toxicity	1	0.24	0.24	3.97	0.05	[a]
				Focal toxicity: Competitor toxicity	1	0.00	0.00	0.08	0.78	
				Residuals	68	4.07	0.06			
			20 °C	Focal toxicity	1	0.42	0.42	11.36	<0.05	*
				Competitor toxicity	1	0.01	0.01	0.32	0.57	
				Focal toxicity: Competitor toxicity	1	0.02	0.02	0.59	0.45	
				Residuals	68	2.51	0.04			
			25 °C	Focal toxicity	1	0.21	0.21	1.81	0.18	
				Competitor toxicity	1	0.71	0.71	6.02	<0.05	*a
				Focal toxicity: Competitor toxicity	1	0.00	0.00	0.01	0.93	
				Residuals	68	8.04	0.12			

Supplementary Table 6.6. Summary statistics of the analysis of variance (ANOVA) conducted to determine the effect of temperature, taxonomic identity, and toxicity on growth of dinoflagellates in co-cultures using the full datasets. Notes: asterisk * indicates significance at 95% confidence interval.

ANOVA	Model	Data separation		Terms	df	Sum Sq.	Mean Sq.	F value	p-value	
			Prorocentrum sp.	Temperature	2	0.1	0.05	120.88	<0.05	*
				Competitor species	4	0.04	0.01	26.83	<0.05	*
				Temperature: Competitor	8	0.03	0	8.23	<0.05	*
				Residuals	30	0.01	0			
			Prorocentrum micans	Temperature	2	0.14	0.07	175.67	<0.05	*
				Competitor	4	0.05	0.01	28.89	<0.05	*
				Temperature: Competitor	8	0.06	0.01	18.38	<0.05	*
				Residuals	30	0.01	0			
			Alexandrium tamutum	Temperature	2	0.49	0.25	546.62	<0.05	*
				Competitor	4	0.05	0.01	27.25	<0.05	*
	Growth rate ~			Temperature: Competitor	8	0.02	0	5.95	<0.05	*
7	Temperature x	Focal species		Residuals	30	0.01	0			
	Competitor species		*Prorocentrum minimum*	Temperature	2	0.29	0.15	462.72	<0.05	*
				Competitor	4	0.06	0.01	43.79	<0.05	*
				Temperature: Competitor	8	0.08	0.01	30.02	<0.05	*
				Residuals	30	0.01	0			
			Prorocentrum lima	Temperature	2	0.06	0.03	37.27	<0.05	*
				Competitor	4	0.01	0	3.26	<0.05	*
				Temperature: Competitor	8	0.01	0	0.78	0.62	
				Residuals	30	0.02	0			
			Alexandrium minutum	Temperature	2	0.81	0.4	1670.68	<0.05	*
				Competitor	4	0.03	0.01	34.33	<0.05	*
				Temperature: Competitor	8	0.02	0	12.44	<0.05	*
				Residuals	30	0.01	0			
	Growth rate ~		*Prorocentrum*	Temperature	2	0.50	0.25	32.28	<0.05	*
8	Temperature x	Focal genus		Competitor	5	0.07	0.01	1.79	0.12	
	Competitor species			Temperature:	10	0.08	0.01	1.08	0.38	

					Df					
				Competitor Residuals	162	1.25	0.01			
			Alexandrium	Temperature	2	1.28	0.64	308.14	<0.05	*
				Competitor						
				Temperature: Competitor						
				Residuals	87	0.18	0			
9	Growth rate ~ Temperature x Competitor species	Focal toxicity	non-toxic	Temperature	2	0.62	0.31	58.32	<0.05	*
				Competitor	5	0.18	0.04	6.88	<0.05	*
				Temperature: Competitor	10	0.07	0.01	1.34	0.22	
				Residuals	117	0.62	0.01			
			potentially toxic	Temperature	2	0.93	0.47	30.66	<0.05	*
				Competitor	5	0.22	0.04	2.92	<0.05	*
				Temperature: Competitor	10	0.06	0.01	0.39	0.95	
				Residuals	117	1.78	0.02			
10	Growth rate ~ Focal species x Competitor species	Temperature	15 °C	Focal	5	0.19	0.04	175.68	<0.05	*
				Competitor	5	0.05	0.01	51.19	<0.05	*
				Focal: Competitor	19	0.09	0	21.31	<0.05	*
				Residuals	60	0.01	0			
			20 °C	Focal	5	0.95	0.19	400.06	<0.05	*
				Competitor	5	0.02	0	6.77	<0.05	*
				Focal: Competitor	19	0.09	0	9.88	<0.05	*
				Residuals	60	0.03	0			
			25 °C	Focal	5	1.31	0.26	419.71	<0.05	*
				Competitor	5	0.03	0.01	9.3	<0.05	*
				Focal: Competitor	19	0.18	0.01	14.82	<0.05	*
				Residuals	60	0.04	0			
11		Temperature	15 °C	Focal genus	1	0.04	0.04	13.78	<0.05	*
				Competitor genus	1	0.03	0.03	10.81	<0.05	*
				Focal genus: Competitor genus	1	0	0	1.34	0.25	
				Residuals	86	0.26	0			

	Growth rate ~ Focal genus x Competitor genus		20 °C	Focal genus	1	0.53	0.53	84.09	<0.05	*
				Competitor genus	1	0.01	0.01	0.93	0.34	
				Focal genus: Competitor genus	1	0	0	0.24	0.63	
				Residuals	86	0.54	0.01			
			25 °C	Focal genus	1	0.82	0.82	100.02	<0.05	*
				Competitor genus	1	0	0	0.27	0.6	
				Focal genus: Competitor genus	1	0.02	0.02	2.65	0.11	
				Residuals	86	0.71	0.01			
12	Growth rate ~ Focal toxicity x Competitor toxicity	Temperature	15 °C	Focal toxicity	1	0	0	0.45	0.5	
				Competitor toxicity	1	0.01	0.01	3.67	0.06	
				Focal toxicity: Competitor toxicity	1	0	0	0.07	0.8	
				Residuals	86	0.32	0			
			20 °C	Focal toxicity	1	0	0	0.19	0.66	
				Competitor toxicity	1	0	0	0.18	0.67	
				Focal toxicity: Competitor toxicity	1	0.01	0.01	0.95	0.33	
				Residuals	86	1.07	0.01			
			25 °C	Focal toxicity	1	0.04	0.04	2.34	0.13	
				Competitor toxicity	1	0.01	0.01	0.46	0.5	
				Focal toxicity: Competitor toxicity	1	0	0	0.07	0.8	
				Residuals	86	1.5	0.02			

Supplementary Table 6.7. Summary statistics of the analysis of variance (ANOVA) conducted to determine the effect of temperature, taxonomic identity, and toxicity on relative growth of dinoflagellates using the full datasets. Notes: asterisk * indicates significance at 95% confidence interval.

ANOVA	Model	Data separation		Terms	df	Sum Sq.	Mean Sq.	F value	p-value	
			Prorocentrum sp.	Temperature	2	0.73	0.36	21.13	<0.05	*
				Competitor species	4	1.09	0.27	15.88	<0.05	*
				Temperature: Competitor	8	0.8	0.1	5.84	<0.05	*
				Residuals	30	0.52	0.02			
			Prorocentrum micans	Temperature	2	5.2	2.6	164.27	<0.05	*
				Competitor	4	1.47	0.37	23.2	<0.05	*
				Temperature: Competitor	8	1.79	0.22	14.11	<0.05	*
				Residuals	30	0.48	0.02			
			Alexandrium tamutum	Temperature	2	0.1	0.05	4.89	<0.05	*
				Competitor	4	0.44	0.11	11.26	<0.05	*
				Temperature: Competitor	8	0.13	0.02	1.72	0.13	
	Relative growth ~			Residuals	30	0.29	0.01			
13	Temperature x Competitor species	Focal species	*Prorocentrum minimum*	Temperature	2	0.57	0.28	36.73	<0.05	*
				Competitor	4	0.38	0.1	12.3	<0.05	*
				Temperature: Competitor	8	0.59	0.07	9.52	<0.05	*
				Residuals	30	0.23	0.01			
			Prorocentrum lima	Temperature	2	3.2	1.6	24.07	<0.05	*
				Competitor	4	0.92	0.23	3.45	<0.05	*
				Temperature: Competitor	8	0.43	0.05	0.82	0.6	
				Residuals	30	1.99	0.07			
			Alexandrium minutum	Temperature	2	0.41	0.21	61.94	<0.05	*
				Competitor	4	0.5	0.12	37.32	<0.05	*
				Temperature: Competitor	8	0.57	0.07	21.28	<0.05	*
				Residuals	30	0.1	0			
	Relative growth ~		*Prorocentrum*	Temperature	2	6.00	3.00	50.09	<0.05	*
14	Temperature x	Focal genus		Competitor	5	2.13	0.43	7.11	<0.05	*
	Competitor species			Temperature:	10	3.54	0.35	5.91	<0.05	*

#	Model			Term	Df	Sum Sq	Mean Sq	F	p	
				Competitor						
				Residuals	162	9.71	0.06			
			Alexandrium	Temperature	2	0.11	0.05	1.91	0.15	
				Competitor						
				Temperature: Competitor						
				Residuals	87	2.43	0.03			
15	Relative growth ~ Temperature x Competitor species	Focal toxicity	non-toxic	Temperature	2	2.35	1.18	18.46	<0.05	*
				Competitor	5	1.34	0.27	4.2	<0.05	*
				Temperature: Competitor	10	2.49	0.25	3.9	<0.05	*
				Residuals	117	7.46	0.06			
			potentially toxic	Temperature	2	2.92	1.46	31.12	<0.05	*
				Competitor	5	0.64	0.13	2.74	<0.05	*
				Temperature: Competitor	10	1.15	0.12	2.45	<0.05	*
				Residuals	117	5.49	0.05			
16	Relative growth ~ Focal species x Competitor species	Temperature	15 °C	Focal	5	1.34	0.27	17.19	<0.05	*
				Competitor	5	1.36	0.27	17.48	<0.05	*
				Focal: Competitor	19	2.64	0.14	8.92	<0.05	*
				Residuals	60	0.94	0.02			
			20 °C	Focal	5	0.77	0.15	9.88	<0.05	*
				Competitor	5	0.17	0.03	2.19	0.07	
				Focal: Competitor	19	1.42	0.07	4.77	<0.05	*
				Residuals	60	0.94	0.02			
			25 °C	Focal	5	4.98	1	34.39	<0.05	*
				Competitor	5	1.13	0.23	7.77	<0.05	*
				Focal: Competitor	19	2.4	0.13	4.35	<0.05	*
				Residuals	60	1.74	0.03			
17		Temperature	15 °C	Focal genus	1	0.4	0.4	7.01	<0.05	*
				Competitor genus	1	0.84	0.84	14.52	<0.05	*
				Focal genus: Competitor genus	1	0.08	0.08	1.39	0.24	
				Residuals	86	4.96	0.06			

	Relative growth ~ Focal genus x Competitor genus		20 °C	Focal genus	1	0.06	0.06	1.74	0.19	
				Competitor genus	1	0	0	0.06	0.81	
				Focal genus: Competitor genus	1	0.03	0.03	0.93	0.34	
				Residuals	86	3.19	0.04			
			25 °C	Focal genus	1	1.53	1.53	15.47	<0.05	*
				Competitor genus	1	0.05	0.05	0.54	0.46	
				Focal genus: Competitor genus	1	0.15	0.15	1.55	0.22	
				Residuals	86	8.5	0.1			
18	Relative growth ~ Focal toxicity x Competitor toxicity	Temperature	15 °C	Focal toxicity	1	0.58	0.58	9.52	<0.05	*
				Competitor toxicity	1	0.42	0.42	6.77	<0.05	*
				Focal toxicity: Competitor toxicity	1	0	0	0.01	0.91	
				Residuals	86	5.28	0.06			
			20 °C	Focal toxicity	1	0.42	0.42	13	<0.05	*
				Competitor toxicity	1	0.03	0.03	0.83	0.37	
				Focal toxicity: Competitor toxicity	1	0.08	0.08	2.41	0.12	
				Residuals	86	2.77	0.03			
			25 °C	Focal toxicity	1	0.25	0.25	2.18	0.14	
				Competitor toxicity	1	0.32	0.32	2.86	0.09	
				Focal toxicity: Competitor toxicity	1	0	0	0.03	0.86	
				Residuals	86	9.67	0.11			

SUPPLEMENTARY FIGURES

This page is intentionally left blank.

This page is intentionally left blank.
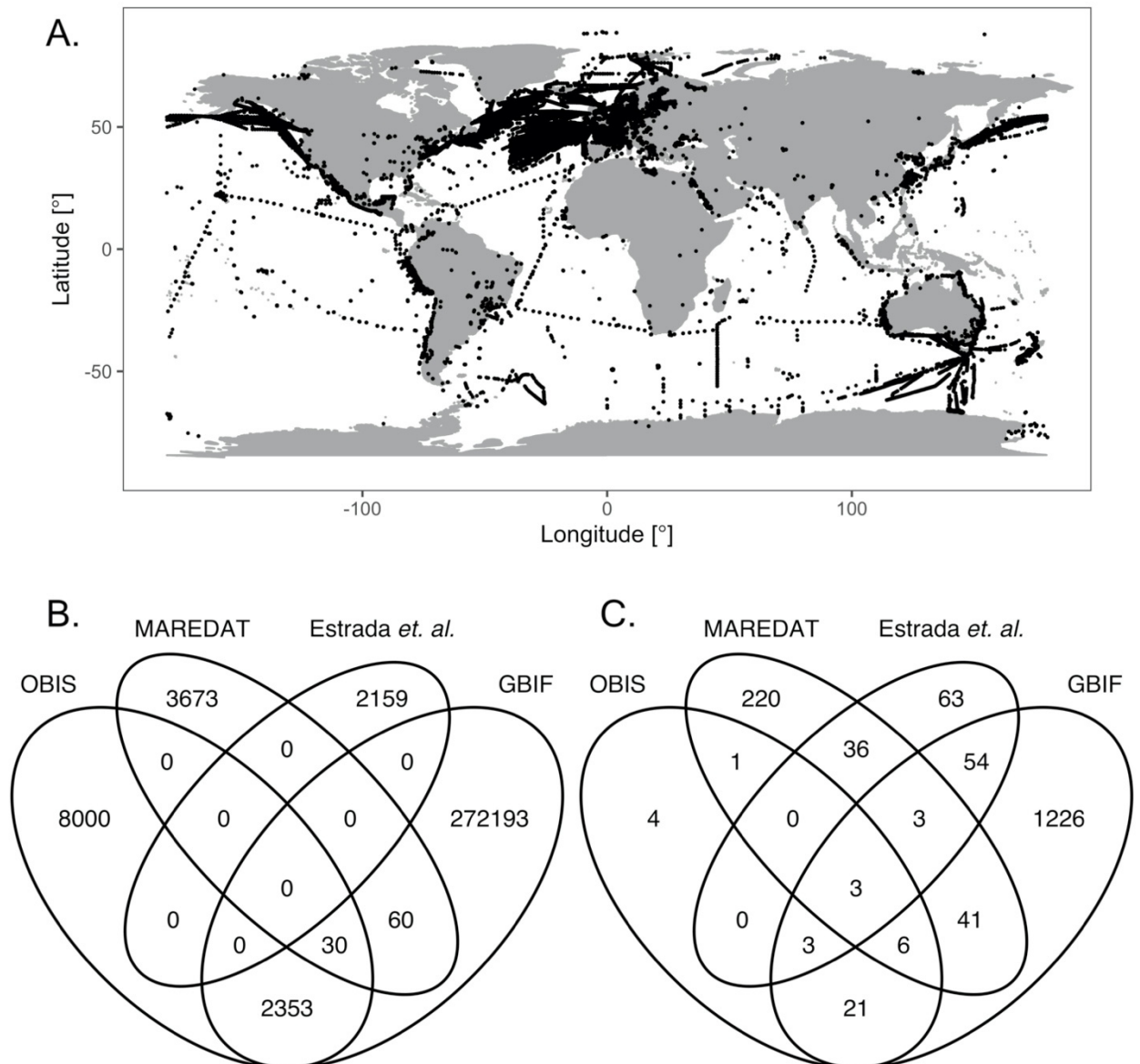
Supplementary Figure 2.1. Geographic locations of the occurrence records of phytoplankton species retrieved from the four data sources used in this study (A). The compiled dataset is comprised of 771,286 observations representing 1,681 species recorded between 2000 and 2014, which were retrieved from *OBIS*, *GBIF*, *MAREDAT*, and Estrada *et. al*. Contribution of sources to the phytoplankton dataset is illustrated in Venn diagrams, showing the number of distinct and common observations (B) and species (C).
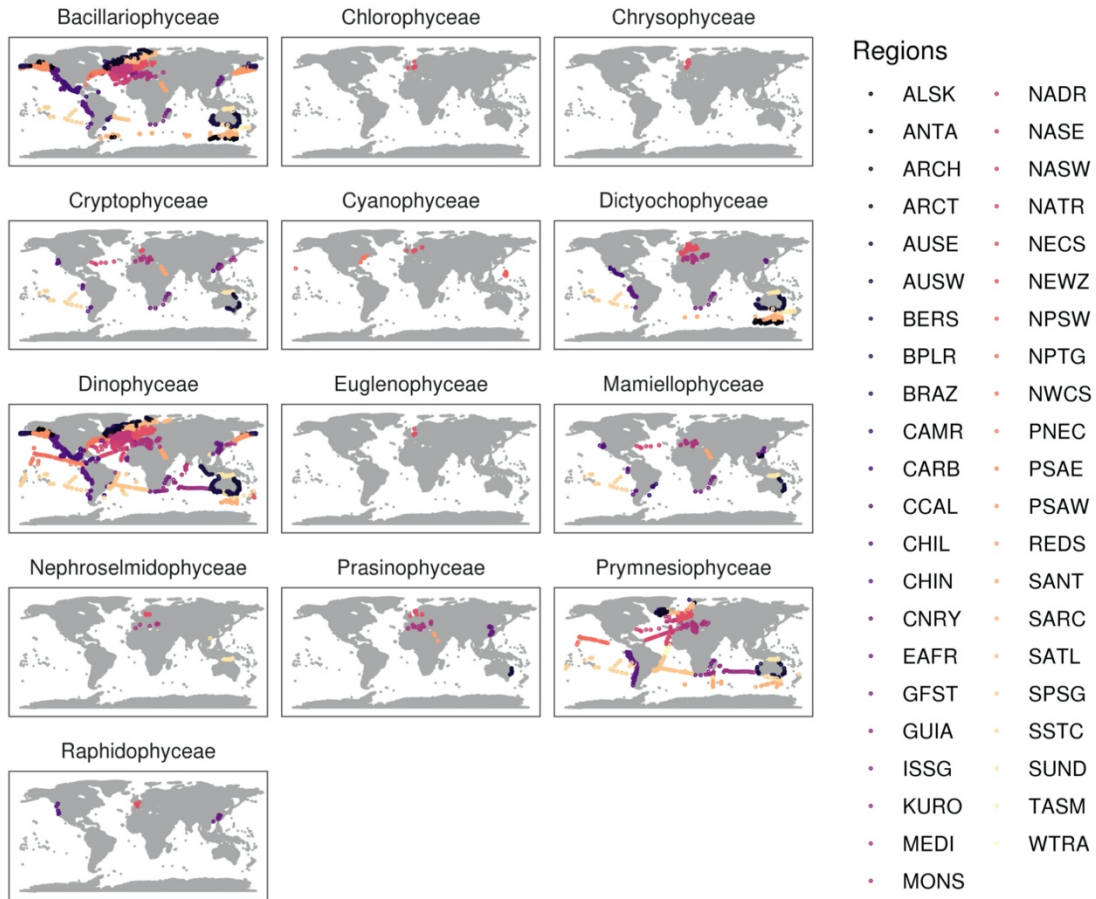
Supplementary Figure 2.2. Occurrence locations of marine phytoplankton. Colour-coded points represent occurrence records of marine phy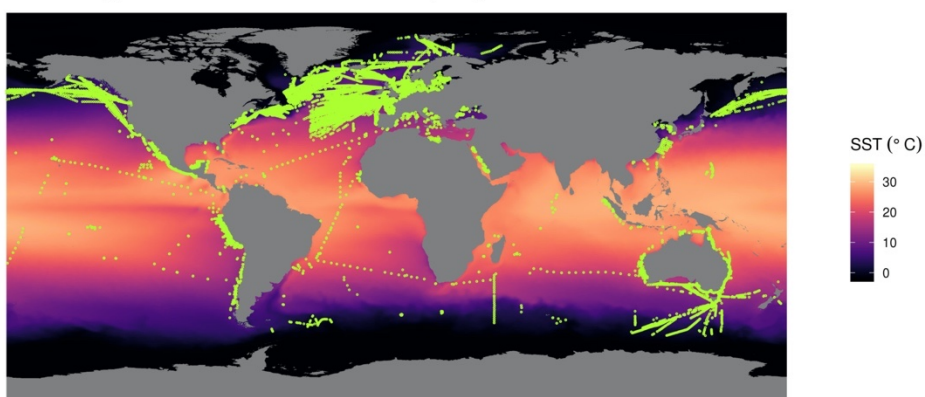toplankton species representing 13 taxonomic classes across 43 ocean regions (see Supplementary Information SI2 for abbreviation).

A. Average annual SST (mean)
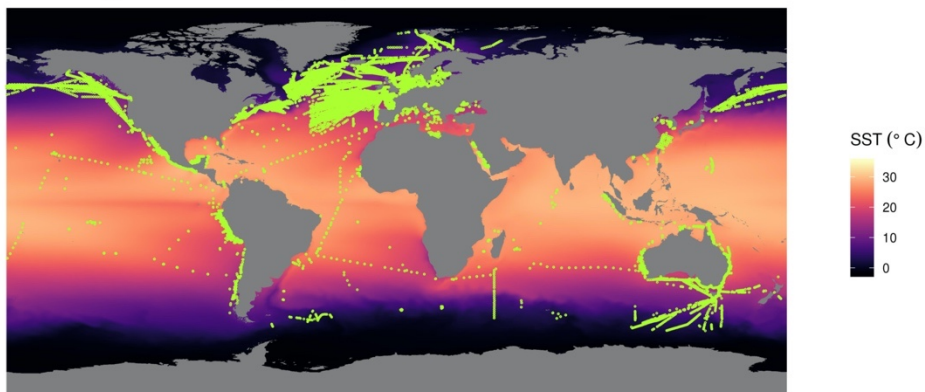
B. Average SST of the coolest months (min)

C. Average SST of the warmest months (min)

Supplementary Figure 2.3. Global sea surface temperature (*SST*,   C) data at 5 arcmin between 2000 and 2014 retrieved from *Bio-ORACLE*. The colour gradients indicate the long-term annual average *SST* (A) and seasonal extreme *SST*, i.e. average *SST* of the coolest months (B) and average *SST* of the warmest months (C). The points represent occurrence records of marine phytoplankton species representing 13 taxonomic classes across 43 ocean regions (see Supplementary Figure 2.2).

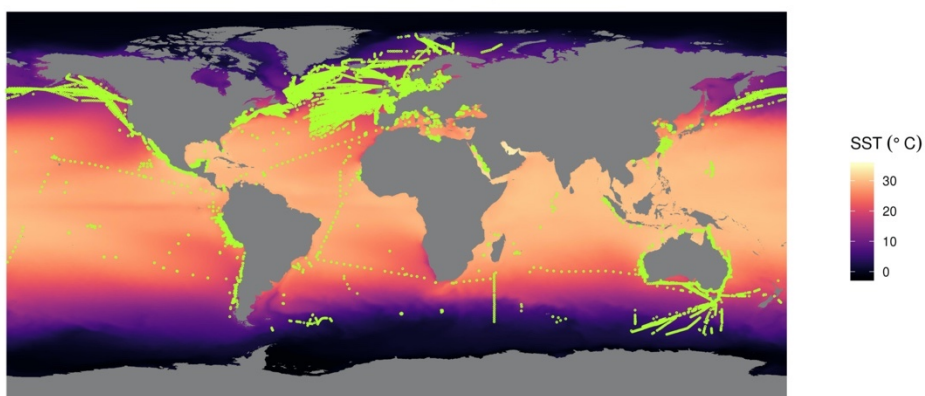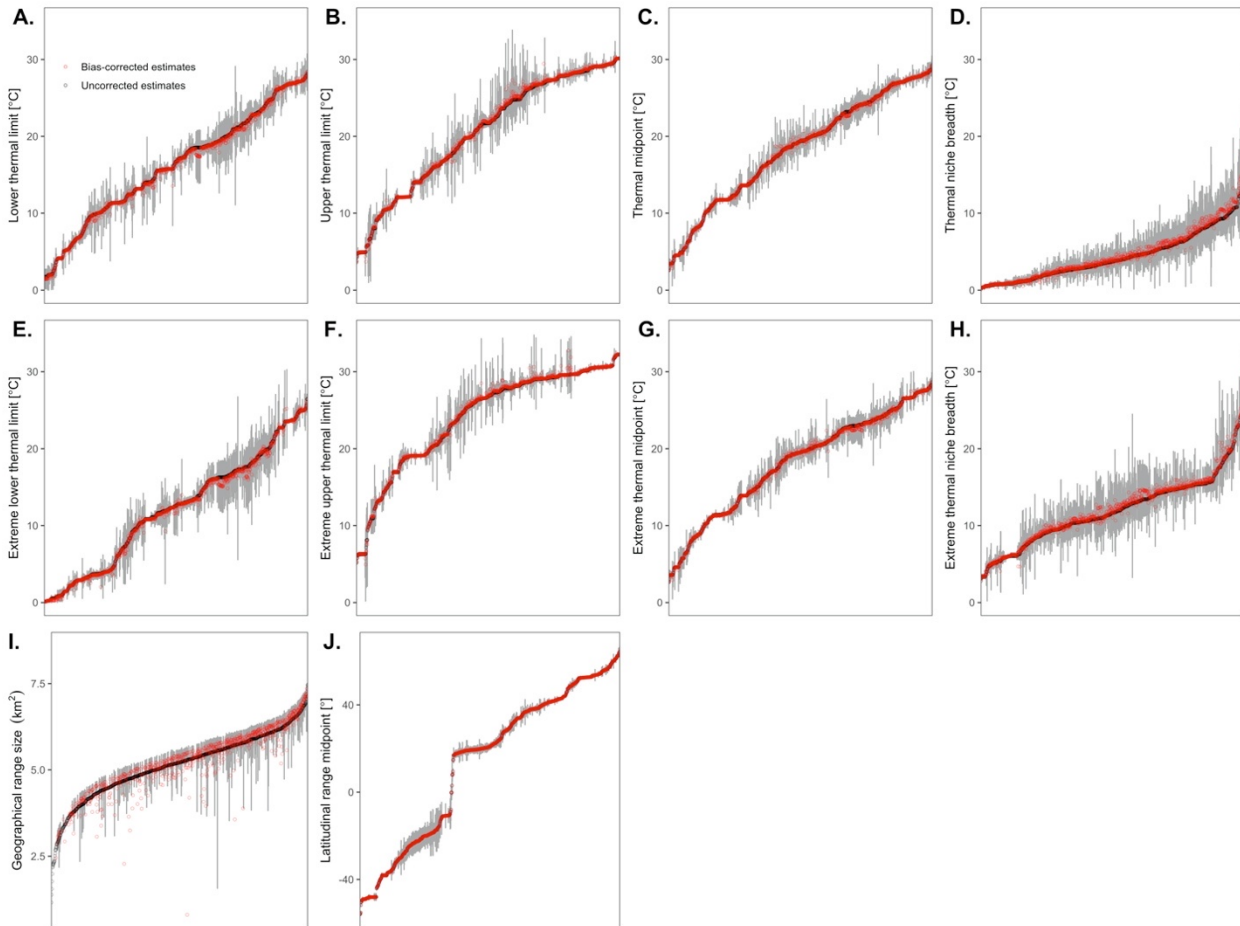**Supplementary Figure 2.4.** Estimates of uncertainty in thermal limits, midpoints, and niche breadth derived from annual average *SST* (A – D) and extreme seasonal *SST* (E – H), geographic range size (I), and latitudinal range midpoint (J), obtained through bootstrapping. Uncorrected estimates are shown as black points and the 95% confidence intervals for the uncorrected estimates are shown by the grey error bars. Bias-corrected estimates, i.e. the difference between uncorrected estimate and bootstrap estimate of bias, are shown as red points. Geographic variants are ranked in ascending order of the traits.
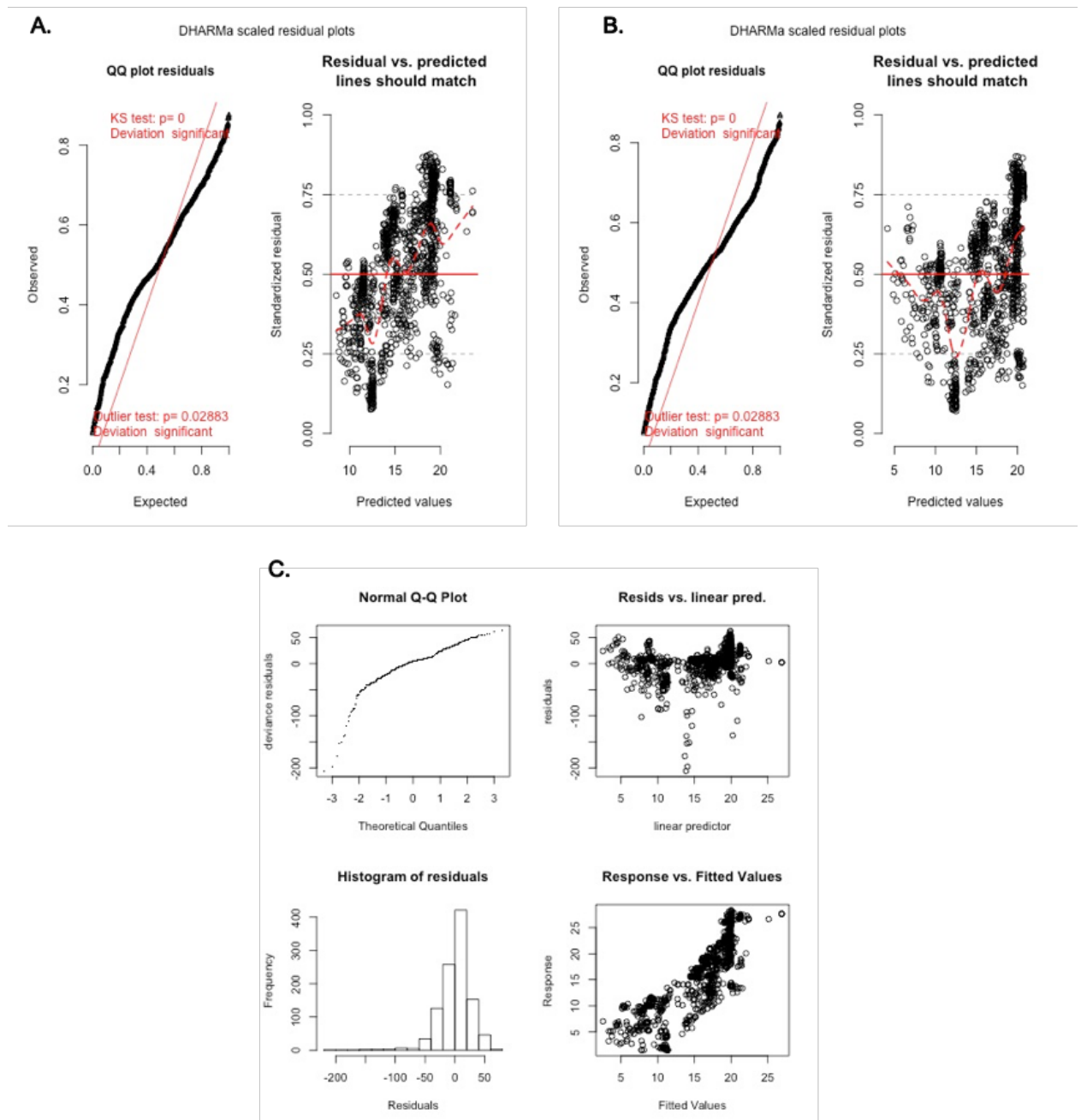
Supplementary Figure 2.5. Sample regression diagnostics plots used to evaluate the residuals of the mixed models. These diagnostics are for *GLMM* with linear term only (A), *GLMM* with both the linear and quadratic terms (B), and *GAMM* with cubic regression splines (C).
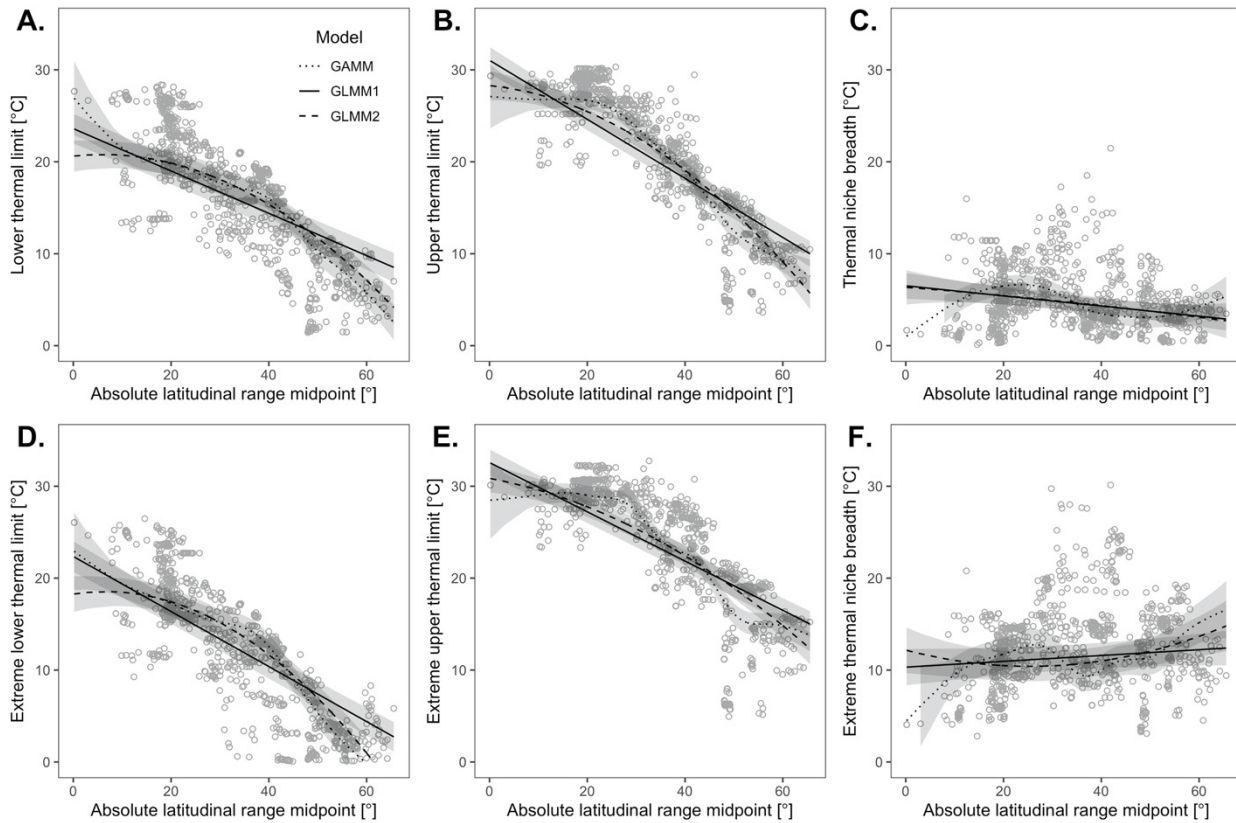
Supplementary Figure 2.6. Latitudinal trend in lower and upper thermal limits, and niche breadth of marine phytoplankton derived from annual average *SST* (A – C) and seasonal extreme *SST* (D – F). The points correspond to estimated thermal traits of geographic variant in phytoplankton fitted against the absolute latitudinal range midpoint, and the regression lines represent the fit from generalised linear mixed model with linear term only (*GLMM1*) and with both the linear and quadratic terms (*GLMM2*), and generalised additive model with cubic regression splines (*GAMM*). The 95% confidence intervals are represented as error of the regression in grey shading.
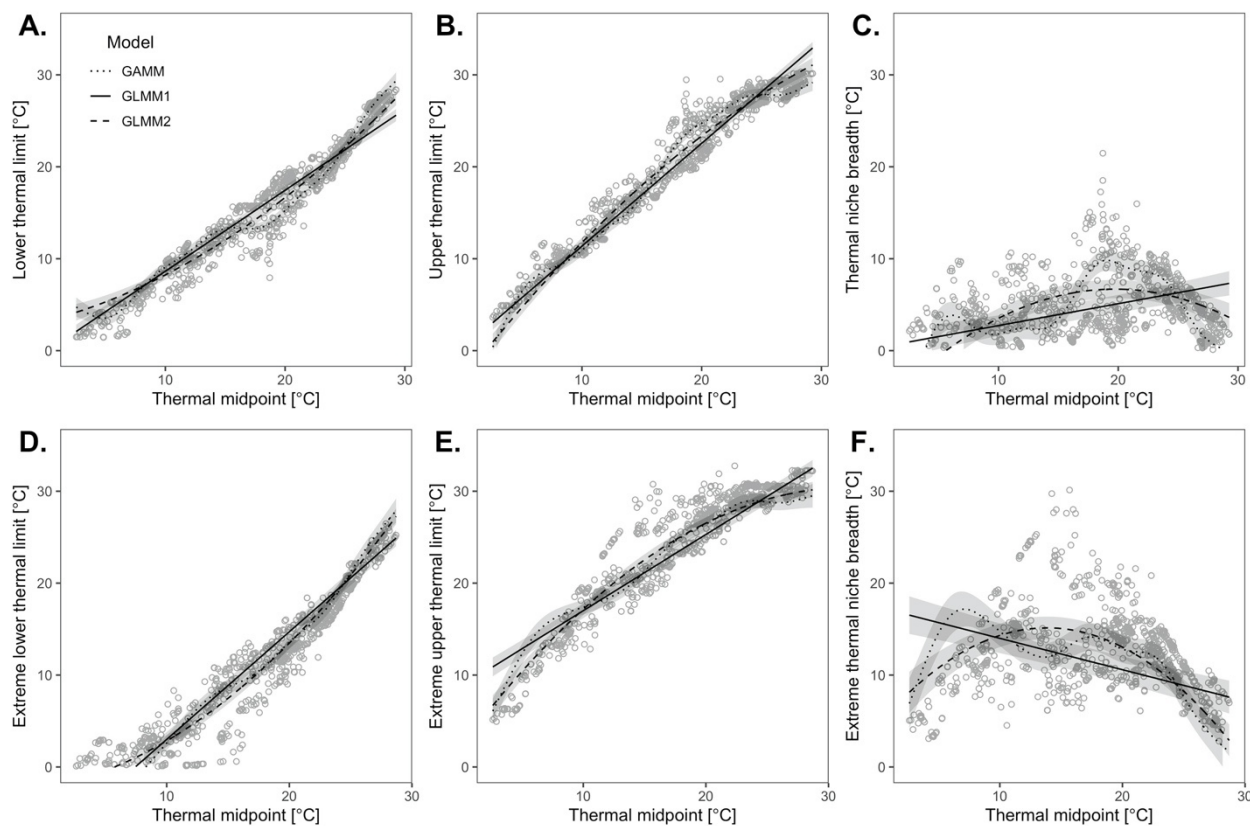
Supplementary Figure 2.7. Thermal trend in lower and upper thermal limits, and niche breadth in marine phytoplankton derived from annual average *SST* (A – C) and seasonal extreme *SST* (D – F). The points correspond to estimated thermal traits of geographic variant in phytoplankton fitted against the thermal midpoint, and the regression lines represent the fit from generalised linear mixed model with linear term only (*GLMM1*) and with both the linear and quadratic terms (*GLMM2*), and generalised additive model with cubic regression splines (*GAMM*). The 95% confidence intervals are represented as error of the regression in grey shading.
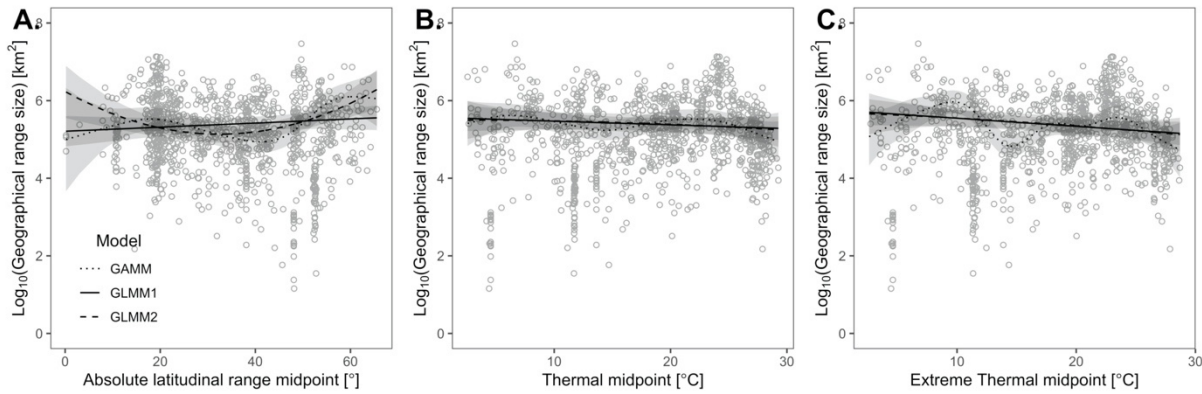
Supplementary Figure 2.8. Trend in geographical range size of marine phytoplankton across the gradient of latitude (A) and temperature (B and C). The points correspond to estimated thermal traits of geographic variant in phytoplankton fitted against the latitudinal and thermal midpoints, and the regression lines represent the fit from generalised linear mixed model with linear term only (*GLMM1*) and with both the linear and quadratic terms (*GLMM2*), and generalised additive model with cubic regression splines (*GAMM*). The 95% confidence intervals are represented as error of the regression in grey shading.
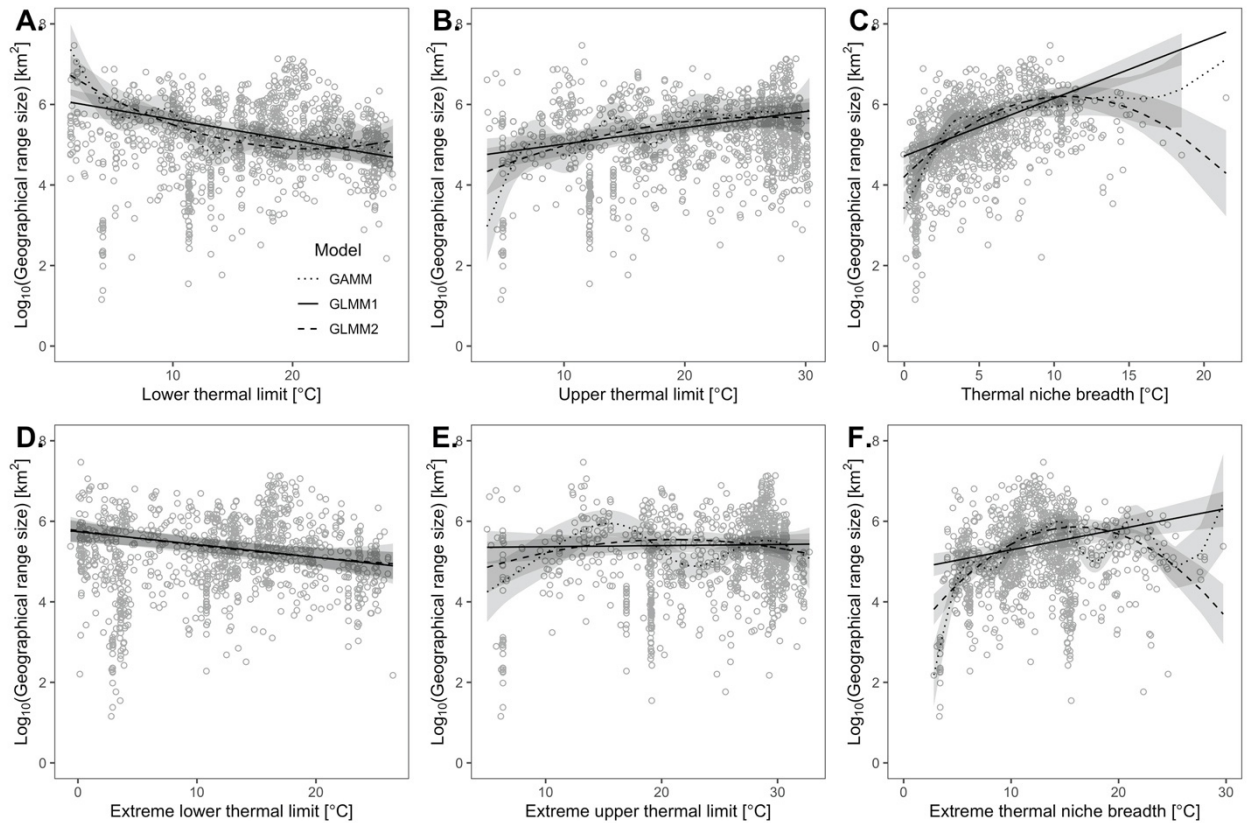
Supplementary Figure 2.9. Relationship between on geographic range size and thermal traits, i.e. lower and upper thermal limits, and geographic range size in marine phytoplankton derived from annual average *SST* (A – C) and seasonal extreme *SST* (D – F). The points correspond to estimated range size of geographic variant in phytoplankton fitted against the estimates of thermal traits, and the regression lines represent the fit from generalised linear mixed model with linear term only (*GLMM1*) and with both the linear and quadratic terms (*GLMM2*), and generalised additive model with cubic regression splines (*GAMM*). The 95% confidence intervals are represented as error of the regression in grey shading.
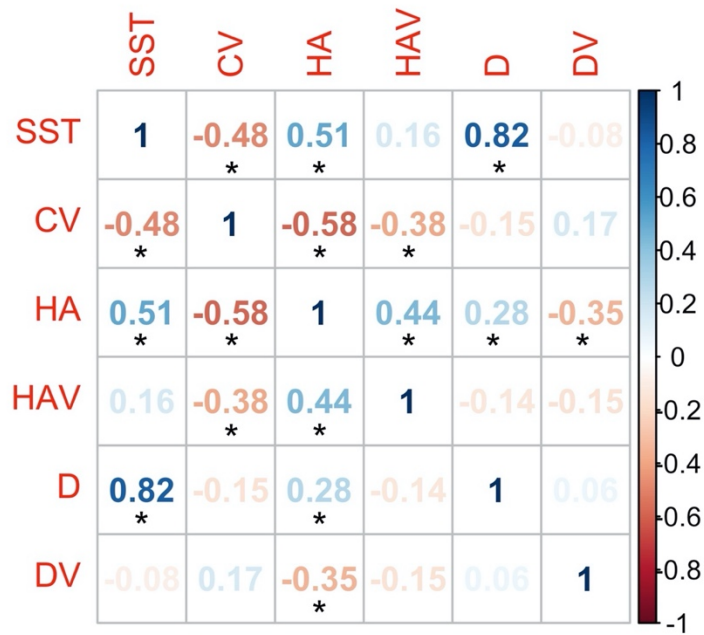
Note: * p value < 0.05

Supplementary Figure 2.10. Correlogram showing the correlation between the environmental variables, including sea surface temperature (*SST*), climate variability (*CV*), habitat availability (*HA*) habitat availability variability (*HAV*), diversity (*D*), and diversity variability (*DV*). Values with an asterisk (*) indicate significance of the correlation 95% confidence level.
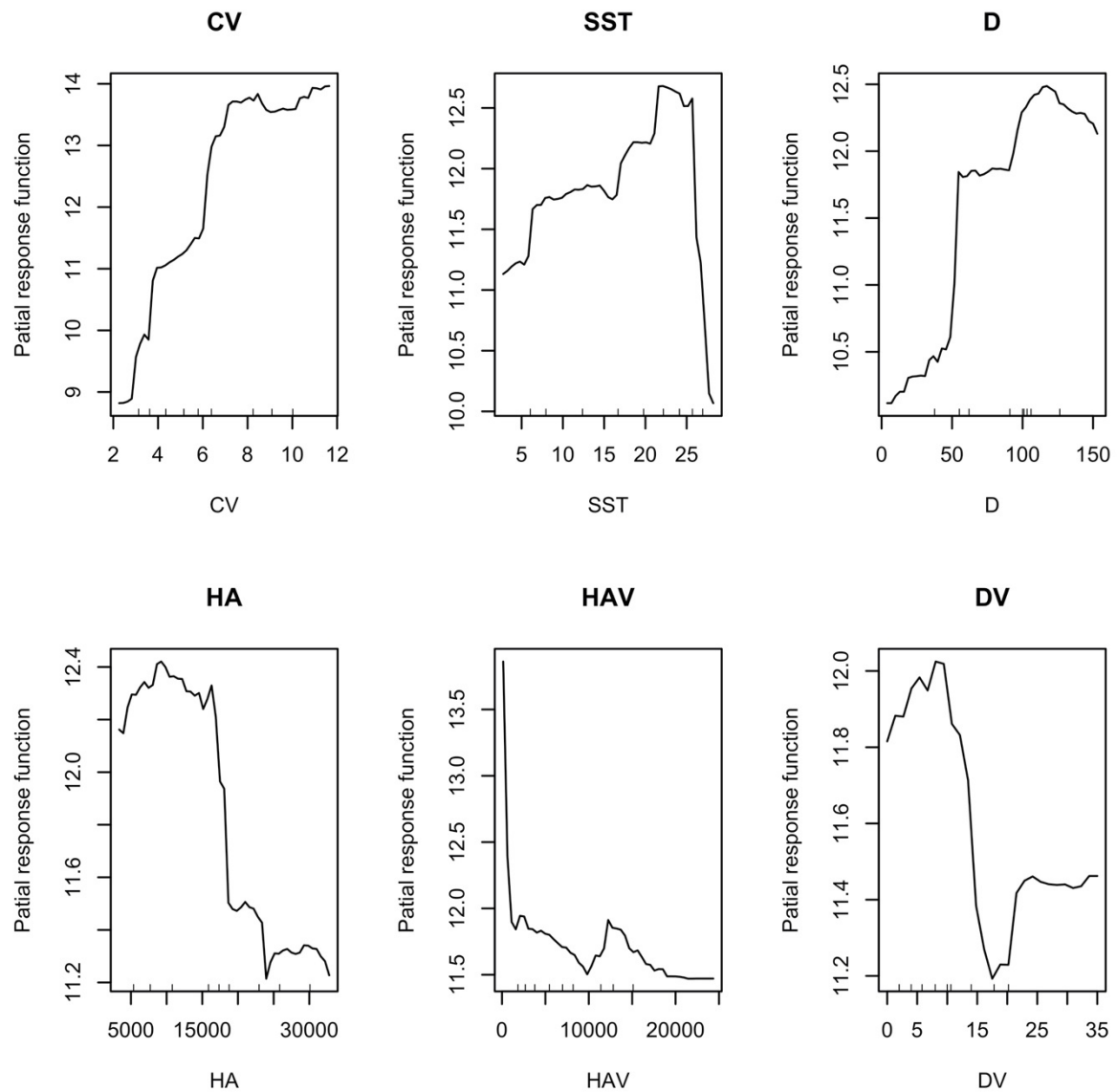
Supplementary Figure 2.11. Partial response plots of explanatory variables for thermal niche breadth such as sea surface temperature (*SST*), climate variability (*CV*), habitat availability (*HA*) habitat availability variability (*HAV*), diversity (*D*), and diversity variability (*DV*). The plots are arranged according to the relative importance of variables as predictors for niche breadth in a random forest model.
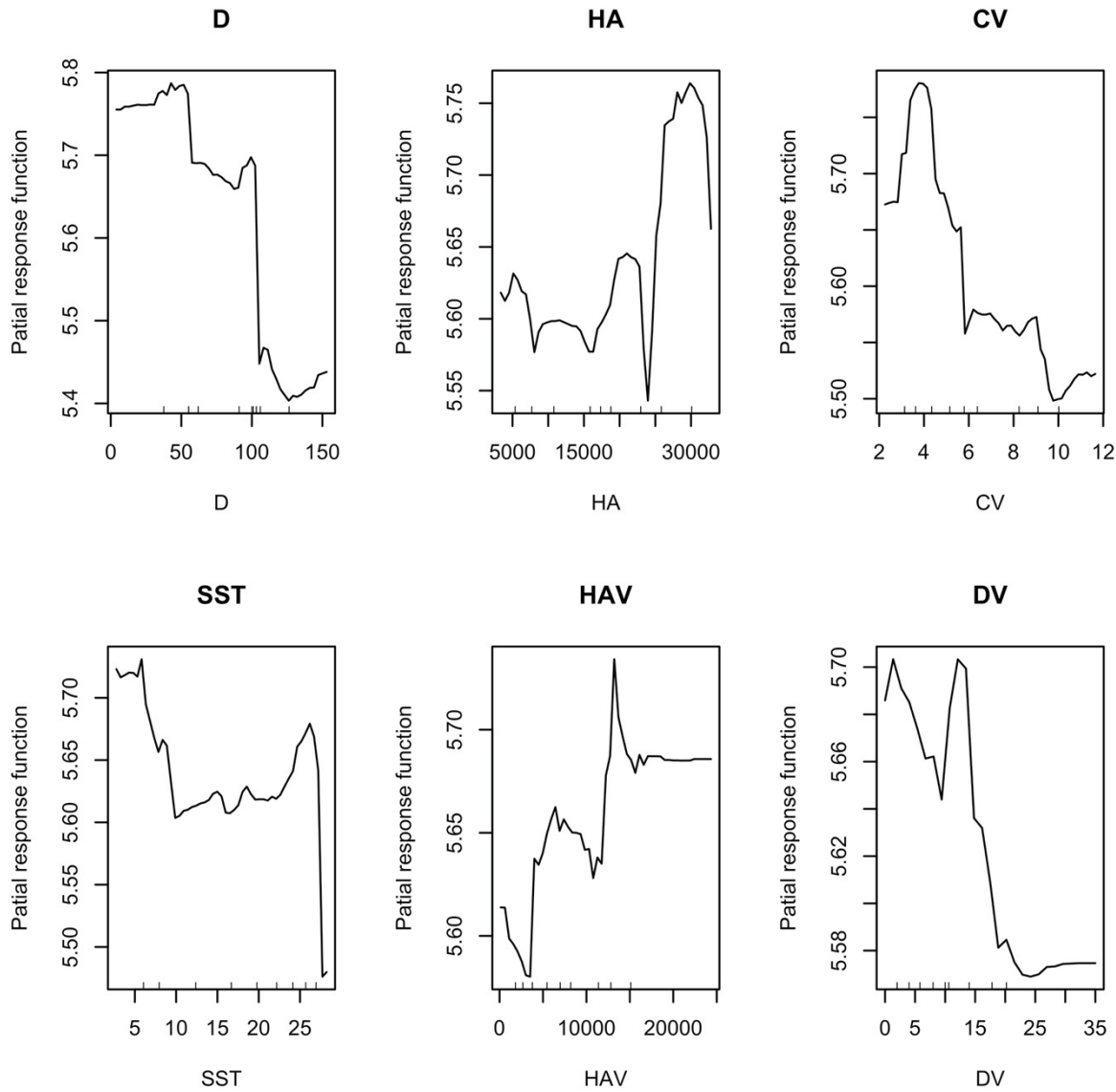
Supplementary Figure 2.12. Partial response plots of explanatory variables for geographic range size such as sea surface temperature (*SST*), climate variability (*CV*), habitat availability (*HA*) habitat availability variability (*HAV*), diversity (*D*), and diversity variability (*DV*). The plots are arranged according to the relative importance of variables as predictors for the range size in a random forest model.
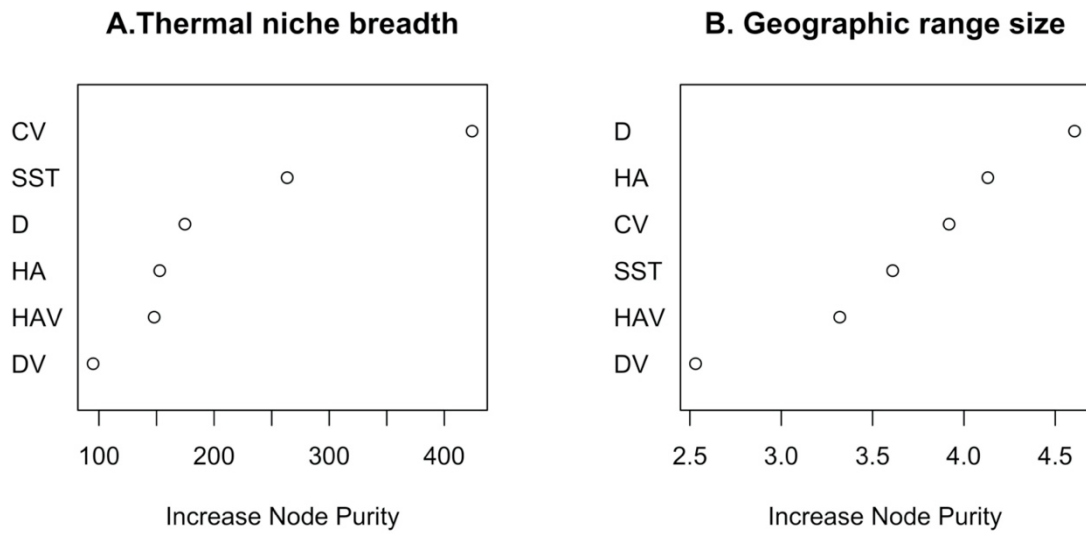
Supplementary Figure 2.13. Relative importance of explanatory variables for thermal niche (A) geographic range size (A) such as sea surface temperature (*SST*), climate variability (*CV*), habitat availability (*HA*) habitat availability variability (*HAV*), diversity (*D*), and diversity variability (*DV*). *CV* and and *SST* are the relatively most important predictors for thermal niche breadth. On the hand, *D* and *HA* are the relatively most important predictors for geographic range size.
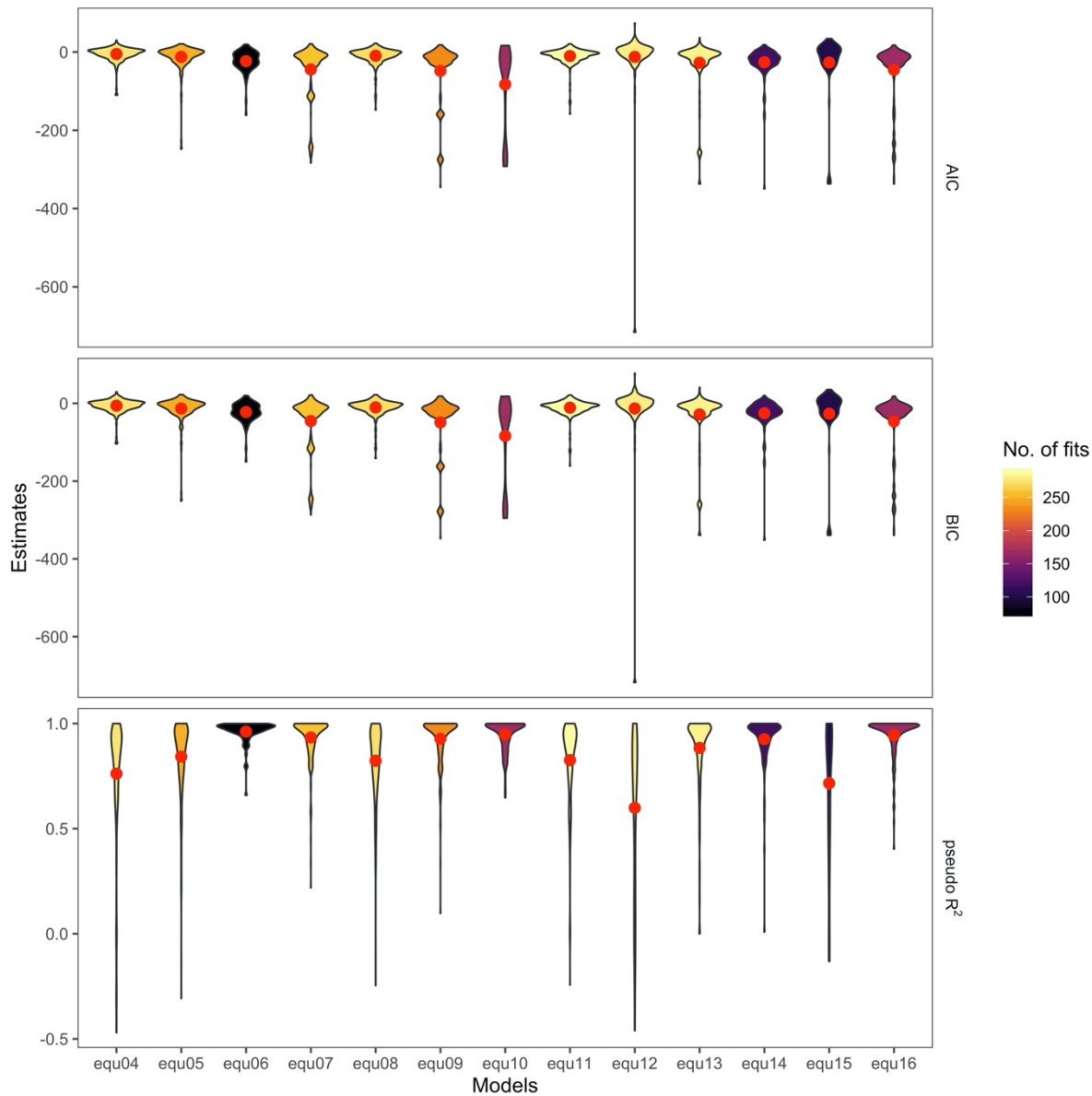
Supplementary Figure 3.1. Akaike Information Criteria (*AIC*), Bayesian Information Criterion (*BIC*), and coefficient of determination (*pseudo R²*) of the non-linear models (i.e. equ04 – equ15 in Low-Décarie *et al.* 2017, and equ16 (i.e. *CTMI* in (Rosso et al., 1993); see Supplementary Information SI2 for description of the models) used to fit growth rates across against temperature. The red point indicates the mean of the statistical estimate. The colour bar indicates the number of successful fits. Both equ10 and equ16 were initially selected as the best models since they had relatively lower *AIC* and *BIC* values and had relatively higher *pseudo R²*.
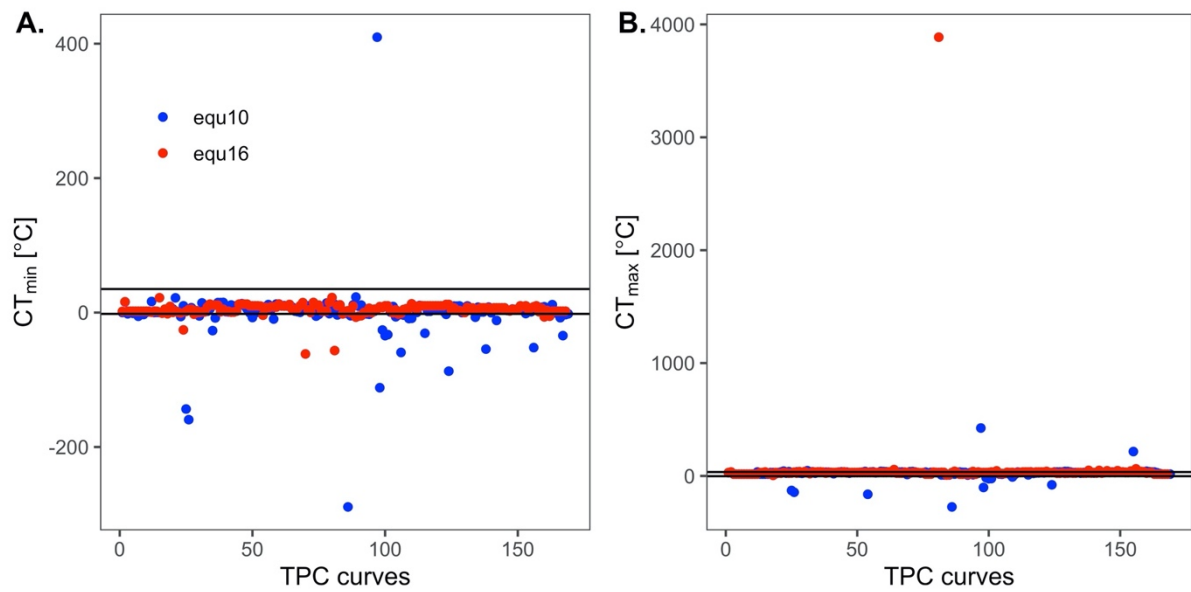
Supplementary Figure 3.2. Critical thermal minimum (CT_{min}) and critical thermal maximum (CT_{max}) predicted from equ10 and equ16. The solid lines indicate the minimum and maximum sea surface temperature ever recorded in 2002 – 2009 (https://earthobservatory.nasa.gov/global-maps/MYD28M). *CTMI* model (i.e. equ16) had produced more realistic estimates of the cardinal temperatures, and hence was preferably used in the succeeding analysis.
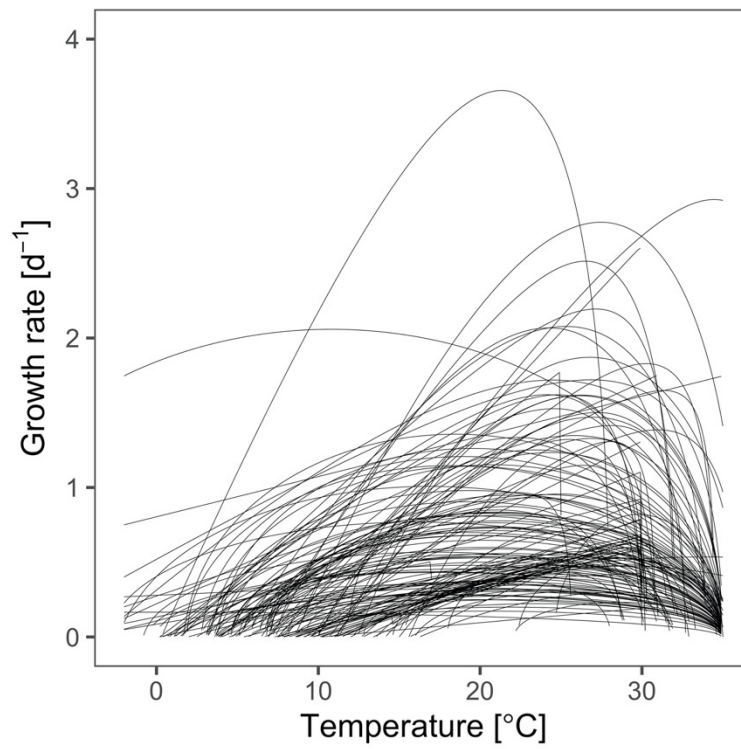
Supplementary Figure 3.3. Thermal performance curves fitted using Cardinal Temperature Model with Inflexion (*CTMI*), which were used to derive the thermal physiology traits.
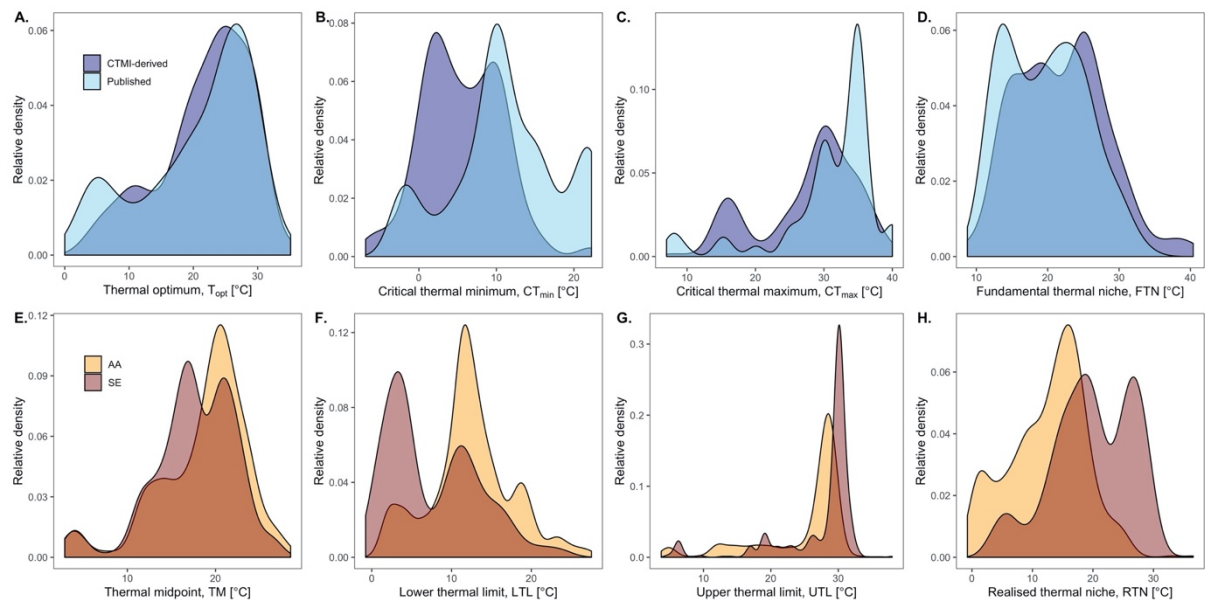
Supplementary Figure 3.4. Density plots illustrating the relative distribution of thermal traits in the *CTMI*-derived and published datasets (A – D) and in species occurrence dataset (E – H). Occurrence-based thermal traits were derived from annual average (*AA*) and seasonal extreme (*SE*) sea surface temperature (*SST*).
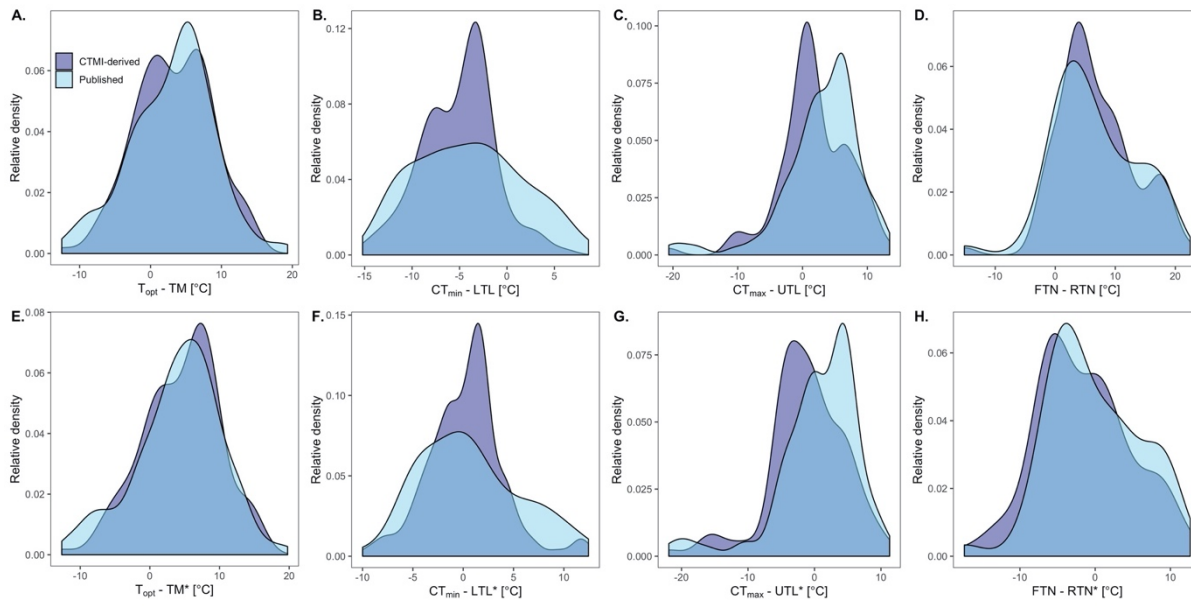
Supplementary Figure 3.5. Density plots illustrating the relative distribution of the difference between physiology- and occurrence-based estimates of thermal traits ($TT_p – TT_o$). Published and *CTMI*-derived TT_p were subtracted by TT_o derived from annual average (A – D) and seasonal extreme (E – H) sea surface temperature (*SST*).
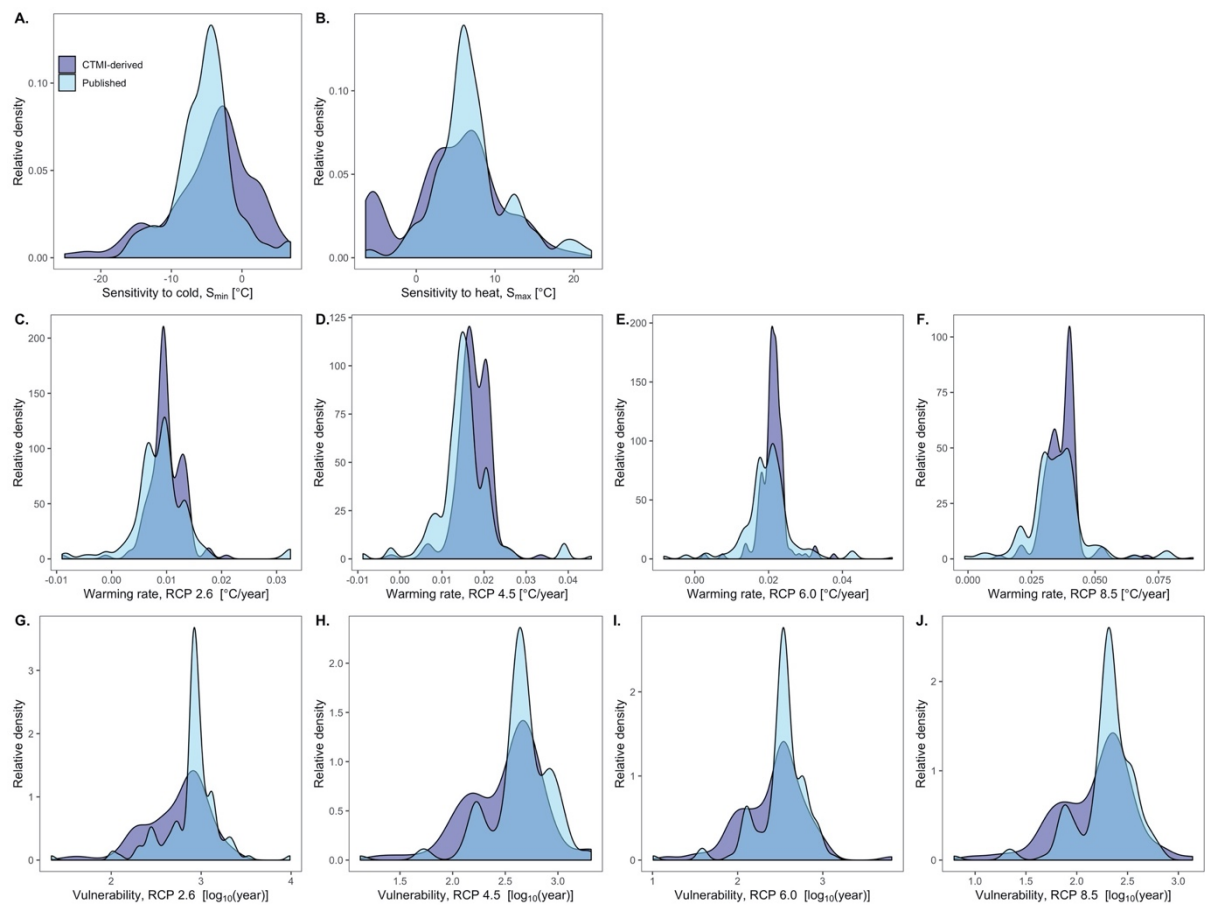
Supplementary Figure 3.6. Density plots illustrating the relative distribution of sensitivity to cold temperature (A) and warm temperature (B), warming exposure (C – F), and vulnerability to warming (G – J). Warming vulnerability are computed based on different climate scenarios (i.e. *RCP 2.6*, *RCP 4.5*, *RCP 6.0*, and *RCP 8.5*).
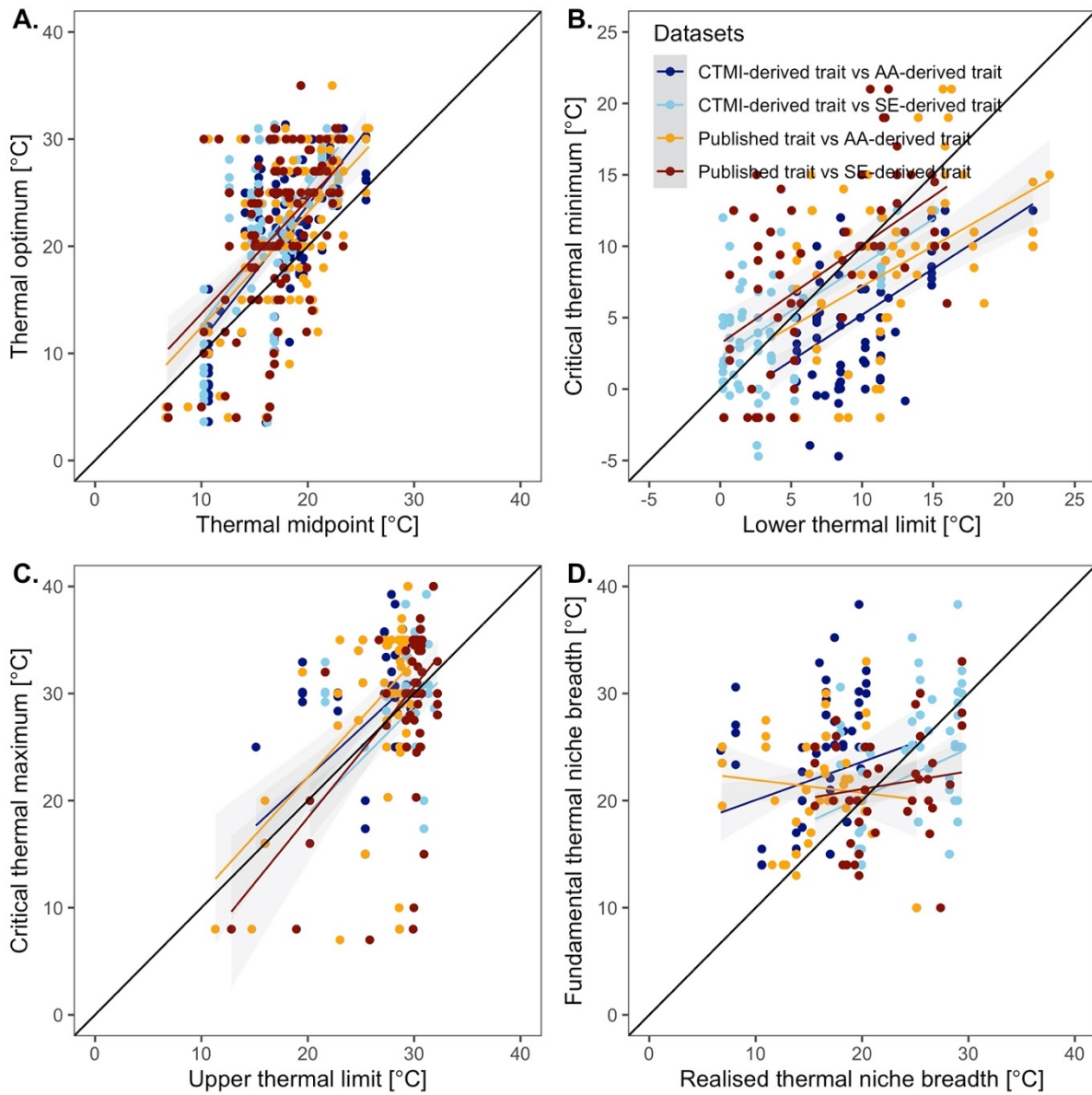
Supplementary Figure 3.7. Relationship between physiology- and occurrence-based estimates of thermal traits (TT_p and TT_o, respectively) in marine phytoplankton. TT_p were fitted against TT_o using generalised linear models (*GLM*; see Supplementary Table 3.1 for the summary statistics). The regression lines are indicated in color solid lines with 95% confidence interval in grey shading. The black solid lines represent equality between TT_p and TT_o.
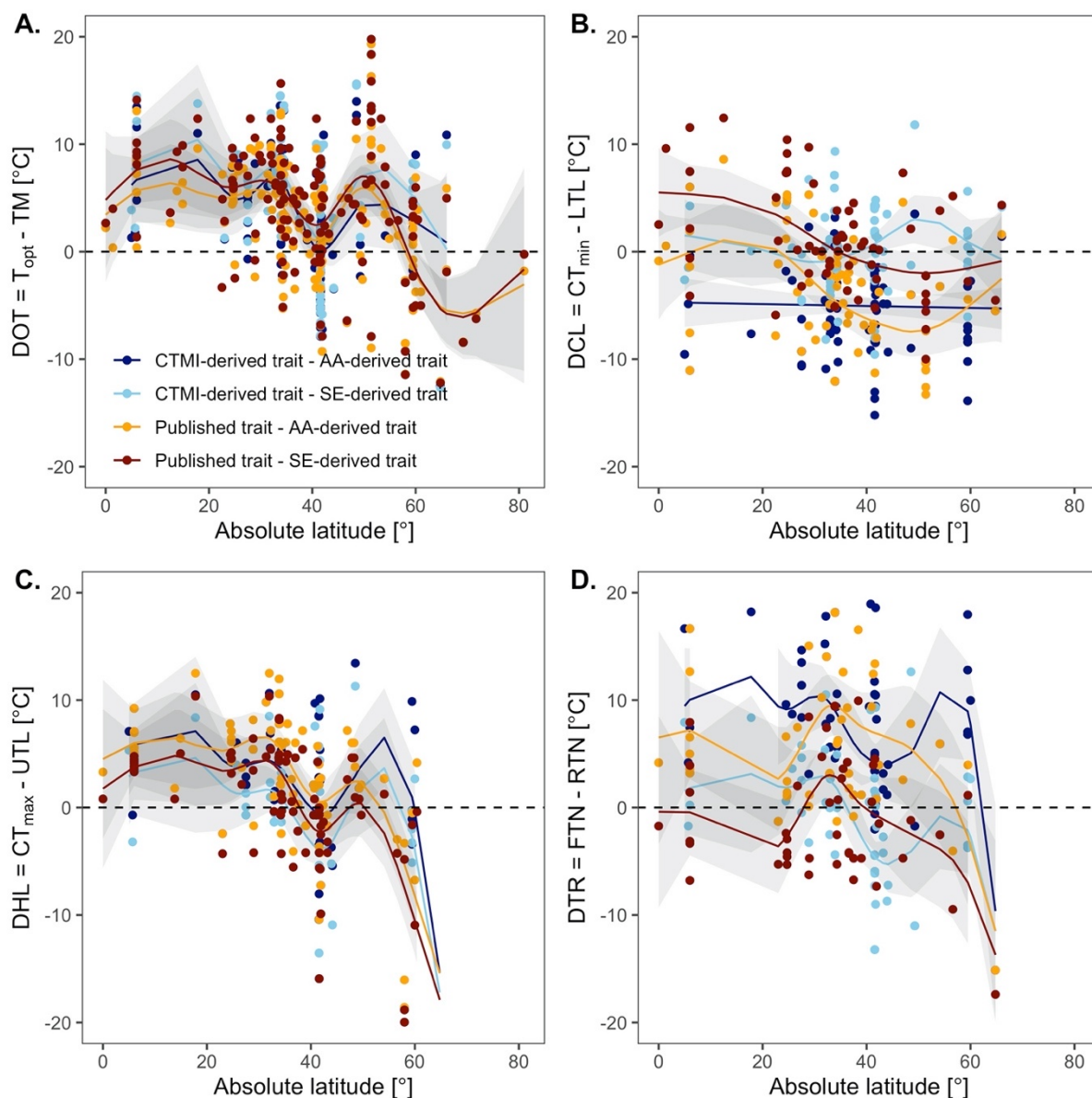
Supplementary Figure 3.8. Latitudinal trends in the difference between physiology- and occurrence-based thermal traits ($TT_p – TT_o$) in marine phytoplankton. The estimates of $TT_p – TT_o$ were fitted against latitude using generalised additive models (*GAM*; see Supplementary Table 3.2 for the summary statistics). The regression lines are indicated in blue solid lines with 95% confidence interval in grey shading. The horizontal broken line indicates the difference is zero.
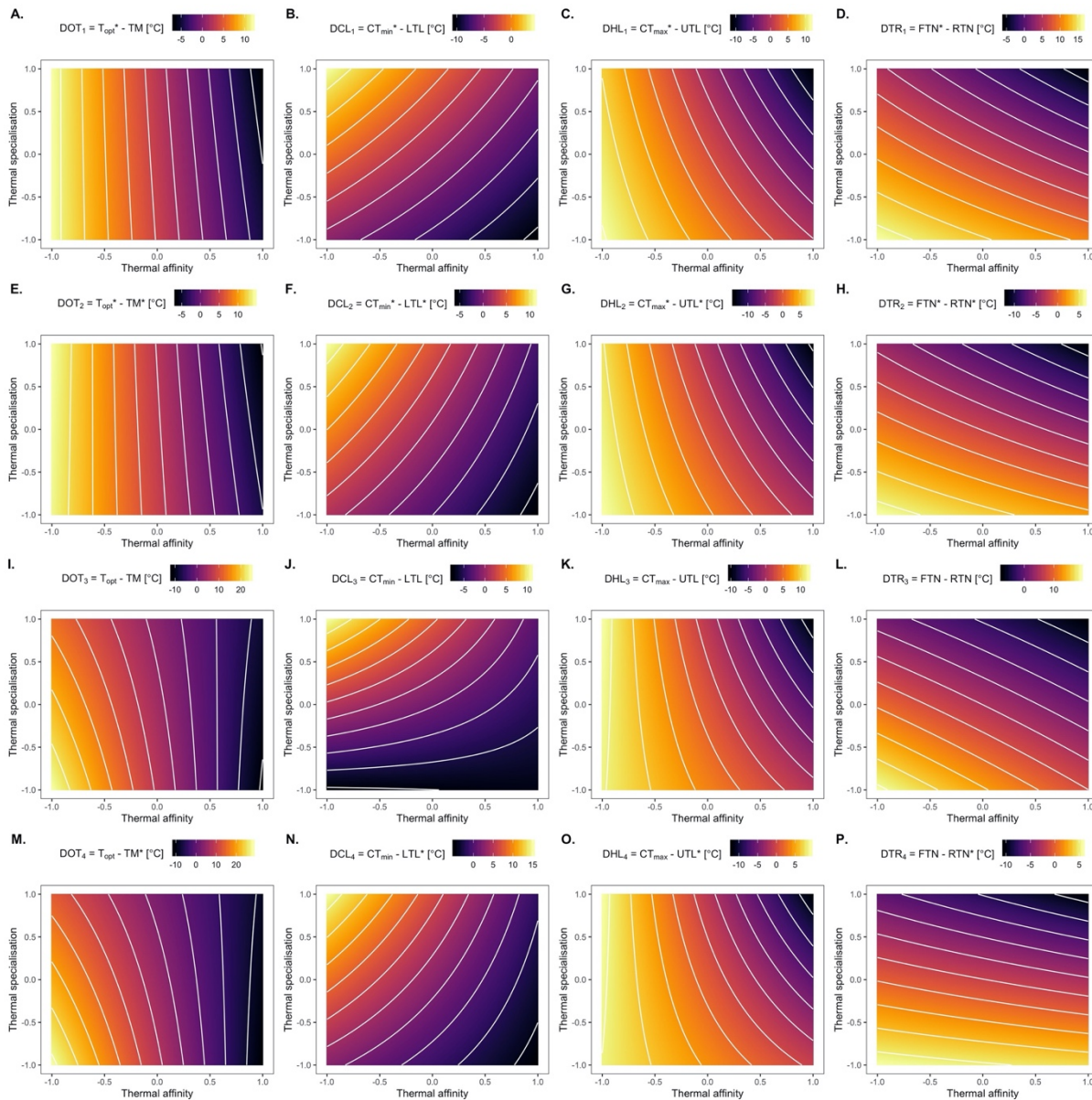
Supplementary Figure 3.9. Contour plots of the difference between physiology- and occurrence-based thermal traits ($TT_p - TT_o$) in marine phytoplankton across thermal affinity and thermal specialisation. The estimates of $TT_p - TT_o$ were fitted against thermal affinity and thermal specialisation using generalised linear models (*GLM*; see Supplementary Table 3.4 for the summary statistics). The *GLMs* were used to construct the contour plots. The colour bars indicate the estimates of $TT_p - TT_o$.
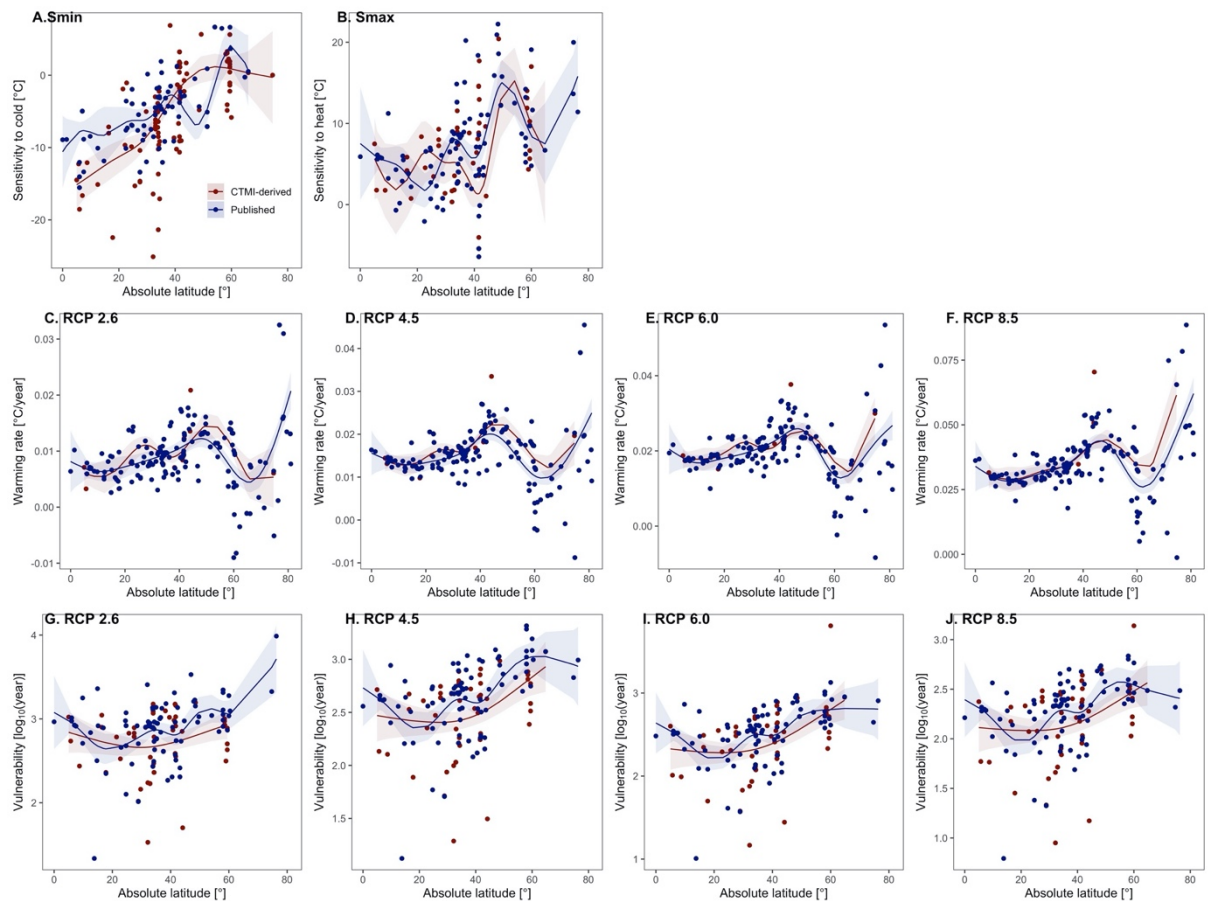
Supplementary Figure 3.10. Latitudinal trends in thermal sensitivity (S_{min} and S_{max}), warming exposure (WR), and vulnerability to warming (V) in marine phytoplankton. The estimates were obtained from *CTMI*-derived dataset (indicated by an asterisk) and published dataset. The warming rate and vulnerability were computed based on different climate scenarios (i.e. *RCP* 2.6, *RCP* 4.5, *RCP* 6.0, and *RCP* 8.5). The estimates were fitted against latitude using generalised additive models (*GAM*; see Supplementary Table 3.3 for the summary statistics). The regression lines are indicated in solid lines with 95% confidence interval in grey shading.
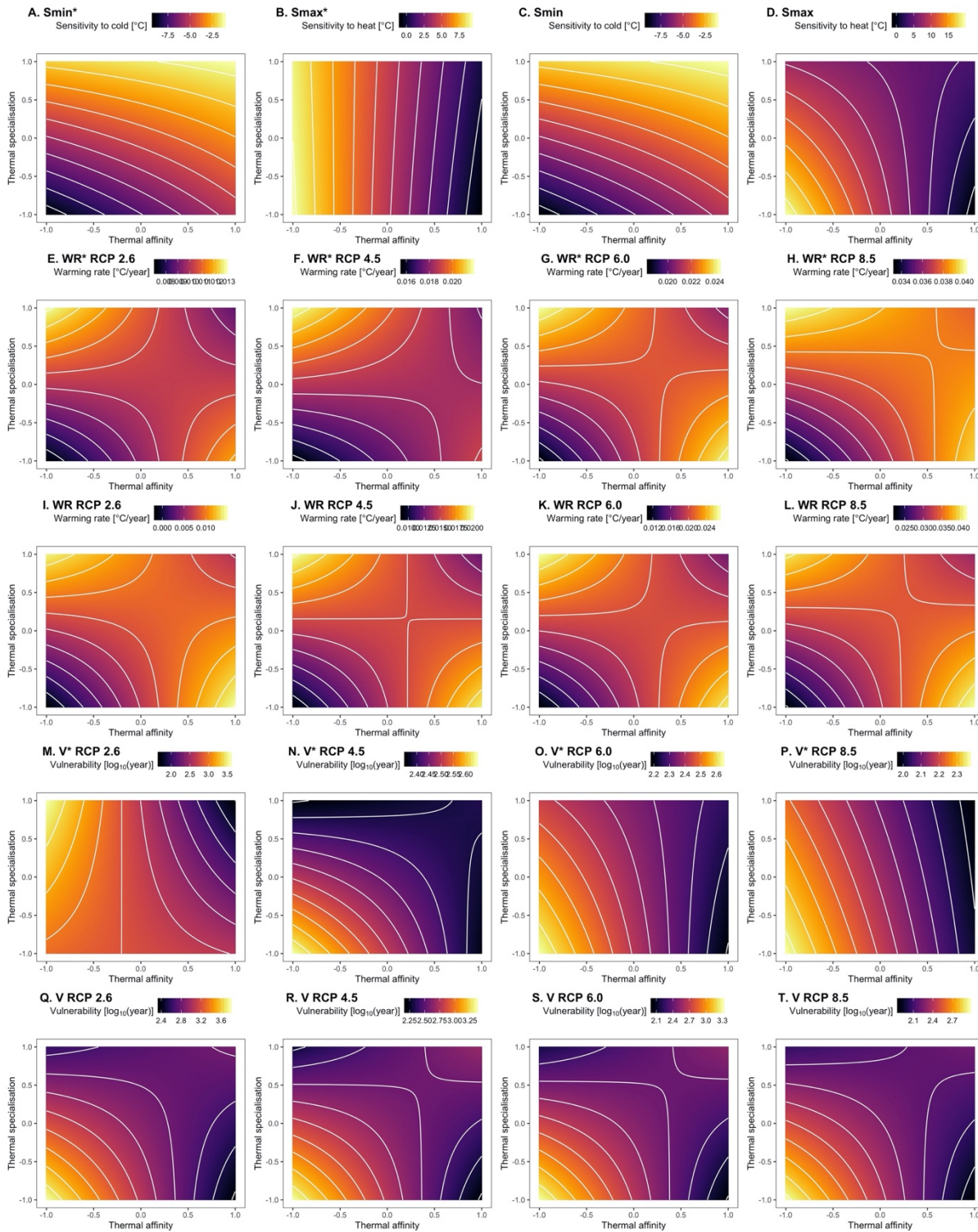
Supplementary Figure 3.11. Contour plots of thermal sensitivity (S_{min} and S_{max}), warming exposure (*WR*), and vulnerability to warming (*V*) in marine phytoplankton across and across thermal affinity and thermal specialisation. The estimates were obtained from *CTMI*-derived dataset (indicated by an asterisk) and published dataset. The warming rate and vulnerability were computed based on different climate scenarios (i.e. *RCP* 2.6, *RCP* 4.5, *RCP* 6.0, and *RCP* 8.5). The estimates were fitted against thermal affinity and thermal specialisation using generalised linear models (*GLM*; see Supplementary Table 3.5 for the summary statistics). The *GLMs* were used to construct the contour plots.
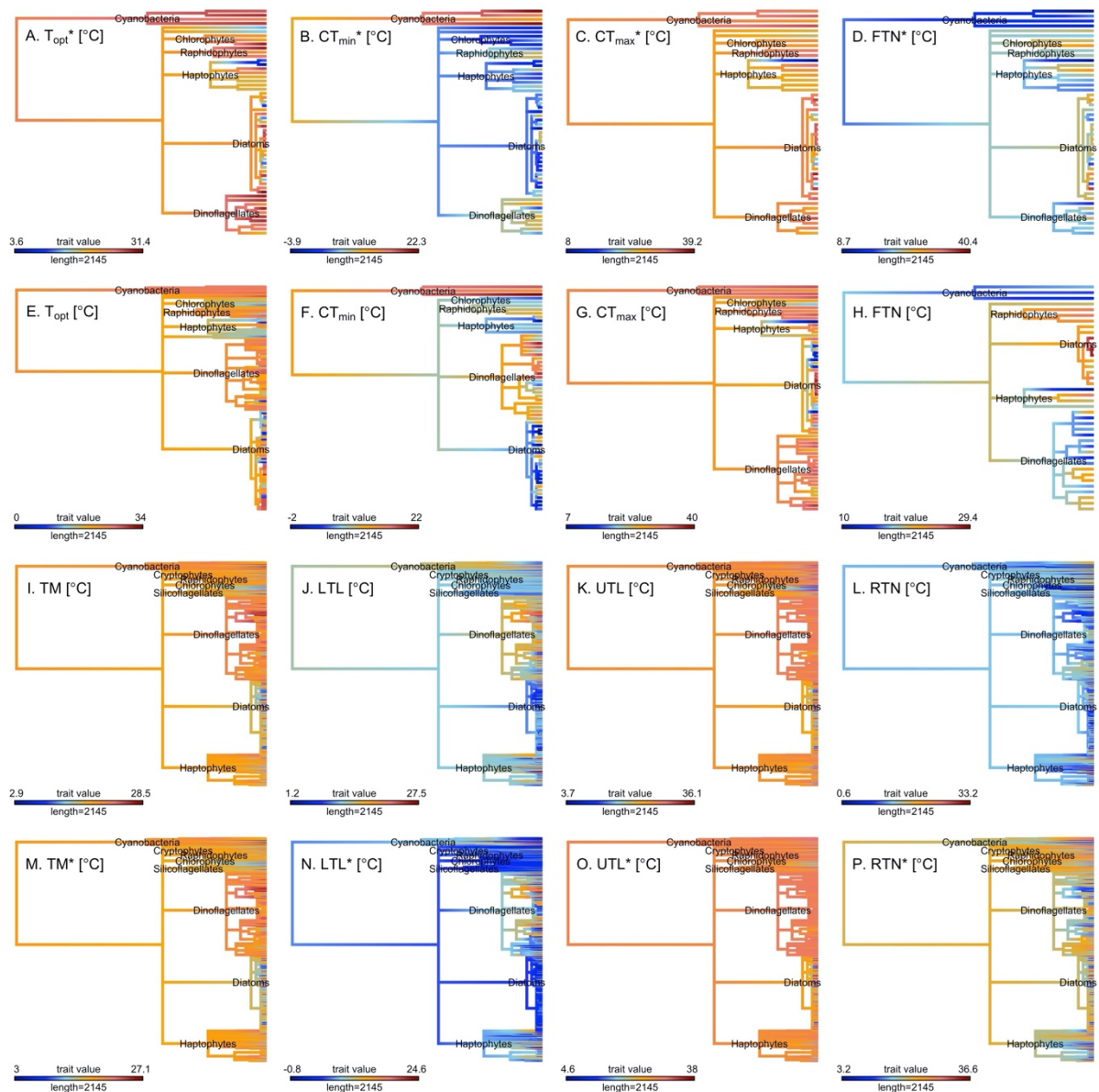
Supplementary Figure 3.12. Phylogenetic distribution of the thermal traits estimated from physiology data (TT_p) and occurrence data (TT_o) in marine phytoplankton. Estimates of TT_p were obtained from *CTMI* fitting (A – D) and published literature (E – H). Estimates of TT_o were derived from annual average *SST* (I – L) and seasonal extreme *SST* (M – P). Colours indicate trait value, as shown by the colour bar below each tree.

Supplementary Figure 3.13. Phylogenetic distribution of the difference between the thermal traits estimated from physiology data (TT_p) and occurrence data (TT_o) in marine phytoplankton. Estimates of TT_p were obtained from *CTMI* fitting (indicated by an asterisk) and published literature, whilst estimates of TT_o were derived from annual average *SST* and seasonal extreme *SST* (indicated by an asterisk). These were merged and matched up by species, resulting to four sets of datasets: (1) TT_p* and TT_o (A – D), (2) TT_p* and TT_o* (E – H), (3) TT_p and TT_o (I – L), and (4) TT_p and TT_o* (M – P). These datasets were used to compute for the difference in optimal temperature (*DOT*), cold tolerance limit (*DCL*), heat tolerance limit (*DHL*), and thermal range (*DTR*). Colours indicate trait value, as shown by the colour bar below each tree.
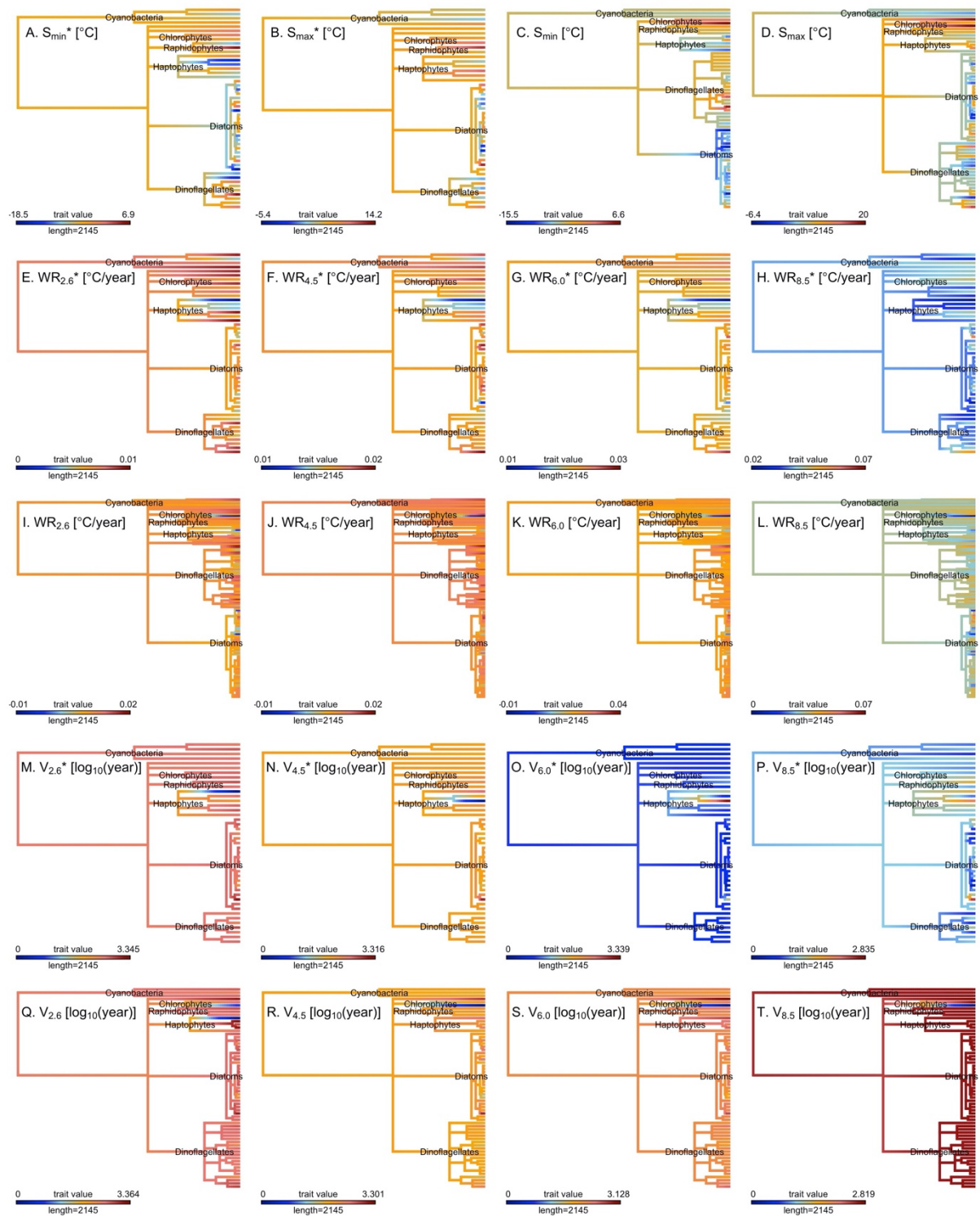
Supplementary Figure 3.14. Phylogenetic distribution of the sensitivity to cold temperature (S_{min}; A and C), sensitivity to warm temperature (S_{max}; B and D), warming exposure (*WR*; E – L), and warming vulnerability (*V*; M – T) in marine phytoplankton. The estimates were obtained from *CTMI*-derived dataset (indicated by an asterisk) and published dataset. The warming rate and vulnerability were computed based on different climate scenarios (i.e. *RCP* 2.6, *RCP* 4.5, *RCP* 6.0, and *RCP* 8.5). Colours indicate trait value, as shown by the colour bar below each tree.

Supplementary Figure 3.15. Percentage of variation in thermal traits estimated from physiology data (TT_p) and occurrence data (TT_o) in marine phytoplankton explained by different taxonomic levels according to a variance partitioning analysis. Estimates of TT_p were obtained from *CTMI* fitting (A – D) and published literature (E – H). Estimates of TT_o were derived from annual average *SST* (I – L) and seasonal extreme *SST* (M – P). Solid points represent the observed values, whilst the boxplots represent the distribution of values generated by the tip randomisation null model. All observed values are significant different from the null model at 95% confidence interval. The red and blue points indicate that observed values are lower and higher than the null model, respectively.

Supplementary Figure 3.16. Percentage of variation in the difference between the thermal traits estimated from physiology data (TT_p) and occurrence data (TT_o) in marine phytoplankton explained by different taxonomic levels according to a variance partitioning analysis. Estimates of TT_p were obtained from *CTMI* fitting (indicated by an asterisk) and published literature, whilst estimates of TT_o were derived from annual average *SST* and seasonal extreme *SST* (indicated by an asterisk). These were merged and matched up by species, resulting to four sets of datasets: (1) TT_p * and TT_o (A – D), (2) TT_p * and TT_o* (E – H), (3) TT_p and TT_o (I – L), and (4) TT_p and TT_o *(M – P). These datasets were used to compute for the difference in optimal temperature (*DOT*), cold tolerance limit (*DCL*), heat tolerance limit (*DHL*), and thermal range (*DTR*). Solid points represent the observed values, whilst the boxplots represent the distribution of values generated by the tip randomisation null model. All observed values are significant different from the null model at 95% confidence interval. The red and blue points indicate that observed values are lower and higher than the null model, respectively.

Supplementary Figure 3.17. Percentage of variation in the sensitivity to cold temperature (S_{min}; A and C), sensitivity to warm temperature (S_{max}; B and D), warming exposure (WR; E – L), and warming vulnerability (V; M – T) in marine phytoplankton explained by different taxonomic levels according to a variance partitioning analysis. The estimates were obtained from *CTMI*-derived dataset (indicated by an asterisk) and published dataset. The warming rate and vulnerability were computed based on different climate scenarios (i.e. *RCP* 2.6, *RCP* 4.5, *RCP* 6.0, and *RCP* 8.5). Solid points represent the observed values, whilst the boxplots represent the distribution of values generated by the tip randomisation null model. All observed values are significant different from the null model at 95% confidence interval. The red and blue points indicate that observed values are lower and higher than the null model, respectively.
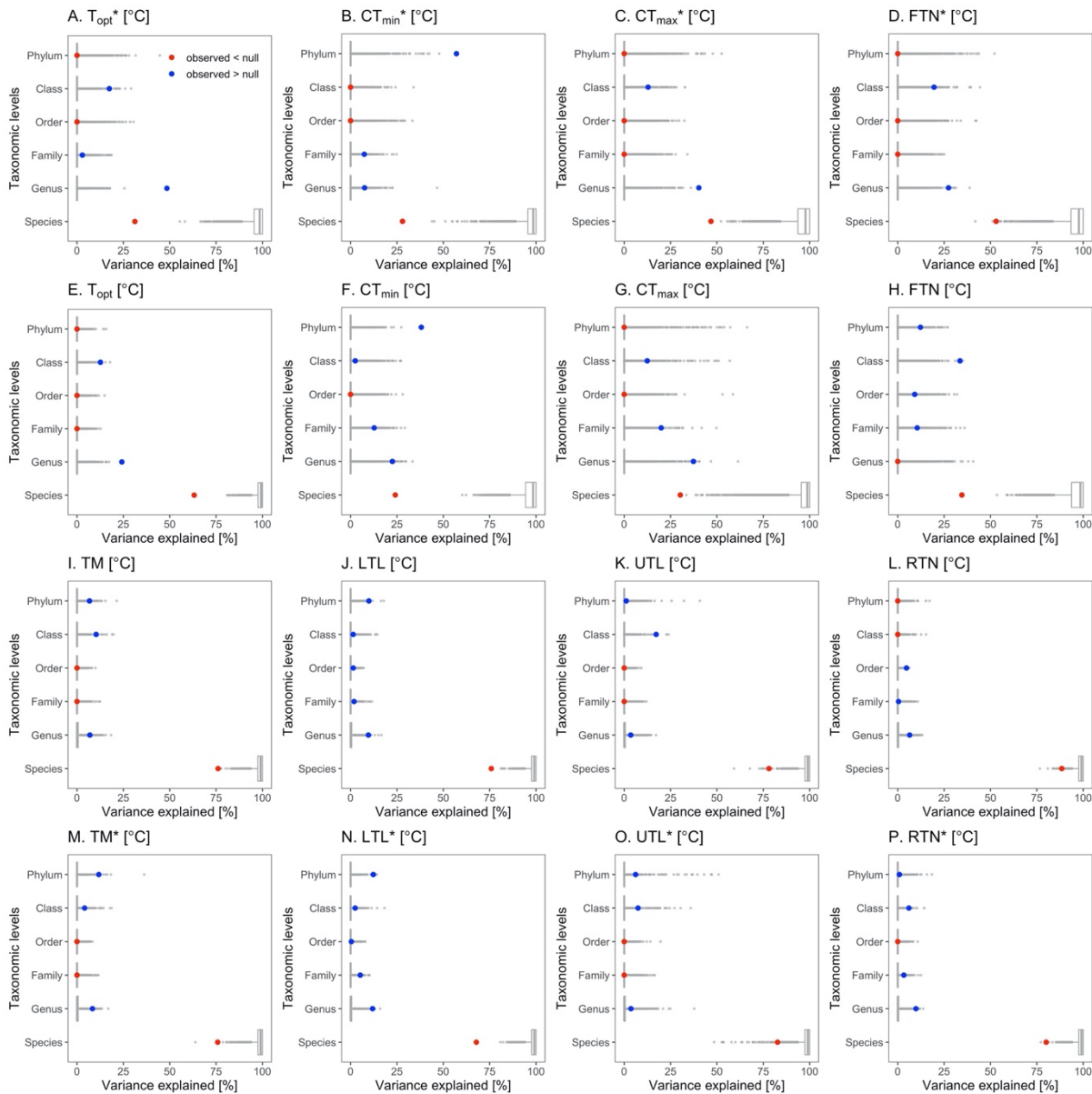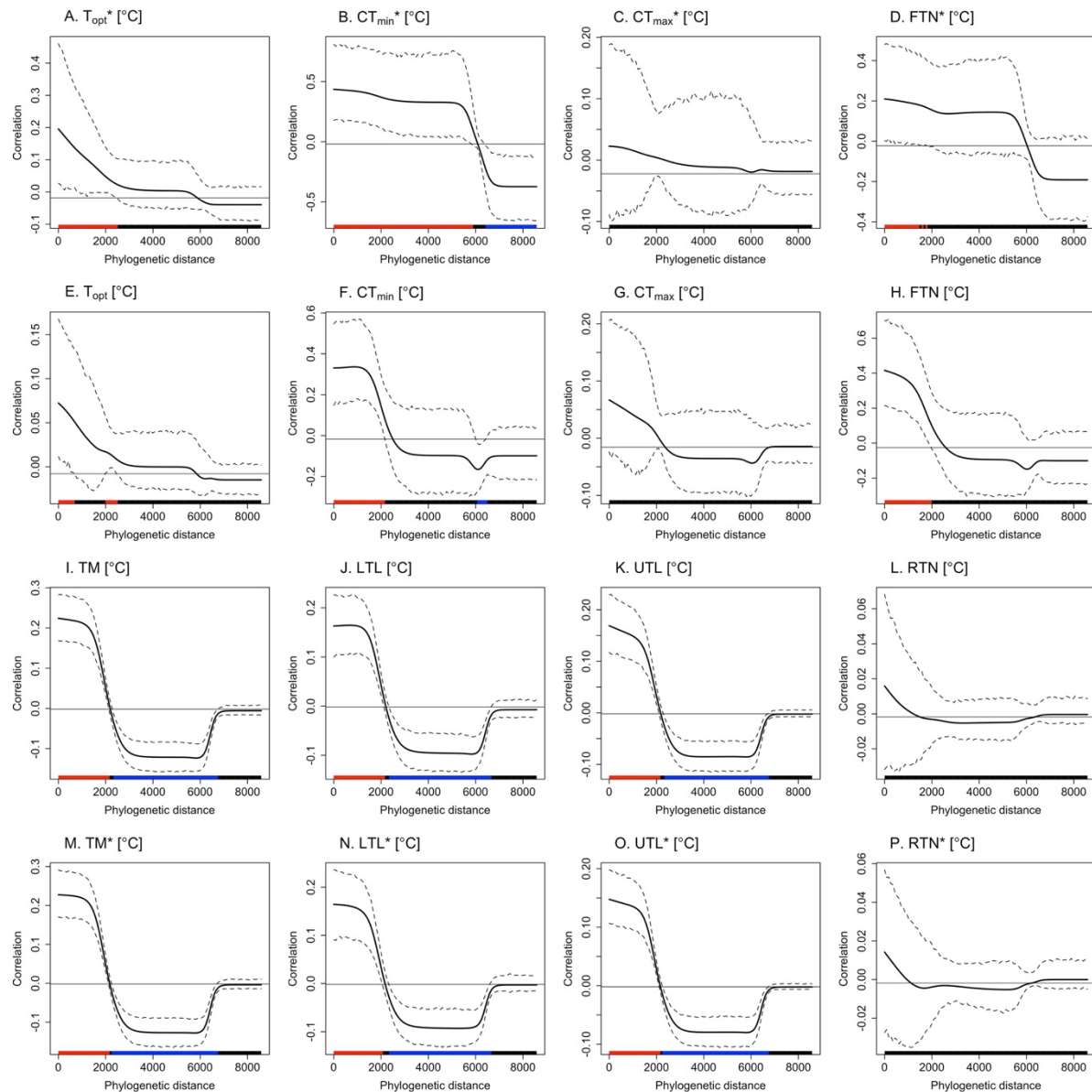
Supplementary Figure 3.18. Phylogenetic correlograms for the thermal traits estimated from physiology data (TT_p) and occurrence data (TT_o) in marine phytoplankton. Estimates of TT_p were obtained from *CTMI* fitting (A – D) and published literature (E – H). Estimates of TT_o were derived from annual average *SST* (I – L) and seasonal extreme *SST* (M – P). The solid black lines indicate the Moran's I index autocorrelation, and the dashed black lines indicate the 95% confidence interval. The horizontal black lines represent the estimated value of Moran's I under the null hypothesis of no phylogenetic autocorrelation. The red and blue colored bars indicate significant positive and negative autocorrelation, respectively; whilst, the black colored bars indicate a non-significant autocorrelation.
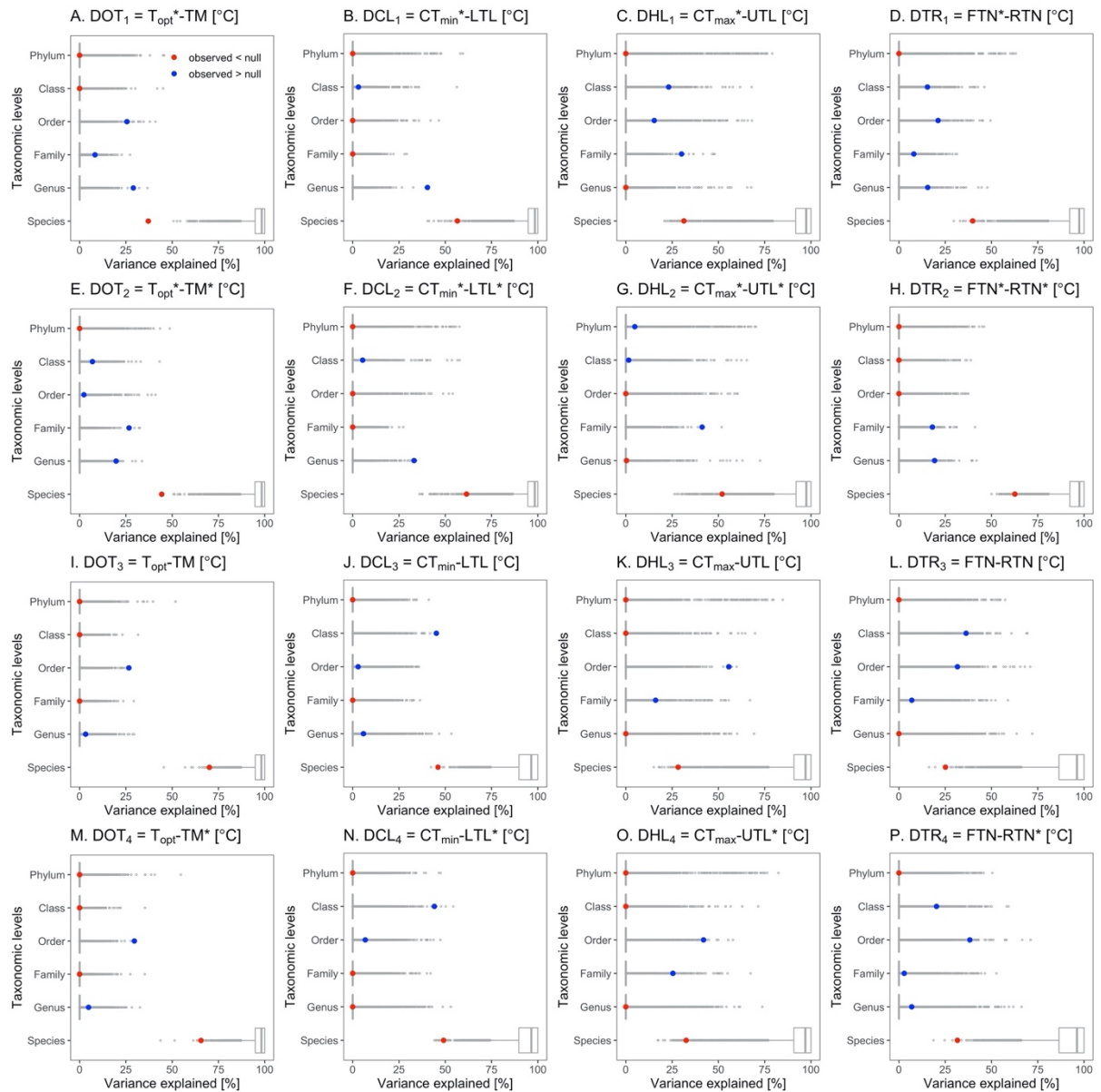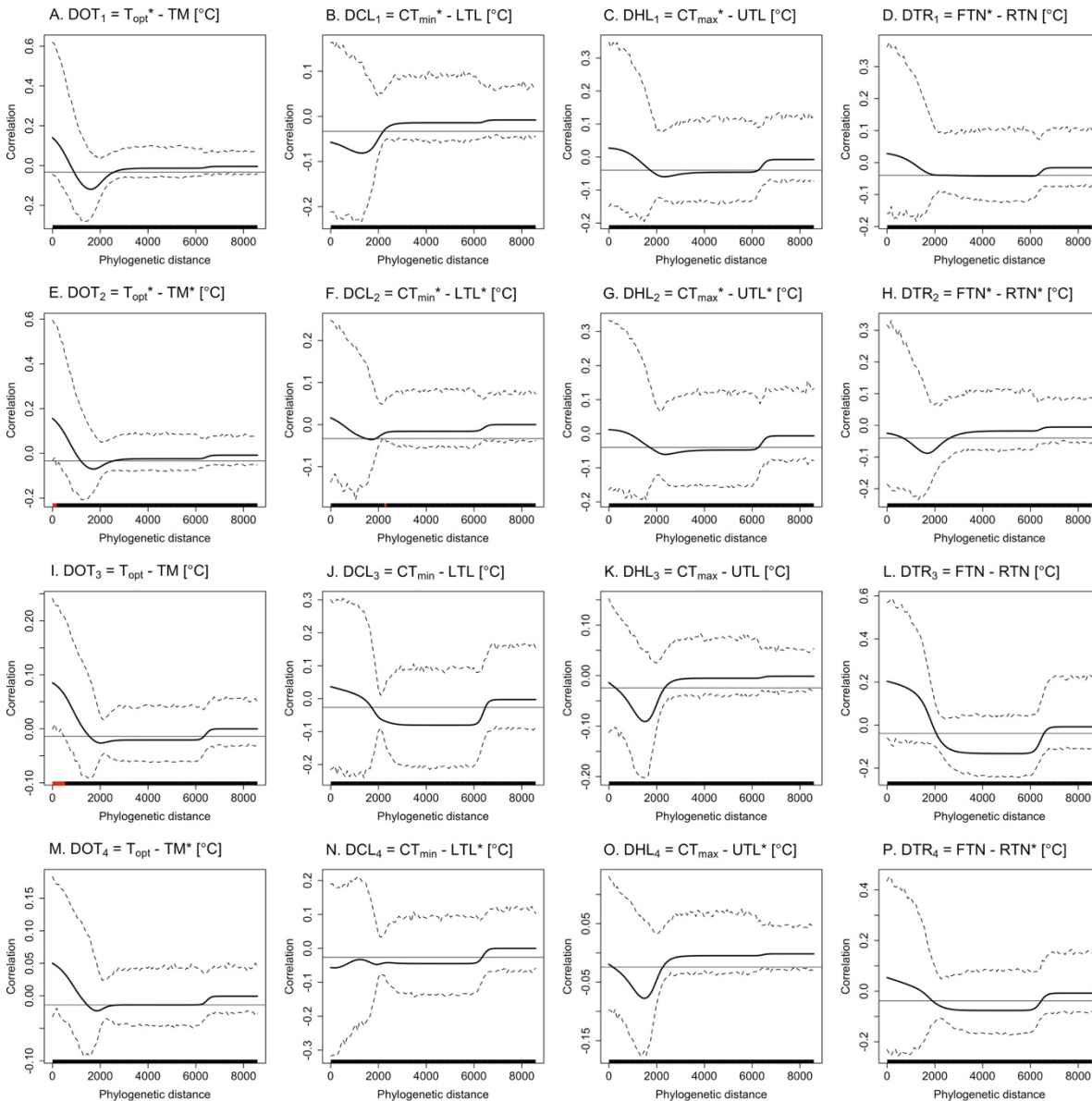
Supplementary Figure 3.19. Phylogenetic correlograms for the difference between the thermal traits estimated from physiology data (TT_p) and occurrence data (TT_o) in marine phytoplankton. Estimates of TT_p were obtained from *CTMI* fitting (indicated by an asterisk) and published literature, whilst estimates of TT_o were derived from annual average *SST* and seasonal extreme *SST* (indicated by an asterisk). These were merged and matched up by species, resulting to four sets of datasets: (1) TT_p * and TT_o (A – D), (2) TT_p * and TT_o * (E – H), (3) TT_p and TT_o (I – L), and (4) TT_p and TT_o * (M – P). These datasets were used to compute for the difference in optimal temperature (*DOT*), cold tolerance limit (*DCL*), heat tolerance limit (*DHL*), and thermal range (*DTR*). The solid black lines indicate the Moran's I index autocorrelation, and the dashed black lines indicate the 95% confidence interval. The horizontal black lines represent the estimated value of Moran's I under the null hypothesis of no phylogenetic autocorrelation. The red and blue colored bars indicate significant positive and negative autocorrelation, respectively; whilst, the black colored bars indicate a non-significant autocorrelation.
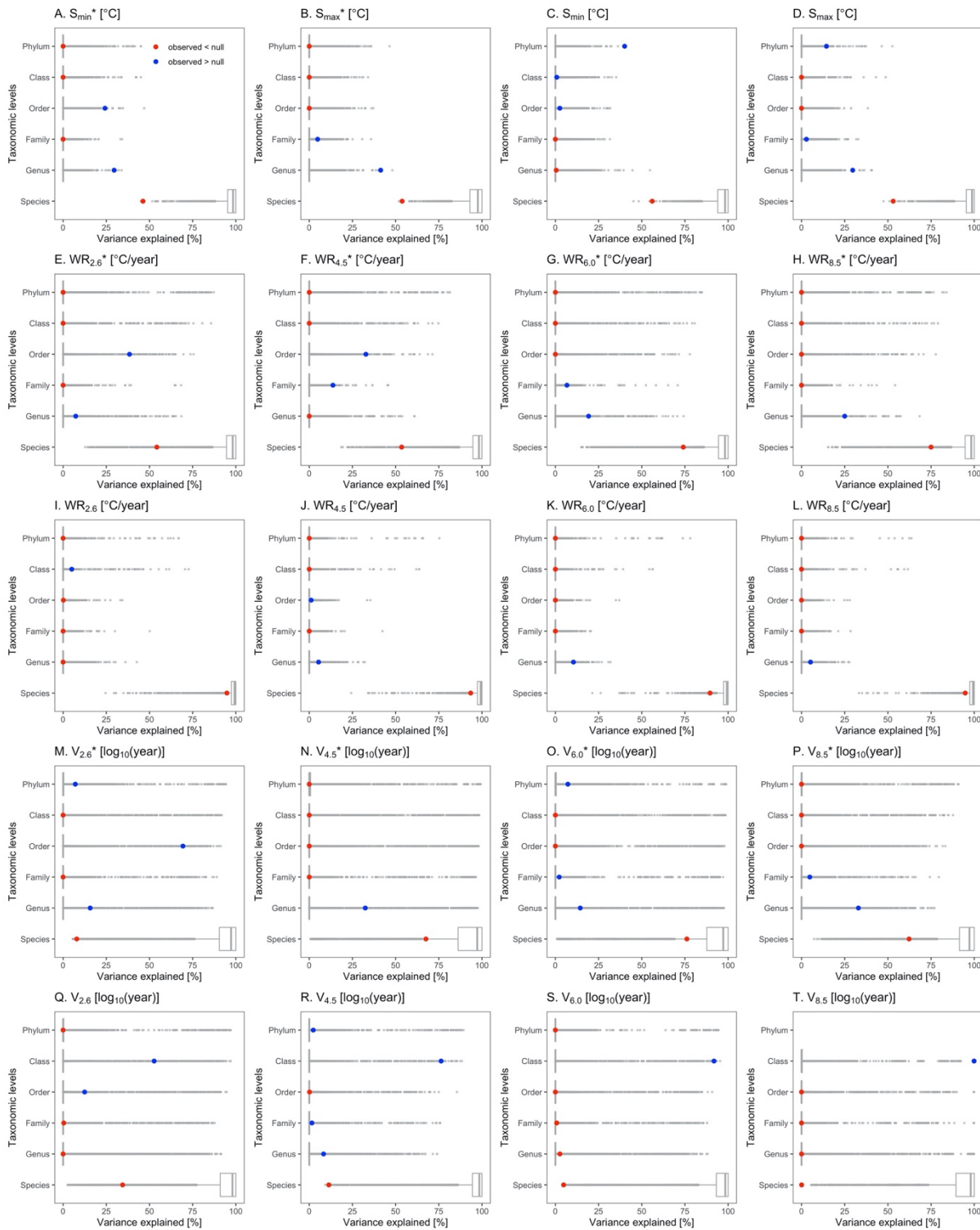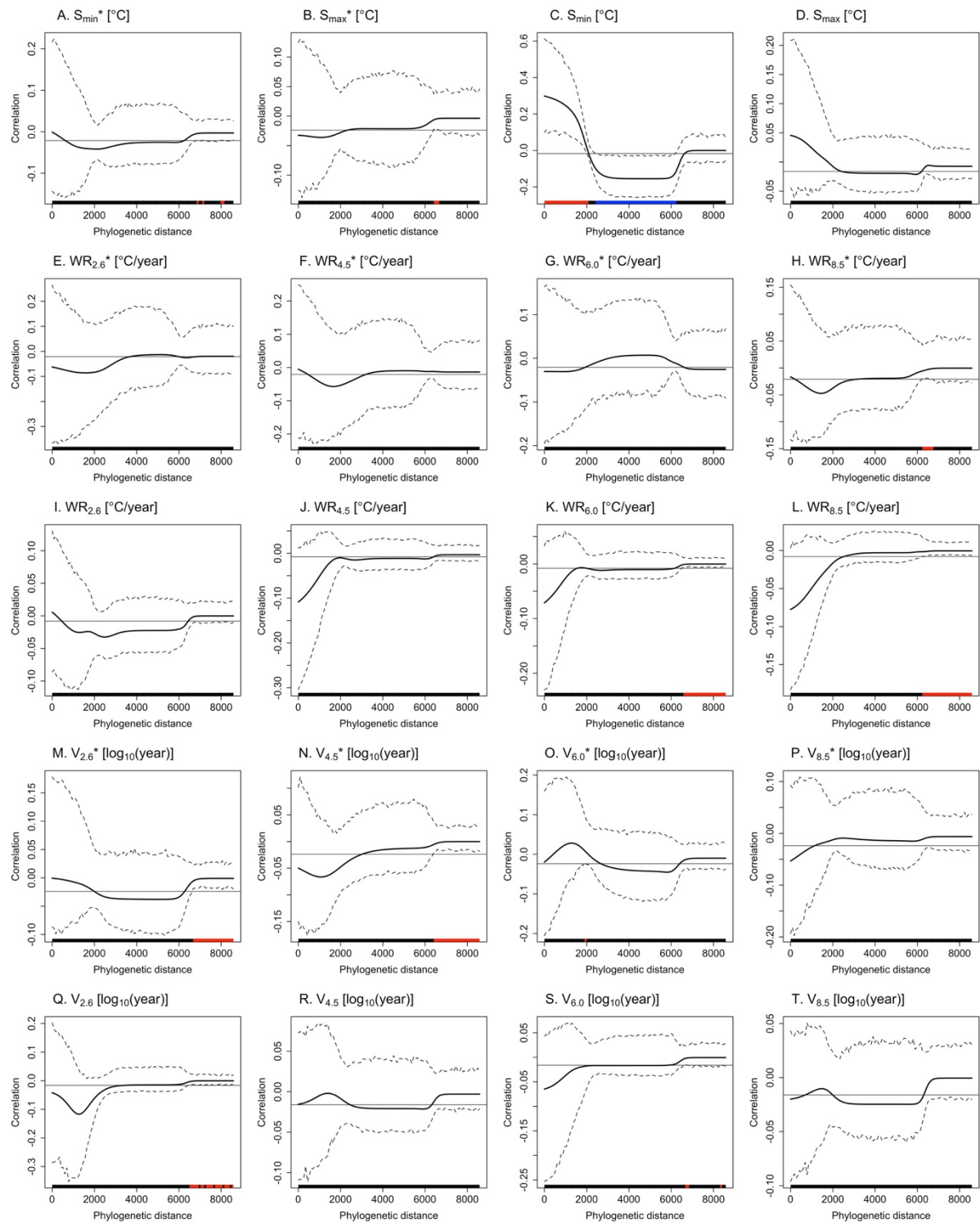
Supplementary Figure 3.20. Phylogenetic correlograms for sensitivity to cold temperature (S_{min}; A and C), sensitivity to warm temperature (S_{max}; B and D), warming exposure (WR; E – L), and warming vulnerability (V; M – T) in marine phytoplankton. The estimates were obtained from *CTMI*-derived dataset (indicated by an asterisk) and published dataset. The warming rate and vulnerability were computed based on different climate scenarios (i.e. *RCP* 2.6, *RCP* 4.5, *RCP* 6.0, and *RCP* 8.5). The solid black lines indicate the Moran's *I* index autocorrelation, and the dashed black lines indicate the 95% confidence interval. The horizontal black lines represent the estimated value of Moran's *I* under the null hypothesis of no phylogenetic autocorrelation. The red and blue colored bars indicate significant positive and negative autocorrelation, respectively; whilst, the black colored bars indicate a non-significant autocorrelation.
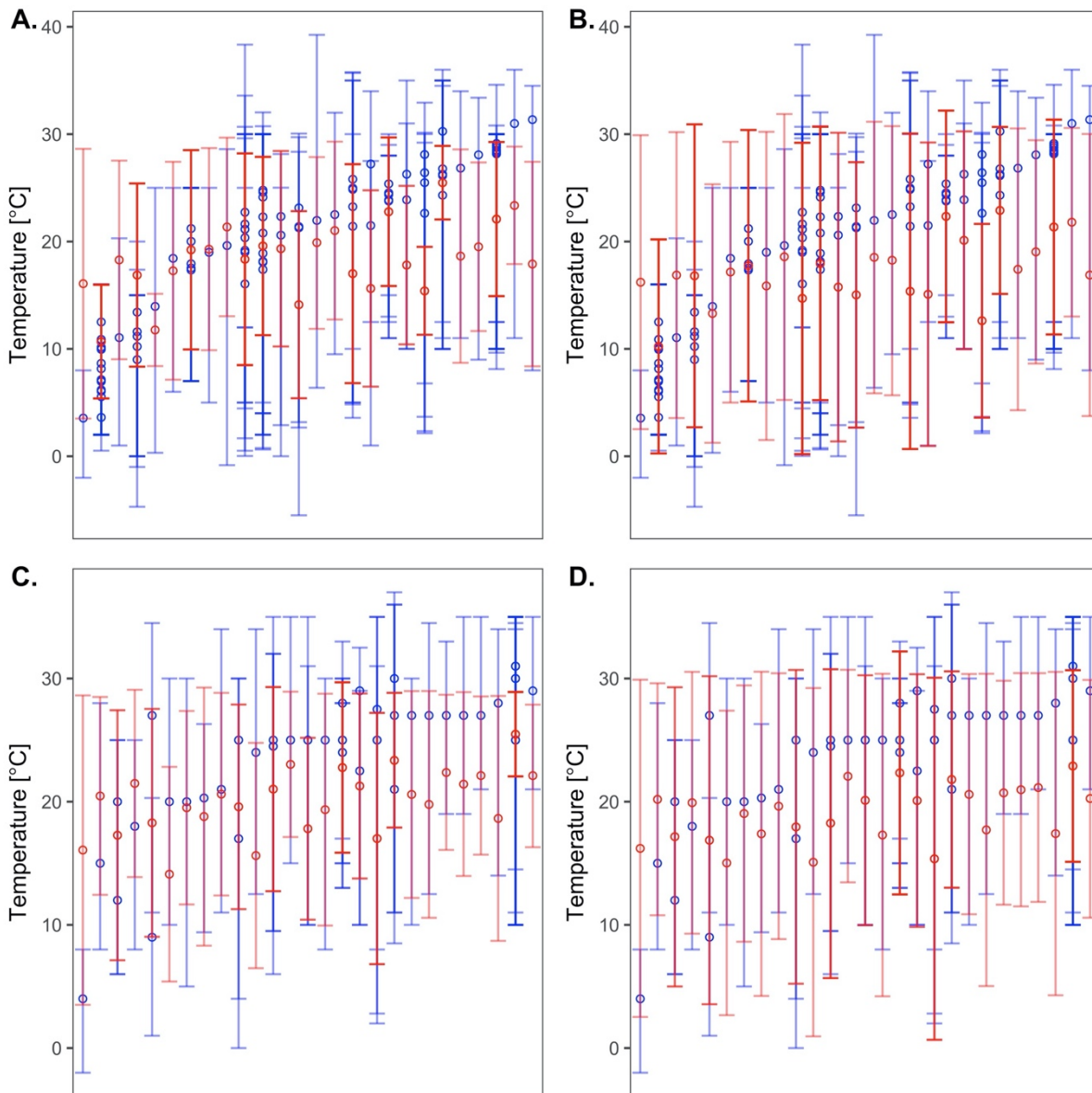
Supplementary Figure 3.21. Temperature limits and ranges in marine phytoplankton species estimated from   physiology (blue) and occurrence (red) data (TT_p and TT_o, respectively). Estimates of TT_p were obtained from *CTMI* fitting (indicated by an asterisk) and published literature, whilst estimates of TT_o were derived from annual average *SST* and seasonal extreme *SST* (indicated by an asterisk). These data were merged and matched up by species, resulting to four sets of datasets: (1) TT_p* and TT_o (A), (2) TT_p* and TT_o*(B), (3) TT_p and TT_o(C), and (4) TT_p and TT_o*(D). The point represents the optimal temperature. The bars indicate the range between cold and heat tolerance limits. Species are ranked in ascending order of optimal temperature.

Supplementary Figure 4.1. Growth of non-toxic (A – C) and potentially toxic (D – F) strains of marine phytoplankton over time (in days) across all assay temperatures in the plate-based experiments. The points represent the phytoplankton biomass that were indirectly measured using optical density (*OD660*), which were quality controlled. The red points represent the omitted data points and the black points represent the data points that were in the subsequent analysis. Natural logarithm of *OD660* estimates were fitted against time (in days) using linear regression to estimate the growth rate. The regression lines are indicated in black solid lines with 95% confidence interval in grey shading.
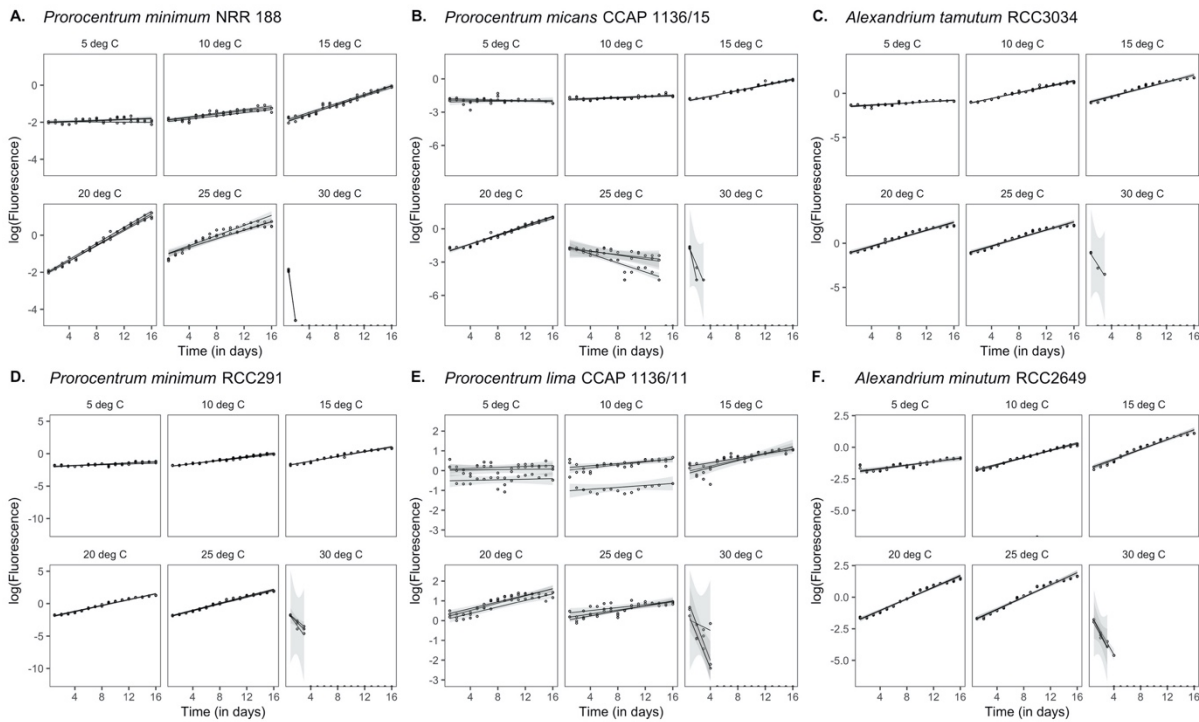
Supplementary Figure 4.2. Growth of non-toxic (A – C) and potentially toxic (D – F) strains of marine phytoplankton over time (in days) across all assay temperatures in the first tube-based experiments. The points represent the estimates of phytoplankton biomass that were indirectly measured using *in vivo* fluorescence. Natural logarithm of fluorescence estimates were fitted against time (in days) using linear regression to estimate the growth rate. The regression lines are indicated in black solid lines with 95% confidence interval in grey shading.
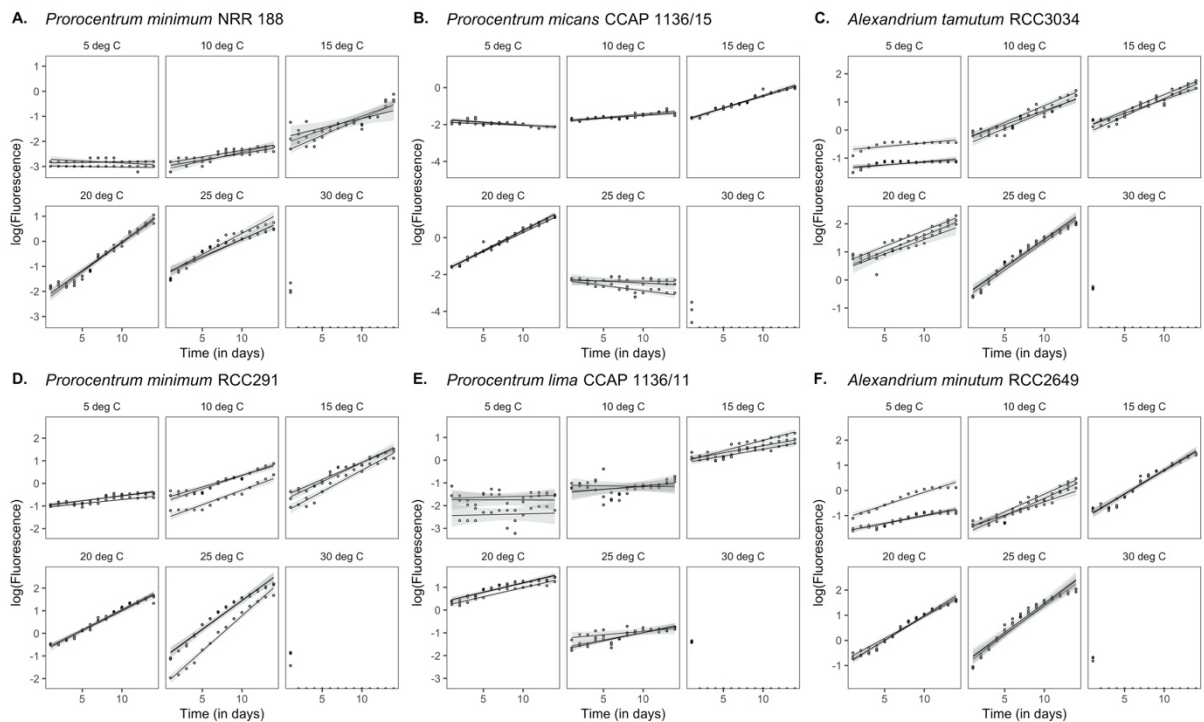
Supplementary Figure 4.3. Growth of non-toxic (A – C) and potentially toxic (D – F) strains of marine phytoplankton over time (in days) across all assay temperatures in the second tube-based experiments during the acclimatisation. The points represent the estimates of phytoplankton biomass that were indirectly measured using *in vivo* fluorescence. Natural logarithm of fluorescence estimates were fitted against time (in days) using linear regression to estimate the growth rate. The regression lines are indicated in black solid lines with 95% confidence interval in grey shading.
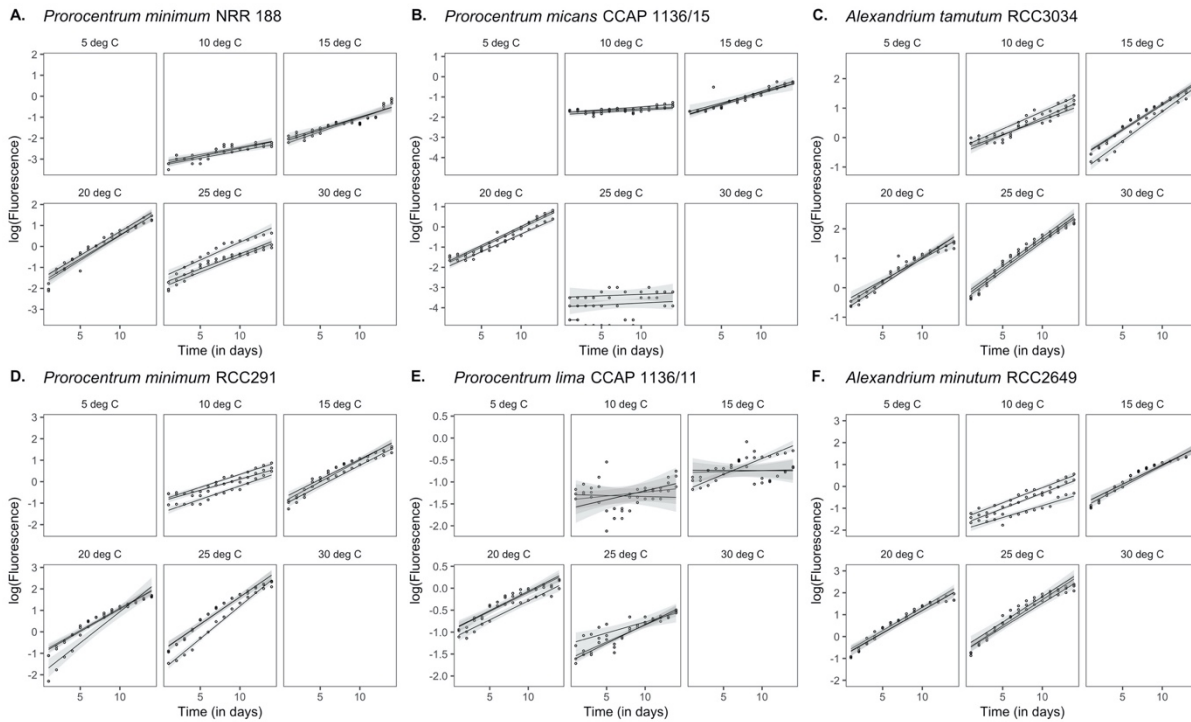
Supplementary Figure 4.4. Growth of non-toxic (A – C) and potentially toxic (D – F) strains of marine phytoplankton over time (in days) across all assay temperatures in the second tube-based experiments after the acclimatisation. The points represent the estimates of phytoplankton biomass that were indirectly measured using *in vivo* fluorescence. Natural logarithm of fluorescence estimates were fitted against time (in days) using linear regression to estimate the growth rate. The regression lines are indicated in black solid lines with 95% confidence interval in grey shading.
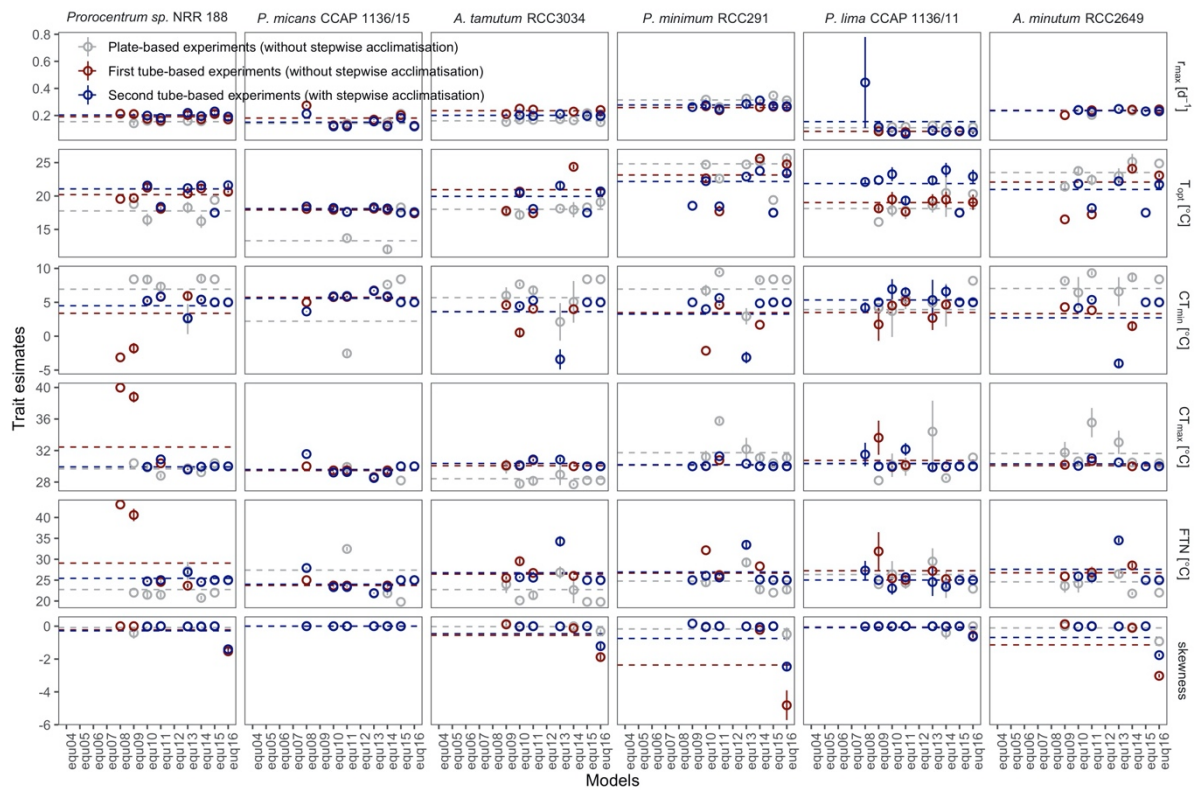
Supplementary Figure 4.5. Variation in thermal traits estimated from the different non-linear functions (equ04 – equ16; refer to Table 4.3 for description) used to fit growth rates against temperature obtained in plate- and tube-based growth experiments. The circles indicate the mean estimates of the thermal traits and the error bars indicate the standard error of the mean. The horizontal lines indicate the average trait values weighted by BIC rank.
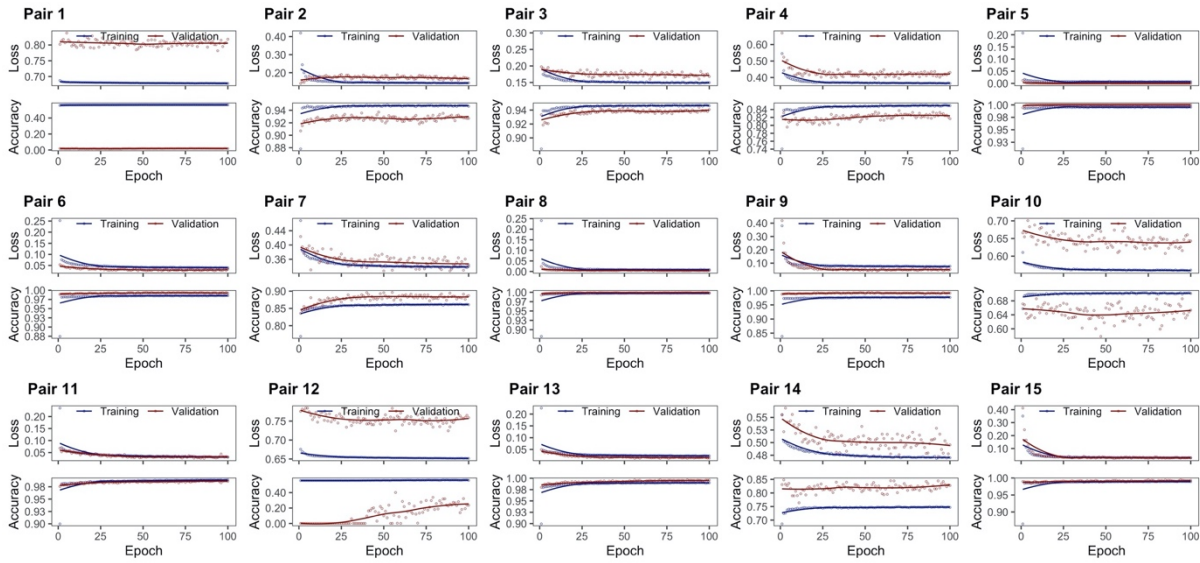
Supplementary Figure 6.1. Model performance of deep learning models used to classify species in pairwise mixed cultures incubated at 15 °C. The line plots showing the cross-entropy loss and classification accuracy over epochs for the training (blue) and validation (red) datasets.
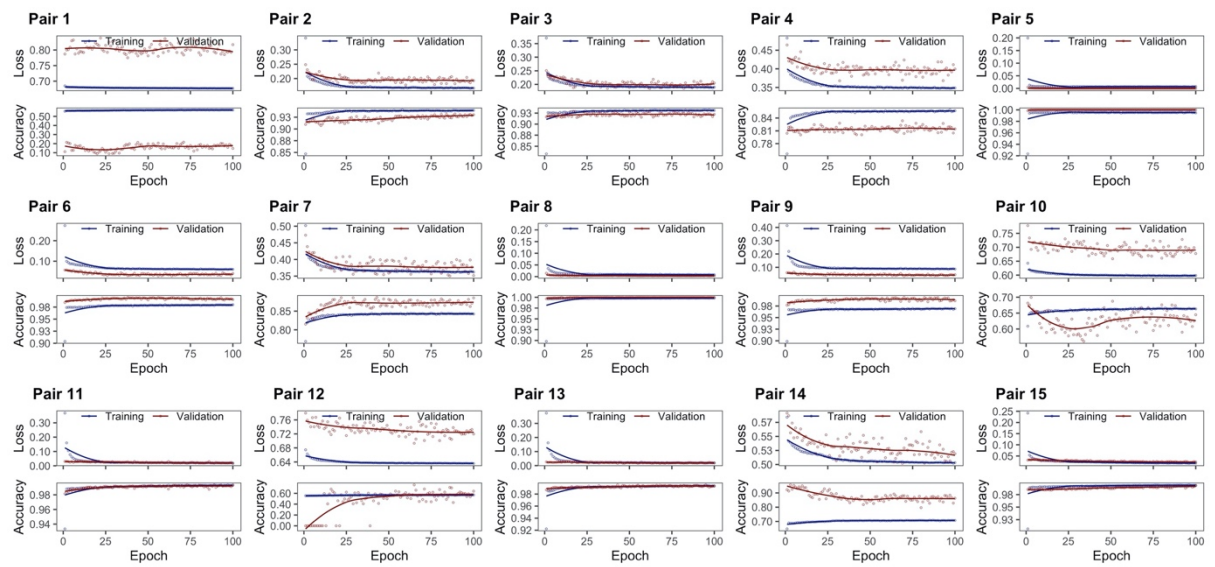
Supplementary Figure 6.2. Model performance of deep learning models used to classify species in pairwise mixed cultures incubated at 20 °C. The line plots showing the cross-entropy loss and classification accuracy over epochs for the training (blue) and validation (red) datasets.
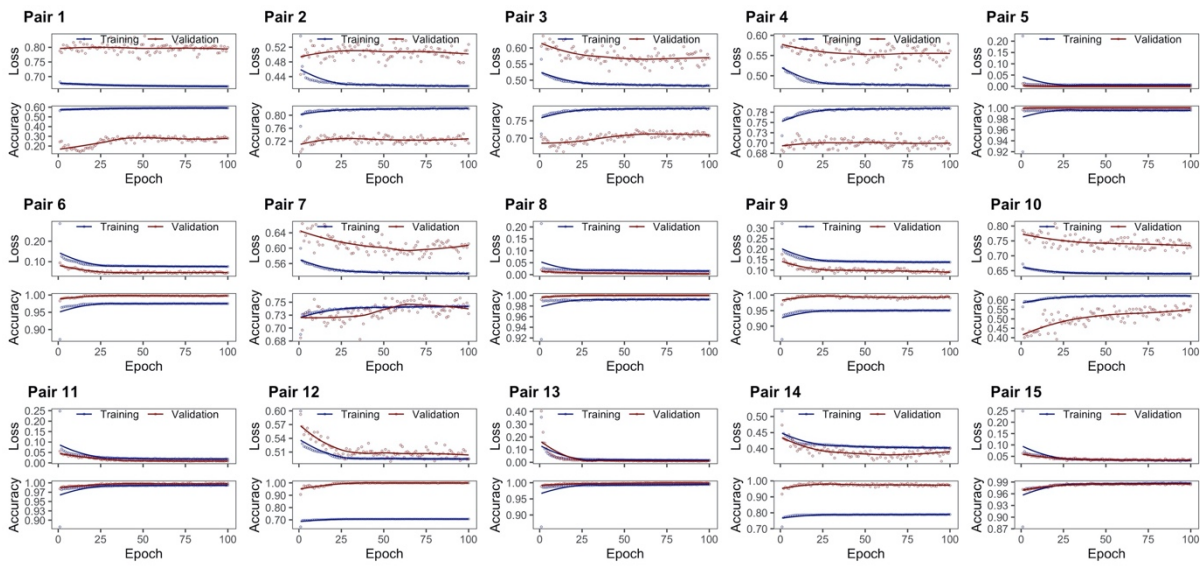
Supplementary Figure 6.3. Model performance of deep learning models used to classify species in pairwise mixed cultures incubated at 25 °C. The line plots showing the cross-entropy loss and classification accuracy over epochs for the training (blue) and validation (red) datasets.
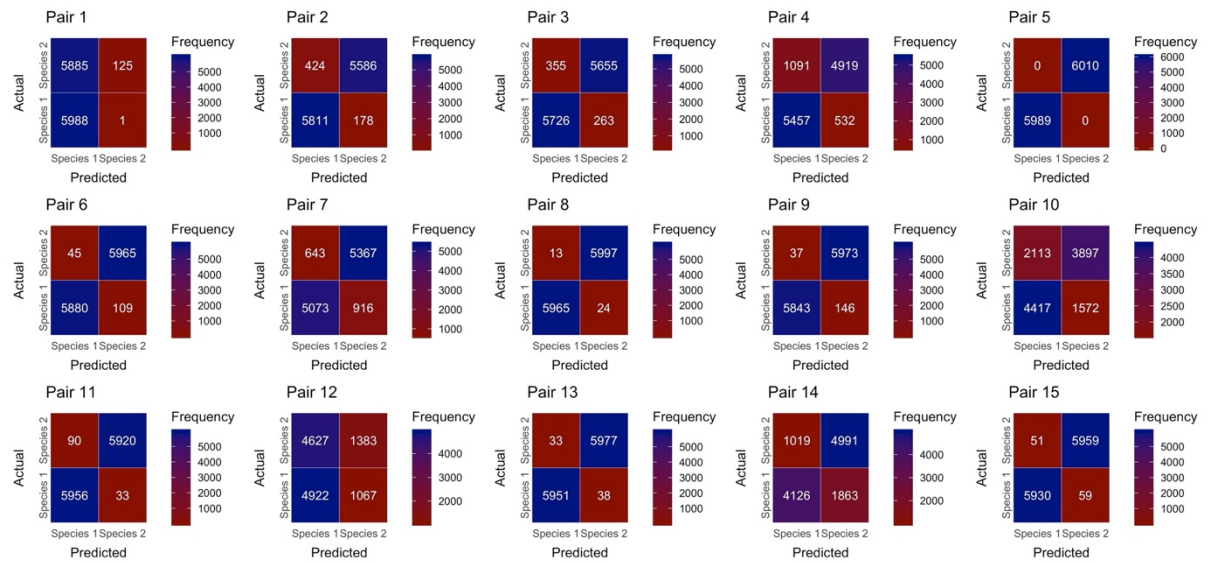
Supplementary Figure 6.4. Confusion matrix heat map showing the frequency of correct and incorrect classification of species in pairwise mixed-species cultures incubated at 15 °C.
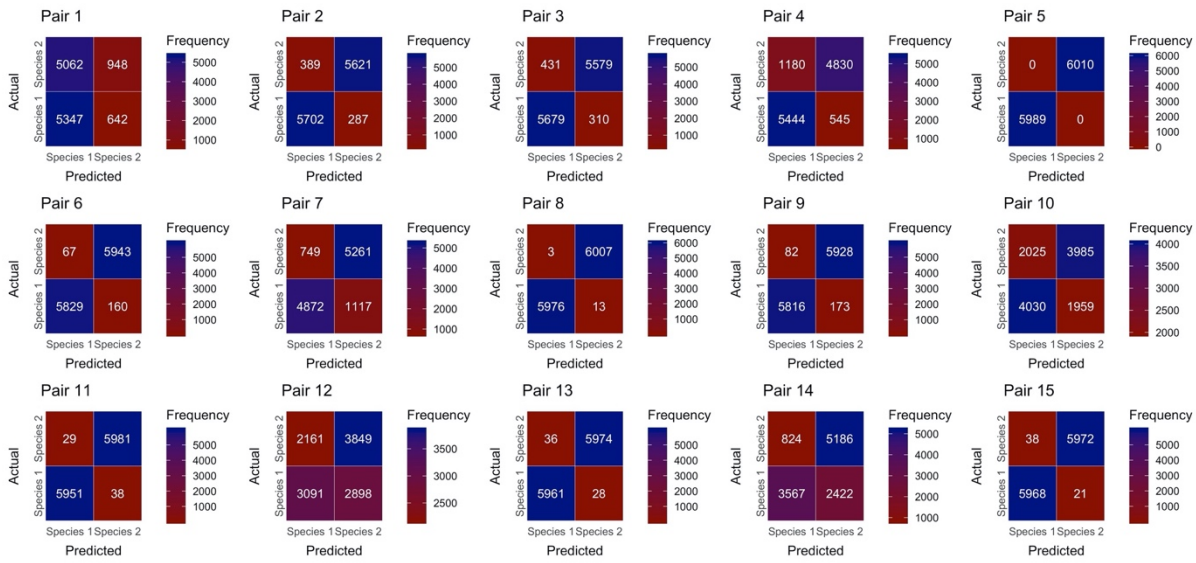
Supplementary Figure 6.5. Confusion matrix heat map showing the frequency of correct and incorrect classification of species in pairwise mixed-species cultures incubated at 20 °C.
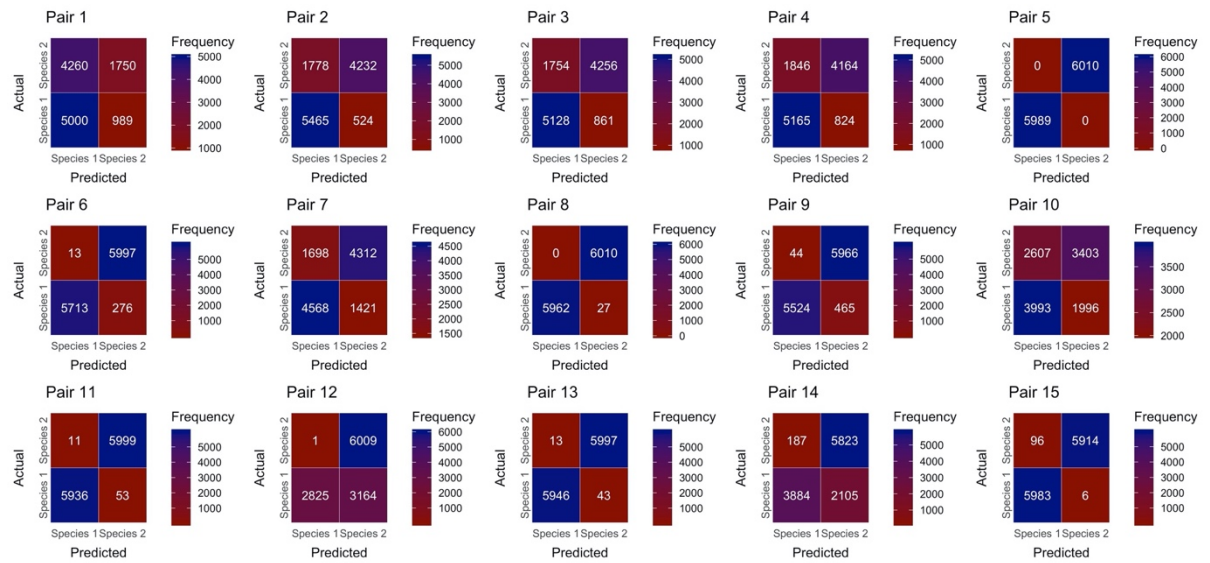
Supplementary Figure 6.6. Confusion matrix heat map showing the frequency of correct and incorrect classification of species in pairwise mixed-species cultures incubated at 25 °C.
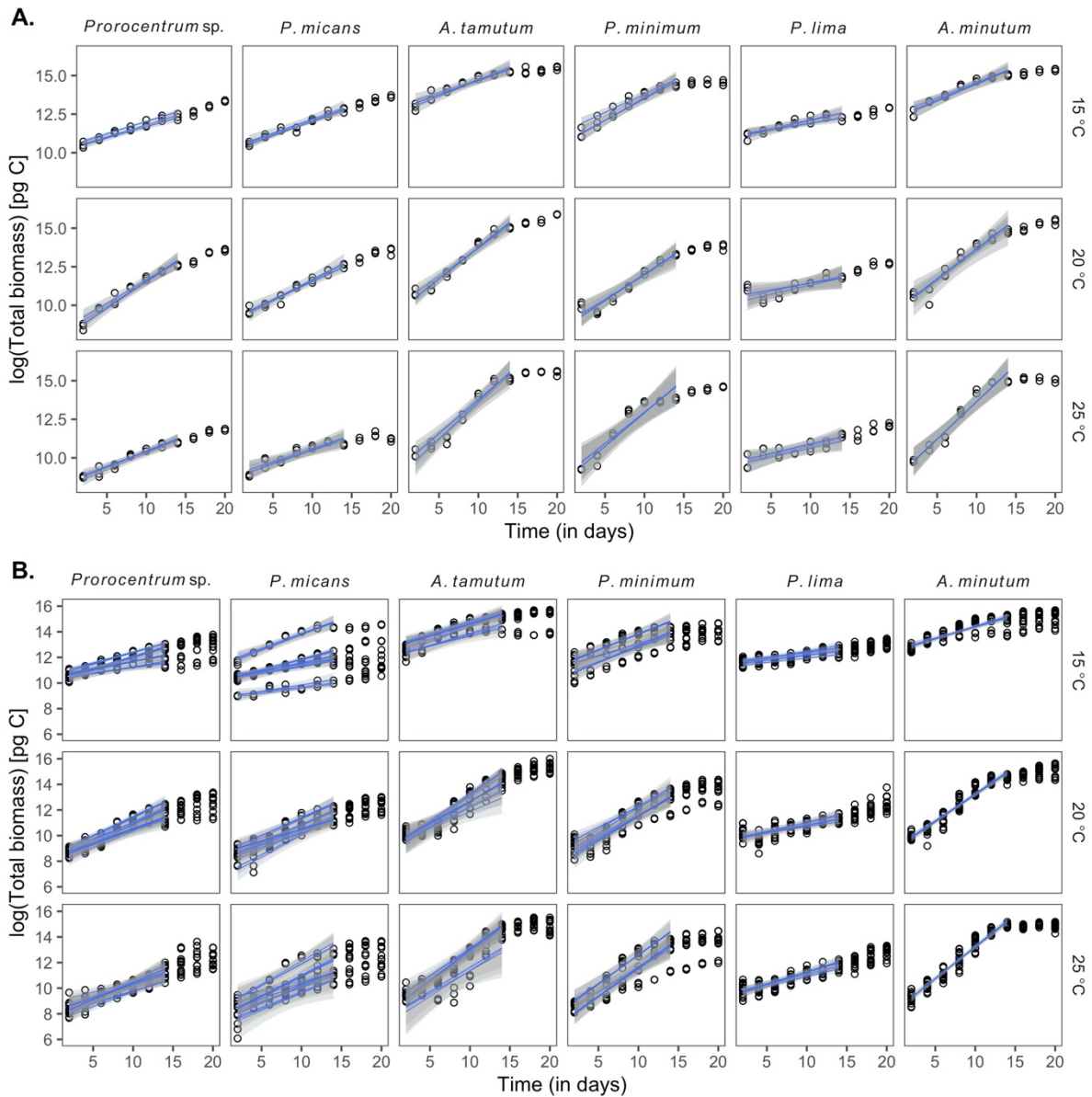
Supplementary Figure 6.7. Growth of non-toxic and potentially toxic dinoflagellates over time in monocultures and co-cultures across three assay temperatures. The points represent the total biomass (pg C). Natural logarithm of the total biomass estimates were fitted against time (in days) using linear regression to estimate the growth rate in monocultures and co-cultures (A and B, respectively). The regression lines are indicated in black solid lines with 95% confidence interval in grey shading.
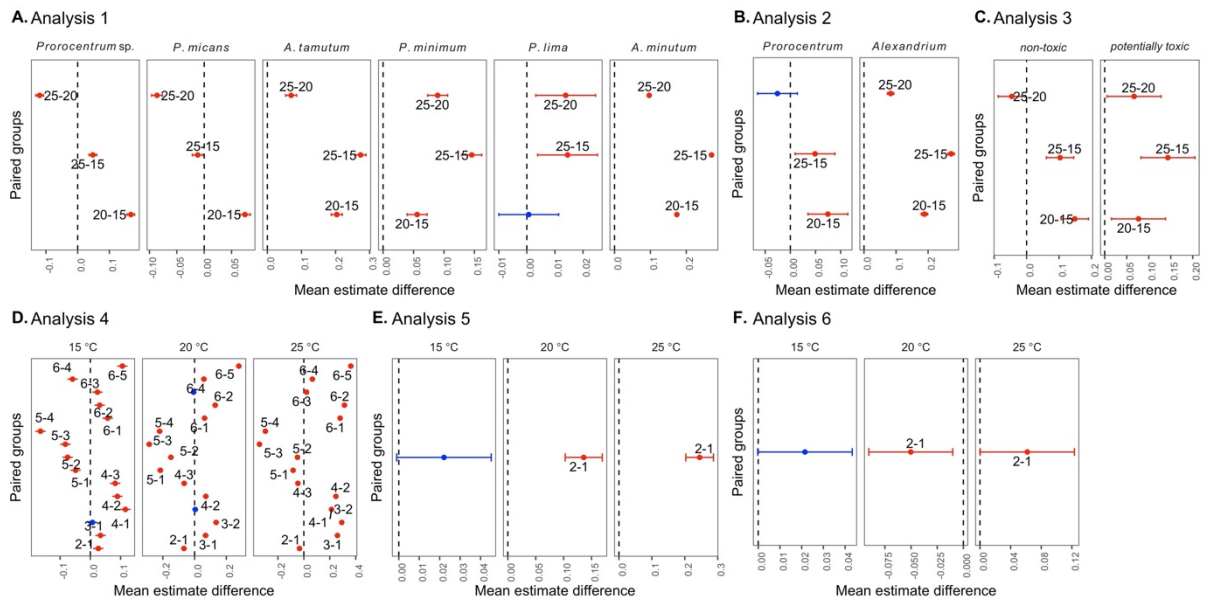
Supplementary Figure 6.8. Significant difference in mean estimates of growth rates of non-toxic and potentially toxic dinoflagellates in monocultures between paired groups based on post hoc Tukey tests for different analyses (see Table 1 for description). Variation in the mean estimates between paired groups of temperature treatments (15, 20, 25 °C), species (1 = *Prorocentrum* sp., 2 = *Prorocentrum micans*, 3 = *Alexandrium tamutum*, 4 = *Prorocentrum minimum*, 5 = *Prorocentrum lima*, and 6 = *Alexandrium minutum*), genus (1 = *Prorocentrum* and 2 = *Alexandrium*), and toxicity (1 = non-toxic and 2 = potentially toxic) are presented. Each point indicates a mean estimate difference with error bar represents the lower and upper limits, colored red indicates significant difference at 95% confidence interval whilst colored blue indicate non-significance. Paired groups with significant difference are labelled.

Supplementary Figure 6.9. Significant difference in mean estimates of growth rates of non-toxic and potentially toxic dinoflagellates in co-cultures between paired groups based on post hoc Tukey tests for different analyses (see Supplementary Table 5.2 for description) using the filtered datasets. Variation in the mean estimates between paired groups of temperature treatments (15, 20, 25 °C), species (1 = *Prorocentrum* sp., 2 = *Prorocentrum micans*, 3 = *Alexandrium tamutum*, 4 = *Prorocentrum minimum*, 5 = *Prorocentrum lima*, and 6 = *Alexandrium minutum*), genus (1 = *Prorocentrum* and 2 = *Alexandrium*), and toxicity (1 = non-toxic and 2 = potentially toxic) are presented. Each point indicates a mean estimate difference with error bar represents the lower and upper limits, colored red indicates significant difference at 95% confidence interval whilst colored blue indicate non-significance. Paired groups with significant difference are labelled.
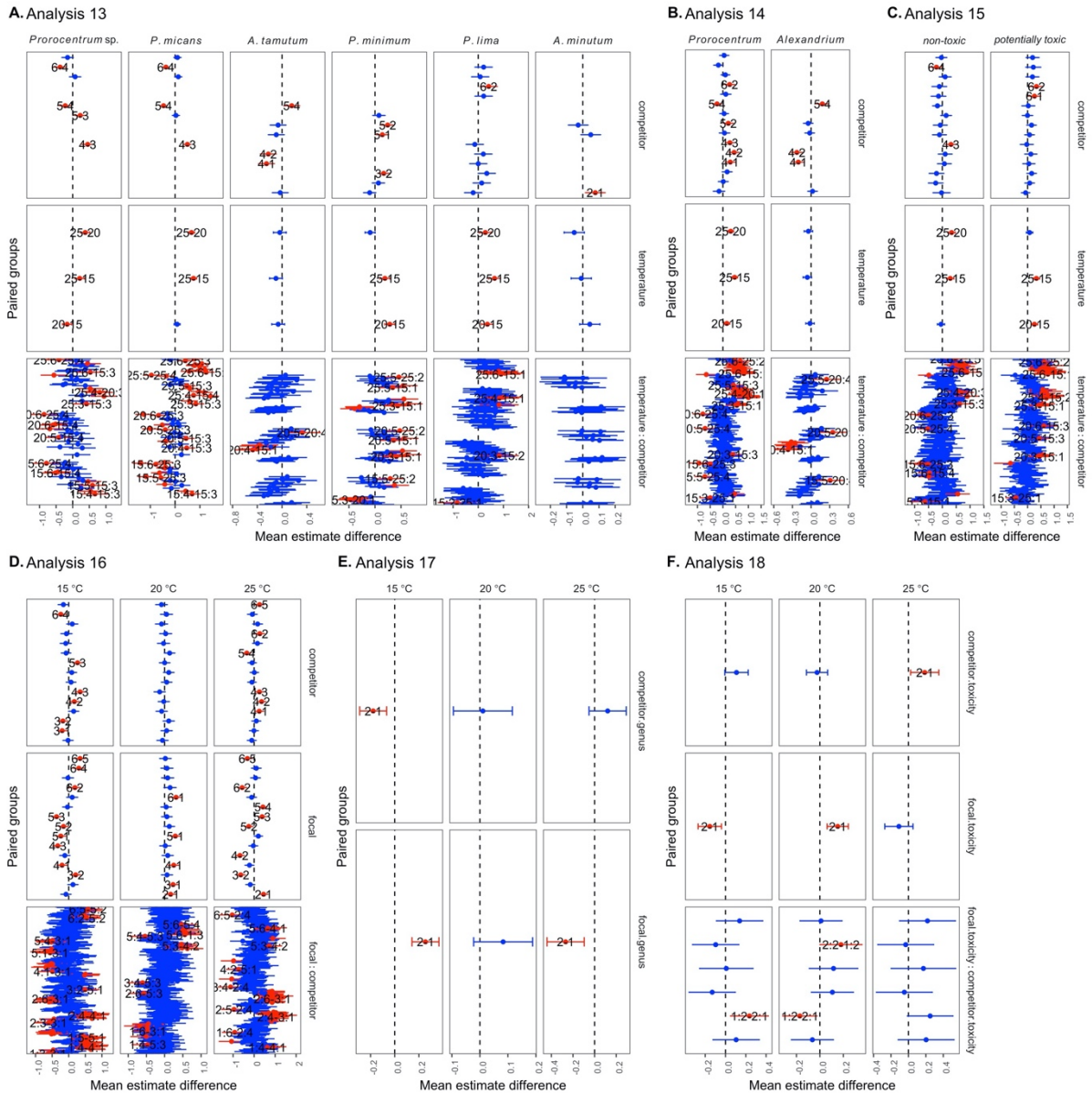
Supplementary Figure 6.10. Significant difference in mean estimates of relative growth rates of non-toxic and potentially toxic dinoflagellates between paired groups based on post hoc Tukey tests for different analyses (see Supplementary Table 5.2 for description) using the filtered datasets. Variation in the mean estimates between paired groups of temperature treatments (15, 20, 25 °C), species (1 = *Prorocentrum* sp., 2 = *Prorocentrum micans*, 3 = *Alexandrium tamutum*, 4 = *Prorocentrum minimum*, 5 = *Prorocentrum lima*, and 6 = *Alexandrium minutum*), genus (1 = *Prorocentrum* and 2 = *Alexandrium*), and toxicity (1 = non-toxic and 2 = potentially toxic) are presented. Each point indicates a mean estimate difference with error bar represents the lower and upper limits, colored red indicates significant difference at 95% confidence interval whilst colored blue indicate non-significance. Paired groups with significant difference are labelled.

Supplementary Figure 6.11. Significant difference in mean estimates of growth rates of non-toxic and potentially toxic dinoflagellates in co-cultures between paired groups based on post hoc Tukey tests for different analyses (see Supplementary Table 5.2 for description) using the full datasets. Variation in the mean estimates between paired groups of temperature treatments (15, 20, 25 °C), species (1 = *Prorocentrum* sp., 2 = *Prorocentrum micans*, 3 = *Alexandrium tamutum*, 4 = *Prorocentrum minimum*, 5 = *Prorocentrum lima*, and 6 = *Alexandrium minutum*), genus (1 = *Prorocentrum* and 2 = *Alexandrium*), and toxicity (1 = non-toxic and 2 = potentially toxic) are presented. Each point indicates a mean estimate difference with error bar represents the lower and upper limits, colored red indicates significant difference at 95% confidence interval whilst colored blue indicate non-significance. Paired groups with significant difference are labelled.

Supplementary Figure 6.12. Significant difference in mean estimates of relative growth rates of non-toxic and potentially toxic dinoflagellates between paired groups based on post hoc Tukey tests for different analyses (see Supplementary Table 5.2 for description) using the full datasets. Variation in the mean estimates between paired groups of temperature treatments (15, 20, 25 °C), species (1 = *Prorocentrum* sp., 2 = *Prorocentrum micans*, 3 = *Alexandrium tamutum*, 4 = *Prorocentrum minimum*, 5 = *Prorocentrum lima*, and 6 = *Alexandrium minutum*), genus (1 = *Prorocentrum* and 2 = *Alexandrium*), and toxicity (1 = non-toxic and 2 = potentially toxic) are presented. Each point indicates a mean estimate difference with error bar represents the lower and upper limits, colored red indicates significant difference at 95% confidence interval whilst colored blue indicate non-significance. Paired groups with significant difference are labelled.

This page is intentionally left blank.

SUPPLEMENTARY INFORMATION

This page is intentionally left blank.

Supplementary Information 1.1. Review of the evolution and ecology of toxin production by phytoplankton

ABSTRACT

The effects of toxic algal blooms to humans and to other organisms and the potential impacts of climate change on toxic blooms in the future have generated ongoing interests in understanding the evolution and ecophysiology of toxin production. This trait is only known to a few phytoplankton species despite its advantage as anti-predation. Despite the rarity, phycotoxins are diverse in terms of chemical structure and property. In this review, we examined how the diversity of phycotoxins is associated with a wide diversity of toxic phytoplankton and infer patterns in phylogenetic distribution that may shed light to the origin and evolution of toxin production. We argued that the rarity and ubiquity of toxin production in the phytoplankton lineage may indicate non-essentiality of this trait for survival and the diversification may have rendered adaptive advantage to the producers. We also argued that the toxin production may have originated from a toxic ancestor that have evolved under selective pressure. We evaluated the existing evolutionary theories to supplement our arguments. Regardless of their evolutionary history, toxic species must have taken the advantage of keeping the complex and costly biosynthesis of toxins. We argued that toxins have multiple roles and have evolved in response to abiotic and biotic pressures to improve efficiency in cellular and ecological functions beyond defense against predators. Finally, we discussed how the multiplicity of roles of toxins may provide an ecophysiological advantage to toxic species in the changing environment.

INTRODUCTION

Phytoplankton are ecologically important as primary producers and biological carbon pump regulators (e.g. Behrenfeld et al., 2006; Falkowski, 2012; Falkowski and Oliver, 2007). However, some phytoplankton species may form harmful algal blooms (HAB) that are often produce toxins, posing a risk to public health, environment, and economy (Berdalet et al., 2015; Hallegraeff et al., 2004). Toxic blooms are already a global problem and their current distribution is alarming (Figure 1). Climate change may contribute to this trend by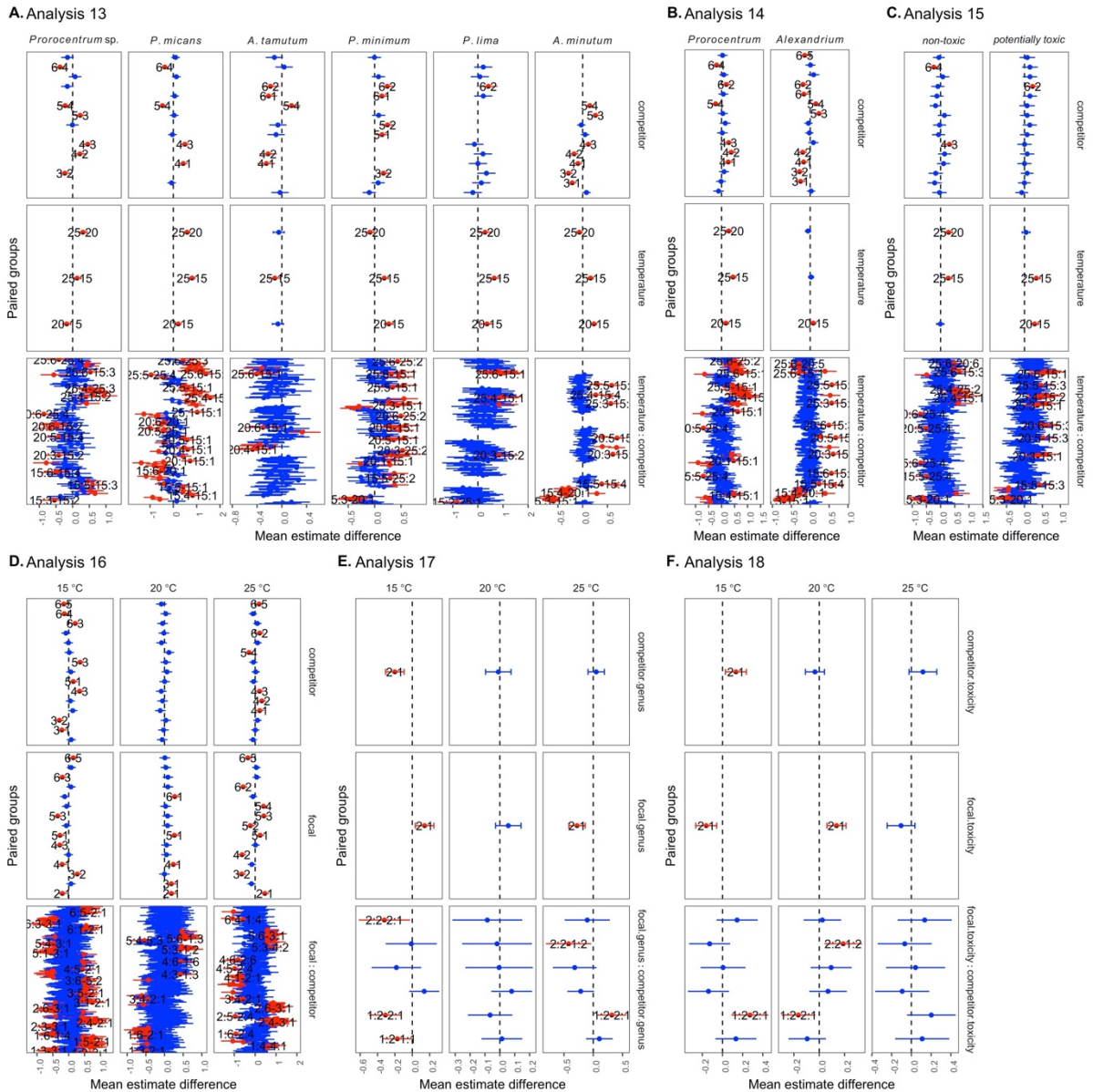 providing favourable conditions for toxic algae to occur (Hallegraeff, 2010). It is likely that toxic blooms and their impacts may be exacerbated in the future where their duration, intensity, and frequency may increase in response to changes in the climate (Moore et al., 2008; Tatters et al., 2013). The well-documented effects of toxins to humans and to other organisms (Berdalet et al., 2016; Hallegrae, 2014; Lee *et al.*, 2016) and the potential effect of climate change on toxic blooms in the future (Fu et al., 2012) have generated ongoing interests in the ecophysiology of toxic phytoplankton (e.g. Kellmann et al., 2010a; Perini et al., 2014; Ramsey et al., 1998; Stüken et al., 2011). However, research has focused on individual toxins and taxa, and we know relatively little about the overall evolutionary history and ecological role of toxicity, a surprisingly rare trait among phytoplankton taxa.

The advantages of toxin production would lead to the expectation of the ubiquity of toxicity in phytoplankton. Surprisingly toxin production is only known for few phytoplankton species (150 species in 50 genera listed in Moestrup et al. (2009)). Despite the rarity of toxicity in phytoplankton lineage, the toxins are diverse with distinct chemical structure, biosynthetic pathways and mode of actions (Rossini and Hess, 2010). The toxin diversity may be attributed

to its widespread distribution in phytoplankton lineage and may reveal putative physiological and ecological roles beyond their assumed primary role as a defense mechanism. However, there is no clear evidence to explain why some phytoplankton species are toxic while others are not. There are theories that attempt to explain the evolutionary history of toxins in phytoplankton (Kellmann et al., 2010; Murray et al., 2015), but are often challenged by lack of evidence. Despite recent progress in biosynthesis and molecular genetics of toxins in phytoplankton (Kellmann et al., 2010; Murray et al., 2011; Orr et al., 2013; Stüken et al., 2011), our knowledge of their origin and eco-evolutionary roles is limited (Hallegrae, 2014), and the link between the ecophysiological and evolutionary aspects of toxin production remain unclear despite its widespread implications.

In this review, we summarised our current knowledge on the evolution and ecology of toxin production by phytoplankton, and provided ecophysiological insights into the expected change in toxic bloom formation with climate change, which brings issues to the debate whether toxin production may provide a competitive advantage in phytoplankton in the future climate scenarios.
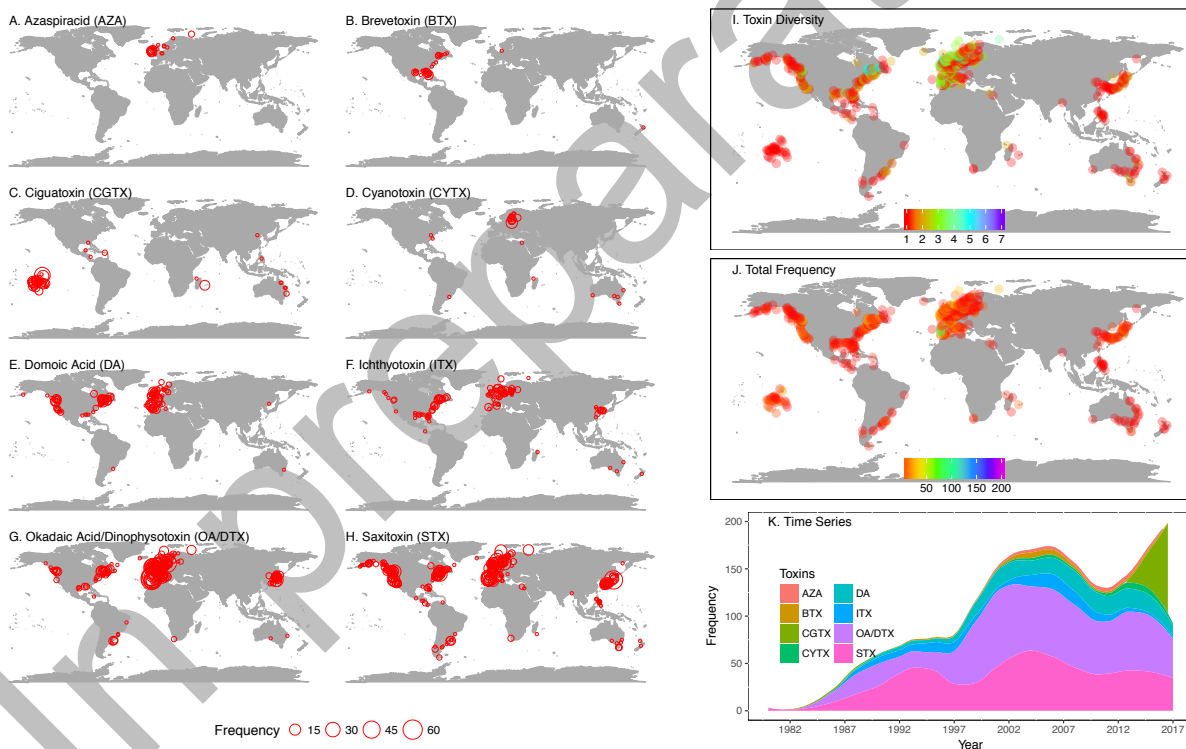
Figure 1. Global distribution of toxins detected during harmful algal events in the last 35 years (A –H). As shown, some toxins are reported frequently in the tropics and/or temperate, which entails different threats to the regions. This also presents diversity of toxins (I) and the total frequency of toxic blooms (J) reported in each site. It is alarming that toxic blooms appear to be more frequent globally (K), which may be attributed to anthropogenic activities (e.g. increased number of observations, cultural eutrophication, transport toxic species via ships' ballast water, and translocation of shellfish stocks, and climate change (Anderson et al., 2012)). This figure is drawn from the data obtained from Harmful Algal Information System (HAIS), http://haedat.iode.org/.

DIVERSITY OF PHYCOTOXINS

Phycotoxins are complex compounds that are synthesized through the secondary metabolic pathways in microalgae and cyanobacteria. They are structurally diverse compounds, which have different biosynthetic pathways and distinct mode of actions (Table 1). Phycotoxins range from small to medium-sized compounds and weigh from ~300 to over 3000 Da (Rossini and Hess, 2010). They belong to diverse groups of chemical compounds (e.g. kainoid, perhydropurine, polyethers). Each group has numerous compounds that shared similar backbone and typically has several derivatives (Rasmussen et al., 2016; Rossini and Hess, 2010). Homology in chemical structure among toxins may indicate shared elements of biosynthetic pathways (Wright and Cembella, 1998). Phycotoxins are not primary gene products (Wright and Cembella, 1998), but there are genes that are known to be involved in their biosynthesis. These genes code for the enzymes necessary for the biosynthesis of toxins that is assumed to be costly as the pathways utilise precursors derived from primary metabolic processes. Furthermore, phycotoxins have distinctive mode of actions that are linked to their toxicity (Hallegraeff, 2014). The better known molecular activities of phycotoxins are (1) alteration of ion channels (Cusick and Sayler, 2013; Ramsdell, 2007), (2) inhibition of phosphoprotein phosphatases (Garibo et al., 2013), and (3) modification of cytoskeletal elements (Allingham et al., 2007).

Table 1. Chemical classification and mode of action of toxins produced by toxic phytoplankton. Information of this table is obtained from Shimizu (1996), Cembella (2003), Moestrup *et al.* (2009) and Rossini and Hess (2010).

Classification	Toxins	Mode of action	Producers
Kanoid	Domoic acid	glutamate receptor agonist	*Pseudo-nitzschia spp.* *Nitzschia spp.* *Halamphora coffeiformis?*
Perhydropurine	Saxitoxin and derivatives	Na^+-channel blocker	*Alexandrium spp.* *Pyrodinium bahamense* *Gymnodinium catenatum* *Anabaena spp.* *Aphanizomenon spp.* *Cylindrospermopsis spp.* *Lyngbya spp.* *Planktothrix spp.* *Oscillatoria spp.*
Linear polyethers	Okadaic acid and derivatives	Protein phosphatase inhibitor	*Dinophysis spp.* *Prorocentrum spp.*
	Azaspracid	hERG voltage-gated potassium channels inhibitor	*Azadinium* spp. *Amphidoma* spp.
	Prymnesin	Ca^{2+}-channel effector	*Prymnesium parvum*
	Ostreocin	Na^+/K^+ ATPase disruptor	*Ostreopsis siamensis*
	Palytoxin	?	*Ostreopsis lenticularis* *Ostreopsis ovata* *Ostreopsis siamensis*

	Karlotoxin	?	*Karlodinium australe* *Karlodinium conicum* *Karlodinium veneficum*
	Scytophycin	?	*Scytonema spp.*
	Tolytoxin	Microfilament-depolymerizing agent	*Tolypothrix conglutinata*
	Debromoaplysiatoxin	Protein kinase C activator	*Lyngbya majuscula*
Macrocyclic polyethers	Pectenotoxin	Actin depolymerizing agent	*Dinophysis fortii* *Dinophysis acuta*
	Spirolide	Muscarinic receptor or cholinesterase inhibitor	*Alexandrium ostenfeldii*
	Amphidinolide	?	*Amphidinium spp.*
	Caribenolide	?	*Amphidinium spp.*
	Goniodomin	?	*Alexandrium spp.*
	Prorocentrolide	?	*Prorocentrium lima*
Ladder-frame polyethers	Ciguatoxin	Na$^+$-channel activator	*Gambierdiscus toxicus*
	Gambieric acid	?	*Gambierdiscus toxicus*
	Maitotoxin	Ca^{2+}-channel effector	*Gambierdiscus toxicus*
	Ostreotoxin	Na$^+$-channel activator?	*Ostreopsis lenticularis*
	Cooliatoxin	?	*Coolia monotis*
	Brevetoxin	Na$^+$-channel activator	*Karenia brevis,* *Karenia brevi-sulcata* *Chatonella marina,* *Chatonella antiqua* *Chatonella cf. verruculosa*
	Yessotoxin	Affects cyclic AMP	*Protoceratium reticulatum* *Lingulodinium polyedrum*
	Brevisulcenal	?	*Karenia brevisulcata*
	Brevisulcatic acid		*Karenia brevisulcata*
	Gymnocin	?	*Karenia mikimotoi*
Open-chain polyketides	Majusculamide	Microtubulin assembly inhibitor	*Lyngbya majuscula*
	Curacin	Microtubulin assembly inhibitor	*Lyngbya majuscula*
	Amphidinol	?	*Amphidinium spp.*
	Amphiketide	?	*Amphidinium spp.*
Cyclic imine	Gymnodimine	?	*Karenia selliformis*
	Pinnatoxin	?	*Vulcanodinium rugosum*
Prenylated amino acid	Lyngbyatoxin	Protein kinase C activator	*Lyngbya majuscula*
Oxylipins	Bacillariolide	Phospholipase A2 inhibitor	*Pseudo-nitzschia multiseries*

Understanding the structural and functional homology and biosynthesis of phycotoxins is a key
in elucidating the phylogenetic origin of toxin production in phytoplankton. Here, we briefly
describe the chemical structure, biosynthesis, and mode of the main groups of phycotoxins.

Domoic acid (DA) belong to kainoid, a class of non-proteigenous amino acids (Wood and Fryer, 1998), which are produced exclusively by diatoms. Three DA derivative (i.e. isodomoic acids A, B, and C) have been identified in toxic diatoms (Holland et al., 2005; Kotaki et al., 2005), and most species do not produce all of them (Bajarias et al., 2006). Whilst it has been suggested that DA is synthesized from the fusion of two precursors derived from the citric acid cycle (i.e. glutamate) and isoprenoid pathways (i.e. geranyl diphosphate), later stage of its biosynthesis is still unclear. A most recent study isolated six novel DA intermediates that could elucidate the biosynthesis of DA and possibly contribute to the identification of biosynthetic genes that have not yet been discovered in diatoms (Maeno et al., 2018). Its structure is homologous to glutamate (Ohfune and Tomita, 1982), and hence it can bind to glutamate receptors and activate the influx of calcium. This action results in nerve damage in humans, causing amnestic shellfish poisoning (Ramsdell, 2007).

Saxitoxin (STX) is comprised of a tri-cyclic perhydropurine, a nitrogen-rich alkaloid (Gupta et al., 1989). Despite its similarity to purines of primary metabolism, STX and its derivatives appears to be synthesized by a totally different pathway (Shimizu et al., 1984). It has been suggested that arginine, acetate, and methionine serve as the building blocks of this compound (Gupta et al., 1989; Shimizu et al., 1984). The biosynthesis of saxitoxin is catalysed by an enzyme coded from *sxt* genes which were found in toxigenic cyanobacteria and dinoflagellates (Moustafa et al., 2009; Orr et al., 2013). Similar to DA, STX also modifies ion channels specifically by binding to voltage-gated sodium channels. It blocks the opening and prevents the sodium ion flux across the membrane. This neurotoxin alters the propagation of action potential generated across the nerve membrane and thus prevents normal nerve function. STX is the causative agent for paralytic shellfish poisoning (PSP) (Cusick and Sayler, 2013).

The majority of the toxic compounds in dinoflagellate and other ichthyotoxic phytoplankton are either linear, macrocyclic or ladder-frame polyethers. These polyether compounds are derived from the successive addition of acetate units to a growing polyketide chain, which is catalysed by the polyketide synthase (PKS) (Staunton and Weissman, 2001). It has been suggested that the polyketides in dinoflagellates are produced by modular type I PKS enzymes in certain cases with involvement of non-ribosomal peptide synthase (NRPS) (Kellmann et al., 2010).

Azaspiracid (AZA) is a linear polyether toxin that inhibits hERG voltage-gated potassium channels by blocking the cytoplasmic mouth of the open pore in the cell (Twiner et al., 2012). This toxin is the cause of azaspiracid shellfish poisoning (AZP) (Rossini and Hess, 2010).

Okadaic acid (OA) and dinophysistoxin (DTX) are also linear polyethers that are linked to diarrhetic shellfish poisoning (DSP) (Hackett et al., 2009; Quilliam et al., 1996). These toxins are known to bind to the phosphatase proteins, specifically serine/threonine phosphatases, and inhibit the activity of the protein by hyperphosphorylation. The inhibition eventually modifies secretion of sodium ions and cell permeability of solutes (Garibo et al., 2013). Pectenotoxin (PTX) is a macrocyclic polyether and also associated with DSP (Amzil et al., 2007). Unlike OA and DTX, PTX binds to actin filaments and modify cytoskeletal elements in the cell (Allingham et al., 2007).

Brevetoxins (BTX) and ciguatoxin (CGTX) are both known neurotoxins that belong to ladder-frame polyether class. These neurotoxins are sodium channel activator. They bind to voltage-

sensitive sodium channels and opening it that cause depolarization (Rossini and Hess, 2010). BTX cause neurotoxic shellfish poisoning (NSP) (Watkins et al., 2008), whilst CGTX is responsible for ciguatera fish poisoning (CFP) (Crump et al., 1999).

Cyanotoxins (CYTX) are group of toxins produced exclusively by freshwater cyanobacteria. Unlike marine phycotoxins, freshwater toxins are more structurally diverse that distinctively include peptides, phosphate esters, and chlorinated diaryllactones. Also, they are more functionally diverse and widely known as either dermatotoxic, hepatotoxic, or neurotoxic.

The diversity of phycotoxins in terms of structure, biosynthesis, and mode of actions may reveal interesting pattern in the phylogeny of toxin production in phytoplankton. First, this trait is rare, but ubiquitous in their lineage. Second, most toxins are exclusively found in specific groups (e.g. DA production by diatom), and few are produced by phytoplankton that are phylogenetically distant (e.g. STX production by cyanobacteria and dinoflagellates). These patterns provide insights to the heritability of this trait and its diversification to provide an adaptive advantage to the producers.

ORIGIN AND EVOLUTION OF TOXINS IN PHYTOPLANKTON

The diversity of phycotoxins is associated with a wide diversity of toxic phytoplankton lineage (Figure 2). Oddly, toxicity is a rare trait among phytoplankton taxa. Toxicity may have arisen multiple independent times, however, there is some evidence that part of the diversity in toxins arise through subsequent diversification. In some cases, the algae toxicity may not even be attributed to the algae itself, but to bacteria in its associated microbiome. Here, we summarised our current knowledge on the phylogenetic distribution and origin of toxins in phytoplankton, and explore the different theories that may suggest putative alternate roles of phycotoxins.
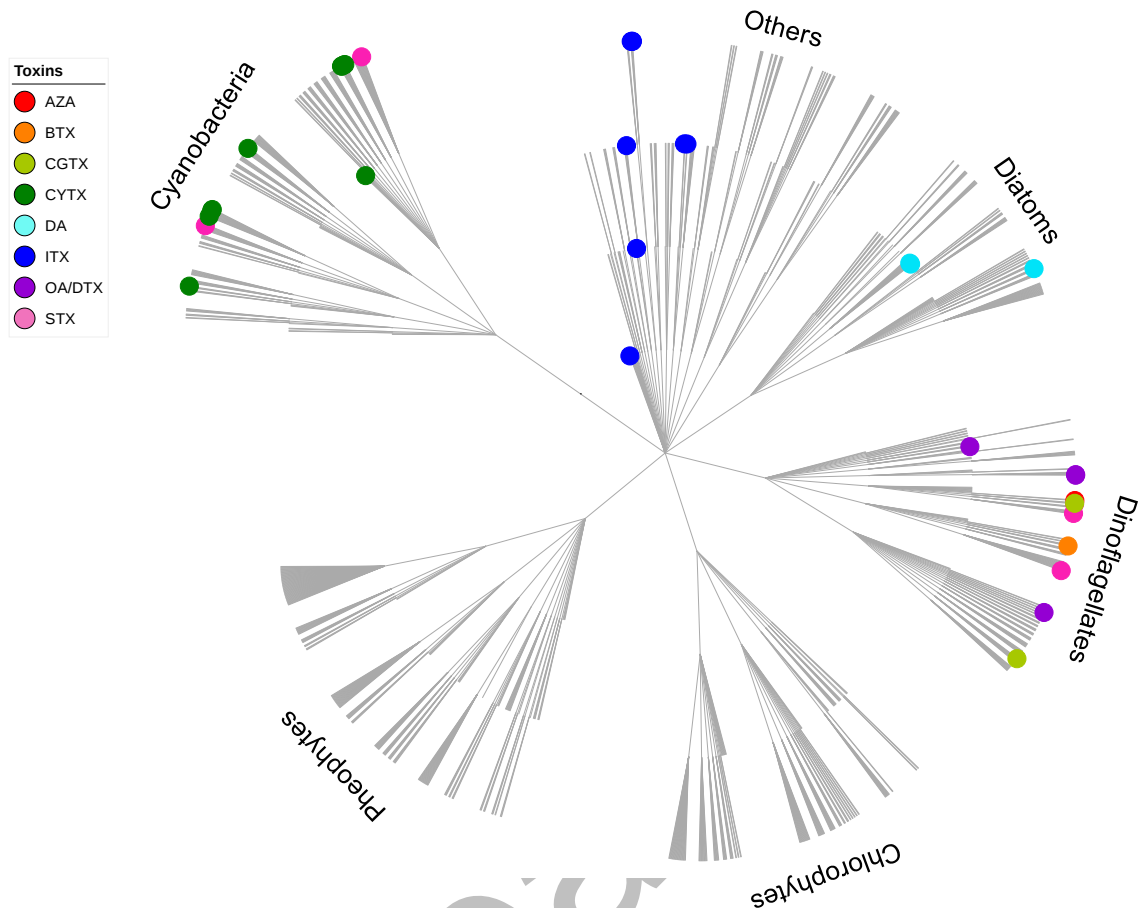
Figure 2. A phylogenetic tree of the phytoplankton within the major taxonomic group. The points represents toxic phytoplankton listed in IOC-UNESCO Taxonomic Reference List of Harmful Micro Algae (Moestrup et al., 2009). The colors represent the different toxins that are produced by the toxic phytoplankton at general. This phylogenetic relationship of phytoplankton is based on the molecular National Center for Biotechnology Information (NCBI) databases constructed using iTOL v.3 developed by Letunic & Bork (2016).

Rarity and ubiquity of toxin production

Toxin production is only found for few phytoplankton species (currently, 150 species in 50 genera listed in Moestrup et al. (2009)) but are present in most major phytoplankton groups. All major groups of phytoplankton, except for cholorphytes, contain at least one species that produces a toxin. Phycotoxins are mainly produced by dinoflagellates (82 species in 24 genera mostly from the genera *Alexandrium*, *Gambierdiscus*, *Prorocentrum*, *Dinophysis, Karenia* and *Azadinium*), diatoms (26 species in 3 genera, mostly from the genus *Pseudo-nitzschia*) and cyanobacteria (25 species in 13 genera, mostly from the genera *Microcystis* and *Dolichospermum*), and few representatives (≤ 8 species in ≤ 3 genera) of haptophytes, raphidophytes, dictyochophytes, and pelagophytes. Approximation of the species richness of toxic phytoplankton is undoubtedly underestimated as (1) many phytoplankton that belong to toxic taxa remain to be examined and (2) novel compounds that may have putative toxic effects are also continuously being discovered in phytoplankton, for example, derivatives of maitotoxin, pectenotoxin, and spirolides (e.g. Ajani et al., 2017; Amzil et al., 2007; Pisapia et al., 2017). It is

plausible that many more toxins will be discovered and more toxic phytoplankton will be identified as our scientific awareness and monitoring effort increases.

Exclusivity and cross-taxa distribution of toxin production

Toxin type appears to be a phylogenetically conserved trait among toxic phytoplankton. For instance, DA production is exclusively found in toxic diatoms. Whilst, production of STX is found in the cyanobacteria and dinoflagellate lineage. In cyanobacteria, it is found in *Cylindrospermum* and *Phormidium*, whilst in dinoflagellates, this trait is shared by *Alexandrium*, *Pyrodinium,* and Gymnodinium within the orders Gonyaulacales and Gymnodiniales. On the other hand, most polyether toxins producers exclusively belong to dinoflagellates. Among the dinoflagellates toxins, AZA and BTX are exclusively found in the order Gonyaulacales and Gymnodiniales, respectively. OA/DTX production is shared by *Prorocentrum*, *Dinophysis*, *Phalacroma*, and *Coolia* within the order Prorocentrales, Dinophysiales, Peridiniales. CGTX production is known in *Gambierdiscus* and *Fukuyoa* within the order of Gonyaulacales and Peridiniales, respectively.

There is no clear evidence to explain why some phytoplankton species or even strains of the same species are toxic while others are not. The pattern in the distribution of toxin production in phytoplankton lineage may give insights on the origin and evolution of phycotoxins.

Heritability of toxin production

The rarity of toxin production may suggest that this trait may not be essential for phytoplankton survival, and hence only a few species may have evolved to produce toxins. It is also plausible that toxin may not be produced by the phytoplankton, but by the co-cultured bacteria. This co-cultured bacteria theory is supported by the evidence from several studies on saxitoxin biosynthesis in dinoflagellates (Kodama et al., 1988; Silva, 1990) but is challenged by some (Baker et al., 2003; Hold et al., 2001; Martins et al., 2003). Less support is given to this theory since the discovery of the *sxt* genes in dinoflagellates (Russell J.S. Orr et al., 2013; Stüken et al., 2011). No evidence that DA can be autonomously produced by intracellular or isolated extracellular bacteria (Bates, 1998). However, it has been suggested that bacteria may play a role in the production of DA by toxic diatoms, but the link between DA production and physiology needs further investigations (Lelong et al., 2014). The discovery of genes that code for enzymes which are essential for the biosynthesis of phycotoxin (Kimura et al., 2015; Russell J.S. Orr et al., 2013; Perini et al., 2014) may give us the certainty that toxin production is a heritable trait in phytoplankton.

Diversification of toxin production

The widespread distribution of toxicity in phytoplankton lineage may indicate that toxin may have diversified to provide an adaptive advantage to the producers, which lead to expectations of the perpetuity of toxicity and similarity of toxin profiles in all toxic strains of the same species. The conservatism and cross-taxa distribution of this trait may suggest that the recent toxic species may have acquired this trait from a toxic ancestor that may have undergone a convergent or divergent evolution. The convergent evolution theory postulates that production of toxin has a polyphyletic origin. For instance, STX biosynthesis occurred independently in the lineages of cyanobacteria and dinoflagellate, converging on the same toxic compound

(Cembella, 1998). However, this theory is challenged by the confirmation of multiple *sxt* homologues with a high sequence which suggest that convergent evolution of STX biosynthesis is unlikely (Orr et al., 2013). Also, the lack of evidence of their eco-evolutionary roles and selective pressure implies that convergence is unlikely to have happened (Orr et al., 2013).

The most established theory is the horizontal gene transfer (De la Cruz and Davies, 2000). It suggests that genes for biosynthesis of toxin originate from ancestral bacteria and introduce to toxic phytoplankton genome via horizontal gene transfer (HGT) event. For example, cyanobacteria and dinoflagellates obtained the STX biosynthetic genes from an ancestral bacteria via HGT event (Plumey, 2001), which is supported by the evidence that most of the sxt homologues in cyanobacteria have an origin in other bacterial genomes (Moustafa et al., 2009). It postulated that sxt genes identified in dinoflagellates have been introduced via HGT from a STX-producing cyanobacterial origin, which probably happened before the divergence of Alexandrium and Pyrodinium within the order Gonyaulacales, and some descendant species may have lost these genes (Russell J.S. Orr et al., 2013). Moreover, structural alignment of 28S rDNA sequences from diatoms, including toxic species, provides insights into the phylogeny of DA synthesis (Lundholm et al., 2002), which suggests that production of DA has either evolved independently many times, or the necessary genes have been laterally transferred, and that multiple losses have happened (Janson and Hayes, 2006). Furthermore, it has been observed that polyketide biosynthesis by type I PKS are found in a few bacteria (Broadhurst et al., 2003; Chen and Du, 2016; Moss et al., 2004), which implies that the biosynthetic genes in eukaryotes may have come from prokaryotes (Kellmann et al., 2010; Kroken et al., 2003). This bacterial origin theory suggests that genes for biosynthesis of polyethers toxins have been introduced to dinoflagellates genome via HGT, with the successive alteration that results to diverse polyketide-derived polyether compounds (Kellmann et al., 2010; Wright and Cembella, 1998).

ROLES OF TOXIN PRODUCTION IN PHYTOPLANKTON

Regardless of the origin of toxin production in phytoplankton, toxic species must have benefitted from keeping the complex and costly biosynthesis of toxins. Algal toxins have generally been considered as secondary metabolites that do not directly involved in the primary metabolism of the organism (Bates, 1998; Cembella, 1998; Wright and Cembella, 1998). They were once thought as waste products but were later given putative roles as they have costly biosynthesis and regulatory mechanism that may indicate that they have evolved to benefit the cell (Vining, 1990). They were several hypotheses that have based their assumptions on the chemical properties, structural homology, and mode of action of toxins, which may suggest their putative ecophysiological functions. However, the functional significance of toxins remained ambiguous due to weak or lack of evidence.

The toxic property of toxin may give us the intuition to attribute reduction of predation as its primary role. However, this hypothesis is challenged by the contrasting results of the effects of the toxin on many predators/grazers (Breier and Buskey, 2007; Koski et al., 1999; Prince et al., 2006). Many toxic algae have other ecophysiological adaptations that are highly effective at reducing predation, such as the production of less costly metabolites (i.e. ROS and PUFA) (Ianora et al., 2011) and chain formation (Selander et al., 2011). Some toxins are not harmful to the direct grazers that may have evolved to

ingest toxin-producing species. For instance, grazers may have mutated their voltage-gated ion channels allowing them to ingest STX producers (Finiguerra et al., 2015) and to integrate the acquired toxins as their defense mechanism against their natural predators. Furthermore, it is likely that toxicity is not related to the main function/s of the toxin. It is possible that toxins have physiological and ecological roles beyond defense against predators/grazers given that their production has been kept over long evolutionary periods despite their biosynthetic costs. Physiological roles of toxins may have evolved in response to stressful abiotic conditions to improve efficiency in nutrient acquisition and storage, excretion, osmoregulation, scavenging mechanisms, biosynthesis, structural organisation, and cell signaling. Ecological roles of toxins may have evolved from the need for communication chemicals (semiochemicals) for biotic interaction to improve efficiency in mating, alarm signals, defense/offense mechanism, and symbiosis.

Putative physiological roles

Nutrient acquisition. Toxins may provide assistance in nutrient uptake during nutrient limitation. Recent evidence has shown that the presence of cyanobacterial toxins triggers other phytoplankton to secrete alkaline phosphatase that can be used by the toxic producers to maximise the uptake of inorganic phosphate (Bar-Yosef et al., 2010).

Nutrient storage. Toxins may serve as a nutrient reserve for remobilization during nutrient limitation (Loeblich & Loeblich, 1984). It has been suggested that STX may perform as nitrogen storage since it known to have a N-rich structure (Cembella, 1998).

Excretion. Toxin synthesis may provide an alternative pathway to dispense excess resources (Bates, 1998; Cembella, 1998). For instance, the structural feature of STX leads to a hypothesis that their biosynthesis may serve as a shunt to prevent NH_4^+ toxicity in a high nutrient condition (Cembella, 1998) and a mechanism to deposit excess N to the sediments (Wyatt and Jenkinson, 1997). Furthermore, DA production is postulated to dispense with excess photosynthetic energy when growth is no longer optimal (Bates, 1998), which is supported by the hypothesis that phosphorylation-derived ATP is not used for primary production during biosynthesis of DA (Pan et al., 1996).

Osmoregulation. Toxins may regulate the osmotic pressure to maintain homeostasis in toxic species. DA may serve as an osmolyte in response to increasing salinity (Bates, 1998) as suggested by its chemical structure that is derived from amino acids (Savage et al., 2012). Furthermore, STX may block sodium channels to maintain sodium homeostasis and reduce salt stress in toxic phytoplankton (Soto-Liebe et al., 2012).

Scavenging mechanism. Toxins may serve as an iron-scavenging molecule and deactivator of free intracellular iron in response to iron stress. This function has been suggested on the evidence that toxic cyanobacterial species have more iron uptake systems and the production of toxin appear to be regulated by the free intracellular iron (Utkilen and Gjølme, 1995). Also, toxins may also act as reactive oxygen species (ROS) scavengers in response to oxidative stress. Several studies have shown that toxin

production may protect the cell from oxidative damage due to excessive production of ROS (Alexova et al., 2011; Zilliges et al., 2011).

Other intracellular processes. Toxins may participate in other cellular processes. For example, polyether toxins may serve as signaling factors or cell regulators (Wright and Cembella, 1998). STX may play a role in the ancestral pathway of nucleic acid biosynthesis as suggested by their structural affinity with purine (Cembella, 1998). STX may also have a functional role in chromosome structural organization as implied by their proximity to chromosomes (Anderson and Cheng, 1988).

Putative ecological roles

Mating. Toxins may facilitate sexual reproduction in toxic phytoplankton species. For instance, STX is postulated to serve as sex pheromones, which is released in senescence via leakage, excretion, or cell lysis plausibly during the bloom decline (Wyatt and Jenkinson, 1997), as supported by experimental findings that toxin content per cell is maximal at exponential growth phase and declines at stationary phase (Prakash, 1967; White and Maranda, 1978). These toxins may have evolved to facilitate the success of mating by improving the ability of gametes to find each other and by allowing recognition of the correcting mating types (Wyatt and Jenkinson, 1997). Furthermore, the quanidium groups of STX may function as a surface recognition site for cell mating (Cembella, 1998).

Defense/offense. Toxins, especially those that are known to be effective Na^+ channel blockers, may serve as allomones that can be used for chemical defense by toxic phytoplankton species against predators (i.e. copepods, ciliates, and heterotrophic dinoflagellates) by deterring grazing and reducing grazer's reproductive viability (Cembella, 1998).

Chemical cues. Toxins may be used by toxic species as alarm pheromones. This is in response to the threat of grazing pressure and/or resource competition in order to warn conspecifics of the presence of danger and cooperatively reduce the risk of predation and competition. Moreover, STX may also have similar function to a compound linked to bioluminescence as suggested by their structural resemblance (Cembella, 1998). This may attract potential mate, lure prey, or scare predators. However, there is no evidence to support these hypotheses.

Symbiosis. It is also plausible that toxins may act as synmones, where toxins benefit both the producers and recipients. For instance, toxic algal epiphytes may use their toxins to compete on the limited macro algal space more effectively with other epiphytes, and in return the toxins may provide the macroalgae a mechanism to deter herbivory.

ECOPHYSIOLOGICAL ADVANTAGE OF TOXIN PRODUCTION IN THE CHANGING OCEAN

Toxin production may be a plastic trait and is influenced by a number of abiotic factors such as temperature, pH, light, nutrients and biotic factors such as competition and grazing. It is likely that toxin production may arise from the interaction between abiotic and biotic pressures, and hence may serve multiple functions acting at intracellular and intercellular levels. This multi-functionality of toxins may provide toxic species an ecophysiological advantage over non-toxic species, and have an overall positive feedback on their fitness in the changing environment.

For instance, the temperature is one of the most fundamental abiotic factors that may have a direct effect, or an indirect effect if growth and toxin production is uncoupled (Cembella, 1998). Temperature-dependent effect of toxin production is associated with species-specific growth rate, and hence production of toxins is dependent on the thermal tolerance of the species. Growth at the sub-optimal thermal range was observed to favor a high cell PSP toxin quota in *Alexandrium* spp. (Usup et al., 1994), which may suggest that cellular nitrogen is more allocated to toxin synthesis than protein biosynthesis at this condition (Anderson et al., 1990). The same observation was found in *Pseudo-nitzchia seriata* where growth at lower temperature produce higher levels of cellular DA, but it is still unclear whether this is due to physiological stress at this condition (Bates, 1998). It is also observed that cellular OA/DTX content is increased in *Prorocentrum lima* at lower temperature which may be also attributed to a division rate rather an increase in production (Wright and Cembella, 1998). Furthermore, cell growth in *Pseudo-nitzchia multiseries* at higher temperature and light did increase the cellular DA content, which may suggest increase supply of photosynthetic energy to enhance DA production (Bates, 1998). Some species produce toxin in response to stressful thermal conditions when growth is strongly inhibited (Aquino-Cruz, 2012). Long-term starvation allows toxic species to accumulate toxins (Lee et al., 2016), which can be induced when increased temperature limits their capacity to uptake nutrients (Sterner and Grover, 1998). Thermal plasticity of toxin production may have a positive (benefit) and negative (cost) outcomes to the producers at the intracellular level, and at the same time may place a benefit (positive externality) or a cost (negative externality) to other organisms at the intercellular level. Two ecological scenarios can be postulated to arise under non-optimal condition. First is that toxic species might reduce their production of the toxins to redirect their energy for cell growth. However, this could increase their vulnerability to grazing and competition; hence, could provide more resources to their enemies (i.e. grazers/predators or competitors). Second is that they might enhance their toxin production to influence their external environment. In this scenario, toxic species could exploit more resource and could better defend themselves against their enemies, however at the expense of high metabolic cost. Both scenarios have a potential implication on how toxin production could influence the structure and function of marine ecosystems in the future climate scenario.

CONCLUSION

Further work is needed to address the following questions: (1) How does toxigenicity spread in phytoplankton lineage? (2) How toxin production responds to individual and combined effects of biotic and abiotic pressures? (3) How toxin production influences the structure and function of the aquatic ecosystem? The "omics" technology (i.e. genomics, transcriptomics, proteomics, metabolomics, metagenomics) is a promising tool to elucidate the biosynthesis and regulation of toxins in phytoplankton and may shed light on the origin and evolutionary history of toxin production. This technology can also be applied to study the ecophysiological dynamics of toxin production which may lead to a new understanding in the evolution and ecology of toxic phytoplankton species.

REFERENCES

Ajani, P., Harwood, D., Murray, S., 2017. Recent Trends in Marine Phycotoxins from Australian Coastal Waters. Mar. Drugs 15, 33. https://doi.org/10.3390/md15020033

Alexova, R., Haynes, P.A., Ferrari, B.C., Neilan, B.A., 2011. Comparative protein expression in different strains of the bloom-forming cyanobacterium Microcystis aeruginosa. Mol. Cell. Proteomics 10, M110.003749. https://doi.org/10.1074/mcp.M110.003749

Allingham, J.S., Miles, C.O., Rayment, I., 2007. A Structural Basis for Regulation of Actin Polymerization by Pectenotoxins. J. Mol. Biol. 371, 959–970. https://doi.org/10.1016/j.jmb.2007.05.056

Amzil, Z., Sibat, M., Royer, F., Masson, N., Abadie, E., 2007. Report on the First Detection of Pectenotoxin-2, Spirolide-A and Their Derivatives in French Shellfish. Mar. Drugs 5, 168–179. https://doi.org/10.3390/md504168

Anderson, D.M., Cembella, A.D., Hallegraeff, G.M., 2012. Progress in understanding harmful algal blooms: paradigm shifts and new technologies for research, monitoring, and management. Ann. Rev. Mar. Sci. 4, 143–76. https://doi.org/10.1146/annurev-marine-120308-081121

Anderson, D.M., Cheng, T.P.-O., 1988. Intracellular localization of saxitoxins in the dinoflagellate Gonyaulax tamarensis. J. Phycol. 24, 17–22. https://doi.org/10.1111/j.1529-8817.1988.tb04451.x

Anderson, D.M., Kulis, D.M., Sullivan, J.J., Hall, S., Lee, C., 1990. Dynamics and physiology of saxitoxin production by the dinoflagellates Alexandrium spp. Mar. Biol. https://doi.org/10.1007/BF01314358

Aquino-Cruz, A., 2012. Effect of increasing sea water temperature on the growth and toxin production of three harmful benthic dinoflagellates isolated from the fleet lagoon, dorset, uk. PQDT - UK Irel.

Bajarias, F.F.A., Yuichi, K., Relox Jr., J.R., Romero, M.L.J., Furio, E.F., Lundholm, N., Kazuhiko, K., Yasuwo, F., Masaaki, K., 2006. Screening of diatoms producing domoic acid and its derivatives in the Philippines. Coast. Mar. Sci. 30, 121–129.

Baker, T.R., Doucette, G.J., Powell, C.L., Boyer, G.L., Plumley, F.G., 2003. GTX4 imposters: Characterization of fluorescent compounds synthesized by Pseudomonas stutzeri SF/PS and Pseudomonas/Alteromonas PTB-1, symbionts of saxitoxin-producing Alexandrium spp. Toxicon 41, 339–347. https://doi.org/10.1016/S0041-0101(02)00314-8

Bar-Yosef, Y., Sukenik, A., Hadas, O., Viner-Mozzini, Y., Kaplan, A., 2010. Enslavement in the Water Body by Toxic Aphanizomenon ovalisporum, Inducing Alkaline Phosphatase in Phytoplanktons. Curr. Biol. 20, 1557–1561. https://doi.org/10.1016/j.cub.2010.07.032

Bates, S.S., 1998. Ecophysiology and Metabolism of ASP Toxin Production, in: Anderson, D.M., Cembella, A.D., Hallegraeff, G.M. (Eds.), Physiological Ecology of Harmful Algal Blooms. Springer-Verlag, Heidelberg (1998), pp. 405–426.

Behrenfeld, M.J., O'Malley, R.T., Siegel, D.A., McClain, C.R., Sarmiento, J.L., Feldman, G.C., Milligan, A.J., Falkowski, P.G., Letelier, R.M., Boss, E.S., 2006. Climate-driven trends in contemporary ocean productivity. Nature 444, 752–755. https://doi.org/10.1038/nature05317

Berdalet, E., Fleming, L.E., Gowen, R., Davidson, K., Hess, P., Backer, L.C., Moore, S.K., Hoagland, P., Enevoldsen, H., 2015. Marine harmful algal blooms, human health and wellbeing: challenges and opportunities in the 21st century. J. Mar. Biol. Assoc. U.K.. 2015. https://doi.org/10.1017/S0025315415001733

Breier, C.F., Buskey, E.J., 2007. Effects of the red tide dinoflagellate, Karenia brevis, on grazing and fecundity in the copepod Acartia tonsa. J. Plankton Res. 29, 115–126. https://doi.org/10.1093/plankt/fbl075

Broadhurst, R.W., Nietlispach, D., Wheatcroft, M.P., Leadlay, P.F., Weissman, K.J., 2003. The structure of docking domains in modular polyketide synthases. Chem. Biol. 10, 723–731. https://doi.org/10.1016/S1074-5521(03)00156-X

Cembella, A., 1998. Ecophysiology and Metabolism of Paralytic Shellfish Toxins in Marine Microalgae, in: Anderson, D.M., Cembella, A.D., Hallegraeff, G.M. (Eds.), Physiological Ecology of Harmful Algal Blooms. NATO-Advanced Study Institute Series, Springer-Verlag, Heidelberg, pp. 381–404.

Cembella, A.D., 2003. Chemical ecology of eukaryotic microalgae in marine ecosystems. Phycologia 42, 420–447. https://doi.org/10.2216/i0031-8884-42-4-420.1

Chen, H., Du, L., 2016. Iterative polyketide biosynthesis by modular polyketide synthases in bacteria. Appl. Microbiol. Biotechnol. 100, 541–57. https://doi.org/10.1007/s00253-015-7093-0

Crump, J.A., McLay, C.L., Chambers, S.T., 1999. Ciguatera fish poisoning. Postgrad. Med. J. 75, 678–9.

Cusick, K., Sayler, G., 2013. An Overview on the Marine Neurotoxin, Saxitoxin: Genetics, Molecular Targets, Methods of Detection and Ecological Functions. Mar. Drugs 11, 991–1018. https://doi.org/10.3390/md11040991

De la Cruz, F., Davies, J., 2000. Horizontal gene transfer and the origin of species: Lessons from bacteria. Trends Microbiol. https://doi.org/10.1016/S0966-842X(00)01703-0

Falkowski, P., 2012. Ocean science: the power of plankton. Nature 483, S17–S20.

Falkowski, P.G., Oliver, M.J., 2007. Mix and match: how climate selects phytoplankton. Nat. Rev. Microbiol. 5, 813–819. https://doi.org/10.1038/nrmicro1751

Fu, F.X., Tatters, A.O., Hutchins, D.A., 2012. Global change and the future of harmful algal blooms in the ocean. Mar. Ecol. Prog. Ser. 470, 207–233. https://doi.org/10.3354/meps10047

Garibo, D., de la Iglesia, P., Diogène, J., Campàs, M., 2013. Inhibition Equivalency Factors for Dinophysistoxin-1 and Dinophysistoxin-2 in Protein Phosphatase Assays: Applicability to the Analysis of Shellfish Samples and Comparison with LC-MS/MS. J. Agric. Food Chem. 61, 2572–2579. https://doi.org/10.1021/jf305334n

Gupta, S., Norte, M., Shimizu, Y., 1989. Biosynthesis of saxitoxin analogues: the origin and introduction mechanism of the side-chain carbon. J. Chem. Soc., Chem. Commun. 0, 1421–1424. https://doi.org/10.1039/C39890001421

Hackett, J.D., Tong, M., Kulis, D.M., Fux, E., Hess, P., Bire, R., Anderson, D.M., 2009. DSP toxin production de novo in cultures of Dinophysis acuminata (Dinophyceae) from North America. Harmful Algae 8, 873–879. https://doi.org/10.1016/j.hal.2009.04.004

Hallegraeff, G.M., 2014. Harmful Algae and their Toxins: Progress, Paradoxes and Paradigm Shifts, in: Rossini, G.P. (Ed.), Toxins and Biologically Active Compounds from Microalgae. CRC Press, pp. 3–20. https://doi.org/10.1201/b16569-3

Hallegraeff, G.M., 2010. Ocean climate change, phytoplankton community responses, and harmful algal blooms: A formidable predictive challenge. J. Phycol. https://doi.org/10.1111/j.1529-8817.2010.00815.x

Hallegraeff, G.M., Anderson, D.M., Cembella, A.D. (Eds.), 2004. Manual on Harmful Marine Microalgae, Monographs on Oceanographic Methodology. https://doi.org/10.1097/00000433-198206000-00020

Hold, G.L., Smith, E.A., Harry Birkbeck, T., Gallacher, S., 2001. Comparison of paralytic shellfish toxin (PST) production by the dinoflagellates Alexandrium lusitanicum NEPCC 253 and Alexandrium tamarense NEPCC 407 in the presence and absence of bacteria. FEMS Microbiol. Ecol. 36, 223–234. https://doi.org/10.1111/j.1574-6941.2001.tb00843.x

Holland, P.T., Selwood, A.I., Mountfort, D.O., Wilkins, A.L., McNabb, P., Rhodes, L.L., Doucette, G.J., Mikulski, C.M., King, K.L., 2005. Isodomoic Acid C, an Unusual Amnesic Shellfish Poisoning Toxin from *Pseudo-nitzschia australis* [†]. Chem. Res. Toxicol. 18, 814–816. https://doi.org/10.1021/tx0496845

Ianora, A., Bentley, M.G., Caldwell, G.S., Casotti, R., Cembella, A.D., Engström-Öst, J., Halsband, C., Sonnenschein, E., Legrand, C., Llewellyn, C.A., Paldavičienë, A., Pilkaityte, R., Pohnert, G., Razinkovas, A., Romano, G., Tillmann, U., Vaiciute, D., 2011. The Relevance of Marine Chemical Ecology to Plankton and Ecosystem Function: An Emerging Field. Mar. Drugs 9, 1625–1648. https://doi.org/10.3390/md9091625

Janson, S., Hayes, P.K., 2006. Molecular Taxonomy of Harmful Algae, in: Ecology of Harmful Algae. Springer Berlin Heidelberg, pp. 9–21. https://doi.org/10.1007/978-3-540-32210-8_2

Kellmann, R., Stüken, A., Orr, R.J.S., Svendsen, H.M., Jakobsen, K.S., 2010. Biosynthesis and molecular genetics of polyketides in marine dinoflagellates. Mar. Drugs 8, 1011–1048. https://doi.org/10.3390/md8041011

Kimura, K., Okuda, S., Nakayama, K., Shikata, T., Takahashi, F., Yamaguchi, H., Skamoto, S., Yamaguchi, M., Tomaru, Y., 2015. RNA Sequencing Revealed Numerous Polyketide Synthase Genes in the Harmful Dinoflagellate Karenia mikimotoi. https://doi.org/10.1371/journal.pone.0142731

Kodama, M., Ogata, T., Sato, S., 1988. Bacterial production of saxitoxin. Agric. Biol. Chem. 52, 1075–1077. https://doi.org/10.1271/bbb1961.52.1075

Koski, M., Rosenberg, M., Viitasalo, M., Tanskanen, S., Sjölund, U., 1999. Is Prymnesium patelliferum toxic for copepods? – Grazing, egg production, and egestion of the calanoid copepod Eurytemora affinis in mixtures of "'good'" and " 'bad'" food. ICES J. Mar. Sci. 56, 131–139. https://doi.org/DOI 10.1006/jmsc.1999.0621

Kotaki, Y., Furio, E.F., Satake, M., Lundholm, N., Katayama, T., Koike, K., Fulgueras, V.P., Bajarias, F.A., Takata, Y., Kobayashi, K., Sato, S., Fukuyo, Y., Kodama, M., 2005. Production of isodomoic acids A and B as major toxin components of a pennate diatom Nitzschia navis-varingica. Toxicon 46, 946–953. https://doi.org/https://doi.org/10.1016/j.toxicon.2005.09.004

Kroken, S., Glass, N.L., Taylor, J.W., Yoder, O.C., Turgeon, B.G., 2003. Phylogenomic analysis of type I polyketide synthase genes in pathogenic and saprobic ascomycetes. Proc. Natl. Acad. Sci. U. S. A. 100, 15670–5. https://doi.org/10.1073/pnas.2532165100

Lee, T., Fong, F., Ho, K.-C., Lee, F., 2016. The Mechanism of Diarrhetic Shellfish Poisoning Toxin Production in Prorocentrum spp.: Physiological and Molecular Perspectives. Toxins (Basel). 8, 272. https://doi.org/10.3390/toxins8100272

Lelong, A., Hégaret, H., Soudant, P., 2014. Link between domoic acid production and cell physiology after exchange of bacterial communities between toxic Pseudo-nitzschia multiseries and non-toxic Pseudo-nitzschia delicatissima. Mar. Drugs 12, 3587–607. https://doi.org/10.3390/md12063587

Letunic, I., Bork, P., 2016. Interactive tree of life (iTOL) v3: an online tool for the display and annotation of phylogenetic and other trees. Nucleic Acids Res. 44, W242–W245. https://doi.org/10.1093/nar/gkw290

Lundholm, N., Daugbjerg, N., Moestrup, Ø., 2002. Phylogeny of the Bacillariaceae with emphasis on the genus *Pseudo - nitzschia* (Bacillariophyceae) based on partial LSU rDNA. Eur. J. Phycol. 37, 115–134. https://doi.org/10.1017/S096702620100347X

Maeno, Y., Kotaki, Y., Terada, R., Cho, Y., Konoki, K., Yotsu-Yamashita, M., 2018. Six domoic acid related compounds from the red alga, Chondria armata, and domoic acid biosynthesis by the diatom, Pseudo-nitzschia multiseries. Sci. Rep. 8, 356. https://doi.org/10.1038/s41598-017-18651-w

Martins, C.A., Alvito, P., Tavares, M.J., Pereira, P., Doucette, G., Franca, S., 2003. Reevaluation of production of paralytic shellfish toxin by bacteria associated with dinoflagellates of the Portuguese coast. Appl. Environ. Microbiol. 69, 5693–8. https://doi.org/10.1128/AEM.69.9.5693-5698.2003

Moestrup, Ø., Akselmann, R., Fraga, S., Hoppenrath, M., Iwataki, M., Komárek, J., Larsen, J., Lundholm, N., Zingone, A., 2009. IOC-UNESCO Taxonomic Reference List of Harmful Micro Algae (HABs) [WWW Document]. URL http://www.marinespecies.org/hab/index.php (accessed 10.12.17).

Moore, S.K., Trainer, V.L., Mantua, N.J., Parker, M.S., Laws, E.A., Backer, L.C., Fleming, L.E., 2008. Impacts of climate variability and future climate change on harmful algal blooms and human health. Environ. Health 7 Suppl 2, S4. https://doi.org/10.1186/1476-069X-7-S2-S4

Moss, S.J., Martin, C.J., Wilkinson, B., 2004. Loss of co-linearity by modular polyketide synthases: a mechanism for the evolution of chemical diversity. Nat. Prod. Rep. 21, 575–593. https://doi.org/10.1039/b315020h

Moustafa, A., Loram, J.E., Hackett, J.D., Anderson, D.M., Plumley, F.G., Bhattacharya, D., 2009. Origin of Saxitoxin Biosynthetic Genes in Cyanobacteria. PLoS One 4, e5758. https://doi.org/10.1371/journal.pone.0005758

Murray, S., Diwan, R., Orr, R., Kohli, G., John, U., Eddy, S., Skamoto, S., Yamaguchi, M., Tomaru, Y., 2015. Gene duplication, loss and selection in the evolution of saxitoxin biosynthesis in alveolates. Mol phylogenet evol 92, e0142731.

https://doi.org/10.1371/JOURNAL.PONE.0142731

Murray, S.A., Wiese, M., Stüken, A., Brett, S., Kellmann, R., Hallegraeff, G., Neilan, B.A., 2011. sxtA-Based Quantitative Molecular Assay To Identify Saxitoxin-Producing Harmful Algal Blooms in Marine Waters. Appl. Environ. Microbiol. 77, 7050–7057. https://doi.org/10.1128/AEM.05308-11

Ohfune, Y., Tomita, M., 1982. Total synthesis of (-)-domoic acid. A revision of the original structure. J. Am. Chem. Soc. 104, 3511–3513. https://doi.org/10.1021/ja00376a048

Orr, R.J.S., Stüken, A., Murray, S.A., Jakobsen, K.S., 2013. Evolution and distribution of saxitoxin biosynthesis in dinoflagellates. Mar. Drugs. https://doi.org/10.3390/md11082814

Orr, R.J.S., Stüken, A., Murray, S.A., Jakobsen, K.S., 2013. Evolutionary acquisition and loss of saxitoxin biosynthesis in dinoflagellates: The second "core" gene, sxtG. Appl. Environ. Microbiol. 79, 2128–2136. https://doi.org/10.1128/AEM.03279-12

Pan, Y., Subba Rao, D. V., Mann, K.H., 1996. Changes in domoic acid production and cellular chemical composition of the toxigenic diatom Pseudo-nitschia multiseries under phosphate limitation. J. Phycol. 32, 371–381. https://doi.org/10.1111/j.0022-3646.1996.00371.x

Perini, F., Galluzzi, L., Dell'Aversano, C., Iacovo, E., Tartaglione, L., Ricci, F., Forino, M., Ciminiello, P., Penna, A., 2014. SxtA and sxtG Gene Expression and Toxin Production in the Mediterranean Alexandrium minutum (Dinophyceae). Mar. Drugs 12, 5258–5276. https://doi.org/10.3390/md12105258

Pisapia, F., Sibat, M., Herrenknecht, C., Lhaute, K., Gaiani, G., Ferron, P.-J., Fessard, V., Fraga, S., Nascimento, S.M., Litaker, R.W., Holland, W.C., Roullier, C., Hess, P., 2017. Maitotoxin-4, a Novel MTX Analog Produced by Gambierdiscus excentricus. Mar. Drugs 15, 220. https://doi.org/10.3390/md15070220

Plumey, F.G., 2001. Purification of an enzyme involved in saxitoxin synthesis. J. Phycol. 37, 926–928. https://doi.org/10.1046/j.1529-8817.2001.37601.x

Prakash, A., 1967. Growth and Toxicity of a Marine Dinoflagellate, *Gonyaulax tamarensis*. J. Fish. Res. Board Canada 24, 1589–1606. https://doi.org/10.1139/f67-131

Prince, E.K., Lettieri, L., McCurdy, K.J., Kubanek, J., 2006. Fitness consequences for copepods feeding on a red tide dinoflagellate: deciphering the effects of nutritional value, toxicity, and feeding behavior. Oecologia 147, 479–488. https://doi.org/10.1007/s00442-005-0274-2

Quilliam, M.A., Hardstaff, W.R., Ishida, Noriko, 2, McLachlan, J.L., Reeves, A.R., Ross, N.W., Windust, A.J., 1996. Production of Diarrhetic Shellfish Poisoning (DSP) toxins by Prorocentrum lima in culture and development of analytical methods, in: Yasumoto, T., Oshima, Y., Fukuyo, Y. (Eds.), Harmful and Toxic Algal Blooms,. IOC/UNESCO, Paris, pp. 289–92.

Ramsdell, J.S., 2007. The Molecular and Integrative Basis to Domoic Acid Toxicity, in: Phycotoxins: Chemistry and Biochemistry. Blackwell Publishing, Ames, Iowa, USA, pp. 223–250. https://doi.org/10.1002/9780470277874.ch13

Ramsey, U.P., Douglas, D.J., Walter, J.A., Wright, J.L., 1998. Biosynthesis of domoic acid by the diatom Pseudo-nitschia multiseries. Nat. Toxins 6, 137–146. https://doi.org/10.1002/(SICI)1522-7189(199805/08)6:3/4<137::AID-NT28>3.0.CO;2-L

Rasmussen, S.A., Andersen, A.J.C., Andersen, N.G., Nielsen, K.F., Hansen, P.J., Larsen, T.O., 2016. Chemical Diversity, Origin, and Analysis of Phycotoxins. J. Nat. Prod. 79, 662–673. https://doi.org/10.1021/acs.jnatprod.5b01066

Rossini, G.P., Hess, P., 2010. Phycotoxins: chemistry, mechanisms of action and shellfish poisoning. EXS 100, 65–122.

Savage, T.J., Smith, G.J., Clark, A.T., Saucedo, P.N., 2012. Condensation of the isoprenoid and amino precursors in the biosynthesis of domoic acid. Toxicon 59, 25–33. https://doi.org/10.1016/j.toxicon.2011.10.010

Selander, E., Jakobsen, H.H., Lombard, F., Kiorboe, T., 2011. Grazer cues induce stealth behavior in marine dinoflagellates. Proc. Natl. Acad. Sci. 108, 4030–4034. https://doi.org/10.1073/pnas.1011870108

Shimizu, Y., 1996. Microalgal metabolites: a new perspective. Annu. Rev. Microbiol. 50, 431–465. https://doi.org/10.1146/annurev.micro.50.1.431

Shimizu, Y., Norte, M., Hori, A., Genenah, A., Kobayashi, M., 1984. Biosynthesis of Saxitoxin

Analogues: The Unexpected Pathway. J. Am. Chem. Soc. 106, 6433–6434. https://doi.org/10.1021/ja00333a062

Silva, E.S., 1990. Intracellular bacteria: the origin of dinoflagellate toxicity. J. Environ. Pathol. Toxicol. Oncol. 10, 124–128.

Soto-Liebe, K., Méndez, M.A., Fuenzalida, L., Krock, B., Cembella, A., Vásquez, M., 2012. PSP toxin release from the cyanobacterium Raphidiopsis brookii D9 (Nostocales) can be induced by sodium and potassium ions. Toxicon 60, 1324–1334. https://doi.org/10.1016/j.toxicon.2012.09.001

Staunton, J., Weissman, K.J., 2001. Polyketide biosynthesis: a millennium review. Nat. Prod. Rep. 18, 380–416. https://doi.org/10.1039/a909079g

Sterner, R.W., Grover, J.P., 1998. Algal growth in warm temperate reservoirs: kinetic examination of nitrogen, temperature, light, and other nutrients. Water Res. 32, 3539–3548. https://doi.org/10.1016/S0043-1354(98)00165-1

Stüken, A., Orr, R.J.S., Kellmann, R., Murray, S.A., Neilan, B.A., Jakobsen, K.S., 2011. Discovery of Nuclear-Encoded Genes for the Neurotoxin Saxitoxin in Dinoflagellates. PLoS One 6, e20096. https://doi.org/10.1371/journal.pone.0020096

Tatters, A.O., Flewelling, L.J., Fu, F., Granholm, A.A., Hutchins, D.A., 2013. High CO2 promotes the production of paralytic shellfish poisoning toxins by Alexandrium catenella from Southern California waters. Harmful Algae 30, 37–43. https://doi.org/10.1016/j.hal.2013.08.007

Twiner, M.J., Doucette, G.J., Rasky, A., Huang, X.-P., Roth, B.L., Sanguinetti, M.C., 2012. Marine algal toxin azaspiracid is an open-state blocker of hERG potassium channels. Chem. Res. Toxicol. 25, 1975–84. https://doi.org/10.1021/tx300283t

Usup, G., Kulis, D.M., Anderson, D.M., 1994. Growth and toxin production of the toxic dinoflagellate Pyrodinium bahamense var. compressum in laboratory cultures. Nat. Toxins 2, 254–62.

Utkilen, H., Gjølme, N., 1995. Iron-stimulated toxin production in Microcystis aeruginosa. Appl. Environ. Microbiol. 61, 797–800.

Vining, L.C., 1990. Functions of Secondary Metabolites. Annu. Rev. Microbiol. 44, 395–427. https://doi.org/10.1146/annurev.mi.44.100190.002143

Watkins, S.M., Reich, A., Fleming, L.E., Hammond, R., 2008. Neurotoxic shellfish poisoning. Mar. Drugs 6, 431–55. https://doi.org/10.3390/md20080021

White, A.W., Maranda, L., 1978. Paralytic Toxins in the Dinoflagellate *Gonyaulax excavata* and in Shellfish. J. Fish. Res. Board Canada 35, 397–402. https://doi.org/10.1139/f78-070

Wood, M.E., Fryer, A.M., 1998. Synthesis of kainoids and kainoid analogues, in: Moody, C.J. (Ed.), Advances in Nitrogen Heterocycles. Volume 3. Jai.

Wright, J.L.C., Cembella, A.D., 1998. Ecophysiology and biosynthesis of polyether marine biotoxins., in: Physiological Ecology of Harmful Algal Blooms. pp. 427–451.

Wyatt, T., Jenkinson, I.R., 1997. Notes on Alexandrium population dynamics. J. Plankton Res. 19, 551–575. https://doi.org/10.1093/plankt/19.5.551

Zilliges, Y., Kehr, J.-C., Meissner, S., Ishida, K., Mikkat, S., Hagemann, M., Kaplan, A., Börner, T., Dittmann, E., 2011. The cyanobacterial hepatotoxin microcystin binds to proteins and increases the fitness of microcystis under oxidative stress conditions. PLoS One 6, e17615. https://doi.org/10.1371/journal.pone.0017615

This page is intentionally left blank.

Supplementary information 2.1. *R* packages used in the data processing and analyses.

1. Provoost P, S Bosch. 2019 robis: R Client to access data from the OBIS API.
2. Chamberlain S, Barve V, Mcglinn D, Oldoni D. 2019 rgbif: Interface to the Global Biodiversity Information Facility API. See https://cran.r-project.org/package=rgbif.
3. Chamberlain S *et al.* 2018 taxize: Taxonomic information from around the web. *R Packag. version 0.9.3*.
4. Broennimann O, Di Cola V, Guisan A. 2018 ecospat: Spatial Ecology Miscellaneous Methods.
5. Samuel Bosch. 2018 sdmpredictors: Species Distribution Modelling Predictor Datasets.
6. Harrell Jr FE, with contributions from Charles Dupont, many others. 2019 Hmisc: Harrell Miscellaneous.
7. Hijmans RJ. 2017 geosphere: Spherical Trigonometry.
8. Canty A, Ripley BD. 2019 boot: Bootstrap R (S-Plus) Functions.
9. Bates D, Mächler M, Bolker B, Walker S. 2015 Fitting Linear Mixed-Effects Models Using lme4. *J. Stat. Softw.* **67**, 1–48. (doi:10.18637/jss.v067.i01)
10. Wood S. 2019 Mixed GAM Computation Vehicle with Automatic Smoothness Estimation.
11. Bartoń K. 2019 MuMIn: Multi-Model Inference.
12. Hartig F. 2019 DHARMa: Residual Diagnostics for Hierarchical (Multi-Level / Mixed) Regression Models.
13. Wickham H. 2017 tidyverse: Easily Install and Load the 'Tidyverse'.
14. Hijmans RJ. 2019 raster: Geographic Data Analysis and Modeling.
15. Bivand R, Lewin-Koh N. 2019 maptools: Tools for Handling Spatial Objects.
16. Lüdecke D. 2018 ggeffects: Tidy Data Frames of Marginal Effects from Regression Models. *J. Open Source Softw.* **3**, 772. (doi:10.21105/joss.00772)
17. Wickham H. 2016 *ggplot2: Elegant Graphics for Data Analysis*. Springer-Verlag New York. See https://ggplot2.tidyverse.org.
18. Arnold JB. 2019 ggthemes: Extra Themes, Scales and Geoms for 'ggplot2'.
19. Robinson D, Hayes A. 2019 broom: Convert Statistical Analysis Objects into Tidy Tibbles.
20. Wilke CO. 2019 cowplot: Streamlined Plot Theme and Plot Annotations for 'ggplot2'.

Supplementary information 2.2. Longhurst provinces code and description.

Code	Description
BPLR	Polar - Boreal Polar Province (POLR)
ARCT	Polar - Atlantic Arctic Province
SARC	Polar - Atlantic Subarctic Province
NADR	Westerlies - N. Atlantic Drift Province (WWDR)
GFST	Westerlies - Gulf Stream Province
NASW	Westerlies - N. Atlantic Subtropical Gyral Province (West) (STGW)
NATR	Trades - N. Atlantic Tropical Gyral Province (TRPG)
WTRA	Trades - Western Tropical Atlantic Province
ETRA	Trades - Eastern Tropical Atlantic Province
SATL	Trades - South Atlantic Gyral Province (SATG)
NECS	Coastal - NE Atlantic Shelves Province
CNRY	Coastal - Canary Coastal Province (EACB)
GUIN	Coastal - Guinea Current Coastal Province
GUIA	Coastal - Guianas Coastal Province
NWCS	Coastal - NW Atlantic Shelves Province
MEDI	Westerlies - Mediterranean Sea, Black Sea Province
CARB	Trades - Caribbean Province
NASE	Westerlies - N. Atlantic Subtropical Gyral Province (East) (STGE)
BRAZ	Coastal - Brazil Current Coastal Province
FKLD	Coastal - SW Atlantic Shelves Province
BENG	Coastal - Benguela Current Coastal Province
MONS	Trades - Indian Monsoon Gyres Province
ISSG	Trades - Indian S. Subtropical Gyre Province
EAFR	Coastal - E. Africa Coastal Province
REDS	Coastal - Red Sea, Persian Gulf Province
ARAB	Coastal - NW Arabian Upwelling Province
INDE	Coastal - E. India Coastal Province
INDW	Coastal - W. India Coastal Province
AUSW	Coastal - Australia-Indonesia Coastal Province
BERS	Polar - N. Pacific Epicontinental Province
PSAE	Westerlies - Pacific Subarctic Gyres Province (East)
PSAW	Westerlies - Pacific Subarctic Gyres Province (West)
KURO	Westerlies - Kuroshio Current Province
NPPF	Westerlies - N. Pacific Polar Front Province
NPSW	Westerlies - N. Pacific Subtropical Gyre Province (West)
TASM	Westerlies - Tasman Sea Province
SPSG	Westerlies - S. Pacific Subtropical Gyre Province
NPTG	Trades - N. Pacific Tropical Gyre Province
PNEC	Trades - N. Pacific Equatorial Countercurrent Province
PEQD	Trades - Pacific Equatorial Divergence Province

WARM   Trades - W. Pacific Warm Pool Province
ARCH   Trades - Archipelagic Deep Basins Province
ALSK   Coastal - Alaska Downwelling Coastal Province
CCAL   Coastal - California Upwelling Coastal Province
CAMR   Coastal - Central American Coastal Province
CHIL   Coastal - Chile-Peru Current Coastal Province
CHIN   Coastal - China Sea Coastal Province
SUND   Coastal - Sunda-Arafura Shelves Province
AUSE   Coastal - East Australian Coastal Province
NEWZ   Coastal - New Zealand Coastal Province
SSTC   Westerlies - S. Subtropical Convergence Province
SANT   Westerlies - Subantarctic Province
ANTA   Polar - Antarctic Province
APLR   Polar - Austral Polar Province

Supplementary Information 3.1. Description of physiology- and occurrence based thermal traits, their differences, thermal sensitivity, vulnerability to warming, thermal affinity, and thermal specialisation.

Parameters		Symbols	Unit	Description
Physiology-based thermal traits (TT_p)	Optimal temperature	$T_{opt}^{(*)}$	$^\circ C$	temperature that corresponds to maximum growth rate (r_{max}, d^{-1}); obtained from published literature or derived from Cardinal Temperature Model with Inflexion (*CTMI*; indicated by asterisk *), respectively
	Critical thermal minimum	$CT_{min}^{(*)}$	$^\circ C$	lowest temperature at which growth rate = 0; obtained from published literature or *CTMI*-derived (indicated by asterisk *), respectively
	Critical thermal maximum	$CT_{max}^{(*)}$	$^\circ C$	highest temperature at which growth rate = 0; obtained from published literature or *CTMI*-derived (indicated by asterisk *), respectively
	Fundamental thermal niche	$FTN^{(*)}$	$^\circ C$	physiological range of tolerance to temperature in the absence of biotic interactions and is derived by the difference between $CT_{max}^{(*)}$ and $CT_{min}^{(*)}$; obtained from published literature or *CTMI*-derived (indicated by asterisk *), respectively
Occurrence-based thermal traits (TT_o)	Lower thermal limit	$LTL^{(*)}$	$^\circ C$	the lowest temperature experienced by a species across its geographic range, and is derived from the 5th percentiles of average annual *SST* and long-term minimum *SST* (indicated by asterisk *), respectively
	Upper thermal limit	$UTL^{(*)}$	$^\circ C$	the highest temperature experienced by a species across its geographic range, and is derived from the 95th percentiles of average annual *SST* and long-term maximum *SST* (indicated by asterisk *), respectively
	Thermal midpoint	$TM^{(*)}$	$^\circ C$	midpoint between the lower and upper thermal limits derived from annual average and seasonal extreme SST (indicated by asterisk *), respectively; central tendency of the realised thermal distribution of the species and is considered a proxy for optimal temperature for the ecological success of the species
	Realised thermal niche	$RTN^{(*)}$	$^\circ C$	physiological range of tolerance to temperature in the presence of biotic interactions $RTN = UTL - LTL$ $RTN^* = UTL^* - LTL^*$
Difference between physiology- and occurrence-based thermal traits	Difference in optimal temperature	DOT	$^\circ C$	a measure of the ability of species to thrive in optimal thermal conditions than estimated by physiology $DOT_1 = T_{opt} - TM$ $DOT_2 = T_{opt} - TM^*$ $DOT_3 = T_{opt}^* - TM$ $DOT_4 = T_{opt}^* - TM^*$
	Difference in cold tolerance limit	DCL	$^\circ C$	a measure of the ability of species to thrive in colder conditions than estimated by physiology $DCL_1 = CT_{min} - LTL$ $DCL_2 = CT_{min} - LTL^*$ $DCL_3 = CT_{min}^* - LTL$ $DCL_4 = CT_{min}^* - LTL^*$
	Difference in heat tolerance limit	DHL	$^\circ C$	a measure of the ability of species to thrive in hotter conditions than estimated by physiology $DHL_1 = CT_{max} - UTL$ $DHL_2 = CT_{max} - UTL^*$

				$DHL_3 = CT_{max}* - UTL$ $DHL_4 = CT_{max}* - UTL*$
	Difference in thermal range	DTR	$°C$	a measure of the congruence in the thermal tolerances obtained from the two approaches $DTR_1 = FTN - RTN$ $DTR_2 = FTN - RTN*$ $DTR_3 = FTN* - RTN$ $DTR_4 = FTN* - RTN*$
Thermal sensitivity and warming vulnerability	Sensitivity to cold temperature	$S_{min}{}^{(*)}$	$°C$	proximity between the species critical thermal minimum (CT_{min}) and the minimum ambient sea surface temperature extremes it experiences in its local habitat (H_{min}). $S_{min} = CT_{min} - H_{min}$ $S_{min}* = CT_{min}* - H_{min}$
	Sensitivity to warm temperature	$S_{max}{}^{(*)}$	$°C$	proximity between the species critical thermal maximum (CT_{max}) and the maximum ambient sea surface temperature extremes it experiences in its local habitat (H_{max}). $S_{max} = CT_{max} - H_{max}$ $S_{max}* = CT_{max}* - H_{max}$
	Vulnerability to warming	$V^{(*)}$	year	a function of inherent sensitivity to warm temperature ($S_{max}{}^{(*)}$) and warming exposure (WR) in a given location; this describes the number of years prior the local temperatures are expected to exceed CT_{max} in a given location; warming vulnerability ($V_{i,j}$) of a species in location i based on climate scenario j (i.e. *RCP 2.6, RCP 4.5, RCP 6.0,* and *RCP 8.5*) is expressed as: $$V_{i,j} = S_{max_i}/WR_{i,j}$$ where $WR_{i,j}$ is the warming exposure in a location i based on the *RCP* climate scenario j, which is expressed as: $$WR_{i,j}$$ $$= \frac{\dfrac{H_{max2050_{i,j}} - H_{max_i}}{2050 - [(2014 - 2000)/2]} + \dfrac{H_{max2100_{i,j}} - H_{max2050}}{2100 - 2050}}{2}$$ where H_{max_i} is the average SST of the warmest month recorded in 2000 – 2014 in location i, and $H_{max2050_{i,j}}$ and $H_{max2100_{i,j}}$ are the SST of the warmest month predicted in the year 2050 and 2010 based on the *RCP* climate scenario j
Thermal affinity and specialisation	Thermal affinity	$TA^{(*)}$	au	degree of affinity of species to warm or cold temperatures relative to the average affinity of all species in the pool; thermal affinity of species s is expressed as: $$TA_s = log\left[\frac{(TM^*{}_s)^2/T_{opt_s}}{(TM^*{}_{\bar{x}})^2/T_{opt_{\bar{x}}}}\right]$$ where $TM^*{}_s$ and T_{opt_s} are the extreme thermal midpoint ($TM*$) and thermal optimum ($T_{opt}{}^{(*)}$) of species s, respectively, whereas $TM^*{}_{\bar{x}}$ and $T_{opt_{\bar{x}}}$ are the average $TM*$ and $T_{opt}{}^{(*)}$ of all species in the pool

347

Thermal specialisation	$TS^{(*)}$	au	degree of species thermal tolerance relative to the average tolerance of all species in the pool; thermal specialisation of species s is expressed as: $$TS_s = log\left[\frac{(RTN^*{}_s)^2/FTN_s}{(RTN^*{}_{\bar{x}})^2/FTN_{\bar{x}}}\right]$$ where $RTN^*{}_s$ and FTN_s are the extreme realised and fundamental thermal niche (RTN^* and $FTN^{(*)}$) of species s, respectively, whereas $RTN^*{}_{\bar{x}}$ and $FTN_{\bar{x}}$ are the RTN^* and $FTN^{(*)}$ of all species in the pool

Note*: au* is arbitrary unit

Supplementary Information 3.2. List of equations used to fit growth or metabolic rates (r) against temperature (T). Abbreviations: $a - f$ are the model coefficients; R is the universal gas (Boltzmann) constant; T_{ref} is reference temperature; CT_{min} is the critical thermal minimum; CT_{max} is the critical thermal maximum; T_{opt} is the thermal optimum; r_{max} is the maximum growth rate.

ID	Formula	References
equ04	$r = a \cdot exp\left(\frac{-b}{R \cdot T}\right) - c \cdot exp\left(\frac{-d}{R \cdot T}\right)$	[1] citing [2,3]
equ05	$r = \dfrac{a \cdot T \cdot exp\left(\frac{-b}{R \cdot T}\right)}{1 + exp\left(\frac{-c}{R}\right) \cdot exp\left(\frac{-d}{R \cdot T}\right)}$	[1] citing [2,4]
equ06	$r = \dfrac{a \cdot \left(\frac{T}{298.15}\right) \cdot exp\left(\frac{b}{R} \cdot \left(\frac{1}{298.15} - \frac{1}{T}\right)\right)}{1 + exp\left[\frac{c}{R} \cdot \left(\frac{1}{d} - \frac{1}{T}\right)\right] + exp\left[\frac{e}{R}\left(\frac{1}{f} - \frac{1}{T}\right)\right]}$	[1] citing [5]
equ07	$r = \dfrac{a \cdot \left(\frac{T}{293.15}\right) \cdot exp\left(\frac{b}{R} \cdot \left(\frac{1}{293.15} - \frac{1}{T}\right)\right)}{1 + exp\left[\frac{c}{R} \cdot \left(\frac{1}{d} - \frac{1}{T}\right)\right]}$	[1] citing [6,7]
equ08	$r = a \cdot exp\left[-0.5 \cdot \left(\frac{[T - T_{ref}]}{b}\right)^2\right]$	[1] citing [2,8]
equ09	$r = a \cdot exp\left[-0.5 \cdot \left(\frac{abs[T - T_{ref}]}{b}\right)^c\right]$	[1] citing [6]
equ10	$r = a \cdot \exp\left(c \cdot T\right)\left[1 - \left(\frac{T - T_{ref}}{b}\right)^2\right]$	[1] citing [9,10]
equ11	$r = a + b \cdot T + c \cdot T^2$	[1] citing [6]
equ12	$r = \dfrac{1}{1 + (a + b \cdot T + c \cdot T^2)}$	[1] citing [6,11]
equ13	$r = [a \cdot (T - CT_{min})]^2 \cdot \left[1 - exp\left(b \cdot (T - CT_{max})\right)\right]^2$	[1] citing [12]
equ14	$r = a \cdot \{1 - exp[-b \cdot (T - CT_{min})]\} \cdot \{1 - exp[-c \cdot (CT_{max} - T)]\}$	[1] citing [13]
equ15	$r = r_{max} \cdot \left\{ sin\left[\pi \cdot \left(\frac{T - CT_{min}}{CT_{max} - CT_{min}}\right)^a\right]\right\}^b$	[1] citing [14]

$$\begin{cases} r = 0 \ , if \ T < CT_{min} \\ r = r_{max} \cdot \theta, if \ CT_{max} \ \leq T \leq CT_{max} \\ r = 0 \ , if \ T > CT_{max} \end{cases}$$

with:

equ16 $\qquad \theta = \dfrac{(T - CT_{max}) \cdot (T - CT_{min})^2}{(T_{opt} - CT_{min}) \cdot [(T_{opt} - CT_{min}) \cdot (T - T_{opt}) - (T_{opt} - CT_{max}) \cdot (T_{opt} + CT_{min} - 2T)]}$ $\qquad$ [15]

under the condition:

$$T_{opt} > \frac{CT_{min} + CT_{max}}{2}$$

References:
1. Low-Décarie E, Boatman TG, Bennett N, Passfield W, Gavalás-Olea A, Siegel P, Geider RJ. 2017 Predictions of response to temperature are contingent on model choice and data quality. *Ecol. Evol.* , 1–15. (doi:10.1002/ece3.3576)
2. Li WK, Dickie PM. 1987 Temperature characteristics of photosynthetic and heterotrophic activities: seasonal variations in temperate microbial plankton. Appl. Environ. Microbiol. 53, 2282–95.
3. Hinshelwood CN. 1947 Presidential address. Some observations on present day chemical kinetics. J. Chem. Soc. , 694. (doi:10.1039/jr9470000694)
4. Johnson FH, Eyring H, Williams RW. 1942 The nature of enzyme inhibitions in bacterial luminescence: Sulfanilamide, urethane, temperature and pressure. J. Cell. Comp. Physiol. 20, 247–268. (doi:10.1002/jcp.1030200302)
5. Heitzer A, Kohler HP, Reichert P, Hamer G. 1991 Utility of phenomenological models for describing temperature dependence of bacterial growth. Appl. Environ. Microbiol. 57, 2656–65.
6. Montagnes DJS, Morgan G, Bissinger JE, Atkinson D, Weisse T. 2008 Short-term temperature change may impact freshwater carbon flux: A microbial perspective. Glob. Chang. Biol. 14, 2823–2838. (doi:10.1111/j.1365-2486.2008.01700.x)
7. Schoolfield RM, Sharpe PJH, Magnuson CE. 1981 Non-linear regression of biological temperature-dependent rate models based on absolute reaction-rate theory. J. Theor. Biol. 88, 719–731. (doi:10.1016/0022-5193(81)90246-0)
8. Stoermer EF, Ladewski TB. 1976 Apparent optimal temperatures for the occurrence of some common phytoplankton species in southern Lake Michigan. University of Michigan.
9. Thomas MK, Kremer CT, Klausmeier C a., Litchman E. 2012 A global pattern of thermal adaptation in marine phytoplankton. Science (80-.). 338, 1085–1088. (doi:10.1126/science.1224836)
10. Norberg J. 2004 Biodiversity and ecosystem functioning: A complex adaptive systems approach. Limnol. Oceanogr. 49, 1269–1277. (doi:10.4319/lo.2004.49.4_part_2.1269)
11. Flinn PW. 1991 Temperature-Dependent Functional Response of the Parasitoid Cephalonomia waterstoni (Gahan) (Hymenoptera: Bethylidae) Attacking Rusty Grain Beetle Larvae (Coleoptera: Cucujidae). Environ. Entomol. 20, 872–876. (doi:10.1093/ee/20.3.872)
12. Ratkowsky DA, Lowry RK, McMeekin TA, Stokes AN, Chandler RE. 1983 Model for bacterial culture growth rate throughout the entire biokinetic temperature range. J. Bacteriol. 154, 1222–1226.
13. Kamykowski D. 1986 A survey of protozoan laboratory temperature studies applied to marine dinoflagellate behavior from a field perspective. Contrib Mar Sci 27, 176–194.
14. Boatman TG, Lawson T, Geider RJ. 2017 A key marine diazotroph in a changing ocean: The interacting effects of temperature, CO_2 and light on the growth of trichodesmium erythraeum IMS101. PLoS One 12. (doi:10.1371/journal.pone.0168796)
15. Rosso L, Lobry JR, Flandrois JP. 1993 An unexpected correlation between cardinal temperatures of microbial growth highlighted by a new model. J. Theor. Biol. 162, 447–463. (doi:10.1006/jtbi.1993.1099)

Supplementary Information 3.3. Estimated divergence time (in million years ago, *MYA*) of major taxon in marine phytoplankton.

Taxon name	Taxonomic rank	Estimated divergence time (*MYA*)	References
Alexandrium	genus	77	[1]
Aphanothece	genus	927	[2]
Bacillariophyceae	class	75	[3]
Bacillariophyta	phylum	139.4	[4]
Bacillariophyta	phylum	183	[3]
Bacillariophyta	phylum	227.9	[5]
Bacillariophyta	phylum	201	[6]
Bacillariophyta	phylum	330	[7]
Bacillariophyta	phylum	380	[7]
Blennothrix	genus	150.3	[2]
Brasilonema	genus	93.1	[2]
Calciodinellum	genus	12	[8]
Calothrix	genus	1280.6	[2]
Chlamydomonadales	order	756.3	[9]
Chlorophyta	phylum	848.1	[5]
Chlorophyta	phylum	613	[10]
Chlorophyta	phylum	1574.7	[6]
Chlorophyta	phylum	1116.6	[9]
Chlorophyta	phylum	1030	[11]
Chroococcus	genus	652.6	[2]
Cyanobacteria	kingdom	931.8	[12]
Cyanobacteria	kingdom	1039	[13]
Cyanobacteria	kingdom	2686	[14]
Cyanobacteria	kingdom	2629.8	[15]
Cyanobacteria	kingdom	1720	[16]
Cyanobacteria	kingdom	2539.8	[6]
Cyanobacteria	kingdom	2594	[17]
Cyanobacteria	kingdom	2104.3	[2]
Cylindrotheca	genus	9	[3]
Dinophyceae	class	669	[18]
Eukaryota	kingdom	1558	[19]
Eukaryota	kingdom	1956	[20]
Eukaryota	kingdom	1545	[21]
Eukaryota	kingdom	1781.1	[5]
Eukaryota	kingdom	2002	[6]
Eunotia	genus	16	[3]
Gonyaulacaceae	family	180	[1]
Haptophyceae	class	800	[22]
Haptophyceae	class	805	[19]
Haptophyceae	class	520.9	[23]
Haptophyceae	class	341.5	[24]
Haptophyceae	class	675	[5]
Haptophyceae	class	870	[25]
Haptophyceae	class	1000	[25]
Haslea	genus	30	[3]
Isochrysidales	order	130	[22]
Isochrysidales	order	119.2	[23]
Isochrysidales	order	94.7	[24]
Isochrysidales	order	226.4	[5]
Isochrysidales	order	130	[25]
Isochrysidales	order	60	[25]
Lyngbya	genus	689	[2]
Lyngbya	genus	616	[2]
Mamiellaceae	family	66.1	[26]
Mediophyceae	class	141	[3]
Merismopedia	genus	792.1	[2]
Navicula	genus	15	[3]

Nitzschia	genus	24	[3]
Nitzschia	genus	50	[3]
Nitzschia	genus	16	[3]
Nodularia	genus	154	[16]
Nodularia	genus	16	[16]
Nodularia	genus	41.1	[2]
Nodularia	genus	10.9	[2]
Okeania	genus	39.6	[2]
Oscillatoria	genus	892.2	[14]
Oscillatoria	genus	1653.1	[17]
Oscillatoria	genus	927	[2]
Oscillatoriales	order	2508.5	[14]
Oscillatoriales	order	2340.5	[15]
Oscillatoriales	order	1671.5	[6]
Oscillatoriales	order	2352.3	[17]
Oscillatoriales	order	2104.3	[2]
Peridiniales	order	136	[18]
Phacotaceae	family	175.7	[9]
Phaeocystis	genus	120	[22]
Phormidium	genus	689	[2]
Prymnesiales	order	200	[22]
Pseudanabaena	genus	927	[2]
Pseudo-nitzschia	genus	6.6	[27]
Rivulariaceae	family	1037	[14]
Rivulariaceae	family	1720	[16]
Rivulariaceae	family	1385.5	[17]
Rivulariaceae	family	1280.6	[2]
Schizothrix	genus	927	[2]
Scytonema	genus	246.7	[2]
Scytonemataceae	family	927	[2]
Skeletonema	genus	13	[3]
Skeletonema	genus	18.2	[28]
Symploca	genus	131.4	[2]
Syracosphaeraceae	family	195	[22]
Syracosphaeraceae	family	31.7	[23]
Syracosphaeraceae	family	44.1	[24]
Syracosphaeraceae	family	65	[25]
Syracosphaeraceae	family	20	[25]
Thalassiosira	genus	32	[3]
Thalassiosira	genus	29.8	[29]
Thalassiosira	genus	70.3	[28]
Thalassiosirales	order	74	[3]
Thalassiosirales	order	83.3	[28]
root	root	4290	[18]

References:
1. John U, Fensome RA, Medlin LK. 2003 The application of a molecular clock based on molecular sequences and the fossil record to explain biogeographic distributions within the Alexandrium tamarense 'species complex' (Dinophyceae). Mol. Biol. Evol. 20, 1015–1027. (doi:10.1093/molbev/msg105)
2. Marin J, Battistuzzi FU, Brown AC, Hedges SB. 2016 The timetree of prokaryotes: New insights into their evolution and speciation. Mol. Biol. Evol. 34, msw245. (doi:10.1093/molbev/msw245)
3. Sorhannus U. 2007 A nuclear-encoded small-subunit ribosomal RNA timescale for diatom evolution. Mar. Micropaleontol. 65, 1–12. (doi:10.1016/j.marmicro.2007.05.002)
4. Matari NH, Blair JE. 2014 A multilocus timescale for oomycete evolution estimated under three distinct molecular clock models. BMC Evol. Biol. 14, 101. (doi:10.1186/1471-2148-14-101)
5. Parfrey LW, Lahr DJG, Knoll AH, Katz LA. 2011 Estimating the timing of early eukaryotic diversification with multigene molecular clocks. Proc. Natl. Acad. Sci. 108, 13624–13629. (doi:10.1073/pnas.1110633108)
6. Blank CE. 2013 Origin and early evolution of photosynthetic eukaryotes in freshwater environments: reinterpreting proterozoic paleobiology and biogeochemical processes in light of trait evolution. J. Phycol. 49, 1040–1055. (doi:10.1111/jpy.12111)
7. Sorhannus U. 1997 The origination time of diatoms: An analysis based on ribosomal RNA data. Micropaleontology 43, 215–218. (doi:10.2307/1485785)
8. Gottschling M, Renner SS, Sebastian Meier KJ, Willems H, Keupp H. 2008 Timing deep divergence events in calcareous dinoflagellates. J. Phycol. 44, 429–438. (doi:10.1111/j.1529-8817.2008.00479.x)

9. Munakata H, Nakada T, Nakahigashi K, Nozaki H, Tomita M. 2016 Phylogenetic position and molecular chronology of a colonial green flagellate, Stephanosphaera pluvialis (Volvocales, Chlorophyceae), among unicellular algae. J. Eukaryot. Microbiol. 63, 340–348. (doi:10.1111/jeu.12283)

10. Lang D, Weiche B, Gerrittimmerhaus, Richardt S, Riano-Pachon DM, Correak LGG, Reski R, Mueller-Roeber B, Rensing SA. 2010 Genome-wide phylogenetic comparative analysis of plant transcriptional regulation: A timeline of loss, gain, expansion, and correlation with complexity. Genome Biol. Evol. 2, 488–503. (doi:10.1093/gbe/evq032)

11. Herron MD, Hackett JD, Aylward FO, Michod RE. 2009 Triassic origin and early radiation of multicellular volvocine algae. Proc. Natl. Acad. Sci. 106, 3254–3258. (doi:10.1073/pnas.0811205106)

12. Sjöstrand J, Tofigh A, Daubin V, Arvestad L, Sennblad B, Lagergren J. 2014 A bayesian method for analyzing lateral gene transfer. Syst. Biol. 63, 409–420. (doi:10.1093/sysbio/syu007)

13. Battistuzzi FU, Feijao A, Hedges SB. 2004 A genomic timescale of prokaryote evolution: insights into the origin of methanogenesis, phototrophy, and the colonization of land. BMC Evol. Biol. 4, 44. (doi:10.1186/1471-2148-4-44)

14. Sánchez-Baracaldo P, Ridgwell A, Raven JA. 2014 A neoproterozoic transition in the marine nitrogen cycle. Curr. Biol. 24, 652–657. (doi:10.1016/j.cub.2014.01.041)

15. Cornejo-Castillo FM et al. 2016 Cyanobacterial symbionts diverged in the late Cretaceous towards lineage-specific nitrogen fixation factories in single-celled phytoplankton. Nat. Commun. 7, 11071. (doi:10.1038/ncomms11071)

16. Ortiz-Álvarez R, de los Ríos A, Fernández-Mendoza F, Torralba-Burrial A, Pérez-Ortega S. 2015 Ecological specialization of two photobiont-specific maritime Cyanolichen species of the Genus Lichina. PLoS One 10, e0132718. (doi:10.1371/journal.pone.0132718)

17. Sánchez-Baracaldo P. 2015 Origin of marine planktonic cyanobacteria. Sci. Rep. 5, 17418. (doi:10.1038/srep17418)

18. Hedges SB, Marin J, Suleski M, Paymer M, Kumar S. 2015 Tree of life reveals clock-like speciation and diversification. Mol. Biol. Evol. 32, 835–845. (doi:10.1093/molbev/msv037)

19. Yoon HS, Hackett JD, Ciniglia C, Pinto G, Bhattacharya D. 2004 A molecular timeline for the origin of photosynthetic eukaryotes. Mol. Biol. Evol. 21, 809–818. (doi:10.1093/molbev/msh075)

20. Hedges S, Blair JE, Venturi ML, Shoe JL. 2004 A molecular timescale of eukaryote evolution and the rise of complex multicellular life. BMC Evol. Biol. 4, 2. (doi:10.1186/1471-2148-4-2)

21. Feng DF, Cho G, Doolittle RF. 1997 Determining divergence times with a protein clock: update and reevaluation. Proc. Natl. Acad. Sci. U. S. A. 94, 13028–33.

22. Medlin LK, Sáez AG, Young JR. 2008 A molecular clock for coccolithophores and implications for selectivity of phytoplankton extinctions across the K/T boundary. Mar. Micropaleontol. 67, 69–86. (doi:10.1016/J.MARMICRO.2007.08.007)

23. Liu H, Aris-Brosou S, Probert I, De Vargas C. 2010 A time line of the environmental genetics of the haptophytes. Mol. Biol. Evol. 27, 161–176. (doi:10.1093/molbev/msp222)

24. Decelle J, Probert I, Bittner L, Desdevises Y, Colin S, De Vargas C, Galí M, Simó R, Not F. 2012 An original mode of symbiosis in open ocean plankton. Proc. Natl. Acad. Sci. U. S. A. 109, 18000–18005. (doi:10.1073/pnas.1212303109)

25. De Vargas C, Aubry M-P, Probert I, Young J. 2007 Origin and evolution of coccolithophores: From coastal hunters to oceanic farmers. Evol. Prim. Prod. Sea , 251–285. (doi:10.1016/B978-012370518-1/50013-8)

26. Šlapeta J, López-García P, Moreira D. 2006 Global dispersal and ancient cryptic species in the smallest marine eukaryotes. Mol. Biol. Evol. 23, 23–29. (doi:10.1093/molbev/msj001)

27. Casteleyn G, Leliaert F, Backeljau T, Debeer A-E, Kotaki Y, Rhodes L, Lundholm N, Sabbe K, Vyverman W. 2010 Limits to gene flow in a cosmopolitan marine planktonic diatom. Proc. Natl. Acad. Sci. 107, 12952–12957. (doi:10.1073/pnas.1001380107)

28. Alverson AJ. 2014 Timing marine–freshwater transitions in the diatom order Thalassiosirales. Paleobiology 40, 91–101. (doi:10.1666/12055)

29. Whittaker KA, Rignanese DR, Olson RJ, Rynearson TA. 2012 Molecular subdivision of the marine diatom Thalassiosira rotula in relation to geographic distribution, genome size, and physiology. BMC Evol. Biol. 12, 209. (doi:10.1186/1471-2148-12-209)

353

Supplementary information 3.4. *R* packages used in the data processing and analyses.

1. Wickham et al., (2019). Welcome to the tidyverse. Journal of Open Source Software, 4(43), 1686, https://doi.org/10.21105/joss.01686
2. Low-Decarie E, Boatman TG, Bennett N, Passfield W, Gavalas-Olea A, Siegel P, Geider RJ (2017). "Predictions of response to temperature are contingent on model choice and data quality."
3. Samuel Bosch (2018). sdmpredictors: Species Distribution Modelling Predictor Datasets. R package version 0.2.8. https://CRAN.R-project.org/package=sdmpredictors
4. Robert J. Hijmans (2019). raster: Geographic Data Analysis and Modeling. R package version 3.0-7. https://CRAN.R-project.org/package=raster
5. Provoost P, Bosch S (2019). "robis: R Client to access data from the OBIS API." Ocean Biogeographic Information System. Intergovernmental Oceanographic Commission of UNESCO. R package version 2.1.8, <URL: https://cran.r-project.org/package=robis>.
6. Chamberlain S, Barve V, Mcglinn D, Oldoni D, Desmet P, Geffert L, Ram K (2019). rgbif: Interface to the Global Biodiversity Information Facility API. R package version 1.4.0, <URL: https://CRAN.R-project.org/package=rgbif>.
7. Chamberlain S, Boettiger C (2017). "R Python, and Ruby clients for GBIF species occurrence data." PeerJ PrePrints. <URL: https://doi.org/10.7287/peerj.preprints.3304v1>.
8. Garrett Grolemund, Hadley Wickham (2011). Dates and Times Made Easy with lubridate. Journal of Statistical Software, 40(3), 1-25. URL http://www.jstatsoft.org/v40/i03/.
9. Pebesma, E.J., R.S. Bivand, 2005. Classes and methods for spatial data in R. R News 5 (2), https://cran.r-project.org/doc/Rnews/.
10. Roger S. Bivand, Edzer Pebesma, Virgilio Gomez-Rubio, 2013. Applied spatial data analysis with R, Second edition. Springer, NY. http://www.asdar-book.org/
11. Roger Bivand, Tim Keitt and Barry Rowlingson (2019). rgdal: Bindings for the 'Geospatial' Data Abstraction Library. R package version 1.4-7.https://CRAN.R-project.org/package=rgdal
12. Olivier Broennimann, Valeria Di Cola and Antoine Guisan (2018). ecospat: Spatial Ecology Miscellaneous Methods. R package version 3.0. https://CRAN.R-project.org/package=ecospat
13. Angelo Canty and Brian Ripley (2019). boot: Bootstrap R (S-Plus) Functions. R package version 1.3-23.
14. Davison, A. C. & Hinkley, D. V. (1997) Bootstrap Methods and Their Applications. Cambridge University Press, Cambridge. ISBN 0-521-57391-2
15. Frank E Harrell Jr, with contributions from Charles Dupont and many others. (2019). Hmisc: Harrell Miscellaneous. R package version 4.3-0. https://CRAN.R-project.org/package=Hmisc
16. Robert J. Hijmans (2019). geosphere: Spherical Trigonometry. R package version 1.5-10. https://CRAN.R-project.org/package=geosphere
17. David Robinson and Alex Hayes (2019). broom: Convert Statistical Analysis Objects into Tidy Tibbles. R package version 0.5.2. https://CRAN.R-project.org/package=broom

18. Scott Chamberlain and Eduard Szocs (2013). taxize - taxonomic search and retrieval in R. F1000Research,2:191. URL: http://f1000research.com/articles/2-191/v2.

19. Scott Chamberlain, Eduard Szoecs, Zachary Foster, Zebulun Arendsee, Carl Boettiger, Karthik Ram, Ignasi Bartomeus, John Baumgartner, James O'Donnell, Jari Oksanen, Bastian Greshake Tzovaras, Philippe Marchand, Vinh Tran, Maëlle Salmon, Gaopeng Li, and Matthias Grenié. (2019) taxize: Taxonomic information from around the web. R package version 0.9.9. https://github.com/ropensci/taxize

20. Jeffrey B. Arnold (2019). ggthemes: Extra Themes, Scales and Geoms for 'ggplot2'. R package version 4.2.0. https://CRAN.R-project.org/package=ggthemes

21. Simon Garnier (2018). viridis: Default Color Maps from 'matplotlib'. R package version 0.5.1. https://CRAN.R-project.org/package=viridis

22. Wood, S.N. (2011) Fast stable restricted maximum likelihood and marginal likelihood estimation of semiparametric generalized linear models. Journal of the Royal Statistical Society (B) 73(1):3-36

23. Wood S.N., N. Pya and B. Saefken (2016) Smoothing parameter and model selection for general smooth models (with discussion). Journal of the American Statistical Association 111:1548-1575.

24. Wood, S.N. (2004) Stable and efficient multiple smoothing parameter estimation for generalized additive models. Journal of the American Statistical Association. 99:673-686.

25. Wood, S.N. (2017) Generalized Additive Models: An Introduction with R (2nd edition). Chapman and Hall/CRC.

26. Wood, S.N. (2003) Thin-plate regression splines. Journal of the Royal Statistical Society (B) 65(1):95-114.

27. Dabao Zhang (2018). rsq: R-Squared and Related Measures. R package version 1.1. https://CRAN.R-project.org/package=rsq

28. Lüdecke D (2018). "ggeffects: Tidy Data Frames of Marginal Effects from Regression Models." Journal of Open Source Software, 3:(26), 772. doi: 10.21105/joss.00772 (URL: https://doi.org/10.21105/joss.00772).

29. Keck F., Rimet F., Bouchez A., and Franc A. (2016). phylosignal: an R package to measure, test, and explore the phylogenetic signal. Ecology and Evolution, 6(9), 2774-2780. doi:10.1002/ece3.2051

30. R Hackathon et al. (2019). phylobase: Base Package for Phylogenetic Structures and Comparative Data. R package version 0.8.6. https://CRAN.R-project.org/package=phylobase

31. Revell, L. J. (2012) phytools: An R package for phylogenetic comparative biology (and other things). Methods Ecol. Evol. 3 217-223. doi:10.1111/j.2041-210X.2011.00169.x

32. Jeroen Ooms and Scott Chamberlain (2019). phylocomr: Interface to 'Phylocom'. R package version 0.2.0. https://CRAN.R-project.org/package=phylocomr

33. LG Wang, TTY Lam, S Xu, Z Dai, L Zhou, T Feng, P Guo, CW Dunn, BR Jones, T Bradley, H Zhu, Y Guan, Y Jiang, G Yu. treeio: an R package for phylogenetic tree input and output with richly annotated and associated data. Molecular Biology and Evolution 2019, accepted. doi: 10.1093/molbev/msz240

34. Guangchuang Yu, David Smith, Huachen Zhu, Yi Guan, Tommy Tsan-Yuk Lam. ggtree: an R package for visualization and annotation of phylogenetic trees with their covariates and other associated data. Methods in Ecology and Evolution 2017, 8(1):28-36

35. Guangchuang Yu, Tommy Tsan-Yuk Lam, Huachen Zhu, Yi Guan. Two methods for mapping and visualizing associated data on phylogeny using ggtree. Molecular Biology and Evolution 2018, 35(2):3041-3043. doi:10.1093/molbev/msy194

36. Claus O. Wilke (2019). cowplot: Streamlined Plot Theme and Plot Annotations for 'ggplot2'. R package version 1.0.0. https://CRAN.R-project.org/package=cowplot

37. Oswaldo Santos Baquero (2019). ggsn: North Symbols and Scale Bars for Maps Created with 'ggplot2' or 'ggmap'. R package version 0.5.0. https://CRAN.R-project.org/package=ggsn

38. Roger Bivand and Nicholas Lewin-Koh (2019). maptools: Tools for Handling Spatial Objects. R package version 0.9-8. https://CRAN.R-project.org/package=maptools

Supplementary information 6.1. ImageJ Macro script used to process the image data acquired in this study.

```
path = "/Volumes/Seagate Backup Plus Drive/Competition_Experiment/Data/Temp15/20190418/"

//setBatchMode(true);
wells = getFileList(path);
for (j = 0; j < wells.length; j++) {
        input = path + "/" + wells[j];
        output = input;
        list = getFileList(input);
        for (i = 0; i < list.length; i++) {
                filename = list[i];
                if (endsWith(list[i], "bmp")) {
                        action(input, output, filename);
                        }
        }
}
//setBatchMode(false);

function action(input, output, image) {
    setBatchMode(true);
    nameOfFile = File.getName(image);
    dotIndex = indexOf(nameOfFile, ".");
    nameOfFile = substring(nameOfFile, 0, dotIndex);
    open(input + image);
    run("Duplicate...", " ");
        run("Enhance Contrast", "saturated=0.35");
        run("8-bit");
        run("Invert LUT");
        setAutoThreshold("MaxEntropy dark");
        run("Convert to Mask");
        run("Open");
        run("Fill Holes");
        run("Watershed");
        run("Set Measurements...", "area mean standard modal min centroid center perimeter
bounding fit shape feret's integrated median skewness kurtosis area_fraction stack limit display
redirect=None decimal=4");
        run("Analyze Particles...", "size=50-Infinity circularity=0.50-1.00 show=Outlines display
exclude clear");
        selectWindow("Drawing of " + nameOfFile + "-1.bmp");
        run("Invert LUT");
        selectWindow(image);
        run("Duplicate...", " ");
        run("Add Image...", "image=" + "[Drawing of " + nameOfFile + "-1.bmp] x=0 y=0
opacity=100 zero");
        run("Flatten");
        saveAs("Tiff", output + "/" + nameOfFile + ".tif");
        saveAs("Results", output + "/" + nameOfFile + ".csv");
        run("Close All");
}
```

This page is intentionally left blank.

This page is intentionally left blank.

LITERATURE CITED

Abdenadher, M., Hamza, A., Fekih, W., Hannachi, I., Zouari Bellaaj, A., Bradai, M.N., Aleya, L., 2012. Factors determining the dynamics of toxic blooms of *Alexandrium minutum* during a 10-year study along the shallow southwestern Mediterranean coasts. Estuar. Coast. Shelf Sci. 106, 102–111. https://doi.org/10.1016/j.ecss.2012.04.029

Abouheif, E., 1999. A method for testing the assumption of phylogenetic independence in comparative data, Evol. Ecol. Res. 1, 895–909.

Acevedo-Trejos, E., Brandt, G., Bruggeman, J., Merico, A., Barlow, R., 2015. Mechanisms shaping size structure and functional diversity of phytoplankton communities in the ocean. Sci. Rep. 5, 8918. https://doi.org/10.1038/srep08918

Addo-Bediako, A., Chown, S.L., Gaston, K.J., 2000. Thermal tolerance, climatic variability and latitude. Proc. R. Soc. B Biol. Sci. 267, 739–745. https://doi.org/10.1098/rspb.2000.1065

Ajani, P.A., McGinty, N., Finkel, Z. V., Irwin, A.J., 2018. Phytoplankton realized niches track changing oceanic conditions at a long-term coastal station off Sydney Australia. Front. Mar. Sci. 5, 285. https://doi.org/10.3389/fmars.2018.00285

Alexova, R., Haynes, P.A., Ferrari, B.C., Neilan, B.A., 2011. Comparative protein expression in different strains of the bloom-forming cyanobacterium *Microcystis aeruginosa*. Mol. Cell. Proteomics 10, M110.003749. https://doi.org/10.1074/mcp.M110.003749

Allaire, J.J., Chollet, F., 2019. keras: R Interface to "Keras."

Allen, A.P., Brown, J.H., Gillooly, J.F., 2002. Global biodiversity, biochemical kinetics, and the energetic-equivalence rule. Science. 297, 1545–1548. https://doi.org/10.1126/science.1072380

Amarasekare, P., 2007. Trade-offs, temporal variation, and species coexistence in communities with intraguild predation. Ecology 88, 2720–2728. https://doi.org/10.1890/06-1515.1

Amarasekare, P., 2008. Coexistence of intraguild predators and prey in resource-rich environments. Ecology 89, 2786–2797. https://doi.org/10.1890/07-1508.1

Amarasekare, P., Savage, V., 2011. A framework for elucidating the temperature dependence of fitness. https://doi.org/10.1086/663677

Anderson, C.R., Kudela, R.M., Benitez-Nelson, C., Sekula-Wood, E., Burrell, C.T., Chao, Y., Langlois, G., Goodman, J., Siegel, D.A., 2011. Detecting toxic diatom blooms from ocean color and a regional ocean model. Geophys. Res. Lett. 38, L04603. https://doi.org/10.1029/2010GL045858

Anderson, D.M., Cembella, A.D., Hallegraeff, G.M., 2012. Progress in understanding harmful algal blooms: Paradigm shifts and new technologies for research, monitoring, and management. Annu. Rev. Mar. Sci 4, 143–76. https://doi.org/10.1146/annurev-marine-120308-081121

Anderson, D.M., Hoagland, P., Kaoru, Y., White, A.W., 2000. Estimated annual economic impacts from harmful algal blooms (HABs) in the United States WHOI-2000-11.

Anderson, D.M., Kulis, D.M., Sullivan, J.J., Hall, S., Lee, C., 1990. Dynamics and physiology of saxitoxin production by the dinoflagellates *Alexandrium* spp. Mar. Biol. 104, 511–524. https://doi.org/10.1007/BF01314358

Anderson, D.M., Stock, C.A., Keafer, B.A., Bronzino Nelson, A., Thompson, B., McGillicuddy, D.J., Keller, M., Matrai, P.A., Martin, J., 2005. *Alexandrium fundyense*

cyst dynamics in the Gulf of Maine. Deep Sea Res. Part II Top. Stud. Oceanogr. 52, 2522–2542. https://doi.org/10.1016/j.dsr2.2005.06.014

Andrade, J.M., Estévez-Pérez, M.G., 2014. Statistical comparison of the slopes of two regression lines: A tutorial. Anal. Chim. Acta. https://doi.org/10.1016/j.aca.2014.04.057

Angielczyk, K.D., Burroughs, R.W., Feldman, C.R., 2015. Do turtles follow the rules? Latitudinal gradients in species richness, body size, and geographic range area of the world's turtles. J. Exp. Zool. Part B Mol. Dev. Evol. 324, 270–294. https://doi.org/10.1002/jez.b.22602

Angilletta, M., 2009. Thermal adaptation: A theoretical and empirical synthesis. Oxford University Press. https://doi.org/10.1093/acprof:oso/9780198570875.001.1

Anholt, B.R., Werner, E.E., 1995. Interaction between food availability and predation mortality mediated by adaptive behavior. Ecology 76, 2230–2234. https://doi.org/10.2307/1941696

Anselin, L., 2010. Local indicators of spatial association-LISA. Geogr. Anal. 27, 93–115. https://doi.org/10.1111/j.1538-4632.1995.tb00338.x

Aquino-Cruz, A., 2012. Effect of increasing sea water temperature on the growth and toxin production of three harmful benthic dinoflagellates isolated from the Fleet Lagoon, Dorset, UK. PQDT - UK Irel. University of Southampton.

Araújo, M.B., Ferri-Yáñez, F., Bozinovic, F., Marquet, P.A., Valladares, F., Chown, S.L., 2013. Heat freezes niche evolution. Ecol. Lett. 16, 1206–1219. https://doi.org/10.1111/ele.12155

Araújo, M.B., Guisan, A., 2006. Five (or so) challenges for species distribution modelling. J. Biogeogr. 33, 1677–1688. https://doi.org/10.1111/j.1365-2699.2006.01584.x

Araújo, M.B., Luoto, M., 2007. The importance of biotic interactions for modelling species distributions under climate change. Glob. Ecol. Biogeogr. 16, 743–753. https://doi.org/10.1111/j.1466-8238.2007.00359.x

Arrhenius, S., 1915. Quantitative laws in biological chemistry. G. Bell, London : https://doi.org/10.5962/bhl.title.4661

Ashton, M., Tosteson, T., Tosteson, C., 2003. The effect of elevated temperature on the toxicity of the laboratory cultured dinoflagellate *Ostreopsis lenticularis* (Dinophyceae). Rev. Biol. Trop. 51 Suppl 4, 1–6.

Assis, J., Tyberghein, L., Bosch, S., Verbruggen, H., Serrão, E.A., De Clerck, O., 2018. Bio-ORACLE v2.0: Extending marine data layers for bioclimatic modelling. Glob. Ecol. Biogeogr. 27, 277–284. https://doi.org/10.1111/geb.12693

Atkinson, D., Morley, S.A., Hughes, R.N., 2006. From cells to colonies: at what levels of body organization does the "temperature-size rule" apply? Evol. Dev. 8, 202–214. https://doi.org/10.1111/j.1525-142X.2006.00090.x

Austin, M., 2006. Species distribution models and ecological theory: A critical assessment and some possible new approaches. https://doi.org/10.1016/j.ecolmodel.2006.07.005

Austin, M.P., 2002. Spatial prediction of species distribution: An interface between ecological theory and statistical modelling. Ecol. Modell. 157, 101–118. https://doi.org/10.1016/S0304-3800(02)00205-3

Baker, K.G., Robinson, C.M., Radford, D.T., McInnes, A.S., Evenhuis, C., Doblin, M.A., 2016. Thermal performance curves of functional traits aid understanding of thermally induced changes in diatom-mediated biogeochemical fluxes. Front. Mar. Sci. 3, 44. https://doi.org/10.3389/fmars.2016.00044

Baker, R.L., 1982. Effects of food abundance on growth, survival, and use of space by nymphs of *Coenagrion resolutum* (Zygoptera). Oikos 38, 47. https://doi.org/10.2307/3544566

Bar-Yosef, Y., Sukenik, A., Hadas, O., Viner-Mozzini, Y., Kaplan, A., 2010. Enslavement in the water body by toxic *Aphanizomenon ovalisporum*, inducing alkaline phosphatase in phytoplanktons. Curr. Biol. 20, 1557–1561. https://doi.org/10.1016/j.cub.2010.07.032

Barbier, M., Amzil, Z., Mondeguer, F., Bhaud, Y., Soyer-Gobillard, M.O., Lassus, P., 1999. Okadaic acid and PP2A cellular immunolocalization in *Prorocentrum lima* (Dinophyceae). Phycologia 38, 41–46. https://doi.org/10.2216/i0031-8884-38-1-41.1

Barsanti, L., Gualtieri, P., 2005. Algae: anatomy, biochemistry, and biotechnology. CRC Press, Boca Raton, Florida. https://doi.org/10.1201/9780203492598

Barton, A.D., Irwin, A.J., Finkel, Z. V, Stock, C.A., 2016. Anthropogenic climate change drives shift and shuffle in North Atlantic phytoplankton communities. Proc. Natl. Acad. Sci. U. S. A. 113, 2964–9. https://doi.org/10.1073/pnas.1519080113

Barton, S., Jenkins, J., Buckling, A., Schaum, C.-E., Smirnoff, N., Yvon-Durocher, G., 2018. Universal metabolic constraints on the thermal tolerance of marine phytoplankton. bioRxiv 358002. https://doi.org/10.1101/358002

Bates, A.E., Pecl, G.T., Frusher, S., Hobday, A.J., Wernberg, T., Smale, D.A., Sunday, J.M., Hill, N.A., Dulvy, N.K., Colwell, R.K., Holbrook, N.J., Fulton, E.A., Slawinski, D., Feng, M., Edgar, G.J., Radford, B.T., Thompson, P.A., Watson, R.A., 2014. Defining and observing stages of climate-mediated range shifts in marine systems. Glob. Environ. Chang. 26, 27–38. https://doi.org/10.1016/J.GLOENVCHA.2014.03.009

Bates, S.S., 1998. Ecophysiology and metabolism of ASP toxin production, in: Anderson, D.M., Cembella, A.D., Hallegraeff, G.M. (Eds.), Physiological ecology of harmful algal blooms. Springer-Verlag, Heidelberg (1998), pp. 405–426.

Behrenfeld, M.J., O'Malley, R.T., Boss, E.S., Westberry, T.K., Graff, J.R., Halsey, K.H., Milligan, A.J., Siegel, D.A., Brown, M.B., 2015. Revaluating ocean warming impacts on global phytoplankton. Nat. Clim. Chang. 1–27. https://doi.org/10.1038/nclimate2838

Behrenfeld, M.J., O'Malley, R.T., Siegel, D.A., McClain, C.R., Sarmiento, J.L., Feldman, G.C., Milligan, A.J., Falkowski, P.G., Letelier, R.M., Boss, E.S., 2006. Climate-driven trends in contemporary ocean productivity. Nature 444, 752–755. https://doi.org/10.1038/nature05317

Bellard, C., Bertelsmeier, C., Leadley, P., Thuiller, W., Courchamp, F., 2012. Impacts of climate change on the future of biodiversity. Ecol. Lett. https://doi.org/10.1111/j.1461-0248.2011.01736.x

Ben-Gharbia, H., Yahia, O.K.D.O.K., Amzil, Z., Chomérat, N., Abadie, E., Masseret, E., Sibat, M., Triki, H.Z.H.Z., Nouri, H., Laabir, M., 2016. Toxicity and growth assessments of three thermophilic benthic dinoflagellates (*Ostreopsis* cf. *ovata*, *Prorocentrum lima* and *Coolia monotis*) developing in the Southern Mediterranean basin, Toxins. https://doi.org/10.3390/toxins8100297

Bennett, S., Duarte, C.M., Marbà, N., Wernberg, T., 2019. Integrating within-species variation in thermal physiology into climate change ecology. Philos. Trans. R. Soc. B Biol. Sci. 374, 20180550. https://doi.org/10.1098/rstb.2018.0550

Bennington, V., McKinley, G.A., Dutkiewicz, S., Ullman, D., 2009. What does chlorophyll variability tell us about export and air-sea CO_2 flux variability in the North Atlantic? Global Biogeochem. Cycles 23. https://doi.org/10.1029/2008GB003241

Benson, D.A., Karsch-Mizrachi, I., Lipman, D.J., Ostell, J., Sayers, E.W., 2009. GenBank. Nucleic Acids Res. 37, D26–D31. https://doi.org/10.1093/nar/gkn723

Berdalet, E., Fleming, L.E., Gowen, R., Davidson, K., Hess, P., Backer, L.C., Moore, S.K., Hoagland, P., Enevoldsen, H., 2015. Marine harmful algal blooms, human health and wellbeing: challenges and opportunities in the 21st century. J. Mar. Biol. Assoc. U.K. 2015, 61–91. https://doi.org/10.1017/S0025315415001733

Berges, J.A., Franklin, D.J., Harrison, P.J., 2001. Evolution of an artificial seawater medium: Improvements in enriched seawater, artificial water over the last two decades. J. Phycol. 37, 1138–1145. https://doi.org/10.1046/j.1529-8817.2001.01052.x

Bestion, E., García-Carreras, B., Schaum, C.-E., Pawar, S., Yvon-Durocher, G., 2018. Metabolic traits predict the effects of warming on phytoplankton competition. Ecol. Lett. 1–19. https://doi.org/10.1111/ele.12932

Bissinger, J.E., Montagnes, D.J.S., Sharples, J., Atkinson, D., 2008. Predicting marine phytoplankton maximum growth rates from temperature: Improving on the Eppley curve using quantile regression. Limnol. Oceanogr. 53, 487–493. https://doi.org/10.4319/lo.2008.53.2.0487

Blackburn, T.M., Gaston, K.J., 1998. Some methodological issues in macroecology. Am. Nat. 151, 68–83. https://doi.org/10.1086/286103

Blomberg, S.P., Garland, T., Ives, A.R., 2003. Testing for phylogenetic signal in comparative data: behavioral traits are more labile. Evolution. 57, 717–745. https://doi.org/10.1111/j.0014-3820.2003.tb00285.x

Bolker, B.M., Brooks, M.E., Clark, C.J., Geange, S.W., Poulsen, J.R., Stevens, M.H.H., White, J.S.S., 2009. Generalized linear mixed models: a practical guide for ecology and evolution. Trends Ecol. Evol. 24, 127–135. https://doi.org/10.1016/J.TREE.2008.10.008

Boria, R.A., Olson, L.E., Goodman, S.M., Anderson, R.P., 2014. Spatial filtering to reduce sampling bias can improve the performance of ecological niche models. Ecol. Modell. 275, 73–77. https://doi.org/10.1016/j.ecolmodel.2013.12.012

Bourdelais, A.J., Tomas, C.R., Naar, J., Kubanek, J., Baden, D.G., 2002. New fish-killing alga in coastal Delaware produces neurotoxins. Environ. Health Perspect. 110, 465–70.

Boyd, P.W., Rynearson, T.A., Armstrong, E.A., Fu, F., Hayashi, K., Hu, Z., Hutchins, D.A., Kudela, R.M., Litchman, E., Mulholland, M.R., Passow, U., Strzepek, R.F., Whittaker, K.A., Yu, E., Thomas, M.K., Kudela, R.M., Passow, U., Hayashi, K., Armstrong, E.A., Rynearson, T.A., Fu, F., Hutchins, D.A., Litchman, E., Hu, Z., Boyd, P.W., Yu, E., Strzepek, R.F., Whittaker, K.A., Rynearson, T.A., Armstrong, E.A., Fu, F., Hayashi, K., Hu, Z., Hutchins, D.A., Kudela, R.M., Litchman, E., Mulholland, M.R., Passow, U., Strzepek, R.F., Whittaker, K.A., Yu, E., Thomas, M.K., 2013. Marine phytoplankton temperature versus growth responses from polar to tropical waters - Outcome of a scientific community-wide study. PLoS One 8, e63091. https://doi.org/10.1371/journal.pone.0063091

Boyd, P.W., Strzepek, R., Fu, F., Hutchins, D.A., 2010. Environmental control of open-ocean phytoplankton groups: Now and in the future. Limnol. Oceanogr. https://doi.org/10.4319/lo.2010.55.3.1353

Bravo, I., Fernández, M.L., Ramilo, I., Martínez, A., 2001. Toxin composition of the toxic dinoflagellate Prorocentrum lima isolated from different locations along the Galician coast (NW Spain). Toxicon 39, 1537–1545. https://doi.org/10.1016/S0041-0101(01)00126-X

Brown, J.H., Gillooly, J.F., Allen, A.P., Savage, V.M., West, G.B., 2004. Toward a metabolic theory of ecology. Ecology 85, 1771–1789. https://doi.org/10.1890/03-9000

Brun, P., Vogt, M., Payne, M.R., Gruber, N., O'brien, C.J., Buitenhuis, E.T., Le Qu Er, C., Leblanc, K., Luo, Y.-W., 2015. Ecological niches of open ocean phytoplankton taxa. Limnol. Oceanogr. 60, 1020–1038. https://doi.org/10.1002/lno.10074

Brush, M.J., Brawley, J.W., Nixon, S.W., Kremer, J.N., 2002. Modeling phytoplankton production: Problems with the Eppley curve and an empirical alternative. Mar. Ecol. Prog. Ser. 238, 31–45. https://doi.org/10.3354/meps238031

Buitenhuis, E., Vogt, M., Moriarty, R., Bednarsek, N., Doney, S.C., Leblanc, K., Le Quéré, C., Luo, Y.-W., O'brien, C., O'brien, T., Buitenhuis, E.T., Bednaršek, N., Peloquin, J., Schiebel, R., Swan, C., 2013. MAREDAT: towards a world atlas of MARine Ecosystem DATa Earth System Science Data MAREDAT: towards a world atlas of MARine Ecosystem DATa. Earth Syst. Sci. Data 5, 227–239. https://doi.org/10.1594/PANGAEA.779970ï

Cahill, A.E., Aiello-Lammens, M.E., Caitlin Fisher-Reid, M., Hua, X., Karanewsky, C.J., Ryu, H.Y., Sbeglia, G.C., Spagnolo, F., Waldron, J.B., Warsi, O., Wiens, J.J., 2013. How does climate change cause extinction? Proc. R. Soc. B Biol. Sci. https://doi.org/10.1098/rspb.2012.1890

Cembella, A., 1998. Ecophysiology and metabolism of paralytic shellfish toxins in marine microalgae, in: Anderson, D.M., Cembella, A.D., Hallegraeff, G.M. (Eds.), Physiological ecology of harmful algal blooms. NATO-Advanced Study Institute Series, Springer-Verlag, Heidelberg, pp. 381–404.

Chaudhary, C., Saeedi, H., Costello, M.J., 2016. Bimodality of latitudinal gradients in marine species richness. Trends Ecol. Evol. https://doi.org/10.1016/j.tree.2016.06.001

Chen, B., 2015. Patterns of thermal limits of phytoplankton. J. Plankton Res. 37, 285–292. https://doi.org/10.1093/plankt/fbv009

Chen, B., Laws, E.A., 2016. Is there a difference of temperature sensitivity between marine phytoplankton and heterotrophs? Limnol. Oceanogr. https://doi.org/10.1002/lno.10462

Chesson, P., 2000. Mechanisms of maintenance of species diversity. Annu. Rev. Ecol. Syst. 31, 343–366. https://doi.org/10.1146/annurev.ecolsys.31.1.343

Chu, C., Ludford, P.M., Ozbun, J.L., Sweet, R.D., 1978. Effects of temperature and competition on the establishment and growth of redroot pigweed and common lambsquarters. Crop Sci. 18, 308–310. https://doi.org/10.2135/cropsci1978.0011183x001800020029x

Chust, G., Allen, J.I., Bopp, L., Schrum, C., Holt, J., Tsiaras, K., Zavatarelli, M., Chifflet, M., Cannaby, H., Dadou, I., Daewel, U., Wakelin, S.L., Machu, E., Pushpadas, D., Butenschon, M., Artioli, Y., Petihakis, G., Smith, C., Garçon, V., Goubanova, K., Le Vu, B., Fach, B.A., Salihoglu, B., Clementi, E., Irigoien, X., 2014. Biomass changes and trophic amplification of plankton in a warmer ocean. Glob. Chang. Biol. 20, 2124–2139. https://doi.org/10.1111/gcb.12562

Clusella-Trullas, S., Blackburn, T.M., Chown, S.L., 2011. Climatic predictors of temperature performance curve parameters in ectotherms imply complex responses to climate change. Am. Nat. 177, 738–751. https://doi.org/10.1086/660021

Coello-Camba, A., Agustí, S., 2017. Thermal thresholds of phytoplankton growth in polar waters and their consequences for a warming polar ocean. Front. Mar. Sci. 4, 168. https://doi.org/10.3389/fmars.2017.00168

Coello-Camba, A., Agustí, S., Vaqué, D., Holding, J., Arrieta, J.M., Wassmann, P., Duarte, C.M., 2015. Experimental assessment of temperature thresholds for arctic phytoplankton communities. Estuaries and Coasts 38, 873–885. https://doi.org/10.1007/s12237-014-9849-7

Colwell, R.K., Rangel, T.F., 2009. Hutchinson's duality: The once and future niche. Proc. Natl. Acad. Sci. U. S. A. 106, 19651–19658. https://doi.org/10.1073/pnas.0901650106

Connell, S.D., Russell, B.D., 2010. The direct effects of increasing CO_2 and temperature on non-calcifying organisms: increasing the potential for phase shifts in kelp forests. Proc. R. Soc. B Biol. Sci. 277, 1409–1415. https://doi.org/10.1098/rspb.2009.2069

Crombie, A.C., 1947. Interspecific Competition. J. Anim. Ecol. 16, 44. https://doi.org/10.2307/1506

Davis, A.J., Jenkinson, L.S., Lawton, J.H., Shorrocks, B., Wood, S., 1998. Making mistakes when predicting shifts in species range in response to global warming. Nature 391, 783–786. https://doi.org/10.1038/35842

de Boer, M.K., Koolmees, E.M., Vrieling, E.G., Breeman, A.M., van Rijssel, M., 2004. Temperature responses of three *Fibrocapsa japonica* strains (Raphidophyceae) from different climate regions. J. Plankton Res. 27, 47–60. https://doi.org/10.1093/plankt/fbh149

Delgado, G., Popowski, G., García, C., Lagos, N., Lechuga-Devéze, C.H., 2005. Presence of DSP-toxins in *Prorocentrum lima* (Ehrenberg) Dodge in Cuba. Rev. Investig. Mar. 26, 229–234.

Dell, A.I., Pawar, S., Savage, V.M., 2014. Temperature dependence of trophic interactions are driven by asymmetry of species responses and foraging strategy. J. Anim. Ecol. 83, 70–84. https://doi.org/10.1111/1365-2656.12081

Deutsch, C.A., Tewksbury, J.J., Huey, R.B., Sheldon, K.S., Ghalambor, C.K., Haak, D.C., Martin, P.R., 2008. Impacts of climate warming on terrestrial ectotherms across latitude 105, 6668–6672.

Dhanji-Rapkova, M., O'Neill, A., Maskrey, B.H., Coates, L., Swan, S.C., Teixeira Alves, M., Kelly, R.J., Hatfield, R.G., Rowland-Pilgrim, S.J., Lewis, A.M., Turner, A.D., 2019. Variability and profiles of lipophilic toxins in bivalves from Great Britain during five and a half years of monitoring: azaspiracids and yessotoxins. Harmful Algae 87. https://doi.org/10.1016/j.hal.2019.101629

Dhanji-Rapkova, M., O'Neill, A., Maskrey, B.H., Coates, L., Teixeira Alves, M., Kelly, R.J., Hatfield, R.G., Rowland-Pilgrim, S.J., Lewis, A.M., Algoet, M., Turner, A.D., 2018. Variability and profiles of lipophilic toxins in bivalves from Great Britain during five and a half years of monitoring: Okadaic acid, dinophysis toxins and pectenotoxins. Harmful Algae 77, 66–80. https://doi.org/10.1016/j.hal.2018.05.011

Diamond, S.E., Sorger, D.M., Hulcr, J., Pelini, S.L., Toro, I. Del, Hirsch, C., Oberg, E., Dunn, R.R., 2012. Who likes it hot? A global analysis of the climatic, ecological, and evolutionary determinants of warming tolerance in ants. Glob. Chang. Biol. 18, 448–456. https://doi.org/10.1111/j.1365-2486.2011.02542.x

Dieckmann, U., Law, R., 1996. The dynamical theory of coevolution: A derivation from stochastic ecological processes. J. Math. Biol. 34, 579–612. https://doi.org/10.1007/BF02409751

Dunson, W.A., Travis, J., 1991. The role of abiotic factors in community organization. Am. Nat. 138, 1067–1091. https://doi.org/10.1086/285270

Durant, J.M., Krasnov, Y. V., Nikolaeva, N.G., Stenseth, N.C., 2012. Within and between species competition in a seabird community: Statistical exploration and modeling of time-series data. Oecologia 169, 685–694. https://doi.org/10.1007/s00442-011-2226-3

Edwards, M., Richardson, A.J., 2004. Impact of climate change on marine pelagic phenology and trophic mismatch. Nature 430, 881–884. https://doi.org/10.1038/nature02808

Elith, J., H. Graham, C., P. Anderson, R., Dudík, M., Ferrier, S., Guisan, A., J. Hijmans, R., Huettmann, F., R. Leathwick, J., Lehmann, A., Li, J., G. Lohmann, L., A. Loiselle, B., Manion, G., Moritz, C., Nakamura, M., Nakazawa, Y., McC. M. Overton, J., Townsend Peterson, A., J. Phillips, S., Richardson, K., Scachetti-Pereira, R., E. Schapire, R., Soberón, J., Williams, S., S. Wisz, M., E. Zimmermann, N., 2006. Novel methods improve prediction of species' distributions from occurrence data. Ecography (Cop.). 29, 129–151. https://doi.org/10.1111/j.2006.0906-7590.04596.x

Elton, C.S., 1927. Animal Ecology. University of Chicago Press.

Eppley, R.W., 1972. Temperature and phytoplankton growth in the sea. Fish. Bull. Nat. Ocean. Atmos. Adm. 70, 1063–85.

Eppley, R.W., Reid, F.M.H., Strickland, J.D.H., 1970. Estimates of phytoplankton crop size, growth rate, and primary production. Bull. Scripps Inst. Oceanogr. 17, 33–42.

Estrada, M., Delgado, M., Blasco, D., Latasa, M., Cabello, A.M., Benítez-Barrios, V., Fraile-Nuez, E., Mozetič, P., Vidal, M., 2016. Phytoplankton across tropical and subtropical regions of the Atlantic, Indian and Pacific oceans. PLoS One 11. https://doi.org/10.1371/journal.pone.0151699

Falkowski, P., 2012. Ocean science: The power of plankton. Nature 483, S17–S20. https://doi.org/10.1038/483S17a

Falkowski, P.G., Katz, M.E., Knoll, A.H., Quigg, A., Raven, J.A., Schofield, O., Taylor, F.J.R., 2004. The evolution of modern eukaryotic phytoplankton. Science. 305, 354–360. https://doi.org/10.1126/science.1095964

Falkowski, P.G., Oliver, M.J., 2007. Mix and match: how climate selects phytoplankton. Nat. Rev. Microbiol. 5, 813–819. https://doi.org/10.1038/nrmicro1751

Falkowski, P.G., Raven, J.A., 2007. Aquatic Photosynthesis, Second Edi. ed. Princeton University Press, New Jersey.

Felsenstein, J., 1985. Phylogenies and the comparative method. Am. Nat. 125(1), 1 – 15.

Feng, Y., Hare, C.E., Leblanc, K., Rose, J.M., Zhang, Y., DiTullio, G.R., Lee, P.A., Wilhelm, S.W., Rowe, J.M., Sun, J., Nemcek, N., Gueguen, C., Passow, U., Benner, I., Brown, C., Hutchins, D.A., 2009. Effects of increased pCO_2 and temperature on the north atlantic spring bloom. I. The phytoplankton community and biogeochemical response. Mar. Ecol. Prog. Ser. 388, 13–25. https://doi.org/10.3354/meps08133

Feng, Y., Warner, M.E., Zhang, Y., Sun, J., Fu, F.-X., Rose, J.M., Hutchins, D.A., 2008. Interactive effects of increased pCO_2, temperature and irradiance on the marine coccolithophore *Emiliania huxley*i (Prymnesiophyceae). Eur. J. Phycol. 43, 87–98. https://doi.org/10.1080/09670260701664674

Fiorini, S., Middelburg, J., Gattuso, J., 2011. Effects of elevated CO_2 partial pressure and temperature on the coccolithophore *Syracosphaera pulchra*. Aquat. Microb. Ecol. 64, 221–232. https://doi.org/10.3354/ame01520

Flanders Marine Institute, 2009. Longhurst Provinces. http://www.marineregions.org/gazetteer.php?p=details&id=22538

Flores-Moya, A., Rouco, M., García-Sánchez, M.J., García-Balboa, C., González, R., Costas, E., López-Rodas, V., 2012. Effects of adaptation, chance, and history on the evolution of the toxic dinoflagellate *Alexandrium minutum* under selection of increased temperature and acidification. Ecol. Evol. 2, 1251–9. https://doi.org/10.1002/ece3.198

Foden, J., Purdie, D.A., Morris, S., Nascimento, S., 2005. Epiphytic abundance and toxicity of *Prorocentrum lima* populations in the Fleet Lagoon, UK. Harmful Algae 4, 1063–1074. https://doi.org/10.1016/j.hal.2005.03.004

Freckleton, Harvey, Pagel, 2002. Phylogenetic analysis and comparative data: A test and review of evidence. Am. Nat. 160, 712–726. https://doi.org/10.2307/3078855

Freckleton, R.P., Cooper, N., Jetz, W., 2011. Comparative methods as a statistical fix: The dangers of ignoring an evolutionary model. Am. Nat. 178. https://doi.org/10.1086/660272

Fritschie, K.J., Cardinale, B.J., Alexandrou, M.A., Oakley, T.H., 2014. Evolutionary history and the strength of species interactions: Testing the phylogenetic limiting similarity hypothesis. Ecology. https://doi.org/10.1890/13-0986.1

Fu, F.X., Warner, M.E., Zhang, Y., Feng, Y., Hutchins, D.A., 2007. Effects of increased temperature and CO_2 on photosynthesis, growth, and elemental ratios in marine Synechococcus and Prochlorococcus (Cyanobacteria). J. Phycol. 43, 485–496. https://doi.org/10.1111/j.1529-8817.2007.00355.x

Fu, F.X., Tatters, A.O., Hutchins, D.A., 2012. Global change and the future of harmful algal blooms in the ocean. Mar. Ecol. Prog. Ser. 470, 207–233. https://doi.org/10.3354/meps10047

Garibo, D., de la Iglesia, P., Diogène, J., Campàs, M., 2013. Inhibition equivalency factors for dinophysistoxin-1 and dinophysistoxin-2 in protein phosphatase assays: Applicability to the analysis of shellfish samples and comparison with LC-MS/MS. J. Agric. Food Chem. 61, 2572–2579. https://doi.org/10.1021/jf305334n

Gaston, K.J., Chown, S.L., Calosi, P., Bernardo, J., Bilton, D.T., Clarke, A., Clusella-Trullas, S., Ghalambor, C.K., Konarzewski, M., Peck, L.S., Porter, W.P., Pörtner, H.O., Rezende, E.L., Schulte, P.M., Spicer, J.I., Stillman, J.H., Terblanche, J.S., van Kleunen, M., 2009. Macrophysiology: a conceptual reunification. Am. Nat. 174, 595–612. https://doi.org/10.1086/605982

Gaylord, Gaines, 2000. Temperature or transport? Range limits in marine species mediated solely by flow. Am. Nat. 155, 769. https://doi.org/10.2307/3079099

GBIF Secretariat, 2019. GBIF Backbone Taxonomy. https://doi.org/10.15468/39omei

GBIF.org, 2018. The Global Biodiversity Information Facility. https://doi.org/10.1145/1185448.1185493

Geider, R.J., MacIntyre, H.L., Kana, T.M., 1997. Dynamic model of phytoplankton growth and acclimation: Responses of the balanced growth rate and the chlorophyll *a*: carbon ratio to light, nutrient-limitation and temperature. Mar. Ecol. Prog. Ser. 148, 187–200. https://doi.org/10.3354/meps148187

Gerssen, A., Mulder, P.P.J., McElhinney, M.A., de Boer, J., 2009. Liquid chromatography-tandem mass spectrometry method for the detection of marine lipophilic toxins under alkaline conditions. J. Chromatogr. A 1216, 1421–1430. https://doi.org/10.1016/j.chroma.2008.12.099

Gessner, B.D., Middaugh, J.P., 1995. Paralytic shellfish poisoning in Alaska: a 20-year retrospective analysis. Am. J. Epidemiol. 141, 766–70.

Gillooly, J.F., 2001. Effects of size and temperature on metabolic rate. Science. 293, 2248–2251. https://doi.org/10.1126/science.1061967

Gilman, S.E., Urban, M.C., Tewksbury, J., Gilchrist, G.W., Holt, R.D., 2010. A framework for community interactions under climate change. Trends Ecol. Evol. 25, 325–331. https://doi.org/10.1016/j.tree.2010.03.002

Gittleman, J.L., Kot, M., 1990. Adaptation: Statistics and a null model for estimating phylogenetic effects. Syst. Zool. 39, 227. https://doi.org/10.2307/2992183

Goldberg, D.E., Landa, K., 1991. Competitive effect and esponse: Hierarchies and correlated traits in the early stages of competition. J. Ecol. 79, 1013. https://doi.org/10.2307/2261095

Graham, C.H., Ferrier, S., Huettman, F., Moritz, C., Peterson, A.T., 2004. New developments in museum-based informatics and applications in biodiversity analysis. Trends Ecol. Evol. https://doi.org/10.1016/j.tree.2004.07.006

Gran, H.H., Braarud, T., 1935. A quantitative study of the phytoplankton in the Bay of Fundy and the Gulf of Maine (including observations on hydrography, chemistry and turbidity). J. Biol. Board Canada 1, 279–467. https://doi.org/10.1139/f35-012

Grimaud, G.M., 2016. Modelling the temperature effect on phytoplankton: from acclimation to adaptation.

Grimaud, G.M., Mairet, F., Sciandra, A., Bernard, O., 2017. Modeling the temperature effect on the specific growth rate of phytoplankton: a review. Rev. Environ. Sci. Bio/Technology 16, 625–645. https://doi.org/10.1007/s11157-017-9443-0

Grinnell, J., 1917. The Niche-relationships of the California thrasher. Auk 34, 427–433. https://doi.org/10.2307/4072271

Gross, S.J., Price, T.D., 2000. Determinants of the northern and southern range limits of a warbler. J. Biogeogr. 27, 869–878. https://doi.org/10.1046/j.1365-2699.2000.00440.x

Grover, J.P., 2000. Resource competition and community structure in aquatic micro-organisms: experimental studies of algae and bacteria along a gradient of organic carbon to inorganic phosphorus supply. J. Plankton Res. 22, 1591–1610. https://doi.org/10.1093/plankt/22.8.1591

Grzebyk, D., Denardou, A., Berland, B., Pouchus, Y.F., 1997. Evidence of a new toxin in the red-tide dinoflagellate *Prorocentrum minimum*. J. Plankton Res. 19, 1111–1124. https://doi.org/10.1093/plankt/19.8.1111

Guisan, A., Thuiller, W., 2005. Predicting species distribution: Offering more than simple habitat models. Ecol. Lett. https://doi.org/10.1111/j.1461-0248.2005.00792.x

Guisan, A., Zimmermann, N.E., 2000. Predictive habitat distribution models in ecology. Ecol. Modell. 135, 147–186. https://doi.org/10.1016/S0304-3800(00)00354-9

Gunderson, A.R., Stillman, J.H., 2015. Plasticity in thermal tolerance has limited potential to buffer ectotherms from global warming. Proc. R. Soc. B Biol. Sci. 282, 20150401. https://doi.org/10.1098/rspb.2015.0401

Häder, D.-P., Gao, K., 2015. Interactions of anthropogenic stress factors on marine phytoplankton. Front. Environ. Sci. 3, 14. https://doi.org/10.3389/fenvs.2015.00014

Hackett, J.D., Tong, M., Kulis, D.M., Fux, E., Hess, P., Bire, R., Anderson, D.M., 2009. DSP toxin production de novo in cultures of *Dinophysis acuminata* (Dinophyceae) from North America. Harmful Algae 8, 873–879. https://doi.org/10.1016/j.hal.2009.04.004

Hales, S., Weinstein, P., Woodward, A., 1999. Ciguatera (Fish Poisoning), El Niño, and Pacific Sea Surface Temperatures. Ecosyst. Heal. 5, 20–25. https://doi.org/10.1046/j.1526-0992.1999.09903.x

Hallegraeff, G.M., 2010. Ocean climate change, phytoplankton community responses, and harmful algal blooms: A formidable predictive challenge. J. Phycol. https://doi.org/10.1111/j.1529-8817.2010.00815.x

Hallegraeff, G.M., Anderson, D.M., Cembella, A.D. (Eds.), 2004. Manual on harmful marine microalgae, Monographs on Oceanographic Methodology. https://doi.org/10.1097/00000433-198206000-00020

Hanelt, D., Wiencke, C., Bischof, K., 2003. Photosynthesis in marine macroalgae, in: Larkum, A., Douglas, S., Raven, J. (Eds.), Photosynthesis in algae. Kluwer Academic Publishers, Amsterdam, pp. 413–435.

Heredia-Tapia, A., Arredondo-Vega, B.O., Nuñez-Vázquez, E.J., Yasumoto, T., Yasuda, M., Ochoa, J.L., 2002. Isolation of *Prorocentrum lima* (Syn. *Exuviaella lima*)

and diarrhetic shellfish poisoning (DSP) risk assessment in the Gulf of California, Mexico. Toxicon 40, 1121–127. https://doi.org/10.1016/s0041-0101(02)00111-3

Hernández-Carrasco, I., Orfila, A., Rossi, V., Garçon, V., 2018. Effect of small scale transport processes on phytoplankton distribution in coastal seas. Sci. Rep. 8, 8613. https://doi.org/10.1038/s41598-018-26857-9

Hijmans, R.J., Graham, C.H., 2006. The ability of climate envelope models to predict the effect of climate change on species distributions. Glob. Chang. Biol. 12, 2272–2281. https://doi.org/10.1111/j.1365-2486.2006.01256.x

Hikosaka, K., Ishikawa, K., Borjigidai, A., Muller, O., Onoda, Y., 2005. Temperature acclimation of photosynthesis: mechanisms involved in the changes in temperature dependence of photosynthetic rate. J. Exp. Bot. 57, 291–302. https://doi.org/10.1093/jxb/erj049

Hochachka, P.W., Somero, G.N., 2002. Biochemical adaptation : mechanism and process in physiological evolution. Oxford University Press.

Hodge, A., Fitter, A.H., 2013. Microbial mediation of plant competition and community structure. Funct. Ecol. 27, 865–875. https://doi.org/10.1111/1365-2435.12002

Hoegh-Guldberg, O., Bruno, J.F., 2010. The impact of climate change on the world's marine ecosystems. Science. https://doi.org/10.1126/science.1189930

Holt, R.D., 2003. On the evolutionary ecology of species' ranges.

Huertas, I.E., Rouco, M., López-Rodas, V., Costas, E., 2011. Warming will affect phytoplankton differently: Evidence through a mechanistic approach. Proc. R. Soc. B Biol. Sci. 278, 3534–3543. https://doi.org/10.1098/rspb.2011.0160

Huertas, I.E., Rouco, M., López-Rodas, V., Costas, E., 2011. Warming will affect phytoplankton differently: evidence through a mechanistic approach. Proceedings. Biol. Sci. 278, 3534–43. https://doi.org/10.1098/rspb.2011.0160

Huey, R.B., Deutsch, C.A., Tewksbury, J.J., Vitt, L.J., Hertz, P.E., Pérez, H.J.Á., Garland, T., 2009. Why tropical forest lizards are vulnerable to climate warming. Proc. R. Soc. B Biol. Sci. 276, 1939–1948. https://doi.org/10.1098/rspb.2008.1957

Hughes, T.P., Rodrigues, M.J., Bellwood, D.R., Ceccarelli, D., Hoegh-Guldberg, O., McCook, L., Moltschaniwskyj, N., Pratchett, M.S., Steneck, R.S., Willis, B., 2007. Phase shifts, herbivory, and the resilience of coral reefs to climate change. Curr. Biol. 17, 360–5. https://doi.org/10.1016/j.cub.2006.12.049

Hutchins, D.A., Fu, F.-X., Zhang, Y., Warner, M.E., Feng, Y., Portune, K., Bernhardt, P.W., Mulholland, M.R., 2007. CO_2 control of *Trichodesmium* N_2 fixation, photosynthesis, growth rates, and elemental ratios: Implications for past, present, and future ocean biogeochemistry. Limnol. Ocean. 52, 1293–1304.

Hutchinson, G.E., 1957. Concluding Remarks. Cold Spring Harb. Symp. Quant. Biol. 22, 415–427. https://doi.org/10.1101/sqb.1957.022.01.039

Iglesias-Prieto, R., Matta, J.L., Robins, W.A., Trench, R.K., 1992. Photosynthetic response to elevated temperature in the symbiotic dinoflagellate *Symbiodinium microadriaticum* in culture. Ecology 89, 10302–10305.

IPCC, 2013. Climate Change 2013: The Physical Science Basis. Contribution of Working Group I to the Fifth Assessment Report of the Intergovernmental Panel on Climate Change. Cambridge University Press, Cambridge, United Kingdom and New York, NY, USA. https://doi.org/10.1017/CBO9781107415324.Summary

Irwin, A.J., Nelles, A.M., Finkel, Z. V., 2012. Phytoplankton niches estimated from field data. Limnol. Oceanogr. 57, 787–797. https://doi.org/10.4319/lo.2012.57.3.0787

Isaac, N.J.B., Pocock, M.J.O., 2015. Bias and information in biological records. Biol. J. Linn. Soc. 115, 522–531. https://doi.org/10.1111/bij.12532

Ives, A.R., Midford, P.E., Garland, T., 2007. Within-species variation and measurement error in phylogenetic comparative methods. Syst. Biol. 56, 252–270. https://doi.org/10.1080/10635150701313830

Jackson, A.E., Marr, J.C., McLachalan, J.L., 1993. Production of diarrhetic shellfish toxins by an isolate of *Prorocentrum lima* from Nova Scotia, Canada, in: Smayda, T., Shimizu, Y. (Eds.), Toxic phytoplankton blooms in the Sea. Elsevier, Amsterdam, The Netherlands, pp. 513–518.

Jackson, S.T., Overpeck, J., 2000. Responses of plant populations and communities to environmental changes of the late Quaternary. Paleobiology 26, 194–220.

Jankowski, J.E., Londoño, G.A., Robinson, S.K., Chappell, M.A., 2013. Exploring the role of physiology and biotic interactions in determining elevational ranges of tropical animals. Ecography (Cop.). 36, 1–12. https://doi.org/10.1111/j.1600-0587.2012.07785.x

Janzen, D.H., 1967. Why mountain passes are higher in the tropics. Am. Nat. 101, 233–249. https://doi.org/10.1086/282487

Jiménez-Valverde, A., Lobo, J.M., Hortal, J., 2008. Not as good as they seem: the importance of concepts in species distribution modelling. Divers. Distrib. 14, 885–890. https://doi.org/10.1111/j.1472-4642.2008.00496.x

Johannes, R., Wiebe, W., Crossland, C., Rimmer, D., Smith, S., 1983. Latitudinal limits of coral reef growth. Mar. Ecol. Prog. Ser. 11, 105–111. https://doi.org/10.3354/meps011105

Kamiyama, T., Nagai, S., Suzuki, T., Miyamura, K., 2010. Effect of temperature on production of okadaic acid, dinophysistoxin-1, and pectenotoxin-2 by Dinophysis acuminata in culture experiments. Aquat. Microb. Ecol. 60, 193–202. https://doi.org/10.3354/ame01419

Karney, C.F.F., 2013. Algorithms for geodesics 87, 43–55. https://doi.org/10.1007/s00190-012-0578-z

Kearney, M., 2006. Habitat, environment and niche: What are we modelling? Oikos. https://doi.org/10.1111/j.2006.0030-1299.14908.x

Kearney, M., Porter, W., 2009. Mechanistic niche modelling: combining physiological and spatial data to predict species' ranges. Ecol. Lett. 12, 334–350. https://doi.org/10.1111/j.1461-0248.2008.01277.x

Kearney, M., Porter, W.P., 2004. Mapping the fundamental niche: Physiology, climate, and the distribution of a nocturnal lizard. Ecology 85, 3119–3131. https://doi.org/10.1890/03-0820

Keck, F., Rimet, F., Bouchez, A., Franc, A., 2016. phylosignal: an R package to measure, test, and explore the phylogenetic signal. Ecol. Evol. 6, 2774–80. https://doi.org/10.1002/ece3.2051

Keddy, P.A., 2001. Competition, 2nd ed. Kluwer Academic Publishers.

Keller, M.D., Selvin, R.C., Claus, W., Guillard, R.R.L., 1987. Media for the culture of oceanic ultraphytoplankton. J. Phycol. 23, 633–638.

Kellmann, R., Stüken, A., Orr, R.J.S., Svendsen, H.M., Jakobsen, K.S., 2010. Biosynthesis and molecular genetics of polyketides in marine dinoflagellates. Mar. Drugs 8, 1011–1048. https://doi.org/10.3390/md8041011

Kennedy, P., 2010. Ectomycorrhizal fungi and interspecific competition: Species interactions, community structure, coexistence mechanisms, and future research directions. New Phytol. https://doi.org/10.1111/j.1469-8137.2010.03399.x

Kent, M.L., Whytel, J.N.C., Latrace, C., 1995. Gill lesions and mortality in seawater pen-reared Atlantic salmon Salmo salar associated with a dense bloom *of Skeletonema costatum* and *Thalassiosira species* 22, 77–81.

Kingsolver, J.G., 2009. The well-temperatured biologist. (American Society of Naturalists Presidential Address). Am. Nat. 174, 755–68. https://doi.org/10.1086/648310

Knies, J.L., Kingsolver, J.G., 2010. Erroneous Arrhenius: Modified Arrhenius model best explains the temperature dependence of ectotherm fitness. Am. Nat. 176, 227–233. https://doi.org/10.1086/653662

Koike, K., Sato, S., Yamaji, M., Nagahama, Y., Kotaki, Y., Ogata, T., Kodama, M., 1998. Occurrence of okadaic acid-producing *Prorocentrum lima* on the Sanriku coast, northern Japan. Toxicon 36, 2039–42. https://doi.org/10.1016/s0041-0101(98)00132-9

Kordas, R.L., Harley, C.D.G., O'Connor, M.I., 2011. Community ecology in a warming world: The influence of temperature on interspecific interactions in marine systems. J. Exp. Mar. Bio. Ecol. https://doi.org/10.1016/j.jembe.2011.02.029

Krasnov, B.R., Poulin, R., Mouillot, D., 2011. Scale-dependence of phylogenetic signal in ecological traits of ectoparasites. Ecography (Cop.). 34, 114–122. https://doi.org/10.1111/j.1600-0587.2010.06502.x

Kremer, C.T., Thomas, M.K., Litchman, E., 2017. Temperature- and size-scaling of phytoplankton population growth rates: Reconciling the Eppley curve and the metabolic theory of ecology. Limnol. Oceanogr. 62, 1658–1670. https://doi.org/10.1002/lno.10523

Kremp, A., Anderson, D.M., 2000. Factors regulating germination of resting cysts of the spring bloom dinoflagellate *Scrippsiella hangoei* from the northern Baltic Sea. J. Plankton Res. 22, 1311–1327. https://doi.org/10.1093/plankt/22.7.1311

Kremp, A., Godhe, A., Egardt, J., Dupont, S., Suikkanen, S., Casabianca, S., Penna, A., 2012. Intraspecific variability in the response of bloom-forming marine microalgae to changed climate conditions. Ecol. Evol. 2, 1195–207. https://doi.org/10.1002/ece3.245

Krol, M., Maxwell, D.P., Huner, N.P.A., 1997. Exposure of *Dunaliella salina* to low temperature mimics the high light-induced accumulation of carotenoids and the carotenoid binding protein (Cbr). Plant Cell Physiol 38, 213–216.

Kuhn, M., Chow, F., Wickham, H., 2019. rsample: General resampling infrastructure.

Kuhn, M., Vaughan, D., 2020. yardstick: Tidy characterizations of model performance.

Kuhn, M., Wickham, H., 2019. recipes: Preprocessing tools to create design matrices.

Kumar, S., Stecher, G., Suleski, M., Hedges, S.B., 2017. TimeTree: A resource for timelines, timetrees, and divergence times. Mol. Biol. Evol. 34, 1812–1819. https://doi.org/10.1093/molbev/msx116

Laffoley, D., Baxter, J.M. (Eds.), 2016. Explaining ocean warming: Causes, scale, effects and consequences. Gland, Switzerland.

Lang, B., Rall, B.C., Brose, U., 2012. Warming effects on consumption and intraspecific interference competition depend on predator metabolism. J. Anim. Ecol. 81, 516–523. https://doi.org/10.1111/j.1365-2656.2011.01931.x

Leblanc, K., Arístegui, J., Armand, L., Assmy, P., Beker, B., Bode, A., Breton, E., Cornet, V., Gibson, J., Gosselin, M.P., Kopczynska, E., Marshall, H., Peloquin, J., Piontkovski, S., Poulton, A.J., Quéguiner, B., Schiebel, R., Shipe, R., Stefels, J., Van Leeuwe, M.A., Varela, M., Widdicombe, C., Yallop, M., 2012. A global diatom database- Abundance, biovolume and biomass in the world ocean. Earth Syst. Sci. Data 4, 149–165. https://doi.org/10.5194/essd-4-149-2012

Lee, J.S., Igarashi, T., Fraga, S., Dahl, E., Hovgaard, P., Yasumoto, T., 1989. Determination of diarrhetic shellfish toxins in various dinoflagellate species. J. Appl. Phycol. 1, 147–152. https://doi.org/10.1007/BF00003877

Lee, T., Fong, F., Ho, K.C., Lee, F., 2016. The mechanism of diarrhetic shellfish poisoning toxin production in *Prorocentrum* spp.: Physiological and molecular perspectives. Toxins (Basel). 8, 272. https://doi.org/10.3390/toxins8100272

Levasseur, M.E., Morissette, J.-C., Popovic, R., Harrison, P.J., 1990. Effects of long term exposure to low temperature on the photosynthetic apparatus of *Dunaliella tertiolecta* (Chlorophyceae). J. Phycol. 26, 479–484. https://doi.org/10.1111/j.0022-3646.1990.00479.x

Levitan, O., Kranz, S.A., Spungin, D., Prášil, O., Rost, B., Berman-Frank, I., 2010. Combined effects of CO_2 and Light on the N_2-fixing cyanobacterium *Trichodesmium* IMS101: A mechanistic view. Plant Physiol. 154, 346–356. https://doi.org/10.1104/pp.110.159285

Li, Y., Gao, K., Villafañe, V.E., Helbling, E.W., 2012. Ocean acidification mediates photosynthetic response to UV radiation and temperature increase in the diatom *Phaeodactylum tricornutum*. Biogeosciences 9, 3931–3942. https://doi.org/10.5194/bg-9-3931-2012

Lima, F.P., Ribeiro, P.A., Queiroz, N., Xavier, R., Tarroso, P., Hawkins, S.J., Santos, A.M., 2007. Modelling past and present geographical distribution of the marine gastropod *Patella rustica* as a tool for exploring responses to environmental change. Glob. Chang. Biol. 13, 2065–2077. https://doi.org/10.1111/j.1365-2486.2007.01424.x

Litchman, E., Edwards, K.F., Klausmeier, C.A., Thomas, M.K., 2012. Phytoplankton niches, traits and eco-evolutionary responses to global environmental change. Mar. Ecol. Prog. Ser. 470, 235–248. https://doi.org/10.3354/meps09912

Litchman, E., Klausmeier, C., 2014. Laboratory results on marine phytoplankton growth rates, temperatures, and isolation locations collected at Michigan State University in 2012. Biol. Chem. Oceanogr. Data Manag. Off. (BCO-DMO). Dataset version 2014-12-22. URL http://lod.bco-dmo.org/id/dataset/544814 (accessed 11.1.17).

Longhurst, A.R., 2007. Ecological geography of the sea. Elsevier. https://doi.org/10.1016/B978-0-12-455521-1.X5000-1

López-Rosales, L., Gallardo-Rodríguez, J.J., Sánchez-Mirón, A., Cerón-García, M. del C., Belarbi, E.H., García-Camacho, F., Molina-Grima, E., 2013. Simultaneous effect of temperature and irradiance on growth and okadaic acid production from the marine dinoflagellate *Prorocentrum belizeanum*. Toxins (Basel). 6, 229–253. https://doi.org/10.3390/toxins6010229

Lord, J., Whitlatch, R., 2015. Predicting competitive shifts and responses to climate change based on latitudinal distributions of species assemblages, Ecology. 96(5), 1264 – 1274.

Low-Décarie, E., Boatman, T.G., Bennett, N., Passfield, W., Gavalás-Olea, A., Siegel, P., Geider, R.J., 2017. Predictions of response to temperature are contingent on model choice and data quality. Ecol. Evol. 1–15. https://doi.org/10.1002/ece3.3576

Low-Decarie, E., Fussman, G.F., Bell, G., 2011. The effect of elevated CO_2 on growth and competition in experimental phytoplankton communities. Glob. Chang. Biol. 17, 2525–2535. https://doi.org/10.1111/j.1365-2486.2011.02402.x

Loza, M.I., Jiménez, I., Jørgensen, P.M., Arellano, G., Macía, M.J., Torrez, V.W., Ricklefs, R.E., 2017. Phylogenetic patterns of rarity in a regional species pool of tropical woody plants. Glob. Ecol. Biogeogr. 26, 1043–1054. https://doi.org/10.1111/geb.12615

Lutz, M.J., Caldeira, K., Dunbar, R.B., Behrenfeld, M.J., 2007. Seasonal rhythms of net primary production and particulate organic carbon flux to depth describe the efficiency of biological pump in the global ocean. J. Geophys. Res. Ocean. 112. https://doi.org/10.1029/2006JC003706

Machac, A., Zrzavý, J., Storch, D., 2011. Range size heritability in carnivora is driven by geographic constraints. Am. Nat. 177, 767–779. https://doi.org/10.1086/659952

MacKenzie, L.A., Selwood, A.I., McNabb, P., Rhodes, L., 2011. Benthic dinoflagellate toxins in two warm-temperate estuaries: Rangaunu and Parengarenga Harbours, Northland, New Zealand. Harmful Algae 10, 559–566. https://doi.org/10.1016/j.hal.2011.02.007

Magozzi, S., Calosi, P., 2015. Integrating metabolic performance, thermal tolerance, and plasticity enables for more accurate predictions on species vulnerability to acute and chronic effects of global warming. Glob. Chang. Biol. 21, 181–194. https://doi.org/10.1111/gcb.12695

Marañón, E., Cermeño, P., Huete-Ortega, M., López-Sandoval, D.C., Mouriño-Carballido, B., Rodríguez-Ramos, T., 2014. Resource supply overrides temperature as a controlling factor of marine phytoplankton growth. PLoS One 9, e99312. https://doi.org/10.1371/journal.pone.0099312

Márcia Barbosa, A., Sillero, N., Martínez-Freiría, F., Real, R., 2012. Ecological niche models in Mediterranean herpetology: Past, present and future, in: Zhang, W.-J. (Ed.), Ecological niche models in Mediterranean herpetology. Nova Publishers, pp. 173–204.

Marr, J.C., Jackson, A.E., McLachlan, J.L., 1992. Occurrence of *Prorocentrum lima*, a DSP toxin-producing species from the Atlantic coast of Canada. J. Appl. Phycol. 4, 17–24. https://doi.org/10.1007/BF00003956

Martine Morlaix, Patrick Lassus, 1992. Influence de l'azote et du phosphore sur la croissance et la toxicité de *Prorocentrum lima* (Ehrenberg) Dodge. Cryptogam. Algol 13, 187–195.

Masuda, R., 2008. Seasonal and interannual variation of subtidal fish assemblages in Wakasa Bay with reference to the warming trend in the Sea of Japan. Environ. Biol. Fishes 82, 387–399. https://doi.org/10.1007/s10641-007-9300-z

Maxwell, D.P., Falk, S., Trick, C.G., Huner, N., 1994. Growth at low temperature mimics high-light acclimation in *Chlorella vulgaris*. Plant Physiol. 105, 535–543.

McCarty, J.P., 2001. Ecological consequences of recent climate change. Conserv. Biol. 15, 320–331. https://doi.org/10.1046/j.1523-1739.2001.015002320.x

Milazzo, M., Mirto, S., Domenici, P., Gristina, M., 2013. Climate change exacerbates interspecific interactions in sympatric coastal fishes. J. Anim. Ecol. 82, 468–477. https://doi.org/10.1111/j.1365-2656.2012.02034.x

Mittelbach, G.G., Schemske, D.W., Cornell, H. V., Allen, A.P., Brown, J.M., Bush, M.B., Harrison, S.P., Hurlbert, A.H., Knowlton, N., Lessios, H.A., McCain, C.M., McCune, A.R., McDade, L.A., McPeek, M.A., Near, T.J., Price, T.D., Ricklefs, R.E., Roy, K., Sax, D.F., Schluter, D., Sobel, J.M., Turelli, M., 2007. Evolution and the latitudinal diversity gradient: speciation, extinction and biogeography. Ecol. Lett. 10, 315–331. https://doi.org/10.1111/j.1461-0248.2007.01020.x

Moenickes, S., Frassl, M., Schlief, J., Kupisch, M., Mutz, M., Suhling, F., Richter, O., 2012. Temporal patterns of populations in a warming world: A modelling framework. Mar. Biol. 159, 2605–2620. https://doi.org/10.1007/s00227-012-1996-4

Moestrup, Ø., Akselmann, R., Fraga, S., Hoppenrath, M., Iwataki, M., Komárek, J., Larsen, J., Lundholm, N., Zingone, A., 2009. IOC-UNESCO Taxonomic Reference List of Harmful Micro Algae (HABs). http://www.marinespecies.org/hab/index.php

Molnár, P.K., Kutz, S.J., Hoar, B.M., Dobson, A.P., 2013. Metabolic approaches to understanding climate change impacts on seasonal host-macroparasite dynamics. Ecol. Lett. 16, 9–21. https://doi.org/10.1111/ele.12022

Montoya, J.P., Holl, C.M., Zehr, J.P., Hansen, A., Villareal, T.A., Capone, D.G., 2004. High rates of N_2 fixation by unicellular diazotrophs in the oligotrophic Pacific Ocean. Nature 430, 1027–1031. https://doi.org/10.1038/nature02824

Moore, S.K., Trainer, V.L., Mantua, N.J., Parker, M.S., Laws, E.A., Backer, L.C., Fleming, L.E., 2008. Impacts of climate variability and future climate change on harmful algal blooms and human health. Environ. Health 7 Suppl 2, S4. https://doi.org/10.1186/1476-069X-7-S2-S4

Moore, S.K., Mantua, N.J., Kellogg, J.P., Newton, J.A., Moore, S.K., Mantua, N.J., Kellogg, J.P., Newton, J.A., 2008. Local and large-scale climate forcing of Puget Sound oceanographic properties on seasonal to interdecadal timescales. Limnol. Oceanogr. 53, 1746–1758.

Moran, P.A.P., 1948. The Interpretation of statistical maps. J. R. Stat. Soc. Ser. B. https://doi.org/10.2307/2983777

Moran, P.A.P., 1950. Notes on continuous stochastic phenomena. Biometrika 37, 17. https://doi.org/10.2307/2332142

Morin, X., Lechowicz, M.J., 2008. Contemporary perspectives on the niche that can improve models of species range shifts under climate change. Biol. Lett. https://doi.org/10.1098/rsbl.2008.0181

Mortain-Bertrand, A., Descolas-Gros, C., Jupin, H., 1988. Growth, photosynthesis and carbon metabolism in the temperate marine diatom *Skeletonema costatum* adapted to low temperature and low photon-flux density. Mar. Biol. 100, 135–141. https://doi.org/10.1007/BF00392963

Morton, S.L., Tindall, D.R., 1995. Morphological and biochemical variability of the toxic dinoflagellate *Prorocentrum lima* isolated from three locations at Heron island, Australia. J. Phycol. 31, 914–921. https://doi.org/10.1111/j.0022-3646.1995.00914.x

Münkemüller, T., Lavergne, S., Bzeznik, B., Dray, S., Jombart, T., Schiffers, K., Thuiller, W., 2012. How to measure and test phylogenetic signal. Methods Ecol. Evol. 3, 743–756. https://doi.org/10.1111/j.2041-210X.2012.00196.x

Murphy, H.T., Lovett-Doust, J., 2007. Accounting for regional niche variation in habitat suitability models. Oikos 116, 99–110. https://doi.org/10.1111/j.2006.0030-1299.15050.x

Nakagawa, S., Schielzeth, H., 2013. A general and simple method for obtaining R^2 from generalized linear mixed-effects models. Methods Ecol. Evol. 4, 133–142. https://doi.org/10.1111/j.2041-210x.2012.00261.x

Nascimento, S.M., Purdie, D.A., Morris, S., 2005. Morphology, toxin composition and pigment content of *Prorocentrum lima* strains isolated from a coastal lagoon in southern UK. Toxicon 45, 633–649. https://doi.org/10.1016/j.toxicon.2004.12.023

Nedwell, D.B., Rutter, M., 1994. Influence of temperature on growth rate and competition between two psychrotolerant antarctic bacteria: Low temperature diminishes affinity for substrate uptake. Appl. Environ. Microbiol. 60, 1984–1992. https://doi.org/10.1128/aem.60.6.1984-1992.1994

Nilsson-Örtman, V., Stoks, R., Johansson, F., 2014. Competitive interactions modify the temperature dependence of damselfly growth rates. Ecology 95, 1394–1406. https://doi.org/10.1890/13-0875.1

O'Brien, C.J., Peloquin, J.A., Vogt, M., Heinle, M., Gruber, N., Ajani, P., Andruleit, H., Arístegui, J., Beaufort, L., Estrada, M., Karentz, D., Kopczyńska, E., Lee, R., Poulton, A.J., Pritchard, T., Widdicombe, C., 2013. Global marine plankton functional type biomass distributions: Coccolithophores. Earth Syst. Sci. Data 5, 259–276. https://doi.org/10.5194/essd-5-259-2013

OBIS, 2018. Ocean Biogeographic Information System. Intergov. Oceanogr. Comm. UNESCO. URL www.iobis.org

Ooms, J., Chamberlain, S., 2019. phylocomr: Interface to "Phylocom".

Orr, R.J.S., Stüken, A., Murray, S.A., Jakobsen, K.S., 2013. Evolutionary acquisition and loss of saxitoxin biosynthesis in dinoflagellates: The second "core" gene, sxtG. Appl. Environ. Microbiol. 79, 2128–2136. https://doi.org/10.1128/AEM.03279-12

Pacifici, M., Foden, W.B., Visconti, P., Watson, J.E.M., Butchart, S.H.M., Kovacs, K.M., Scheffers, B.R., Hole, D.G., Martin, T.G., Akçakaya, H.R., Corlett, R.T., Huntley, B., Bickford, D., Carr, J.A., Hoffmann, A.A., Midgley, G.F., Pearce-Kelly, P., Pearson, R.G., Williams, S.E., Willis, S.G., Young, B., Rondinini, C., 2015. Assessing species vulnerability to climate change. Nat. Clim. Chang. https://doi.org/10.1038/nclimate2448

Padfield, D., Buckling, A., Warfield, R., Lowe, C., Yvon-Durocher, G., 2018. Linking phytoplankton community metabolism to the individual size distribution. Ecol. Lett. 21, 1152–1161. https://doi.org/10.1111/ele.13082

Pagel, M., 1999. Inferring the historical patterns of biological evolution. Nature 401, 877–884. https://doi.org/10.1038/44766

Palevsky, H.I., Quay, P.D., 2017. Influence of biological carbon export on ocean carbon uptake over the annual cycle across the North Pacific Ocean. Global Biogeochem. Cycles 31, 81–95. https://doi.org/10.1002/2016GB005527

Pan, Y., Cembella, A.D., Quilliam, M.A., 1999. Cell cycle and toxin production in the benthic dinoflagellate *Prorocentrum lima*. Mar. Biol. 134, 541–549. https://doi.org/10.1007/s002270050569

Pan, Y., Subba Rao, D. V., Mann, K.H., 1996. Changes in domoic acid production and cellular chemical composition of the toxigenic diatom *Pseudo-nitschia multiseries* under phosphate limitation. J. Phycol. 32, 371–381. https://doi.org/10.1111/j.0022-3646.1996.00371.x

Pardew, J., Blanco Pimentel, M., Low-Decarie, E., 2018. Predictable ecological response to rising CO_2 of a community of marine phytoplankton. Ecol. Evol. 4292–4302. https://doi.org/10.1002/ece3.3971

Park, T., 1954. Experimental studies of interspecies competition II. Temperature, humidity, and competition in two Species of *Tribolium*. Physiol. Zool. 27, 177–238. https://doi.org/10.1086/physzool.27.3.30152164

Parmesan, C., Gaines, S., Gonzalez, L., Kaufman, D.M., Kingsolver, J., Townsend Peterson, A., Sagarin, R., 2005. Empirical perspectives on species borders: from traditional biogeography to global change. Oikos 108, 58–75. https://doi.org/10.1111/j.0030-1299.2005.13150.x

Parmesan, C., Yohe, G., Andrus, J.E., 2003. A globally coherent fingerprint of climate change impacts across natural systems.

Payne, N.L., Smith, J.A., 2017. An alternative explanation for global trends in thermal tolerance. Ecol. Lett. 20, 70–77. https://doi.org/10.1111/ele.12707

Pearson, R.G., 2007. Species' distribution modeling for conservation educators and practitioners. Synthesis. Am. Museum Nat. Hist. 3, 1–50.

Pearson, R.G., Dawson, T.P., 2003. Predicting the impacts of climate change on the distribution of species: Are bioclimate envelope models useful? Glob. Ecol. Biogeogr. 12, 361–371. https://doi.org/10.1046/j.1466-822X.2003.00042.x

Pecl, G.T., Araújo, M.B., Bell, J.D., Blanchard, J., Bonebrake, T.C., Chen, I.C., Clark, T.D., Colwell, R.K., Danielsen, F., Evengård, B., Falconi, L., Ferrier, S., Frusher, S., Garcia, R.A., Griffis, R.B., Hobday, A.J., Janion-Scheepers, C., Jarzyna, M.A., Jennings, S., Lenoir, J., Linnetved, H.I., Martin, V.Y., McCormack, P.C., McDonald,

J., Mitchell, N.J., Mustonen, T., Pandolfi, J.M., Pettorelli, N., Popova, E., Robinson, S.A., Scheffers, B.R., Shaw, J.D., Sorte, C.J.B., Strugnell, J.M., Sunday, J.M., Tuanmu, M.N., Vergés, A., Villanueva, C., Wernberg, T., Wapstra, E., Williams, S.E., 2017. Biodiversity redistribution under climate change: Impacts on ecosystems and human well-being. Science. https://doi.org/10.1126/science.aai9214

Pedersen, E.J., Miller, D.L., Simpson, G.L., Ross, N., 2019. Hierarchical generalized additive models in ecology: an introduction with mgcv. PeerJ 7, e6876. https://doi.org/10.7717/peerj.6876

Perini, F., Galluzzi, L., Dell'Aversano, C., Iacovo, E., Tartaglione, L., Ricci, F., Forino, M., Ciminiello, P., Penna, A., 2014. *sxtA* and *sxtG* gene expression and toxin production in the Mediterranean *Alexandrium minutum* (Dinophyceae). Mar. Drugs 12, 5258–5276. https://doi.org/10.3390/md12105258

Peter, K.H., Sommer, U., 2013. Phytoplankton cell size reduction in response to warming mediated by nutrient limitation. PLoS One 8, e71528. https://doi.org/10.1371/journal.pone.0071528

Peterson, A.T., 2006. Uses and requirements of ecological niche models and related distributional models. Biodivers. Informatics 59–72.

Pohnert, G., Steinke, M., Tollrian, R., 2007. Chemical cues, defence metabolites and the shaping of pelagic interspecific interactions. Trends Ecol. Evol. https://doi.org/10.1016/j.tree.2007.01.005

Poloczanska, E.S., Brown, C.J., Sydeman, W.J., Kiessling, W., Schoeman, D.S., Moore, P.J., Brander, K., Bruno, J.F., Buckley, L.B., Burrows, M.T., Duarte, C.M., Halpern, B.S., Holding, J., Kappel, C. V., O'Connor, M.I., Pandolfi, J.M., Parmesan, C., Schwing, F., Thompson, S.A., Richardson, A.J., 2013. Global imprint of climate change on marine life. Nat. Clim. Chang. 3, 919–925. https://doi.org/10.1038/nclimate1958

Poloczanska, E.S., Burrows, M.T., Brown, C.J., Molinos, J.G., Halpern, B.S., Hoegh-Guldberg, O., Kappel, C. V., Moore, P.J., Richardson, A.J., Schoeman, D.S., Sydeman, W.J., 2016. Responses of marine organisms to climate change across oceans. Front. Mar. Sci. https://doi.org/10.3389/fmars.2016.00062

Pörtner, H.O., 2002. Climate variations and the physiological basis of temperature dependent biogeography: systemic to molecular hierarchy of thermal tolerance in animals. Comp. Biochem. Physiol. A. Mol. Integr. Physiol. 132, 739–61.

Price, T.D., Kirkpatrick, M., 2009. Evolutionarily stable range limits set by interspecific competition. Proc. R. Soc. B Biol. Sci. 276, 1429–1434. https://doi.org/10.1098/rspb.2008.1199

Prinzing, A., Durka, W., Klotz, S., Brandl, R., 2001. The niche of higher plants: Evidence for phylogenetic conservatism. Proc. R. Soc. B Biol. Sci. 268, 2383–2389. https://doi.org/10.1098/rspb.2001.1801

Pulliam, H.R., 2000. On the relationship between niche and distribution. Ecol. Lett. https://doi.org/10.1046/j.1461-0248.2000.00143.x

Quilliam, M.A., Hardstaff, W.R., Ishida, Noriko, 2, McLachlan, J.L., Reeves, A.R., Ross, N.W., Windust, A.J., 1996. Production of Diarrhetic Shellfish Poisoning (DSP) toxins by *Prorocentrum lima* in culture and development of analytical methods, in: Yasumoto, T., Oshima, Y., Fukuyo, Y. (Eds.), Harmful and toxic algal blooms. IOC/UNESCO, Paris, pp. 289–92.

R Core Team, 2019. R: A language and environment for statistical computing.

Ramsey, U.P., Douglas, D.J., Walter, J.A., Wright, J.L., 1998. Biosynthesis of domoic acid by the diatom *Pseudo-nitzschia multiseries*. Nat. Toxins 6, 137–146.

https://doi.org/10.1002/(SICI)1522-7189(199805/08)6:3/4<137::AID-NT28>3.0.CO;2-L

Ras, M., Steyer, J.-P., Bernard, O., 2013. Temperature effect on microalgae: a crucial factor for outdoor production. Rev. Environ. Sci. Bio/Technology 12, 153–164. https://doi.org/10.1007/s11157-013-9310-6

Rasmussen, S.A., Andersen, A.J.C., Andersen, N.G., Nielsen, K.F., Hansen, P.J., Larsen, T.O., 2016. Chemical diversity, origin, and analysis of phycotoxins. J. Nat. Prod. 79, 662–673. https://doi.org/10.1021/acs.jnatprod.5b01066

Ratkowsky, D.A., Olley, J., Ross, T., 2005. Unifying temperature effects on the growth rate of bacteria and the stability of globular proteins. J. Theor. Biol. 233, 351–362. https://doi.org/10.1016/j.jtbi.2004.10.016

Raven, J.A., Geider, R.J., 1988. Temperature and algal growth. New Phytol. 110, 441–461. https://doi.org/10.1111/j.1469-8137.1988.tb00282.x

Regaudie-De-Gioux, A., Duarte, C.M., 2012. Temperature dependence of planktonic metabolism in the ocean. Global Biogeochem. Cycles 26, n/a-n/a. https://doi.org/10.1029/2010GB003907

Reuman, D.C., Holt, R.D., Yvon-Durocher, G., 2014. A metabolic perspective on competition and body size reductions with warming. J. Anim. Ecol. 83, 59–69. https://doi.org/10.1111/1365-2656.12064

Rhein, M., Rintoul, S., Aoki, S., Campos, E., Chambers, D., Feely, R., Gulev, S., Johnson, G., Josey, S., Kostianoy, A., Mauritzen, C., Roemmich, D., Talley, L., Wang, F., 2013. Observations: Ocean, in: Stocker, T.F., Qin, D., Plattner, G.K., Tignor, M., Allen, S.K., Boschung, J., Nauels, A., Xia, Y., Bex, V., Midgley, P.M. (Eds.), Climate Change 2013: The Physical Science Basis. Contribution of Working Group I to the Fifth Assessment Report of the Intergovernmental Panel on Climate Change. Cambridge University Press, Cambridge, United Kingdom and New York, NY, USA.

Righetti, D., Vogt, M., Gruber, N., Psomas, A., Zimmermann, N.E., 2019. Global pattern of phytoplankton diversity driven by temperature and environmental variability. Sci. Adv. 5. https://doi.org/10.1126/sciadv.aau6253

Rohlf, F.J., 2001. Comparative methods for the analysis of continuous variables: Geometric interpretations. Evolution (N. Y). 55, 2143–2160. https://doi.org/10.1111/j.0014-3820.2001.tb00731.x

Root, T.L., Price, J.T., Hall, K.R., Schneider, S.H., Rosenzweig, C., Pounds, J.A., 2003. Fingerprints of global warming on wild animals and plants. Nature 421, 57–60. https://doi.org/10.1038/nature01333

Rosenzweig, C., Casassa, D., Karoly, A., Imeson, C., Liu, A., Menzel, S., Tyrjanowski, P., 2007. Impacts, adaptation and vulnerability. Contribution of Working Group II to the Fourth Assessment Report of the Intergovernmental Panel on Climate Change. O. Parry, J. Canz. P. Palutikof, C. van Der Linden C. Hanson 79–131.

Rosenzweig, M.L., 1995. Species-area curves: large issues, in: Species diversity in space and time. https://doi.org/10.1017/CBO9780511623387

Rossini, G.P., Hess, P., 2010. Phycotoxins: chemistry, mechanisms of action and shellfish poisoning. EXS 100, 65–122.

Rosso, L., Lobry, J.R., Flandrois, J.P., 1993. An unexpected correlation between cardinal temperatures of microbial growth highlighted by a new model. J. Theor. Biol. 162, 447–463. https://doi.org/10.1006/jtbi.1993.1099

Roy, K., Jablonski, D., Valentine, J.W., 1994. Eastern Pacific molluscan provinces and latitudinal diversity gradient: No evidence for "Rapoport's rule." Proc. Natl. Acad. Sci. U. S. A. 91, 8871–8874. https://doi.org/10.1073/pnas.91.19.8871

Rushton, S.P., Ormerod, S.J., Kerby, G., 2004. New paradigms for modelling species distributions? J. Appl. Ecol. https://doi.org/10.1111/j.0021-8901.2004.00903.x

Salvador, G.-R.J., Jiménez, L., Quiroz-Reyes, A.P., Sotelo-Pedroza, S.C., Jorge, S., 2019. On some problems of estimating fundamental niche from physiological data. bioRxiv 716688. https://doi.org/10.1101/716688

Sánchez-Fernández, D., Aragón, P., Bilton, D.T., Lobo, J.M., 2012. Assessing the congruence of thermal niche estimations derived from distribution and physiological data. A test using diving beetles. PLoS One 7, e48163. https://doi.org/10.1371/journal.pone.0048163

Sánchez-Fernández, D., Rizzo, V., Cieslak, A., Faille, A., Fresneda, J., Ribera, I., 2016. Thermal niche estimators and the capability of poor dispersal species to cope with climate change. Sci. Rep. 6. https://doi.org/10.1038/srep23381

Savage, V.M., Gillooly, J.F., Brown, J.H., West, G.B., Charnov, E.L., 2004. Effects of body size and temperature on population growth, Am. Nat.

Sayers, E.W., Barrett, T., Benson, D.A., Bryant, S.H., Canese, K., Chetvernin, V., Church, D.M., DiCuccio, M., Edgar, R., Federhen, S., Feolo, M., Geer, L.Y., Helmberg, W., Kapustin, Y., Landsman, D., Lipman, D.J., Madden, T.L., Maglott, D.R., Miller, V., Mizrachi, I., Ostell, J., Pruitt, K.D., Schuler, G.D., Sequeira, E., Sherry, S.T., Shumway, M., Sirotkin, K., Souvorov, A., Starchenko, G., Tatusova, T.A., Wagner, L., Yaschenko, E., Ye, J., 2009. Database resources of the National Center for Biotechnology Information. Nucleic Acids Res. 37, D5–D15. https://doi.org/10.1093/nar/gkn741

Schiebel, R., 2002. Planktic foraminiferal sedimentation and the marine calcite budget. https://doi.org/10.1029/2001GB001459

Schindelin, J., Arganda-Carreras, I., Frise, E., Kaynig, V., Longair, M., Pietzsch, T., Preibisch, S., Rueden, C., Saalfeld, S., Schmid, B., Tinevez, J.Y., White, D.J., Hartenstein, V., Eliceiri, K., Tomancak, P., Cardona, A., 2012. Fiji: An open-source platform for biological-image analysis. Nat. Methods. https://doi.org/10.1038/nmeth.2019

Sett, S., Bach, L.T., Schulz, K.G., Koch-Klavsen, S., Lebrato, M., Riebesell, U., 2014. Temperature modulates coccolithophorid sensitivity of growth, photosynthesis and alcification to increasing seawater pCO_2. PLoS One 9, e88308. https://doi.org/10.1371/journal.pone.0088308

Sexton, J.P., McIntyre, P.J., Angert, A.L., Rice, K.J., 2009. Evolution and ecology of species range limits. Annu. Rev. Ecol. Evol. Syst. 40, 415–436. https://doi.org/10.1146/annurev.ecolsys.110308.120317

Silvertown, J., McConway, K., Gowing, D., Dodd, M., Fay, M.F., Joseph, J.A., Dolphin, K., 2006. Absence of phylogenetic signal in the niche structure of meadow plant communities. Proc. R. Soc. B Biol. Sci. 273, 39–44. https://doi.org/10.1098/rspb.2005.3288

Simó, R., 2001. Production of atmospheric sulfur by oceanic plankton: Biogeochemical, ecological and evolutionary links. Trends Ecol. Evol. https://doi.org/10.1016/S0169-5347(01)02152-8

Simon, N., Cras, A.L., Foulon, E., Lemée, R., 2009. Diversity and evolution of marine phytoplankton. Comptes Rendus - Biol. https://doi.org/10.1016/j.crvi.2008.09.009

Slatyer, R.A., Hirst, M., Sexton, J.P., 2013. Niche breadth predicts geographical range size: a general ecological pattern. Ecol. Lett. 16, 1104–1114. https://doi.org/10.1111/ele.12140

Soberón, J., 2007. Grinnellian and Eltonian niches and geographic distributions of species. Ecol. Lett. https://doi.org/10.1111/j.1461-0248.2007.01107.x

Soberon, J., Arroyo-Peña, B., 2017. Are fundamental niches larger than the realized? Testing a 50-year-old prediction by Hutchinson. PLoS One 12. https://doi.org/10.1371/journal.pone.0175138

Soberón, J., Nakamura, M., 2009. Niches and distributional areas: Concepts, methods, and assumptions. Proc. Natl. Acad. Sci. U. S. A. 106, 19644–19650. https://doi.org/10.1073/pnas.0901637106

Sorte, C.J.B., Williams, S.L., Carlton, J.T., 2010. Marine range shifts and species introductions: comparative spread rates and community impacts. Glob. Ecol. Biogeogr. 19, 303–316. https://doi.org/10.1111/j.1466-8238.2009.00519.x

Staehr, P.A., Birkeland, M.J., 2006. Temperature acclimation of growth, photosynthesis and respiration in two mesophilic phytoplankton species. Phycologia 45, 648–656. https://doi.org/10.2216/06-04.1

Steele, J.H., 1985. A comparison of terrestrial and marine ecological systems. Nature. https://doi.org/10.1038/313355a0

Stenseth, N.C., Durant, J.M., Fowler, M.S., Matthysen, E., Adriaensen, F., Jonzén, N., Chan, K.S., Liu, H., De Laet, J., Sheldon, B.C., Visser, M.E., Dhondt, A.A., 2015. Testing for effects of climate change on competitive relationships and coexistence between two bird species. Proc. R. Soc. B Biol. Sci. 282. https://doi.org/10.1098/rspb.2014.1958

Sterner, R.W., Grover, J.P., 1998. Algal growth in warm temperate reservoirs: kinetic examination of nitrogen, temperature, light, and other nutrients. Water Res. 32, 3539–3548. https://doi.org/10.1016/S0043-1354(98)00165-1

Stevens, G.C., 1989. The latitudinal gradient in geographical range: How so many species coexist in the tropics. Am. Nat. 133, 240–256. https://doi.org/10.1086/284913

Stuart-Smith, R.D., Edgar, G.J., Barrett, N.S., Kininmonth, S.J., Bates, A.E., 2015. Thermal biases and vulnerability to warming in the world's marine fauna. Nature 528, 88–92. https://doi.org/10.1038/nature16144

Stuart-Smith, R.D., Edgar, G.J., Bates, A.E., 2017. Thermal limits to the geographic distributions of shallow-water marine species. Nat. Ecol. Evol. 1, 1846–1852. https://doi.org/10.1038/s41559-017-0353-x

Stüken, A., Orr, R.J.S., Kellmann, R., Murray, S.A., Neilan, B.A., Jakobsen, K.S., 2011. Discovery of nuclear-encoded genes for the neurotoxin saxitoxin in dinoflagellates. PLoS One 6, e20096. https://doi.org/10.1371/journal.pone.0020096

Sun, J., Liu, D., 2003. Geometric models for calculating cell biovolume and surface area for phytoplankton. J. Plankton Res. 25, 1331–1346. https://doi.org/10.1093/plankt/fbg096

Sunday, J.M., Bates, A.E., Dulvy, N.K., 2011. Global analysis of thermal tolerance and latitude in ectotherms. Proc. R. Soc. B Biol. Sci. 278, 1823–1830. https://doi.org/10.1098/rspb.2010.1295

Sunday, J.M., Bates, A.E., Dulvy, N.K., 2012. Thermal tolerance and the global redistribution of animals. Nat. Clim. Chang. 2, 686–690. https://doi.org/10.1038/nclimate1539

Sunday, J.M., Bates, A.E., Kearney, M.R., Colwell, R.K., Dulvy, N.K., Longino, J.T., Huey, R.B., 2014. Thermal-safety margins and the necessity of thermoregulatory behavior across latitude and elevation. Proc. Natl. Acad. Sci. U. S. A. 111, 5610–5615. https://doi.org/10.1073/pnas.1316145111

Sutherst, R.W., Maywald, G.F., Bourne, A.S., 2007. Including species interactions in risk assessments for global change. Glob. Chang. Biol. 13, 1843–1859. https://doi.org/10.1111/j.1365-2486.2007.01396.x

Tatters, A.O., Flewelling, L.J., Fu, F., Granholm, A.A., Hutchins, D.A., 2013. High CO_2 promotes the production of paralytic shellfish poisoning toxins by *Alexandrium catenella* from Southern California waters. Harmful Algae 30, 37–43. https://doi.org/10.1016/j.hal.2013.08.007

Tester, P.A., 1994. Harmful marine phytoplankton and shellfish toxicity. Potential consequences of climate change. Ann. N. Y. Acad. Sci. 740, 69–76.

Thomas, C.D., Cameron, A., Green, R.E., Bakkenes, M., Beaumont, L.J., Collingham, Y.C., Erasmus, B.F.N., Ferreira De Siqueira, M., Grainger, A., Hannah, L., Hughes, L., Huntley, B., Van Jaarsveld, A.S., Midgley, G.F., Miles, L., Ortega-Huerta, M.A., Peterson, A.T., Phillips, O.L., Williams, S.E., 2004. Extinction risk from climate change. Nature 427, 145–148. https://doi.org/10.1038/nature02121

Thomas, M.K., Aranguren-Gassis, M., Kremer, C.T., Gould, M.R., Anderson, K., Klausmeier, C.A., Litchman, E., 2017. Temperature-nutrient interactions exacerbate sensitivity to warming in phytoplankton. Glob. Chang. Biol. 23, 3269–3280. https://doi.org/10.1111/gcb.13641

Thomas, M.K., Kremer, C.T., Klausmeier, C.A., Litchman, E., 2012. A global pattern of thermal adaptation in marine phytoplankton. Science. 338, 1085–1088. https://doi.org/10.1126/science.1224836

Thomas, M.K., Kremer, C.T., Litchman, E., 2016. Environment and evolutionary history determine the global biogeography of phytoplankton temperature traits. Glob. Ecol. Biogeogr. 25, 75–86. https://doi.org/10.1111/geb.12387

Tilman, D., 1981. Tests of resource competition theory using four species of Lake Michigan Algae. Ecology 62, 802–815. https://doi.org/10.2307/1937747

Tittensor, D.P., Mora, C., Jetz, W., Lotze, H.K., Ricard, D., Berghe, E. Vanden, Worm, B., 2010. Global patterns and predictors of marine biodiversity across taxa. Nature 466, 1098–1101. https://doi.org/10.1038/nature09329

Tomas, C.R., Baden, D.G., 1993. The influence of phosphorus source on the growth and cellular toxin content of the benthic dinoflagellate *Prorocentrum lima*, in: Smayda, T., Shimizu, Y. (Eds.), Toxic phytoplankton blooms in the Sea. Elsevier, Amsterdam, The Netherlands, pp. 565–570.

Tomašových, A., Kennedy, J.D., Betzner, T.J., Kuehnle, N.B., Edie, S., Kim, S., Supriya, K., White, A.E., Rahbek, C., Huang, S., Price, T.D., Jablonski, D., 2016. Unifying latitudinal gradients in range size and richness across marine and terrestrial systems. Proc. R. Soc. B Biol. Sci. 283. https://doi.org/10.1098/rspb.2015.3027

Toseland, A., Daines, S.J., Clark, J.R., Kirkham, A., Strauss, J., Uhlig, C., Lenton, T.M., Valentin, K., Pearson, G.A., Moulton, V., Mock, T., 2013. The impact of temperature on marine phytoplankton resource allocation and metabolism. Nat. Clim. Chang. 3, 979–984. https://doi.org/10.1038/nclimate1989

Touzet, N., Franco, J.M., Raine, R., 2007. Characterization of nontoxic and toxin-producing strains of *Alexandrium minutum* (Dinophyceae) in Irish coastal waters. Appl. Environ. Microbiol. 73, 3333–3342. https://doi.org/10.1128/AEM.02161-06

Tozzi, S., Schofield, O., Falkowski, P., 2004. Historical climate change and ocean turbulence as selective agents for two key phytoplankton functional groups. Mar. Ecol. Prog. Ser. 274, 123–132. https://doi.org/10.3354/meps274123

Tréguer, P.J., De La Rocha, C.L., 2013. The World Ocean Silica Cycle. Ann. Rev. Mar. Sci. 5, 477–501. https://doi.org/10.1146/annurev-marine-121211-172346

Turner, A.D., Dhanji-Rapkova, M., Fong, S.Y.T., Hungerford, J., McNabb, P.S., Boundy, M.J., Harwood, D.T., 2019. Ultrahigh-Performance Hydrophilic Interaction Liquid Chromatography with Tandem Mass Spectrometry Method for the determination of Paralytic Shellfish Toxins and Tetrodotoxin in mussels, oysters, clams, cockles, and

scallops: Collaborative study. J. AOAC Int. 103, 1–30. https://doi.org/10.5740/jaoacint.19-0240

Tylianakis, J.M., Didham, R.K., Bascompte, J., Wardle, D.A., 2008. Global change and species interactions in terrestrial ecosystems. Ecol. Lett. https://doi.org/10.1111/j.1461-0248.2008.01250.x

Usup, G., Kulis, D.M., Anderson, D.M., 1994. Growth and toxin production of the toxic dinoflagellate *Pyrodinium bahamense* var. *compressum* in laboratory cultures. Nat. Toxins 2, 254–62.

Vale, P., Veloso, V., Amorim, A., 2009. Toxin composition of a *Prorocentrum lima* strain isolated from the Portuguese coast. Toxicon 54, 145–152. https://doi.org/10.1016/j.toxicon.2009.03.026

Van Der Meer, J., 2006. Metabolic theories in ecology. Trends Ecol. Evol. 21, 136–140. https://doi.org/10.1016/j.tree.2005.11.004

Vanucci, S., Guerrini, F., Milandri, A., Pistocchi, R., 2010. Effects of different levels of N- and P-deficiency on cell yield, okadaic acid, DTX-1, protein and carbohydrate dynamics in the benthic dinoflagellate *Prorocentrum lima*. Harmful Algae 9, 590–599. https://doi.org/10.1016/j.hal.2010.04.009

Varkitzi, I., Pagou, K., Granéli, E., Hatzianestis, I., Pyrgaki, C., Pavlidou, A., Montesanto, B., Economou-Amilli, A., 2010. Unbalanced N:P ratios and nutrient stress controlling growth and toxin production of the harmful dinoflagellate *Prorocentrum lima* (Ehrenberg) Dodge. Harmful Algae 9, 304–311. https://doi.org/10.1016/j.hal.2009.12.001

Vázquez, D.P., Stevens, R.D., 2004. The latitudinal gradient in niche breadth: concepts and evidence. Am. Nat. 164. https://doi.org/10.1086/421445

Vlamis, A., Katikou, P., Rodriguez, I., Rey, V., Alfonso, A., Papazachariou, A., Zacharaki, T., Botana, A.M., Botana, L.M., 2015. First detection of tetrodotoxin in Greek shellfish by UPLC-MS/MS potentially linked to the presence of the dinoflagellate *Prorocentrum minimum*. Toxins (Basel). 7, 1779–1807. https://doi.org/10.3390/toxins7051779

Vogt, M., O'Brien, C., Peloquin, J., Schoemann, V., Breton, E., Estrada, M., Gibson, J., Karentz, D., Van Leeuwe, M.A., Stefels, J., Widdicombe, C., Peperzak, L., 2012. Global marine plankton functional type biomass distributions: *Phaeocystis* spp. Earth Syst. Sci. Data 4, 107–120. https://doi.org/10.5194/essd-4-107-2012

Waldron, A., 2007. Null models of geographic range size evolution reaffirm its heritability evidence for ecosystem services & conservation land management view project. https://doi.org/10.1086/518963

Walther, G.R., Post, E., Convey, P., Menzel, A., Parmesan, C., Beebee, T.J.C., Fromentin, J.M., Hoegh-Guldberg, O., Bairlein, F., 2002. Ecological responses to recent climate change. Nature. https://doi.org/10.1038/416389a

Wang, L., Yan, T., Yu, R., Zhou, M., 2005. Experimental study on the impact of dinoflagellate *Alexandrium* species on populations of the rotifer *Brachionus plicatilis*. Harmful Algae 4, 371–382. https://doi.org/10.1016/j.hal.2004.06.014

Wang, Q., Lyu, Z., Omar, S., Cornell, S., Yang, Z., Montagnes, D.J.S., 2018. Predicting temperature impacts on aquatic productivity: Questioning the metabolic theory of ecology's "canonical" activation energies. Limnol. Oceanogr. https://doi.org/10.1002/lno.11105

Webb, C.O., Ackerly, D.D., Kembel, S.W., 2008. Phylocom: software for the analysis of phylogenetic community structure and trait evolution. Bioinformatics 24, 2098–2100. https://doi.org/10.1093/bioinformatics/btn358

Webb, C.O., Donoghue, M.J., 2005. Phylomatic: tree assembly for applied phylogenetics. Mol. Ecol. Notes 5, 181–183. https://doi.org/10.1111/j.1471-8286.2004.00829.x

Wernberg, T., Smale, D.A., Thomsen, M.S., 2012. A decade of climate change experiments on marine organisms: Procedures, patterns and problems. Glob. Chang. Biol. 18, 1491–1498. https://doi.org/10.1111/j.1365-2486.2012.02656.x

Wiens, J.J., 2011. The niche, biogeography and species interactions. Philos. Trans. R. Soc. Lond. B. Biol. Sci. 366, 2336–50. https://doi.org/10.1098/rstb.2011.0059

Wiens, J.J., Graham, C.H., 2005. Niche conservatism: Integrating evolution, ecology, and conservation biology. Annu. Rev. Ecol. Evol. Syst. 36, 519–539. https://doi.org/10.1146/annurev.ecolsys.36.102803.095431

Willig, M.R., Kaufman, D.M., Stevens, R.D., 2003. Latitudinal gradients of biodiversity: Pattern, process, scale, and synthesis. Annu. Rev. Ecol. Evol. Syst. https://doi.org/10.1146/annurev.ecolsys.34.012103.144032

Willig, M.R., Lyons, S.K., 1998. An analytical model of latitudinal gradients of species richness with an empirical test for marsupials and bats in the New World. Oikos 81, 93. https://doi.org/10.2307/3546471

Willig, M.R., Presley, S.J., 2018. Latitudinal gradients of biodiversity: Theory and empirical patterns, in: Encyclopedia of the Anthropocene. pp. 13–19. https://doi.org/10.1016/b978-0-12-809665-9.09809-8

Woods, A., 2016. Domoic acid production in *Pseudo-nitzschia* (Bacillariophyceae) as a general response to unbalanced growth : The role of photo-oxidative stress. California State University, Monterey Bay.

Woodward, G., Benstead, J.P., Beveridge, O.S., Blanchard, J., Brey, T., Brown, L.E., Cross, W.F., Friberg, N., Ings, T.C., Jacob, U., Jennings, S., Ledger, M.E., Milner, A.M., Montoya, J.M., O'Gorman, E., Olesen, J.M., Petchey, O.L., Pichler, D.E., Reuman, D.C., Thompson, M.S.A., Van Veen, F.J.F., Yvon-Durocher, G., 2010. Ecological networks in a changing climate, Advances in Ecological Research. Academic Press. https://doi.org/10.1016/B978-0-12-381363-3.00002-2

Wright, J.L.C., Cembella, A.D., 1998. Ecophysiology and biosynthesis of polyether marine biotoxins., in: Anderson, D.M., Cembella, A.D., Hallegraeff, G.M. (Eds.), Physiological ecology of harmful algal blooms. pp. 427–451.

Yang, C.Z., Albright, L.J., 1992. Effects of the harmful diatom *Chaetoceros concavicornis* on respiration of rainbow trout *Oncorhynchus mykiss*. Dis. Aquat. Organ. 14, 105–114.

Yang, I., John, U., Beszteri, S., Glöckner, G., Krock, B., Goesmann, A., Cembella, A.D., 2010. Comparative gene expression in toxic versus non-toxic strains of the marine dinoflagellate *Alexandrium minutum*. BMC Genomics 11. https://doi.org/10.1186/1471-2164-11-248

Zou, D., Gao, K., Luo, H., 2011. Short- and long-term effects of elevated CO_2 on photosynthesis and respiration in the marine macroalga *Hizikia fusiformis* (Sargassaceae, Phaeophyta) grown at low and high N supplies. J. Phycol. 47, 87–97. https://doi.org/10.1111/j.1529-8817.2010.00929.x